Ehsan Noroozinejad Farsangi ·
Izuru Takewaki · Tony Y. Yang ·
Abolhassan Astaneh-Asl · Paolo Gardoni
Editors

Resilient Structures and Infrastructure

Springer

Resilient Structures and Infrastructure

Ehsan Noroozinejad Farsangi ·
Izuru Takewaki · Tony Y. Yang ·
Abolhassan Astaneh-Asl ·
Paolo Gardoni
Editors

Resilient Structures and Infrastructure

≜ Springer

Editors
Ehsan Noroozinejad Farsangi
School of Civil and Surveying Engineering
Graduate University of Advanced
Technology
Kerman, Iran

Izuru Takewaki
Department of Architecture and
Architectural Engineering
Kyoto University
Kyoto, Japan

Tony Y. Yang
Department of Civil Engineering
The University of British Columbia
Vancouver, BC, Canada

Abolhassan Astaneh-Asl
Department of Civil and Environmental
Engineering
University of California, Berkeley
Berkeley, CA, USA

Paolo Gardoni
Department of Civil and Environmental
Engineering
University of Illinois at Urbana-Champaign
Urbana, IL, USA

Preface

Over the last decade, the concept of resilience has gained considerable attention recognizing the fact that all hazards or threats cannot be averted. The efforts of communities around the world have been to clearly define and enhance their resilience against extreme disasters. The resilience of structures and infrastructure is becoming an important issue for developed countries accepting the fact that they cannot prevent future hazards, but rather they have to manage and minimize their impacts on humans and assets. There is a large debate in the literature on how to define resilience. The concept of resilience does not have a unique meaning and implication in all fields of science and engineering due to its broad use. This edited book is mainly focused on resilience related topics in the field of engineering. In this context, the word resilience can be defined as the capability of a system to maintain or promptly recover its functionality in the face of extreme events.

A growing number of structures are built in disaster-prone areas. To this, when a natural or anthropogenic hazard occurs, structures and infrastructure have to be not only capable of withstanding them but they also have to be resilient. In this context, the concept of resilience-based design can be regarded as a prerequisite to enhance the sustainability of modern societies through a multiscale approach: from a single structure scale to urban environment scale.

The objective of this book is to highlight criticalities in current structural design practice and to provide guidelines to help researchers, engineers, and policy-makers toward more resilient structures and infrastructure. To this aim, the book content is divided into three sections. The first part contains 11 chapters discussing the resilient-based design in structures with an emphasis on buildings. The content covers a wide range of topics including the resilient structural elements and fuses, resilience-based design against earthquake, blast, flooding and other hazards, risk management, and proposed hazard mitigation frameworks. The second part presents contributions on the resilience of infrastructure. The content covers the resilience issues related to mitigation schemes, bridging multi-hazard, and critical infrastructure. The last part presents fundamental works related to the concept of resilience and its mathematical formulation.

It is our hope that this book, which integrates the concept and theoretical aspects of resilience, will serve as a comprehensive guide and reference for practicing engineers, researchers, educators, and recent graduates entering the civil engineering profession by assuring them that they have discovered an exciting world of challenges and opportunities.

Kerman, Iran   Ehsan Noroozinejad Farsangi
Kyoto, Japan   Izuru Takewaki
Vancouver, Canada   Tony Y. Yang
Berkeley, USA   Abolhassan Astaneh-Asl
Urbana, USA   Paolo Gardoni
January 2019

Contents

Contributors

Taiwo J. Adedeji Faculty of Computing, Engineering and the Built Environment, Birmingham City University, Birmingham, UK

Rabindra Adhikari Department of Civil Engineering, Cosmos College of Management and Technology, Pokhara University, Pokhara, Nepal; Interdisciplinary Research Institute for Sustainability (IRIS), Kathmandu, Nepal

Athanasios Agalianos ETH Zurich, Zurich, Switzerland

Ioannis Anastasopoulos ETH Zurich, Zurich, Switzerland

Bikalpa Aryal Department of Civil Engineering, Cosmos College of Management and Technology, Pokhara University, Pokhara, Nepal

Abolhassan Astaneh-Asl University of California, Berkeley, USA

Ersin Aydin Nigde Ömer Halisdemir University, Nigde, Turkey

Aleksandra Bogdanovic Institute of Earthquake Engineering and Engineering Seismology, Skopje, Macedonia

Henry V. Burton Department of Civil and Environmental Engineering, University of California Los Angeles, Los Angeles, USA

Manuel Campidelli Institute for Multi-Hazard Systemic Risk Studies—Interface, Department of Civil Engineering, McMaster University, Hamilton, ON, Canada

G. P. Cimellaro Politecnico di Torino, Turin, Italy

Shahrzad Dastmalchi Department of Civil and Environmental Engineering, University of California Los Angeles, Los Angeles, USA

M. De Iuliis Politecnico di Torino, Turin, Italy

Raffaele De Risi Department of Civil Engineering, University of Bristol, Bristol, UK

You Dong Department of Civil Engineering, The Hong Kong Polytechnic University, Kowloon, Hong Kong, China

Maciej Dutkiewicz University of Science and Technology, Bydgoszcz, Poland

Wael W. El-Dakhakhni Institute for Multi-Hazard Systemic Risk Studies—Interface, Department of Civil Engineering, McMaster University, Hamilton, ON, Canada

Ehsan Noroozinejad Farsangi Graduate University of Advanced Technology, Kerman, Iran

Tiago Miguel Ferreira ISISE, Institute of Science and Innovation for Bio-Sustainability (IB-S), Department of Civil Engineering, University of Minho, Guimarães, Portugal

Kohei Fujita Department of Architecture and Architectural Engineering, Kyoto University, Kyoto, Japan

Paolo Gardoni Department of Civil and Environmental Engineering, MAE Center, University of Illinois at Urbana-Champaign, Urbana, IL, USA

Dipendra Gautam Structural and Geotechnical Dynamics Laboratory, StreGa, University of Molise, Campobasso, Italy

Thomas Gernay Department of Civil Engineering, Johns Hopkins University, Baltimore, MD, USA

Kamal Ghalan Department of Civil Engineering, Cosmos College of Management and Technology, Pokhara University, Pokhara, Nepal

Paul Gharzouzi Department of Civil and Environmental Engineering, MAE Center, University of Illinois at Urbana-Champaign, Urbana, IL, USA

Katsuichiro Goda Department of Earth Sciences, Western University, London, Canada

Héctor Hernández-Ramírez Mexico City, Mexico

Pratyush Jha Digicon Engineering Consult, Lalitpur, Nepal

Liam Jones ETH Zurich, Zurich, Switzerland

Innocent Kafodya University of Malawi, The Polytechnic, Blantyre, Malawi

O. Kammouh Politecnico di Torino, Turin, Italy

Negar Elhami Khorasani Department of Civil, Structural and Environmental Engineering, University at Buffalo NY, Buffalo, NY, USA

Panos Kloukinas Faculty of Engineering & Science, University of Greenwich, Chatham, UK

Kotaro Kojima Faculty of Design and Architecture, Kyoto Institute of Technology, Kyoto, Japan

Wolfgang Kröger ETH Zurich, Zürich, Switzerland

Ji Yun Lee Department of Civil and Environmental, Washington State University, Pullman, USA

Paulo B. Lourenço ISISE, Institute of Science and Innovation for Bio-Sustainability (IB-S), Department of Civil Engineering, University of Minho, Guimarães, Portugal

John Macdonald Department of Civil Engineering, University of Bristol, Bristol, UK

Scott J. Menegon Swinburne University of Technology, Melbourne, VIC, Australia;
Wallbridge Gilbert Aztec, Melbourne, VIC, Australia

Saber Moradi Department of Civil Engineering, Ryerson University, Toronto, USA

Gokarna Motra Department of Civil Engineering, Institute of Engineering, Pulchowk Campus, Lalitpur, Nepal

Aman Mwafy United Arab Emirates University, Al-Ain, UAE

Horacio de Jesús Nangullasmú-Hernández Posgrado en Ingeniería Estructural, Universidad Autónoma Metropolitana—Azcapotzalco, Mexico City, Mexico

Ignasio Ngoma University of Malawi, The Polytechnic, Blantyre, Malawi

Viviana Novelli Department of Civil Engineering, University of Bristol, Bristol, UK

Victor O. Oladokun Industrial and Production Engineering, University of Ibadan, Ibadan, Nigeria

Baki Öztürk Hacettepe University, Ankara, Turkey

David G. Proverbs Faculty of Computing, Engineering and the Built Environment, Birmingham City University, Birmingham, UK

Xin Qian John A. Martin Associates Structural Engineers, Los Angeles, USA

Saim Raza Swinburne University of Technology, Melbourne, VIC, Australia

Hugo Rodrigues RISCO-School of Management and Technology, Polytechnic Institute of Leiria, Leiria, Portugal

Jayant Kumar Routray Regional and Rural Development Program, Asian Institute of Technology, Khlong Luang, Thailand

Rajesh Rupakhety Earthquake Engineering Research Center, University of Iceland, Selfoss, Iceland

Lampros Sakellariadis ETH Zurich, Zurich, Switzerland

Shady Salem Civil Engineering Department, The British University in Egypt, El-Sherouk City, Cairo, Egypt;
Department of Civil Engineering, McMaster University, Hamilton, ON, Canada

Yongjiu Shi Tsinghua University, Beijing, China

Michael J. Tait Institute for Multi-Hazard Systemic Risk Studies—Interface, Department of Civil Engineering, McMaster University, Hamilton, ON, Canada

Izuru Takewaki Department of Architecture and Architectural Engineering, Kyoto University, Kyoto, Japan

Arturo Tena-Colunga Departamento de Materiales, Universidad Autónoma Metropolitana—Azcapotzalco, Mexico City, Mexico

S. Tesfamariam The University of British Columbia, Vancouver, Canada

Hing-Ho Tsang Swinburne University of Technology, Melbourne, VIC, Australia

Md. Shahab Uddin Disaster Preparedness, Mitigation and Management, Asian Institute of Technology, Khlong Luang, Thailand

Pennung Warnitchai School of Engineering & Technology, Asian Institute of Technology, Khlong Luang, Thailand

John L. Wilson Swinburne University of Technology, Melbourne, VIC, Australia

Hong Xiao Faculty of Computing, Engineering and the Built Environment, Birmingham City University, Birmingham, UK

Part I
Resilience in Structures

Application of Steel Shear Walls Toward More Resilient Structures

Abolhassan Astaneh-Asl, Xin Qian and Yongjiu Shi

1 Introduction

Steel shear wall systems are one of the main steel lateral force-resisting systems in buildings. Other commonly used steel lateral force resisting systems are the moment frame, concentrically braced frame, and eccentrically braced frame. Figure 1 shows the main components of a steel plate shear wall, which are the steel infill plate, the surrounding boundary beams and boundary columns, connections of the infill plate to boundary columns and beams, beam-to-column connections, stiffeners if any, the base connections of the columns, and the splices of the boundary columns.

Steel shear walls are divided into *stiffened* and *unstiffened*. In unstiffened shear walls, the infill plate has no stiffeners, as shown in Fig. 2a, while in the stiffened steel shear walls, there are horizontal or vertical stiffeners on one side, or both horizontal and vertical stiffeners either on one side or each on one side of the steel infill plate, Fig. 2b.

Early steel shear walls used in the 1960s and '70s were stiffened to prevent buckling of relatively thin infill plates until the plate yields in shear. Later, during the 1980s, the thin unstiffened steel plate shear walls became popular after the post-buckling capacity from the diagonal tension field action of the unstiffened infill plates was recognized. The superior shear resistance, stable hysteresis behavior, high-energy dissipation capability, and high ductility, as well as the inherent redundancy, have made the steel plate shear walls a promising alternative to conventional lateral load-resisting systems in high seismic and wind regions. Unstiffened shear

A. Astaneh-Asl (✉)
University of California, Berkeley, USA
e-mail: astaneh@berkeley.edu

X. Qian
John A. Martin Associates Structural Engineers, Los Angeles, USA

Y. Shi
Tsinghua University, Beijing, China

3

Steel Beam

Steel Infill Plate

Steel Column

Column Splice

Beam-to-Column
Connection

Corner Brackets

Fin Plates

Stiffeners in
"Stiffened"
Shear Walls

Base Beam

Column Base
Connection

Fin
Plates   Infill
                          Plate

Beam Section

Column Section

Example of
Column Splice

Field Fillet
Welds

Example of
Beam-to-Column Connection
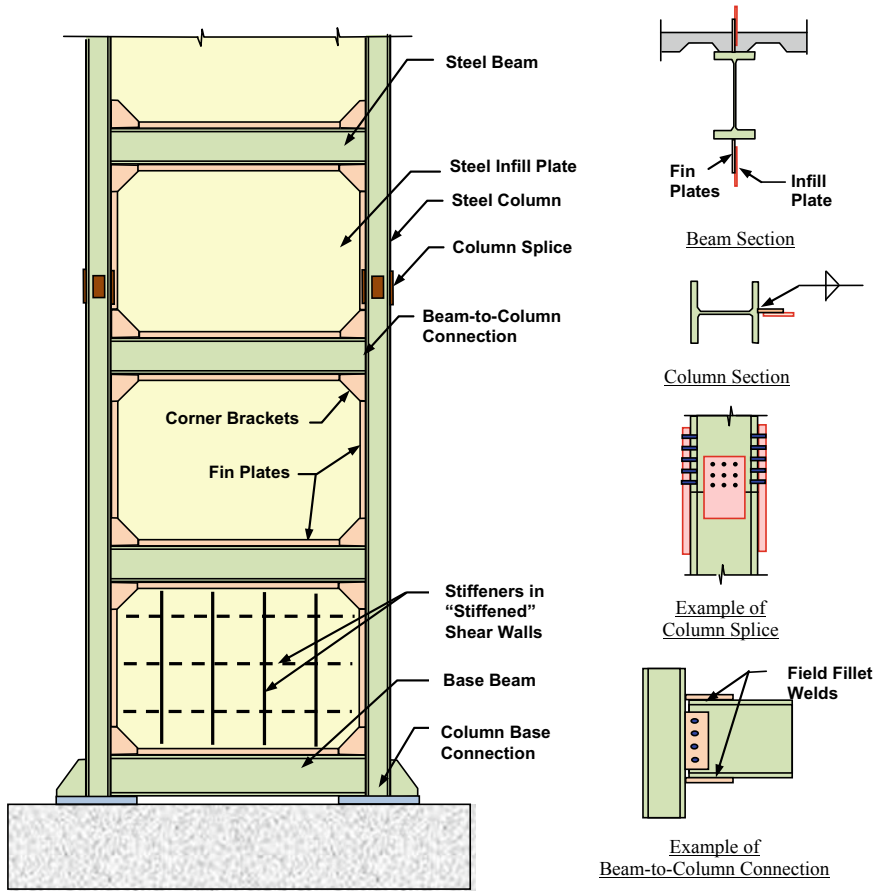
Fig. 1 Main components of a typical steel shear wall system

Steel Plate

Fin Plates

Steel Infill Plate

Boundary Column

Boundary Beam
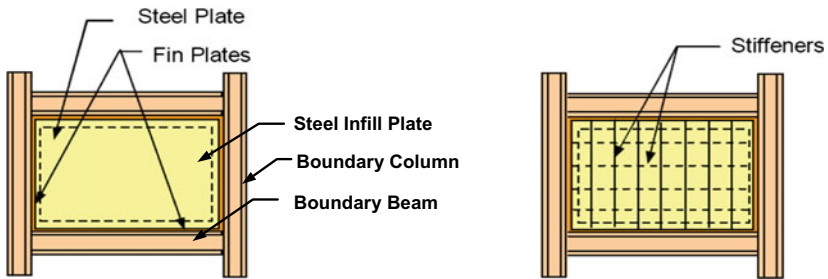
Stiffeners

(a) *Unstiffened* Steel Shear Wall   (b) *Stiffened* Steel Shear Wall

Fig. 2 Components of typical unstiffened and stiffened steel shear walls
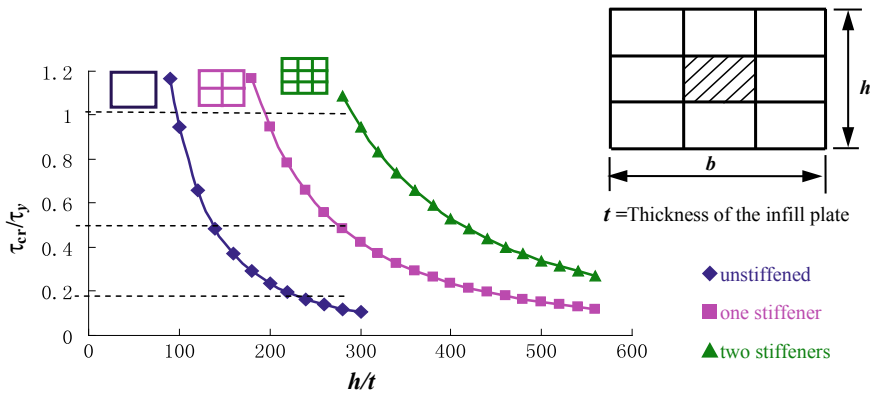
Fig. 3 Shear buckling strength of unstiffened and stiffened steel shear walls

walls are quite popular in the U.S. and Canada, while the steel shear walls used in China and Japan are often stiffened.

The stiffened steel shear walls, compared to unstiffened steel shear walls are more expensive, due to the added cost of stiffeners, and occupy more floor space, again, because of the presence of stiffeners. The loss of usable space can result in a substantial financial loss, especially in high rise buildings.

Figure 3 shows the increase in shear strength of the unstiffened steel plate shear wall when stiffeners added (Shi and Astaneh-Asl 2008). The study indicated that for unstiffened shear walls when height-to-thickness ratio, h/t, is more than 300, the critical buckling stress of the wall is less than 10% of its shear yield stress. In most applications, today, the height/thickness ratio of unstiffened shear walls is much more than 300 and in the order of 700–1000. The current U.S. code for unstiffened steel shear walls (AISC 2016a) ignores the buckling capacity of the unstiffened shear walls, and only considers the diagonal tension field capacity in the design. As Fig. 3 (Shi and Astaneh-Asl 2008) shows, for h/t of 300 adding one or two stiffeners in vertical and horizontal directions, increased the shear buckling stress to 45 and 95% of the shear yield stress respectively. The curves indicate that to achieve a critical shear buckling stress equal to yield stress, which will result in yielding of the panel before its buckling, the height to thickness ratio of the unstiffened wall needs to be 100 or less. For stiffened walls, to ensure yielding of the panels before buckling, the same limitation applies but this time to the height-to-thickness of the panel bounded by the stiffeners.

2 Steel Shear Wall Systems

Steel shear walls are usually placed around the elevator and staircase core of the building, although in some cases they have been placed in the other bays even on the façade. Figure 4 shows common steel shear wall systems, which are single bay,

Single Bay
Steel Shear Wall

Coupled Steel Shear
Walls

Outrigger Steel Shear Walls

Steel Shear Wall System with Coupled
Bays & CFT Columns
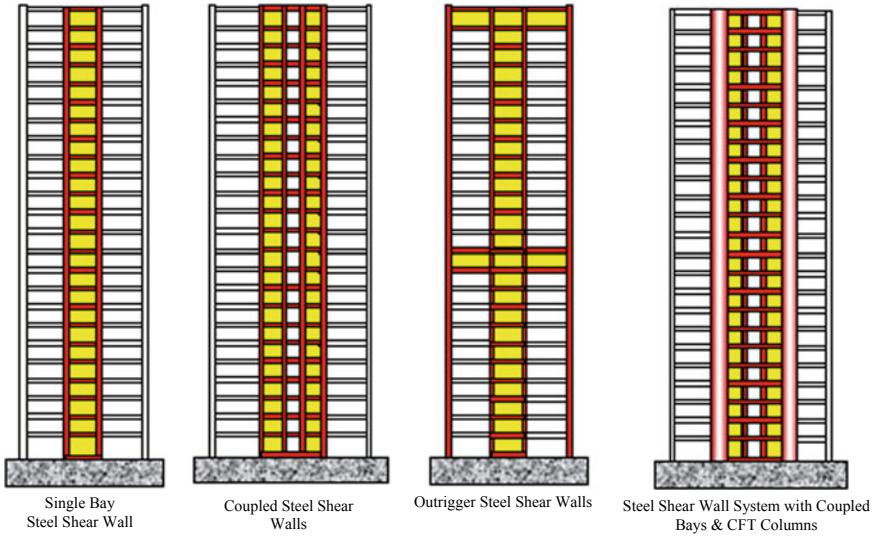
Fig. 4 Typical steel shear wall systems

coupled, outrigger and coupled bays and concrete-filled tubes, respectively. The shear wall in these systems can be either stiffened or unstiffened. The columns and the beams are usually I-section wide flanges with the web of the section in the plane of the steel plate, and the wall connected to the flanges of the columns and beams. The reason for the use of wide flange beams and columns is because of almost all early tests of steel shear walls in North America are done using such wide flange sections. However, in Japan, concrete-filled or hollow structural steel round columns are used as the boundary columns of steel shear wall systems.

The beam-to-column connections in a steel shear wall system are usually a rigid connection required by the current seismic codes. More information on beam-to-column connections in steel shear wall systems is given later in this chapter.

The most common steel shear wall system is the single bay system, where steel plate shear wall is field-welded or bolted to boundary columns and beams. In this system, the steel plate shear wall is designed to resist the entire story shear and the boundary moment frame is designed to resist overturning moment. If the steel shear wall is unstiffened, it resists the story shear by developing a diagonal tension field. The tension field action applies lateral forces to the boundary columns and beams causing shear forces and bending moments in them. The lateral forces applied to the beams from the story below and above are usually slightly different and almost cancel each other, except the roof and base beams that are subjected to lateral load only from below or above respectively. If the steel shear wall is stiffened such that the steel plate within the stiffened panels will yield before buckling, there will be no tension field action and no lateral load on the boundary beams and columns.

In a *single bay steel shear wall*, the steel plate is connected to the vertical boundary columns and horizontal boundary beams. The beam-to-column connections are generally moment connections as required by the seismic design codes such as the AISC-341 standard (AISC 2016a). The moment connections do not need to be a "Special" moment connections capable of accommodating story drift angle of at least 0.04 radians and can be "Intermediate" moment connections. Seismic design codes such as the AISC-341 standard (AISC 2016a) define the Special and Intermediate moment connections. The shear wall is designed to resist the story shear. The entire moment frame resists overturning moment as well as the gravity loads.

In a *coupled steel shear wall system*, two or more single bay steel shear walls are connected with coupling beams. The connections of coupling beams are rigid ductile moment connection. In high seismic areas, the connections should be "Special" moment connections as defined in seismic codes such as the AISC-341 standard (AISC 2016a) and are developed and expected to undergo cyclic plastic rotations of at least 0.03 radians. In coupled shear wall system, the single bay shear walls together with the coupling beams are designed to resist the story shear, and the tension and compression in the single bay shear walls resist overturning moment.

In an *outrigger steel shear wall system*, in a few floors, horizontal shear walls, or trusses, connect the shear wall to the exterior columns. The connections of the outriggers to the columns are usually rigid, but if the length of the outrigger is relatively short, the connections of the outrigger to the exterior columns can be simple (i.e., shear) connections to save in the cost of design, construction, and inspection associated with moment connections. In high seismic areas, the beam-to-column connections should be "Special" moment connections as per governing seismic code such as the AISC-341 standard (AISC 2016a). In an outrigger steel shear wall, the single bay shear walls are designed to resist the story shear only. The entire moment frame including the axial strength of the exterior columns, brought into action by the outriggers, resists the overturning moment as well as the gravity loads.

A *Coupled Bays and Concrete-Filled Tube (CFT) Columns* is an efficient steel shear wall system, originally developed and used by MKA structural engineering firm (Seilie and Hooper 2005) Zhao and Astaneh-Asl (2004, 2008) tested the system under cyclic loading and established its behavior. The system is different from the three systems mentioned above. The two large Concrete Filled Tube (CFT) columns on the right and left side of the system carry a relatively large seismic shear and vertical gravity load. The columns, beams and steel plate shear walls between the two CFT columns primarily carry the seismic load and a negligible amount of gravity load. Unlike all systems mentioned above, where the rule of "strong-column, weak beam requires that the columns remain elastic, in this system the steel columns between the two CFT composite columns are allowed to undergo significant yielding and plastification. More information on this system is provided later in this chapter.

3 Advantages and Disadvantages of Steel Plate Shear Walls

3.1 Advantages of Steel Plate Shear Walls

Compared to other lateral force resisting systems for buildings, such as steel braced or moment frames, or reinforced concrete shear wall or moment frame systems, the main advantages of steel shear wall systems are:

1. Steel shear wall systems have a relatively high shear strength-to-weight ratio compared to reinforced concrete shear walls, which results in significant reduction of the self-weight of the structure reducing gravity and seismic forces in the structure and its foundations.
2. The high ductility and energy dissipation capacity of steel shear walls makes them one of the most efficient lateral force resisting systems in high seismic areas.
3. Since steel shear walls, especially the unstiffened shear walls, have a very small footprint, the thickness of the finished wall is relatively small compared to other systems, enabling more plan areas used as the occupiable floor areas. The increase in useful floor areas can be quite significant in high-rise buildings.
4. Through prefabrication of the steel shear wall units in the shop and having bolted field splices, the costly and time-consuming field weldings can be avoided. Also, eliminating field welding enables the system to be constructed efficiently in cold weather.
5. The infill plates in a steel shear wall system are the elements that experience buckling and yielding during a major seismic event with some yielding expected in the boundary beams as well. The damaged panels can be easily replaced with new panels, and seismic resistance of the steel shear wall system can be restored relatively rapidly and economically.
6. Steel shear walls can be used in new steel and composite structures and even in new reinforced concrete buildings as the main lateral force resisting system. Also, as the past applications indicate, steel shear walls can be used efficiently in the retrofit of existing seismically deficient structures such as non-ductile reinforced concrete and masonry buildings. Examples are Veterans Administration Medical Center and Oregon State Library (Baldelli 1983; Robinson and Ames 2000).
7. As for stiffness, the shear stiffness of the stiffened shear walls, where buckling of the plate is prevented until shear yielding of the plate occurs, can be quite high. However, for unstiffened steel shear walls, due to diagonal buckling of the unstiffened plate under relatively small story drift values of about 0.005, the stiffness can be reduced considerably. The unstiffened steel plate shear wall is stiffer than a steel moment frames but is more flexible than a typical steel braced frame.

3.2 Issues in Using Steel Shear Walls

The following items are important issues in selecting steel shear walls as the lateral force resisting system.

1. A typical steel shear wall covers the entire width and height of the bay. From the architectural point of view, this can be considered as a disadvantage, especially if compared to moment frames where the bay is not obstructed. For this reason, in many applications, steel shear walls are placed around the elevator/staircase core of the buildings. If necessary, steel shear walls can have openings and penetrations as shown in Fig. 5 with added vertical and horizontal members as boundary elements at the openings. The openings that are outside the diagonal tension and compression fields are preferred.

2. Unstiffened shear walls, in general, end-up being relatively thin. Handling large and thin steel plates during construction, especially field welding of the thin plates to the boundary columns and beams can pose some difficulty. Also, welding very thin plates, even in the shop can be somewhat difficult.

3. Unstiffened shear walls need to be checked for stiffness, to ensure that under the service design wind load the diagonal buckling of the shear wall will not occur, and the stiffness of the shear wall after buckling is sufficient to satisfy the inter-story drift limits for wind and earthquakes.

4. Unstiffened steel shear walls create relatively large bending moments, axial force, and shear in the boundary columns due to tension field forces applied to the columns, making the boundary columns quite large. The solution is to eliminate the lateral forces, which can be done by using a stiffened shear walls, composite shear walls, and the High-Performance Steel Plate Shear Wall (Qian 2017; Qian and Astaneh-Asl 2016a, 2017) where the unstiffened steel plate is not connected to the boundary columns. Also, by using slit shear walls (Cortes and Liu 2011a, b), the lateral forces applied to the columns can be reduced. More on the new high-performance steel plate shear wall and slit shear wall are given later in this chapter.
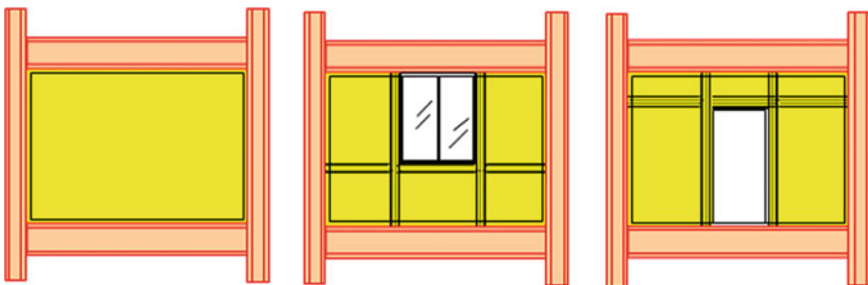
Fig. 5 Openings in steel shear walls and boundary elements around the openings

4 Examples of Constructed Steel Plate Shear Wall Buildings

Since the 1960s, stiffened steel shear walls have been used in Japan for new construction, and since the 1970s, they also found application in the U.S. in both seismic retrofit projects and new buildings. Later in the 1980s and 1990s, unstiffened steel shear walls became popular in the U.S and Canada, and recently in China. The first major tall steel plate shear wall building was the 53-story Shinjuku Nomura Building in Tokyo completed in 1978. The shear walls in this steel structure were stiffened (Astaneh-Asl 2002b). Currently, the tallest steel shear wall building in the world is the 74-story Tianjin World Financial Center in China (Sarkisian and Mathias 2012; Lee et al. 2010). More information on this structure and its design are provided later in this chapter.

In the United States, currently, the tallest steel shear wall building is the 52-story Los Angeles Convention Center Hotel (Youssef et al. 2010, 2011). Steel shear walls occasionally have been used in low rise residential building successfully to control stiffness (Eatherton 2006; Eatherton and Johnson 2004). Steel shear walls have also been used in retrofit projects. One example is the Veterans Administration Medical Center in Charleston, South Carolina. The decision to use steel shear walls instead of concrete walls was based on the need to minimize the disruption of services in the hospital, which justified the higher cost of using steel shear walls instead of concrete shear walls. The designers pointed out that wall stiffness requirements governed the design and prevented the use of thinner walls (Baldelli 1983). The stiffness of unstiffened steel shear walls can be an issue and was also mentioned in Design Guide 20 (AISC 2007). Oregon State Library is an example of retrofit of reinforced concrete moment frame with steel plate shear walls. The steel plate shear wall was chosen because book relocation could be avoided during steel construction. Bolted splices were used to minimize the risk of fire from welding in the library (Robinson and Ames 2000). Steel shear walls have also been used to strengthen steel moment frames that were damaged during the 1994 Northridge earthquake.

5 Actual Performance of Steel Shear Wall Buildings During Earthquakes

5.1 The Sylmar County Hospital (Old Olive View Medical Center), 1994 Northridge Earthquake

The Olive View Medical Center shown in Fig. 6, is a 6-story steel structure with reinforced concrete shear walls in the lower two floors and steel shear walls in the four upper floors. The floor system is a concrete slab on the steel deck. The bottom two floors have a rectangular plan, and the plan of the upper four floors is a cross

https://www.pererainc.com/healthcare-construction/olive-view-medical-center
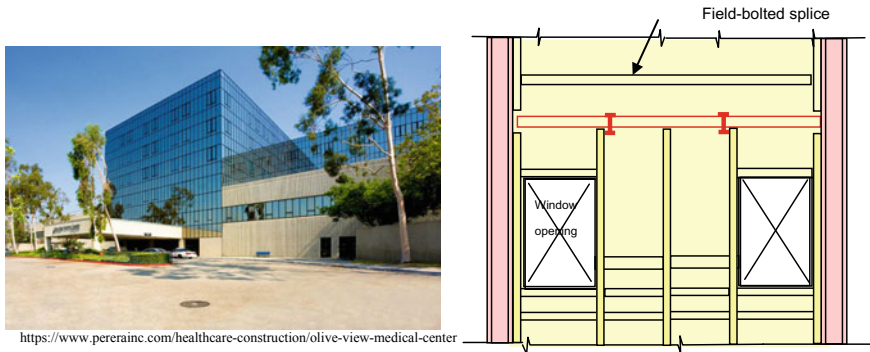
Fig. 6 The Olive View Medical Center and view of its typical shear walls

shape with stiffened steel shear walls in its perimeter (Troy and Richard 1979). During the 1994 Northridge earthquake, the building sustained serious damage to its sprinkler systems and fixed-in-place equipment, and the hospital could not function even though no damage was reported to its structure. The California Strong, Motion Instrumentation Program, instrumented the building.

The records obtained from the instrumentation indicated that on the East wall, the ground acceleration was 0.8 g, and at the roof, was 1.5 g (Astaneh-Asl 2002b). The investigation of damage to this building in the aftermath of the 1994 Northridge earthquake, by the first author, indicated that there was severe damage to some non-structural elements such as suspended ceilings and sprinkler system resulting in breakage of some sprinklers and flooding of some floors. Also, most TV sets bolted to the wall of the patient rooms had broken the connections to the wall and were thrown to the floor. The non-structural damage was an indicator of the relatively high stiffness of this structure, which was also the cause of relatively large amplification of accelerations from the ground to roof level. More information on seismic responses of this structure can be found in (Celebi 1997).

5.2 The 35-Story Office Building, 1995 Kobe Earthquake

One of the most important buildings with steel plate shear wall, subjected to a relatively strong earthquake, was the 35-story high-rise in Kobe, Japan, Fig. 7, which was subjected to the 1995 Kobe earthquake. The study of this building by Fujitani et al. (1996) indicated that the damage consisted of local buckling of the stiffened steel plate shear walls on the 26th story, Fig. 7, and a permanent roof drift of 225 mm in northerly and 35 mm in westerly directions. The results of inelastic analyses of this structure reported in Fujitani et al. (1996) indicates that soft stories may have formed at floors between 24th and 28th level of the building (Fujitani et al. 1996). A
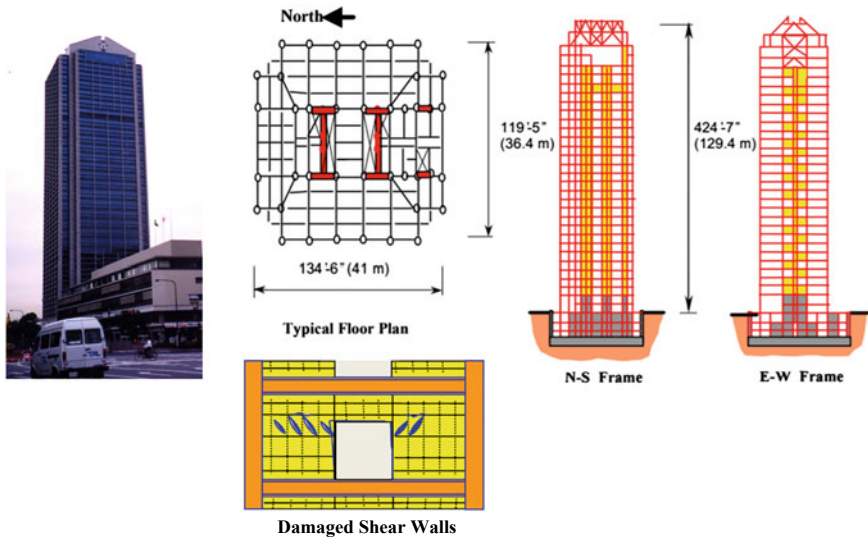
Fig. 7 The 38-story steel shear wall building and damage during the 1995 Kobe earthquake (Astaneh-Asl and Zhao 2000)

visual inspection of the structure two weeks after the earthquake by the first author did not show any sign of visual damage from outside.

6 A Brief Summary of the Past Research

Basler and Thurlimann (1961) proposed a theory for calculating the shear capacity of steel plate girders, which served as the basis of several analytical models developed later for the unstiffened steel plate shear wall system (SPSWs). Starting in the early 1980s, the post-buckling strength of steel plate shear walls was investigated at the University of Alberta, where Thorburn et al. (1983), Timler and Kulak (1983) and Tromposch and Kulak (1987) tested several single and multi-story specimens under quasi-static cyclic load, and proposed the use of a strip model to compute the post-buckling shear strength of the steel plate shear walls (Thorburn et al. 1983; Tromposch and Kulak 1987; Timler and Kulak 1983). The initial strip model proposed by Thorburn et al. (1983) was found to be capable of predicting the overall force-displacement response well but tended to overestimate the elastic stiffness. Based on test results, Timler and Kulak (1983) modified the tension field action equation proposed by Thorburn et al. (1983) for multi-story systems and included the effect of flexural stiffness of the columns.

Caccese et al. (1993) conducted tests for a series of three-story quarter-scale specimens to study the effects of different parameters on the behavior of SPSWs.

They recognized the difference in the governing limit state for thin and thick infill plates—the former is governed by yielding of infill plates, and the latter is governed by the instability of columns. Lubell (1997) tested two single panel specimens and one four-story specimen under fully reversed cyclic quasi-static loading. They found that the infill plates significantly reduced the rotational demand on the beam-to-column connections by providing a redundant lateral force resisting mechanism. The simplified strip model was again reported to be adequate in predicting post-yield strength, but not the elastic stiffness.

Driver (1997) tested a four-story-one bay specimen including gravity effects under cyclic loading. They reported that most of the energy dissipation occurred by the plates yielding with limited yielding at the beam-to-column moment connections. The strip model was found to be adequate for predicting ultimate strength but underestimated the initial stiffness. A revision of the hysteretic model proposed by Tromposch and Kulak (1987) was also proposed, in which the contributions from the moment frame and the infill panels were explicitly separated. Schumacher et al. (1999) studied four infill plate-to-boundary element connection details. The load-displacement responses of all four specimens had similar force-displacement and energy-dissipation behavior regardless of the plate-to-boundary detailing. Tears were concentrated in the corner region of three specimens.

Lubell et al. (2000) pointed out that the Canadian code provision at that time, CAN/CSA-S16.2-M94 (CSA 1994), may not be adequate for multi-story steel shear wall frames since it fails to incorporate the effects of (1) large overturning moments of multi-story frames, (2) infill panel aspect ratio and (3) the undesirable yielding sequences of the system components.

Astaneh-Asl (2002b) developed seismic design procedures for steel shear walls, which included Response Modification Factor, Displacement Amplification Factor, and Overstrength Factor. Zhao and Astaneh-Asl (2004a) tested two specimens of an innovative coupled steel shear walls system developed and used by Skilling, Ward, Magnussen, and Berkshire, now as Magnusson Klemencic Associates, a structural engineering firm in Seattle. This innovative system was used in at least one tall building. In this system, the boundary columns are relatively large concrete-filled tube composite section easily capable of resisting lateral forces of the tension field forces applied to them. Between these two boundary columns, there are two steel wide flange columns. These steel columns are not gravity columns and are allowed to yield during large seismic events. Horizontal beams are connected to all four columns. Steel shear walls are used in the two side panels. The shear walls act as coupled shear walls. The results indicated that the system has relatively high strength, high stiffness, ductility, and energy dissipation-capacities, reaching larger than 0.03-radian inter-story drift and up to 15 inelastic cycles. More information on these tests is provided later in this chapter.

Sabouri-Ghomi et al. (2005) presented a new method for calculating the shear capacity of the steel shear walls. In their method, the shear capacity of the wall was the sum of the shear capacity of the steel plate and the columns. They provided a simple, mechanics-based equation to calculate these two shear capacities and then

compared the prediction of the model to available test results, showing that the predictions are quite close to test results.

The behavior of steel plate shear wall with reduced beam section connections and composite floors was studied by Qu et al. (2008) through a two-phase experimental program on a full-scale two-story specimen. The buckled panels due to progressively increasing ground motions in Phase I was replaced by new panels before applying additional shakings in Phase II. The study verified the reparability and redundancy of the SPSW such that the repaired specimen can survive a subsequent earthquake without severe boundary frame damages or overall strength degradation, and could achieve story drifts up to 5.2% (Qu et al. 2008).

Park et al. (2007) tested five single-bay three-story specimens. They found that the shear strength and energy dissipation capacity of the steel plate walls increased in proportion to the width of the infill steel plate. Different infill plate-to-boundary connections details were also studied, and the advantages and disadvantages of each alternative were discussed (Choi and Park 2009).

Researchers proposed a plastic design method for the SPSW (Berman and Bruneau 2003), and studied many other code-based design aspects of the steel plate shear walls, such as the capacity design method for the boundary column (Qu and Bruneau 2010), how to avoid in-span hinges in the boundary beams (Qu and Bruneau 2009) and the method to reduce the system over-strength by using the balanced design concept (Purba and Bruneau 2014). By using the proposed plastic and capacity design methods, it was shown that the behavior of the SPSW system could be improved.

Shi and Astaneh-Asl (2008) investigated the design of steel plate shear walls using different design philosophies. They found that the plate girder design procedures applied to steel plate shear walls can predict the shear strength of the walls reasonably well and can lead to more economical designs. The study also established that the lateral stiffness of the wall decreases considerably as the diagonal buckling of the wall occurs at relatively small lateral drifts.

Bhowmick et al. (2009) studied strain rate and P–Δ effects and found that the loading rate increases flexural demand mostly at the base of the steel plate shear wall but has limited effects on the inelastic seismic demands for a suite of spectrum compatible earthquake records for Vancouver. They also pointed out the conservative nature of the current National Building Code of Canada stability factor approach to include the P–Δ effects for steel plate shear walls, and that P–Δ has small effects on seismic demand estimations.

Two-phase pseudo-dynamic tests on a two-story steel plate shear wall system conducted by Lin et al. (2010) showed that the steel shear wall specimens could withstand three earthquakes without significant wall fracture or overall strength deterioration, but with reduced energy-dissipating capacity when subjected to the same ground motions again in Phase II. The horizontal restrainers used in Phase I design were found to be effective in improving the serviceability of the steel plate shear wall systems. The use of a strip model and equivalent brace model was also reported to be adequate in predicting global system response provided that the boundary elements are properly designed based on capacity design principle. Habashi and Alinia (2010) examined the wall frame interaction for the system. They concluded that with prac-

tical steel plate shear wall dimensions (Length/Height < 2), if the system is designed as per the AISC Design Guide 20 rules, the frame behavior is independent of the infill plate; therefore the shear capacity of the system can be calculated by simply adding frame and the infill plate capacities. Baldvins et al. (2012) proposed a set of fragility functions for steel plate shear walls for use in the performance-based design applications.

Kharmale and Ghosh (2013) proposed a performance-based plastic design method for steel plate shear walls with rigid beam-to-column connections, where a specific ductility demand and a preferred yield mechanism are chosen as the performance target. Before this work, Ghosh et al. (2009) proposed a ductility or displacement-based design methodology for SPSW systems with simple beam-to-column connections. They considered the target displacement ductility ratio and pre-selected yield mechanism with inelastic energy balance concept in the formulation. Plastic design is performed to detail the frame members and connections to achieve the target ductility ratio and yield mechanism.

Hosseinzadeh and Tehranizadeh (2014) reviewed the code-designed SPSW system and found that the boundary frames are effective in resisting story shear only in a few lower stories, while in the upper stories the bulk of the story shear is taken by the infill plates. They also found that about 70–80% of the compressive axial force in the boundary columns results from plate tension field action. Zhang and Guo (2014) established a reduction coefficient for the shear capacity of the system considering the pre-compression effect from the shortening of the boundary columns.

7   Behavior of Typical Steel Plate Shear Walls

Figure 8 shows the results of the inelastic push-over of a typical unstiffened steel plate shear wall designed according to the AISC-341 standard (AISC 2016a) and reported in the Design Guide 20 (AISC 2007).
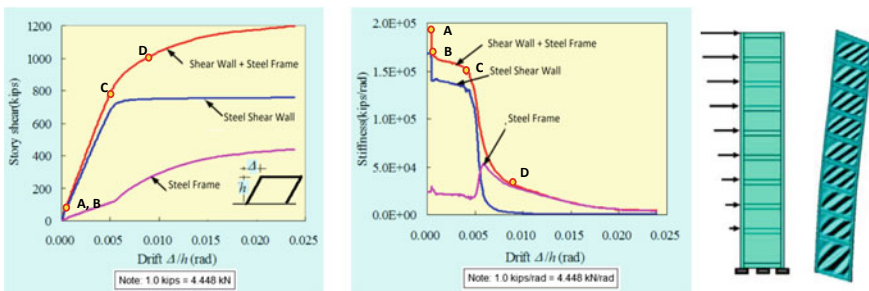

Fig. 8 Variation of story shear (left) and story lateral stiffness (right) versus story drift for a typical unstiffened single-bay steel shear wall (Shi and Astaneh-Asl 2008)

During the first phase of a pushover, the steel shear wall, and the boundary steel frame are elastic. At Point A, diagonal buckling of the unstiffened plate occurs. Due to the relatively high height-to-thickness ratio of typical steel plate shear walls, diagonal buckling occurs under relatively small story drift in the order of 0.001 radians. The shear force causing diagonal buckling was about 12% of shear yield strength of the shear wall. After diagonal buckling of the wall, lateral stiffness of the wall drops from Point A to Point B, Fig. 8 (right). The drop is about 10% of the initial stiffness of the wall. After buckling, the wall continues to resist the applied shear due to development of the tension field action. At point C the diagonal tension field yield, which causes a significant drop of lateral stiffness of the system to about 20% of the initial stiffness. At the point of yielding of the tension field area, the story drift is about 0.005 radians which is relatively small.

The lateral stiffness of steel plate shear wall designed according to the current AISC-341 standard (AISC 2016a) can be a concern and may require adding to the thickness of the wall or adding more moment frame bays as is done in Design Guide 20 (AISC 2007) Adding to the thickness of the wall will result in the development of larger tension field actions, which in turn will subject the columns to even larger lateral loads, forcing the designer to increase the size of the columns. Adding more bays of moment frames will result in higher costs since the design, construction and inspection of moment connections is quite high and can add to the cost of the structure significantly. Such solutions, which require using material and labor to increase the stiffness to satisfy the story drift limitation of the seismic codes without a need for such increase for strength purposes, can result in making the unstiffened steel shear wall uneconomical compared to other lateral force resisting systems, especially the concentrically braced frames.

As we will show later in the chapter, one solution to this problem can be to separate the steel shear wall from the columns so that the lateral forces due to tension field action do not act directly on the columns. Doing so will result in selecting the thickness of the steel shear wall to satisfy both strength and stiffness requirements without being forced to increase the size of the columns or making the shear beam-to-column connections outside the boundary frame rigid moment connections. Another solution to the problem of stiffness demand is instead of using unstiffened, use stiffened steel shear walls, where the stiffeners are designed such that the buckling of the steel panels will not occur before the yielding of the steel plate, then the system will remain elastic until the wall has yielded in shear. In this case, also, there will be no significant lateral loads acting on the columns, and the thickness of the plate can be adjusted to satisfy the strength and stiffness requirements without changing the size of the columns.

8   Modeling Steel Shear Walls

The history of analytical models and design concepts for steel shear walls dates back to the 1960s and design of steel plate girders when Basler and Thurlimann (1961), proposed analytical models and design procedures for the steel plate girders.

These plate girder design procedures served as the basis for many analytical models developed later for the steel plate shear walls.

In Japan, steel shear walls were modeled as concentrically braced frames, where the shear wall infill plates were replaced with X-bracing. During 1980s research in Canada (Tromposch and Kulak 1987; Timler and Kulak 1983; Thorburn et al. 1983) resulted in the development of the "strip" model where the steel shear wall panel was replaced with parallel diagonal truss members. The finite element models of the steel shear walls have also been used in the design of steel shear walls in important buildings such as the 73-story Jinta Building (Lee et al. 2010). In the following, the plate girder model, the shell finite element model, the strip model, and the diagonal truss model are summarized.

8.1   The Plate Girder Model and Design Procedure

Steel plate girders were studied during the 1960s by (Basler et al. 1960; Basler and Thuerlimann 1961) resulting in design procedures that recognized the development of diagonal buckling of the web plate, followed by the development of tension field action as the mechanisms of shear resistance in plate girders with relatively high height/thickness ratio of the web. Shi and Astaneh-Asl (2008) showed that the prediction of the shear strength of steel plate shear wall, modeled as plate girder and designed using the plate girder design equations closely matched the test results of steel shear walls, making the application of the plate girder design equations in the ASIC-360 standard (AISC 2016b) to design of steel shear walls a viable option.

Figure 9 shows the similarities between a plate girder and a steel shear wall. The columns in steel shear wall act as the flange of a plate girder and the beams in the steel shear wall act as stiffeners in a plate girder. Similar to plate girders, unstiffened steel plate shear walls under the applied load develop diagonal shear buckling at relatively small loads. After buckling, the applied shear is resisted primarily by the diagonal tension field action of the shear wall.

8.2   The Shell Elements Model

Currently, one of the most common methods of analysis to establish seismic forces is to model the structure elastically and subject it to "equivalent" static force established by governing codes such as the ASCE-7 (ASCE 2016). Since the analysis is elastic, the buckling phenomenon cannot be modeled directly. For design purposes, the steel shear wall can be modeled as elastic "shell" elements and the boundary beams and columns as elastic "beam" elements. The shell elements can be assigned isotropic properties to simulate the stiffness of the wall before diagonal buckling occurs. Then, a second analysis needs to be done by assigning the shell elements orthotropic
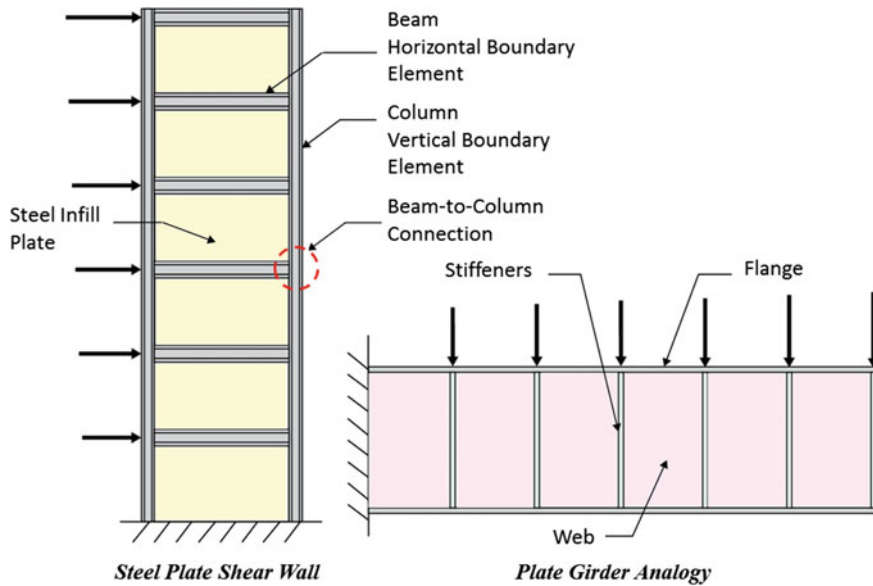
Fig. 9 Analogous relationship of the steel plate shear wall and the plate girder

properties, with the stiffness along the compression field much smaller than the stiffness along the tension field.

For important structures, such as high-rise buildings in high seismic areas, and especially when performance-based design procedures are used, (Lee et al. 2010) inelastic shell elements are used to model the steel infill plates, and inelastic beam-column members are used to model boundary beams and columns (Fig. 10 as an example). The boundary columns and beams can also be modeled using inelastic shell elements. Several past studies (Elgaaly et al. 1993; Shi and Astaneh-Asl 2008; Qian and Astaneh-Asl 2017) have shown that such "all-shell" modeling of steel shear walls predicted the stiffness and yield capacity of the shear wall, the two most important design parameters, quite accurately, although the strain hardening and failure of the first floor columns, during the late stages of the loading was not predicted by the model as accurately. Refining the material stress-strain curve and introducing initial imperfections in the columns, can improve the prediction of strain hardening and column failure.

8.3   The Strip Truss Modelling and Design

In 1980s researchers at the University of Alberta, investigated the actual behavior of steel shear wall specimens subjected to monotonic and cyclic story shear (Thorburn et al. 1983; Timler and Kulak 1983; Tromposch and Kulak 1987). They proposed
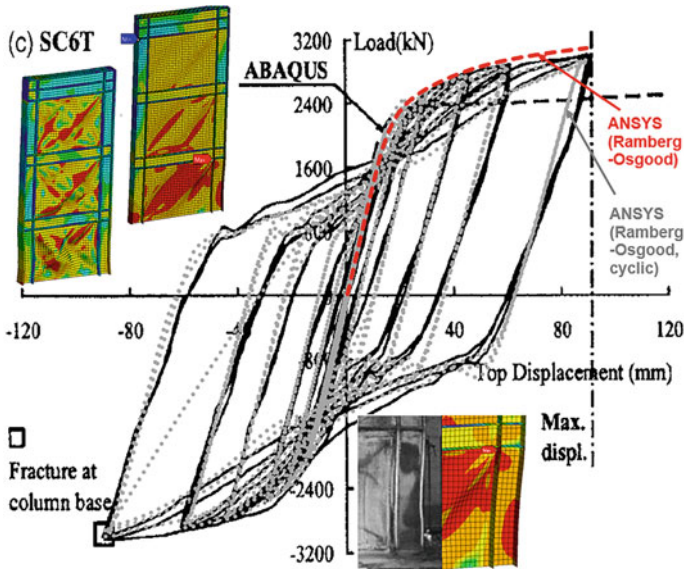
Fig. 10 Monotonic and cyclic pushover curves obtained from inelastic FE analysis compared to test results by Park et al. (2007) (Qian and Astaneh-Asl 2017)

a strip model, shown in Fig. 11a to be used for the shear wall in the analysis of the structure to establish forces developed in the components of the steel shear wall system. The walls in these studies were all unstiffened. The strip model is currently included in the North American design codes; AISC341 standard (AISC 2016a) and CAN/CSA S16-14 (CSA 2014). In this model of steel shear wall, the buckling capacity of the steel shear wall is ignored, and the steel plate is replaced by 10 or more diagonal parallel plate strips acting as pin-ended truss elements. The angle α of the strips with the vertical boundary elements, i.e., columns. The AISC-341 standard (AISC 2016a) has an equation to calculate α and also allows the angle α be taken as 40°. It was shown the strength of SPSW designed in compliance with current AISC requirements is not substantially sensitive to the angle of inclination and using a value of 40° will generally lead to slightly conservative results (Dastfan and Driver 2008).

The strip model represents the post-buckling condition of the wall and ignores the diagonal compression capacity of the wall. The model is reasonable for predicting maximum forces in the diagonal tension field as well as the lateral forces applied to boundary elements only in relatively slender walls. However, by ignoring the strength and stiffness of the compression field, the model underestimates the lateral stiffness of the shear wall system. Since seismic forces, in reality, are dynamic forces, underestimating stiffness of a system subjected to dynamic forces, will result in underestimating the actual dynamic forces generated in the system, especially in tall buildings, where the walls are relatively thick in lower floors, and their strength and stiffness in diagonal compression field cannot be ignored.

(a) Strip Model in the Current North American Design Codes

(b) Strip Model in the Current North American Design Codes
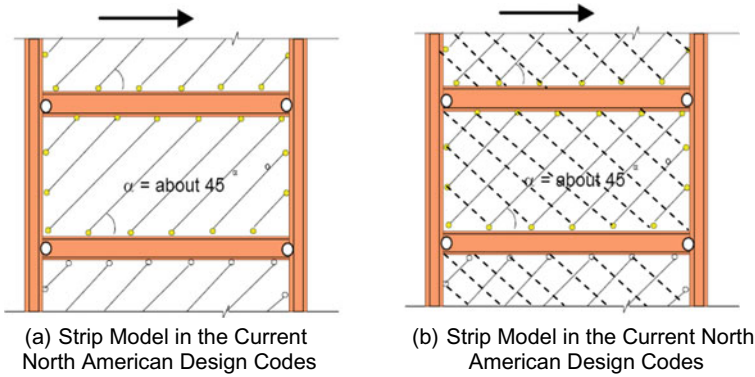
Fig. 11 The strip model of the steel shear wall

As Fig. 3 earlier shows, for unstiffened steel shear walls with height/thickness ratio of 300 or more, the shear buckling stress is 10% or less of the shear yield stress, therefore, conservatively can be ignored. A modification of the strip model is shown in Fig. 11b, where diagonal compression strips are also added. This model can correct the shortcoming of the strip-model for walls with a height/thickness ratio of more than 300. The width of compression strips can be equal to the width of tension strips times the ratio of shear buckling stress to shear yield stress given in Fig. 3 earlier.

Topkaya and Atasoy (2009) studied pre- and post-buckling shear stiffness of steel shear walls using nonlinear finite element analysis of the wall as well as the results obtained from the strip model. They concluded that (a) the lateral stiffness obtained from the finite element method is higher than the test results and can be considered an upper bound solution; (b) the strip method of analysis offers less stiffness than the test results and can be considered as a lower bound solution. Topkaya and Atasoy (2009) proposed an equation to establish pre- and post-buckling stiffness of the unstiffened steel shear walls.

8.4 The Diagonal Truss Model

The equivalent brace (EB) model shown in Fig. 12 was first proposed and recommended by Thorburn et al. (1983) for preliminary design purposes and is included in the Canadian standard CAN/CSA-S16. The inherent assumption of EB model is that all tension strips develop the same strain and can be replaced by a single diagonal truss member. The properties of the equivalent brace are related to the properties of the infill plate by matching the shear strength and stiffness of the equivalent brace to the original steel shear wall. Due to its simplicity, the EB model has also been commonly used in the analysis of SPSWs. However, certain phenomena cannot be captured by the EB model such as the tension field effects on the columns and the

Fig. 12 The equivalent brace model of the steel shear wall
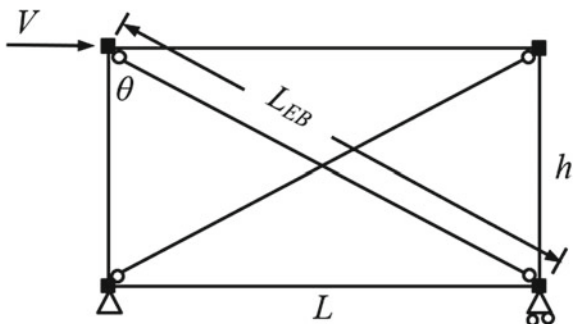
compression resistance of the panel near the corners. These concerns will be less of an issue if the infill panels are connected to the beam only since the column is no longer subjected to the distributed lateral tension field forces.

The brace area and yield stress for conventional unstiffened steel plate shear walls are shown in Eqs. 1 and 2.

$$A_{EB} = \frac{t_p L}{2} \frac{\sin^2(2\alpha)}{\sin\theta \sin(2\theta)} \tag{1}$$

$$f_{yEB} = \frac{\sin(2\theta)}{\sin(2\alpha)} \frac{L_{cf}}{L} f_{yp} \tag{2}$$

where α is the angle of inclination defined earlier, which can be taken as 40°, θ is the angle between the diagonal brace and columns; t_p is the infill plate thickness, and f_{yp} is the minimum specified yielding stress of infill plate. L is the center to center distance between columns, L_{cf} is the clear distance between column faces, and h is story height.

9 Design of Steel Shear Walls

The steel shear walls currently covered by design codes such as the AISC-341 standard (AISC 2016a) and called Special Plate Shear Walls (SPSW) consists of unstiffened steel *infill plates* connected to the *boundary steel moment frame*. The design procedures for the SPSW in the AISC-341 standard (AISC 2016a) are formulated to make the system to behave in a ductile manner under cyclic lateral forces by primarily shear yielding of the steel infill plates and development of plastic hinges at the ends of the horizontal boundary elements, i.e., beams. The boundary columns and all connections in the system are expected to remain essentially elastic. To achieve the desirable ductile behavior, the unstiffened infill plates are designed to yield in shear under the maximum applied shear force. Since the infill plates are quite slender,

they buckle diagonally during early stages of application of the shear and develop diagonal tension field action, which resists the applied shear.

9.1 Design of the Infill Plate Using Plate Girder Equations

The infill plates in early steel shear walls were designed using equations developed for steel plate girders and given in design specifications such as the AISC-341 standard (AISC 2016a). Shi and Astaneh-Asl (2008) took the 9-story steel shear walls given in the design example in AISC Design Guide 20 (AISC 2007) and redesigned them using the steel plate girder equations. The shear walls in the AISC Design Guide were designed using the "Strip" model procedures currently in the AISC-341 standard (AISC 2016a). Figure 13 shows the two design cases. Case 1A is the frame included in the AISC Design Guide 20 (AISC 2007) and designed following the procedures in the current AISC-341 standard (AISC 2016a).
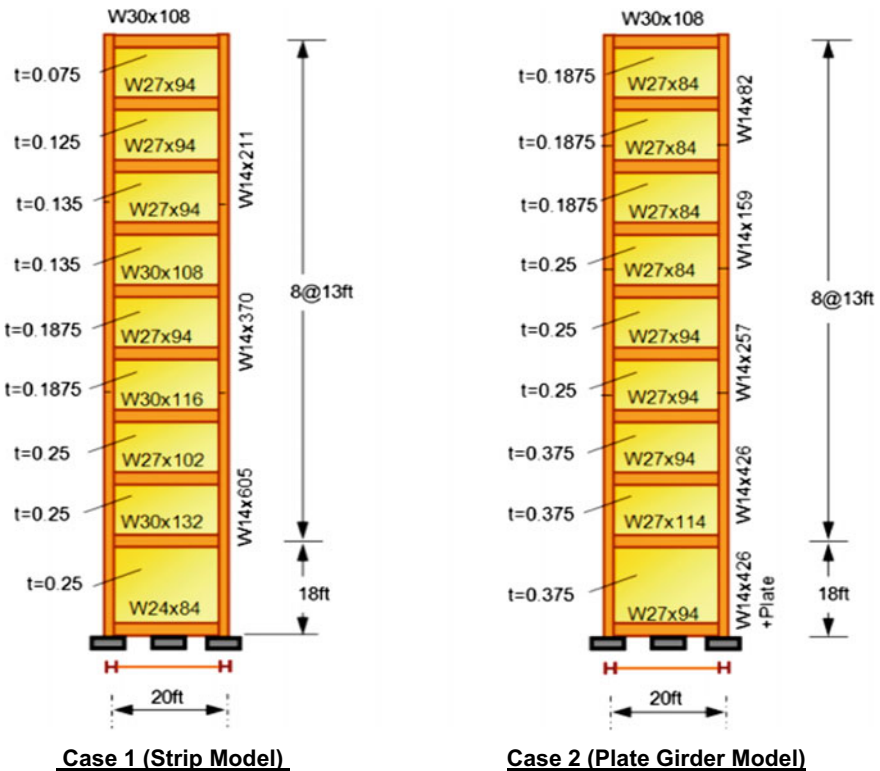
Fig. 13 Shear wall designed using "strip model" (left), and plate girder model (right) (Shi and Astaneh-Asl 2008)

Case 2A is designed following the procedures proposed by Astaneh-Asl and Shi (2008). The main difference between these two cases is that the columns in Case 1A are much heavier than the Columns in Case 2A while the walls in Case 1A are much thinner than the walls in Case 2A. The beams in Case 1A are also heavier than the beams in Case 2A. The infill wall thickness for Case 1A was less than the wall thickness for Case 2A. In both cases, all beam-to-column connections are moment connections. The weight of the 9-story shear wall and boundary columns and beams for Case 2A, designed using plate girder equations was 85% of the weight of Case 1A, which was designed using the strip model currently in the AISC-341 standard (AISC 2016a). Since the fabrication costs for both cases were almost the same, the comparison of the weight is a good measure of construction costs savings. By using the plate girder equations to design the shear wall, we could save about 15% in the cost; now, the question is what the performance of these two designs under lateral forces.

Figure 14a shows the variation of stiffness versus story drift for the shear wall in the 4th floor of both designs. The design Case 1A, the Strip Model design, shows higher initial stiffness until the infill plate buckles. The slightly high initial stiffness is due to the stiffness of relatively heavy beams and columns in the boundary frame. However, both design cases buckle diagonally at a drift level of about 0.0007. As mentioned before, diagonal buckling of the unstiffened shear wall under such relatively small drift values is a concern that is not addressed in the current AISC-341 standard (AISC 2016a). After buckling of the diagonal, tension field action develops and continues to resist shear. Case 1 design based on the current Strip Model and procedures in the AISC-341 standard (AISC 2016a) yields under a story drift of about 0.004 and drops the lateral stiffness abruptly, while the design based on the plate girder model yields at 0.0055 story drift and drop of the lateral stiffness is more gradual. Figure 14b shows the variation of story shear versus story drift. Even though, Case 2A design, based on the "Plate Girder Model" was 15% lighter than the design using the strip model, the shear yield capacity of the Case 2 shear wall was about 25% higher than
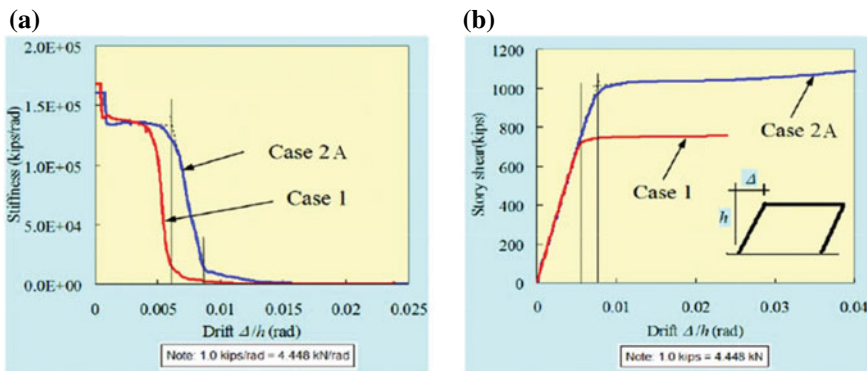
Fig. 14   a Lateral stiffness versus story drift, and **b** story shear versus story drift

the shear wall designed in AISC Design Guide 20 (AISC 2007) using the AISC (2016a) strip model procedures.

The studies by Shi and Astaneh-Asl (2008) summarized above indicated that using the plate girder equations to design steel shear walls results in a system that behaves better than a system designed using the strip model and provisions in the current AISC Seismic Provisions (AISC 2016a), has about 12% higher yield strength and is 15% lighter than the system designed using strip model.

9.2 Design of the Infill Plate Using the Strip Model

In this approach, which is currently in the AISC-341 standard (AISC 2016a), the nominal shear strength of the Special Plate Shear Walls is established by the following equation, using only tension field action and ignoring shear buckling capacity of the infill panel.

$$V_n = 0.42 f_{yp} t_p L_{cf} \sin 2\alpha \tag{3}$$

where α is the angle of infill plate yielding measured relative to the vertical defined by Eq. 3 given earlier, f_{yp} is the specified minimum yield stress of infill plate, t_p is the thickness of the infill plate, and L_{cf} is the clear distance between column flanges. In this method, there are limitations on the moment of inertia of the boundary columns and beams. The moment of inertia of the boundary column should be larger than $0.00307 \, t_w h^4 / L$. A ϕ-factor of 0.90 is used in Load and Resistance Factor (LRFD) to compare the above shear strength to the applied shear strength resulting from the application of factored lateral forces to the system.

While the plate girder equations can be applied to all values of depth-to-thickness ratio, the strip model is developed using experimental data on highly slender shear walls. It is suggested that the use of the strip model should be limited to shear walls with a height-to-depth ratio more than 500. For walls with h/t less than 500, the plate girder procedure can be used or a realistic inelastic finite element analysis or testing be conducted to establish their actual behavior.

9.3 Design of the Infill Plate Using Finite Element Model

In this method of analysis of shear wall, the infill plate is modeled as elastic or inelastic shell elements. If elastic shell elements are used, to incorporate the diagonal buckling of the infill plate, the material of the plate can be orthotropic and rotated 45° with respect to the beams. The modulus of elasticity of the diagonal tension direction can be the full elastic modulus, and for the compression diagonal direction, the modulus of elasticity can be 10% of the full modulus of elasticity.
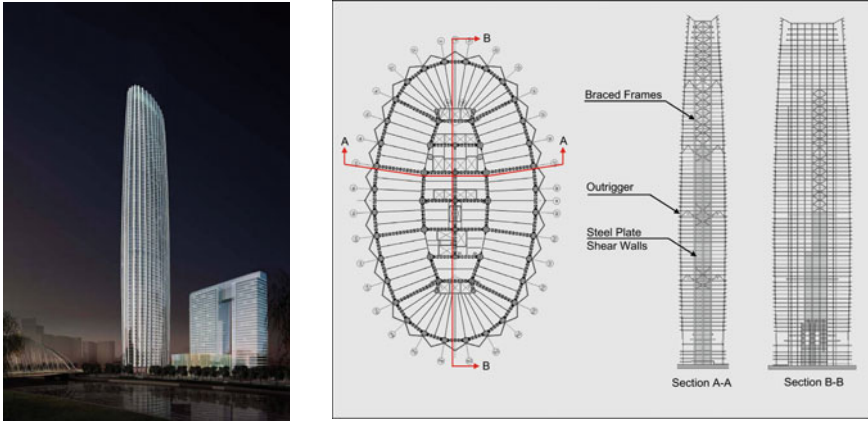
(Photo courtesy of SOM)

Fig. 15 The Tianjin World Financial Center and its structural system (Lee et al. 2010)

In the past decade, two high-rise buildings have been designed and constructed using steel plate shear walls. One is the 74-story Tianjin World Financial Center in China, which has vertically stiffened steel shear walls. The other steel shear wall tall building is the 55-story Los Angeles Convention Center Hotel, which has unstiffened steel plate shear walls (Youssef et al. 2010). Both have heavily used finite element methods in the analysis of the steel shear walls. In the following design procedures used in the design of the 74-story Tianjin Building is summarized. The building is located in high seismic and high wind area.

Design procedures used in the design of 74-story Tianjin World Financial Center

Figure 15 shows a view of the Tianjin-WFC building, its framing plan and elevation view of its typical shear wall frames. The steel shear walls in this building are vertically stiffened outrigger, steel shear walls for lower 2/3 of the height and outrigger concentrically braced frames for the top 1/3 of the height. The columns are concrete-filled composite round tube members and the beams are I-shaped girders acting compositely with the floors. All beam-to-column connections in steel shear wall system are rigid moment connections.

The designers (Lee et al. 2010) state that in this case, they studied other options such as concrete shear walls, composite shear walls, and dual concentrically braced frames. The concrete shear walls were ruled out because of the large dimensions of the concrete walls taking too much of occupiable floor area. The composite shear walls were not selected since the designers felt there would be a need for a significant amount of cost and time to be spent to conduct testing and research to establish the performance. The dual braced frame system proved to require 20–25% more steel than the steel shear walls to satisfy the performance requirements.

Figure 16 shows a view of the shear walls in the Tianjin WFC building and the von Mises stresses acting on a typical infill panel. In this case, the vertical stiffeners
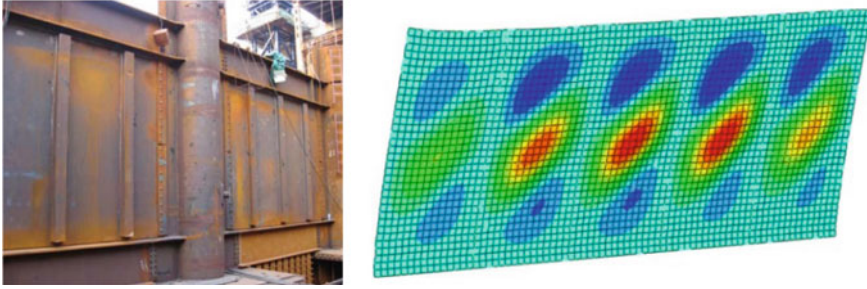
(a) **Buckling restrained SPSW : channel stiffener with a gap between end of stiffeners to
the boundary beams by Lee et al. (2010)**

Fig. 16 Steel shear walls of the Tianjin WFC building and von Mises stresses (Lee et al. 2010)

were designed to prevent buckling of the infill panels under the code design wind
load and the "frequent" earthquakes.

The general design philosophy for steel plate shear walls in this building was
established to satisfy the requirement of the Chinese code JGJ 99-98, which requires
that the steel plates be designed not to buckle under frequent earthquakes and winds
and have the strength to resist the strong earthquakes without exceeding the limit
of inter-story drift. For the strong earthquake level, buckling of the steel plates and
the utilization of tension field action is allowed. Following is a summary of main
design considerations and limitations in the design of steel plate shear walls as given
in Lee et al. (2010).

- The structure was designed to satisfy the Chinese code JGJ 99-98 for gravity, wind,
  and earthquakes with regards to strength as well as stiffness.
- The structure was designed to carry gravity loads without the contribution of the
  shear walls.
- The code design procedures utilize 50-year return wind and seismic loads. The
  seismic event corresponding to this recurrence period is termed the "frequent
  earthquake."
- For wind effects, the building was designed to satisfy the code drift requirement
  of 1/400 for 50-year wind (63.5% probability of exceedance in 50 years) which
  corresponded to a basic wind pressure 0.5 kN/m^2 in Tianjin, and strength require-
  ments under the 100-year wind (basic wind pressure 0.6 kN/m^2 in Tianjin). Damp-
  ing ratio was set at 3.5% considering the composite effect of the CFT columns.
  The building was also designed to satisfy the code wind acceleration perception
  requirements based on a 10-year return event (basic wind pressure 0.3 kN/m^2 in
  Tianjin) with damping ratio set at 1.5% by code, once again considering the CFT
  columns. Acceleration was limited by code to 0.28 m/s^2 at the highest occupied
  floor. Wind tunnel testing was required. By local practice, wind speeds used in the
  tests were at least as high as those stipulated in the codes in the predominant wind
  direction, but directional effects were permitted to be considered.

- The tower is located in a high seismic area, with a peak ground acceleration of 0.15 g specified in the local code for this site. Inter-story drift was 1/300 for this seismic event. A damping ratio of 3.5% was used. Also, the codes required that time-history analysis of the building be performed using two recorded and one simulated site-specific ground motions.
- Cyclic tests of scaled steel shear wall specimens were conducted to establish actual behavior of specimens.
- The steel shear walls were designed to remain elastic and not to buckle during the frequent earthquake and design wind loads. The steel shear walls were also designed to be the primary lateral load resisting system during moderate or rare earthquakes. The thickness of the infill plate satisfied the strength requirements of the Chinese code as well as the AISC-341 standard (AISC 2016a).
- For the elastic analysis, the infill panel was modeled using full isotropic shell elements. For inelastic time history analysis, a dual strip model, shown in Fig. 11b earlier was used.
- The boundary beams and columns of the steel shear walls were designed for the forces determined from elastic analyses to satisfy the Chinese code provisions.
- Development of plastic hinges at the end of boundary beams was allowed at the moderate and rare earthquake demand levels.
- As per the requirement of the seismic experts, the first author is one of them, some minor yielding but no plastic hinging was allowed in the boundary columns at moderate earthquake levels, and, in the lower 16 stories, some minor yielding but no plastic hinging was allowed in the boundary columns at rare earthquake levels.
- Because of the newness of the structural system, as the Chinese code requires, at the end of the design process, the seismic and wind performance of the building were reviewed by a panel of experts and additional requirements were imposed on the design.

10 Material Used in Steel Shear Wall Systems

The material of steel shear wall is usually ASTM A36 steel, with a specified minimum yield stress of 36 ksi (248 MPa), which was used in most of the steel shear wall specimens tested in the past by researchers. The use of higher grade of steel is not prohibited by seismic design codes. However, the use of high strength steel plate can result in reduced ductility of steel shear wall systems. The lateral stiffness of steel shear wall is directly proportional to the thickness of the infill plate (Thorburn et al. 1983; Sabouri-Ghomi et al. 2005), and by using higher strength steel and the associated reduced thickness, the stiffness of the shear wall will be reduced.

As mentioned under Construction Issues later, one of the problems with the fabrication of steel shear wall systems is handling and welding thin steel plate shear walls. Using higher strength steel and having even thinner walls can create problems with handling and welding in the field. Analytical studies and cyclic tests of steel

stiffened and unstiffened shear walls using low yield steel has shown very ductile and desirable performance.

Chen and Jhang (2011) conducted cyclic testing of one- and two-story steel shear walls and concluded that the specimens could tolerate cyclic lateral story drifts exceeding 0.05 radians. The test specimens had rigid as well as pin connections between the beams and columns of the boundary frames. They concluded that the specimens with shear (pin) connections had 28% less strength and 18% less energy dissipation capacity than the specimens with moment connections and recommended the use of moment connections in steel shear walls with low yield steel. However, considering the current relatively high cost of design, fabrication, and inspection of the field-welded moment connections compared to shear connections, it seems that the above reduction in the strength and energy dissipation can be easily compensated for by either adding to the length or thickness of the steel shear wall itself and using shear connections instead of moment beam-to-column connections.

To satisfy strong column-weak beam design requirement, the columns in the boundary frame are usually ASTM A913 Grade 65 or ASTM A992 Grade 65 with a minimum specified yield stress of 448.5 MPa (65 ksi). The beams in the boundary frame are usually ASTM A992 Grade 50, with a minimum specified yield stress of 345 MPa (50 ksi). Using grade 65 steel for columns and grade 50 steel for beams results in satisfying the "strong column-weak beam" requirement for the boundary frame easier.

In unstiffened steel shear walls, relatively large lateral forces act on the boundary columns creating relatively large bending moments in the boundary columns. One of the efficient ways to resist such bending moments is the use of the concrete-filled tube or built-up box sections as the boundary columns. The columns of the 73-story and 55-story steel shear wall building shown in Fig. 15 are concrete-filled tube and built-up box sections respectively.

11   Design of Members and Connections

The boundary columns and beams in a steel shear wall are capacity-designed to resist gravity alone and gravity plus seismic or wind load combinations. The seismic load combinations should include *overstrength* load equal to strain-hardened, expected yield strength of the tension filed equal to 1.1 $R_y F_y t_w$. The width-to-thickness, the *b/t* ratios of the elements of the cross sections of the boundary beams and columns should be such that these members do not develop local buckling under cyclic loading until they yield. The AISC-341 standard (AISC 2016a) designates such members as *highly ductile members* and provides the limiting values of the *b/t* ratio in its Table D1.1.

For the connections, like other steel systems, the type and detailing of the connections of steel shear walls play a major role in the cyclic behavior of the system. The main connections of steel shear wall system are infill plate-to-boundary element connections, splices in the steel plate and columns, beam to column connections, the column base connections, floor to girder connections and the connections of the

collectors to the steel shear wall system. The following sections provide information on the design, detailing, and construction aspects of these connections.

11.1 Infill Plate-to-Boundary Element Connection

The infill steel plate is connected to the boundary either by welds, bolts or their combination. The elements of the connection are designed following capacity design concepts to develop the strength of the steel plate using the expected yield strength of the infill plate $R_y F_y t_w$.

In fully welded option, "fin" plates are fillet-welded to the columns and beams in the shop. Then, the steel infill plate is welded to the fin plates with continuous fillet welds in the field. This option is used quite often, and almost all cyclic test specimens of steel shear walls have used this detail validating its desirable performance. In welded-bolted option, the fin plates are still welded to the boundary elements, but the infill plate is bolted to the fin plates by one or if needed more rows of bolts. In bolted-bolted detail, instead of fin plates, a tee section or double-angle section can be used, where the flange of the tee or the outstanding legs of the double-angle are bolted to flanges of the boundary columns and beams, and the stem of the tee or the back-to-back legs of the double angles are bolted to the steel infill plate. The bolted-bolted detail seems to be a viable option for stiffened shear walls where negligible tension field action forces are applied to the columns. In using this detail in unstiffened steel shear walls, the prying action on the bolts on the column flange needs to be considered in the design. No experimental results on the actual behavior of bolted-bolted connections of the infill plate-to-boundary element could be located at this writing.

Past cyclic tests of the unstiffened steel shear walls (Timler and Kulak 1983) have shown that during the cyclic loading the corners of the wall plate fractured due to the relatively large cyclic strain concentrations at the corners. To prevent the corner fracture, researchers have recommended adding welded strap plates to fill the gap between the horizontal and vertical fin plate (Tromposch and Kulak 1987), to provide corner cut-outs (Schumacher et al. 1999), or to incorporate special corner brackets and connecting the horizontal and vertical fin plates away from the corner (Choi and Park 2008). It appears that adding corner brackets can be an effective and economical solution, which was done for the 73-story Tianjin-WFC building.

11.2 Splices in the Infill Plate

In many applications, the size of the infill panel is such that the steel infill plates need to be spliced. The splices typically consist of shop-welding steel plates directly to each other or field-bolted using two splice plates one on each side of the infill plate. Figure 17 shows a view of a typical bolted splice. The splices of steel plate shear

Fig. 17 A bolted steel plate splice
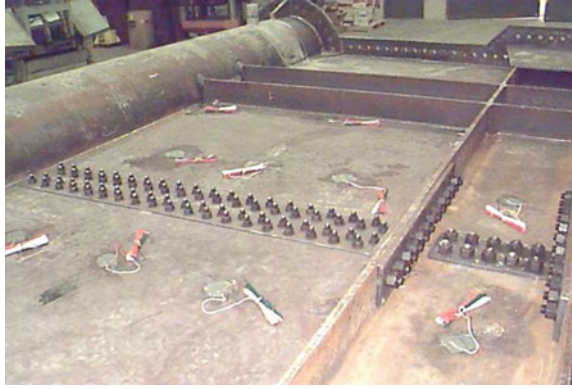
walls need to be designed for the strain-hardened expected yield strength of the wall equal to 1.1 $R_y F_y t_w$.

11.3 Beam-to-Column Connections

Beam-to-column connections in steel shear walls can be rigid, partially restrained (i.e., semi-rigid), or simple shear connections. The current AISC-341 standard (AISC 2016a) specifies the use of rigid moment connections but does not specify whether the connections should be *Ordinary, Intermediate,* or *Special.* In the Commentary part of the AISC-341 standard (AISC 2016a), it is mentioned that the moment connections are *Intermediate.* For more details on the beam-to-column connections design requirements and definition of the Intermediate Moment Frames; the readers are referred to the provisions of the AISC-341 standard (AISC 2016a). The seismic provisions ensure minimal ductility in the connection to enable the girders to develop plastic moment and to prevent brittle fracture in the connection area when steel shear wall undergoes large cyclic story drifts.

Cyclic tests done by Tromposch and Kulak (1987) showed that steel shear wall specimen with a fully restrained beam-to-column connection could dissipate as much as three times more energy than the system using similar frames but with bolted simple connections. The tests showed a robust rotation capacity of the bolted simple beam-to-column shear connections. Caccese et al. (1993) found that the rigidity of beam-to-column connections had a minor effect on the overall load-displacement behavior of the system. Sabouri-Ghomi and Gholhaki (2008) conducted cyclic tests of steel shear walls with the fully restrained and simple shear connection. Both specimens were able to reach story drift of 2.7%, where the shear wall developed corner tearing, and the tests stopped (Sabouri-Ghomi and Gholhaki 2008).

In their studies summarized in Shi and Astaneh-Asl (2008), the researchers conducted nonlinear push-over analyses of two steel shear walls to compare the behavior
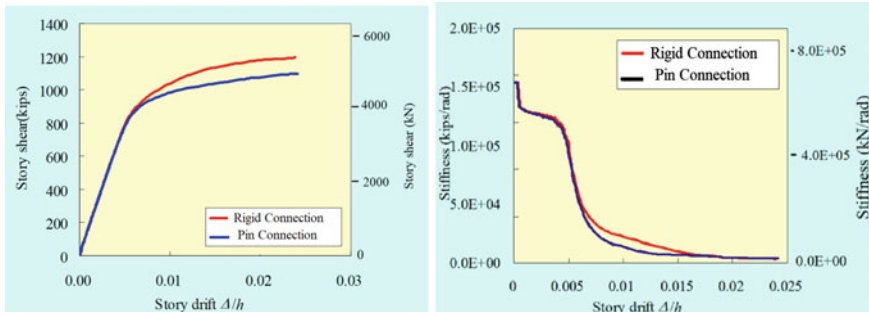
Fig. 18 Variations of story shear and lateral stiffness versus story drift for frames with rigid and pin connections

of steel shear walls with rigid and pin beam-to-column connections. One frame was the 9-story steel shear wall in the AISC Design Guide 20 (AISC 2007), which has rigid moment connections and the other was the same frame, but the beam-to-column connections were pin connections. Figure 18 shows the variation of the lateral stiffness versus story drift and variation of story shear versus story drift curves for the two frames. Both frames, one with the moment and the other with pin connections showed almost the same initial stiffness and yield point. After yielding of the shear wall; the frame with rigid connection showed more strain hardening.

Qu et al. (2008) and Vian et al. (2009) based on their studies of shear walls have recommended the use of Special Moment Connections in the steel shear walls. Higher ductility and energy-dissipation capacity of special moment connections is a desirable property; however, the beam-to-column connections are not the main source of energy-dissipation in a steel shear wall system and the rotational demand on the connections of steel shear walls are less than the demand in moment frames. The use of simple shear connection (Xue and Lu 1994; Cortes and Liu 2011b) and bolted plate moment connection (Vatansever and Yardimci 2011; Caccese et al. 1993) in the SPSW system should be re-visited, and development of new beam-to-column connections that fit the steel shear wall system should be encouraged. The potential savings gained by replacing a special or an intermediate moment connection by some other simpler and more cost-efficient beam-to-column connection need to be considered.

One of the innovative moment connections developed recently by Qian and Astaneh-Asl (2017) is the Gusset Plate Moment Connection (GPMC). Figure 19 shows the main elements of the new Gusset Plate Moment Connection (GPMC). The connection has two versions: welded and bolted.

The gusset plate in the new Gusset Plate Moment Connection is a vertical flat plate in the plane of the column and beam web. The gusset plate is mainly subjected to bending and shear, and a small amount of axial force. The plastic hinge formation is expected to occur in the gusset plate primarily due to in-plane yielding of the gusset plate. The gusset plate is designed to yield within a specified area—the gap between

Welded Version of the New Gusset Plate Moment Connection

Bolted Version of the New Gusset Plate Moment Connection
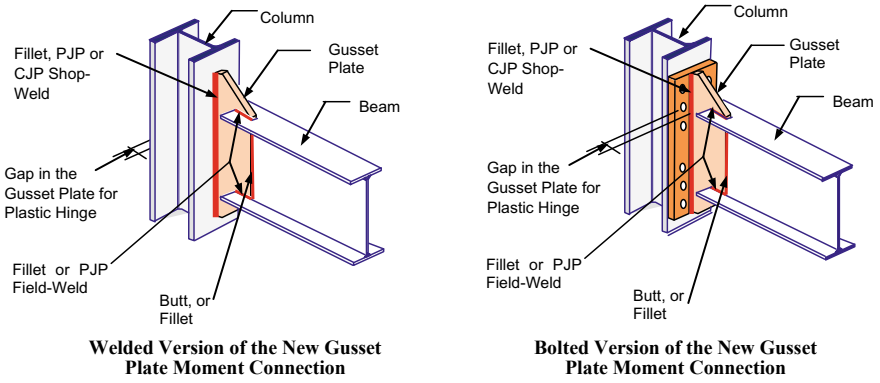
Fig. 19 Welded (left), and bolted (right) versions of the new Gusset Plate Moment Connection (Qian and Astaneh-Asl 2017)
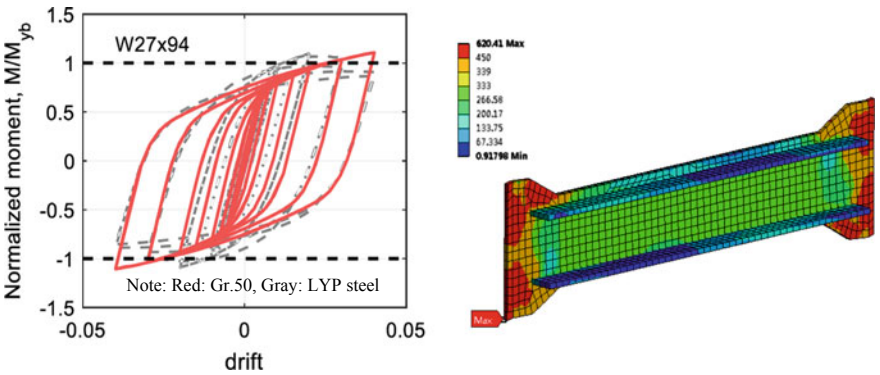
Fig. 20 Hysteresis curves (left) and von Mises stresses for a Gusset Plate Moment Connection

the face of the column flange and end of the beam, Fig. 19—and is the only inelastic element of the connection. The gusset plate, being the only element of the connection that yields and dissipates energy, acts as a "fuse" and protects all other elements of the joint such as the beam, column, welds and bolts, which are designed to remain essentially elastic during the seismic event. More information on the behavior and design of new Gusset Plate Moment Connection is in Qian and Astaneh-Asl (2017).

Figure 20 shows the cyclic behavior of a gusset Plate Moment Connection with gusset plate made of grade 50 steel (Fy = 345 MPa or 50 ksi) and low yield steel (F$_y$ = 131 MPa or 19 ksi).

The new connection utilizes highly ductile gusset plates to provide the necessary bending strength, rotational stiffness, required plastic rotation, and sufficient energy dissipation capacity. Based on the extensive analytical studies performed, the new connection has proven to be highly ductile, easy to fabricate, and potentially cost-effective. The proposed connection has a wide range of applications in steel and

composite moment frames, and composite and steel shear walls (such as the new *High Performance Steel Plate Shear Wall* discussed later in this chapter), as well as in dual steel systems composed of special concentrically braced frames and moment frames. It can be used for seismic as well as wind and gravity resistance. The most important advantage over the field-welded moment connections used in the current steel plate shear wall is that the new connection does not incorporate Complete Joint Penetration (CJP) field-welds, which not only are relatively expensive to fabricate but require costly field-inspection using ultrasonic testing equipment and expert operators. Another Advantage is that using this connection the *strong column-weak beam design* is no longer required, see Qian and Astaneh-Asl (2017).

11.4   Column Splices

Column splices in steel shear wall systems should be designed to resist at least 50% of the bending strength of the smaller of the column section being spliced AISC-341 standard (AISC 2016a). The nominal shear strength of the splice should be equal or greater than the $\Sigma M_{pc}/H_c$ where ΣM_{pc} is the plastic moment capacity of the cross sections of the columns above and below the splice, and H_c is the clear height of the column between beam-to-column connections. If welds are used in the splice, they should be complete joint penetration groove welds AISC-341 standard (AISC 2016a).

11.5   Collectors Connections

Collectors are the girders connected to the sides of the steel shear wall columns to transfer the inertia forces from the floors to the walls. The main force to be transferred is an axial force in the connector. The connection should be designed to have large axial force capacity but relatively small bending moment capacity so that the boundary columns are not subjected to additional bending. Details suggested by Astaneh-Asl (2008) for connections of collectors to the columns of concentrically braced frames can also be used for steel shear wall columns.

11.6   Column Base Connections

Columns in steel shear walls should remain essentially elastic. The only exception is that they can develop plastic hinges at their base above the base plate. The base connections of the boundary columns should be designed to transfer combined axial and bending as well as shear strength of the plastic hinge formed at the base of the column. The yield stress of the column used in establishing the axial, bending and

shear strength of the column should be 1.1 $R_y F_y$. It is recommended that the transfer of shear from the base plate to the foundation be done by using shear keys under the base plate instead of anchor rods. The role of anchor rods should be to resist tension due to overturning and uplift of the base plates. The grout under the base plate should be high strength grout, not thicker than 2-in. (50 mm) and preferably be fiber-reinforced concrete to prevent cracking of the grout under compression as was observed in the thick unreinforced grouts under the base plates of the Northridge State University Library during the 1994 Northridge earthquake. In this case, eventually the library had to be demolished and rebuilt since unlike damage to other elements of a steel structure, that in most cases can be easily repaired, the damage to the grout under a base plate, or even damage to a base plate or anchor rods is very difficult and costly to repair.

11.7   The Connection of Infill Plate to the Foundation

The connection of steel shear wall to the foundation should be capable of resisting the shear force in the infill plate connected to the foundation. The AISC-341 standard (AISC 2016a) does not provide specific provisions on what should be the required strength of the base connection of the steel infill plate. However, applying the provisions for the fin-plates connecting the infill plate to the boundary beams and columns, the base connection of the infill plate, should be designed to resist tensile yield strength of the tension field calculated using *expected yield* strength of the infill plate, $R_y F_y$ of the steel infill plate. Due to the importance of the base connection of the infill plate to the foundation, the authors recommend that the connection be designed to resist the tensile yield capacity of the tension field using *strain-hardened, expected yield strength,* 1.1 $R_y F_y$.

The base beam is optional. If only shear studs are used, then the base beam is allowed to bend upward due to tension field action and should be capacity-designed to resist the *expected yield strength* of the infill plate. If anchor rods are used and designed to resist the expected yield strength of the infill plate, then the base of the shear wall can be considered fixed.

Figure 21 shows examples of details of the connection of the steel infill plate to the foundation.

12   Construction Considerations

Currently, to construct steel shear walls, first, the boundary columns and beams are fabricated in the shop and then erected in the filed using field-welded and bolted moment connections. The steel infill plates are then welded to the fin plates on the boundary beams and columns using fillet welds. Due to the relatively thin character of the unstiffened plates, an attempt should be made to reduce the gravity loads

supported by the unstiffened steel shear walls. Gravity loads can cause buckling of the thin unstiffened shear walls even during construction. In the design stage, an attempt should be made to put as little floor gravity load as possible on the horizontal boundary elements of the shear wall system. Even if the steel shear wall is not directly subjected to gravity loads, in highrise buildings, the possibility of column shortening causing buckling of the unstiffened steel shear walls should be investigated.

To prevent buckling of unstiffened steel shear walls, the top of the steel plate can be left unwelded to the horizontal beam and the welding be done after several floors above the weld line are constructed. By doing this the effects of floor gravity load, as well as column shortening in pushing down the thin steel plate, will be significantly reduced.

The potential problem of burning of the infill plate during the upward field welding has been reported (Eatherton 2006). Difficulties were also encountered in constructing the infill plate-to-column connection at the column splice location. Sometimes, relatively large holes had to be cut in the infill plates to provide space and access to the column splice connection (Youssef et al. 2011).

Steel shear walls can be prefabricated in modules in the shop and assembled in the field. Zhao and Astaneh-Asl (2004a) tested a shop-welded, field-bolted modular steel shear wall system, which was used in a 24-story building and proved to be a viable option. Driver and Moghimi (2011) investigated the modular construction of steel shear walls and proposed three different concepts. The concept of mid-height continuous splices, similar to that shown in Fig. 17, and tested by Zhao and Astaneh-Asl (2004a) was considered one of the most promising configurations regarding practicality and economics.
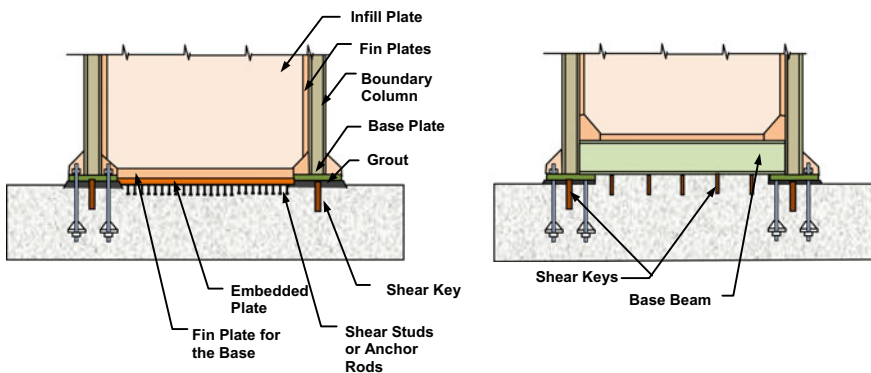
Fig. 21 Suggested details for the base connection of steel shear walls

13   Recent New Developments

The current code procedure for the design of steel shear walls utilizes the post-buckling tension field action. The use of tension field action results in the relatively large lateral and axial forces applied to the boundary beams and especially to the boundary columns. For columns, such lateral forces are applied only from one side, the infill plate side, resulting in relatively large bending moments in the columns. Such large lateral forces applied to the column make the boundary columns quite large and costly. In recent years, a few attempts have been made to develop new and more efficient steel shear wall systems. Two attempts focused on decreasing the lateral loads applied to the boundary columns (Corts and Liu 2011a, b; Qian and Astaneh-Asl 2016, 2017). The new High Performance Steel Plate Shear Wall system, developed by Qian and Astaneh-Asl is summarized in Sect. 13.2 of this chapter.

13.1   Coupled Bays and CFT Columns

This system was developed by Skilling Ward Magnusson Barkshire (now Magnusson Klemencic Associates) and was tested and studied at the University of California Berkeley by the first author and his research Associates (Zhao and Astaneh-Asl 2008, 2004b). Figure 22 shows components of the system. Specimen One, which has a height to width ratio of 1.5 for the infill plate, yielded at the inter-story drift of 0.006 and showed very high cyclic ductility and was able to reach cyclic inter-story drift of about ±3.3% after undergoing 79 cycles, 35 of the cycles being inelastic. The maximum shear force reached was about 4079 kN (917 kips) during the 79th cycle. Throughout the test, the gravity load carrying concrete-filled steel tube remained essentially elastic while non-gravity carrying lateral load resisting elements underwent well-distributed and desirable yielding. The specimen failed during the 80th cycle due to a fracture of the top coupling beam due to low-cycle fatigue fracture of the web. Figure 23 shows Specimen One before testing and its cyclic behavior.

Similar to Specimen One, Specimen Two also behaved in a ductile and desirable manner. Up to inter-story drifts of about 0.7%, the specimen was almost elastic. At this drift level, some yield lines appeared on the wall plate, and the force-displacement curve started to deviate from the straight elastic line. During later cycles, a distinct X-shaped yield line was visible on the steel plate shear wall. The specimen could tolerate 79 cycles, out of which 30 cycles were inelastic. The specimen reached an inter-story drift of more than 2.2% and maximum shear force of 5449 kN (1,225 kips). At this level of drift, the upper floor-coupling beam fractured at the face of the column (due to low-cycle fatigue), and the shear strength of the specimen dropped to about 88% of the maximum shear force reached in previous cycles (5449 kN or 1,225 kips). Testing continued, and when inter-story drift reached about 3.2%, the load dropped to below 75% of maximum load and test stopped.

Large concrete-filled steel tubes for lateral loads plus gravity load

Steel shear walls, beams and columns for lateral load resistance only

Steel beams and columns carrying gravity load only

Steel Plate

Bolted Splice

Rigid Moment Connection

Steel columns and beams are for seismic resistance and not for carrying gravity load

Large concrete-filled steel tubes for lateral loads plus gravity load

Fig. 22 Components of innovative coupled wall with CFT columns
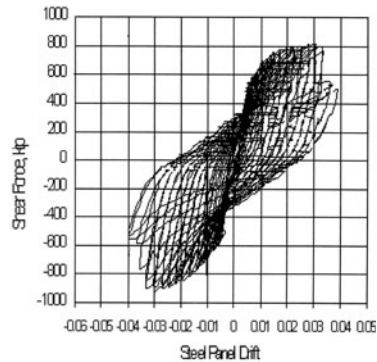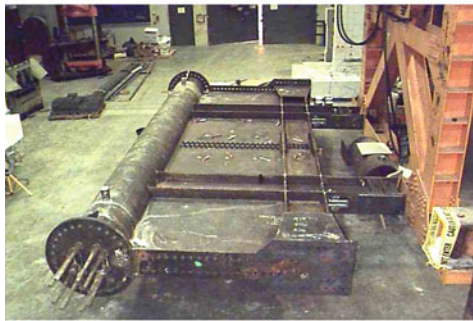
Fig. 23 Specimen one, and its shear force-drift relation

13.2   The High-Performance Steel Plate Shear Wall (Qian and Astaneh-Asl 2017)

Figure 24 shows the main elements of the new *High-Performance Steel Plate Shear Wall* (*HPSPSW*) system, as well as its main advantages compared to the current steel plate shear walls in the current design codes such as the AISC-341 standard (AISC 2016a).

The main elements of the new HPSPSW are:

a. **Unstiffened steel plate shear wall**: the unstiffened steel plate is designed to satisfy two levels of performance: (1) to resist the story shear under the ultimate factored load primarily by the strength of the tension field action; and (2) to remain essentially elastic under the service wind and service level lateral seismic

code design forces. The main innovation in this system is that the steel infill plate is not connected to the boundary columns; instead, the infill plate is connected to a vertical stiffener, usually a T-section next to the column. Separating the steel infill plate from the column in this system frees the columns from the lateral forces of the tension field action reducing bending moment in the columns significantly.

b. **Vertical side stiffeners**: As shown in Fig. 24, two vertical steel plates, T-sections, or another steel shape, are shop-welded to the vertical sides of the infill steel plate and are next to but not connected to the columns. These side stiffeners are located between floors and play three important roles: (1) to prevent lateral forces of the tension field action acting on the columns, (2) to provide out-of-plane buckling restraint to the steel infill plate, and (3) to provide in-plane boundary constraint to the tension field action;

c. **Beam-to-column moment connections**: The beam-to-column connections in the new *HPSPSW* system presented here are the new innovative Gusset Plate Moment Connection (GPMC), which is also developed by the authors (Qian and Astaneh-Asl 2016b, 2017) and discussed in the previous section.

d. **Boundary columns**: The boundary columns in the *HPSPSW* are not connected to the steel shear wall between the floor beams, preventing the steel plate from applying lateral force to the columns. Since columns are not connected to the infill plate directly, the columns can be steel rolled or built-up open or closed sections, steel-concrete composite sections, or even reinforced concrete sections. There is no restriction on the column orientation. The role of the column in this system is similar to the role of the columns in concentrically braced frames—to carry primarily axial loads; and

e. **Boundary beams**: in the new *HPSPSW* system, the boundary beams can be fillet-welded or bolted to the steel infill panel. If welds are used, welding can

(1) No lateral forces due to tension field action act on the columns.

(2) No vertical welds connect the shear wall to the columns.

(3) Design of columns does not depend on the design of the steel shear wall.

(4) Gusset plates prevent fracture at the corners.

(5) Steel plate does not buckle under "service" loads.

(6) Wall thickness can be increased to satisfy drift limitations without a need to increase column size.

Boundary Column

Gusset Plate Connection

Boundary Beam

Fin Plate

Side Stiffener (T-Section)

Base Beam

(7) No need to satisfy "strong-column, weak-beam" design since plastic hinge forms in the gusset and both beam and column remain elastic.

(8) No CJP field-welded beam-to-column moment connections are used.

(9) No doubler-plates are generally required for panel zone.

(10) No continuity-plates are generally required since beam flange is not welded to column flange.

Fig. 24 The new HPSPSW with its advantages
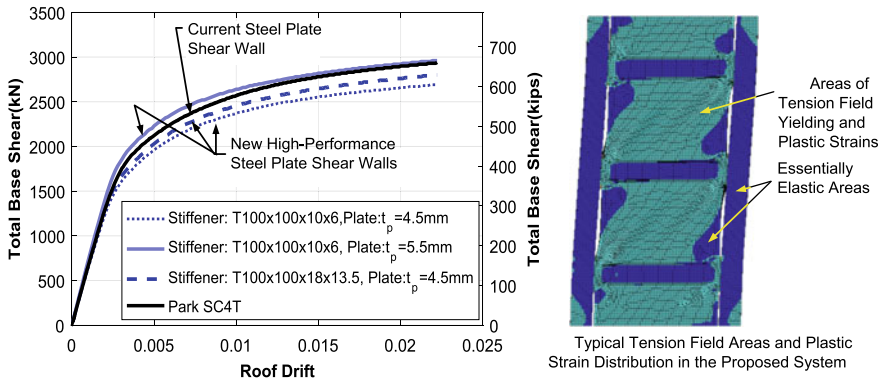
Fig. 25 Pushover curve and von Mises stresses in the innovative, high-performance steel plate shear wall

be done in the field or the shop in the "modular" construction option of the new system. These welds are fillet welds, requiring only visual inspections and not ultrasonic testing. The beams in the new system do not need to be wide flange shape as is the case in the current SPSW system; they can be angles, channels, or even simple flanges as long as they are strong enough to carry the gravity loads and the tension field forces from the wall.

Figure 25 shows a comparison of pushover curves in a Steel Plate Shear Wall system designed according to the AISC-341 standard (AISC 2016a) and same system designed as a High-Performance Steel Plate Shear Wall as shown in Fig. 24. As also shown in Fig. 25, the columns and beams in the HPSPSW remain essentially elastic, very small bending moments are generated in the columns, and the bulk of yielding takes place in the steel infill plate and some yielding in the connection gusset plate as per intended design. More information on the behavior and design of HPSPSW is in Qian and Astaneh-Asl (2017). To compare the HPSPSW to current SPSW system included in the AISC-341 standard AISC-341 standard (AISC 2016a) using the 9-story SPSW building in the AISC Design Guide 20 (AISC 2007) the SPSW shear walls were redesigned as HPSPSW system to resist the same lateral forces with the same inter-story drift limitations. It was shown that the HPSPSW designs could be 20% (code-based designed) to 10% (performance-based design) lighter than the AISC SPSW design in the AISC Design Guide 20 (AISC 2007), not including the additional savings on fabrication. The HPSPSW system had much lighter column sections compared to the AISC SPSW design. The comparison between the performance of the new system and the current AISC steel plate shear wall system (Qian and Astaneh-Asl 2016a, b, 2017) showed that the new system reduces the structural weight and column over-stress significantly, eases the design iterations and improves the constructability, material-utilization ratio, and economy of the system efficiently with enhanced seismic performance.

The High-Performance Steel Plate Shear Wall system has high potential to be an efficient, economical and easy to design, construct and inspect the system. There is a need for actual cyclic tests of the system to establish its performance under cyclic loading.

13.3 Buckling Restrained Steel Shear Walls

Another solution to reduce the tension field forces acting on the boundary columns has been to add buckling-restraining braces to the steel infill plate to delay or prevent its buckling before its yielding in shear (Nie et al. 2012; Tsai et al. 2007, 2010; Li et al. 2010). The major forms of existing buckling restrainers published in the literature include

a. channels welded to the infill plate but with a gap left between the restrainer and the boundary beam (Nie et al. 2012; Lee et al. 2010),
b. square tubes bolted on both sides of the infill plate using enlarged bolt holes to allow the relative movement of the infill plate and the buckling restrainers (Li et al. 2010; Tsai et al. 2007, 2010),
c. concrete cover plates added to the steel shear wall infill plate, where there is a gap around the concrete wall to prevent engagement of concrete with the boundary frames during small and moderate, but more frequent earthquakes (Zhao and Astaneh-Asl 2004a; Astaneh-Asl 2002a) The concrete plate engages with the steel shear wall making the wall a composite shear wall during major seismic events.
d. An infill steel panel sandwiched between two concrete cover plates similar to that in a composite shear wall but with enlarged bolt holes so that the concrete cover could slide freely relative to the steel plate (Guo et al. 2009).

13.4 Steel Slit Panel-Frame Shear Walls

Hitaka and Matsui (2003) were the first to introduce a series of slits in the unstiffened steel shear wall. The use of a series of slits on the infill panel enables the formation of a series of flexural links in between the slits and allows the system to provide a fairly ductile response without the need of substantial stiffening (Hitaka and Matsui 2003). Cortes and Liu (2011a, b) further improved this concept and studied steel slit panel—the frame, a new steel shear wall system, and developed design procedures for the system. The main components of the systems are columns and beams and Steel Slit Panels (SSPs). The beam-to-column connections are simple shear connections. The panels are not connected to the column, thus preventing the development and application of the tension field action forces to the columns. The Steel Slit Panel has some vertical slit cuts. The slit cuts convert the steel infill plate into a series of vertical

beam. The story shear is resisted by vertical beams bending in double curvature and forming plastic hinges at the top and bottom ends of the vertical beams. The panels have stiffeners in their vertical edges to prevent out of plane buckling of the panels.

Based on their analytical and actual cyclic testing of scaled specimens, the researchers concluded that all specimens were able to undergo cyclic inter-story drifts of at least 5% without the peak strength at each cycle dropping below 80% of the maximum strength reached during the first cycle. The proposed analytical equation could predict the stiffness and strength of the SSPF. The results also indicated that the stiffness is significantly reduced by the characteristics and properties of the boundary frames, especially by the flexural rigidity of the boundary beams. The researchers state that "The experimental results suggest that the SSPF system has high potential, with ductile and predictable behavior. Further studies confirming the performance of this system must be conducted before the SSPF may be used for lateral resistance in seismic regions."

13.5 Perforated Steel Shear Walls

Vian et al. (2009) tested steel perforated shear walls, where multiple circular holes were cut out of the infill plate. The holes were arranged in regularly spaced diagonal strips within the infill panel. One of the objectives of cutting out the circular holes was to reduce the strength and stiffness of the infill panel. The researchers stated that: "This option may be beneficial to designers who feel an SPSW system is suited to a particular structure, but the required solid infill plate thickness is unreasonably small." The steel used in the perforated panel was low yield steel, and the beam-to-column connections were special "reduced beam section" moment connections. The tested specimens behaved in a ductile manner and resisted cyclic lateral story drifts of 3% or greater. The researchers state that the perforation holes reduce the capacity of the tension field and to achieve the same shear strength for the infill panel the thickness is increased. Ignoring the additional cost of cutting multiple holes in the infill plate, the concept does not reduce significantly, the lateral forces acting on boundary elements, especially columns, which is the main reason for making the traditional steel shear walls not as cost-efficient as they can be.

14 Summary

Since 1960s steel shear walls are used as an efficient lateral force resisting system. Steel shear walls consist of a steel infill plate connected to boundary columns and beams by welded or bolted connections. The connection of the boundary columns and beams are usually moment connections making the boundary frame a moment frame. The steel plate is designed to resist the story shear, while the entire system consisting of the steel infill plate and boundary frame resists overturning moments.

Steel infill plate can have only horizontal or vertical stiffeners or both. Without stiffeners, due to relatively large height-to-thickness ratio, the unstiffened steel infill plate buckles diagonally under relatively small shear and after buckling resists the applied shear by diagonal tension field action. Unstiffened steel shear walls are popular in North America with a 55-story building in Los Angeles currently being the tallest steel shear wall building in the world.

Two issues make the unstiffened steel shear walls relatively expensive compared to the stiffened shear walls. One is that buckling of steel infill plate can occur under service loads which is currently an unacceptable performance in some countries like China. By adding stiffeners to the steel infill plates, we can delay the diagonal buckling of the steel infill plate under service load, and even avoid the buckling until the infill plate yields in shear during ultimate design loads. The second issue with unstiffened steel shear walls is that the development of tension field action after buckling of the compression diagonals results in the application of relatively large lateral tension field action forces to the columns making the columns relatively heavy. Stiffened shear walls are popular in Asia, and currently, a 73-story high-rise building in China is the tallest steel shear wall building in the world. The building has stiffened shear walls designed to prevent diagonal buckling of the wall under more frequent earthquakes, but allow buckling of compression diagonal and development of tension field action during severe earthquakes. This dual design criterion appears to be more rational than the current approach in the North American design codes that only considers designing the steel infill panel to resist the shear forces expected during the strong earthquakes without any consideration given to the performance of the wall during small but more frequent earthquakes and wind loads.

There is a great potential for new research and development activities in this area to develop more efficient steel shear wall systems as well as more rational seismic design procedures and modeling technics. Several new steel shear wall systems have been developed in recent years primarily to address the main issue with the current unstiffened steel shear wall systems which is the buckling of the diagonal compression field and development of the tension field action, which in turn results in the application of relatively large lateral forces to the boundary columns. Two examples of such systems are the High-Performance Steel Shear Wall System (HPSSWS) (Qian and Astaneh-Asl 2016a, b, 2017), and the steel slit panel frame shear walls (Cortes and Liu 2011a, b). In the HPSSWS the infill plate is connected to the boundary beams but not to the boundary columns eliminating any lateral force applied to the columns. In this system, the vertical edges of the steel infill plate, instead of being connected to the columns, are connected to the plate or Tee-section stiffeners. In the steel slit panel-frame shear wall systems, the steel infill plate is connected to the boundary beams and columns, but the infill wall has a series of vertical slits cut into it making the plate act as a collection of vertical columns acting primarily in bending.

At this time, steel plate shear walls are one of the most resilient lateral load resisting systems, with sufficient initial stiffness, yield strength, and ductility to resist lateral loads of winds and earthquakes in a cost-efficient manner. Still, there is plenty of

room for innovative ideas to make the system more efficient by developing new and cost-efficient concepts and detailings in the following areas:

1. More analytical and especially experimental research is needed on the two promising steel shear wall systems, the High-Performance Steel Plate Shear Walls (Qian and Astaneh-Asl 2016a, b, 2017) and the Slit Panel-Frames (Cortes and Liu 2011a, b), to establish their performance and to develop design procedures for these and other future systems that can eliminate the lateral tension field action on the columns.
2. More analytical and experimental research is needed to establish which of the simple, partially restrained and rigid moment connections are more efficient for the beam-to-column and column-base connections. Then, based on the findings of such research, new or improved cost efficient beam-to-column and column-base connections can be developed.
3. There is a need for current codes such as the AISC-341 standard (AISC 2016a) to have a design procedure that includes satisfactory performance under both frequent but medium size seismic events and less frequent but large earthquakes. This is the case in Chinese code but not in the U.S., Canada, and Eurocode.
4. There is a need to develop details that prevent the transfer of gravity loads to the steel shear walls.
5. There is a need to develop construction procedures that increases pre-fabrication and shop work as much as possible and reduces field work, especially field welding, inspection, as well as erection time.

References

AISC. (2007). *Steel design guide 20: Steel plate shear walls*. American Institute of Steel Construction, Chicago, IL.

AISC. (2016a). *Seismic provisions for structural steel buildings.* ANSI/AISC 341-16, American Institute of Steel Construction, Chicago, IL.

AISC. (2016b). *Specification for structural steel buildings.* ANSI/AISC 360-16, American Institute of Steel Construction, Chicago, IL.

ASCE. (2016). Minimum design loads and associated criteria for buildings and other structures. Reston (VA): American Society of Civil Engineers.

Astaneh-Asl, A. (2002a). Seismic behavior and design of composite steel plate shear walls. *Steel Technical Information and Product Services (Steel TIPS) Report*. Structural Steel Educational Council (www.steeltips.org), CA.

Astaneh-Asl, A. (2002b). Seismic behavior and design of steel shear walls. *Steel Technical Information and Product Services (Steel TIPS) Report*. Structural Steel Educational Council (www.steeltips.org), CA.

Astaneh-Asl, A. (2008). Seismic behavior and design of base plates in braced frames. *Steel Technical Information and Product Services (Steel TIPS) Report*. Structural Steel Educational Council (www.steeltips.org), CA.

Astaneh-Asl, A., & Zhao, Q. H. (2000). Seismic studies of an innovative and traditional composite shear walls. In *6th ASCCS International Conference on Steel-Concrete Composite Structures*, Los Angeles, CA.

Baldelli, J. A. (1983). Steel shear walls for existing buildings. *AISC Engineering Journal, Second Quarter*, 70–77.

Baldvins, N. M., Berman, J. W., Lowes, L. N., Janes, T. M., & Low, N. A. (2012). Fragility functions for steel plate shear walls. *Earthquake Spectra, 28,* 405–426.

Basler, K., & Thuerlimann, A. (1961). Strength of plate girders in bending. *Journal of the Structural Division, 87,* 153–184.

Basler, K., Yen, B., Mueller, J., & Thurlimann, B. (1960). *Web buckling tests on welded plate girders*. Fritz Engineering Laboratory, Lehigh University.

Berman, J., & Bruneau, M. (2003). Plastic analysis and design of steel plate shear walls. *Journal of Structural Engineering, 129,* 1448–1456.

Bhowmick, A. K., Driver, R. G., & Grondin, G. Y. (2009). Seismic analysis of steel plate shear walls considering strain rate and—Delta effects. *Journal of Constructional Steel Research, 65,* 1149–1159.

Caccese, V., Elgaaly, M., & Chen, R. (1993). Experimental study of thin steel-plate shear walls under cyclic load. *Journal of Structural Engineering, 119,* 573–587.

Celebi, M. (1997). Response of olive view hospital to Northridge and Whittier earthquake. *Journal of Structural Engineering, ASCE, 123,* 389–396.

Chen, S.-J., & Jhang, C. (2011). Experimental study of low-yield-point steel plate shear wall under in-plane load. *Journal of Constructional Steel Research, 67,* 977–985.

Choi, I.-R., & Park, H.-G. (2008). Ductility and energy dissipation capacity of shear-dominated steel plate walls. *Journal of Structural Engineering, 134,* 1495–1507.

Choi, I.-R., & Park, H.-G. (2009). Steel plate shear walls with various infill plate designs. *Journal of Structural Engineering, 135,* 785–796.

Cortes, G., & Liu, J. (2011a). Analysis and design of steel slit panel frames (SSPFs) for seismic areas. *Engineering Journal-Chicago, 48,* 1.

Cortes, G., & Liu, J. (2011b). Experimental evaluation of steel slit panel–frames for seismic resistance. *Journal of Constructional Steel Research, 67,* 181–191.

CSA. (1994). *Limit state design of steel structures, CAN/CSA-S16.2-M94*. Canadian Standard Association, Toronto, Ontario.

CSA. (2014). *Limit state design of steel structures, CAN/CSA-S16-14*. Canadian Standard Association, Toronto, Ontario.

Dastfan, M., & Driver, R. G. (2008). Flexural stiffness limits for frame members of steel plate shear wall systems. In *Annual Stability Conference* (pp. 321–334). Nashville, TN: Structural Stability Research Council.

Driver, R. G. (1997). *Seismic behaviour of steel plate shear walls*. Department of Civil and Environmental Engineering, University of Alberta.

Driver, R. G., & Moghimi, H. (2011). Modular construction of steel plate shear walls for low and moderate seismic regions. In *Structures Congress*. Structural Engineering Institute, American Society of Civil Engineers, Las Vegas, NV.

Eatherton, M. (2006). Design and construction of steel plate shear walls. In *Proceedings of the Eighth US National Conference on Earthquake Engineering*, San Francisco, California, USA.

Eatherton, M., & Johnson, K. (2004). High-end residence using steel plate shear walls in Woodside, California. In *SEAOC 2004 Convention: 75th Anniversary Celebration*, Monterey, CA.

Elgaaly, M., Caccese, V., & Du, C. (1993). Postbuckling behavior of steel-plate shear walls under cyclic loads. *Journal of Structural Engineering, 119,* 588–605.

Fujitani, H., Yamanouchi, H., Okawa, I., Sawai, N., Uchida, N., & Matsutani, T. (1996). Damage and performance of tall buildings in the 1995 Hyogoken Nanbu earthquake. In *67th Regional Conference (in conjunction with ASCE Structures Congress XIV)*. Chicago: Council on Tall Buildings and Urban Habitat.

Ghosh, S., Adam, F., & Das, A. (2009). Design of steel plate shear walls considering inelastic drift demand. *Journal of Constructional Steel Research, 65,* 1431–1437.

Guo, Y., Dong, Q., & Zhou, M. (2009). Tests and analysis on hysteretic behavior of buckling restrained steel plate shear wall. *Journal of Building Structures, 30,* 10.

Habashi, H. R., & Alinia, M. M. (2010). Characteristics of the wall–frame interaction in steel plate shear walls. *Journal of Constructional Steel Research, 66,* 150–158.

Hitaka, T., & Matsui, C. (2003). Experimental study on steel shear wall with slits. *Journal of Structural Engineering, 129,* 586–595.

Hosseinzadeh, S. A. A., & Tehranizadeh, M. (2014). Behavioral characteristics of code designed steel plate shear wall systems. *Journal of Constructional Steel Research, 99,* 72–84.

Kharmale, S. B., & Ghosh, S. (2013). Performance-based plastic design of steel plate shear walls. *Journal of Constructional Steel Research, 90,* 85–97.

Lee, S., Wang, D., Liao, Y., & Mathias, N. (2010). Performance based seismic design of a 75 story buckling restrained slender steel plate shear wall tower. In *Structures Congress*. ASCE, Orlando, Florida.

Li, C. H., Tsai, K. C., Lin, C. H., & Chen, P. C. (2010). Cyclic tests of four two-story narrow steel plate shear walls. Part 2: Experimental results and design implications. *Earthquake Engineering and Structural Dynamics, 39,* 801–826.

Lin, C.-H., Tsai, K.-C., Qu, B., & Bruneau, M. (2010). Sub-structural pseudo-dynamic performance of two full-scale two-story steel plate shear walls. *Journal of Constructional Steel Research, 66,* 1467–1482.

Lubell, A. S. (1997). *Performance of unstiffened steel plate shear walls under cyclic quasi-static loading*. University of British Columbia.

Lubell, A. S., Prion, H. G., Ventura, C. E., & Rezai, M. (2000). Unstiffened steel plate shear wall performance under cyclic loading. *Journal of Structural Engineering, 126,* 453–460.

Nie, J., Fan, J., Liu, X., & Huang, Y. (2012). Comparative study on steel plate shear walls used in a high-rise building. *Journal of Structural Engineering, 139,* 85–97.

Park, H.-G., Kwack, J.-H., Jeon, S.-W., Kim, W.-K., & Choi, I.-R. (2007). Framed steel plate wall behavior under cyclic lateral loading. *Journal of Structural Engineering, 133,* 378–388.

Purba, R., & Bruneau, M. (2014). Seismic performance of steel plate shear walls considering various design approaches. *Technical Report MCEER-14-0005*. Buffalo, New York: Multidisciplinary Center for Earthquake Engineering Research, State Univ. of New York at Buffalo.

Qian, X. (2017). *Development of a high-performance steel plate shear wall system with an innovative gusset plate moment connection* (Ph.D. dissertation, University of California Berkeley).

Qian, X., & Astaneh-Asl, A. (2016a). Development of a high-performance steel plate shear wall system. *International Journal of Earthquake and Impact Engineering, 1*, 57–80 (Inderscience Publishers).

Qian, X., & Astaneh-Asl, A. (2016b). Introducing a new ductile and economical steel moment connection. In *2016 SEAOC Convention*, October 12–15, Maui, Hawaii.

Qian, X., & Astaneh-Asl, A. (2017). Development of a high-performance steel shear wall and a new moment connection. *Final Report, Report Number UCB/CEE-STEEL-12/2017*. Department of Civil and Environmental Engineering, University of California, Berkeley.

Qu, B., & Bruneau, M. (2009). Capacity design of intermediate horizontal boundary elements of steel plate shear walls. *Journal of Structural Engineering, 136,* 665–675.

Qu, B., & Bruneau, M. (2010). Behavior of vertical boundary elements in steel plate shear walls. *Engineering Journal (Chicago), 47*, 109–122.

Qu, B., Bruneau, M., Lin, C.-H., & Tsai, K.-C. (2008). Testing of full-scale two-story steel plate shear wall with reduced beam section connections and composite floors. *Journal of Structural Engineering, 134,* 364–373.

Robinson, K., & Ames, D. (2000). Steel plate shear walls: Library seismic upgrade. In *Modern steel construction.* Chicago, IL: AISC.

Sabouri-Ghomi, S., & Gholhaki, M. (2008). Tests of two three-story ductile steel plate shear walls. In *ASCE Structures Congress 2008: Crossing Borders*. Vancouver, British Columbia, Canada.

Sabouri-Ghomi, S., Ventura, C. E., & Kharrazi, M. H. (2005). Shear analysis and design of ductile steel plate walls. *Journal of Structural Engineering, 131,* 878–889.

Sarkisian, M. P., & Mathias, N. J. (2012). Testing as a validation tool for tall, non-prescriptive buildings in China. In *Structures Congress 2012*, American Society of Civil Engineers.

Schumacher, A., Grondin, G. Y., & Kulak, G. L. (1999). Connection of infill panels in steel plate shear walls. *Canadian Journal of Civil Engineering, 26,* 549–563.

Seilie, I., & Hooper, J. D. (2005). Steel plate shear walls: practical design and construction. In Modern Steel Construction, American Institute of Steel Construction.

Shi, Y., & Astaneh-Asl, A. (2008). Lateral stiffness of steel shear wall systems. In *Structures Congress*. ASCE, April 24–26, Vancouver, Canada.

Thorburn, L. J., Kulak, G. L., & Montgomery, C. (1983). Analysis of steel plate shear walls.

Timler, P., & Kulak, G. L. (1983). *Experimental study of steel plate shear walls*. Edmonton, Alberta: Department of Civil Engineering, University of Alberta.

Topkaya, C., & Atasoy, M. (2009). Lateral stiffness of steel plate shear wall systems. *Thin-Walled Structures, 47,* 827–835.

Tromposch, E., & Kulak, G. L. (1987). *Cyclic and static behaviour of thin panel steel plate shear walls*. Department of Civil Engineering, University of Alberta, Edmonton, Canada.

Troy, R. G., & Richard, R. M. (1979). Steel plate shear walls resist lateral load, cut costs. *Civil Engineering, ASCE, 49,* 3.

Tsai, K., Lin, Y., & Lin, C. (2007). Seismic responses and design of steel plate shear wall. *Progress in Steel Building Structures, 9,* 19–25.

Tsai, K. C., Li, C. H., Lin, C. H., Tsai, C. Y., & Yu, Y. J. (2010). Cyclic tests of four two-story narrow steel plate shear walls—Part 1: Analytical studies and specimen design. *Earthquake Engineering and Structural Dynamics, 39,* 775–799.

Vatansever, C., & Yardimci, N. (2011). Experimental investigation of thin steel plate shear walls with different infill-to-boundary frame connections. *Steel and Composite Structures, 11,* 251–271.

Vian, D., Bruneau, M., Tsai, K., & Lin, Y.-C. (2009). Special perforated steel plate shear walls with reduced beam section anchor beams. I: Experimental investigation. *Journal of Structural Engineering, 135,* 211–220.

Xue, M., & Lu, L.-W. (1994). Monotonic and cyclic behavior of infilled steel shear panels. In *Proceedings of 17th Czech and Slovak International Conference on Steel Structures and Bridges* (pp. 152–160).

Youssef, N., Wilkerson, R., Fischer, K., & Tunick, D. (2010). Seismic performance of a 55-storey steel plate shear wall. *The Structural Design of Tall and Special Buildings, 19,* 139–165.

Youssef, N., Wilkerson, R., & Tunick, D. (2011). Thin steel plate shear walls: Performance based design. *Steel Tips*.

Zhang, X., & Guo, Y. (2014). Behavior of steel plate shear walls with pre-compression from adjacent frame columns. *Thin-Walled Structures, 77,* 17–25.

Zhao, Q., & Astaneh-Asl, A. (2004a). Cyclic behavior of traditional and innovative composite shear walls. *Journal of Structural Engineering, 130,* 271–284.

Zhao, Q. H., & Astaneh-Asl, A. (2004b). Cyclic behavior of an innovative steel shear wall system. In *13th World Conference on Earthquake Engineering*, August 1–6, Vancouver, Canada.

Zhao, Q. H., & Astaneh-Asl, A. (2008). Experimental and analytical studies of a steel plate shear wall system. In *Structures Congress*. ASCE, April 24–26, Vancouver, Canada.

Resilience of the Built Environment: A Methodology to Estimate the Downtime of Building Structures Using Fuzzy Logic

M. De Iuliis, O. Kammouh, G. P. Cimellaro and S. Tesfamariam

1 Introduction

Natural and man-disasters have a serious impact on countries, in terms of number of affected people and in terms of economic damages. Building and communities are often not enough resilient to extreme natural disasters, such as earthquakes, tsunamis, hurricanes, etc.; they can't completely prevent all the risk but they need to be "*prepared*" and less "*vulnerable*" in order to achieve a high "*resilience*" (Cimellaro 2016). Resilience is a measure of the ability of a system exposed to hazards to resist and recover its functionality in a timely and efficient manner (ISDR 2009).

Bruneau et al. (2003) defined seismic resilience as "the ability of both physical and social systems to reduce the impact of a shock, to absorb such a shock if it occurs, and to quickly re-establish normal performance". Cimellaro et al. (2010) introduced the concept of functionality recovery and suggested that resilience is "the ability of social units (e.g. organizations, communities) to mitigate hazards, contain the effects of disasters when they occur, and carry out recovery activities in ways to minimize social disruption and mitigate the effects of further earthquakes". In the context of this work, resilience is defined as the ability of engineering and socio-economic systems to rebound after severe events, or disasters, such as earthquakes (Cimellaro et al. 2008).

Estimating resilience has been performed in different fields, from engineering to economics. Several resilience frameworks can be found in literature. Some tackled the engineering resilience on the country level (Kammouh et al. 2017a, b) and some on the local and community levels (Kammouh et al. 2017c; Kammouh et al. 2018b; Kammouh and Cimellaro 2018; Kammouh et al. 2019). A quantitative method to

M. De Iuliis · O. Kammouh · G. P. Cimellaro (✉)
Politecnico di Torino, Turin, Italy
e-mail: gianpaolo.cimellaro@polito.it

S. Tesfamariam
The University of British Columbia, Vancouver, Canada

evaluate the resilience at the state level was introduced in Kammouh et al. (2017b). In their approach, the data provided by the Hyogo Framework for Action (HFA) (ISDR 2005), which is a work developed by the United Nations (UN), is used in the analysis. Another quantitative framework for evaluating community resilience is the PEOPLES framework (Cimellaro et al. 2016a). PEOPLES is an expansion of the resilience research at the Multidisciplinary Center of Earthquake Engineering Research (MCEER). PEOPLES framework involves seven dimensions: Population, Environment, Organized government services, Physical infrastructures, Lifestyle, Economic, and Social capital (Renschler et al. 2010).

The absence of a concise approach makes resilience difficult to determine, especially because the concept of resilience involves different aspects, such as seismic prediction, vulnerability assessment, and downtime estimation (Cimellaro et al. 2016a; Chang et al. 2014; Bonstrom and Corotis 2014). In the context of seismic risk assessment, quantifying downtime is of importance to decision makers and owners (Cimellaro et al. 2016b).

In the seismic resilience evaluation, downtime is "*the time necessary to plan, finance, and complete repair facilities damaged by earthquakes or other disasters and is composed by rational and irrational components*" (Comerio 2006). The "rational" components are predictable and easily quantifiable, such as construction costs and the time needed to repair damaged facilities. The "irrational" components, on the other hand, consider the time required to start repairs (financing, workforce availability, and regulatory and economic uncertainty).

The Federal Emergency Management Agency (FEMA) has performed several studies focusing on developing earthquake loss estimation techniques. These studies have resulted in the development of a loss estimation software "HAZUS" (Kircher et al. 2006). HAZUS 97 was the first edition of the risk assessment software, built using GIS technology. HAZUS, in which downtime depends on structural and non-structural damage probabilities, provides an estimate for the damage caused by extreme events. Moreover, an electronic tool called the P*erformance Assessment Calculation Tool* (PACT) was released by FEMA. The tool aims at implementing probabilistic computation and accumulation of losses for individual buildings (FEMA 2012b). It also provides a methodology to evaluate the seismic performance of buildings in situations with high uncertainty. The methodology defines the expected building damage and the consequences of such damage.

Currently, existing methodologies are carried out through a probabilistic approach. Using such methodologies, quantification of downtime, and therefore resilience, uses historical data and resources that are usually not readily available. The main reason is that, such parameters (e.g. topology and site seismic characteristics) are not simple to capture using traditional models because they are different in nature and lead to complex mathematical formulation. Therefore, a simple prediction method for the downtime and resilience of building structures needs to be developed.

This chapter proposes a new methodology to evaluate the downtime for three recovery states (e.g. re-occupancy, functional and full recovery) of building structures after earthquakes. The methodology permits a fast and economical estimation of downtime parameters that involve uncertainties using the Fuzzy Logic hierarchi-

cal scheme (Tesfamariam and Saatcioglu 2010) in which information of damaged buildings is combined. Such information is obtained from a Rapid Visual Screening, which is a questionnaire carried out by a screener to identify the design and the components of the damaged buildings. Moreover, the use of a fuzzy inference system allows the estimation of building damageability, which is the main parameter to quantify downtime. The methodology can be used by owners, engineers, architects, and decision makers for managing earthquakes consequences, minimizing the impacts of the earthquakes, and allowing the damaged buildings to recover as soon as possible.

2 Fuzzy Logic

The fuzzy logic concept was first introduced by Zadeh (1965). The idea behind the fuzzy theory is that systems with high complexity cannot be analyzed using classical mathematical methods because they are not expressive to characterize the relationships between input and output, especially in the situation where there is imprecision and uncertainty. While classical binary logic evaluates a statement by an integer number, zero or one, which corresponds to true or false. The fuzzy logic uses membership grades (μ) ranging between 0 and 1, which indicate whether a variable x belongs to a fuzzy set. That is, 0 indicates that x does not belong to the fuzzy set and 1, instead, shows that x completely belongs to the fuzzy set (Tesfamariam and Saatcioglu 2008).

Later on, fuzzy sets were implemented to new approaches in which numerical variables are replaced by linguistic variables (Zadeh 1973). The use of the linguistic values changed completely the way of considering the human systems. The first application of the fuzzy logic was in the design of Fuzzy Logic Controller (FLC) for industrial plants. Mamdani (1974) showed that the hierarchical approach and the fuzzy rules need to be set. Fuzzy logic became a key factor in several fields such as industrial applications in the early 1980s in Europe and Japan and, Machine Intelligence Quotient (MIQ) to mimic the ability of human, and earthquake engineering.

As shown in Fig. 1, the fuzzy logic consists of three main steps: (1) Fuzzification; (2) Fuzzy Inference System; and (3) Defuzzification.

2.1 Fuzzification

Every basic input parameter has a range of values that can be clustered into linguistic terms, such as very low (VL), low (L), medium (M), high (H) and very high (VH), which are assigned through a procedure called *granulation*. According to their granularities, the input values are converted or fuzzified into a comparable scale by assigning corresponding membership functions (Tesfamariam and Saatcioglu 2008).
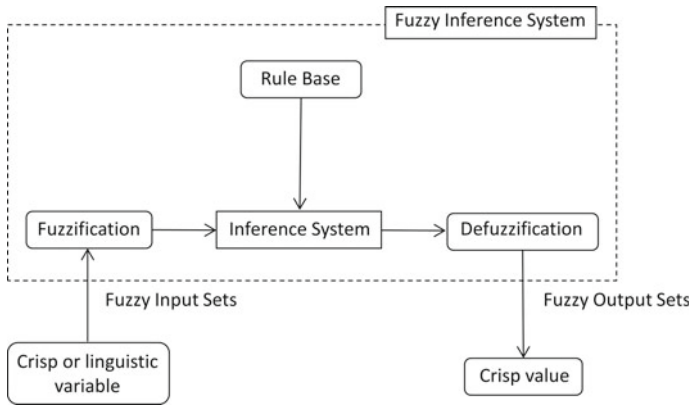
Fig. 1 Fuzzy inference system (FIS)
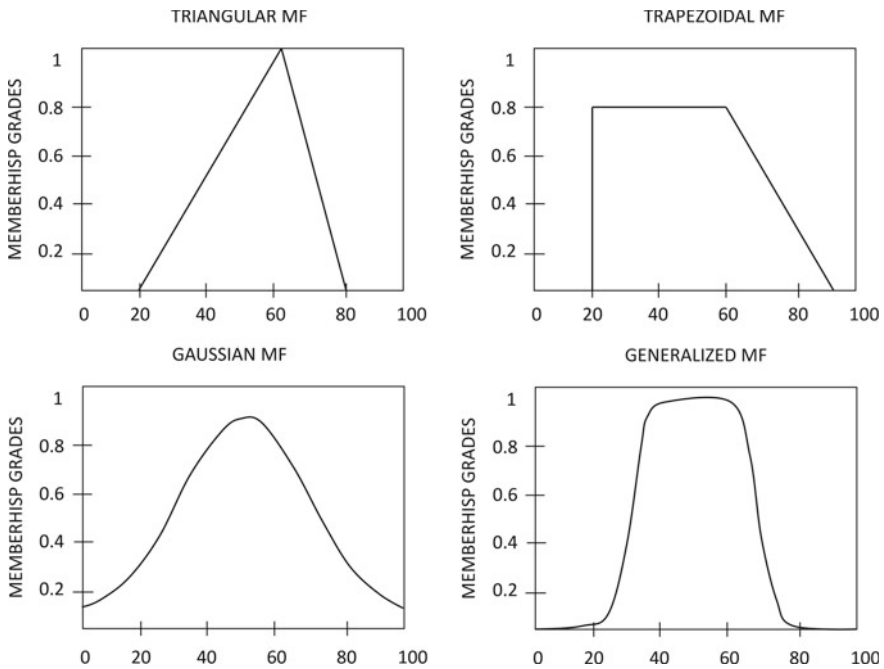
Fig. 2 Different shapes of membership functions

A membership function defines how input point is represented by a membership value between 0 and 1, and it is used to quantify a linguistic term. In literature, different forms of membership functions are presented (e.g. the triangular, trapezoidal, and Gaussian shapes (Fig. 2), which are the most common used). The choice of the membership function is related to the user experience (Mendel 1995).

2.2 Fuzzy Rules

The *fuzzy rule base* (FRB) is defined from expert knowledge and/or historical data (*fuzzy knowledge base*). The *fuzzy rule base* consists of statements called rules that express the decision maker's opinion or judgment about an uncertain situation. The fuzzy rule is mainly represented by the *Mamdani* type (Mamdani 1976), which is a simple IF-THEN rule, which associates a condition described using linguistic variables and fuzzy sets to an output or a conclusion. For instance, considering two inputs x_i and x_2, the ith rule R_i, is shown as follows:

$$R_i : IF \ x_1 \ is \ A_{i1} \ AND \ x_2 \ is \ A_{i2} \ THEN \ y \ is \ B_i \quad i = 1, \dots, n \tag{1}$$

where x_1 and x_2 are the input linguistic variables (antecedent), A_{i1} and A_{i2} are the input sets, n is the total number of rules, y is the output linguistic variable (consequent), B_i is the consequent fuzzy set.

In the methodology, the fuzzy rules are defined using a proposed weighted average method in order to systematize the process. A weighting factor W, for instance 1 or 2, defined using experts judgement, is assigned to each input. This value represents the impact of the input towards the output (e.g. a weighting factor 2 signifies a higher impact of the input towards the output). The output is then identified by considering the weights of the inputs. This is mathematically represented in Eq. 3, where L_{out} refers to the level of the output (*low, medium or high*, which can be mathematically represented as 1, 2, and 3 respectively), $L_{inp,i}$ is the level if input i, $W_{inp,i}$ is the weight of input i.

Consider the following example of a fuzzy rule base: IF input x_1 is *Low* ($L_{inp,1}$=1) AND input x_2 is *Medium* ($L_{inp,2}$= 2) and the corresponding weights are $W_{inp,1} = 1$ and $W_{inp,2} = 2$ respectively THEN the output y is L_{out}= 1.67 (using Eq. 2) which can be rounded to 2. Therefore, the level of the output y is *medium* (2 corresponds to *medium*). Once Fuzzy rules are obtained, they are assigned to each parameter required for the downtime assessment.

$$L_{out} = \frac{\sum_{i=1}^{n} L_{inp,i} \times W_{inp,i}}{\sum_{i=1}^{n} W_{inp,i}} \tag{2}$$

2.3 Fuzzy Inference System (FIS)

The results of the rules are combined to obtain a final output through a process called *inference*. The evaluations of the fuzzy rules and the combination of the results of the individual rules are performed using fuzzy set operations to describe the behavior of a complex system for all values of the inputs. Different aggregation procedures are available: intersection, minimum, product, union, maximum, and summation (Klir and Yuan 1995). For example, in Mamdani's inference system, three connectives can
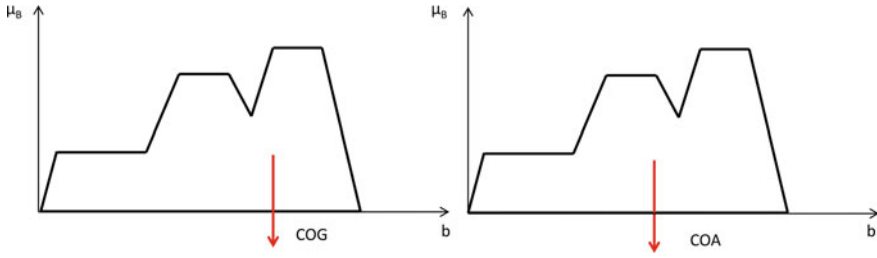
Fig. 3 Different defuzzification methods

be used: the aggregation of antecedents in each rule (AND connectives), implication (IF-THEN connectives), and aggregation of the rules (ALSO connectives).

2.4 Defuzzification

Defuzzification represents the inverse of the fuzzification process. It is performed according to the membership function of the output variable. The purpose of the defuzzifier component of a fuzzy logic system (FLS) is to defuzzify the fuzzy output and obtain a final crisp output. Many different techniques to perform defuzzification are available in the literature, such as: center of the area, center of gravity, bisector of area, etc. (Fig. 3) (Klir and Yuan 1995).

3 Methodology to Quantify the Downtime and Seismic Resilience

The methodology starts with a Rapid Visual Screening (RVS) of the buildings. The RVS survey form, which is performed by an expert, aims to collect information on the building's components that could be damaged. Building's information from the RVS is incorporated through a comprehensive hierarchical structure, which follows a logical order that combines specific contributors (e.g. site seismic hazard and building vulnerability modules) to estimate the building damage. A Fuzzy system is implemented in the procedure to translate the RVS results from linguistic terms into numerical data.

The building damageability is carried out as five-tuple membership values (μ_{VL}^{BD}, μ_L^{BD}, μ_M^{BD}, μ_H^{BD}, μ_{VH}^{BD}) and each membership value is associated with five damage states, *very low* (VL), *low* (L), *medium* (M), *high* (H), and *very high* (VH). The building membership can be considered as the limit state in which the structure may be for a given site seismic hazard and building vulnerability. For this reason, the downtime analysis is carried out for the degrees of damage membership that are greater than zero, which represents the possibility of the building being in a limit

Building Damageability
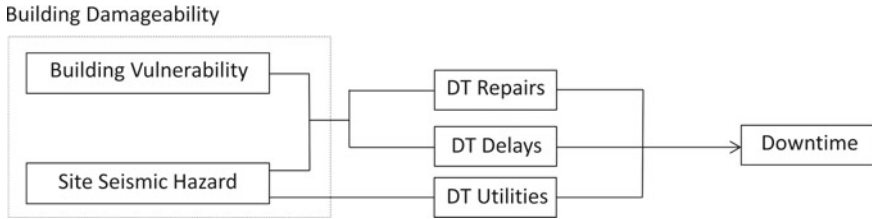
Fig. 4 Evaluation of downtime

state. For instance, if the damage membership is $(\mu_{VL}^{BD}, \mu_{L}^{BD}, \mu_{M}^{BD}, \mu_{H}^{BD}, \mu_{VH}^{BD}) = (0, 0, 0.37, 0.63, 0)$, the downtime is quantified for damage $= Medium$ (0.37) and damage $= High$ (0.63) (Tesfamariam and Sanchez-Silva 2011). These fuzzy numbers describe the damage expected as a result of a given earthquake and are used to calculate the *repairs, delays,* and *utilities disruption.* That is, the downtime is the combination of the time required for *repairs* (rational components), *delays* (irrational components), and the time of *utilities* disruption Fig. 4, as follows:

$$DT = \max((DT\ repairs + DT\ delays); DT\ utilities) \tag{3}$$

The combination of the three parameters depends on the chosen recovery state (i.e. re-occupancy recovery, functional recovery, and full recovery) (Bonowitz 2010). For example, in the re-occupancy recovery state, consideration of *utilities* disruption is not required, thus the downtime is the result of the time required for *repairs* and *delays* only.

To estimate the downtime due to *repairs*, it is necessary to define the repair time for each component of the analyzed building and the number of workers assigned for the repair. Downtime due to *delays* is based on irrational components (Comerio 2006), which are a selection from the components used by REDI™: post-earthquake inspection, engineering mobilization, financing, contractor's mobilization, and permitting. Downtime due to *utilities* depends on the site seismic hazard and on infrastructure systems that are likely to be disrupted after an earthquake (e.g. electricity, water, gas, etc.).

Finally, once the rational components, the irrational components, and the utilities disruption are known, the total repair time can be estimated. A downtime value is computed for each damage membership as follows:

$$DT = \sum_{i=1}^{n} DT_i * \mu_i \tag{4}$$

where DT_i is the downtime for a certain granulation, i is the granulation assigned to the damage membership, μ_i is the damage membership degree of granulation i. The Seismic Resilience of a damaged building is computed through the aggregation of the downtime and building damageability by applying the Fuzzy logic steps defined before.

3.1 Damage Estimation

The building damage is estimated through a hierarchical scheme that includes all variables contributing to the building damage (Fig. 5). The proposed hierarchical scheme for building damageability is an adaptation from Tesfamariam and Saatcioglu (2008), in which the variables are aggregated through the fuzzy model introduced before and the granularity assigned to the fuzzification is associated with the level of damage state. In the methodology, the Fuzzy Logic is applied using a heuristic model to assign membership values starting from linguistic information, which can generate membership functions using our intelligence. The membership functions considered in the methodology are introduced by Tesfamariam and Saatcioglu (2008) and are based on triangular fuzzy numbers (TFNs) that are expressed by three vertices (a; b; c) where a, b, and c represent the minimum and the maximum, respectively. The triangular fuzzy numbers are suitable to describe linguistic param-
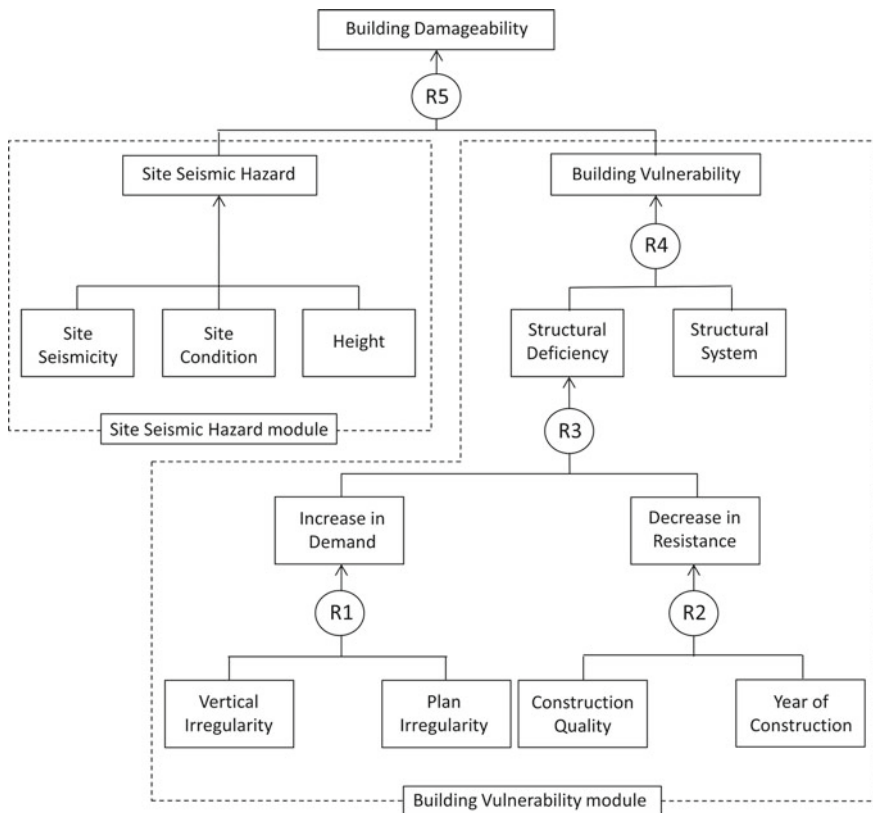
Fig. 5 The building damageability hierarchical scheme, adapted from Tesfamariam and Saatcioglu (2008)

eters since they can refer to three possible scenarios: pessimistic, most probable and optimistic. Finally, at each level of the hierarchical scheme (Fig. 5), the weighted average method is used for the defuzzification to obtain an index I, as follows:

$$I = \sum_{i=1}^{n} q_i * \mu_{R,i} \tag{5}$$

where q_i is the quality-ordered weights, $\mu_{R,i}$ is the degree of membership, i is the tuple fuzzy set (Sadiq et al. 2004; Liou and Lo 2005). The 1991 Northridge Earthquake damage observations are used to calibrate the quality-ordered weights in the methodology (Tesfamariam and Saatcioglu 2008).

The defuzzification process is not required for the Building Damageability. That is, each damage membership grade that is greater than zero is used independently in the downtime analysis. The resulting downtimes corresponding to the different memberships are combined to obtain a final downtime value, as described before.

Following the proposed hierarchical scheme, the Building Damageability index (I^{BD}) is evaluated by combining Site Seismic Hazard (SSH) and Building Vulnerability (BV). Building Vulnerability index (I^{BV}) is obtained through the integration
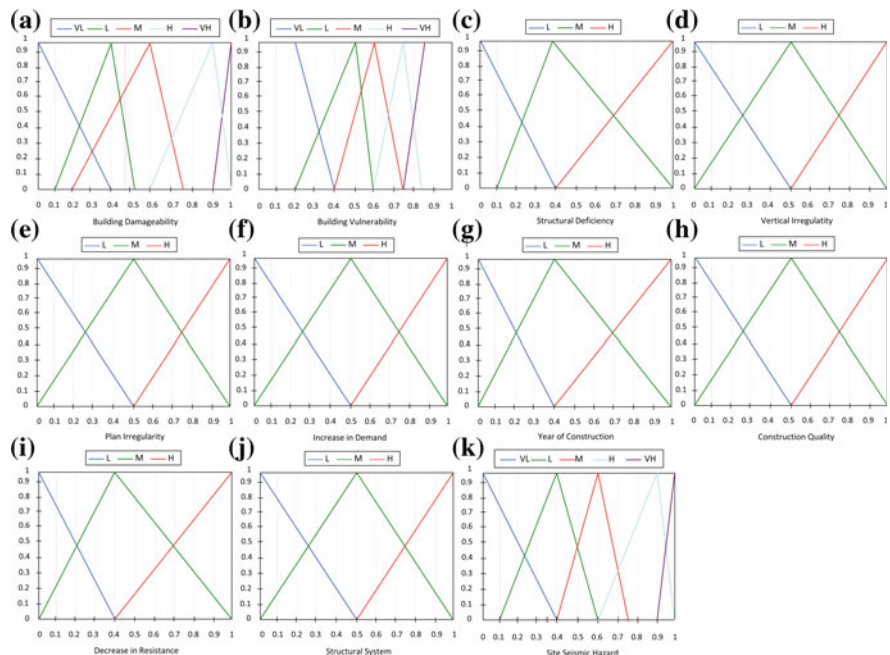
Fig. 6 Membership functions and granulation for: **a** Building damageability *BD*; **b** Building vulnerability *BV*; **c** Structural deficiency *SD*; **d** Vertical irregularity *VI*; **e** Plan irregularity *PI*; **f** Increase in demand *ID*; **g** Year of construction *YC*; **h** Construction quality *CQ*; **i** Decrease in resistance *DR*; **j** Structural system *SS*; **k** Site seismic hazard *SSH*

Table 1 Fuzzy rules for building damageabilty

Rule	SSH W = 2	BV W = 1	BD
1	VL	VL	VL
2	VL	L	VL
3	VL	M	L
4	VL	H	L
5	VL	VH	L
6	L	VL	L
7	L	L	L
8	L	M	L
9	L	H	M
10	L	VH	M
11	M	VL	L
12	M	L	M
13	M	M	M
14	M	H	M
15	M	VH	H
16	H	VL	M
17	H	L	M
18	H	M	H
19	H	H	H
20	H	VH	H
21	VH	VL	H
22	VH	L	H
23	VH	M	H
24	VH	H	VH
25	VH	VH	VH

Table 2 Fuzzy rules for building vulnerability

Rule	SD W = 2	SS W = 1	BV
1	L	L	L
2	L	M	L
3	L	H	M
4	M	L	M
5	M	M	M
6	M	H	M
7	H	L	M
8	H	M	H
9	H	H	H

Table 3 Fuzzy rule for increase in demand

Rule	VI W = 2	PI W = 1	ID
1	L	L	L
2	L	M	L
3	L	H	M
4	M	L	M
5	M	M	M
6	M	H	M
7	H	L	M
8	H	M	H
9	H	H	H

Table 4 Fuzzy rules for decrease in resistance

Rule	CQ W = 2	YC W = 1	DR
1	L	L	L
2	L	M	L
3	L	H	M
4	M	L	M
5	M	M	M
6	M	H	M
7	H	L	M
8	H	M	H
9	H	H	H

Table 5 Fuzzy rules for structural deficiency

Rule	ID W = 1	DR W = 2	SD
1	L	L	L
2	L	M	M
3	L	H	M
4	M	L	L
5	M	M	M
6	M	H	H
7	H	L	M
8	H	M	M
9	H	H	H

Table 6 Fuzzy rules for seismic resilience

Rule	DT W = 2	BD W = 1	R
1	VL	VL	VL
2	VL	L	VL
3	VL	M	L
4	VL	H	L
5	VL	VH	L
6	L	VL	L
7	L	L	L
8	L	M	L
9	L	H	M
10	L	VH	M
11	M	VL	L
12	M	L	M
13	M	M	M
14	M	H	M
15	M	VH	H
16	H	VL	M
17	H	L	M
18	H	M	H
19	H	H	H
20	H	VH	H
21	VH	VL	H
22	VH	L	H
23	VH	M	H
24	VH	H	VH
25	VH	VH	VH

of the two components: Structural Deficiency (SD) and Structural System (SS). On the other hand, the Site Seismic Hazard index (I^{SH}) is computed by combining the earthquake source conditions, source-to-site transmission path properties, and site conditions. I^{SH} is expressed in terms of building response acceleration, which can be obtained as a function of the building fundamental period (T).

Structural Deficiency is characterized by two categories (Saatcioglu et al. 2001): factors that increase the seismic demand (*Increase in Demand*) and factors contributing to a reduction in ductility and energy absorption (*Decrease in Resistance*). Parameters that contribute to the decrease in resistance are Construction Quality (CQ) and Year of Construction (YC). In general, the year of construction can be classified into three distinct states (Hazus 1999): low code (YC $\leq$ 1941), moderate code (1941 $\leq$ YC $\geq$ 1975), and high code (YC $\geq$ 1975). These thresh-

old values are derived from the North America practice. Year of Construction (YC) is used to convey important information about the seismic design code provision. Such information allows identifying the building behavior in ductility, strength and detailing. Parameters that contribute to the increase in seismic demand are Vertical Irregularity (VI) and Plan Irregularities (PI).

Three popular reinforced concrete building types are identified for the evaluation of the structural system component: moment resisting frames (C1), shear walls (C2), and moment resisting frames with infill masonry walls (C3). Moment resisting frame (C1) is a rectilinear structure with beams and columns rigidly connected, in which the resistance to lateral forces is provided by rigid frame action (Bruneau et al. 2011). Shear wall (C2) is a structural system with shear panels used to resist lateral forces. Moment resisting frames with infill masonry walls (C3) are largely presented in older buildings. They may work as shear walls in controlling deformations until the elastic limit of non-ductile concrete frames is exceeded. The granulation assigned to each parameter is shown in Fig. 6. The Fuzzy rules assigned to each parameter are listed in Tables 1, 2, 3, 4, 5, and 6.

4 Downtime Due to Repairs

Downtime due to repairs considers rational parameters: the state of the damaged components and the number of workers assigned (Fig. 7).

4.1 State of Components

Repair times are evaluated and collected from an electronic tool developed by FEMA (2012a), the *Performance Assessment Calculation Tool* (PACT). It provides repair times through functions that represent the distribution of losses as a function of damage state. In this work, only data representing the 50th and 90th percentile is used, as the 10th percentile is not desirable for downtime assessment.
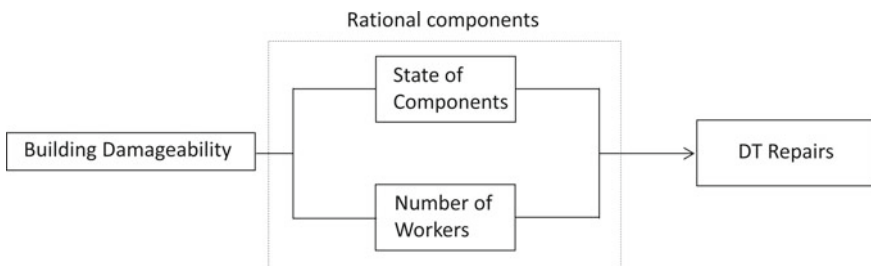
Fig. 7 Downtime due to repairs (rational components)
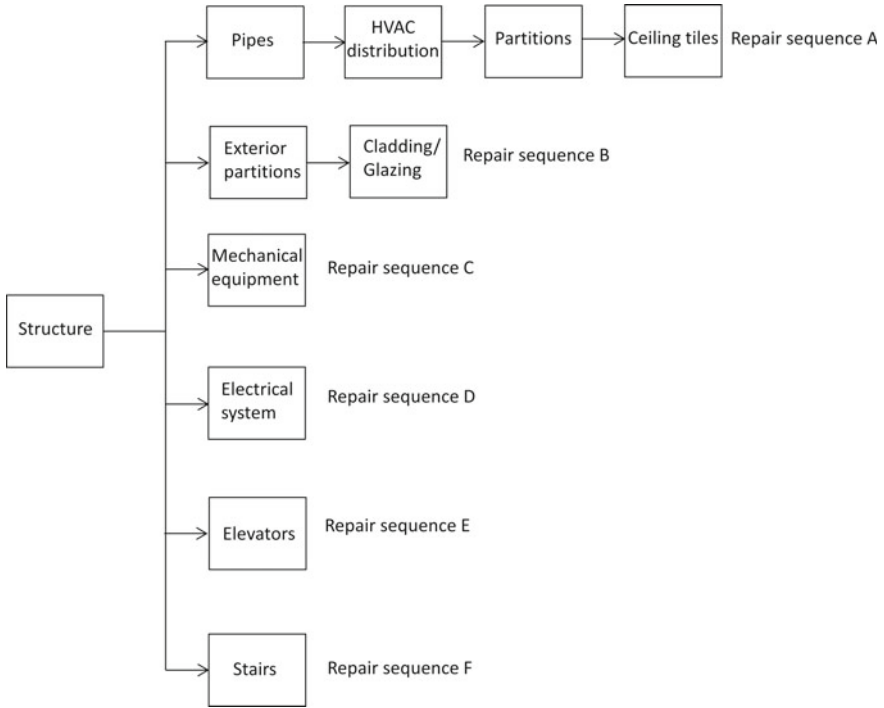
Fig. 8 Repair sequences from REDi

Once component repair times for each damage state are known, the values can be used to compute total component repair time by defuzzifying the component repair times using the corresponding membership values, as follows:

$$RT = \sum_{i=1}^{n} rt_{,i} * \mu_{R,i} \tag{6}$$

where RT is the component total repair time, rt_i is the repair time of the component considered, i is the damage state level, $\mu_{R,I}$ represents the damage membership value considered in the analysis. In this methodology, the repairs sequence presented in REDI™ (Almufti and Willford 2013), which defines the order of repairs (Fig. 8), is used to quantify the repair time and depends on the building damage state. That is, if the building damage state is classified as *Medium*, structural components can be repaired simultaneously (in parallel); if the building damage state is classified as *High* or *Very High*, structural repairs are done for one floor at a time (in series). Depending on the repair scheme and on the number of floors in the building, repair times may be in order of months (parallel repair scheme) and/or years (series repair scheme).

4.2 Number of Workers

Repairs can be carried faster or slower, depending on the crew number. Information about the number of workers is obtained from FEMA P-58 and from REDi™. The maximum number of workers indicated in FEMA P-58 ranges between 1 worker per 250 ft². and 1 worker per 2000 ft² (FEMA 2012b). Following the REDi™ instructions, repairs for structural components have a labor allocation limitation of 1 worker per 500 ft² per floor. For non-structural repairs, REDi™ recommends using 1 worker per 1000 ft².

The number of workers assigned to each repair sequence is determined through the average number of workers from RS Means (Alterman et al. 2013). Equation (7) computes the maximum number of workers for structural repairs in a building for a gross area:

$$N_{\max} = 2.5 \times 10^{-4} A_{tot} + 10 \tag{7}$$

where N_{max} is the maximum number of workers on site, A_{tot} is the total floor area of the building (ft²).

5 Downtime Due to Delays

Downtime due to delays is largely based on the building damage. That is, in buildings where the expected damage state is *Low*, less downtime due to delays is likely to occur. Downtime due to delays derived from several irrational components, which were introduced by Comerio (2006).

The irrational components used in the methodology are a selection from the components used by REDi™: Financing, Post-earthquake inspection, Engineer mobilization, Contractor mobilization, and Permitting (Fig. 9).

REDi™ guidelines define the irrational components as "*impeding factors*", as they increase the time required to start repairs. Irrational components are presented in the form of lognormal cumulative distribution functions, which are based on data from previous earthquakes provided by engineers, contractors, bankers, and cost estimators. In the proposed methodology, the "best estimate" approximation of delays is used.

5.1 Financing

Delay due to financing depends on the method of financing, which can be: private loans (e.g. bank loans), Small Business Administration (SBA), insurance, and pre-
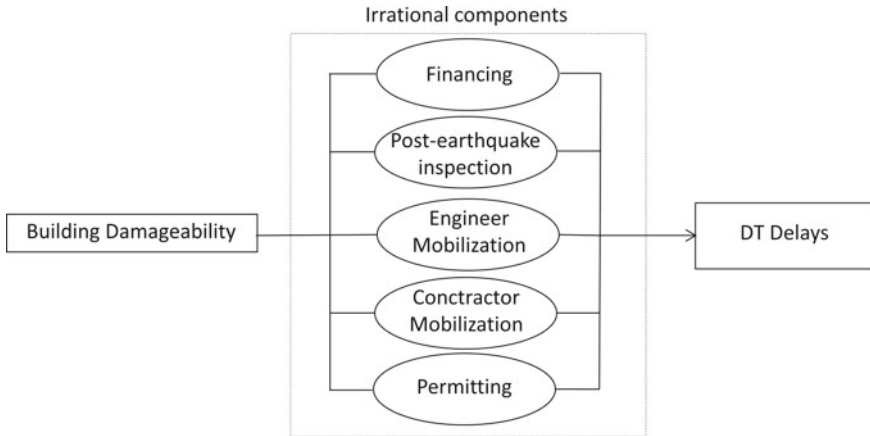
Fig. 9 Downtime due to delays (irrational components)

arranged credit line. Delays due to financing need to be considered in case that the building damage membership state is greater than or equal to *High*.

5.2 Post-earthquake Inspection

Delays due to post-earthquake inspection depend basically on the building use. For instance, if the building is an essential facility, inspectors are expected to arrive earlier due to the importance of the building in the community. In order to reduce the downtime significantly, owners can enroll in different programs, such as the *Building Occupancy Resumption Program* (BORP) (Mayes et al. 2011) where there is no necessity of official city-inspectors.

Post-earthquake inspection delays are considered for every recovery state if the membership of building damage state is higher than *Medium*. Otherwise they are not included as there would be no structural damage.

5.3 Engineer Mobilization

Delays due to engineer mobilization are mostly the time required for finding engineers plus the time needed to carry out engineering review and/or re-design. It depends on the level of structural damage and the size of the building. Such delays are considered in the analysis if the membership of building damage state is *Medium*, *High* and/or *Very High*. For instance, if the building damage membership is defined as *Medium*, minor structural repairs should be approved by an engineer and structural calculations

are not necessary, or if the building damage membership is classified as *High* the building should be re-designed due to the high level of the damage. Thus, the time required for engineer mobilization is the time necessary for a new building project.

5.4 Contractor Mobilization

Different factors contribute to the increase in delays due to contractor mobilization, such as the lack of availability contractors, materials, and equipment after the earthquake event. Their consideration depends on the building damage state in each recovery state: *High* in re-occupancy, *Medium* in functional recovery, and *Low* in full recovery state.

5.5 Permitting

Permitting is the time needed for the local building jurisdiction to review and approve the proposed repairs. Delays due to permitting are included in the downtime analysis if the membership of building damage state is *High* for re-occupancy and functional recovery states, and/or *Medium* for full recovery state.

6   Downtime Due to Utilities Disruption

Consideration of utilities service, and consequently utilities disruption is needed only in functional and full recovery states (Fig. 10).

Utilities disruption times are defined from data about past earthquakes (Kammouh et al. 2018a), where the authors introduces a simplified empirical model based on real data of past earthquakes to estimate the downtime of different types of infrastructures. Disruption of utilities should be considered if the membership value of site seismic hazard is greater than or equal to *Medium.*
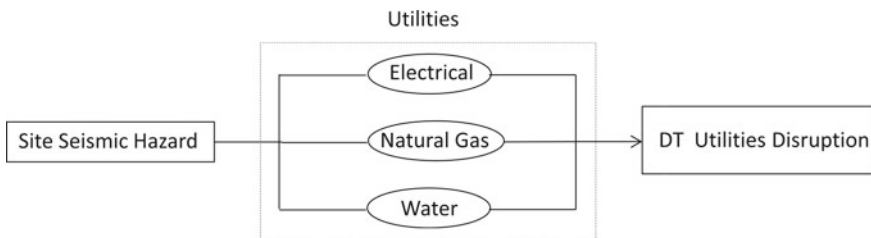
Fig. 10 Downtime due to utilities disruption

6.1 Electricity

The recover time of electricity systems ranges from 2 to 14 days for full recovery. They generally recover faster than other utility systems due to their high level of redundancy.

6.2 Natural Gas

Natural gas systems tend to require a longer time for restoration (from 7 to 84 days). That's because the gas services need to be re-lighted and re-pressurized after the gas shuts off for safety purpose.

6.3 Water

Time to recover the water system is usually considerable in all earthquakes and ranges between 6 days and 10 weeks for full restoration. The methodology used for determining the water disruption time follows the same criteria of natural gas disruption.

7 Illustrative Example

The case study consists of a hypothetical three-story residential building with floor area A = 4800 ft^2, structural system SS = C1, and fundamental period T_1 = 0.38 s. The 1994 Northridge Earthquake has been selected as the hazard event. From the walk down survey (RVS), information about the analyzed building has been collected and presented in Table 7. In addition, from the response spectrum of the 1994 Northridge Earthquake, the spectral acceleration S_a has been identified as 0.50 g. In the following, the downtime and resilience estimation procedure are illustrated in detail.

Table 7 Basic risk items and transformation

Basic risk item	Field observation	Transformation
Structural system (SS)	C1	0.70
Vertical irregularity (VI)	Yes	0.80
Plan irregularity (PI)	Yes	0.80
Construction quality (CQ)	Poor	0.99
Year of construction (YC)	1960	−0.01*YC + 20,25

7.1   The Northridge Earthquake Scenario

The earthquake that hit Northridge on January 17 in 1994 is considered as the most damaging earthquake in the history of the United States. The magnitude 6.7 earthquake Northridge occurred on a fault under the San Ferdinando Valley and extended under the Santa Susana Mountains (Stein 1994). Preliminary data on the emergency response and on the social impacts of the Northridge earthquake highlights that structural failure was the underlying cause of facilities directly assigned to the earthquake.

The earthquake caused significant damage to health facilities, such as non-structural damage to pipes and other utilities. For example, the damage of a rooftop water tank induced the evacuation of a psychiatric hospital, and other facilities were left without water or power (Comerio and Blecher 2010).

Data from the Association of Bay Area Governments (ABAG) and from Assessor for the Northridge-affected areas (Los Angeles city, Los Angeles County and the City of Santa Monaca) estimated the status of residential building damaged by the Northridge earthquake as repaired, demolished, or rebuilt. The building evaluation was carried out with a red (unsafe for re-occupancy or entry) and yellow (limited entry) indicator. Such data estimated that 3127 residential buildings were repaired, 126 were demolished, and 378 were rebuilt.

Later, around three weeks from the seismic event, FEMA received applications for assistance through the Disaster Housing Program, the Small Business Administration (SBA), which provide housing assistance and, if it is necessary, funds for temporary housing.

The Northridge earthquake illustrates that the post-disaster recovery activity started almost immediately after the hazard event. The high-priority activities included: providing water to areas where that utility was damaged; developing an alternative transportation system to reduce congestion; and making plans to deal with the school-system disruption (Tierney et al. 1995).

Real data for damaged structural and non-structural components are not available, unfortunately. Thus, in the illustrative case study, unreal information about the building's components has been used.

7.2   Damage Estimation

STEP 1: Transformation

The first step is to transform the basic risk items into a comparable number, which is mainly based on expert knowledge. The 1991 Northridge Earthquake damage database is adopted to calibrate the transformation values for VI, PI, and CQ are (Tesfamariam and Saatcioglu 2008). The transformation values are listed in Table 7.

Table 8 Fuzzification process

Basic risk items	Fuzzification
Vertical irregularity	$(\mu_L^{VI}, \mu_M^{VI}, \mu_H^{VI}) = (0, 0.40, 0.60)$
Plan irregularity	$(\mu_L^{VI}, \mu_M^{VI}, \mu_H^{VI}) = (0, 0.40, 0.60)$
Construction quality	$(\mu_L^{CQ}, \mu_M^{CQ}, \mu_H^{CQ}) = (0, 0.01, 0.99)$
Year of construction	$(\mu_L^{YQ}, \mu_M^{YQ}, \mu_H^{YQ}) = (0, 0.60, 0.40)$
Structural system	$(\mu_L^{SS}, \mu_M^{SS}, \mu_H^{SS}) = (0, 0.50, 0.50)$
Site seismic hazard	$(\mu_{VL}^{SSH}, \mu_L^{SSH}, \mu_M^{SSH}, \mu_H^{SSH}, \mu_{VH}^{SSH}) = (0, 0.50, 0.50, 0, 0)$

STEP 2: Fuzzification

Fuzzification is the conversion of input values into corresponding membership with respect of their granulation. That is, after selecting a transformation value for each parameter (Table 7), one can enter into the corresponding fuzzy sets graph and obtain the degree of membership for each parameter. The results are presented in Table 8.

STEP 3: Inference

Mamdani's inference system is performed through the hierarchical scheme (Fig. 5). It is implemented using a bottom up approach, starting with R_1 and R_2 till R_5. An example of inference for the Increase in Demand index (I^S) is given in this section. The inference of other indices is done in a similar fashion. As mentioned before, the increase in demand index (I^{ID}) is the combination of vertical and plan irregularities. Using the fuzzy rule base, I^{ID} is computed to be:

$$
ID = \begin{array}{l}
\mu_L^{ID} = max(min(0, 0), min(0, 0.40)) = 0 \\
\mu_M^{ID} = max(min(0, 0.60), min(0.40, 0), min(0.40, 0.40), min(0.40, 0.60), min(0.60, 0)) = 0.4 \\
\mu_H^{ID} = max(min(0.60, 0.40), min(0.60, 0.60)) = 0.60
\end{array}
$$

(8)

STEP 4: Defuzzification

Using the previously introduced quality-ordered weights factors, q_i ($i = 1, 2, 3$)=[0.25, 0.5, 1], the I^{ID} is defuzzified as follows:

$$
ID = \sum_{i=1}^{n} q_i \cdot \mu_i = 0.25 \times 0 + 0.5 \times 0.4 + 1 \times 0.6 = 0.80
$$

(9)

Defuzzification of other indexes is given in Table 9.

For the Building Damageability index (I^{BD}), defuzzification is not performed because the membership values are used in the subsequent analysis (i.e., components repair time evaluation), as we mentioned before. The membership of I^{BD} is given through inferencing the Site seismic hazard index (I^{SSH}) and the Building vulnerability index (I^{BV}) as

Table 9 Defuzzification process

Index	Inference/Aggregation	Defuzzification
I^{DR}	(R2) = YC + CQ	0.77
I^{SD}	(R3) = I^{ID} + I^{DR}	0.63
I^{BV}	(R4) = I^{SD} + I^{SS}	0.54

$$\left(\mu_{VL}^{BD}, \mu_{L}^{BD}, \mu_{M}^{BD}, \mu_{H}^{BD}, \mu_{VH}^{BD}\right) = (0, \mathbf{0.35}, \mathbf{0.65}, 0, 0)$$

Since the memberships that are greater than zero are associated with μ_{L}^{BD} (0.35) and μ_{M}^{BD} (0.65), the downtime analysis for $I^{BD} = Low$ and $I^{BD} = Medium$ is carried out. According to the membership degrees results, the downtime is quantified for re-occupancy recovery state.

7.3 Downtime Due to Repairs

Repair times for each type of damaged component are provided in terms of 'worker-days' from PACT. Tables 10 and 11 present the process for obtaining this information and summarize repair times for building components related to *Low* and *Medium* damage state in a repair sequence. The number of 'worker-days' of each component is computed by multiplying the unitary worker-days value provided by PACT by the corresponding number of units (EA, units) or area (SF, square feet), whichever relevant. Once component repair times are known, they are defuzzified with the corresponding membership degrees of the building damage state (in the case study 0.35 and 0.65), using Eq. (6).

7.3.1 Structural Repairs

Low and *Medium* building damage states implies that the structural components can be repaired in parallel. Considering that all floors have the same area, the number of workers required in each floor is:

$$no.\,of\,workers = (4800\,\text{ft}^2)(1\,worker/(500\,\text{ft}^2)) = 10\,workers \qquad (10)$$

Equation (7) shows that the maximum number of workers allowed to execute structural repairs at any time is 22 workers. Thus, the number of workers computed in Eq. (10) is considered acceptable because it is less than the maximum number allowed. Adding up the numbers of defuzzified 'worker-days' related to structural components at floor 1, floor 2 and floor 3 and dividing by the number of workers defined using Eq. (10), one can obtain the days required for structural repairs. The results are 2.2, 1.4, and 2.4 days, respectively for the *Low* damage analysis. Instead,

Table 10 Component repair times and worker days for *Low* damage

Floor	Repair	Component type	Worker-days per unit or area	EA or SF	Total worker-days	Defuzzification
Floor 1	Structural repairs	Concrete beam	22.758	2 units	45.5	15.93
		Link beams <16″	17.358	1 units	17.358	6.08
	Repair sequence A	Interior partitions	5	215.3 ft²	1076.4	376.74
		Ceiling	17	30 ft²	510	178.50
	Repair sequence B	Exterior partitions	32	20 ft²	640	224
	Repair sequence D	Transformer <100 kVA	1.818	1 unit	1.818	0.64
		Low voltage switchgear	2.226	1 unit	2.226	0.78
	Repair sequence F	Stairs	13.965	4 units	55.86	19.55
Floor 2	Structural repairs	Concrete beam	22.758	1 unit	22.758	7.97
		Link beams <16″	17.358	1 unit	17.358	6.08
	Repair sequence A	Interior partitions	5	220 ft²	1100	385
		Ceiling	17	10 ft²	170	59.5
	Repair sequence B	Exterior partitions	32	5 ft²	160	56
	Repair sequence D	Transformer <100 kVA	1.818	1 unit	1.818	0.64
		Low voltage switchgear	2.226	1 unit	2.226	0.78
	Repair sequence F	Stairs	13.965	4 units	55.86	19.55
Floor 3	Structural repairs	Concrete beam	22.758	3 units	68.27	23.89
	Repair sequence A	Interior partitions	5	190 ft²	950	332.5
		Ceiling	17	15 ft²	255	89.25
	Repair sequence D	Transformer <100 kVA	1.818	1 unit	1.818	0.64
		Low voltage switchgear	2.226	1 unit	2.226	0.78
	Repair sequence F	Stairs	13.965	4 units	55.86	19.55
Roof	Repair sequence C	Chiller	11.088	1 unit	11.088	3.88

Table 11 Component repair times and worker days for *Medium* damage

Floor	Repair	Component type	Worker-days per unit or area	EA or SF	Total worker-days	Defuzzification
Floor 1	Structural repairs	Concrete beam	22.758	2 units	45.5	29.58
		Link beams <16″	17.358	1 unit	17.358	11.28
	Repair sequence A	Interior partitions	5	215.3 ft²	1076.4	699.66
		Ceiling	17	30 ft²	510	331.50
	Repair sequence B	Exterior partitions	32	20 ft²	640	416
	Repair sequence D	Transformer <100 kVA	1.818	1 unit	1.818	1.18
		Low voltage switchgear	2.226	1 unit	2.226	1.45
	Repair sequence F	Stairs	13.965	4 units	55.86	36.31
Floor 2	Structural repairs	Concrete beam	22.758	1 unit	22.758	14.79
		Link beams <16″	17.358	1 unit	17.358	11.28
	Repair sequence A	Interior partitions	5	220 ft²	1100	715
		Ceiling	17	10 ft²	170	110.5
	Repair sequence B	Exterior partitions	32	5 ft²	160	104
	Repair sequence D	Transformer <100 kVA	1.818	1 unit	1.818	1.18
		Low voltage switchgear	2.226	1 unit	2.226	1.45
	Repair sequence F	Stairs	13.965	4 units	55.86	36.31
Floor 3	Structural repairs	Concrete beam	22.758	3 units	68.27	44.38
	Repair sequence A	Interior partitions	5	190 ft²	950	617.5
		Ceiling	17	15 ft²	255	165.75
	Repair sequence D	Transformer <100 kVA	1.818	1 unit	1.818	1.18
		Low voltage switchgear	2.226	1 unit	2.226	1.45
	Repair sequence F	Stairs	13.965	4 units	55.86	36.31
Roof	Repair sequence C	Chiller	11.088	1 unit	11.088	7.21

Table 12 Number of workers for non-structural repairs

Repair sequence	Number of workers per floor	Max number of worker per component type
Repair sequence A	#workers = (4800 ft^2) (1 worker/1000 ft^2) = 5 workers	15
Repair sequence B	#workers = (4800 ft^2) (1 worker/1000 ft^2) = 5 workers	15
Repair sequence C	#workers = (1 damaged unit) (3 workers/damaged unit) = 3 workers	9
Repair sequence D	#workers = (1 damaged unit) (3 workers/damaged unit) = 2 workers	9
Repair sequence F	#workers = (4 damaged unit) (2 workers/damaged unit) = 8 workers	6

the results are 4, 2.6, and 4.4 day, respectively for *Medium* damage analysis. Thus, all the floors can be repaired in parallel in around 2.4 days (*Low* damage) and 4.4 days (*Medium* damage).

7.3.2 Non-structural Repairs

After all structural repairs have been completed, non-structural repairs can begin. Repair sequences considered in the case study are Repair Sequence A, B, C, D, and F, and they are summarized in Table 12, in which the number of workers per floor and the corresponding maximum number of workers allowed are presented.

Table 12 shows that repair sequence F requires a larger number of workers per floor (8 workers) than the maximum allowed per Repair sequence (6 workers). When the number of workers per floor is higher than the maximum number of worker, the maximum number allowed is considered in the methodology (in the illustrative example 6 workers). Summing the worker-days and dividing by the number of workers assigned to the repair sequence, the repair time for each repair sequence is calculated (Tables 13 and 14).

7.4 Downtime Due to Delays

The downtime analysis due to delays is carried out only for the *Medium* damage. That is, delays can increase the downtime if the building damage is greater than *Low*, otherwise irrational components don't influence the result. The following delays are considered: post-earthquake inspection and engineer mobilization (Table 15).

Table 13 Repair time for each repair sequence for *Low* damage

Floor 1	Repair sequence A	RT = (555.34 worker days)/5 workers = 111.05 days
	Repair sequence B	RT = (224 worker days)/5 workers = 45 days
	Repair sequence D	RT = (1.42 worker days)/2 workers = 0.71 day
	Repair sequence F	RT = (19.55 worker days)/6 workers = 2.76 days
Floor 2	Repair sequence A	RT = (444.5 worker days)/5 workers = 88.9 days
	Repair sequence B	RT = (56 worker days)/5 workers = 11.2 days
	Repair sequence D	RT = (1.42 worker days)/2 workers = 0.71 day
	Repair sequence F	RT = (19.55 worker days)/6 workers = 2.76 days
Floor 3	Repair sequence A	RT = (421.75 worker days)/5 workers = 84.4 days
	Repair sequence D	RT = (1.42 worker days)/2 workers = 0.71 day
	Repair sequence F	RT = (19.55 worker days)/6 workers = 2.76 days
Roof	Repair sequence C	RT = (3.88 worker days)/3 workers = 1.3 days

Table 14 Repair time for each Repair sequence for *Medium* damage

Floor 1	Repair sequence A	RT = (1031.16 worker days)/5 workers = 206.23 days
	Repair sequence B	RT = (416 worker days)/5 workers = 83.2 days
	Repair sequence D	RT = (2.63 worker days)/2 workers = 1.31 day
	Repair sequence F	RT = (36.31 worker days)/6 workers = 6.05 days
Floor 2	Repair sequence A	RT = (825.5 worker days)/5 workers = 165.1 days
	Repair sequence B	RT = (104 worker days)/5 workers = 20.8 days
	Repair sequence D	RT = (2.63 worker days)/2 workers = 1.31 day
	Repair sequence F	RT = (36.31 worker days)/6 workers = 6.05 days
Floor 3	Repair sequence A	RT = (783.25 worker days)/5 workers = 156.65 days
	Repair sequence D	RT = (2.64 worker days)/2 workers = 1.31 day
	Repair sequence F	RT = (36.31 worker days)/6 workers = 6.05 days
Roof	Repair sequence C	RT = (7.21 worker days)/3 workers = 2.40 days

Table 15 Impeding factors delays

	Post-earthquake inspection		Engineer mobilization	
Building type	Delays P50		Max buil. damage	Delays P50
BORP	1 days		Medium	6 weeks

7.5 Downtime Due to Utilities Disruption

Utilities disruption is not considered in downtime assessment for re-occupancy recovery state because this only affects building functionality.

7.6 Total Repair Time

As mentioned before, in the re-occupancy recovery state, downtime calculation is carried out by aggregating DT repairs and DT delays, as follows:

$$DT(damage = Low) = DT\ repairs + DT\ delays = 284.3 + 0 = 284.3\ \text{days}$$
$$DT(damage = Medium) = DT\ repairs + DT\ delays = 527.98 + 43 = 571\ \text{days}$$
(11)

Once the downtimes for each damage state have been calculated, the final results can be weighted with the damage membership values defined above, as follows:

$$DT = \sum_{i=1}^{n} DT_i * \mu_i = (284.3 * 0.35) + (571 * 0.65) = 470.6\ \text{days} \tag{12}$$

Equation (12) shows that the final downtime of the residential building is around 470.6 days.

7.7 Seismic Resilience Estimation

STEP 1: Transformation

The downtime can be classified as *Short, Average,* and *Long*, and the corresponding transformation values are 0.2, 0.5, and 0.8 respectively. The downtime resulted from the previous analysis is about 471 days, thus it can be classified as *Average* total repair time with a transformation value of 0.5.

STEP 2: Fuzzification

The granulation assigned for the fuzzification consists of five granules (*Very Low, Low, Medium, High,* and *Very High*). The downtime fuzzy sets are illustrated in Fig. 11.

The membership function of downtime is the following:

$$\left(\mu_{VL}^{DT}, \mu_{L}^{DT}, \mu_{M}^{DT}, \mu_{H}^{DT}, \mu_{VH}^{DT}\right) = (0,\ 0.25,\ 1,\ 0,\ 0)$$

The building damageability membership function, which has been obtained from inferencing the site seismic hazard and the building vulnerability, is given as follows:

Fig. 11 Downtime fuzzy sets
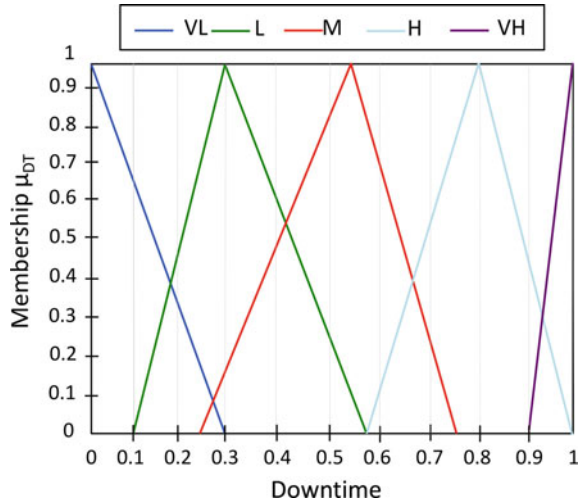
$$\left(\mu_{VL}^{BD}, \mu_{L}^{BD}, \mu_{M}^{BD}, \mu_{H}^{BD}, \mu_{VH}^{BD}\right) = (0, \ 0.35, \ 0.65, \ 0, \ 0)$$

STEP 3: Inference

Downtime is a key aspect of resilience. In this work, downtime is considered more influential than the building damageability and thus assigned a higher weight. Using the fuzzy rule base listed in Table 6, the I^R is computed:

$$I^R = \left(\mu_{VL}^{R}, \mu_{L}^{R}, \mu_{M}^{R}, \mu_{H}^{R}, \mu_{VH}^{R}\right) = (0, \ 0.20, \ 0.65, \ 0, \ 0)$$

STEP 4: Defuzzification

The resilience index I^R can be defuzzified using the quality-ordered weights factors adopted from those introduced by (Tesfamariam and Saatcioglu 2008), as follows:

$$I^R = \sum_{i=1}^{n} q_i * \mu_i = 0 * 0 + 0.25 * 0.20 + 0.5 * 0.65 + 0.75 * 0 + 1 * 0 = 0.38$$

(13)

8 Summary and Remarks

The current chapter presented a new methodology for quantifying the downtime and consequently the resilience of residential buildings against earthquake events. This helps in the decision-making process during the planning phase. In the resilience analysis, decision-making is an uncertain process since it requires complex analysis

of parameters that contribute towards uncertainties, such as building irregularities (topography), construction quality, and the relationship between the building damage and the seismic hazards.

A new methodology for three recovery states (e.g. re-occupancy, functional and full recovery), in which the Fuzzy logic is applied to overcome the uncertainty issues, is proposed. Unlike the traditional probabilistic methodologies, the advantage of the proposed Fuzzy method is that it is simpler and faster for the assessment and decision-making; it accepts imprecise and fuzzy data, which includes linguistic parameters; it can provide a downtime and resilience evaluation of buildings under different hazards.

The methodology can be divided into five main modules: quantification of building damage, evaluation of repairs (rational components), delays (irrational components) and utilities disruption, and evaluating the Resilience parameter.

Results from the case study show that irrational components increase the total downtime. In specific, delays before construction, such as financing and engineer mobilization, contribute significantly to the total repair time after a disastrous event.

The goal of the presented research has been to develop a new methodology for downtime and resilience analysis. In pursuit of this goal, different implications were taken, that although acceptable for this work, may be improved upon in future. Some of the mentioned limitations are the building structures (only three building structural types are considered), component repair times, and delays (limited to the U.S.A). Therefore, the authors propose as future directions to extend the methodology in order to cover more structural types as light wood-frame system or mixed structures made of timber framing and masonry; to expand the library of building components, delays, and utilities repair times to apply the methodology in other countries, and finally to apply different fuzzy membership shapes from those used in the methodology and compare the resulted effects.

References

Almufti, I, & Willford, M. (2013). *Resilience-based earthquake design (REDi) rating system, version 1.0*. Arup.

Alterman, T., Luckhaupt, S. E., Dahlhamer, J. M., Ward, B. W., & Calvert, G. M. (2013). Prevalence rates of work organization characteristics among workers in the US: Data from the 2010 National Health Interview Survey. *American Journal of Industrial Medicine, 56*(6), 647–659.

Bonowitz, D. (2010). Resilience criteria for seismic evaluation of existing buildings: A proposal to supplement ASCE 31 for intermediate performance objectives. In *Improving the Seismic Performance of Existing Buildings and Other Structures*, pp. 477–488.

Bonstrom, H., & Corotis, R. B. (2014). First-order reliability approach to quantify and improve building portfolio resilience. *Journal of Structural Engineering, 142*(8), C4014001.

Bruneau, M., Chang, S. E., Eguchi, R. T., Lee, G. C., O'Rourke, T. D., Reinhorn, A. M., et al. (2003). A framework to quantitatively assess and enhance the seismic resilience of communities. *Earthquake Spectra, 19*(4), 733–752.

Bruneau, M., Uang, C.-M., & Sabelli, S. R. (2011). *Ductile design of steel structures*. McGraw Hill Professional.

Chang, S. E., McDaniels, T., Fox, J., Dhariwal, R., & Longstaff, H. (2014). Toward disaster-resilient cities: Characterizing resilience of infrastructure systems with expert judgments. *Risk Analysis, 34*(3), 416–434.

Cimellaro, G. P. (2016). *Urban resilience for emergency response and recovery*. Springer.

Cimellaro, G. P., Fumo, C., Reinhorn, A., Bruneau, M. (2008). Seismic resilience of health care facilities. In *14th World Conference on Earthquake Engineering (14WCEE)*, Beijing, China, October 2008, pp. 12–17.

Cimellaro, G. P., Reinhorn, A. M., & Bruneau, M. (2010). Framework for analytical quantification of disaster resilience. *Engineering Structures, 32*(11), 3639–3649.

Cimellaro, G. P., Renschler, C., Reinhorn, A. M., & Arendt, L. (2016a). PEOPLES: A framework for evaluating resilience. *Journal of Structural Engineering, 142*(10), 04016063.

Cimellaro, G. P., Zamani-Noori, A., Kammouh, O., Terzic, V., & Mahin, S. A. (2016b). *Resilience of critical structures, infrastructure, and communities*. Berkeley, California: Pacific Earthquake Engineering Research Center (PEER).

Comerio, M. C. (2006). Estimating downtime in loss modeling. *Earthquake Spectra, 22*(2), 349–365.

Comerio, M. C., & Blecher, H. E. (2010). Estimating downtime from data on residential buildings after the Northridge and Loma Prieta Earthquakes. *Earthquake Spectra, 26*(4), 951–965.

FEMA (2012a) Seismic performance assessment of buildings, "Implementation Guide". vol 2. Applied Technology Council for the Federal Emergency Management Agency, CA, USA.

FEMA (2012b) Seismic performance assessment of buildings, "Methodology". vol 1. Applied Technology Council for the Federal Emergency Management Agency, CA, USA.

Hazus, M. (1999). *Earthquake loss estimation methodology technical and user manual*.

ISDR U Hyogo framework for action 2005–2015: building the resilience of nations and communities to disasters. In: Extract from the final report of the World Conference on Disaster Reduction (A/CONF. 206/6), 2005.

ISDR U (2009) Global assessment report on disaster risk reduction. United Nations International Strategy for Disaster Reduction (UN ISDR), Geneva, Switzerland ISBN/ISSN 980852698:207.

Kammouh, O., Cimellaro, G. P. (2018). PEOPLES: A tool to measure community resilience. In: J. G. Soules (Ed.) *Proceedings of 2018 Structures Congress (SEI2018). ASCE—American Society of Civil Engineering*, Fort Worth, Texas. April 19–21, pp. 161–171. https://doi.org/10.1061/9780784481349.015.

Kammouh, O., Cimellaro, G. P., & Mahin, S. A. (2018a). Downtime estimation and analysis of lifelines after an earthquake. *Engineering Structures, 173,* 393–403.

Kammouh, O., Dervishaj, G., Cimellaro, G. P. (2017a). A new resilience rating system for countries and states. *Procedia Engineering, 198*(Supplement C), 985–998. https://doi.org/10.1016/j.proeng.2017.07.144.

Kammouh, O., Dervishaj, G., & Cimellaro, G. P. (2017b). Quantitative framework to assess resilience and risk at the country level. *ASCE-ASME Journal of Risk and Uncertainty in Engineering Systems, Part A: Civil Engineering, 4*(1), 04017033. https://doi.org/10.1061/ajrua6.0000940.

Kammouh, O., Noori, A. Z., Taurino, V., Mahin, S. A., & Cimellaro, G. P. (2018b). Deterministic and fuzzy-based methods to evaluate community resilience. *Earthquake Engineering and Engineering Vibration, 17*(2), 261–275. https://doi.org/10.1007/s11803-018-0440-2.

Kammouh, O., Noori, A. Z., Cimellaro, G. P., & Mahin, S. A. (2019). Resilience assessment of urban communities. *ASCE-ASME Journal of Risk and Uncertainty in Engineering Systems, Part A: Civil Engineering, 5*(1), 04019002. https://doi.org/10.1061/AJRUA6.0001004

Kammouh, O., Zamani-Noori, A., Renschler, C., & Cimellaro, G. P. (2017c). Resilience quantifi-
cation of communities based on peoples framework. In *16th World Conference on Earthquake
Engineering (16WCEE)*, Santiago, Chile, January 9–13, 2017. IAEE, Santiago, Chile.

Kircher, C. A., Whitman, R. V., & Holmes, W. T. (2006). HAZUS earthquake loss estimation
methods. *Natural Hazards Review, 7*(2), 45–59.

Klir, G., & Yuan, B. (1995). *Fuzzy sets and fuzzy logic* (Vol. 4). Prentice hall, New Jersey.

Liou, Y.-T., & Lo, S.-L. (2005). A fuzzy index model for trophic status evaluation of reservoir
waters. *Water Research, 39*(7), 1415–1423.

Mamdani, E. H. (1974). Application of fuzzy algorithms for control of simple dynamic plant. In
Proceedings of the Institution of Electrical Engineers, vol. 12, pp. 1585–1588. IET.

Mamdani, E. H. (1976). Application of fuzzy logic to approximate reasoning using linguistic synthe-
sis. In *Proceedings of the Sixth International Symposium on Multiple-Valued Logic*, pp. 196–202.
IEEE Computer Society Press.

Mayes, C., Hohbach, D., Bello, M., Bittleston, M., Bono, S., Bonowitz, D., et al., (2011). SEAONC
rating system for the expected earthquake performance of buildings. In *SEAOC Convention Pro-
ceedings*, 2011.

Mendel, J. M. (1995). Fuzzy logic systems for engineering: A tutorial. *Proceedings of the IEEE,
83*(3), 345–377.

Renschler, C. S., Frazier, A. E., Arendt, L. A., Cimellaro, G. P., Reinhorn, A. M., & Bruneau, M.
(2010). *A framework for defining and measuring resilience at the community scale: The PEOPLES
resilience framework*. MCEER Buffalo.

Saatcioglu, M., Mitchell, D., Tinawi, R., Gardner, N. J., Gillies, A. G., Ghobarah, A., et al. (2001).
The August 17, 1999, Kocaeli (Turkey) earthquake damage to structures. *Canadian Journal of
Civil Engineering, 28*(4), 715–737.

Sadiq, R., Al-Zahrani, M. A., Sheikh, A. K., Husain, T., & Farooq, S. (2004). Performance evaluation
of slow sand filters using fuzzy rule-based modelling. *Environmental Modelling and Software,
19*(5), 507–515.

Stein, R. (1994). *The Northridge, California earthquake of January 1994 a computer animation
and paper model*. US Geological Survey.

Tesfamariam, S., & Saatcioglu, M. (2008). Risk-based seismic evaluation of reinforced concrete
buildings. *Earthquake Spectra, 24*(3), 795–821.

Tesfamariam, S., & Saatcioglu, M. (2010). Seismic vulnerability assessment of reinforced concrete
buildings using hierarchical fuzzy rule base modeling. *Earthquake Spectra, 26*(1), 235–256.

Tesfamariam, S., & Sanchez-Silva, M. (2011). A model for earthquake risk management based on
the life-cycle performance of structures. *Civil Engineering and Environmental Systems, 28*(3),
261–278.

Tierney, K., Blair-Tyler, M., Blais, N., Bolin, R., Borden, F., Bourque, L. B., et al. (1995). Societal
impacts and emergency response. *Earthquake Spectra, 11*(S2), 373–418.

Zadeh, L. A. (1965). Information and control. *Fuzzy Sets, 8*(3), 338–353.

Zadeh, L. A. (1973). Outline of a new approach to the analysis of complex systems and decision
processes. *IEEE Transactions on Systems, Man and Cybernetics, 1100,* 38–45.

Resilient Design of Buildings with Hysteretic Energy Dissipation Devices as Seismic Fuses

Arturo Tena-Colunga, Héctor Hernández-Ramírez
and Horacio de Jesús Nangullasmú-Hernández

1 Introduction

Modern seismic design methodologies based upon the collapse prevention limit state were proposed since the 1960s and are available in most seismic design codes worldwide since the 1970s. To date, this design philosophy is still available in most seismic code worldwide, including the most recent versions of the United States of America (ASCE 7-16 2016; IBC-18 2017) and Mexico (MDOC-15 2015; NTCS-17 2017). However, in recent strong earthquakes worldwide occurred in this century, it has been observed that buildings designed for the collapse prevention limit state since the late 1970s to date developed extensive nonstructural and structural damage, even when the intensity of the ground shaking was reasonable covered by the corresponding design spectrum for the site of interest.

For example, during the September 19, 2017 Puebla-Morelos Earthquake ($M_w = 7.1$), in Mexico City alone, 54 recent buildings designed with NTCS-04 (2004) experienced important damage, from moderate to severe; two of them collapsed and three of them have been already demolished (Fig. 1). It is extremely unacceptable that 53 of these 54 buildings were for residential use. The corresponding building height ranges are identified in Fig. 2, where it can be observed that most of the severely damaged buildings were low and medium-rise buildings between 5

A. Tena-Colunga (✉)
Departamento de Materiales, Universidad Autónoma Metropolitana—Azcapotzalco, Mexico City, Mexico
e-mail: atc@correo.azc.uam.mx

H. Hernández-Ramírez
Mexico City, Mexico
e-mail: hhruam@hotmail.com

H. de J. Nangullasmú-Hernández
Posgrado en Ingeniería Estructural, Universidad Autónoma Metropolitana—Azcapotzalco, Mexico City, Mexico
e-mail: hnangu@hotmail.com
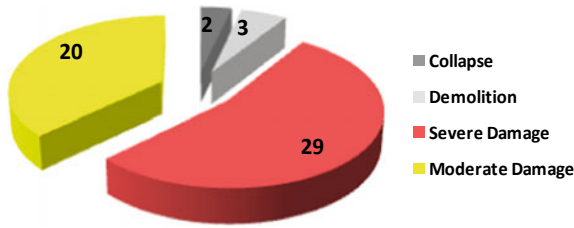
Fig. 1 Extent of damage of buildings built after 2004 in Mexico City during the September 19, 2017 earthquake
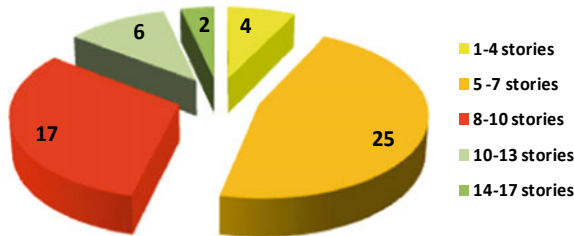
Fig. 2 Range for the number of stories of buildings built after 2004 in Mexico City and damaged during the September 19, 2017 earthquake
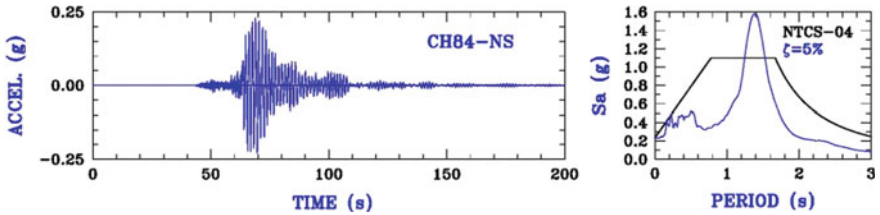
Fig. 3 Accelerations recorded in station CH84 in Mexico City during the September 19, 2017 earthquake. Comparison of their corresponding response spectrum for 5% equivalent viscous damping with respect to the design spectrum for the site according to NTCS-04

and 10 stories, but there were at least eight buildings taller than 10 stories and up to 17 stories that experienced moderate or severe damage.

If one takes aside the four damaged buildings located in Tlalpan and Coyoacán Districts, where ground motions were very intense and their corresponding response spectra even surpassed the design spectra for those sites (i.e., Tena-Colunga 2018, Fig. 3) and then, the extent of damage for the collapse prevention limit state was expected for those buildings, it was unacceptable that the remaining 50 buildings built according to NTCS-04 experienced such extent of damage.

For illustration purposes, in Figs. 4 and 5 two buildings classified by the city authorities (https://plataforma.cdmx.gob.mx/) as having severe damaged are shown, together with the corresponding elastic design spectrum for the site according to
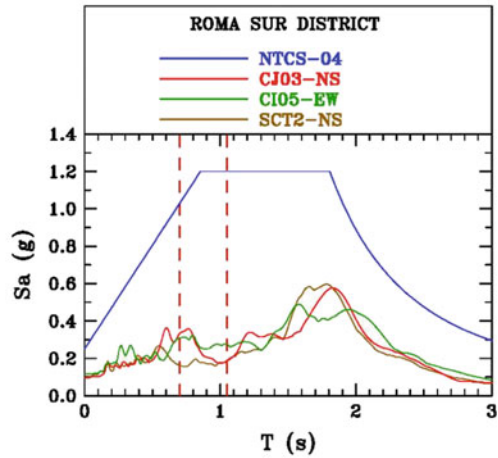
(a) 6-story building   (b) site response and design spectra

Fig. 4 Apartment building at Roma Sur District built in 2008 and severely damaged during the September 19, 2017 earthquake. Comparison of the design spectrum for the site according to NTCS-04 with respect to the response spectra for 5% equivalent viscous damping for the closest stations to the site. The expected natural period range is marked with vertical dashed lines

NTCS-04, as well as the response spectrum for 5% damping for the closest recording station(s) from the site. As it is observed, spectral ordinates close to both sites were well covered by the elastic design spectra established by NTCS-04 for those sites, yet, both buildings were severely damaged. It is worth noting that the observed interior damage was much worse than the exterior one, particularly for the Moderna District building.

It can be concluded that the observed extent of damage in many recent buildings designed according to modern codes such as NTCS-04 (2004) in the September 19, 2017 earthquake is unacceptable for the society. The extent of damage seems to be a direct consequence of both: (a) abusing on nonlinear responses (allow important damage) in buildings in terms of the response modification factor that accounts for "ductile" behavior and, (b) the perennial problem of allowing large story drifts in the structural design without directly considering the participation of infill walls and detail them properly (Figs. 4a and 5a).

Therefore, in order to satisfy today´s society need for resilient cities in seismic zones, building codes worldwide should move forward to resilient-based seismic design. One way to achieve a resilient seismic design is using passive energy dissipation devices as structural fuses, as explained in following sections.

(a) 17-story building   (b) site response and design spectra

Fig. 5 Apartment building at Moderna District built in 2007 and severely damaged during the September 19, 2017 earthquake. Comparison of the design spectrum for the site according to NTCS-04 with respect to the response spectra for 5% equivalent viscous damping for the closest stations to the site. The expected natural period range is marked with vertical dashed lines
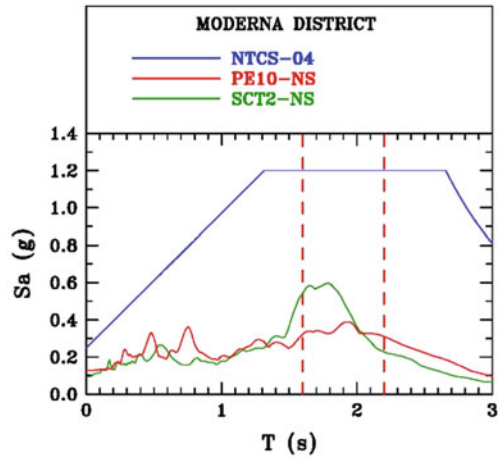
2 Seismic Fuse Concept

For an efficient and resilient seismic design, it is required that the structural system which carries the gravitational loads (primary system) should remain essentially elastic after a strong earthquakes. At the same time, it is required to have a secondary system that would be activated when an earthquake strikes, and it should be able to withstand the earthquake ground motions in a stable manner, protecting the primary system to remain essentially elastic or with at most an incipient damage. This secondary system should be easily replaceable after the action of a strong earthquake, in case that the developed damage within this system is important. Therefore, this secondary system acts as an structural fuse during the earthquake, as it takes most of the earthquake action and, if damaged, it could be easily replaced, then minimizing interruptions on the building usage after an strong earthquake.

Then, passive energy dissipation devices are solid candidates to be used in resilient-based seismic design, as they can be designed as structural fuses. Among all the passive energy dissipation devices that are now available (viscous dampers, viscoelastic dampers, dry friction devices, hysteretic devices, etc.) and that can be used, hysteretic energy devices are attractive because: (a) their design properties can be easily assessed and, (b) maintenance costs may be lower than for other options.

2.1 Pioneering Research and Applications

Hysteretic passive energy dissipation devices were proposed since they were developed to perform as seismic fuses, even when they were not named in such manner. For example, the well-known shaking table tests at the University of California at Berkeley for a steel moment frame with ADAS devices mounted on chevron braces were developed under a seismic fuse concept: the frame members and supporting braces remained elastic whereas the ADAS devices responded in the nonlinear range in a controlled manner and behaved as seismic fuses (Whittaker et al. 1989). Other pioneering experimental works in shaking tables, such as those conducted at Taiwan for the TADAS devices, followed the same design philosophy (Tsai et al. 1993).

First applications of hysteretic energy dissipation devices designed as structural fuses in existing buildings date back from the early 1990s. Perry et al. (1993) reported the seismic retrofit of the 2-story Wells Fargo bank building at San Francisco damaged during the 1989 Loma Prieta Earthquake using ADAS energy dissipation devices as structural fuses. Martínez-Romero (1993) reported the seismic retrofit and upgrading of three reinforced concrete buildings in soft soil sites of Mexico City using ADAS devices as structural fuses: the Izazaga building (Fig. 6a), the Cardiology Hospital and the IMSS Reforma Headquarters (Fig. 6b). The three aforementioned buildings remained undamaged during the September 19, 2017 earthquake. It is worth noting that the Izazaga building was under a façade renovation process when the earthquake stroke, but as it can be observed, there was no damage within the structural elements (Fig. 6a).

(a) Izazaga Building   (b) IMSS Reforma Headquarters

Fig. 6 Pictures taken shortly after the September 19, 2017 earthquake for two office buildings in Mexico City retrofitted during the 1990s with ADAS energy dissipation devices as structural fuses. The buildings survived the earthquake with no damage

2.2 Proposed Resilient-Based Design Methods

Resilient-based design methods for new structures with metallic fuses have been already proposed, both using code-oriented force-based methods and variations of performance-based and displacement-based methods.

It is worth noting the study reported by Vargas and Bruneau (2006, 2009a, b), as they proposed a design procedure based upon single degree of freedom (SDOF) systems for the design of hysteretic devices as structural fuses. Nonlinear results were then reported in graphs normalized to the following parameters: (a) the design base shear versus the stiffness ratio, in the elastic range, between the bracing-fuse and the moment frame (α) and, (b) the maximum displacement ductility (μ_d) for the structural fuse that assures that the frame remains elastic. In the design process, allowable story drift was introduced as an upper bound limit. They corroborated their method with the design and shaking table tests of a 3-story frame with bucking-restrained braces (BRBs) acting as seismic fuses.

About the same time, Chen et al. (2007) presented a performance-based design method for steel frames with hysteretic devices as structural fuses using also an equivalent SDOF methodology with a strength-demanded spectra and close-form equations for the allocation of strength and stiffness supplied in the structure by the hysteretic energy dissipation devices. This procedure was successfully applied to the design of single-deck and double-deck steel portal frame piers.

Malakoutian et al. (2013) used a forced-design method for the linked column frame (LCF) system, which included replaceable links (structural fuses) located between tightly spaced columns, used together with a moment frame (secondary structure) where the fuses were designed to develop plastic hinges earlier than the beams of the moment frame. The LCF system has also been studied by Dimakogianni et al. (2015). Shoeibi et al. (2017) proposed an alternate design for the LCF system using the performance-based plastic design (PBPD) method.

Bai and Ou (2016) tested the PBPD method for buckling-restrained braced reinforced concrete moment-resisting frames (RC-BRBFs). This design method was successfully verified with a five-story and ten-story RC frames with BRBs placed in a chevron configuration.

Yang et al. (2018) proposed an equivalent energy design procedure (EEDP) for the seismic design of fused structures in a performance-based format. The EEDP directly takes into consideration the structural strength and ductility and it allows designers to select multiple performance objectives at different earthquake shaking intensities. This procedure was illustrated with the design of an earthquake resilient fused truss moment frame.

Liu et al. (2018) have recently presented a direct displacement-based design method who they successfully applied for the design of steel braced frame structures with self-centering buckling-restrained braces (SCBRBs).

Most of the proposed design methods have a performance-based format and are based on extensive nonlinear SDOF simulations to adjust design variables such as yield strength, yield displacement, hysteretic energy, ductility, etc. There are fewer

studies on hand where global design parameters appropriate to be implemented in the force-based design methods available in most building codes format have been evaluated.

Vargas and Bruneau (2006 and 2009a) proposed some global design parameters based upon SDOF simulations. Extensive parametric studies using multi-degree of freedom (MDOF) models were used to assess global design parameters for low to medium rise regular: (a) reinforced concrete intermediate moment-resisting frames (RC-IMRFs) with steel fuses mounted on chevron steel bracing (Tena-Colunga and Nangullasmú-Hernández 2015; Nangullasmú-Hernández and Tena-Colunga 2016; Tena-Colunga and Gama-Contreras 2017) and, (b) special moment-resisting steel frames (SMRSFs) with steel fuses mounted on chevron steel bracing (Tena-Colunga and Hernández-Ramírez 2017). The principal objective of the cited studies was to evaluate global seismic design parameters that could be effortlessly introduced in the design philosophy of Mexican codes for a resilient seismic design. Various elastic stiffness ratios between the moment frame structure and the complete structure (α) and between the structural fuses and the bearing braces (β) were studied, among other pertinent structural parameters, as described in following sections.

3 Code-Oriented Resilient Design Method

3.1 Evaluation of Global Design Parameters

For an efficient and resilient seismic design under a code-oriented force-based format, global design structural parameters need to be available to warrant that the primary system should remain essentially elastic after a strong earthquake while the secondary system would be active and act as structural fuses (Fig. 7).

For this purpose, comprehensive parametric studies (Fig. 8) for building models where the structural system was composed of moment-resisting frames with hysteretic energy devices (seismic fuses) mounted on chevron steel braces were con-
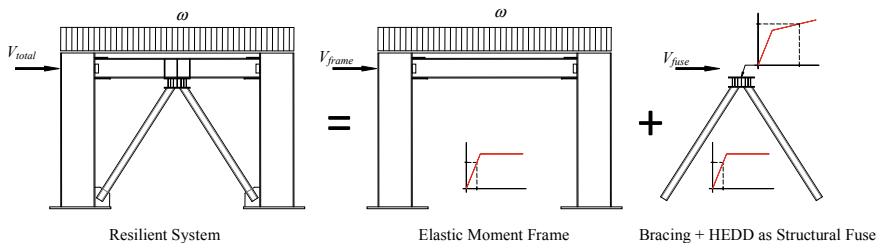
Fig. 7 Schematic representation of a seismic resilient structural system composed of a moment frame which should respond essentially elastic during a strong earthquake and HEDD as structural fuses supported on elastic chevron braces
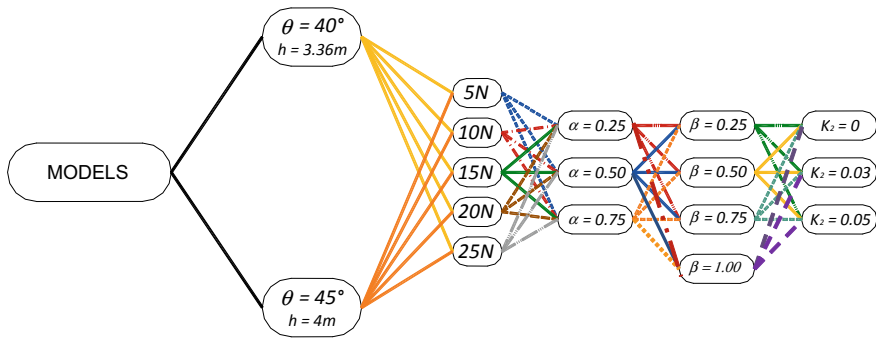
Fig. 8 Schematic tree diagram to summarize the conducted parametric studies on steel and reinforced concrete moment-resisting buildings models with structural fuses (HEDDs) to define global design parameters

ducted to define the following design parameters: (a) global ductility deformation capability for the structure (R factor), (b) global overstrength factor for the structure (Ω factor), (c) story drifts related to the peak ductility demand of the HEDD where a resilient mechanism is achieved for the system (Δ_u) and, (d) story drifts linked to the first yielding (Δ_y).

Buildings models ranged from 5 to 25 stories were selected with a common distribution in plan used in Mexico City for reinforced concrete (Tena-Colunga and Nangullasmú-Hernández 2015; Nangullasmú-Hernández and Tena-Colunga 2016; Tena-Colunga and Gama-Contreras 2017) and steel buildings (Tena-Colunga and Hernández-Ramírez 2017). Four structural parameters (three stiffness-related) were evaluated with the purpose of measuring their level of application for seismic regions where the effective design base shear (after reductions for ductility, overstrength, redundancy, soil-structure interaction, etc.) should be close to $V/W_t = 0.10$, a value that mostly covers the most demanded zones in soft soils in Mexico City and many cities in the Mexican Pacific Coast where the earthquake hazard is high. Of course, global design parameters also depend on the value of the effective base shear (Vargas and Bruneau 2006). The considered structural design parameters were (for example, Tena-Colunga and Nangullasmú-Hernández 2015; Nangullasmú-Hernández and Tena-Colunga 2016; Tena-Colunga and Hernández-Ramírez 2017):

(a) The stiffness parameter α, described as the quotient between the global average elastic lateral stiffness for the frame (K_{frame}) and the global average lateral stiffness of the complete frame-bracing-fuse system (K_{total}).
(b) The stiffness parameter β, the quotient between the elastic stiffness for the HEDDs (K_{ELD}) and the elastic lateral stiffness of the supporting chevron braces (K_{diag}).
(c) The stiffness parameter k_2, the post to pre yielding stiffness ratio for the HEDDs.

Table 1 Range for structural design parameters to achieve a full resilient design for RC-IMRBFs with ductile confinement when $\theta = 45°$ and $V/W_t = 0.10$

Stories	α	K_2/K_{ELD}	β	μ_d
	0.25		0.50–1.0	10–8
5	0.50	0.05	0.50–1.0	10–6
	0.75		0.50–1.0	12–8
	0.25		0.50–1.0	12–8
10	0.50	0.05	0.50–1.0	10–8
	0.75		0.50–1.0	10–8
15	0.50	0.05	0.50–1.0	12–8
	0.75		0.50–1.0	12–8
20	0.50	0.05	0.50–1.0	12–8
	0.75		0.50–1.0	12–8
25	0.50	0.05	0.50–1.0	12–8
	0.75		0.50–1.0	12–10

(d)   The angle of inclination of the chevron bracing regarding the horizontal plane (θ) was assessed because it has an impact on the equivalent instantaneous nonlinear effective stiffness which it is reduced as θ is smaller.

From the extensive parametric studies, it was possible to define ranges of application and global structural design parameters for all the studied systems: (a) reinforced concrete intermediate moment-resisting braced frames (RC-IMRBFs) with steel structural fuses (Tena-Colunga and Nangullasmú-Hernández 2015), (b) reinforced concrete intermediate moment-resisting braced frames (RC-IMRBFs) with steel structural fuses, where ductile detailing in RC beams and columns are voluntary applied (Nangullasmú-Hernández and Tena-Colunga 2016), (c), reinforced concrete special moment-resisting braced frames (RC-SMRBFs) with steel structural fuses (Tena-Colunga and Gama-Contreras 2017) and, (d) steel special moment-resisting braced frames (SMRSBFs) with structural fuses (Tena-Colunga and Hernández-Ramírez 2017). The details on the assessment and specific values for those parameters for each structural system are discussed in greater detail in the cited publications.

For illustration purposes, in this chapter are only discussed the results obtained for the structural systems that may be more attractive to apply the resilient design methodology and mostly for the worst-case scenarios where a 100% or close to 100% resilient design could be achieved.

According to the results reported by Nangullasmú-Hernández and Tena-Colunga (2016) for RC-SMRBFs with voluntary ductile detailing for RC beams and columns, full resilient seismic designs could be achieved for the combination of global structural parameters identified in Table 1 when $\theta = 45°$. The best balances are identified in bold letters.

As it can be observed, the application range is wide even for a relatively large design base shear $V/W_t = 0.10$. For these stiffness balances, a global ductility $R = 4$ could be used for building with global slenderness ratio (total height over minimum

Table 2 Range for structural design parameters to achieve a full resilient design for SMRSBFs when $\theta = 40°$ and $V/W_t = 0.10$

Stories	α	K_2/K_{ELD}	R (Q)		
			$\beta = 0.25$	$\beta = 0.5$	$\beta = 0.75$
5	0.25–0.75	0.00	5.8	4.3–4.5	3.7–4.2
		0.03	5.4–6.4	4.9	4.2–4.5
		0.05	5.6–6.4	5.0–5.2	4.4–4.7
10	0.25–0.75	0.00	3.7–3.9	3.7	3.4
		0.03	4.0–4.4	4.1–4.3	3.7–3.9
		0.05	4.3–4.6	4.3–4.6	3.9–4.1
15	0.25–0.75	0.00	3.2	3.0–3.1	2.9–3.1
		0.03	3.6	3.4–3.5	3.3–3.6
		0.05	3.4–3.8	3.6–3.9	3.5–3.9
20	0.25–0.50	0.00	2.9	2.8–2.6	2.7–2.6
		0.03	3.2	3.1–2.8	3.0–2.9
		0.05	3.4–2.8	3.3–3.1	3.2
25	0.25–0.50	0.00	2.8	2.6	2.5–2.6
		0.03	2.9	2.7–2.8	2.7–2.8
		0.05	3.0	2.9–2.9	2.9

dimension in plan) H/B ≤ 2.0. Global ductility for the system is reduced as the height increases, but for the 25 story buildings (H/B $= 3.2$) it was reduced to $R = 3.5$. Global overstrength factors mostly ranged from 1.5 to 1.8, so for practical and conservative purposes, one could use $\Omega = 1.5$ in the design process. Peak story drifts related to the resilient mechanism can be warranted when $\Delta_u \leq 0.015$ (1.5%) and story drifts associated to the first yielding should be $\Delta_y \leq 0.003$ (0.3%) for practical design purposes.

According to the results obtained by Tena-Colunga and Hernández-Ramírez (2017) for SMRSBFs, full resilient seismic designs could be achieved for the combination of global structural parameters identified in Table 2 when $\theta = 40°$ and in Table 3 when $\theta = 45°$.

As it can be observed, the application range is wide even for a relatively large design base shear $V/W_t = 0.10$ for $\theta = 40°$ and for $\theta = 45°$, although as the angle of inclination of the chevron braces (θ) increases, yielding demands on beams increase and that is why the application range is somewhat reduced for $\theta = 45°$ as the number of stories increases. For these stiffness balances, a global ductility $R = 4$ could be used up to 10-story buildings. Global ductility for the system is reduced when the number of stories augments, and for the 25-story buildings it was reduced to $R = 2.5$.

As expected, higher overstrengths were obtained for these code-designed SMRSFs structures with structural fuses compared to those obtained for RC-SMRBFs with structural fuses. Assessed overstrength factors fluctuated from $1.7 \leq \Omega \leq 2.4$ for

Table 3 Range for structural design parameters to achieve a full resilient design for SMRSBFs when θ = 45° and V/W$_t$ = 0.10

Stories	α	K_2/K_{ELD}	R (Q)		
			β = 0.25	β = 0.5	β = 0.75
5	0.25–0.75	0.00	4.7–5.2	4.0–4.1	3.8–3.5
		0.03	5.1–5.6	4.5–4.7	4.2–4.0
		0.05	5.3–5.7	4.7–5.0	4.4–4.2
10	0.25–0.50	0.00	3.5	3.3	3.2
		0.03	4.0	3.7	3.6
		0.05	4.3	4.0	3.9
15	0.25–0.50	0.00	2.9	2.8	2.7
		0.03	3.3	3.1	3.1
		0.05	3.5	3.3	3.4
20	0.25–0.50	0.00	2.6	2.5	2.6
		0.03	3.0	2.9	2.8
		0.05	3.2	3.0	2.9
25	0.25–0.50	0.00	–	–	–
		0.03	–	2.6	2.5
		0.05	–	2.6	2.5

SMRSFs with $\alpha = 0.25$, $2.4 \leq \Omega \leq 3.0$ if $\alpha = 0.50$, and $3.0 \leq \Omega \leq 4.0$ when $\alpha = 0.75$ (Tena-Colunga and Hernández-Ramírez 2017). The most prominent stiffness balance on overstrength is α, since as α increases, this system takes a larger portion of the lateral load. Peak story drifts related to the resilient mechanism can be warranted when $\Delta_u \leq 0.013$ (1.3%) and story drifts related to the first yielding should vary in the following range: $0.0008 \Delta_y \leq 0.0043$. For this parameter, it was observed that Δ_y increases as: (a) α increases, (b) β decreases, (c) the number of stories increases and, (d) θ increases.

3.2 Code-Oriented Design Procedure

A general design procedure suited for building codes is schematically summarized in Fig. 9 and described in greater detail somewhere else (Tena-Colunga and Nangullasmú-Hernández 2015; Tena-Colunga and Hernández-Ramírez 2017).

The first step is to define the design base shear using methods prescribed by building codes. One can obtain the design forces from the code design spectrum (step 1, Fig. 1) and reduce them with the global design parameters R and Ω, as outlined by the code (step 2, Fig. 9). An assumption is taken for the elastic lateral stiffness ratio α, (step 3, Fig. 9). The design base shear that the moment frame must

1.- Selection of design spectrum.

2.- Assess V_{total}
$$V_{total} = \frac{Sa}{R\Omega} W_{total}$$

3.- Selection of α.
$$\alpha = \begin{cases} 25\% & K_{b-H} > K_{frame} \\ 50\% & K_{b-H} = K_{frame} \\ 75\% & K_{b-H} < K_{frame} \end{cases} \quad \alpha = \frac{K_{frame}}{K_{total}}$$

4.-Compute V_{frame} without considering the bracing - HEDDs system.
$$V_{frame} = \alpha V_{total}$$

5.- Distribute V_{frame} at each level.
$$V_i = \frac{V_{frame} W_i H_i}{\Sigma W_i H_i}$$

6.- Analyze the frame only for all load combinations. Pre-dimensioning of beams and columns.

7.a.-Beam Design o.k.? | 7.b.-Column design o.k.? | 7.c.-Joint design o.k.?
NO | NO | NO
YES | YES
YES

8.- Assess K_{frame}.
$$K_{frame} = \begin{cases} \text{Wilbur's formula} \\ \text{Rigorous software modelling} \end{cases}$$

9.- Assess K_{eq}.
$$K_{eq} = \frac{K_{frame}(1-\alpha)}{\alpha}$$

10.-Selection of design parameters for HEDDs.
β, μ and $\eta = k_2/K_{ELD}$

11.- Assess the bracing stiffness K_{brace}.
$$K_{brace} = \frac{K_{eq}\{\mu+\beta[1+\eta(\mu-1)]\}}{\beta[1+\eta(\mu-1)]}$$

12.- Pre-dimensioning of brace.
$$A_{brace} = \frac{K_{brace} L_{brace}}{N_{brace} E cos^2\theta} \quad A_{brace} \approx A^*_{brace}$$

13.- Assessment of elastic stiffness for HEDDs.
$$K^*_{brace} = \frac{2A^*_{brace} E cos^2\theta}{L_{brace}} \quad K_{ELD} = \beta K^*_{brace}$$

14.- Predimensioning of HEDDs.

15.- Distribute V_{total} at each level.
$$V_i = \frac{V_{total} W_i H_i}{\Sigma W_i H_i}$$

16.-Analyze the complete system for all load combinations. Check proposed sections.

17.a.-HEDD design o.k.? | 17.b.-Bracing design o.k.? | 17.c.-Beam checking o.k.?
NO | NO | NO
YES | YES
YES

17.d.-Column checking o.k.? | 17.e.-Joint checking o.k.?
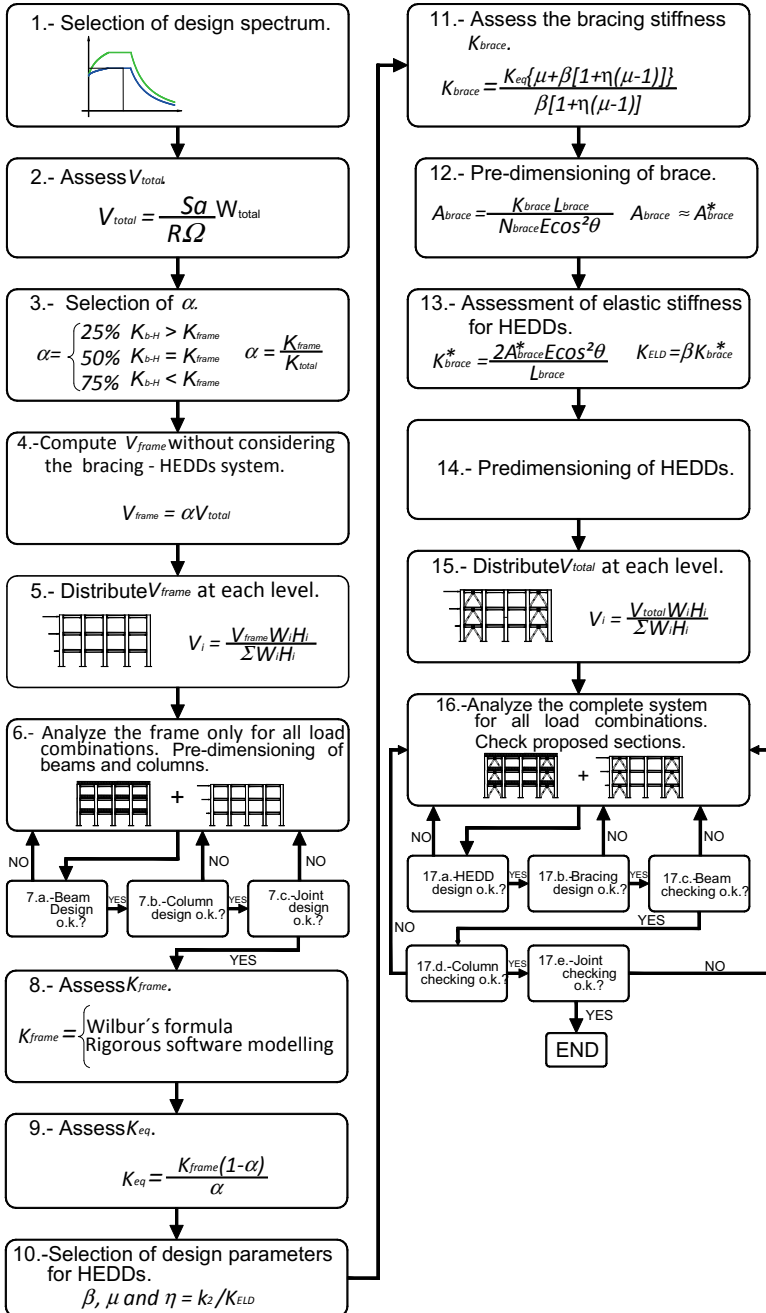NO
YES | YES
NO

END

Fig. 9 Flow chart summarizing the general proposed resilient design procedure suited for building codes for moment frames with structural fuses (HEDDs)

take to respond elastically in lack of the bracing-fuse substructure is calculated (step 4, Fig. 9). Lateral forces should be then allocated along the height (step 5, Fig. 9). Beam and column sections should be preliminary designed for gravitational loads together with their portion of lateral loads in lack of the bracing-fuse system (steps 6 and 7, Fig. 9). The frame must fulfill also with all limits for serviceability under gravitational loads that apply.

Once beam and column elements were pre-dimensioned, the lateral stiffness for the moment frame (K_{frame}) might be assessed with any recognized procedure already on hand in the literature (step 8, Fig. 9). Next, the stiffness of an equivalent global bracing (nK_{eq}) is computed (step 9, Fig. 9), where n is the number of braces needed to mount hysteretic structural fuses. The stiffness K_{eq} takes into account the elastic stiffness for each axial element (K_{brace}) and the effective stiffness of the structural fuse at the objective maximum local displacement ductility μ. Assumptions must be done regarding the design parameters for the structural fuses: β, μ and $\eta = k_2/k_{ELD}$ (step 10, Fig. 9). Then, the required elastic stiffnesses for the steel braces and the structural fuses are computed (step 11, Fig. 9). The steel braces are then pre-designed taking into consideration strength and stiffness (step 12, Fig. 9) criteria. An elastic performance for the bracing should be insured when the seismic fuses achieve their peak displacement ductility μ, designing the bracing with a rational factor of safety for buckling (Tena-Colunga and Nangullasmú-Hernández 2015).

After the preliminary design for all structural elements is done, a suitable elastic model for the complete building is assembled (step 15, Fig. 9), using the equivalent secant stiffness at the objective ductility μ for the hysteretic structural fuse, that must be analyzed once more subjected to gravitational loads and the lateral load distribution related to the design base-shear (step 16, Fig. 9). Three-dimensional elastic representations can be now used for this objective. All elements must be revised for deformation and strength again in the outlined sequence (step 17, Fig. 9) related to a capacity design methodology to insure a design in agreement to the structural fuse concept: firstly the HEDDs, next the braces (weak fuse—strong brace), afterwards beams, columns and beam-column joints (weak beam—strong column—strongest joint). The whole building must also be revised to satisfy with lateral deformation limits set in code guidelines or for other performance goals. In a successful design procedure, only the structural fuses would behave nonlinearly, keeping beams elements as emergency supply of energy dissipation if anticipated demands are surpassed.

3.3 Verification with Nonlinear Analyses

To illustrate that the proposed method is trustworthy to achieve resilient designs for intense ground motions, pushover and nonlinear dynamic analyses conducted for some of the 270 SMRSBFs models when subjected to an artificial record for station CO56 (Roma Norte District) for a proposed $M_s = 8.1$ subduction earthquake comparable to the September 19, 1985 Michoacán earthquake in soft soils of Mexico
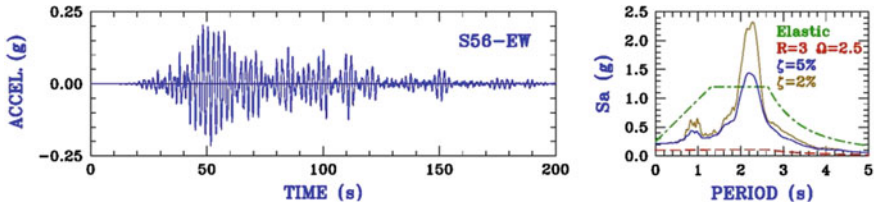
Fig. 10 Simulated S56-EW acceleration record and response spectra for $\zeta = 2$ and 5%. Inelastic and elastic design spectra for NTCS-04 for CO56 site ($T_s = 2.2$ s)

City are presented. The simulated S56-EW record is shown in Fig. 10, together with its response spectra for 2 and 5% equivalent viscous damping.

For the nonlinear dynamic simulations, an equivalent viscous damping ratio $\zeta = 2\%$ was considered for all models, as experimentally, measured values for ζ have ranged from 2 to 4% in existing steel buildings. The site period for CO56 is $T_s = 2.2$ s. The maximum pseudo-acceleration for S56-EW is near to 1.5 g for $\zeta = 5\%$, exceeding in 25% the peak pseudo-acceleration 1.2 g defined in the elastic design spectrum for CO56 site in Mexico´s Federal District Code (NTCS-04 2004). However, considering $\zeta = 2\%$ for steel structures, the maximum pseudo-acceleration is $S_a = 2.32$ g, which exceeds in 93% the design acceleration for the elastic design spectrum, as shown in Fig. 10. As reference, the design spectrum according to NTC-04 considering $R = 3$ and $\Omega = 2.5$ is also depicted in Fig. 10, where the effective design base shear in the plateau of the design spectrum is $S_a = 0.11$ g, 10% higher than the base shear used for designing all reference models ($V/W_t = 0.10$). Then, all models were under designed by 10% if a 5% equivalent viscous damping is considered.

A scale with hot colors was employed to show up the nonlinear demands of all structural elements, as shown in Fig. 11. Elastic responses are identified with no color. Inelastic responses after yielding and up to a reparable damage state for standard structural elements ($\phi/\phi_u \leq 0.25$), and for HEDDs $1 < \mu < 2.5$ are identified with yellow. Moderate inelastic responses for common structural elements ($0.25 < \phi/\phi_u \leq 0.5$) and for hysteretic fuses $2.5 < \mu < 5$ are highlighted in orange. Important inelastic responses for beams and columns (up to peak response, $0.5 < \phi/\phi_u \leq 0.75$) and for structural fuses $5 < \mu < 7.5$ are identified with red. Inelastic responses on the descending branch of moment-curvature curves for beams and columns ($0.75 < \phi/\phi_u \leq 1.0$) and for HEDDs $7.5 < \mu < 10$ are highlighted in brown. Although the nonlinear behavior of brace elements was modeled in all studied buildings, all of them braces remained elastic in all models during the conducted nonlinear static and dynamic analyses.

The dynamic properties of the five selected SMRSBFs to discuss within this chapter are shown in Table 4. As it is seen, one model for studied building height was selected for this purpose.

According to the results obtained from pushover analyses, it is possible to achieve a 100% resilient design for all 5-story models when $\theta = 40°$ and $\theta = 45°$, but higher demands on beams were obtained for $\alpha = 0.75$, $\beta = 0.25$, $k_2/k_{ELD} = 0.05$ and

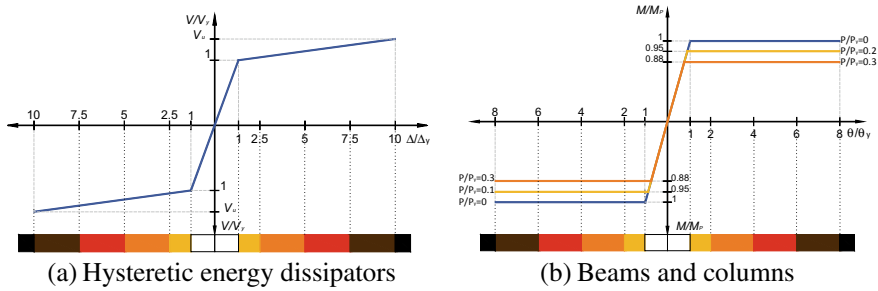(a) Hysteretic energy dissipators   (b) Beams and columns

Fig. 11 Schematic color intensity scale for the inelastic responses of the assessed moment-normalized curvature curves for HEDDs, beams and columns

Table 4 Selected SMRSBFs building models to help illustrate the resilient design with the proposed code-oriented design procedure

Model	θ	Stories	α	β	k_2/k_{ELD}	T (s)
m5α75β25	45°	5	0.75	0.25	0.05	0.762
m10α25β25	45°	10	0.25	0.25	0.00	1.240
m15α50β50	40°	15	0.50	0.50	0.03	1.550
m20α50β75	45°	20	0.50	0.75	0.05	1.773
m25α75β75	40°	25	0.75	0.25	0.03	2.295

$\theta = 45°$ and that is why this model is presented in greater detail. The yielding mappings obtained for model m5α75β25 from pushover analyses (to achieve $\mu = \mu_d = 10$ in critical HEDDs) and from nonlinear dynamic simulations under the action of the acceleration record S56-EW considering equivalent viscous dampings $\zeta = 5\%$ and $\zeta = 2\%$ are shown and compared in Fig. 12. It is observed in Fig. 12 a good agreement between the results obtained from pushover and nonlinear dynamic analyses in both the special distribution and amount of yielding for the HEDDs. Nevertheless, it is worth noting that the intensity of yielding in the results from nonlinear dynamic analyses were smaller than those obtained from pushover analysis because the fundamental natural period for the model (T = 0.762 s) is reasonable away from nonlinear resonant responses. This observation is confirmed with the peak demands shown in Fig. 13 for each analysis (ductility demands of HEDDs μ_d, story drifts Δ and story shears V/W_t), where it can be observed that the curve obtained from pushover analyses basically encloses those obtained from nonlinear dynamic analyses. As expected, higher demands are obtained for $\zeta = 2\%$ than for $\zeta = 5\%$. It is worth noting that ductility demands $\mu_d > 6$ are developed in the HEDDs for story drifts $\Delta < 1\%$. It is confirmed that the developed yielding only in HEDDs is consistent with a 100% resilient design, where these devices act as structural fuses.

It is also worth noting the following aspects, as they are indeed germane for the resilient seismic design of all structural systems, not only those with HEDDs as structural fuses: (a) the convenience in the design process to target the natural elastic
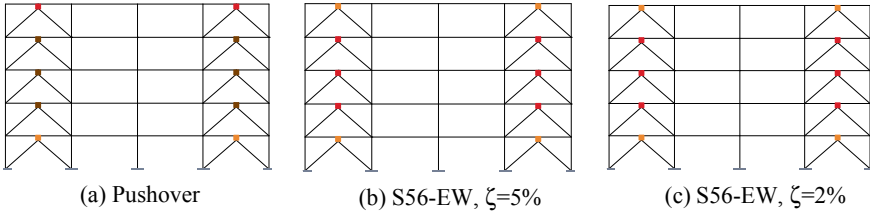
(a) Pushover   (b) S56-EW, ζ=5%   (c) S56-EW, ζ=2%

Fig. 12 Comparison of peak inelastic demands mappings for the 5-story model where $\alpha = 0.75$, $\beta = 0.25$, $k_2/k_{ELD} = 0.05$ and $\theta = 45°$
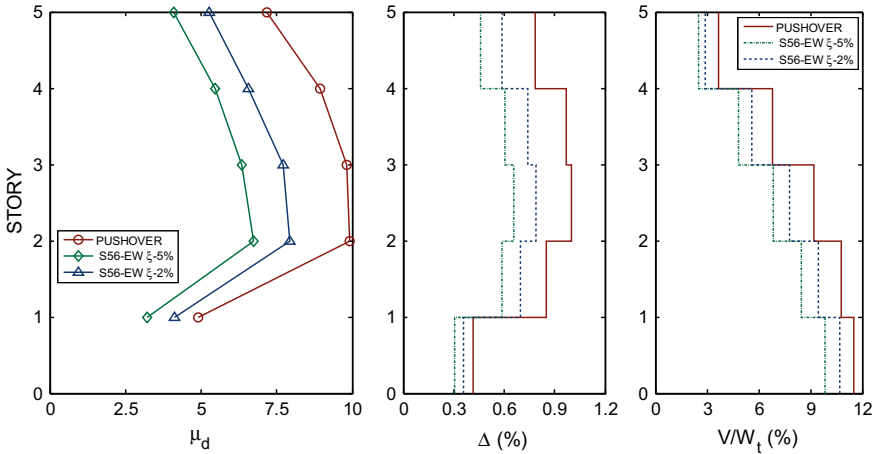

Fig. 13 Comparison of peak ductility demands for the HEDD (μ_d), peak story drifts (Δ) and peak normalized story shears (V/W_t) for the 5-story model where $\alpha = 0.75$, $\beta = 0.25$, $k_2/k_{ELD} = 0.05$ and $\theta = 45°$

period for the structural system (T) away from the dominant period for the site (T_s), to avoid resonant responses in the nonlinear range and, (b) when one designs buildings for high global ductility reduction factors (R), important nonlinear demands (and damage) would be achieved in the structural elements assumed to be the weak links or structural fuses, and adequate detailing is required to avoid that partition walls may be damaged, as they may work as infill walls if not properly separated from the columns and beams of the resisting frames (for example, Figs. 4a and 5a).

For the 10-story model m10α25β25 where $k_2/k_{ELD} = 0$ and $\theta = 45°$, from the observation of obtained yielding mappings from pushover and nonlinear dynamic analysis depicted in Fig. 14, it is confirmed the good agreement between both types of analyses in both the special distribution and intensity of yielding for the structural fuses. Again, the intensity of yielding in the results obtained from nonlinear dynamic analyses were smaller than those obtained from pushover analysis, because the fundamental natural period for the model (T = 1.24 s) is reasonable away from nonlinear resonant responses.
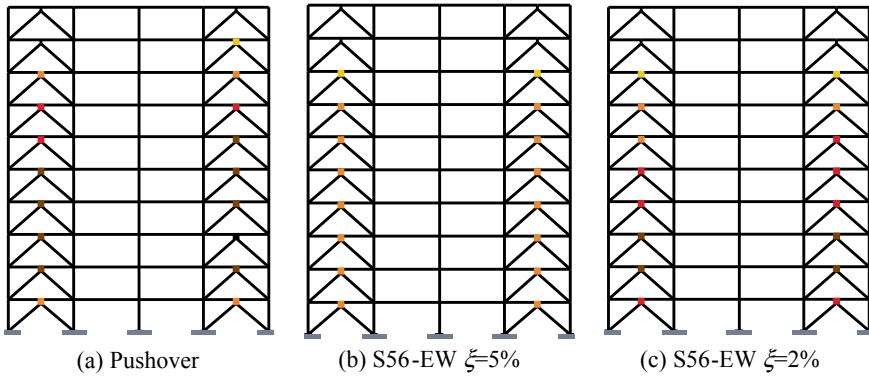
(a) Pushover   (b) S56-EW ξ=5%   (c) S56-EW ξ=2%

Fig. 14 Comparison of peak inelastic demands mappings for the 10-story model where $\alpha = 0.25$, $\beta = 0.25$, $k_2/k_{ELD} = 0$ and $\theta = 45°$

Fig. 15 Comparison of peak ductility demands for the HEDD (μ_d), peak story drifts (Δ) and peak normalized story shears (V/W_t) for the 10-story model where $\alpha = 0.25$, $\beta = 0.25$, $k_2/k_{ELD} = 0$ and $\theta = 45°$

This observation is also confirmed with peak ductility demands for the HEDDs, peak story drifts and peak story shears depicted in Fig. 15 for each analysis, where it is seen that the curve obtained from pushover analyses envelopes those obtained from nonlinear dynamic analyses. Again, a 100% resilient design was achieved and ductility demands $\mu_d > 6$ are obtained in the structural fuses for story drifts $\Delta < 1\%$.

Yielding mappings traced from the results of pushover and nonlinear dynamic analyses for the 15-story model m15α50β50 where $k_2/k_{ELD} = 0.03$ and $\theta = 40°$ and $T = 1.55$ s (Table 4) are depicted in Fig. 16. When $\zeta = 5\%$ is used in the nonlinear dynamic analyses, obtained peak responses (Fig. 16b) are in good agreement with those obtained from pushover analyses (Fig. 16a). In fact, this can be confirmed in

(a) Pushover   (b) S56-EW ξ=5%   (c) S56-EW ξ=2%

Fig. 16 Comparison of peak inelastic demands mappings for the 15-story model where $\alpha = 0.50$, $\beta = 0.50$, $k_2/k_{ELD} = 0.03$ and $\theta = 40°$
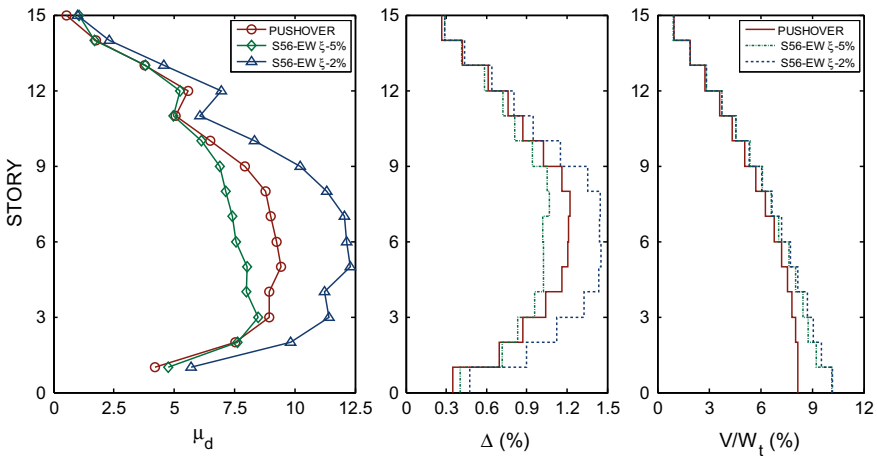
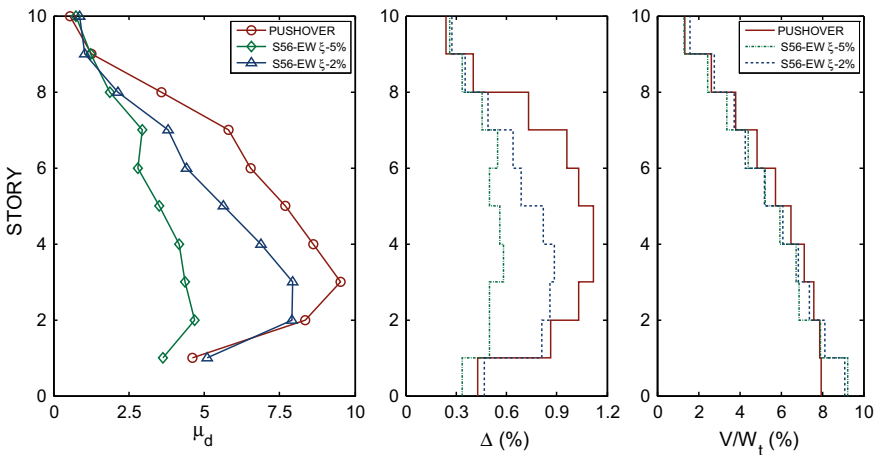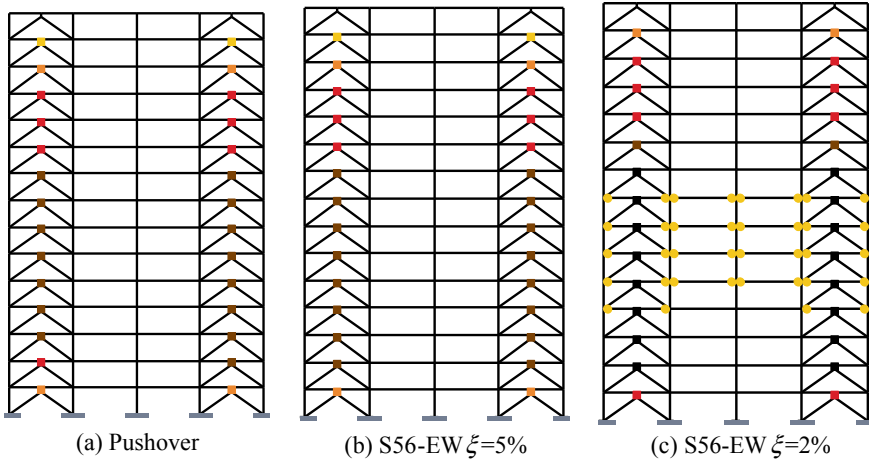**Fig. 17** Comparison of peak ductility demands for the HEDD (μ_d), peak story drifts (Δ) and peak normalized story shears (V/W_t) for the 15-story model where $\alpha = 0.50$, $\beta = 0.50$, $k_2/k_{ELD} = 0.03$ and $\theta = 40°$

Fig. 17, as peak responses in ductility for HEDDs, peak story drifts and peak story shears for $\zeta = 5\%$ are covered by the curves obtained from pushover analyses.

However, when $\zeta = 2\%$ is considered in nonlinear dynamic analyses, obtained peak responses (Figs. 16c and 17) surpassed those obtained from pushover analyses (Figs. 16a and 17), and some incipient beam yielding is developed (Fig. 16c). These results are still consistent with a resilient-based design because of the following reasons. From the elastic response spectrum (Fig. 10), it is observed that: (a) the natural

Fig. 18 Comparison of peak inelastic demands mappings for the 20-story model where $\alpha = 0.50$, $\beta = 0.75$, $k_2/k_{ELD} = 0.05$ and $\theta = 45°$
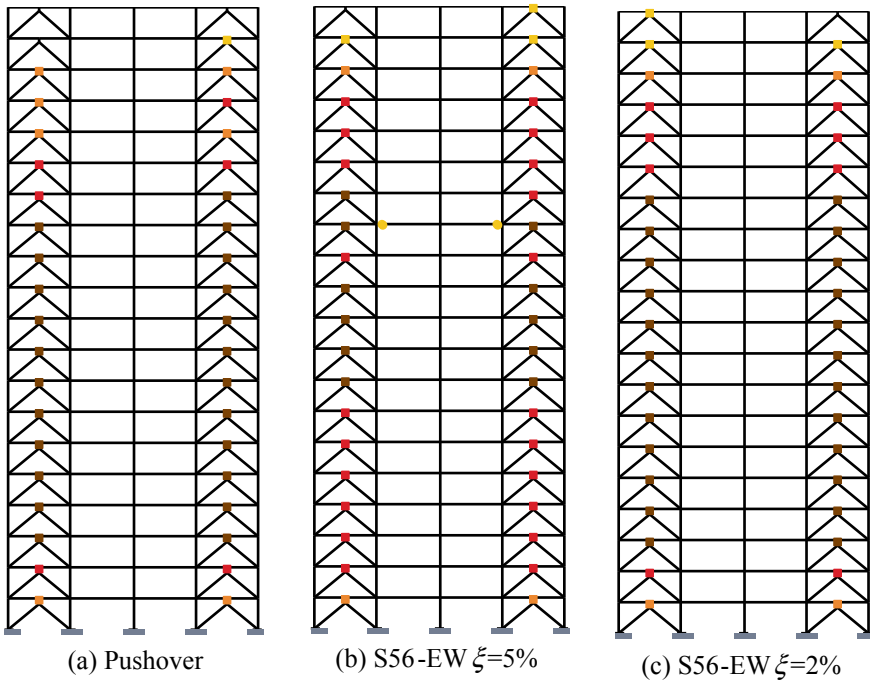
elastic period for the system (T = 1.55 s) is in the ascendant branch of the response spectrum and, (b) peak spectral accelerations for $\zeta = 2\%$ are much higher than those considered in the elastic design spectrum. Then, as an important global ductility reduction factor was considered for the design of the building, this model entered in near-resonant nonlinear responses, which considerably surpassed those assumed in the design process. Nevertheless, the design is still resilient, as the second line of nonlinear defense is activated (the beams), if the earthquake demands considerably surpassed those assumed in the design process. Besides, nonlinear demands in those beams are low. Then, it is confirmed from these results that the suggested code-oriented design procedure is robust and reliable, as the integrity of the structure is warrant, even when the size of the earthquake demands considered in the design are significantly surpassed.

For the 20-story model m20α50β75, where $k_2/k_{ELD} = 0.05$ and $\theta = 45°$, considering elastic dynamic properties only (T = 1.773 s), one may assume near-resonant responses (Fig. 10) that may avert the 100% resilient structural fuse response obtained from pushover analyses (Fig. 18a). Nevertheless, in this case, the nonlinear dynamic response is also 100% resilient for both $\zeta = 5\%$ (Fig. 18b) and $\zeta = 2\%$ (Fig. 18c), as only incipient yielding of two interior beams was developed (Fig. 18b).
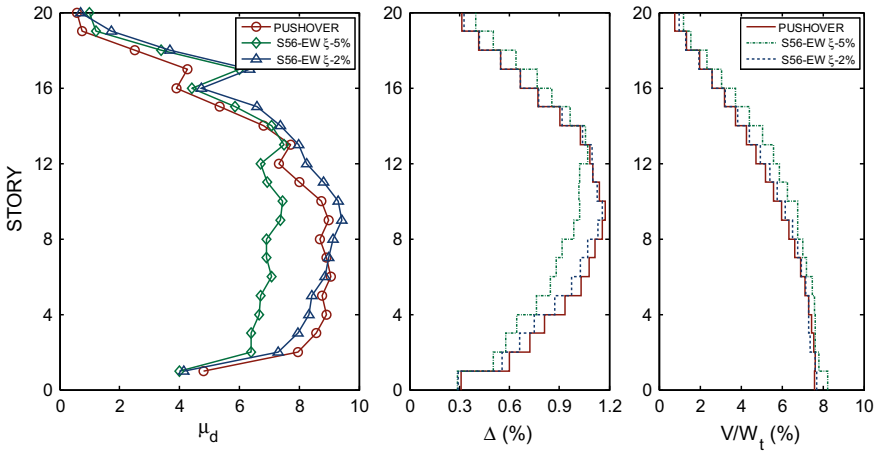
Fig. 19 Comparison of peak ductility demands for the HEDD (μ_d), peak story drifts (Δ) and peak normalized story shears (V/W_t) for the 20-story model where $\alpha = 0.50$, $\beta = 0.75$, $k_2/k_{ELD} = 0.05$ and $\theta = 45°$

It is observed from the peak responses for ductility demands of HEDDs and story drifts depicted in Fig. 19, that pushover curves envelop well the curves for $\zeta = 5\%$ for the first 13 stories, but they are surpassed by the curves of $\zeta = 5\%$ for the remaining stories. This can be explained because the contributions of higher modes in the response of buildings of this size start to be more important than for buildings 15-stories in height or lower.

From the obtained results for this model, it is also observed that for $\zeta = 2\%$, peak demands surpass by a small amount those obtained from the pushover analysis (Fig. 19), yet a 100% resilient yielding mapping is achieved (Fig. 18c). Nevertheless, what attracted the attention of the authors is that, in many stories, computed peak story shears were higher for $\zeta = 5\%$ than for $\zeta = 2\%$ (Fig. 19).

To understand this apparent exception to the rule (from elastic sdof systems dynamics), obtained peak responses were dissected for this more complex structural system. Therefore, peak dynamic story shears resisted by: (a) the frame alone, (b) the bracing-HEDDs system alone and, (c) the complete structure ("Total") are depicted in Fig. 20. It can be observed that the reason that higher peak story shear forces are developed for the whole system ("Total") for $\zeta = 5\%$ are because those higher forces are obtained in the bracing-HEDDs system (fuse system), as they are higher for $\zeta = 5\%$ than for $\zeta = 2\%$ in stories 1–18. However, for most stories, peak shear story forces within the frame system alone are more demanded when $\zeta = 2\%$ instead of when $\zeta = 5\%$.

As a simple explanation with peak story responses may not be enough, the time-history for the story shears were also break-down an analyzed. For illustration purposes, the time vs. story shear forces for the frame alone, the bracing-HEDDs alone and for the whole system for the second story are depicted in Fig. 21. The second
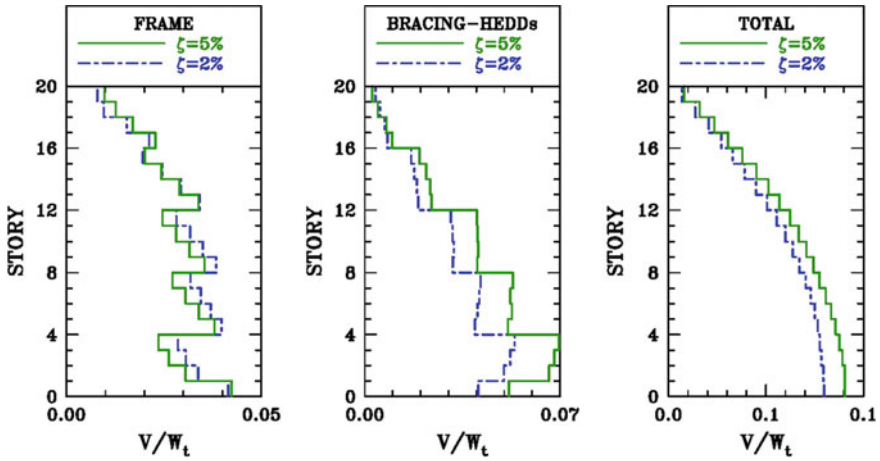
Fig. 20 Comparison of peak story shears (V/W$_t$) for the frame and bracing-HEDD system for the 20-story model where α = 0.50, β = 0.75, k$_2$/k$_{ELD}$ = 0.05 and θ = 45°
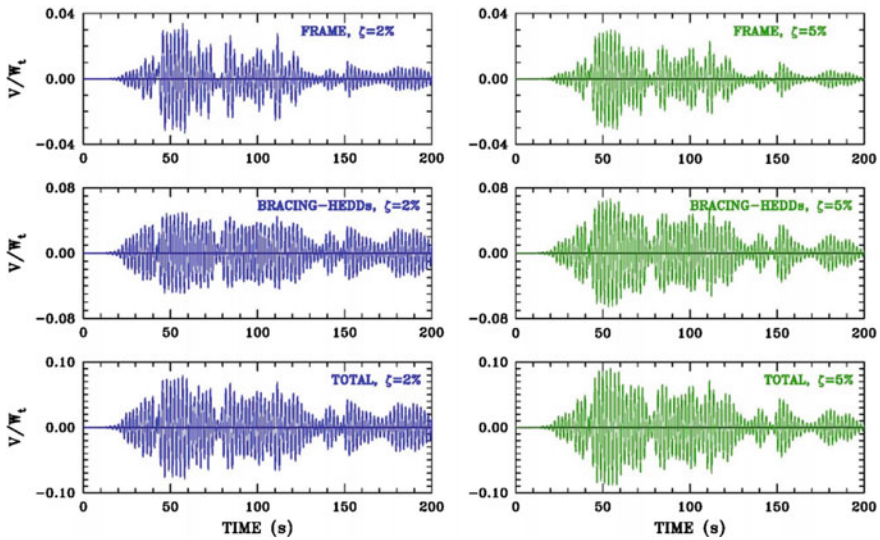
Fig. 21 Comparison of time versus story shears (V/W$_t$) for the frame and bracing-HEDD system for the second story of the 20-story model where α = 0.50, β = 0.75, k$_2$/k$_{ELD}$ = 0.05 and θ = 45°

story was selected as: (a) peak story shears are clearly more demanded for the frame alone when ζ = 2% with respect to ζ = 5% (Fig. 20) and, (b) in contrast, higher peak story shears are developed for the bracing-HEDDs system when ζ = 5% with respect to ζ = 2% (Fig. 20).

From the observation of the time vs. story-shear time-history curves depicted in Fig. 21, it can be corroborated and elementary principle of structural dynamics: when

the seismic excitation is considerably reduced (coda) or it is in free vibration, the amplitudes of response for a system with higher equivalent viscous damping ($\zeta = 5\%$) tend to attenuate or reduce much faster than those for the same system with a smaller equivalent viscous damping ($\zeta = 2\%$). It can be observed in Fig. 21 that this principle is satisfied by the frame, the bracing-HEDDs and the complete structure, primarily after 160 s of dynamic excitation (Fig. 21), when the intensity of S56-EW record is notably reduced (Fig. 10). Therefore, it can be concluded that although *a priori* it is difficult to accept that higher shear forces are developed for a given system when the equivalent viscous damping is increased, for a complex, multi-degree of freedom nonlinear system, this is possible in some circumstances (near resonant responses).

The yielding mappings obtained from pushover and nonlinear dynamic analysis for the 25-story model m25α75β75, where $k_2/k_{ELD} = 0.03$ and $\theta = 40°$ and T = 1.851 s (Table 4), are depicted in Fig. 22. When $\zeta = 5\%$ is considered in the nonlinear dynamic analyses, obtained peak responses (Fig. 22b) are in good agreement with those obtained from pushover analyses (Fig. 22a), with only incipient yielding in two beams of the twelfth story and yielding at corner columns at the base. Peak responses in ductility for HEDDs, peak story drifts and peak story shears for $\zeta = 5\%$ are also mostly enveloped by curves obtained from pushover analysis, except in stories 1–3 and 16–25 (Fig. 23). However, peak story shears for $\zeta = 5\%$ surpassed by 10–20% those obtained from pushover analysis. Nevertheless, it worth noting that models were designed for $V/W_t = 0.10$ (10% less than the required from the design spectrum) and that the design spectrum is surpassed by the response spectrum for S56-EW for $\zeta = 5\%$ (Fig. 10), as the building model is responding in the nonlinear resonant response period range.

From the results obtained for $\zeta = 2\%$, one can confirm the robustness of the proposed code-oriented design procedure to achieve resilient designs. This model also entered in near-resonant nonlinear responses for earthquake actions that considerably surpassed those assumed in the design process and, as consequence, the second line of nonlinear defense was activated, and these beams only developed incipient yielding (Fig. 22c) for such a strong ground shaking.

Finally, to highlight the importance of the post yielding stiffness of the HEDDs, the response maxima obtained for the 15-story models considering $\alpha = 0.50$, $\beta = 0.50$, $\theta = 45°$ and being subjected to the S56-EW record for $\zeta = 2\%$ (extreme condition) are shown in Figs. 24 and 25. It can be observed from the yielding mappings depicted in Fig. 24 that, as expected, if earthquake demands surpass those considered in the design, most demanded HEDDs with a higher post yielding stiffness would lead some beams to yield. This happens because the forces transmitted to the beams would be higher than those considered in the design. In contrast, elastic-perfectly plastic HEDDs would not transfer higher forces to the beams than those considered in the design. Therefore, the practice to model as elastic-perfectly plastic HEDDs which obtained experimental hysteretic behavior is bilinear with a positive post yielding stiffness ($k_2 \neq 0$) is not safe enough. From response maxima envelopes, it is observed for this building model that higher peak ductility demands and story drifts are developed when the post yielding stiffness increases. Also, as a consequence

(a) Pushover (b) S56-EW ξ=5% (c) S56-EW ξ=2%
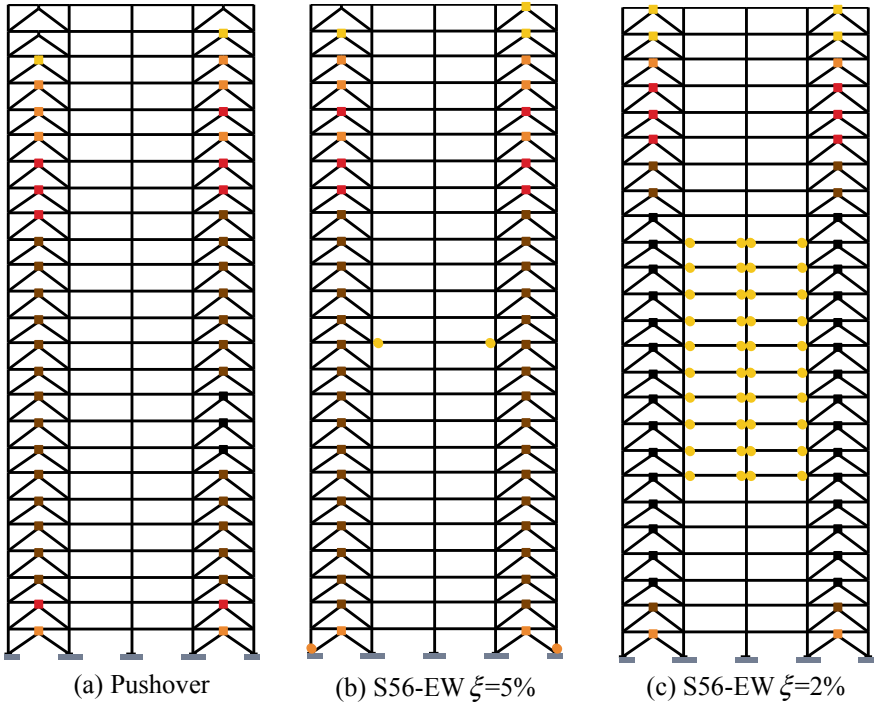
Fig. 22 Comparison of peak inelastic demands mappings for the 25-story model where $\alpha = 0.75$, $\beta = 0.75$, $k_2/k_{ELD} = 0.03$ and $\theta = 40°$
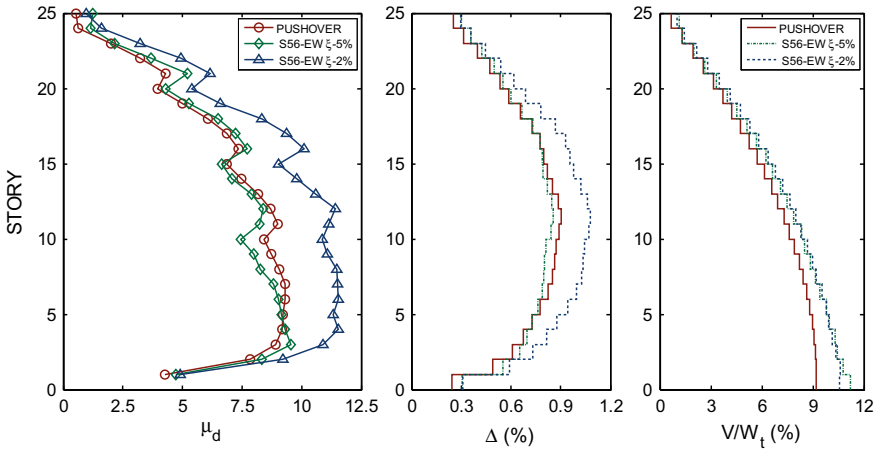
Fig. 23 Comparison of peak ductility demands for the HEDD (μ_d), peak story drifts (Δ) and peak normalized story shears (V/W_t) for the 25-story model where $\alpha = 0.75$, $\beta = 0.75$, $k_2/k_{ELD} = 0.03$ and $\theta = 40°$

(a) $k_2/k_{ELD}=0$ (b) $k_2/k_{ELD}=0.03$ (c) $k_2/k_{ELD}=0.05$
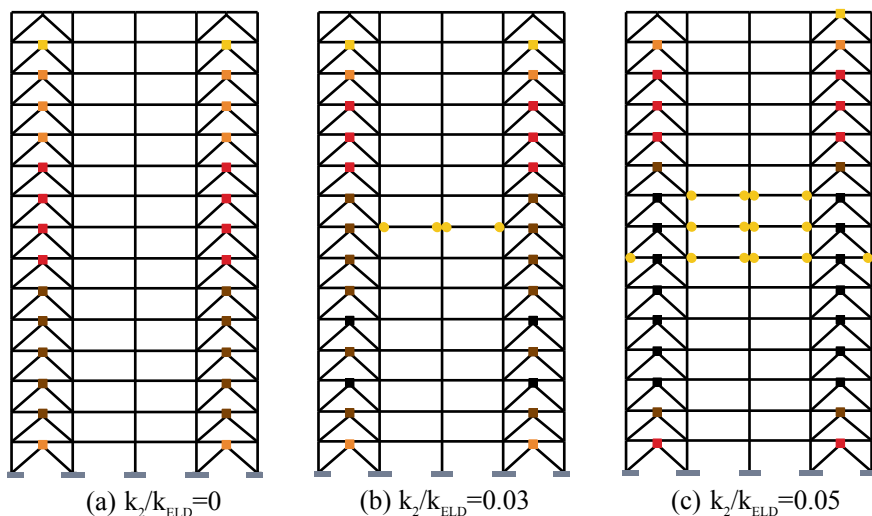
Fig. 24 Comparison of peak inelastic demands mappings for the 15-story model where $\alpha = 0.50$, $\beta = 0.50$, $\theta = 45°$ for S56-EW artificial acceleration record when $\zeta = 2\%$
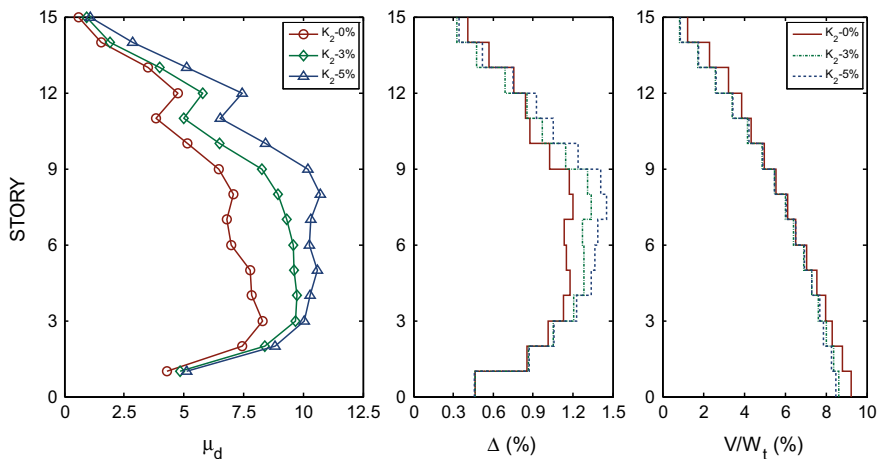
Fig. 25 Comparison of peak ductility demands for the HEDD (μ_d), peak story drifts (Δ) and peak normalized story shears (V/W_t) for the 15-story model where $\alpha = 0.50$, $\beta = 0.50$ and $\theta = 45°$ for S56-EW artificial acceleration record when $\zeta = 2\%$

of the associated higher hysteretic energy dissipation, peak story shear forces are reduced as the post yielding stiffness increases (Fig. 25).

From all the results that have been obtained and briefly presented in this chapter, it can be concluded that resilient seismic designs can be achieved with a code-oriented methodology for moment frames with structural fuses (HEDDs) with a correct selection of global parameters and using the outlined capacity design procedure.

4 Concluding Remarks

A resilient-based, code-oriented seismic design for buildings composed of steel or RC moment frames with hysteretic energy dissipation devices as structural fuses has been presented. The proposed force-design procedure is well suited to be implemented or adapted according to general guidelines available in most seismic buildings codes worldwide.

Global design parameters (R, Ω, Δ_y and Δ_u) were assessed through extensive and detailed parametric studies in building models from five stories to 25 stories in height. It can be concluded from the findings of the parametric studies that a significant global ductility capacity could be achieved for RC-IMRFs and SMRSFs with HEDDs as structural fuses, without obtaining important nonlinear responses in beams for the entire studied range of parameters: (a) $0.25 \leq \alpha \leq 0.75$, (b) $0.25 \leq \beta \leq 0.75$ and, (c) $\mu \leq 10$, when the effective design base shear is $V/W_t = 0.10$.

The subsequent general conclusions can also be extracted for these structural systems:

1. For a given α, ductility demands for the HEDDs increases as β diminishes.
2. For a fixed β, ductility demands for the HEDDs augments as α increases.
3. Few beams begin to yield as the number of stories augments as: (a) β decreases, (b) α increases and/or, (c) k_2 for the HEDDs increases.
4. Best performances for these systems are achieved for the next combination of parameters as the number of stories augments: the minimum value for α and the largest value for β.
5. Worst performances are achieved for the next combination of parameters as the number of stories augments: the largest value for α and the shortest value for β.
6. The participation of higher modes in the nonlinear dynamic response of the studied systems started to be more important for building models 20 stories in height or taller.
7. It was noted that more beam yielding occurred for $\theta = 45°$ than for $\theta = 40°$. Therefore, as the value for θ is increased, the bracing-HEDDs are less effective to inhibit the nonlinear response of beams. Actually, as θ augments, larger tension or compression forces are transmitted at braces and columns for a given β ratio for the bracing-HEDDs substructure.

From all the results that have been obtained and briefly presented in this chapter, it can be concluded that resilient seismic designs can be obtained with the proposed code-oriented design method for moment frames with HEDDs as structural fuses with a correct selection of global parameters for $V/W_t = 0.10$, even when near resonant nonlinear responses may be triggered. It is worth noting that the range of application (effective combinations for parameters α, β, k_2, θ and the number of stories) for a 100% resilient seismic design for this system should: (a) increase for a smaller nominal design base shear ($V/W_t < 0.10$) and, (b) decrease for a higher effective design base shear ($V/W_t > 0.10$). Of course, specific ranges of applicability should be confirmed with additional comprehensive parametric studies. Also, the

effects of soil-structure interaction should be assessed, particularly for soft soils and filled soils. The authors are currently working on this direction.

References

ASCE 7-16. (2016). *Minimum design loads for buildings and other structures*. ASCE Standard ASCE/SEI 7-16, American Society of Civil Engineers, ISBN 0-7844-0809-2.

Bai, J., & Ou, J. (2016). Earthquake-resistant design of buckling-restrained braced RC moment frames using performance-based plastic design method. *Engineering Structures, 107,* 66–79. https://doi.org/10.1016/j.engstruct.2015.10.048.

Chen, Z. Y., Ge, H., Kasai, A., & Usami, T. (2007). Simplified seismic design approach for steel portal frame piers with hysteretic dampers. *Earthquake Engineering and Structural Dynamics, 36*(4), 541–562.

Dimakogianni, D., Dougka, G., & Vayas, I. (2015). Seismic behavior of frames with innovative energy dissipation systems (FUSEIS 1-2). *Engineering Structures, 90,* 83–95. https://doi.org/10.1016/j.engstruct.2015.01.054.

IBC-18. (2017, August). *International Building Code* (2018 ed.). International Code Council. ISBN: 978-1-60983-735-8.

Liu, L., Li, S., & Zhao, J. (2018). A novel non-iterative direct displacement-based seismic design procedure for self-centering buckling-restrained braced framed structures. *Bulletin of Earthquake Engineering.* https://doi.org/10.1007/s10518-018-0408-7.

Malakoutian, M., Berman, J. W., & Dusicka, P. (2013). Seismic response evaluation of the linked column frame system. *Earthquake Engineering and Structural Dynamics, 42*(6), 795–814. https://doi.org/10.1002/eqe.2245.

Martínez-Romero, E. (1993). Experiences on the use of supplementary energy dissipators on building structures. *Earthquake Spectra, 9*(3), 581–626.

MOC-15. (2015). *Manual de diseño de obras civiles. Diseño por sismo*, Comisión Federal de Electricidad e Instituto de Investigaciones Eléctricas, México, noviembre (in Spanish).

Nangullasmú-Hernández, H. J., & Tena-Colunga, A. (2016). Requisitos mínimos de detallado dúctil en marcos de concreto reforzado protegidos con disipadores histeréticos de energía. *Revista de Ingeniería Sísmica, 95,* 1–32. (in Spanish).

NTCS-04. (2004). *Normas Técnicas Complementarias para Diseño por Sismo*, Gaceta Oficial del Distrito Federal, Tomo II, No. 103-BIS, octubre (in Spanish).

NTCS-17. (2017). *Normas Técnicas Complementarias para Diseño por Sismo*, Gaceta Oficial de la Ciudad de México, No. 220-BIS, diciembre (in Spanish).

Perry, C. L., Fierro, E. A., Sedarat, H., & Scholl, R. (1993). Seismic upgrade in San Francisco using energy dissipation devices. *Earthquake Spectra, 9*(3), 559–579.

Shoeibi, S., Kafi, M. A., & Gholhaki, M. (2017). New performance-based seismic design method for structures with structural fuse system. *Engineering Structures, 132,* 745–760. https://doi.org/10.1016/j.engstruct.2016.12.002.

Tena-Colunga, A., & Nangullasmú-Hernández, H. J. (2015). Assessment of seismic design parameters of moment resisting RC braced frames with metallic fuses. *Engineering Structures, 95,* 138–153. https://doi.org/10.1016/j.engstruct.2015.03.062.

Tena-Colunga, A., & Hernández-Ramírez, H. (2017). Code-oriented global design parameters for moment-resisting steel frames with metallic structural fuses. *Frontiers in Built Environment*, *3*(19). https://doi.org/10.3389/fbuil.2017.00019.

Tena-Colunga, A., & Gama-Contreras, A. (2017). Determinación de parámetros de diseño sísmico para marcos dúctiles de concreto reforzado con disipadores de energía histeréticos, *Revista Sulamericana de Engenharia Estrutural*, *14*(1), 36–58. http://dx.doi.org/10535/rsaee.v14i1.6496 (in Spanish).

Tena-Colunga, A. (2018). Algunos aspectos a considerar en el modelado de estructuras para el análisis y diseño por sismo. *Proceedings, XXI Congreso Nacional de Ingeniería Estructural*, Campeche, Campeche, Keynote Conference: 1–100, Noviembre (in Spanish).

Tsai, K. C., Chen, H. W., Hong, C. P., & Su, Y. F. (1993). Design of steel triangular plate energy absorbers for seismic-resistant construction. *Earthquake Spectra, 9*(3), 505–528.

Vargas, R., & Bruneau, M. (2006). *Analytical investigation of the structural fuse concept* Technical Report MCEER-06-004. Multidisciplinary Center for Earthquake Engineering Research, State University of New York at Buffalo.

Vargas, R., & Bruneau, M. (2009a). Analytical response and design of buildings with metallic structural fuses, I. *Journal of Structural Engineering, 135*(4), 386–393.

Vargas, R., & Bruneau, M. (2009b). Experimental response of buildings designed with metallic structural fuses. II. *Journal of Structural Engineering, 135*(4), 394–403.

Whittaker, A., Bertero, VV., Thompson, C., & Alonso, J. (1989). *Earthquake simulator testing of steel plate added damping and stiffness elements*. Report UCB/EERC-89/02. Earthquake Engineering Research Center, University of California at Berkeley.

Yang, T. Y., Tung, D. P., & Li, Y. (2018). Equivalent energy design procedure for earthquake resilient fused structures. *Earthquake Spectra, 34*(2), 1–21. https://doi.org/10.1193/122716EQS254M.

Improvement of Building Resilience by Viscous Dampers

**Ersin Aydin, Ehsan Noroozinejad Farsangi, Baki Öztürk,
Aleksandra Bogdanovic and Maciej Dutkiewicz**

1 Introduction

In the last 20 years, intensive research on structural control conducted in highly developed countries has resulted in different technological solutions, and many of them have been applied to numerous structures, high-rise buildings, large-span bridges and towers. The development of new materials, computer technologies and sensors enables the fast development of structural control, whose philosophy is based on providing stability of systems at any time and under any dynamic excitation.

In addition, devastating earthquake events throughout the world, such as 2018 Fiji earthquake (Mw = 8.2), 2017 Chiapas earthquake (Mw = 8.2), 2015 Illapel earthquake (Mw = 8.3), 2010 Chile earthquake (Mw = 8.8), 2003 Hokkaidō earthquake (Mw = 8.3), 1995 Kobe earthquake (Mw = 6.9) and 1989 Loma Prieta earthquake (Mw = 6.9), have indicated that the current seismic design guidelines may not be very appropriate to isolate the seismic effects on structures/infrastructures, and there may experience extensive damages or fully collapse considering the current code approaches.

E. Aydin (✉)
Nigde Ömer Halisdemir University, Nigde, Turkey
e-mail: eaydin@ohu.edu.tr

E. Noroozinejad Farsangi
Graduate University of Advanced Technology, Kerman, Iran
e-mail: noroozinejad@kgut.ac.ir

B. Öztürk
Hacettepe University, Ankara, Turkey

A. Bogdanovic
Institute of Earthquake Engineering and Engineering Seismology, Skopje, Macedonia

M. Dutkiewicz
University of Science and Technology, Bydgoszcz, Poland

Structures that were designed according to novel approaches by implementing seismic control technologies such as passive, semi-active and active damping systems better withstood such events, as verified by field evidences (Han 2018; Segou and Parsons 2018; Tilmann et al. 2016; Lorito et al. 2011; Yamazaki and Cheung 2011; Takewaki 2011; Spencer and Nagarajaiah 2003; Koketsu et al. 2005; Yamaguchi and Yamazaki 2001; Kasai and Maison 1997). The acceptance of these innovative systems is based on performance enhancement, while considering construction costs and long-term effects. To practically assess the performance of these systems, effective system integration and further development of analytical and experimental techniques are required.

Among the available seismic/vibration control methodologies, passive dampers represent an advantage over the semi-active and active devices, since passive dampers do not need an external source of energy for their operation. Moreover, they can be easily repaired or replaced after a major seismic event (Soong and Costantinou 2014; Suzuki 2008; Housner et al. 1997).

It is necessary to install a large number of additional passive devices to achieve a satisfactory level of response reduction. There are many possible positions for damper placement in a real structure. As the number of dampers planned for installation increases, the number of possible combinations for placement in the structure also increases. Considering this, an important task is to find the optimal damper placements in structures. The search becomes more complicated when dampers are to be placed in few story units out of several stories (Sánchez et al. 2018; Milman and Chu 1994; Horta et al. 1986).

Dampers placement is a critical design concern, as the distribution of damping may greatly affect a building's dynamic response and the necessary damping cost. Gluck et al. (1996) optimised performance cost function for the selection of the most suitable configuration of viscous elastic dampers.

One of the best approaches that have been suggested in the literature is to find the optimal locations by using a transfer function, which is a mathematical model to link the system response to external vibrations. The main advantage of a transfer function is to provide a full description of the dynamic behaviour of the structure without considering the detailed configuration of the system. Takewaki (1997a, b, 1998, 2000a, b) defined a procedure to minimise the amplitude of a transfer function at an undamped natural frequency of a building while implementing passive dampers for vibration control. Wu et al. (1997) investigated the optimal damper placement for torsional-dependent structures to obtain minimal rotations and translations. They used the transfer function method of matrix to obtain the target function; the optimal damper placement corresponded to the places the maximal displacements appeared. In another study, Takewaki and Uetani (1999) developed a methodology to optimise the damper placement based on structural response amplification. Singh and Moreschi (2002) used a genetic algorithm to obtain the optimal damper placement in linear systems. They used the classic viscous dampers and viscous elastic dampers for energy dissipation. Main and Krenk (2005) developed approximate solutions for complex eigenvalue problems resulting from the free vibration of structures with added damping. The best location for dampers was obtained using mode shapes for

undamped structure to get the maximum relative displacement between the two ends of the viscous dumper. Aydin et al. (2007) proposed a new approach to find the optimal location of damping devices by considering the base shear as an objective function. Cimellaro (2007) proposed a procedure in which a generalised objective function that combines displacements, accelerations and the base shear transfer function is used to determine the optimal damper placement. In the work of Kohei et al. (2010), the optimisation technique is based on the Lagrange multipliers method with two limitation conditions in order to minimise the maximum response of the structure. To address the problem of optimal damper placement in steel moment frames, Homayoon and Mohammad (2011) applied a new dynamic procedure, called the endurance time, which reasonably reduces computational effort. Aydin (2012) conducted a study on the location and optimal size of passive dampers in steel structures. In this study, the author evaluated the transfer function in an undamped fundamental frequency condition. Mousavi and Ghorbani-Tanha (2012) developed a systematic procedure for determining the optimal placement and characteristics of different linear velocity-dependent dampers according to modal damping ratios.

Furthermore, Martínez et al. (2013, 2014) have focused on defining the optimal damping coefficients of two types of passive dampers. Sonmez et al. (2013) also performed a similar study on calculating the size and location of passive dampers using artificial intelligence-based techniques. The efficiency of the method was evaluated through the amplitude of the transfer function. A meta-heuristic algorithm was proposed to find the optimal location and sizes of the added dampers by Amini and Ghaderi (2013). Adachi et al. (2013) formulated a practical optimal design method to minimise the maximum inter-storey drift or maximum top storey acceleration under earthquakes for nonlinear oil dampers. To minimise the transfer function of the sum of inter-story drift, Fujita et al. (2010) proposed a procedure to determine the optimal placement of dampers and their supporting members, while Wang et al. (2010) used a penalty function and first-order theory in long suspension bridges.

As earlier mentioned, the effectiveness of damping devices depends not only on their energy dissipating mechanism, but also on their placement in structures. Uetani et al. (2003) developed a novel structural system for building structures implementing viscous and hysteretic dampers. Noroozinejad (2011) and Farsangi and Adnan (2012) implemented a trial and error procedure to determine the best configurations for friction and viscoelastic dampers installed in the cutouts of shear walls in tall buildings.

Uz and Hadi (2014) used soft computing techniques (genetic algorithms) to develop a new design strategy for incorporating passive dampers to reduce damages from pounding in adjunct structures under seismic excitations. In their study, the decrement in the number of used dampers improved the dynamic response of the structures. Murakami et al. (2015) developed an optimisation methodology to optimise the size and location of passive dampers, considering a variable adaptive step length. Pu et al. (2016) improved the structural damping ratio by passive damping devices.

Some other studies have focused on optimal damper design in building structures. Leu and Chang (2011), Garcia (2001) and Landi et al. (2015) developed a simplified

search algorithm to maximise the effect of added dampers. Kim and Bang (2002) investigated the influence of passive dampers on the torsional response of asymmetric structures. Xu et al. (2003, 2004) utilised the simplex method to determine the optimal dampers configuration. The results indicated that the adopted methodology appropriately reduced the seismic response of the considered structure. Lang et al. (2013) studied systems with multiple degrees of freedom to investigate the effectiveness of nonlinear passive dampers compared to linear damping devices. Alibrandi and Falsone (2015) presented a minimisation technique based on the expected value of stochastic dissipated power to determine the optimal number and location of passive damping units. More researchers have investigated this issue, including Bose and Thampan (2018), Bharti et al. (2010) and Singh and Moreschi (2002).

In the present study, the use of transfer functions for the optimisation of viscous dampers is explained in planar frames exposed to earthquake vibrations. It is very important to express the steady-state response of the structures with transfer functions and to define the purpose functions required for optimisation by these tools. To find the optimum viscous damper distribution in planar frames, different objective functions and corresponding designs are examined and compared with each other according to their performance. As mentioned above, there are many damping optimisation methods in the literature. Some methods using transfer functions are selected herein. The equation of motion of the structure is given in the time domain, and the behaviour equations are converted in the frequency domain by Fourier transform. Structural behaviours are defined as top displacement or the sum of the interstorey drifts (Takewaki 2000b), top absolute acceleration (Cimellaro 2007) and base shear force (Aydin et al. 2007). The sensitivities of these behaviours according to the damping coefficients are derived. The top displacement, the top absolute acceleration and the base shear force defined by the transfer functions are selected as the objective functions. Using the Lagrange multipliers method, the optimisation criteria are derived, and optimisation is performed with the steepest direction search algorithm given by Takewaki (2000b).

2   Definition of Structural Behaviour by Transfer Functions

The governing equations for the optimal damping problem in planar frame type structures are given in this section. An N-storey plane frame structure is considered by placing dampers in the middle bay shown in Fig. 1a. The damper type placed in the middle bay in this way is a linear viscous damper with details given in Fig. 1b. The structural elements such as the columns and beams are modelled as frame element and the masses are lumped at the nodes. Figure 1 also shows the degree freedom of models, each storey has a horizontal displacement and four vertical displacement and rotation components. The degree of freedom of the dampers is only in the axial direction. It has a horizontal and vertical displacement component at each endpoint. The subject described in this chapter is to investigate the optimum distribution of a certain amount of dampers available to the locations determined.
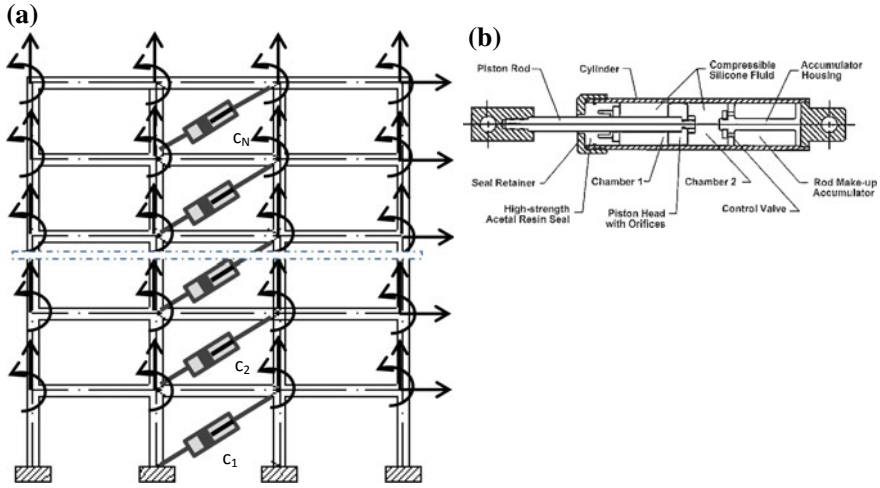
(a)

(b)

Fig. 1 **a** N-storey planar building frame, **b** components of fluid viscous damper

Transfer functions have been widely used to define structural behaviour in damper optimization, and in this study, Takewaki (2000b) has formulated optimum damper distribution on a plane frame. The equations and the method given here are based on this study from Takewaki's study and Aydin et al. (2007) and Cimellaro (2007). The equation of the motion of the N-storey plane frame seen in Fig. 1a under the effect of the earthquake is given as follows

$$M\ddot{x}(t) + C\dot{x}(t) + Kx(t) = -MI\ddot{x}_g(t) \tag{1}$$

The parameters M, C and K refer to the mass, structural damping and stiffness matrices of the structural model and they are constant. I is an influence vector with some elements 1 according to earthquake direction. While $x(t)$ denotes the displacement vector, $\dot{x}(t)$ and $\ddot{x}(t)$ refer to velocity and acceleration vectors. $\ddot{x}_g(t)$ refers to the horizontal acceleration of the earthquake. When Fourier Transform is applied to Eq. (1), which shows the equation of the motion defined in the time domain, it is transformed to the frequency domain. If the Fourier Transforms of the displacement $x(t)$ and the earthquake acceleration $\ddot{x}_g(t)$ are indicated by $X(\omega)$ and $\ddot{X}_g(\omega)$, the transformation of Eq. (1) is given in Eq. (2) below

$$\left(K + i\omega C - \omega^2 M\right)X(\omega) = -MI\ddot{X}_g(\omega) \tag{2}$$

where ω is the circular frequency, and i is the imaginary number. After adding the dampers to the structure, Eq. (2) is converted in the following form

$$\left(K + i\omega(C + C_{VD}) - \omega^2 M\right)X_{VD}(\omega) = -MI\ddot{X}_g(\omega) \tag{3}$$

where the indices of *VD* refers to the viscous damper, while the C_{VD} defines the damping matrix of the supplemental dampers. $X_{VD}(\omega)$ describes the Fourier Transform of the displacement vector in the case of viscous dampers placed. The following quantity is first defined by Takewaki (2000b), which is to make the structural behaviour independent from the external seismic effect. This vector, which can be defined as the transfer function vector of displacements, is found as follows

$$\widehat{X}(\omega) = \frac{X_{VD}(\omega)}{\ddot{X}_g(\omega)} \tag{4}$$

where ω is compressed by frequency ω_1, the structural behaviour is set in the first mode. Using Eqs. (3) and (4), Eq. (5) can be derived as

$$B\widehat{X}(\omega_1) = -MI \tag{5}$$

where $\widehat{X}(\omega_1)$ refers to the vector of the transfer function of the displacements defined according to the first mode. Where the matrix B, which includes the design variables, is written as

$$B = K + i\omega_1(C + C_{VD}) - \omega_1^2 M \tag{6}$$

The stiffness, the damping and the mass matrices are known here. The matrix containing unknown design variables is the C_{VD} matrix and will be optimally designed. The transfer function of the displacements in the first mode by using Eq. (5) can be derived as follows

$$\widehat{X}(\omega_1) = -B^{-1}MI \tag{7}$$

Takewaki (2000b) identified and used the transfer function vector of interstorey drifts by multiplying the equation with a transformation matrix. He aimed at a displacement based method while minimizing the structural behaviour expressed by relative displacements. Aydin et al. (2007) have found a force vector by multiplying the transfer function of the Takewaki (2000b) derived displacements by the stiffness matrix and proposed a force-based method for the optimization of the dampers in the first mode. Equation (7) can be multiplied by the stiffness matrix to obtain this force vector based on the transfer functions

$$F(\omega_1) = -KB^{-1}MI \tag{8}$$

Cimellaro (2007) then found the following equation by deriving the transfer function vector of the absolute acceleration.

$$\ddot{X}(\omega_1) = -M^{-1}BX(\omega_1) \tag{9}$$

In addition, the transfer function of the interstorey drifts presented below is given by Takewaki (2000b), i.e. the transfer function of the displacements is multiplied by the transformation matrix **T**.

$$\delta(\omega_1) = T\widehat{X} \tag{10}$$

3 Configuration of Optimal Damper Problem

In recent years, optimization applications in engineering designs have become widespread. Optimal designs for the placement of the dampers in the structure are developed accordingly. Some methods require gradient and sensitivity calculations, which are called indirect optimization methods. Some other methods, such as various metaheuristic and genetic algorithms, do not need gradient information, which are called direct optimization methods. The method given here is an optimality criteria method and requires sensitivity calculations. Different purpose functions are shown in the damper optimization. Some different types of objective functions such as sum of relative displacements Takewaki (2000b) or peak displacement, base shear (Aydin et al. 2007) or base moment (Aydin 2012), top absolute acceleration (Cimellaro 2007), some damage indexes (Lavan and Levy 2005), energy (Gürgöze and Müller 1992) and cost (Aydin 2013) have been used as the objective function to be minimized for optimum design of dampers. In this study, the closed form of mathematical representation of the objective function can be explained as follows.

$$\text{Min. } J = f(c_1, c_2, c_3, \ldots, c_N) \tag{11}$$

The damping coefficients of the dampers to be placed on the floors can be neither zero nor unlimited. In practice, due to the production standards and limits of the damping coefficients of these technological elements, a restriction of inequality as follows should be defined.

$$0 \le c_j \le \overline{c} \quad (j = 1, 2, \ldots, N) \tag{12}$$

Here it refers to the upper limit of the viscous damper to be added to the $\overline{c}_j$ jth storey. The sum of the design variables, which are the total damping coefficient $(\overline{W})$ of the dampers to be added to the structure, must also be limited, which can be indicated by the following equation

$$c_1 + c_2 + \cdots + c_j + \cdots + c_N = \overline{W} \tag{13}$$

3.1 Objective Functions in Terms of Transfer Function

The first of the selected objective functions to be used in this study is the amplitude of the transfer function of the top displacement in the first mode, which is equal to the sum of the transfer function amplitudes of the interstorey drifts (Takewaki 2000b) and can be given as follows.

$$J_1 = U_T(c_j) = \left| \widehat{X}_{Top} \right| \tag{14}$$

where $\left| \widehat{X}_{Top} \right|$ denotes to the transfer function amplitude of the top displacement evaluated at the first mode. The calculation of $\left| \widehat{X}_{Top} \right|$ is given in the next section. In fact, interstorey drifts are the simplest functions that characterize damage in the structure, and the sum of them gives the top displacement. Minimizing this value by using dampers can mean minimizing damage. The accelerations in the structure are other important behavioural parameters, in particular the top absolute acceleration of the structure is an indication of the earthquake forces coming into the structure and it is also important to reduce it to the minimum value by means of dampers. The minimization of this acceleration is aimed by Cimellaro (2007) and the damper design is also implemented using the transfer functions. Depending on the transfer function amplitude of the absolute acceleration, the second purpose function is given as follows

$$J_2 = A_T(c_j) = \left| \widehat{\ddot{X}}_T \right| \tag{15}$$

Here $\left| \widehat{\ddot{U}}_T \right|$ is the amplitude of the transfer function of the top absolute acceleration and can be calculated with the formula to be given later. The third objective function which is intended in the damper optimization is the base shear force. It can be written in terms of transfer function amplitude as follows

$$J_3 = V_B(c_j) = |F_1| + |F_2| + \cdots + |F_i| + \cdots + |F_N| \tag{16}$$

Here, $|F_i|$ refers to the amplitude of the transfer functions of the ith storey forces, the sum of them which gives transfer function amplitude of the base shear force (Aydin et al. 2007).

3.2 Derivation of Optimality Criteria

Each purpose function and restriction equations using Lagrangian can be written as follows in terms of the Lagrange Multipliers (α, β and γ) and the design variables ($c_1, c_2, c_3, \ldots, c_N$) as

$$L = J_h + \alpha (c_1 + c_2 + \cdots + c_j + \cdots + c_N - \overline{W})$$
$$+ \beta_1 (0 - c_1) + \beta_2 (0 - c_2) + \cdots + \beta_j (0 - c_j)$$
$$+ \cdots + \beta_N (0 - c_N) + \gamma_1 (c_1 - \overline{c}) + \gamma_2 (c_2 - \overline{c})$$
$$+ \cdots + \gamma_j (c_j - \overline{c}) + \cdots + \gamma_N (c_N - \overline{c}) \tag{17}$$

where h refers the number for each objective function. If it derives both Lagrange multipliers and design variables without upper and lower limit of the design variables, the optimality conditions are found as

$$J_{h,j} + \alpha = 0 \; For \; 0 < c_j < \overline{c} \quad (j = 1, 2, \ldots, N) \, \text{and} \, (h = 1, 2 \, \text{and} \, 3) \tag{18}$$

$$c_1 + c_2 + \cdots + c_j + \cdots + c_N - \overline{W} \tag{19}$$

The Lagrange Multipliers can be found from the stationary conditions of the Lagrangian $L(\boldsymbol{\beta} = \boldsymbol{0}, \boldsymbol{\gamma} = \boldsymbol{0})$. $J_{h,j}$ present the first order sensitivity of the objective function with respect to the jth design variable. If the upper and the lower limit of the damping coefficients are active, the Eq. (18) should be modified as follows

$$J_{h,j} + \alpha \geq 0 \quad \text{for} \, c_j = 0 \tag{20}$$

$$J_{h,j} + \alpha \leq 0 \quad \text{for} \, c_j = \overline{c} \tag{21}$$

The Steepest Direction Search Algorithm given by Takewaki (2000b) is used here to find optimum solutions to meet these optimal conditions.

3.3 Derivation of Sensitivities

Sensitivity calculations are needed to solve the above-mentioned optimal conditions. This section describes their derivations. If the partial derivative is obtained according to the design variable jth of the Eq. (5), the following equation is found

$$\boldsymbol{B}_{,j} \widehat{\boldsymbol{X}} + \boldsymbol{B} \widehat{\boldsymbol{X}}_{,j} = \boldsymbol{0} \quad (j = 1, \ldots, N) \tag{22}$$

The first order partial derivative of $\widehat{\boldsymbol{X}}$ according to the jth design variable is as follows

$$\boldsymbol{X}_{,j} = -\boldsymbol{B}^{-1} \boldsymbol{B}_{,j} \widehat{\boldsymbol{X}} \tag{23}$$

Equations (22) and (23) were derived from Takewaki (2000b). Using his method and equations, Aydin et al. (2007) described the first order partial derivative of the storey forces function as follows

$$\boldsymbol{F}_{,j} = -\boldsymbol{K}\boldsymbol{B}^{-1}\boldsymbol{B}_{,j}\widehat{\boldsymbol{X}} \tag{24}$$

Cimellaro (2007) likewise derived first order partial derivatives of absolute accelerations due to transfer functions as

$$\widehat{\ddot{\boldsymbol{X}}}_{,j} = -\boldsymbol{B}^{-1}\boldsymbol{B}_{,j}\omega_1\widehat{\boldsymbol{X}} \tag{25}$$

The ith transfer function values $\widehat{X}_i$, F_i and $\widehat{\ddot{X}}_i$ in the Eqs. (7), (8) and (9) are in a complex form. It can also be written as f_i (i = 1, …, N) and the function f_i is presented in complex form as

$$f_i = Re[f_i] + Im[f_i] \tag{26}$$

where f_i is the value of the *i*th storey displacement, storey forces and storey absolute acceleration, respectively, when the quantities of $\widehat{X}_i$, F_i and $\widehat{\ddot{X}}_i$ are written instead of f_i. The first-order sensitivity of f_i can be written as

$$f_{i,j} = Re[f_{i,j}] + Im[f_{i,j}] \tag{27}$$

The norm of f_i can be given as

$$|f_i| = \sqrt{(Re[f_i])^2 + (Im[f_i])^2} \tag{28}$$

If the norm of f_i is partially differentiated with respect to the *j*th design variable, the first-order sensitivity of $|f_i|$ can be derived as

$$|f_i|_{,j} = \frac{1}{|f_i|}\{Re[f_i](Re[f_{i,j}]) + Im[f_i](Im[f_{i,j}])\} \tag{29}$$

The first-order sensitivity of the base shear force is defined as the sum of $|F_i|_{,j}$ as

$$V_{B,j} = |F_1|_{,j} + |F_2|_{,j} + \cdots + |F_i|_{,j} + \cdots + |F_N|_{,j} \tag{30}$$

If the partial derivative is done according to the *l*th design variable of Eq. (29), the second order sensitivity of $|f_i|$ is derived as follows

$$\begin{aligned}
|f_i|_{,jl} = \frac{1}{|f_i|^2}(|f_i|\{&Re[f_{i,l}]Re[f_{i,j}] + Re[f_i]Re[f_{i,jl}] \\
+&Im[f_{i,l}]Im[f_{i,j}] + Im[f_i]Im[f_{i,jl}]\} \\
-&f_{i,l}\{Re[f_i]Re[f_{i,j}] + Im[f_i]Im[f_{i,j}]\}
\end{aligned} \tag{31}$$

The second order terms ($Re\left[f_{i,jl}\right]$ and $Im\left[f_{i,jl}\right]$) in Eq. (31) is calculated using the Eqs. (32–35).

$$X_{,jl} = B^{-1}B_{,l}B^{-1}B_{,j}\widehat{X} - B^{-1}B_{,j}\widehat{X}_{,l} \tag{32}$$

$$F_{,jl} = K(B^{-1}B_{,l}B^{-1}B_{,j}\widehat{X} - B^{-1}B_{,j}\widehat{X}_{,l}) \tag{33}$$

$$\widehat{\ddot{U}}_{jl} = \left(B^{-1}B_{,l}B^{-1}B_{,j} - B^{-1}B_{,j}B^{-1}B_{,l}\right)\omega_1^2\widehat{X} \tag{34}$$

The second-order sensitivities for base shear is calculated using the second derivative of the transfer function of the storey forces as

$$V_{B,jl} = |F_1|_{,jl} + |F_2|_{,jl} + \cdots + |F_i|_{,jl} + \cdots + |F_N|_{,jl} \tag{35}$$

3.4 Damper Design Algorithm

The steepest direction search algorithm developed by Takewaki (2000b) for the optimization of dampers is used for three different objective functions in this study. This gradient-based optimality criteria method is applied using the equations presented above. Algorithm is given here as flow diagram as shown in Fig. 2. The algorithm shown applies to the absence of a limit to the upper limit of the damper $\left(c_j < \overline{c}\right)$.

The algorithm starts by reading the structural parameters, the constraints of the damper. The eigenvalue analysis has the first frequency of the structure because the behaviour in the first mode state is controlled. Next, the value of all added dampers is zero in the beginning and the amount of damping to be added in each step is calculated by $\overline{W}/m$. Here m is the choice of the designer. The m value indicates the number of steps in the design. In the literature, 300 are commonly used, which is taken in this study. In each step, first-order partial derivatives are calculated and an index is found. ΔW is added to the damping coefficient of kth storey at that stage. Then the objective function and the first derivatives are updated. Thereafter, if there are other derivative values with the same value for the first derivatives, this means that more than one floor will be placed the damper. At this point, the damper coefficients are calculated by using the second derivatives and the equality constraint. If more than one k (k_1, …, k_m) value arises, the objective function and its derivatives are updated as follows

$$f \rightarrow f + f_{,k_1}\Delta c_1 + \cdots + f_{,k_m}\Delta c_{k_m} \tag{36}$$

$$f_{,j} \rightarrow f_{,j} + f_{,1l}\Delta c_l + \cdots + f_{,k_m l}\Delta c_l \tag{37}$$
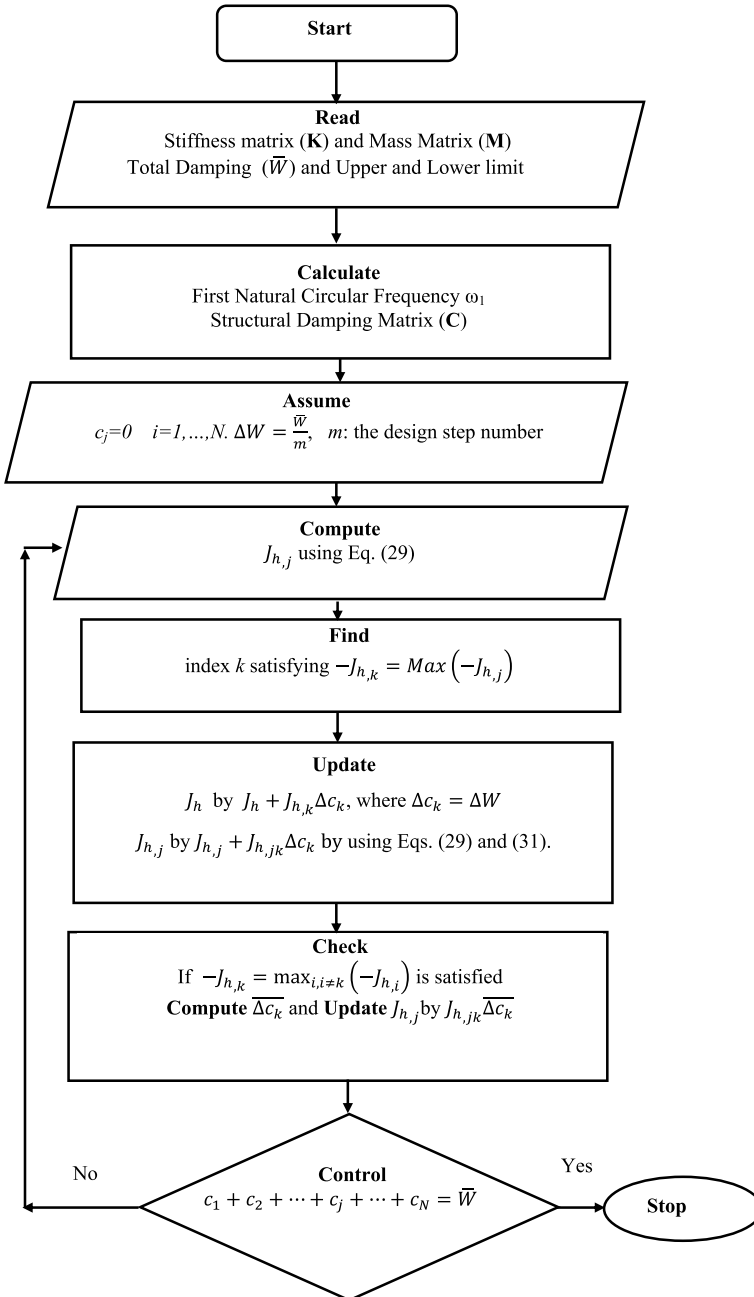
Fig. 2 The flowchart of steepest direction search algorithm

4 Numerical Examples

The mentioned three different objective functions, 5-storey and 10-storey plane frames are chosen to apply the damper optimization to the building models as shown in Fig. 3. The height of each storey and the span of each bay are taken as 4 and 8 m. Young's modulus is 2.06×10^5 MPa in frame elements. While only the bending deformation in beams, both bending and axial deformations in columns are considered, the shear deformation of the members is neglected. The structural properties of frames are given in Table 1. The natural circular frequencies of the planar frames are calculated as $\omega_1 = 7.27$ rad/s in 5-storey building and $\omega_1 = 4.70$ rad/s in 10-storey building. The critical damping ratio of the structure is 0.02 at the fundamental mode for each two models. The effect of stiffness of the supported members is omitted here.
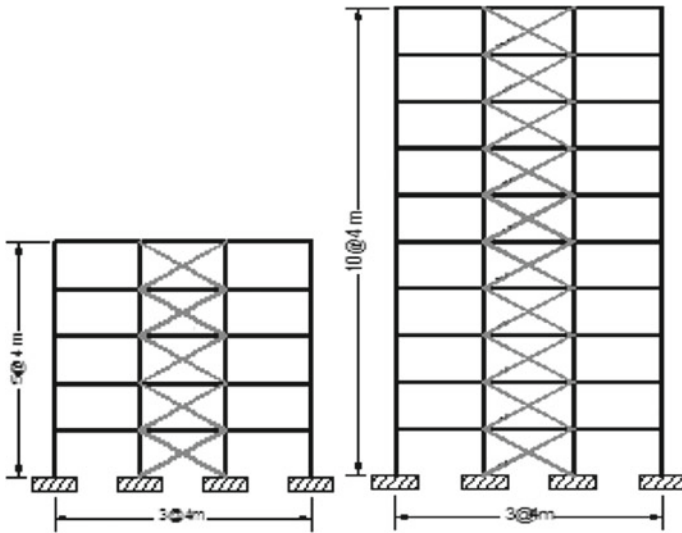
Fig. 3 5-storey and 10-storey planar building frames

Table 1 The properties of the frame elements for 5-storey building frame

Model frame	Beams		Columns		Lumped mass (kg)		Mass moment of inertia (kg m²)	
	A (m²) (10⁻⁴)	I (m⁴) (10⁻⁵)	A (m²) (10⁻⁴)	I (m⁴) (10⁻⁵)	Interior node (10³)	Exterior node (10³)	Interior node (10⁵)	Exterior node (10⁵)
5-storey	365	205	365	205	51.2	25.6	5.46	1.71
10-storey	683	353	683	353	51.2	25.6	5.46	1.71
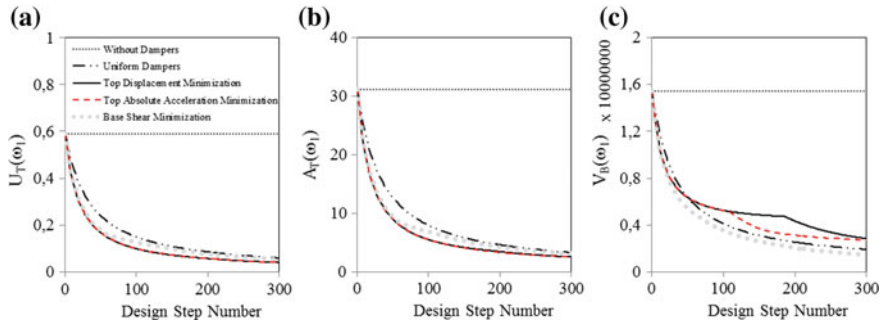
Fig. 4 The variation of the transfer function amplitude of top displacement, top absolute acceleration and base shear for different objective functions in the 5-storey building
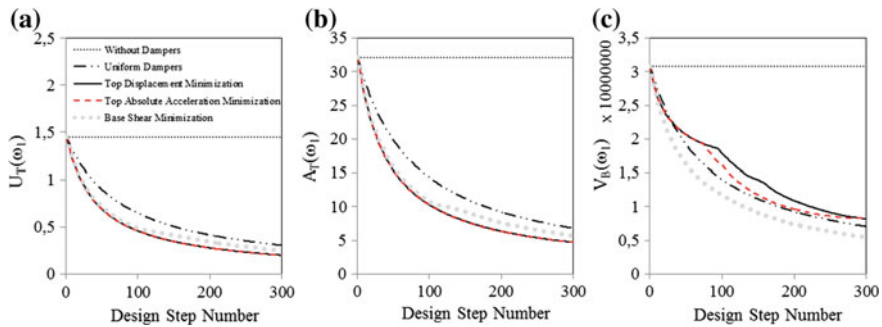
Fig. 5 The variation of the transfer function amplitude of top displacement, top absolute acceleration and base shear for different objective functions in the 10-storey building

The total damping coefficient are assumed to be $\overline{C} = 1.47 \times 10^7$ N s/m of 5-storey model, $\overline{C} = 2.94 \times 10^7$ N s/m of 10-storey model and the increment of damper capacity in each design step is taken $\Delta C = \overline{W}/m$, where design step number (m) is chosen as 300. The upper bounds of the damping coefficients are not active in this examples, i.e. $c_i < \overline{c}$ for all i. Three different objective functions for optimum damper distribution problem based on transfer functions; the amplitude of the transfer function of the top displacement, the amplitude of the top absolute acceleration and the amplitude of the transfer function of the base shear are minimized using steepest direction search algorithm (Takewaki 2000b). The variations of the transfer function amplitude of top displacement (U_T), the top absolute acceleration (A_T) and base shear (V_B) are given in Fig. 4 for 5-storey building and Fig. 5 for 10-storey building during the minimization of each one of the different objective functions.

The changes of functions of 5-storey and 10-storey models are similar. In terms of top displacement, the best performance is presented for the top displacement minimization as expected shown in Figs. 4a and 5a. At the end of the design steps, the optimal design for top displacement has the minimum value in terms of U_T, moreover the values of the acceleration minimization are very close to it. The acceleration

minimization and displacement minimization give very close damper designs and similar structural behaviours. When it is examined in terms of top displacement, the design that provides the most unfavourable result is seen in uniform design, followed by the design which is the result of the base shear optimization as shown in Figs. 4a and 5a. A similar situation applies to changes in the amplitude of the transfer function of the acceleration. Figures 4b and 5b show that the best designs according to the terms of amplitude of top absolute acceleration are the optimal damper design for acceleration minimization and the damper design for top displacement minimization is close to it. Uniform design and base shear design show poor performance in minimizing acceleration. When the variations of the transfer function amplitude of the base shear force are examined in the case of different objective functions, the best damper design in terms of base shear is the design for the base shear minimization for the 5-storey and 10-storey models as shown in Figs. 4c and 5c. The next appropriate damper design is the uniform design. The worst performance in terms of the amplitude of base shear has shown in the damper designs according to the displacement and acceleration minimization.

The obtained damper distributions used by the mentioned method and objective functions are shown in Fig. 6 for 5-storey and 10-storey model buildings. In the 5-storey structure, the dampers which are obtained for displacement and acceleration minimization are distributed on the 2nd and 3rd storeys by decreasing quantity, while the optimum damper design according to the base shear is distributed to the first four storeys with decreasing values as shown in Fig. 6a. In the 10-storey structure, while the designs according to the displacement and acceleration minimization show the damper placement on the 2nd, 3rd and 4th storeys, in the damper design according to the base shear force, the dampers are distributed to the first seven storeys by decreasing values from first storey to the upper storeys. While the damper designs that are found from the displacement and acceleration minimization focus on the storeys with high interstorey drifts, it is clear that the damper design based on the base shear focuses on the lower storey where the storey shear force is large. Optimum damper designs for different purposes minimize their own objectives. However, while the damper designs according to the top displacement and top absolute acceleration give close results, the design of the base shear force is different from them.

Figure 7 shows the changes of first-order sensitivities during optimization for the 5-storey building model and the variation of the first order sensitivities of 10-storey building model with respect to design variables is given in Fig. 8 in each objective function. It can be seen that partial derivatives according to the design variables of all objective functions converge at the end of the design. These changes and observations show the reliability of the results of this gradient based damper optimization method. The optimal damper designs are obtained by taking into account the first mode behaviour. The frequency behaviours of the structures with damper are investigated in terms of the amplitude of three different transfer functions. The change of the transfer function amplitudes of the top displacement, the top absolute acceleration and the base shear force depending on the normalized frequency are shown in Figs. 9 and 10.
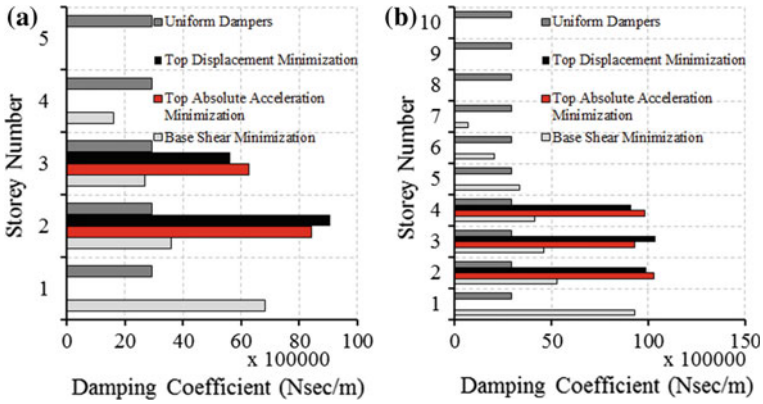
Fig. 6 Optimal damper distributions for different objectives in case of the 5-storey and 10-storey planar building examples
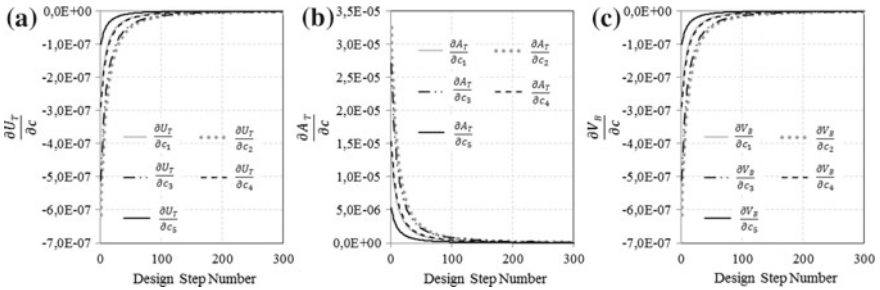
Fig. 7 The variation of the first sensitivities of three objective functions with respect to design step number in case of 5-storey building
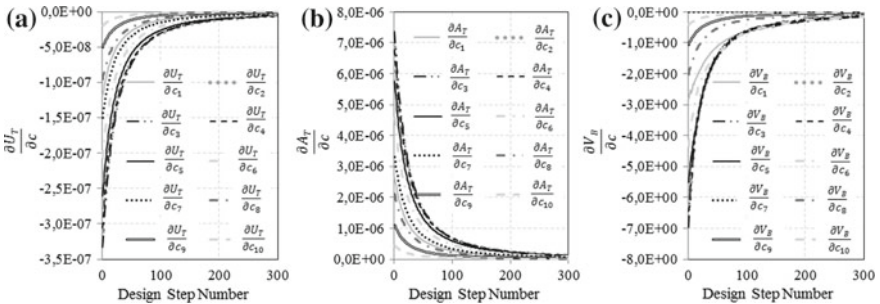
Fig. 8 The variation of the first sensitivities of three objective functions with respect to design step number in case of 10-storey building
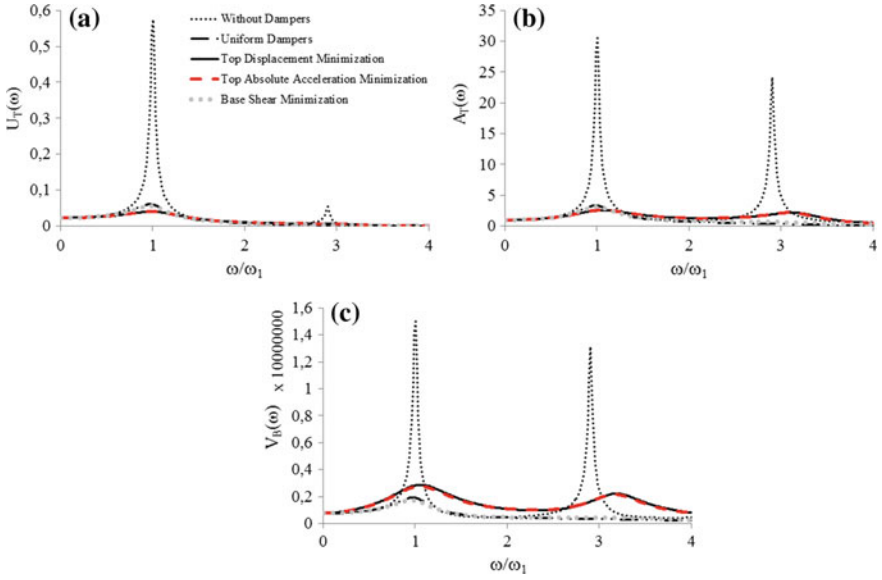
Fig. 9 The transfer function amplitude with respect to normalized frequency for different objectives in case of 5-storey building
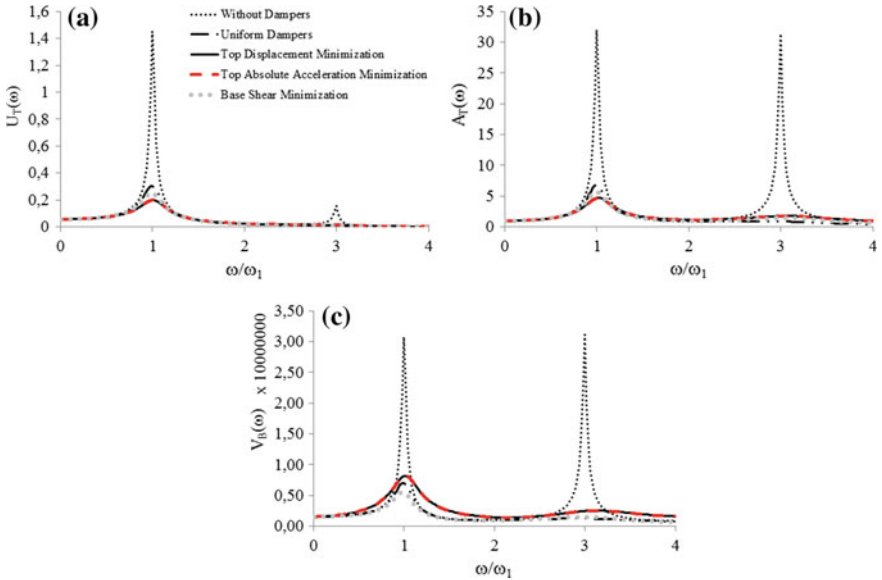
Fig. 10 The transfer function amplitude with respect to normalized frequency for different objectives in case of 10-storey building
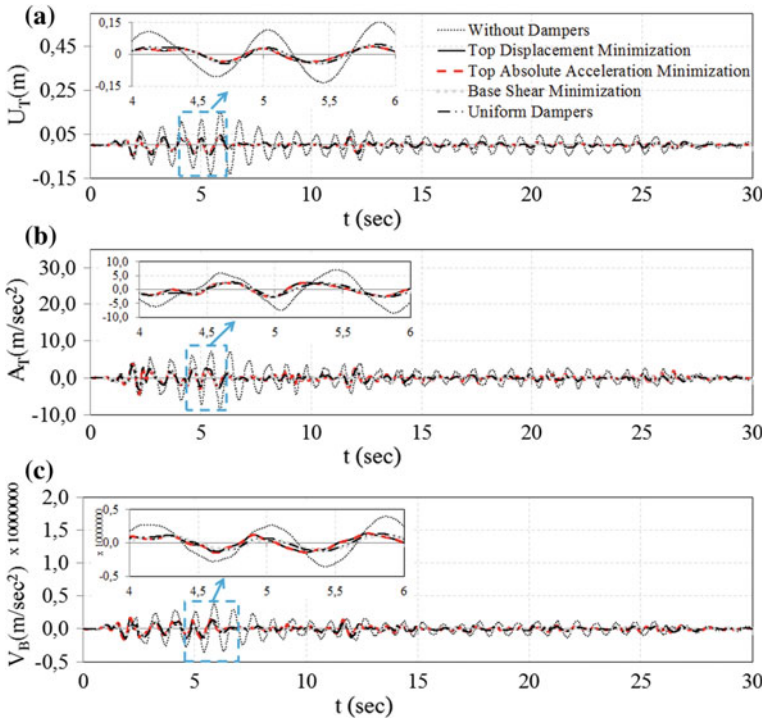
Fig. 11 Time history of top displacement, top absolute acceleration and base shear for different damper designs under El Centro earthquake in case of 5-storey buildings

When Figs. 9 and 10 are examined, all damper designs considerably reduce the top displacement, the top absolute acceleration and the base shear force behaviour. As discussed above, it can be seen that the damper designs according to displacement and acceleration minimization have similar behaviours, while the damper design according to the base shear force and the uniform damper design are closer to each other. Each of these damper designs minimizes its objectives is seen again from these Figs. 9 and 10. It is also worth noting that there is a significant decrease in the values of the amplitudes corresponding to both the first and second mode frequencies. The damper designs obtained are also effective in the second peak region. When the second peaks of the without dampers state are examined as shown in Figs. 9a and 10a, it is seen that the second peak is quite lower level than fundamental frequency level according to the amplitude of the displacement. The amplitudes in this region have been further reduced by the addition of dampers. The peak values of both acceleration and base shear transfer function amplitudes in the second mode region are very close to the peak values in the first mode. The addition of dampers has also resulted in significant drops in these high values. Reductions in the amplitude of the second mode of the acceleration and base shear can be seen in Figs. 9b, c and 10b, c.
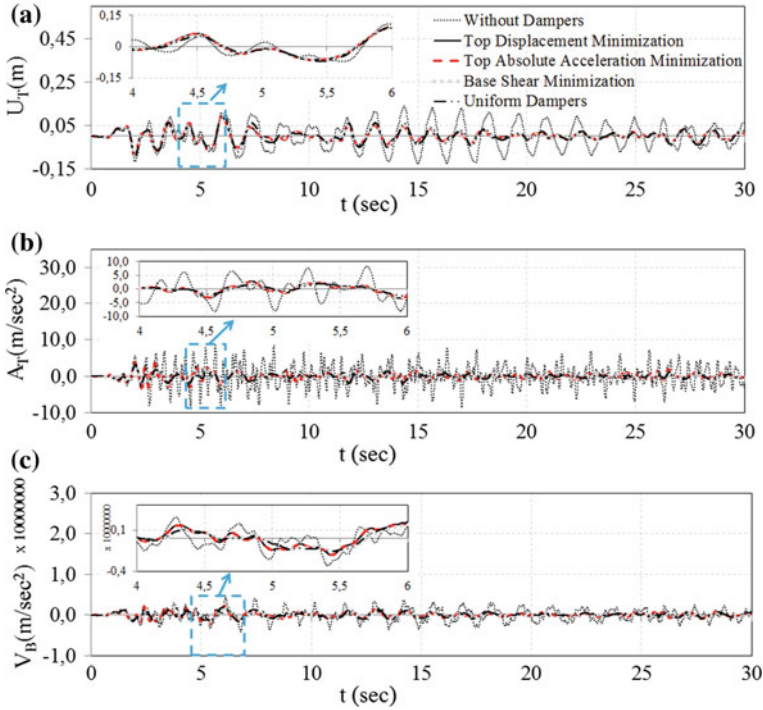
Fig. 12 Time history of top displacement, top absolute acceleration and base shear for different damper designs under El Centro earthquake in case of 10-storey buildings

The damper designs are found by using the transfer functions and the effects of these damper designs in the time domain must be examined. For this purpose, El Centro (NS) earthquake acceleration record is used for time history analyses and the top displacement, the top absolute acceleration and the base shear force are examined by considering actual values. If the top displacement, the top absolute acceleration and the base shear force for both 5-storey structure and 10-storey structure are investigated for different damper designs, all the dampers can effectively reduce the behaviour, however it is the result of displacement optimization which effectively reduces displacement with a little difference. It is seen that the optimal damper design based on acceleration minimization reduces the acceleration most effectively with a little difference and the optimal damper design based on the base shear force decrease more effective the base shear force with a little difference according to the time history analyses shown in Figs. 11 and 12.

5   Conclusions

In this section, the three methods given in the literature for the optimization of viscous dampers based on transfer functions are examined in detail. The governing equations are transformed from time domain to frequency domain by using Fourier Transform. The structural behaviours defined by the transfer functions in the frequency domain are displacements, absolute accelerations and elastic forces. Three different objective functions are defined in the optimization problem using these transfer functions. The amplitude of the top displacement, the top absolute acceleration and the base shear force are selected as the objective functions. The damping coefficients of the dampers added to the structure are chosen as design variables, and an equality constraint is used in the total damping coefficient. In the literature, the damping optimization method proposed by Takewaki (2000b) is given in this study. Based on this method, then top absolute acceleration (Cimellaro 2007) and base shear force (Aydin et al. 2007) were defined and in this study; optimum designs are found with three different purpose functions connected to transfer functions.

The methods shown on two planar frame models, 5-storey and 10-storey, are applied and the designs for different objective functions are compared. Moreover, the uniform damper design, which is common in practical applications, has been compared with optimum damper designs. The results have shown that the dampers should be optimally placed in the structure. When the uniform design is compared with the optimum designs, optimum designs give better results in terms of displacements and accelerations as well as in terms of base shear force. When the optimum designs are compared between each other, according to the analysis of both the transfer function amplitudes and the time domain, each optimum design minimizes its purpose. At this point, the designs can be divided into two groups based on force and displacement. Although the damper designs according to the top displacement and the damper designs based on the top absolute acceleration are quite close to each other, the dampers focus on the floors where the interstorey drifts are high. The optimum damper designs according to the base shear force are distributed from the base storey to the upper storey by decreasing quantity. In this case, the damper places where the coefficients of the dampers take high values in the lower storeys. The dampers focus on the storeys where the storey shear forces are large. When viscous dampers are to be used against earthquakes in buildings, the designers should be directed to an optimum design.

References

Adachi, F., Yoshitomi, S., Tsuji, M., & Takewaki, I. (2013). Nonlinear optimal oil damper design in seismically controlled multi-story building frame. *Soil Dynamics and Earthquake Engineering, 44,* 1–13.

Alibrandi, U., & Falsone, G. (2015). Optimal design of dampers in seismic excited structures by the expected value of the stochastic dissipated power. *Probabilistic Engineering Mechanics, 41,* 129–138.

Amini, F., & Ghaderi, P. (2013). Hybridization of harmony search and ant colony optimization for optimal locating of structural dampers. *Applied Soft Computing, 13,* 2272–2280.

Aydin, E. (2012). Optimal damper placement based on base moment in steel building frames. *Journal of Constructional Steel Research, 79,* 216–225.

Aydın, E. (2013). A simple damper optimization algorithm for both target added damping ratio and interstorey drift ratio. *Earthquakes and Structures, 5*(1), 83–109.

Aydin, E., Boduroglu, M. H., & Guney, D. (2007). Optimal damper distribution for seismic rehabilitation of planar building structures. *Engineering Structures, 29*(2), 176–185.

Bharti, S. D., Dumne, S. M., & Shrimali, M. K. (2010). Seismic response analysis of adjacent buildings connected with MR dampers. *Engineering Structures, 32*(8), 2122–2133.

Bose, A. K., & Thampan, C. P. V. (2018). A review on optimal positioning of X plate damper in concrete frame building. *International Research Journal of Engineering and Technology, 5*(4), 3755–3758.

Cimellaro, G. P. (2007). Simultaneous stiffness-damping optimization of structures with respect to acceleration displacement and base shear. *Engineering Structures, 29,* 2853–2870.

Farsangi, E. N., & Adnan, A. (2012). Seismic performance evaluation of various passive damping systems in high and medium-rise buildings with hybrid structural system. *Gazi University Journal of Science, 25*(3), 721–735.

Fujita, K., Yamamoto, K., & Takewaki, I. (2010). An evolutionary algorithm for optimal damper placement to minimize interstorey-drift transfer function in shear building. *Earthquakes and Structures, 1*(3), 289–306.

Garcia, D. L. (2001). A simple method for the design of optimal damper configurations in MDOF structures. *Earthquake Spectra, 17*(3), 387–398.

Gluck, N., Reinhorn, A. M., Gluck, J., & Levy, R. (1996). Design of supplemental dampers for control of structures. *Journal of Structural Engineering, 122*(12), 1394–1399.

Gürgöze, M., & Müller, P. C. (1992). Optimum position of dampers in multibody systems. *Journal of Sound and Vibration, 158*(3), 517–530.

Han, J. (2018). *Seismic study of tremor, deep long-period earthquakes and basin amplification of ground motion* (Doctoral dissertation).

Homayoon, E., & Mohammad, C. B. (2011). Optimal damper placement in steel frames by the endurance time method. *The Structural Design of Tall Special Buildings, 20,* 612–630.

Horta, L. G., Juang, J. N., & Junkins, J. L. (1986). A sequential linear optimization approach for controller design. *Journal of Guidance, Control and Dynamics, 9*(6), 699–703.

Housner, G. W., Bergman, L. A., Caughey, T. K., Chassiakos, A. G., Claus, R. O., Masri, S. F., … Yao, J. T. (1997). Structural control: Past, present, and future. *Journal of Engineering Mechanics, 123*(9), 897–971.

Kasai, K., & Maison, B. F. (1997). Building pounding damage during the 1989 Loma Prieta earthquake. *Engineering Structures, 19*(3), 195–207.

Kim, J., & Bang, S. (2002). Optimum distribution of added viscoelastic dampers for mitigation of torsional responses of plan-wise asymmetric structures. *Engineering Structures, 24*(10), 1257–1269.

Kohei, F., Abbas, M., & Takewaki, I. (2010). Optimal placement of viscoelastic dampers and supporting members under variable critical excitations. *Earthquake and Structures, 1*(1), 43–67.

Koketsu, K., Hatayama, K., Furumura, T., Ikegami, Y., & Akiyama, S. (2005). Damaging long-period ground motions from the 2003 Mw 8.3 Tokachi-oki, Japan earthquake. *Seismological Research Letters, 76*(1), 67–73.

Landi, L., Conti, F., & Diotallevi, P. P. (2015). Effectiveness of different distributions of viscous damping coefficients for the seismic retrofit of regular and irregular RC frames. *Engineering Structures, 100,* 79–93.

Lang, Z. Q., Guo, P. F., & Takewaki, I. (2013). Output frequency response function based design of additional nonlinear viscous dampers for vibration control of multi-degree-of-freedom systems. *Journal of Sound and Vibration, 332*(19), 4461–4481.

Lavan, O., & Levy, R. (2005). Optimal design of supplemental viscous dampers for irregular shear frames in the presence of the yielding. *Earthquake Engineering and Structural Dynamics, 34,* 889–907.

Leu, L. J., & Chang, J. T. (2011). Optimal allocation of non-linear viscous dampers for three-dimensional building structures. *Procedia Engineering, 14,* 2489–2497.

Lorito, S., Romano, F., Atzori, S., Tong, X., Avallone, A., McCloskey, J., et al. (2011). Limited overlap between the seismic gap and coseismic slip of the great 2010 Chile earthquake. *Nature Geoscience, 4*(3), 173–177.

Main, J. A., & Krenk, S. (2005). Efficiency and tuning of viscous dampers on discrete systems. *Journal of Sound and Vibration, 286*(1–2), 97–122.

Martínez, C. A., Curadelli, O., & Compagnoni, M. E. (2013). Optimal design of passive viscous damping systems for buildings under seismic excitation. *Journal of Constructional Steel Research, 90,* 253–264.

Martínez, C. A., Curadelli, O., & Compagnoni, M. E. (2014). Optimal placement of nonlinear hysteretic dampers on planar structures under seismic excitation. *Engineering Structures, 65,* 89–98.

Milman, M. H., & Chu, C. C. (1994). Optimization methods for passive damper placement and tuning. *Journal of Guidance, Control and Dynamics, 17*(4), 848–856.

Mousavi, S. A., & Ghorbani-Tanha, A. K. (2012). Optimum placement and characteristics of velocity-depend dampers under seismic excitation. *Earthquake Engineering and Engineering Vibration, 11*(3), 403–414.

Murakami, Y., Noshi, K., Fujita, K., Tsuji, M., & Takewaki, I. (2015). *Optimal placement of hysteretic dampers via adaptive sensitivity-smoothing algorithm, engineering and applied sciences optimization* (pp. 233–247). Berlin: Springer.

Noroozinejad, F. E. (2011). Performance evaluation of viscoelastic and friction passive damping systems in vibration control of tall buildings. *International Journal of Advanced Structural Engineering, 3*(2), 187–211.

Pu, W., Liu, C., Zhang, H., & Kasai, K. (2016). Seismic control design for slip hysteretic timber structures based on tuning the equivalent stiffness. *Engineering Structures, 128,* 199–214.

Sánchez, W. E. D., Avila, S. M., & de Brito, J. L. V. (2018). Optimal placement of damping devices in buildings. *Journal of the Brazilian Society of Mechanical Sciences and Engineering, 40*(7), 337.

Segou, M., & Parsons, T. (2018). Testing earthquake links in Mexico from 1978 to the 2017 M = 8.1 Chiapas and M = 7.1 Puebla shocks. *Geophysical Research Letters, 45*(2), 708–714.

Singh, M. P., & Moreschi, L. M. (2002). Optimal placement of dampers for passive response control. *Earthquake Engineering and Structural Dynamics, 31*(4), 955–976.

Sonmez, M., Aydin, E., & Karabork, T. (2013). Using an artificial bee colony algorithm for the optimal placement of viscous dampers in planar building frames. *Structural and Multidisciplinary Optimization, 48*(2), 395–409.

Soong, T. T., & Costantinou, M. C. (2014). *Passive and active structural vibration control in civil engineering*. International Centre for Mechanical Sciences; Course and Lectures No: 345. Berlin: Springer.

Spencer, B. F., Jr., & Nagarajaiah, S. (2003). State of the art of structural control. *Journal of Structural Engineering, 129*(7), 845–856.

Suzuki, K. (2008). Earthquake damage to industrial facilities and development of seismic and vibration control technology. *Journal of System Design and Dynamics, 2*(1), 2–11.

Takewaki, I. (1997a). Efficient redesign of damped structural systems for target transfer functions. *Computer Methods in Applied Mechanics and Engineering, 147*(3–4), 275–286.

Takewaki, I. (1997b). Optimal damper placement for minimum transfer functions. *Earthquake Engineering and Structural Dynamics, 26*(11), 1113–1124.

Takewaki, I. (1998). Optimal damper positioning in beams for minimum dynamic compliance. *Computer Methods in Applied Mechanics and Engineering, 156*(1–4), 363–373.

Takewaki, I. (2000a). Optimal damper placement for critical excitation. *Probabilistic Engineering Mechanics, 15*(4), 317–325.

Takewaki, I. (2000b). Optimum damper placement for planar building frames using transfer functions. *Structural and Multidisciplinary Optimization, 20,* 280–287.

Takewaki, I. (2011). *Building control with passive dampers: Optimal performance-based design for earthquakes*. Hoboken: Wiley.

Takewaki, I., & Uetani, K. (1999). Optimal damper placement for building structures including surface ground amplification. *Soil Dynamics and Earthquake Engineering, 18*(5), 363–371.

Tilmann, F., Zhang, Y., Moreno, M., Saul, J., Eckelmann, F., Palo, M., … Schurr, B. (2016). The 2015 Illapel earthquake, central Chile: A type case for a characteristic earthquake? *Geophysical Research Letters, 43*(2), 574–583.

Uetani, K., Tsuji, M., & Takewaki, I. (2003). Application of an optimum design method to practical building frames with viscous dampers and hysteretic dampers. *Engineering Structures, 25*(5), 579–592.

Uz, M. E., & Hadi, M. N. (2014). Optimal design of semi active control for adjacent buildings connected by MR damper based on integrated fuzzy logic and multi-objective genetic algorithm. *Engineering Structures, 69,* 135–148.

Wang, H., Li, A. Q., Jiao, C. K., & Spencer, B. F. (2010). Damper placement for seismic control of super-long-span suspension bridges based on the first-order optimization method. *Science in China Series E: Technological Sciences, 53*(7), 2008–2014.

Wu, B., Ou, J. P., & Soong, T. T. (1997). Optimal placement of energy dissipation devices for three dimensional structures. *Engineering Structures, 19*(2), 113–125.

Xu, Z. D., Shen, Y. P., & Zhao, H. T. (2003). A synthetic optimization analysis method on structures with viscoelastic dampers. *Soil Dynamics and Earthquake Engineering, 23*(8), 683–689.

Xu, Z. D., Zhao, H. T., & Li, A. Q. (2004). Optimal analysis and experimental study on structures with viscoelastic dampers. *Journal of Sound and Vibration, 273*(3), 607–618.

Yamaguchi, N., & Yamazaki, F. (2001). Estimation of strong motion distribution in the 1995 Kobe earthquake based on building damage data. *Earthquake Engineering and Structural Dynamics, 30*(6), 787–801.

Yamazaki, Y., & Cheung, K. F. (2011). Shelf resonance and impact of near-field tsunami generated by the 2010 Chile earthquake. *Geophysical Research Letters, 38*(12), 1–8.

Earthquake Risk Management Systems and Their Applications for Building Seismic-Resilient Communities

Aman Mwafy (ORCID)

1 Introduction

The earthquake risk represents a challenge in many parts of the world. Several deadly earthquakes were recorded over the past few years, including the 2011 Honshu (Japan), 2010 Haiti, 2008 Sichuan (China), 2005 Kashmir (Pakistan), 2004 Sumatra (Indonesia). In the current and past decades, the most significant earthquakes killed about 800,000 people and cost billions of dollars (USGS 2018). The high losses from previous earthquakes confirm that, although the hazard and vulnerable inventories are recognized, effective strategies for managing seismic risk at the national or regional levels are still missing in some regions. The level of understanding concerning the mechanisms that cause earthquakes, how different components of the built environment respond to the seismic hazard events, and the social and economic consequences from the physical damage caused by earthquakes has advanced in the past few decades. This knowledge has been recently integrated into earthquake risk management systems to help in developing national/regional mitigation plans for minimizing the impacts of earthquakes. These risk management systems provide tools to illustrate the consequences of earthquakes with associated uncertainty and the benefits of mitigation actions.

The regional earthquake risk management framework is a multi-disciplinary concept that incorporates the definition of seismic hazard, exposed inventory, physical damage, and socioeconomic impacts of earthquakes (Hashash et al. 2012). Building inventory, transportation systems, lifeline networks, and emergency facilities should be considered when assessing the physical damage. Short and long-term effects should also be accounted for when estimating the socioeconomic consequences. A visualization platform is essential to integrate all these components. Four of the most common structures proposed in the literature for regional seismic risk management

A. Mwafy (✉)
United Arab Emirates University, P.O. Box 15551, Al-Ain, UAE
e-mail: amanmwafy@uaeu.ac.ae

(a)

(b)
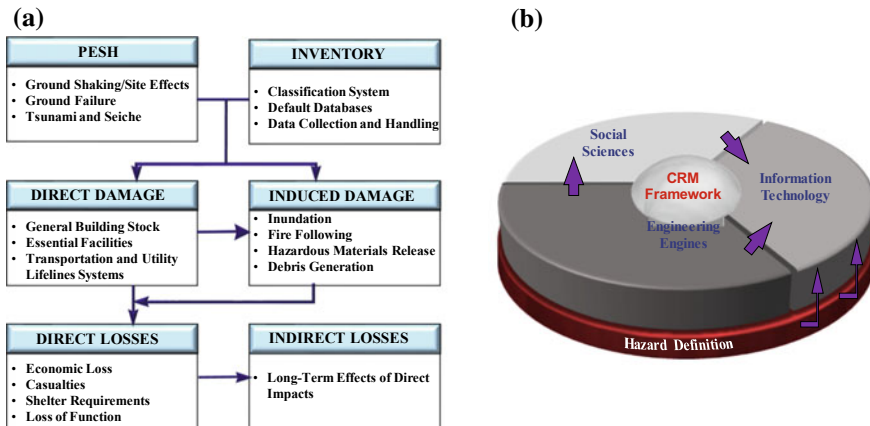
Fig. 1 Examples of earthquake loss estimation and hazard mitigation frameworks: **a** FEMA earthquake loss estimation framework (Kircher et al. 2006; Whitman et al. 1997), and **b** MAE centre consequence-based risk management framework (Elnashai and Hajjar 2006; Hashash et al. 2012)

and seismic resilience of communities are briefly discussed below (e.g. Bruneau et al. 2003; Elnashai and Hajjar 2006; Moehle and Deierlein 2004; Porter 2003; Whitman et al. 1997).

A pioneering framework for seismic loss estimation was developed and released by the Federal Emergency Management Agency (Whitman et al. 1997). The methodology included approaches for seismic hazards characterization; damage and loss estimation; and direct and indirect estimation of socioeconomic losses. The framework incorporated the modules shown in Fig. 1a (Whitman et al. 1997). These six modules may be applied with varying levels of detail. Thus, rapid loss estimations using simplified inventory and analyses or detailed loss estimations based on refined inventory and detailed analyses can be performed (Kircher et al. 2006; Whitman et al. 1997). The ground motion and ground failure are esteemed using the Potential Earth Science Hazards module. The infrastructure and demographic information are described in the Inventory module. Damage estimates for different intensities of ground motion are then provided by the Direct Damage module, while the secondary consequences of earthquakes such as fire are evaluated using the Induced Damage module. The direct and indirect socioeconomic losses are finally estimated through the Direct Loss and Indirect Loss modules. Figure 1 shows that the direct losses are estimated based on direct and induced damage, while indirect losses are the result of the long-term consequences of direct losses.

The framework of the Pacific Earthquake Engineering Research Center was introduced to improve the seismic risk assessment through the Performance-Based Earthquake Engineering approach (Moehle and Deierlein 2004; Porter 2003). The framework involves four main phases related to hazard, structural, damage, and

loss assessment. The process begins with the definition of an earthquake Intensity Measure, use of simulation procedures to establish Engineering Demand Parameter(s), relating EDP to Damage Measure, and finally calculating Decision Variable for use in decision making. The framework is suitable for the detailed performance assessment of a specific facility or for calibrating and improving design provisions. Hence, the performance of existing or new facilities can be improved to reach the target objective(s) efficiently.

The Multi-disciplinary Center for Earthquake Engineering Research Center proposed a framework to assess and improve the seismic resilience of communities. Seismic resilience was described as "the ability of a system to reduce the chances of a shock, to absorb such a shock if it occurs (sudden reduction of performance), and to recover quickly after a shock (reestablish regular performance)" (Bruneau et al. 2003). The measures of resilience of this framework involve: (i) reduced probabilities of failure, (ii) decreased consequences of failure, and (iii) reduced recovery time. The technical, organizational, social, and economic dimensions of community resilience are integrated into this framework to assess and quantify the resilience. This enables comparing between the seismic resilience of different systems and evaluating their resilience with time. This framework is discussed in more details by Bruneau et al. (2003).

The Mid-America Earthquake Centre also developed a framework for seismic risk assessment and mitigation (Elnashai and Hajjar 2006; Hashash et al. 2012). The proposed Consequence-based Risk Management model assesses the interdisciplinary relationship between causes, consequences and mitigation features of seismic events. The risk management framework assists in drawing emergency plans, taking actions during disasters and prioritizing mitigation approaches to reduce losses. As shown in Fig. 1b, the Engineering Engines of the framework estimate the physical damage. The Social Sciences utilize the estimates provided by the physical damage to predict the socioeconomic impacts of earthquakes. Finally, the Information Technology component generates data and provides the visualization of losses and mitigation actions for decision making. Additional information regarding the capabilities of the framework is discussed by Elnashai and Hajjar (2006). It is noteworthy that the focus of MAE center has expanded to cover multi-hazard approaches and promoting the resilience of communities (e.g. Gardoni and LaFave 2016).

The four structures mentioned above of the earthquake risk management framework show that this concept should incorporate four main components, namely the seismic hazard, inventory, vulnerability, and social and economic consequences. A visualization platform then integrates these components. This chapter aims at providing an overview of the earthquake risk management framework and its components and to present case studies and applications of the earthquake risk management process, particularly those related to medium seismicity regions which are represented by UAE.

2   Components of Seismic Risk Management Systems

The main components of a regional seismic risk management system is shown in Fig. 1 (Mwafy 2012a). These components include: (i) seismic hazard, (ii) inventory, and (iii) vulnerability before and after implementing mitigation actions (Elnashai and Di Sarno 2015). Adding social and economic consequences to the above three components enables predicting direct and indirect losses. A risk management platform is essential to integrate the components of the system to assist researchers, practitioners, and policy-makers. A brief review of each of these driving engines is presented below.

2.1   Seismic Hazard

Seismic risk predicts possible losses due to seismic hazard, which is defined as the possibility of potentially damaging earthquake effects taking place at a site (Bommer 2002; Wang 2011). The destructive impact of earthquakes depends on several factors such as their magnitude or intensity, focal depth, duration, epicentral distance, site class, and geological and topographical conditions (e.g. Bozorgnia and Campbell 2004; Hancock and Bommer 2006). The earthquake losses largely depend on the type of constructions and the density of population. Earthquakes may have significant direct and indirect impacts. The direct ground effects involve ground movement, differential settlement, liquefaction, landslides, and rock fall, while the indirect effects include for instance tsunamis (Bolt 1989; Day 2002; Elnashai and Di Sarno 2015). These effects may cause significant structural and non-structural damage, which vary between light damage and collapse. Apart from significant surface fault rupture, the direct damaging effects of seismic events are associated with seismic waves and ground movements. In loss assessment, the ground shaking is typically taken into account because of the decreased impact of secondary hazards such as liquefaction with the increase in the loss model size (Bird and Bommer 2004).

The procedures used to assess the seismic hazard include two options, namely deterministic or probabilistic seismic hazard approaches (DSHA or PSHA; e.g. Kramer 1996; Reiter 1990). The choice between these two approaches is a critical step in hazard assessment. In DSHA, the location and magnitude of the earthquake scenarios that have possible effects on a site are defined. The controlling earthquake is determined using attenuation relations. More than one controlling event could be considered in some cases. This approach is suitable for planning exercises, emergency response and the design of critical facilities such as nuclear power plants.

Since the introduction of PSHA, it has been widely used to determine the characteristics of ground-motion for engineering design (Cornell 1968). Unlike DSHA which is straightforward, PSHA may require clarifications (Abrahamson 2000; Bommer 2002; Hanks and Cornell 1994). The probabilistic approach recognizes all possible seismic events that have possible effects on a site, considering different

combination cases of earthquake distance and magnitude. A recurrence relationship is employed to describe the frequency of different earthquakes, while attenuation relationships are used to calculate the earthquake parameters due to each seismic event. The design earthquake is associated with the value that has a specific annual frequency of occurrence. The issues related to both the PSHA and DSHA approaches include: (i) identifying potential sources of earthquakes, and (ii) modeling of the ground motion using attenuation relationships. Unlike the deterministic approach, PSHA is associated with time (Bommer 2002; Hanks and Cornell 1994).

A brief review of seismic hazard studies related to the UAE, which is a region of medium seismicity subjected to multiple seismic scenarios, is briefly presented below as a case study. Probabilistic seismic hazard maps that represent the soil properties and sets of earthquake records that account for the frequency contents and magnitude of a region are required to define the seismic hazard. Several previous studies were directed to the assessment of seismic hazard in the UAE (e.g. Abdalla and Al-Homoud 2004; Aldama-Bustos et al. 2009; El-Hussain et al. 2012; Irfan et al. 2013; Mwafy et al. 2006; Pascucci et al. 2008; Peiris et al. 2006; Shama 2011; Sigbjornsson and Elnashai 2006). For instance, the seismic events recorded in the UAE and surrounding region from 734 to 2004 is presented in Fig. 2a (Ambraseys 2009; Mwafy et al. 2006; Sigbjornsson and Elnashai 2006). Within or in the proximity of the UAE, about 50 earthquakes were recorded from 1924 to 1999, only three of
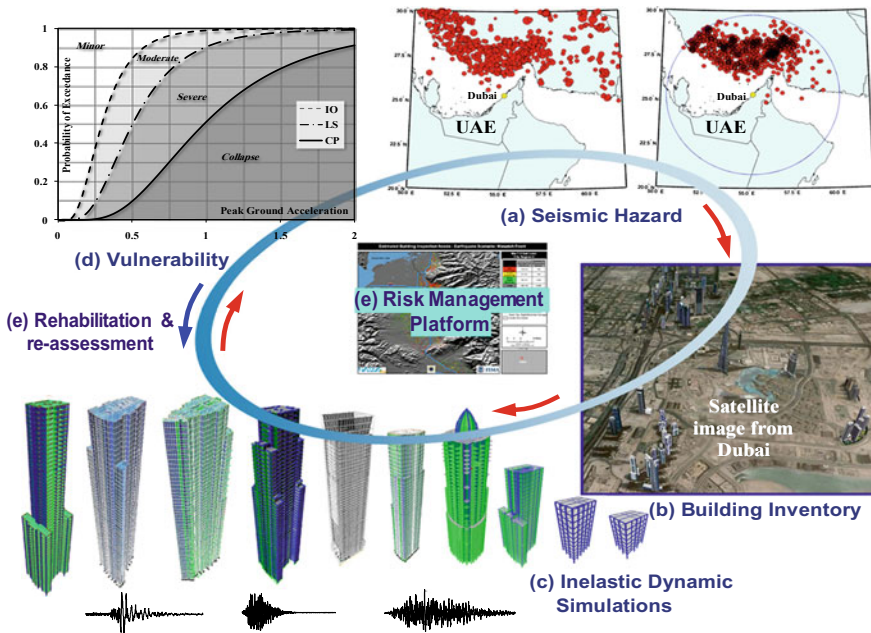
Fig. 2 Main components of a regional seismic risk management system that involves earthquake loss estimation and mitigation (Mwafy 2012a)
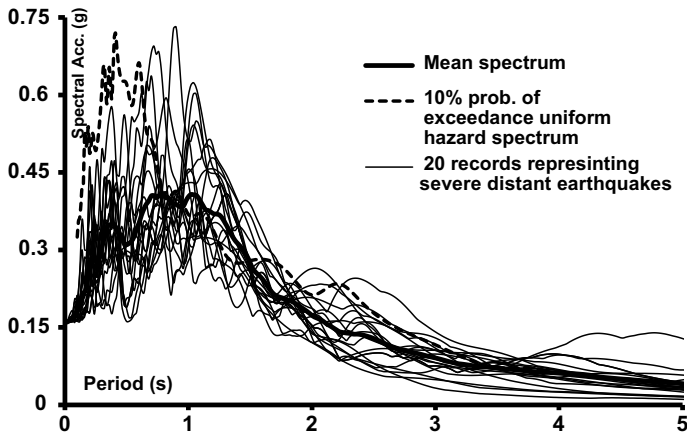
Fig. 3 5% damped response spectra of twenty natural ground motions representing a critical seismic scenario in Dubai

these seismic events were generated in the Arabian Peninsula. More recently from 2000 to 2006, 18 earthquakes were generated, which included eight inland/offshore events (Aldama-Bustos et al. 2009). The recent observations related to increasing the rate of earthquakes emphasize the need for considering recent earthquakes when selecting input ground motions to represent the UAE seismicity reliably.

A sample of the earthquake records employed to represent the seismicity of the UAE in recent studies is shown in Figs. 2c and 3 (Alwaeli et al. 2017a; Mwafy 2013; Mwafy and Khalifa 2017). The most critical seismic scenarios are accounted for through the outcomes of seismic hazard assessment studies and recommended design provisions pertain to the UAE (e.g. Abdalla and Al-Homoud 2004; DMA 2013; Mwafy et al. 2006; Shama 2011). The uncertainty in input ground motions is considered in the vulnerability assessment using diverse sets of earthquake records that were selected according to the latest understanding of the seismicity of the study region. The real earthquake records were selected from the European Strong-Motion and Pacific Earthquake Engineering Research Centre databases (Ambraseys et al. 2004; PEER 2015).

2.2 Inventory

The representation of the exposed built environment is an essential element in seismic risk management systems. The inventory represents the assets that are vulnerable to the seismic hazard (Elnashai and Di Sarno 2015). Assembling an inventory database can be the most demanding process among those needed to conduct loss assessment for a site, and thus it usually among the major constraints (Whitman et al. 1997). The building and infrastructure within the study region must be classified according

to the needs of the framework (Kircher et al. 1997). For instance, the classification of the building inventory should account for occupancy and building characteristics, including the height, structural system, and construction material. Although currently available loss estimation systems such as HAZUS are capable of producing loss estimates based upon default data, the detailed inventory is usually needed in comprehensive studies to reduce uncertainty (Kircher et al. 2006). Information related to the built environment such as location, land use, construction date, and footprint may be available at municipalities and local authorities. However, essential information for structural modeling such as the building height and use, structure system, and configuration are usually difficult to obtain in digital forms for specific regions, particularly for large study areas. Collecting such information from various sources using field survey techniques could be expensive. Hence, researchers need to develop approaches to estimate building inventories from available data.

The Applied Technology Council proposed classifications based on specific criteria such as the use or structure type (ATC-13 1985). Some previous studies relied on tax data to determine different aspects of the built environment (French and Muthukumar 2006). Although this is a realistic approach for certain urban areas in the U.S., this data may not be available in other regions. Some characteristics of the urban building stock such as the height may be obtained from satellite imageries, while others could be obtained from the geometries of building footprints. The estimated characteristics could be used to determine the needed inventory information (French and Muthukumar 2006).

A case study is presented herein for a highly populated seismically vulnerable area in the UAE, which extends from Dubai to Ajman. In considering the potential consequences from natural hazard events, the building inventory is the most important in this area because it represents concentrated economic and human assets. Assembling a realistic building inventory database for this vast area is a significant challenge due to the lack of detailed surveys and continuous changes in the built environment. The existing databases available in municipalities did not provide the structural characteristics needed to classify the building stock correctly for seismic loss assessment. Hence, the inventory database was assembled using high-resolution imageries in addition to several on-site surveys (Elnashai et al. 2008a; Moharram et al. 2008b). Some information was obtained from municipalities in the form of a Geographic Information System (GIS) format. The GIS data was utilized to provide the verification needed for the database collected using imageries and on-site surveys. Thus, the adopted approach to assemble a realistic building inventory involved: (i) dividing the concerned area to zones and small sub-zones, (ii) collecting the needed data from different zones using both imageries and on-site surveys, and (iii) verifying the collected database using the GIS data by comparing the number of building and their heights in various zones. The number of structures in different zones was calculated, and the buildings were classified (Mwafy 2012b).

Owing to the importance of the classification criteria of the inventory in vulnerability analysis, about 30,000 buildings were classified in Dubai using four different criteria, namely: (i) the structure height, (ii) use, (iii) date of construction, and (iv) population intensity of the related site. Ten classes of buildings were selected based
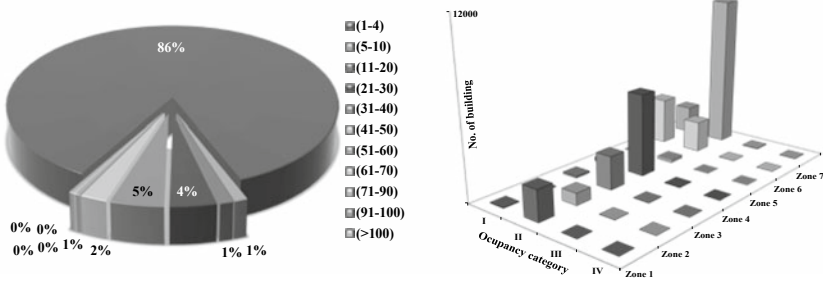
Fig. 4 Sample results depicting the classification of the building inventory in Dubai according to the number of stories (left) and occupancy category (right) (Mwafy 2012b)

on the number of stories to represent this diverse building inventory reliably, as shown in Fig. 4. An emphasis was also given to critical and emergency facilities such as police stations, fire stations, hospitals, and schools that may be used as shelters. The building functionality after seismic events is vital to ensure a successful emergency response. Buildings were thus classified into four categories according to their occupancy, namely I, II, III and IV (ASCE/SEI-7 2010).

Figure 4 shows the classification of the buildings in accordance with the occupancy. Moreover, the study area included several structures that were designed and constructed according to different building codes. Therefore, the building inventory in the study area was divided into two categories according to the date of construction (i.e. before 1991 and after 1991). This allowed classifying the building stock to 'engineered' and 'pre-code' structures. Finally, substantial seismic loss is expected in highly populated areas associated with high seismic hazard. This emphasizes the need for associating the building inventory to population density. The distribution of the population in different study zones was obtained from the official population statistics of the UAE (NMC 2013). Diverse sets of buildings representing the inventory in the study area that extended from Dubai to Ajman were selected from the assembled database for the vulnerability analysis. Owing to the diversity of the building stock in the UAE, the selected benchmark structures for loss assessment comprised of a range of structures of different structural features, as discussed hereafter.

2.3 Vulnerability

Fragility relationships describe the probability of reaching certain limit states as a function of the intensity of input ground motion, as depicted in Fig. 2d (Alwaeli et al. 2017a; Mwafy 2012a). The expected damage ratios obtained from the fragility curves are multiplied by the value of the building or its retrofit costs. Fragility functions are thus essential for seismic loss estimation and retrofit decisions (Ji et al.

2007; Mwafy and Elkholy 2017). Physical damage to buildings has received focused attention since it is the most common form of damage. However, damage to infrastructure, including electric, water, and natural gas distribution systems may also lead to business interruption. Damage to transportation systems is also significant since the emergency response and flow of production supplies will be affected (Elnashai and Di Sarno 2015; Elnashai and Mwafy 2008). Finally, damage to critical facilities such as police stations, fire stations, and hospitals can also result in significant consequences because of the delay in the emergency response system (e.g. Mwafy and Issa 2015).

Different methods are employed in previous studies to develop fragility functions such as: (i) the experimental, (ii) empirical or observational, (iii) analytical, and (iv) hybrid approaches (Calvi et al. 2006; Kwon and Elnashai 2006; Mwafy et al. 2015b; Rossetto and Elnashai 2005). The experimental choice is time-consuming and very costly. Damage probabilities have been derived in several previous studies using observed damage data. The empirical or observational approach was first employed in the U.S., Europe and Japan (e.g. Braga et al. 1982; Scawthorn et al. 1981; Whitman et al. 1973). The original approaches were updated by several researchers (e.g. Di Pasquale et al. 2005; Dolce et al. 2003), while revised approaches were also proposed (e.g. Giovinazzi and Lagomarsino 2004; Orsini 1999; Rossetto and Elnashai 2003; Rota et al. 2008; Shinozuka et al. 1997; Yakut 2004). Although the empirical approach is realistic because the whole inventory is included considering with site properties, collect an observation-based damage data for specific areas such as the UAE is difficult. Therefore, collecting damage data from dynamic response simulations is considered the most effective and practical choice in such regions (Mwafy 2012a). Figure 5 depicts a flowchart describing the process needed for deriving analytical fragility curves (Dumova-Jovanoska 2000).

Several analytical-based techniques for deriving fragility functions have been adopted in the literature, with a diversity in numerical modeling, analysis procedures, and damage models (e.g. Alwaeli et al. 2017a; Jeong et al. 2012; Ji et al. 2009; Kwon and Elnashai 2006; Masi 2003; Mwafy 2012a; Rossetto and Elnashai 2005; Singhal and Kiremidjian 1996; Wen and Ellingwood 2005; Wen et al. 2003). Dynamic response simulation-based approaches are generally computationally demanding because several inelastic response history analyses are needed to account for uncertainties, mostly when adopting inelastic dynamic simulations, which is the most reliable technique and hence is adopted in several research projects. The capacity spectrum method was also adopted in previous studies and loss assessment systems to develop fragility relationships. Under the effect of a specific earthquake scenario, the performance of a structure is obtained from the intersection of an acceleration spectrum representing the seismic demand and a pushover capacity spectrum (ATC 1996; Kircher et al. 1997).

Previous numerical studies also updated analytically-derived fragility functions according to the observational data that were collected from previous earthquakes (e.g. Rossetto and Elnashai 2005; Singhal and Kiremidjian 1998). The hybrid fragility relationships mainly integrate real earthquake damage data with those from analytically-generated damage statistics. This technique is useful when damage data

Selection of earthquake in- tensity indicator	Selection of computational model of structure	Selection of model for defi- nition of damage
Selection of representative set(s) of earthquakes	Definition of random charac- teristics of structural parame- ters	Definition of damage states
	Definition of methodology for nonlinear analysis	Definition of criteria for iden- tification of damage state
	Nonlinear analysis	
	Definition of probabilistic distribution of damage	
Fragility curves		Damage probabilities

Fig. 5 Summary of the process needed for deriving analytically-based fragility curves (Calvi et al. 2006; Dumova-Jovanoska 2000)

at certain intensity is lacking. It also reduces the required computational effort to derive a comprehensive range of fragility relationships (Barbat et al. 1996; Kappos et al. 1998). The main issue in the hybrid technique for deriving fragility functions is associated with the need to calibrate of the analytical-based damage results with those from real earthquakes, considering that the two sets of results involve different sources of uncertainty (Bommer and Crowley 2006; Calvi et al. 2006).

A case study is presented for the development of fragility functions for the building inventory in a highly populated seismically vulnerable area in the UAE. Three-dimensional finite element idealizations were developed for a wide range of structure with different characteristics to represent the diverse building inventory in the UAE. The selected multi-story and high-rise buildings were designed to the codes enforced in the study area. The results of the design process were utilized to model the structures for inelastic dynamic response simulations, which enable the development of a diverse range of fragility functions of the building stock (Mwafy 2012a, b).

The detailed idealizations of the benchmark buildings for dynamic response simulations were performed using a fiber-based analysis platform (Elnashai et al. 2012). This inelastic analysis platform can predict the deformation response of structures under earthquake loading, considering the material inelasticity (Alwaeli et al. 2017b). Several incremental dynamic analyses (IDAs) were carried out to derive the fragility functions of the benchmark buildings (Mwafy and Elnashai 2001). Figure 6 depicts a sample of the dynamic response simulation results under the effect of two earthquake
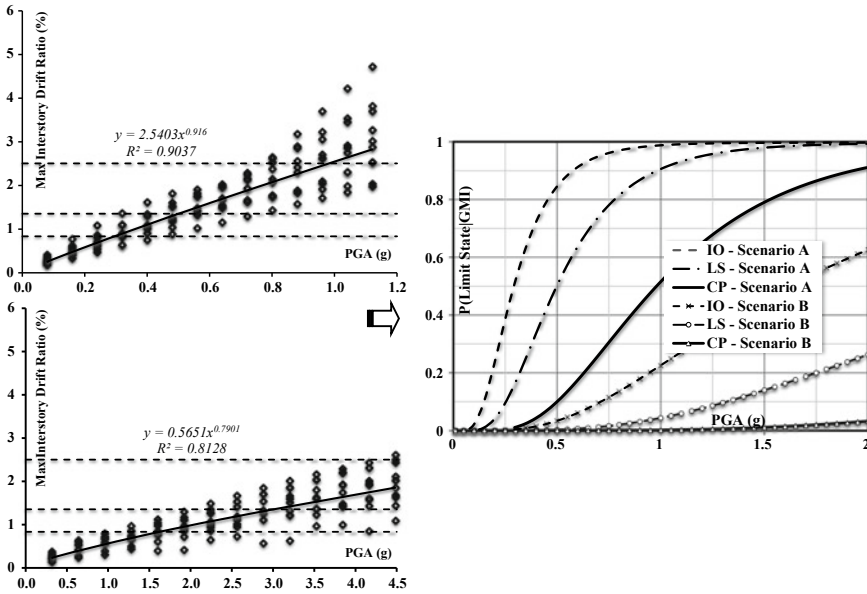
Fig. 6 Damage data and Fragility functions of a 50-story structure calculated under the effect of two earthquake scenarios (Mwafy 2012a, b)

scenarios, including the power law utilized for deriving the fragility functions. The two earthquake scenarios represented both the long-distant and near-source earthquakes (Scenarios A and B, respectively). In total, 280 points representing ground motion intensity-story drift values and generated using IDAs were plotted for each of the considered structures. The results indicated that the damage data from the utilized earthquake scenarios were entirely different. The adopted performance indicators that included Immediate Occupancy, Life Safety, and Collapse Prevention were observed at notably higher intensity levels from Scenario B when compared with Scenario A. This is due to the high spectral amplifications of Scenario A earthquakes, which correspond to the most important modes of vibrations of the benchmark structures. The results highlighted the vulnerability of the inventory in the study region to long distant seismic events and reflected the need to study the seismic loss of different types of structures and infrastructure in the region (Mwafy 2012a).

2.4 Social and Economic Consequences

Based on the physical damage predicted by the fragility relationships, the socioeconomic component quantifies short-term and long-term consequences, including for instance economic losses and business disruption. This component also focuses on illustrating how different people perceive risk and how organizations account for
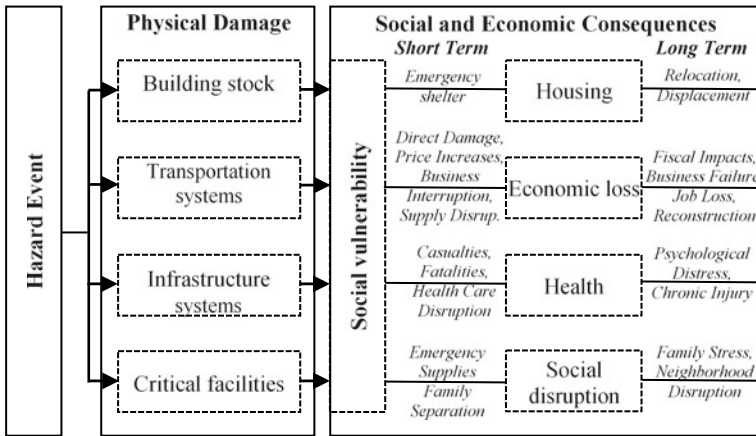
Fig. 7 Social and economic consequences of hazard events (French et al. 2010)

risk. Several previous social science studies were directed toward identifying the social and economic consequences of natural disasters (e.g. Mileti 1999; Tierney et al. 2001). Most of these studies focused on case studies, while few studies were directed to developing models to quantify the short and long-term impacts from a natural hazard that are obtained from physical damage. Figure 7 describes the relationship between natural hazard events and related social and economic consequences (French 2005). It is shown that the actual consequences following an event include different types of damage to buildings, transportation systems, infrastructure, and critical facilities. The social and economic impacts of earthquakes can be classified to: (i) housing, (ii) economic loss, (iii) health and (iv) social disruption, as shown in Fig. 7 (French 2005; French et al. 2010). It is also important to distinguish the social and economic consequences that occur immediately after an earthquake from those that occur over a longer term. Most of the early studies were directed to the direct consequences (Dowrick and Rhoades 1993; French 1995), while more recent studies have focused on accounting for both direct and indirect economic losses (Webb et al. 2000, 2002). A comprehensive literature review on the social and economic consequences is provided by French (French et al. 2010).

3 Risk Management Systems

3.1 Overview

In order to develop a risk management system at a regional scale, seismic hazard for the concerned region must be integrated with the infrastructure and building inventory along with vulnerability characteristics of representative structures for the exposed inventories. Available technologies are used for combining different driving engines

Fig. 8 Integrating different elements of loss assessment and mitigation into a risk management system (e.g. MAE 2006)

of loss assessment and mitigation into a visualization platform. A risk management platform is a data management and visualization system that can generate the loss assessment results to allow for more informed decisions, as illustrated in Fig. 8 (e.g. MAE 2006). The risk management system calculates the seismic hazard of the concerned site and integrates it with the vulnerability of the built environment at risk to predict the loss distribution.

3.2 Earthquake Risk Management Systems

Risk management platforms use different approaches to assess the vulnerability of the built environment. These systems may be classified into: (i) open source, and (ii) closed source that is not available to the public (Daniell 2009). The open source systems are listed in Table 1 with a summary of the applicable region, exposure levels, hazard types, vulnerability types, and complexity of the socioeconomic module (Daniell 2011). The loss estimation platform can be selected based on the case study and required complexity.

In the risk management systems shown in Table 1, the vulnerability can be empirical, analytical or hybrid techniques (Calvi et al. 2006). Structural criteria include the number of floors, material properties, and member dimensions. Quality criteria include the age of the structure and relative quality of construction (Daniell 2011). Socioeconomic losses are related to damage. Simple approaches for estimating social losses (Ss) include direct losses only, while complex methods for social losses (Sc) also involve indirect losses. Similarly, simple economic losses (Es) include direct losses, whereas complex approaches for estimating economic losses (Ec) also include indirect economic losses. A multi-criteria analysis can be used to decide the optimum platform for earthquake risk management (Daniell 2011).

Some of the widely used earthquake loss estimation systems in the U.S., Europe and worldwide are briefly reviewed in the following section, whereas more information related to other platforms are available in Daniell (2009).

Table 1 Earthquake loss estimation and risk mitigation platforms (Daniell 2011)

Platform	Applicable region	Exposure level	Hazard method	Vulnerability type	Socioeconomic loss	Mod.
CAPRA**	Central America	ML	D, P	Both	Unknown	Yes*
CATS	North America	ML	D	Empirical	Ec, Sc	–
DBELA	Worldwide	D, C	D, P	Analytical	Ec, Ss	Yes
ELER	Europe	D, C	D, P	Both	Es, Ss	Yes*
EmerGeo	Worldwide	ML	D	Empirical	Ec, Sc	–
EPEDAT	North America	D, C	D	Empirical	Es, Ss	–
EQRM	Australasia	D, C	D, P	Both	Es, Ss	Yes
EQSIM	Europe	D, C	D	Analytical	Sc	Yes*
Extremum	Worldwide	Ci, R, Cr	D	Empirical	Es, Ss	–
HAZ-Taiwan	Asia	ML	D, P	Analytical	Ec, Sc	–
HAZUS-MH**	North America	ML	D, P	Analytical	Ec, Sc	–
InLET	North America	D, C	D	Empirical	Es, Ss	–
LNECLOSS	Europe	D, C	D	Analytical	Ec, Ss	–
PAGER 2010	Worldwide	ML	D	Both	Es, Ss	Yes*
MAEViz**	North America	D	D, P	Both	Ec, Sc	Yes
OPENRISK	Worldwide	ML	D, P	Empirical	Ec, Ss	Yes
OSRE	Worldwide	ML	D, P	Empirical	Es	Yes
PAGER v1	Worldwide	C, R, Cr	D	Empirical	–	–
QLARM	Worldwide	C, R, Cr	D	Empirical	Es, Ss	–
QL2	Worldwide	C, R, Cr	D	Empirical	Ec, Ss	–
RADIUS	Worldwide	C	D	Empirical	Ss	Yes*

Table 1 (continued)

Platform	Applicable region	Exposure level	Hazard method	Vulnerability type	Socioeconomic loss	Mod.
REDARS	North America	D, C, R	D, P	Empirical	Ec	–
RiskScape	Australasia	D, C, R	D	Empirical	Ec, Sc	Yes*
ROVER-SAT	North America	ML	D	Empirical	–	Yes*
SAFER	Worldwide	D, C	D, P	Both	Es, Ss	–
SELENA**	Worldwide	D, C	D, P	Analytical	Es, Ss	Yes
SES & ESCENARIS	Europe	ML	D, P	Empirical	Es, Ss	–
SIGE	Europe	ML	D	Empirical	Es, Ss	–
SP-BELA**	Europe	D	D, P	Analytical	Es, Ss	Yes
StrucLoss*	Europe	D, C	D, P	Both	Ec, Ss	Ya

Exposure level: *D* related to a district; *C* city; *R* region; *Cr* country; *ML* multi-levels
Hazard method: *D* deterministic; *P* probabilistic
Socioeconomic loss: *Es* simple approach for economic; *Ec* complex; *Ss* simple social; *Sc* complex
Mod. (modification possibility): *Yes** Yes, but subject to availability
**reviewed risk management platforms

3.3　Risk Management Systems in the U.S.

The multi-hazard loss estimation system of the Federal Emergency Management Agency HAZUS combines different loss estimation engines and provides the needed visualization, Fig. 1a (Kircher et al. 1997, 2006; Whitman et al. 1997). The platform was developed for the U.S. states and Puerto Rico. In addition to the earthquake module, HAZUS includes flood and hurricane modules (FEMA 2012; Scawthorn et al. 2006; Vickery et al. 2006). HAZUS provides a platform for more informed decisions regarding disaster response planning and mitigation actions to reduce potential losses. The HAZUS Earthquake module includes an Advanced Engineering Building Module and estimation of losses through ShakeMap (Kircher et al. 2006). This enables constructing damage and loss functions that are utilized to estimate losses. Following a seismic event, earthquake ground motion data are processed by the U.S. Geological Survey to generate ShakeMaps (USGS 2018). Loss estimates recorded ground motions are more reliable for the estimation of the earthquake impacts than those obtained from prediction functions. HAZUS is commonly used to assess losses in the U.S. because of its vast databases, while it may not be applicable for other regions due to the lack of such databases or the differences in building types and construction practice. However, HAZUS was modified and adopted in some regions outside the U.S. (e.g. Shaw et al. 2007; Yeh et al. 2006).

The open source risk management system of the Mid-America Earthquake Center MAEviz is capable of developing risk mitigation strategies to minimize the impacts of seismic events Fig. 1b. MAEviz can be expanded to take into account datasets from regions outside the U.S. such as Turkey (Elnashai et al. 2008b, c). MAEviz was built upon technologies that enable accessing the risk management system in environments ranging from a web portal to a stand-alone software on PC (Myers et al. 2005; Spencer et al. 2005). Damage estimates and socioeconomic consequences can be obtained with various mitigation strategies. The damage analysis estimates the structural damage from a specific hazard. It quantified physical damage and expected overall damage in the study region. MAEviz library includes different fragility functions that represent a range of buildings with different properties (Karaman et al. 2008). MAEviz was designed to meet the evolving needs of researchers and decision-makers (Elnashai et al. 2008b).

3.4　In Europe

The seismic loss estimation using a logic tree approach SELENA was developed by NORSAR, which is a national resource center supported by the Norwegian International Centre for Geohazards. This open source system follows the HAZUS damage probability methodology. The system uses the capacity spectrum method and considers uncertainty (Lang et al. 2008; Molina et al. 2010). Calibrations were conducted to the case study of Oslo, Norway. GIS viewers such as ArcView can be implemented

to display losses. GIS viewer was also integrated with SELENA to enable the direct viewing of the results (Lang and Gutiérrez 2010).

3.5 Worldwide

The Central American Probabilistic Risk Assessment (CAPRA) is a joint project between Central American countries, including Nicaragua, Costa Rica, Honduras, Guatemala, El Salvador, Belize, and Panama. The objective is to produce a region-specific earthquake loss estimation model using a standard methodology and to provide tools through a disaster risk information platform (Anderson 2008; Cardona et al. 2010). CAPRA is an open source that considers different natural hazards by probabilistic risk evaluation using a platform that combines GIS data through a Google Map viewer-type system. The platform can be used for seismic hazard as well as other hazards types.

4 Applications of Earthquake Risk Management Process

4.1 Overview

Several risk management research projects have been conducted in different parts of the world (e.g. Ansal et al. 2009; Cagnan et al. 2008; Costa et al. 2010; Elnashai et al. 2008a; Erberik 2010; Erdik et al. 2010; Kyriakides et al. 2005; Sedan et al. 2013; Vicente et al. 2011). However, few studies were directed to the built environment in some regions such as the Middle East (e.g. Dorra et al. 2013; Moharram et al. 2008b; Mwafy et al. 2015a; Sobaih and Nazif 2012). The following brief review of the studies carried out in the U.S. and the Mediterranean region reflects the urgent need for a global risk management system to provide a platform for formulating realistic risk reduction strategies that can suit different regions' vulnerability and built environment (e.g. GEM 2013; Silva et al. 2014). Furthermore, there is a pressing need for multi-disciplinary graduate courses that prepare students and engineers for addressing complex real-life problems such as earthquake risk management. An example of such multi-disciplinary courses is also reviewed in the following sections.

4.2 Sample of Risk Assessment Studies in the U.S.

Several risk management studies have been carried out in the U.S. (Elnashai et al. 2008a, 2009; Remo and Pinter 2012). For instance, Elnashai et al. (2008a) employed the HAZUS-MH (FEMA 2012) libraries of models. Almost all HAZUS data was

over-written by more comprehensive information. Ten scenarios were used to identify the consequences of earthquakes on eight states in the Central USA. Also, liquefaction susceptibility characterization, inventory updates, and advanced social impact modeling were incorporated to provide a reliable impact assessment. The study concluded that for an earthquake originating in both the northern and southern portions of the New Madrid Seismic Zone, thousands of buildings could be damaged and tens of thousands will be without homes. Critical infrastructure will be heavily damaged. Many hospitals nearest to the rupture zone will not be able to care for patients. The transportation system will not be functioning. Emergency services and schools will be severely affected due to damage. More information related to this study is discussed by Elnashai et al. (2008a).

Elnashai et al. (2009) employed HAZUS (FEMA 2012) again but with more reliable data to determine damage to infrastructure, economic losses, and casualties (Dueñas-Osorio 2005; Genctürk et al. 2007; Kim et al. 2007; Nielson and DesRoches 2006, 2007a, b). MAEviz (2013) was also used to assess transportation and utility networks in the Central U.S. (Kim 2007). Major river crossings, dams, leaves, hazardous materials, and secondary flood risk were assessed. Additional models were utilized to determine various social vulnerabilities, social impacts, and rescue requirements. The results pointed towards considerable infrastructure damage, economic losses, and flood risk. It was also concluded that some consequences might be minimized through retrofit techniques in vulnerable areas. More information related to this comprehensive study was discussed by Elnashai et al. (2009).

4.3 In the Mediterranean Region

Several studies were undertaken to assess the earthquake risk in the Euro-Mediterranean region (e.g. Ansal et al. 2009; Cagnan et al. 2008; Costa et al. 2010; Elnashai et al. 2008a; Erberik 2010; Erdik et al. 2010; Kyriakides et al. 2005; Sedan et al. 2013; Strasser et al. 2008; Vicente et al. 2011). Cagnan et al. (2008) proposed a framework for the assessment of seismic losses in the Euro-Mediterranean region within the project Network of Research Infrastructures for European Seismology. The research project was conducted by research teams from Imperial College London, NORSAR and ETH Zurich. LossMaps provided the required information after an earthquake to European emergency response agencies, like the USGS PAGER system. A pilot application was conducted for Turkey. Loss estimations were calculated for the 1999 Kocaeli earthquake using several approaches and comparisons made with observed values.

A ground-shaking model and an inventory database were developed to assess the earthquake losses for the Greater Cairo (Moharram et al. 2008a, b). The city was divided into several census-tracts of classified building and soil characteristics, which was a fundamental step for developing a loss model. Tectonic configuration, seismicity and hazard studies for the study region were used to define the hazard. This was followed by collating geological and soil condition data using several bore-

holes to classify the soil deposits. The building inventory was prepared using ground surveys and satellite imageries. The vulnerability of representative structures, which were designed according to the design provisions and construction practices, was assessed using static nonlinear analyses. The capacity-spectrum method was used for assessing the structural performance. The results were used to develop a loss model for possible seismic events in the study area. Dorra et al. (2013) also evaluated the vulnerability of the building inventory in the Greater Cairo using available fragility functions. The vulnerability of the infrastructure networks was assessed using fragility curves. Based on the assessment of direct impacts of earthquakes, the results indicated that the losses related to buildings significantly exceeded those related to infrastructure. A macroeconomic model was proposed to account for the damage to the inventory and related indirect economic losses. It was concluded that, for extreme scenarios, indirect losses could exceed direct losses (Dorra et al. 2013).

4.4 Multi-disciplinary Course on Earthquake Risk Management

The development of a multi-disciplinary graduate course related to seismic risk management was discussed in detail by Hashash et al. (2012). The course was developed based on the MAE Center's risk management framework, as explained earlier (Elnashai and Hajjar 2006; MAE 2006). This was a unique course to expose students to advanced multi-disciplinary risk management topics that were taught by experts from various institutions and fields. The course, which was offered successfully at the University of Illinois at Urbana-Champaign, opened new opportunities in teaching the complex seismic risk management topics by the integration of engineering, information technology, and socioeconomic science in a multi-disciplinary graduate course.

Inter-disciplinary course topics were covered, including the seismic risk management framework, earthquake hazards, site effects, ground failure, structural dynamics, fragility assessment, structural retrofit, inventory technologies, socioeconomic consequences of seismic events, vulnerability of networks, and loss assessment techniques. Table 2 provides a summary of the multi-disciplinary risk management course format that was offered at the University of Illinois at Urbana-Champaign. Figure 9 also shows the distribution of the topics covered by the credit course among the main components of the risk management framework. The concepts discussed in each topic of the course were consolidated through assignments that were graded by the instructor of the topic. In addition to group work on topic assignments, students worked in groups on a comprehensive term-long capstone project related to the earthquake risk management.

The capstone project consolidated the concepts related to seismic risk management and emphasized the significance of interdisciplinary collaboration. The comprehensive capstone project focused on assessing the loss of a region and evaluating

Table 2 Different components of the risk management course offered at the University of Illinois at Urbana-champaign by instructors from different universities (Hashash et al. 2012)

Topics/activities	University and lecturer of topic/activity
Introduction to the CRM course	UIUC[2,3,6]
Overview of CRM framework	UIUC[1]
The Kocaeli earthquake	UIUC[1]
The Northridge earthquake	UIUC[1]
Comprehensive project	GT[7] and UIUC[3,6]
Probabilistic decision support	GT[8]
Social and economic impact analysis	GT[9]
Fragility analysis	TAMU[14]
Uncertainty modeling	GT[10]
Seismic hazard assessment	UIUC[3]
Site response effects and analysis	UIUC[3]
Liquefaction and permanent ground deformation	GT[11]
Structural dynamics	GT[12]
Inventory technologies	GT[13]
Term exam	UIUC[2,3,6]
Network performance	GT[7]
Network loss modeling	UTA[15]
Human-computer interaction and user perception	UIUC[4]
Introduction of grid technology	UIUC[4]
Loss estimation tool-MAEviz	UIUC[4]
Mitigation of earthquake losses	UIUC[1]
Mitigation of earthquake losses—land use policy	UIUC[5]
Seminar on the course project	UIUC[2,3,6]
Final exam	UIUC[2,3,6]

UIUC: The University of Illinois at Urbana-Champaign, Profs. [1]A. S. Elnashai, [2]J. F. Hajjar, [3]Y. Hashash, [4]B. F. Spencer, [5]R. Olshansky, and [6]Dr. A. M. Mwafy
GT: Georgia Institute of Technology, Profs. [7]R. DesRoches, [8]A. Bostrom, [9]S. French, [10]B. Ellingwood, [11]G. Rix, [12]B. Goodno, and [13]S. French
TAMU: Texas A&M University, [14]Prof. J. Bracci
UTA: University of Texas Austin, [15]Prof. T. Waller

seismic mitigation approaches. The considered systems for loss assessment were the transportation network and emergency facilities in Charleston, South Carolina, U.S. The project included three phases: (i) Rapid Assessment of losses in the central U.S., (ii) Decision Making to investigate the need for mitigation actions for the existing infrastructure, and (iii) Consequence Minimization to assess the impact of mitigation approaches on reducing seismic losses. The loss estimation tools used were HAZUS-MH and MAEviz (FEMA 2012; MAEviz 2013).
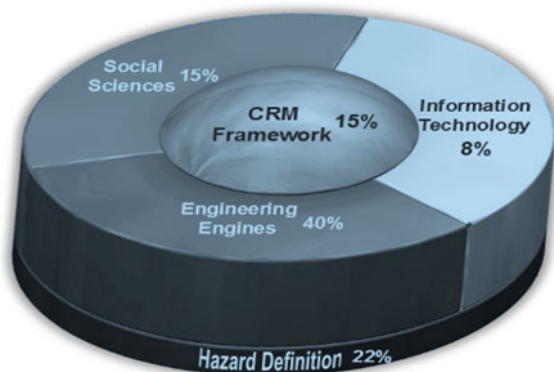
Fig. 9 The contribution of earthquake risk management components to the topics covered by the multi-disciplinary course (Hashash et al. 2012)

In the first assessment step, students learned to estimate seismic hazard using risk management platforms. Estimation of the monetary losses using HAZUS corresponds to another step of the capstone project. Afterward, each participant took a role to ensure seismic safety of the study area. Each student defined the acceptable consequences and studied the impacts of different mitigation actions to minimize the anticipated losses. Students developed their approach to compare the costs and benefits of mitigation approaches. Finally, they recommended a plan for the seismic risk mitigation of the concerned systems in the study area. The seismic risk management course provided an example of multi-disciplinary courses that prepare students for addressing complex problems such as earthquake risk management (Hashash et al. 2012).

5 Conclusions

The earthquake risk represents a challenge in several parts of the world. The high losses from previous earthquakes confirm the needs for earthquake risk management systems in earthquake-prone regions to provide plans and strategies for minimizing the seismic losses. Such plans should include geosciences, engineering, information technology, and socioeconomic sciences to deliver a complete solution to earthquake risk. This chapter provided an overview of the earthquake risk management framework, and briefly reviewed the approaches that were proposed and implemented to mitigate seismic risk in different regions.

Frameworks for seismic loss assessment and for implementing alternatives to minimize the expected losses were reviewed. A regional earthquake risk management system requires a multi-disciplinary framework that incorporates the definition of seismic hazard, physical damage, and socioeconomic consequences. Physical damage should be evaluated for the entire built environment, while long-term impacts of earthquakes should be considered when estimating socioeconomic consequences. This system can provide realistic estimates of losses and mitigation measures with associated uncertainties.

The main components seismic risk management systems were discussed in this chapter. The procedures used to assess the seismic hazard along with a case study for the seismic hazard in the UAE were briefly covered. The description of the built environment at risk, which is the most challenging aspect of performing a loss estimation study, was discussed. Innovative approaches are needed to collect the information needed for loss assessment using existing data and new technologies. A case study was presented for collecting and classifying the building inventory in a highly populated seismically vulnerable area in the UAE. Different approaches and steps for deriving vulnerability relationships were also reviewed. Vulnerability relationships describe the probability of reaching certain limit states as a function of ground motion intensity. The expected damage ratios obtained from fragility curves are multiplied by the value of the structure or an estimate of its repair costs to estimate the losses. The combined physical damage to buildings, infrastructure, transportation systems, and critical facilities should be estimated since it can produce significant consequences. A case study was presented for the development of vulnerability relationships for buildings in the UAE. This included detailed structural design and numerical idealizations of a diverse range of representative structures as well as response history analyses using different sets of input ground motions. Finally, the short- and long-term socioeconomic consequences of earthquakes were highlighted.

The importance of risk management platforms and their classification were briefly discussed. These systems provide data management and visualization that can combine the comprehensive loss assessment and mitigation data to arrive at the most suitable decision for minimizing risk. Commonly used earthquake risk management systems were also reviewed. Different applications of the risk management process were briefly discussed. Several risk management research projects have been conducted in different parts of the world. However, few studies were directed to the built environment in specific regions such as the Middle East. The presented review in this report reflected the pressing need for developing a global risk management system to assist in formulating effective risk reduction strategies in different regions. Multi-disciplinary courses that prepare students and engineers for addressing complex real-life problems such as the earthquake risk management are urgently needed. An example of such multi-disciplinary courses was briefly presented in this chapter.

References

Abdalla, J. A., & Al-Homoud, A. S. (2004). Seismic hazard assessment of United Arab Emirates and its surroundings. *Journal of Earthquake Engineering, 8,* 817–837.

Abrahamson, N. A. (2000). State of the practice of seismic hazard evaluation. In *Proceedings of GEOENG* (Vol. 1, pp. 659–685).

Aldama-Bustos, G., Bommer, J. J., Fenton, C. H., & Stafford, P. J. (2009). Probabilistic seismic hazard analysis for rock sites in the cities of Abu Dhabi, Dubai and Ra's Al Khaymah, United Arab Emirates. *Georisk: Assessment and Management of Risk for Engineered Systems and Geohazards, 3,* 1–29.

Alwaeli, W., Mwafy, A., Pilakoutas, K., & Guadagnini, M. (2017a). A methodology for defining seismic scenario-structure-based limit state criteria for rc high-rise wall buildings using net drift. *Earthquake Engineering and Structural Dynamics, 46,* 1325–1344. https://doi.org/10.1002/eqe.2858.

Alwaeli, W., Mwafy, A., Pilakoutas, K., & Guadagnini, M. (2017b). Multi-level nonlinear modeling verification scheme of RC high-rise wall buildings. *Bulletin of Earthquake Engineering, 15,* 2035–2053. https://doi.org/10.1007/s10518-016-0056-8.

Ambraseys, N. (2009). *Earthquakes in the Mediterranean and Middle East*. New York: Cambridge University Press.

Ambraseys, N. N., Douglas, J., Sigbjornsson, R., Berge-Thierry, C., Suhadolc, P., Costa, G., et al. (2004). *Dissemination of European strong-motion data, vol. 2, using strong-motion datascape navigator, CD ROM collection*. Swindon, UK: Engineering and Physical Sciences Research Council.

Anderson, E. (2008). Central American Probabilistic Risk Assessment (CAPRA): Objectives, applications and potential benefits of an open access architecture. In *Global Risk Forum*. Switzerland: GRF Davos.

Ansal, A., Akinci, A., Cultrera, G., Erdik, M., Pessina, V., Tönük, G., et al. (2009). Loss estimation in Istanbul based on deterministic earthquake scenarios of the Marmara Sea region (Turkey). *Soil Dynamics and Earthquake Engineering, 29,* 699–709.

ASCE/SEI-7. (2010). *Minimum design loads for buildings and other structures, ASCE Standard ASCE/SEI 7-10*. Reston, VA: American Society of Civil Engineers.

ATC-13. (1985). *Earthquake damage evaluation data for California*. Redwood City, CA: Applied Technology Council.

ATC. (1996). *Seismic evaluation and retrofit of concrete buildings, ATC-40*. Redwood City, CA: Applied Technology Council.

Barbat, A. H., Moya, F. Y., & Canas, J. (1996). Damage scenarios simulation for seismic risk assessment in urban zones. *Earthquake Spectra, 12,* 371–394.

Bird, J. F., & Bommer, J. J. (2004). Earthquake losses due to ground failure. *Engineering Geology, 75,* 147–179.

Bolt, B. A. (1989). The nature of earthquake ground motion. In F. Naeim (Ed.), *The seismic design handbook*. Berlin: Springer.

Bommer, J. J. (2002). Deterministic vs. probabilistic seismic hazard assessment: An exaggerated and obstructive dichotomy. *Journal of Earthquake Engineering, 6*, 43–73.

Bommer, J. J., & Crowley, H. (2006). The influence of ground-motion variability in earthquake loss modelling. *Bulletin of Earthquake Engineering, 4,* 231–248.

Bozorgnia, Y., & Campbell, K. W. (2004). Engineering characterization of ground motion. In Y. Bozorgnia & V. V. Bertero (Eds.), *Earthquake engineering from engineering seismology to performance-based engineering*. Boca Raton, Florida: CRC Press LLC.

Braga, F., Dolce, M., & Liberatore, D. (1982). A statistical study on damaged buildings and an ensuing review of the MSK-76 scale. In *Proceedings of the 7th European Conference on Earthquake Engineering*, Athens (pp 431–450).

Bruneau, M., Chang, S. E., Eguchi, R. T., Lee, G. C., O'Rourke, T. D., Reinhorn, A. M., et al. (2003). A framework to quantitatively assess and enhance the seismic resilience of communities. *Earthquake Spectra, 19*, 733–752.

Cagnan, Z., Sesetyan, K., Zulfikar, C. A. N., Demircioglu, M. B., Kariptas, C., Durukal, E., et al. (2008). Development of earthquake lossmap for Europe. *Journal of Earthquake Engineering, 12,* 37–47.

Calvi, G. M., Pinho, R., Magenes, G., Bommer, J. J., Restrepo-Velez, L. F., & Crowley, H. (2006). Development of seismic vulnerability assessment methodologies over the past 30 years. *ISET Journal of Earthquake Technology, 43*, 75–104.

Cardona, O. D., Ordaz Schroder, M. G., Reinoso, E., Yamín, L., & Barbat Barbat, H. A. (2010). Comprehensive Approach for Probabilistic Risk Assessment (CAPRA): International initiative for disaster risk management effectiveness. In *14th European Conference on Earthquake Engineering* (pp. 1–10).

Cornell, C. A. (1968). Engineering seismic risk analysis. *Bulletin of the Seismological Society of America, 58,* 1583–1606.

Costa, A. C., Sousa, M., Carvalho, A., & Coelho, E. (2010). Evaluation of seismic risk and mitigation strategies for the existing building stock: Application of LNECloss to the metropolitan area of Lisbon. *Bulletin of Earthquake Engineering, 8,* 119–134.

Daniell, J. E. (2009). *Comparison and production of open source earthquake loss assessment packages*. ROSE School, European School for Advanced Studies in Reduction of Seismic Risk.

Daniell, J. E. (2011). Open source procedure for assessment of loss using global earthquake modelling software (OPAL). *Natural Hazards and Earth System Science, 11*, 1885–1899.

Day, R. W. (2002). *Geotechnical earthquake engineering handbook*. NY: McGraw-Hill.

Di Pasquale, G., Orsini, G., & Romeo, R. W. (2005). New developments in seismic risk assessment in Italy. *Bulletin of Earthquake Engineering, 3,* 101–128.

DMA. (2013). *Abu Dhabi international building code*. Abu Dhabi, UAE: Department of Municipal Affairs.

Dolce, M., Masi, A., Marino, M., & Vona, M. (2003). Earthquake damage scenarios of the building stock of Potenza (Southern Italy) including site effects. *Bulletin of Earthquake Engineering, 1*, 115–140.

Dorra, E. M., Stafford, P. J., & Elghazouli, A. Y. (2013). Earthquake loss estimation for Greater Cairo and the national economic implications. *Bulletin of Earthquake Engineering*, 1–41.

Dowrick, D. J., & Rhoades, D. A. (1993). Damage costs for commercial and industrial property as a function of intensity in the 1987 Edgecumbe earthquake. *Earthquake Engineering & Structural Dynamics*, *22*, 869–884.

Dueñas-Osorio, L. A. (2005). *Interdependent response of networked systems to natural hazards and intentional disruptions*. Atlanta: Georgia Institute of Technology.

Dumova-Jovanoska, E. (2000). Fragility curves for reinforced concrete structures in Skopje (Macedonia) region. *Soil Dynamics and Earthquake Engineering, 19*, 455–466.

El-Hussain, I., Deif, A., Al-Jabri, K., Toksoz, N., El-Hady, S., Al-Hashmi, S., et al. (2012). Probabilistic seismic hazard maps for the sultanate of Oman. *Natural Hazards*, 1–38.

Elnashai, A. S., Cleveland, L. J., Jefferson, T., & Harrald, J. (2008a). *Impact of earthquakes on the Central USA*. Mid-America earthquake center report 08-02. Urbana, IL: University of Illinois at Urbana-Champaign.

Elnashai, A. S., & Di Sarno, L. (2015). *Fundamentals of earthquake engineering: From source to fragility* (2nd ed.). West Sussex, U.K.: Wiley.

Elnashai, A. S., & Hajjar, J. F. (2006). Mid-America Earthquake (MAE) center program in consequence-based risk management. In: *Eighth National Conference on Earthquake Engineering, 100th Anniversary Earthquake Conference: Managing Risk in Earthquake Country*, San Francisco, California. Oakland: Earthquake Engineering Research Institute.

Elnashai, A. S., Hampton, S., Karaman, H., Lee, J. S., Mclaren, T., Myers, J., et al. (2008b). Overview and applications of Maeviz-Hazturk 2007. *Journal of Earthquake Engineering, 12*, 100–108.

Elnashai, A. S., Hampton, S., Lee, J. S., McLaren, T., Myers, J. D., Navarro, C., et al. (2008c). Architectural overview of MAEviz–HAZTURK. *Journal of Earthquake Engineering, 12*, 92–99.

Elnashai, A. S., Jefferson, T., Fiedrich, F., Cleveland, L. J., & Gress, T. (2009). *Impact of New Madrid seismic zone earthquakes on the central USA* (Vol. I). MAE center report.

Elnashai, A. S., & Mwafy, A. (2008). Seismic response and design. In G. Parke & N. Hewson (Eds.), *ICE manual of bridge engineering* (2nd ed). London, UK: Thomas Telford Ltd., Institution of Civil Engineers. www.icevirtuallibrary.com and www.amazon.co.uk.

Elnashai, A. S., Papanikolaou, V., & Lee, D. (2012). *Zeus-NL—A system for inelastic analysis of structures*. Urbana-Champaign, Urbana, IL: User Manual Mid-America Earthquake Center, University of Illinois.

Erberik, M. A. (2010). Seismic risk assessment of masonry buildings in Istanbul for effective risk mitigation. *Earthquake Spectra, 26,* 967–982.

Erdik, M., Sesetyan, K., Demircioglu, M., Hancilar, U., Zulfikar, C., Cakti, E., et al. (2010). Rapid earthquake hazard and loss assessment for Euro-Mediterranean region. *Acta Geophysica, 58*, 855–892.

FEMA. (2012). *HAZUS-MH 2.1 technical manual—Multi-hazard loss estimation methodology-earthquake model*. Washington, D.C.: Federal Emergency Management Agency.

French, S. P. (1995). Damage to urban infrastructure and other public property from the 1989 Loma Prieta (California) earthquake. *Disasters, 19*, 57–67.

French, S. P. (2005). Estimating the social and economic consequences of earthquakes and other natural hazards. In *46th ACSP Annual Conference*, October 30, Kansas City, Missouri (pp. 1–6).

French, S. P., Lee, D., & Anderson, K. (2010). Estimating the social and economic consequences of natural hazards: Fiscal impact example. *Natural Hazards Review, 11,* 49–57.

French, S. P., & Muthukumar, S. (2006). Advanced technologies for earthquake risk inventories. *Journal of Earthquake Engineering, 10,* 207–236.

Gardoni, P., & LaFave, J. M. (2016). Multi-hazard approaches to civil infrastructure engineering: Mitigating risks and promoting resilence. In *Multi-hazard approaches to civil infrastructure engineering* (pp. 3–12). Berlin: Springer.

GEM. (2013). *Global earthquake model*. GEM Foundation. http://www.globalquakemodel.org/. Accessed November 1, 2013.

Genctürk, B., Elnashai, A., & Song, J. (2007). *Improved fragility relationships for populations of buildings based on inelastic response Urbana (IL)*. Illinois: Department of Civil and Environmental Engineering, University of Illinois at Urbana-Champaign.

Giovinazzi, S., & Lagomarsino, S. A. (2004). Macroseismic method for the vulnerability assessment of buildings. In: *13th World Conference on Earthquake Engineering*, Vancouver, BC, Canada (pp. 1–6).

Hancock, J., & Bommer, J. J. (2006). A state-of-knowledge review of the influence of strong-motion duration on structural damage. *Earthquake Spectra, 22,* 827–845.

Hanks, T. C., & Cornell, C. A. (1994). Probabilistic seismic hazard analysis: A beginner's guide. In: *Proceedings of the Fifth Symposium on Current Issues Related to Nuclear Power Plant Structures, Equipment and Piping* (p. 1).

Hashash, Y. M. A., Mwafy, A., Elnashai, A. S., & Hajjar, J. F. (2012). Development of a multi-disciplinary graduate course on consequence-based earthquake risk management. *International Journal of Continuing Engineering Education and Life Long Learning, 22*, 127–147.

Irfan, M., El-Emam, M., Khan, Z., & Abdalla, J. (2013). *Local site effects on seismic ground response of Dubai-Sharjah metropolitan area*. Paper presented at the GeoCongress.

Jeong, S. H., Mwafy, A., & Elnashai, A. (2012). Probabilistic seismic performance assessment of code-compliant multi-story RC buildings. *Engineering Structures, 34,* 527–537. https://doi.org/10.1016/j.engstruct.2011.10.019.

Ji, J., Elnashai, A. S., & Kuchma, D. A. (2007). An analytical framework for seismic fragility analysis of RC high-rise buildings. *Engineering Structures, 29,* 3197–3209.

Ji, J., Elnashai, A. S., & Kuchma, D. A. (2009). Seismic fragility relationships of reinforced concrete high-rise buildings. *The Structural Design of Tall and Special Buildings, 18,* 259–277.

Kappos, A., Stylianidis, K., & Pitilakis, K. (1998). Development of seismic risk scenarios based on a hybrid method of vulnerability assessment. *Natural Hazards, 17,* 177–192.

Karaman, H., Şahin, M., & Elnashai, A. S. (2008). Earthquake loss assessment features of Maeviz-Istanbul (Hazturk). *Journal of Earthquake Engineering, 12*, 175–186.

Kim, Y. S. (2007). *Seismic loss assessment and mitigation of critical urban infrastructure systems*. Illinois: University of Illinois at Urbana-Champaign.

Kim, Y. S., Spencer, B. F., Song, J., Elnashai, A. S., & Stokes, T. (2007). *Seismic performance assessment of interdependent lifeline systems*, CD Release 07-16. Illinois: Mid-America Earthquake Center, University of Illinois at Urbana-Champaign.

Kircher, C. A., Nassar, A. A., Kustu, O., & Holmes, W. T. (1997). Development of building damage functions for earthquake loss estimation. *Earthquake Spectra, 13,* 663–682.

Kircher, C. A., Whitman, R. V., & Holmes, W. T. (2006). HAZUS earthquake loss estimation methods. *Natural Hazards Review, 7,* 45–59.

Kramer, S. L. (1996). *Geotechnical earthquake engineering*. New Jersey: Prentice Hall.

Kwon, O. S., & Elnashai, A. S. (2006). The effect of material and ground motion uncertainty on the seismic vulnerability curves of RC structure. *Engineering Structures, 28,* 289–303.

Kyriakides, N., Pilakoutas, K., & Kythreoti, S. (2005). Earthquake risk assessment. Case study: Cyprus. In*: IABSE Symposium Report, 2005* (pp. 67–74). International Association for Bridge and Structural Engineering.

Lang, D. H., & Gutiérrez, F. V. (2010). RISe—A Google Earth-based tool to illustrate seismic risk and loss results. *Earthquake Spectra, 26*, 295–307.

Lang, D. H., Molina-Palacios, S., & Lindholm, C. D. (2008). Towards near-real-time damage estimation using a CSM-based tool for seismic risk assessment. *Journal of Earthquake Engineering, 12,* 199–210.

MAE. (2006). Mid-America Earthquake Center Ninth Year Annual Report.

MAEviz. (2013). *MAE Center seismic loss assessment system*. Available at http://mae.cee.illinois.edu/software/software_maeviz.html, last access: October 2013.

Masi, A. (2003). Seismic vulnerability assessment of gravity load designed R/C frames. *Bulletin of Earthquake Engineering, 1,* 371–395.

Mileti, D. (1999). *Disasters by design: A reassessment of natural hazards in the United States*. Washington: National Academies Press.

Moehle, J., & Deierlein, G. G. (2004). A framework methodology for performance-based earthquake engineering. In *Proceedings of the 13th World Conference on Earthquake Engineering* (pp. 3812–3814).

Moharram, A. M., Elghazouli, A. Y., & Bommer, J. J. (2008a). Scenario-based earthquake loss estimation for the city of Cairo, Egypt. *Georisk, 2,* 92–112.

Moharram, A. M., Elghazouli, A. Y., & Bommer, J. J. (2008b). A framework for a seismic risk model for Greater Cairo. *Soil Dynamics and Earthquake Engineering, 28,* 795–811.

Molina, S., Lang, D., & Lindholm, C. (2010). SELENA—An open-source tool for seismic risk and loss assessment using a logic tree computation procedure. *Computers & Geosciences, 36*, 257–269.

Mwafy, A. (2012a). Analytically-derived fragility relationships for the modern high-rise buildings in the UAE. *The Structural Design of Tall and Special Buildings, 21,* 824–843. https://doi.org/10.1002/tal.642.

Mwafy, A. (2012b). Classification and idealization of the building stock in the UAE for earthquake loss estimation. In: *15th World Conference on Earthquake Engineering*, 24–28 September, Lisbon, Portugal. International Association for Earthquake Engineering.

Mwafy, A. (2013). Use of overstrength and inelastic response in seismic design. *Structures and Buildings, The Institution of Civil Engineers (ICE), 166,* 282–297. https://doi.org/10.1680/stbu.11.00022.

Mwafy, A., Ashri, A., & Issa, A. (2015a). Probabilistic vulnerability assessment of the building inventory in an extended seismically active area in the UAE. In *3rd International Conference on Engineering Geophysics*, 15–18 November, Al Ain, UAE.

Mwafy, A., & Elkholy, S. (2017). Performance assessment and prioritization of mitigation approaches for pre-seismic code structures. *Advances in Structural Engineering, 20,* 917–939. https://doi.org/10.1177/1369433216667188.

Mwafy, A., & Elnashai, A. S. (2001). Static pushover versus dynamic collapse analysis of RC buildings. *Engineering Structures, 23,* 407–424. https://doi.org/10.1016/s0141-0296(00)00068-7.

Mwafy, A., Elnashai, A. S., Sigbjornsson, R., & Salama, A. (2006). Significance of severe distant and moderate close earthquakes on design and behavior of tall buildings. *The Structural Design of Tall and Special Buildings, 15,* 391–416. https://doi.org/10.1002/tal.300.

Mwafy, A., Hussain, N., & El-Sawy, K. (2015b). Seismic performance and cost-effectiveness of high-rise buildings with increasing concrete strength. *The Structural Design of Tall and Special Buildings, 24,* 257–279. https://doi.org/10.1002/tal.1165.

Mwafy, A., & Issa, A. (2015). Vulnerability assessment of seismic retrofit measures for frame and wall pre-code buildings. In *Eighth International Structural Engineering and Construction Conference*, 23–28 November, Sydney, Australia.

Mwafy, A., & Khalifa, S. (2017). Effect of vertical structural irregularity on seismic design of tall buildings. *The Structural Design of Tall and Special Buildings, 26,* e1399. https://doi.org/10.1002/tal.1399.

Myers, J., Spencer, B., Jr., & Navarro, C. (2005). Cyberinfrastructure in support of earthquake loss assessment: The MAEviz cyberenvironment. In *Proceedings of the First International Workshop on an Earthquake Loss Estimation Program for Turkey*, HAZTURK-2005, Istanbul, Turkey.

Nielson, B. G., & DesRoches, R. (2006). Influence of modeling assumptions on the seismic response of multi-span simply supported steel girder bridges in moderate seismic zones. *Engineering Structures, 28,* 1083–1092.

Nielson, B. G., & DesRoches, R. (2007a). Analytical seismic fragility curves for typical bridges in the central and southeastern United States. *Earthquake Spectra, 23,* 615–633.

Nielson, B. G., & DesRoches, R. (2007b). Seismic fragility methodology for highway bridges using a component level approach. *Earthquake Engineering & Structural Dynamics, 36,* 823–839.

NMC. (2013). *UAE yearbook*. Dubai, United Arab Emirates: Jumeirah Beach Residence.

Orsini, G. (1999). A model for buildings' vulnerability assessment using the parameterless scale of seismic intensity (PSI). *Earthquake Spectra, 15*, 463–483.

Pascucci, V., Free, M., & Lubkowski, Z. (2008). Seismic hazard and seismic design requirements for the Arabian Peninsula region. In *The 14th World Conference on Earthquake Engineering*.

PEER. (2015). *PEER NGA database*. Berkeley, California: Pacific Earthquake Engineering Research Center, University of California. http://peer.berkeley.edu/nga. Accessed June 2014.

Peiris, N., Free, M., Lubkowski, Z., & Hussein, A. (2006) Seismic hazard and seismic design requirements for the Arabian Gulf region. In *First European Conference on Earthquake Engineering and Seismology* (pp. 4–6).

Porter, K. A. (2003). An overview of PEER's performance-based earthquake engineering methodology. In *Conference on Applications of Statistics and Probability in Civil Engineering* (*ICASP9*) (pp. 6–9). San Francisco, CA: Civil Engineering Risk and Reliability Association (CERRA).

Reiter, L. (1990). *Earthquake hazard analysis: Issues and insights*. New York: Columbia University Press.

Remo, J. W., & Pinter, N. (2012). Hazus-MH earthquake modeling in the central USA. *Natural Hazards, 63,* 1055–1081.

Rossetto, T., & Elnashai, A. (2003). Derivation of vulnerability functions for European-type RC structures based on observational data. *Engineering Structures, 25,* 1241–1263.

Rossetto, T., & Elnashai, A. (2005). A new analytical procedure for the derivation of displacement-based vulnerability curves for populations of RC structures. *Engineering Structures, 27,* 397–409.

Rota, M., Penna, A., & Strobbia, C. (2008). Processing Italian damage data to derive typological fragility curves. *Soil Dynamics and Earthquake Engineering, 28,* 933–947.

Scawthorn, C., Flores, P., Blais, N., Seligson, H., Tate, E., Chang, S., et al. (2006). HAZUS-MH flood loss estimation methodology. II. Damage and loss assessment. *Natural Hazards Review, 7*, 72–81.

Scawthorn, C., Iemura, H., & Yamada, Y. (1981). Seismic damage estimation for low-and mid-rise buildings in Japan. *Earthquake Engineering & Structural Dynamics, 9,* 93–115.

Sedan, O., Negulescu, C., Terrier, M., Roulle, A., Winter, T., & Bertil, D. (2013). Armagedom—A tool for seismic risk assessment illustrated with applications. *Journal of Earthquake Engineering, 17,* 253–281.

Shama, A. A. (2011). Site specific probabilistic seismic hazard analysis at Dubai Creek on the west coast of UAE. *Earthquake Engineering and Engineering Vibration, 10,* 143–152.

Shaw, D., Yeh, C. H., Jean, W. Y., Loh, C. H., & Kuo, Y. L. (2007). A probabilistic seismic risk analysis of building losses in Taipei: An application of Haz-Taiwan with its pre-processor and post-processor. *Journal of the Chinese Institute of Engineers, 30,* 289–297.

Shinozuka, M., Chang, S. E., Eguchi, R. T., Abrams, D. P., Hwang, H. H., & Rose, A. (1997). Advances in earthquake loss estimation and application to Memphis, Tennessee. *Earthquake Spectra, 13,* 739–758.

Sigbjornsson, R., & Elnashai, A. S. (2006). Hazard assessment of Dubai, United Arab Emirates, for close and distant earthquakes. *Journal of Earthquake Engineering, 10,* 749–773.

Silva, V., Crowley, H., Pagani, M., Monelli, D., & Pinho, R. (2014). Development of the OpenQuake engine, the global earthquake model's open-source software for seismic risk assessment. *Natural Hazards, 72,* 1409–1427.

Singhal, A., & Kiremidjian, A. S. (1996). Method for probabilistic evaluation of seismic structural damage. *Journal of Structural Engineering, 122,* 1459–1467.

Singhal, A., & Kiremidjian, A. S. (1998). Bayesian updating of fragilities with application to RC frames. *Journal of Structural Engineering, 124,* 922–929.

Sobaih, M. E., & Nazif, M. A. (2012). A proposed methodology for seismic risk evaluation of existing reinforced school buildings. *HBRC Journal, 8,* 204–211.

Spencer, B., Myers, J., Yang, G., & Navarro, C. (2005). MAEviz/NEESgrid and applications overview. In *Proceedings of the First International Workshop on an Earthquake Loss Estimation Program for Turkey*, HAZTURK-2005, Istanbul, Turkey.

Strasser, F. O., Bommer, J. J., Şeşetyan, K., Erdik, M., Çağnan, Z., Irizarry, J., et al. (2008). A comparative study of European earthquake loss estimation tools for a scenario in Istanbul. *Journal of Earthquake Engineering, 12,* 246–256.

Tierney, K. J., Lindell, M. K., & Perry, R. W. (2001). *Facing the unexpected: Disaster preparedness and response in the United States*. Washington: Joseph Henry Press.

USGS. (2018). *Earthquake hazards program*. United States Geological Survey (USGS). http://earthquake.usgs.gov/. Accessed May 1, 2018.

Vicente, R., Parodi, S., Lagomarsino, S., Varum, H., & Silva, J. M. (2011). Seismic vulnerability and risk assessment: Case study of the historic city centre of Coimbra. *Portugal Bulletin of Earthquake Engineering, 9,* 1067–1096.

Vickery, P. J., Skerlj, P. F., Lin, J., Twisdale, L. A., Jr., Young, M. A., Lavelle, F. M. (2006). HAZUS-MH hurricane model methodology. II: Damage and loss estimation. *Natural Hazards Review, 7*, 94–103.

Wang, Z. (2011). Seismic risk assessment and application in the Central United States. *Geo-Risk*, 1020–1027. https://doi.org/10.1061/41183(418)111.

Webb, G. R., Tierney, K. J., & Dahlhamer, J. M. (2000). Businesses and disasters: Empirical patterns and unanswered questions. *Natural Hazards Review, 1,* 83–90.

Webb, G. R., Tierney, K. J., & Dahlhamer, J. M. (2002). Predicting long-term business recovery from disaster: A comparison of the Loma Prieta earthquake and Hurricane Andrew. *Global Environmental Change Part B: Environmental Hazards, 4,* 45–58.

Wen, Y. K., & Ellingwood, B. R. (2005). The role of fragility assessment in consequence-based engineering. *Earthquake Spectra, 21,* 861–877.

Wen, Y. K., Ellingwood, B. R., Veneziano, D., & Bracci, J. (2003). *Uncertainty modeling in earthquake engineering*. Urbana, IL: University of Illinois at Urbana-Champaign.

Whitman, R. V., Anagnos, T., Kircher, C. A., Lagorio, H. J., Lawson, R. S., & Schneider, P. (1997). Development of a national earthquake loss estimation methodology. *Earthquake Spectra, 13,* 643–661.

Whitman, R. V., Reed, J. W., & Hong, S. (1973). Earthquake damage probability matrices. In *Proceedings of the Fifth World Conference on Earthquake Engineering* (pp. 2540–2531). Rome, Italy: Palazzo Dei Congresi.

Yakut, A. (2004). Preliminary seismic performance assessment procedure for existing RC buildings. *Engineering Structures, 26,* 1447–1461.

Yeh, C.-H., Loh, C.-H., & Tsai, K.-C. (2006). Overview of Taiwan earthquake loss estimation system. *Natural Hazards, 37,* 23–37.

Making Homes More Resilient to Flooding: A New Hybrid Approach

Taiwo J. Adedeji, David G. Proverbs, Victor O. Oladokun and Hong Xiao

1 Introduction

The impact of flooding on the built environment and particularly residential buildings, is severe and far-reaching. The damage caused to buildings through even fairly shallow flooding can take many months to repair and, in the case of deep water flooding, can cause extensive damage to the structure (ODPM 2003). These residential buildings represent a large part of the built environment and play a vital role in meeting one of the basic human needs of providing shelter (Sirochmanova et al. 2016). In Europe, about 75% of the building stock is residential property (Ecofys and BioIntelligence 2010). Due to factors such as urbanization, change in land use patterns and climate change, the number of buildings exposed to flood risk is increasing. According to figures from the Environment Agency (2014), it is estimated that there are 5.4 million properties at risk of flooding in England. Of these, 2.4 million are at risk from rivers or the sea, 3 million from surface water and 600,000 are at risk from both. With this growing flood risk, the need to address these challenges becomes more apparent (Adedeji et al. 2018).

In recent years, UK flood risk management policy has shifted towards recognising that it is no longer considered feasible to prevent all flooding, and instead, efforts should be towards improved management as captured under the 'living with water' philosophy (DEFRA 2005). This approach entails recognising that some flooding will occur and adopting approaches that help to reduce the impacts and improves resilience (Oladokun et al. 2017). For many homes, this largely depends on how well

---

T. J. Adedeji · D. G. Proverbs (✉) · H. Xiao
Faculty of Computing, Engineering and the Built Environment, Birmingham City University, Birmingham, UK
e-mail: David.Proverbs@bcu.ac.uk

V. O. Oladokun
Industrial and Production Engineering, University of Ibadan, Ibadan, Nigeria

prepared the property and homeowners are before a flood event; how these respond and react during flooding; and how they recover after the flood event.

A number of innovative approaches have been developed towards reducing the impacts of flooding on homes (Oladokun et al. 2017). At the outset, structural measures such as flood defences, dams and levees were put in place to provide protection against flooding (Proverbs and Lamond 2017). However, despite the huge investment in structural approaches and engineering measures, flooding still remains as one of the greatest threats to buildings and the wellbeing of humans. More recently, the concept of flood resilience has gained wide recognition in the domain of flood risk management (Oladokun et al. 2017). The concept focuses on the development and adaptation of buildings to the risk of flooding (Wingfield et al. 2005; Kazmierczak and Connelly 2011). This involves constructing buildings that are resilient to flood risk using features that prevent flood damage to the components of a building, such as the sub-structure and super structure, services, fixtures and fittings and the effect that flood water has on them (Jha et al. 2012). Resilient design also ensures that items such as electric sockets and service meters are raised above expected flood levels and the use of resilient materials that do not deform or disintegrate on contact with floodwater.

Much has been done and put in place to ensure the quick recovery of buildings from the impact of flooding through the use of property level flood protection (Lamond, et al. 2016). Meanwhile as important as these measures are, their efficacies to a large extent depends on the characteristics (such as socio-economic factors) of the residents. Humans will continue to interact with buildings and so it becomes essential to recognise the human factors that promote resilience against the impact of flooding within the building. For example, a homeowner's decision to choose a lower flood insurance scheme or exclude content insurance based on their financial capacity will impact the household resilience. Therefore, factors such as financial capacity, level of flood awareness, exposure rate and previous flood experience will influence decisions taken on the level of resilience in the building. That is, the residents have roles to play in determining the degree of resilience present in a building. While much of the research on property flooding is focused on either making the building or the human components resilient (ODPM 2003; Joseph et al. 2015), it is essential to consider both components concurrently in order to improve the resilience of the household. This chapter attempts to further expound the property level flood resilience framework developed earlier by the authors (Adedeji et al. 2018) and then goes on to describe how this framework could be used in practice by a range of stakeholders to improve resilience.

The following narrative explains this in four main sections. The first section discusses the concept of resilience as viewed by disciplines relevant for its application in the purview of property level flood resilience; the following section assesses the impacts of flooding on buildings and humans—which is key to this discourse as the essence of resilience is to minimise flood risk exposure and damage caused; the subse-

quent section focuses on the flood resilience measures within the building alongside the factors that convey resilience in human terms. Finally, the implications of the framework as a tool for use by stakeholders, such as homeowners, property experts, surveyors and insurers, in practice are then described before drawing conclusions.

2 The Concept of Resilience

The concept of resilience focuses on a system's ability to deal with disturbance, surprise and change. The field of resilience is broad and diverse (VanBreda 2001). Areas of application include ecosystem stability (Holling 1973; Gunderson 2010), engineering infrastructure (Tierney and Bruneau 2007), psychology (Fletcher and Sarkar 2013), the behavioural sciences (Norris 2010) and disaster risk reduction (Cutter et al. 2008). In spite of its diversity and lack of specificity in meaning, it has emerged as a fusion of ideas from multiple disciplinary traditions which has encouraged the liberal and enthusiastic use of the concept by policy makers, practitioners and academics (McAslan 2010).

Consequently, the multidisciplinary nature makes the concept a convenient tool to address how both components (building and human) respond and stay fit in the face of adversity. Different disciplines focus on each of the components, with psychological resilience focusing on understanding the behaviour of residents while engineering resilience focusing on building resilience (Adedeji et al. 2018).

2.1 Psychological Resilience

The American Psychological Association has defined resilience as the process of adapting well in the face of adversity, trauma or substantial sources of stress (American Psychological Association 2014). The interest of psychological resilience is mostly human (Adedeji et al. 2018). Moreover, with the exposure to adversity perceived as universal human experience (Fikretoglu and McCreary 2012) and much literature published on the negative psychological impact of experiencing these adversities, the phenomenon of psychological resilience tends to pay attention to the coping capacity, which leads to positive adjustment and healthy developments, even in the face of these massive adversities (Neria et al. 2008). The positive adjustment entails the factors that enable certain individuals to withstand the pressure they experience in their lives (Fletcher and Sarkar 2013; Graber et al. 2015).

Over the past two decades, psychologists' understanding of the way humans function in challenging situations has developed rapidly (Fletcher and Sarkar, 2013). Currently research on human resilience is focused on understanding how individuals overcome the adversities they experience rather than trying to identify protective factors (such as traits) (Luthar et al. 2000). This has prompted researchers to study the characteristics of individuals who thrived while living in difficult circumstances

(Werner and Smith 1992). In the psychology research literature, numerous definitions of resilience have been offered with majority of the definitions centred on two core concepts: adversity and positive adaptation (Fletcher and Sarkar 2013). This makes its application to flooding appropriately forward-looking and result oriented.

2.2 Engineering Resilience

In engineering, the interest in resilience is to ensure stability and guarantee functionality in engineering systems that are confronted by disturbances, which are often associated with low chances of failures or, in the case of failure, quick recovery to functional state (Wang and Blackmore 2009). It is however defined as the ability to maintain stability (Holling 1973). This engineering resilience concept comprises of resistance to, and recovery from disturbances albeit in measurement terms, the focus is apparently on recovery. The sooner the system's functionality is restored, the better the resilience (Hashimoto et al. 1982; Hollnagel et al. 2008).

For instance, the building is an engineering system with different subsystems like the structural, electrical, mechanical parts put together to service the residents. Engineering resilience thus emphasizes the ability of these different parts to bounce back to the normal state when displaced from their position of servicing the residents. Therefore, the concept of engineering resilience provides a rigorous yet valuable way of formalizing resilience which has been helpful in setting up appropriate indicators, standards and norms for infrastructure. According to Bruneau et al. (2003), this kind of resilience depends on four properties: robustness, which reflects the physical strength to cope in the presence of a disturbance without functional degradation; redundancy, which represents the degree to which system's components can be substituted; resourcefulness, which stands for the capacity to recognise problems and assign needed resources; and rapidity, which denotes the capacity to restore the system in good time (Bruneau et al. 2003). However, in an attempt to measure these properties, some basic engineering attributes for fail-safe design, such as predictability, constancy and efficiency, have become the principal focus. According to de Bruijn et al. (2017), sustaining a function and the maintenance of an existing situation are fundamentals to engineering resilience.

3 The Impacts of Flooding

To appreciate resilience, it is important to know what we are building resilience against. The impact of flooding on properties does not affect the building and its contents alone but also the residents since the buildings are designed to accommodate humans. While there is a wide-ranging debatable opinion that flood only causes damage to property, the devastating impact is seen on lives too (Wingfield et al. 2005). Flooding has the potential to inflict both physical and emotional distress on

people (Wingfield et al. 2005). The flood depth, flood duration and the presence of contaminants in the flood water are the main characteristics of flooding that determine the degree of damage caused both to building and humans.. However, the interim guidance for improving the flood resistance of domestic and small business buildings published by the Office of the Deputy Prime Minister reports that the most important aspect to remember is that the damage to property is only a minor part of the true human cost of a flood (ODPM 2003). It identifies the stress that accompanies losing personal possessions, having to live in temporary accommodation while repairs are being done and also the trauma of cleaning up and restoration as huge. Flood losses, both to property and lives, have been categorized as direct and indirect with further classification as tangible and intangible based on whether or not these losses can be assessed in monetary values (Joseph 2014).

3.1 Direct and Indirect Impacts

Direct damage refers to the physical damage by floods to buildings and lives while indirect damage refers to the losses that occur due to the disruption of some activity by the flood, referred to as damage caused by secondary effects. Smith and Ward (1998) argued that direct losses to floods happen immediately after the event as a result of the physical contact of the flood waters with damageable property and with human. However, indirect losses which are less easily connected to the flood disaster and often operate on long time scales, may be equally, or even more important. In order to understand what we are building resilience against, that is the flood impacts, it is essential to view the different category of impacts to buildings and humans. Meanwhile, the losses to each of these components, buildings and humans, require a different mitigation approach (Adedeji et al. 2018) and this is discussed in a latter section. Next section presents details on the classification of these impacts.

3.2 Impacts on Buildings

During floods, water can gain entry into building causing damage to structures, electrical installations, floors and walls, and partial or total destruction of any other item that comes in contact with the water. Even while some furniture, fittings and personal possessions may dry out after being exposed to floodwater, they may be permanently stained (ODPM 2003). This physical damage to buildings and their contents is a direct impact which is considered tangible because it can be measured in terms of replacement or reinstatement cost (Queensland Government 2002). Meanwhile, the other forms of tangible but indirect impacts include the loss of building value, loss of utility supplies like electricity, water and gas which could be fixed. Loss of irreplaceable items like memorabilia is regarded as direct intangible cost. These impacts are shown in Fig. 1 (Table 1).
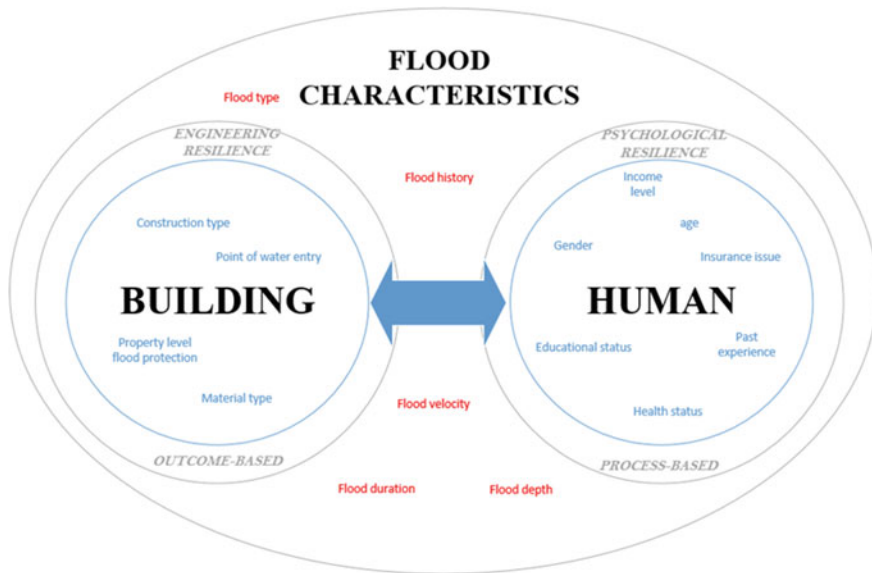
Fig. 1 The property level flood resilience framework. *Source* Adedeji et al. 2018

Table 1 Classification of the flood impacts to the building and human components

	Building		Human	
	Tangible	Intangible	Tangible	Intangible
Direct	Physical damage to building and contents	Loss of irreplaceable items Loss of memorabilia		Injuries and fatalities Hypothermia Ill health
Indirect	Loss of house value Loss of utility supplies (like electricity, gas, water)		Increase travel cost Increase in insurance premium Repair costs	Stress Anxiety Disruption of daily life and normal activities Inconvenience of post flood recovery

Source Adapted from Joseph (2014)

3.3   Impacts on Human Lives

For humans, some of the key direct costs such as loss of life or the resultant ill health of the survivors and also the economic losses are intangible. Also, much of the indirect impact of a flood for a residential property owner will be intangible as it affects their quality of life (Lamond 2008). These indirect, intangible impacts include the

disruption caused to daily life and normal activities, being upset about damage caused to buildings or psychological disorder in the case of recurrent flooding. However, the rise in insurance premium, increased travel cost and cost of reinstating the property are indirect, tangible impacts.

The impacts of flooding on lives, both direct and indirect, is hinged on the combination of different types of impact. According to (McNulty and Rennick, 2015) these combinations are health, social and financial impacts. The effects on health has been widely regarded as an important dimension of the human impact of flooding (Tapsell et al. 2002). Meanwhile, (McNulty and Rennick 2015) have split the effect on health into physical (direct impact) and psychological (indirect) for easy differentiation with 39% of people suffering from physical effects and 67% on their emotional health (Pitt 2008). In a study carried out by Few et al. (2004), the physical health impacts were recognized as fatalities, injuries and the occurrence of disease. Psychological health issues include clinical depression and anxiety, acute stress and post-traumatic stress disorder (McNulty and Rennick 2015). Also, the discomfort caused due to the disruption to domestic life where essential services such as electricity and water supplies are cut off (Lamond 2008) and also children inability to attend school, could be a huge psychological blow on the occupants.

4 Building Resilience Against the Impacts of Flood: A Hybrid Approach

So to think of property flood resilience is to think of minimising the flood risk exposure to both components, the building and its residents. Meanwhile, due to the difference in their nature, each of these components requires a different approach to deal with the pressure that comes from flooding and its impacts. The building is static in nature, and does not have a mind of its own except the design and structure that the engineers and developers put in place (Adedeji et al. 2018). Therefore, its limit is defined by the design specifications. But the human component is dynamic and the flexibility of the human mind and body allows adaptive responses to the impact of flooding. The authors (Adedeji et al. 2018) developed a conceptual framework for property level flood resilience that depicts how these components intend to get protection against flood impact. The framework is described in the following section and the resilience concept adopted for each component is further discussed.

4.1 The Property Level Flood Resilience Framework

The property level flood resilience framework (Fig. 1) was developed to determine the level of protection that is present in the key components. The framework illustrated both components being shielded by an outer circle against the disturbance in

the environment, flood characteristics, in which they are placed. The outer circles represent the resilience concepts and the approaches adopted.

For the building, the engineering resilience is applied with an outcome-based approach which focused on what can be done to protect the building and its contents (Eriksen and Kelly 2007). While for the human, the psychological resilience was applied using the process-based approach which emphasises what should be done to strengthen the residents' capacity to respond and adapt to flood risk exposure. The double-pointed arrow in the centre between the components indicates their interaction. This implies that the decision taken to improve the resilience of one component will affect the other (Adedeji et al. 2018).

4.1.1   The Resilience of the Building Component

For safeguarding the building component, the framework adopted the concept of engineering resilience. This conception corresponds to inanimate, physical objects which can either withstand stress or recover by returning to the equilibrium state of functioning (Kallaos et al. 2014). This resonates with Garvin's (2012) report, that engineering resilience is increasingly being applied in the purview of architecture and building technology. This involves the adoption of flood resilient strategy and technologies to adapt or construct buildings that remain intact or unaffected by flood water (Garvin 2012). That is, equipping the building with the ability to deal with the flood risk prior to flood event, the capacity to cope during flooding and also quick recovery at the aftermath. A lot has been done to ensure the quick recovery of buildings in the event of flooding such as the norms of engineering designs, materials, construction techniques and retrofit strategies developed to protect the physical integrity of building, enhance its ability to withstand flooding and reduce its many impacts described in previous section (Kallaos et al. 2014). The adoption of property-level flood risk adaptation (PLFRA) measures is another means of enhancing the building recovery capacity. It is a process in which physical improvements are made to the building after it has been flooded either through resistance measures (preventing flood water from entering) or resilience measures (minimising the damage when flood water enters) (Joseph et al. 2011). Investing in PLFRA measures has received greater attention in recent years (Kreibich et al. 2005). The outcome-based approach is centred on the resilience outcome obtained through the performance of these strategies.

While these designs and engineering standards are intended to protect the building, they are not sufficient to convene resilience of the entire system of the flooding, made of both the building and its residents (Kallaos et al. 2014). Consequently, this conception does not apply well for complex, dynamic systems and networks such as the human component and societies where recovery does not necessarily imply returning to the initial state (Kallaos et al. 2014). Therefore, to make buildings more resilient, the resilience of the residents must be considered and this requires a different approach because individuals respond to disturbance in different ways.

4.1.2 The Resilience of the Human Component

For the resident, experiencing a flood event is a primary cause of stress, therefore, it is important to realise that the stress and strain which comes as a result of cleaning up of homes and recovery may also be a problem (Lock et al. 2012). This could have profound effects on well-being and mental health of residents that may persist over extended periods of time (Stanke et al. 2012). Notwithstanding, some people have shown to be resilient and cope well with being flooded despite being distressed by it, a form of resilience resulting from individual's ability to recover from stress together with the capacity to anticipate the changing shape of risk before the occurrence of failures and harm. The understanding of this kind of protection is well captured by the psychological resilience.

It has been seen as an individual's tendency to cope with stress caused by flood events on property and their ability to build capacity for learning and adaptation (Folke 2006). The performance of these individuals must continually adjust to changes in the nature and magnitude of the stress component (Hollnagel et al. 2006). According to the Extreme Events and Health Protection (2014), an apt approach for managing people who have been affected by flooding is based on a set of principles and actions, rather than interventions, that anyone can perform. It involves providing support for individuals who are suffering from the impact of flooding. Further, psychological resilience helps to study and understand the response of humans to the flood perturbation. Therefore, at an individual level, the psychological wellbeing of residents confers considerable protection (Friedli 2009; Rose et al. 2016).

4.2 Resilience Measures

The features of building located in high flood risk areas are different from those located in low risk areas, where often the former is designed to accommodate flooding. Many of these features are put in place actively or in standby mode as back-ups to be activated in the event of flooding or its aftermath. These features are listed in Table 2 with their contributions to flood damage reduction. Some of these prevent water from getting into the building such as the resistance measures which could be permanently or temporarily deployed. While others entail the use of materials that will not get damaged in contact with water and designs that promote quick recovery. This is referred to as the resilience measure. The Permanent and temporary resistance measures are designed to stop water from entering into the building either by shutting existing openings such as doors, windows, airbricks, vents and pipes, or by preventing entrance through the walls. For the permanent measures, no action is needed to deploy the device that will stop the water, while the temporary measures will need to be installed before flood water arrives. The measures are designed to reduce the damage flood water can cause by limiting the point of water entry and providing homeowners extra time to move ground floor contents to a safe zone. However, the

measures may only be effective for a limited time and water depth (Dhonau et al. 2016).

In the case of differential head of 0.6 m (USACE 1988) it is recommended to let water into the building to avoid build-up of water pressure outside the building walls that can lead to serious structural damage or collapse. Therefore, features that minimise damage and allow for quick and easy cleaning and drying are considered. The interior of the building, fixtures, fittings, furniture, floor covering and wall hangings are made from materials that are not damaged by water. This is essential because it allows the quick recovery of buildings back to a habitable state (Dhonau et al. 2016).

For the resident, certain factors are considered to influence response to flood risk and flood events. These factors are socio-economic factors, health status and level of flood awareness. For the social dimensions and health status, the following residents: elderly (Age 70+), lone parents, children (Age 12−) and people whose activities are limited by ill-health or disability are more vulnerable to the impact of flooding than others (DEFRA 2006). Financial capacity is another factor that could influence decision making as regards the choice of insurance policy and property level flood protection to acquire. This could affect the coping and recovery capacity of both components and greatly impact resilience. Table 2 shows the human factors that support resilience to flooding and their contributions.

According to Adedeji et al. (2018), the human resilience can be improved by better preparation and building capacity to resist floods or to minimise the impacts. Better preparation could come in the form of flood risk awareness, which implies understanding all actions necessary to minimize the impact of flooding (Jha et al. 2012). Meanwhile, building adaptive capacity could mean the lessons learnt from past flood experience or taking cue from people with past flood experience.

5   Implications of the Framework

This section describes the way in which stakeholders involved with properties would benefit from implementation of the framework. Of course, making properties more resilient to flooding can be of great benefit to homeowners. Furthermore, a tool that captures and quantifies property level flood resilience would be highly valuable to the professional stakeholders (such as property experts, surveyors and insurers). The implications of the property level flood resilience framework and how it might be used in practise are now further explained.

5.1   Homeowners

The framework has the potential to provide valuable information on the flood resilience levels currently present in a home for the benefit of homeowners. This is important as homeowners are partly responsible for protecting their properties

Table 2 Resilience measures and their implications on damage reduction

Measures	Components		Approach	Remark	Implication
	Building	Human			
Flood door	✕		Resistance	Point of water entry	Prevent the entrance of water through door openings
Flood window	✕		Resistance	Point of water entry	Prevent the entrance of water through window openings
Non-return valve on drains and pipes	✕		Resistance	Point of water entry	Prevent the entrance of water through drains and pipes
Water resistant paint	✕		Resistance	Point of water entry	Prevent the entrance of water through walls
Automatic anti-flood airbricks	✕		Resistance	Point of water entry	Prevent the entrance of water through air gaps
Demountable door barriers	✕		Resistance	Point of water entry	Prevent the entrance of water through door openings
Demountable window barriers	✕		Resistance	Point of water entry	Prevent the entrance of water through window openings
Toilet plugs	✕		Resistance	Point of water entry	Prevent the entrance of water through toilet openings
Pipe bungs	✕		Resistance	Point of water entry	Prevent the entrance of water through pipes
Raised service meters	✕		Resistance	Property level flood protection	Access to power and communication during flood event
Sump and pump systems	✕		Resistance	Property level flood protection	Controls the level of water within the building

(continued)

Table 2 (continued)

Measures	Components		Approach	Remark	Implication
	Building	Human			
Raised door threshold	✕		Resistance	Construction type	Prevent the entrance of water into the building
Two or more storeys	✕		Resilience	Construction type	Increases safe indoor flood level and allows the movement of ground floor content to safer floor
Water resistant materials in kitchen and bathroom	✕		Resilience	Material type	Makes cleaning easier and drying faster
Tiled surface	✕		Resilience	Material type	Makes cleaning easier and drying faster
Valuable items kept upstairs	✕	✕	Resilience	Safe storage	Avoid loss of memorabilia
Insurance status	✕	✕	Adaptive	Economic status	Enhance quick recovery
Raised electrics and sockets	✕	✕	Resilience	Property level flood protection	Avoid damage and electrocution
Flood experience		✕	Adaptive	Adaptive capacity	Possess flood memory to learn from
Flood awareness		✕	flood risk intervention	Raising awareness of flood risk	Increased level of preparedness
Income level/employment status		✕	Resilience	Economic/Social status	Improves financial capability
Level of education		✕	Adaptive	Educational status	Ability to develop a flood plan
First aid kit		✕	Resilience	Health status	For emergency treatment of injuries

against the impact of flooding (Joseph et al. 2015). The framework does this through quantifying current resilience levels by identifying any measures that have been put in place to reduce the impact of flooding. The framework will also consider the characteristics of the property, the nature of flood risk exposure for the particular location and the effectiveness of measures put in place.

For example, with low depth flooding (below 0.3 mm), water exclusion approaches (resistance measures) will prove more cost-effective than resilience measures, since in this case water is prevented from getting into the building. However, among the resistance measures, permanent resistance measures tend to be more effective than temporary resistance measures because their deployment do not require human intervention. This is expedient in the case where flooding occurs quickly without warning or when no one is in the building to activate measures. For high depth flooding (above 600 mm), water entry measures (resilience) would read well on the resilience scale than resistance measures since the focus is to reduce damage caused within the building and prevent structural damage. However, it is essential to control the inflow of water and certain resistance measures are required to achieve this. The framework identifies all the paths of water entry, possible flow rates and any resistance measure that applies to each point. This also helps to inform the homeowner in making decisions on which measures to adopt that would lead to the most effective means of improving current resilience. That is, this would allow homeowners to compare and contrast different resilient measures to optimise decision making.

The framework will also provide information on members of the household exposed to flood impacts, and the degree of exposure to the impact through the assessment of their human resilience. This human resilience helps to identify resilience attributes absent or in need of strengthening in residents. This information will enable homeowners to take well calculated steps to anticipate flooding and to protect themselves, their health and well being through interventions such as developing a flood plan, having an emergency pack of food and provisions, or taking steps to develop a better understanding of their risks.

5.2 Property Experts and Surveyors

The framework will be of help to property experts such as surveyors in valuing property and in offering advice to their clients. One of the key factors that influence the value of real estate including homes is flooding or flood risk (Lamond et al. 2010; Kropp 2012). The framework provides information that promulgates a clear understanding of the variables and processes involved in flood risk assessment and property level flood resilience. This will provide property experts with a tool to estimate the resilience levels within a property enabling them to provide impartial and professional advice on risk exposure and which measures might best be adopted to help further protect their properties.

Information on the level of resilience will also help in conducting property valuations at the point of sale and /or for mortgage purposes, enabling any existent

measures that are in place to be considered in this process. Also, through interaction with the framework, surveyors can benefit by carrying out an appraisal of the amount of resilience present in a property. This is essential for surveyors to offer good advice on design interventions to improve resilience and make recommendations on the optimal combination of measures for a particular home.

5.3 Insurers

Insurers will also benefit from the opportunity to apply and use the framework. Often, it can be difficult for insurers to know how to quantify the benefits of any existent resilience measures, particularly those that needs to be proactively deployed (May et al. 2015). However, the framework is designed to provide a means of quantifying the property level flood resilience by demonstrating the effectiveness of any resilient measures in place. This will in turn enable insurers to consider how this might affect insurance premiums and excesses which will in turn improve the role of flood insurance as a market-based incentive.

The framework has the potential to provide an evidence based tool to inform insurers on the levels of resilience present within a given property and how this would reduce the cost of damage. These costs are often shared between the premiums and excesses (Edmonds 2017) and therefore, this improved understanding of flood risk, taking into account any resistance or resilience measures, allows the insurers to value this risk more accurately. In this situation, improving resilience might translate into reductions of premiums and excesses. The improved understanding of flood risk places the insurers in a position to offer premiums that promote property level flood risk adaptation through resilient reinstatement.

5.4 Government/Government Policy

The Government policy as set out in the National Planning Policy Framework, discourages the building of homes in areas with a significant risk of flooding. However, in the case of homes already located in these areas, or where development is necessary, the policy encourages such homes to be designed appropriately with ability to cope with floodwaters and ensure quick recovery after a flooding event. This entails the adoption of the property level flood resistance and resilience measures. Therefore, through the implementation of the framework, the stakeholders involved with properties can encourage the adoption of property level flood resilience thereby promoting this policy. The framework also provide a means by which government could monitor the uptake of property level flood resistance and resilience measures by homeowners and see how the policy is achieving its aim of reducing flood risk exposure.

6   Conclusions

Making a home more resilient entails paying close attention to both human and building components. That is, as much as we design and develop products to reinforce the building against the impact of flooding, we must also learn to identify the qualities and attributes that each resident possesses and where they belong on the resilience scale. The conceptual framework developed will help identify and bring together the resilience measures present in a home including the resilient qualities of the residents. This information is essential to estimate the overall resilience of the property. This will enable us to identify areas with weak resilience and thereby offer advice on design interventions to reinforce such areas.

The implication of the framework entails the provision of an evident-based tool that informs homeowners of the level of resilience present in their home, provides surveyors with information that enable them to give better advice on interventions that can best improve resilience; offers property experts the information required to carry out property valuation; and provides insurers with information that will improve the role of flood insurance as a market-based incentive.

The framework establishes an evidence base for the assessment of property level flood resilience which will in future help inform decisions about the support that homeowners could access from stakeholders for bouncing back from the impacts of flooding in a better way. The framework would help to empower insurers to act as a driver for building adaptive capacity to the changing risk through developing insurance premiums that promote resilient reinstatement. The framework, through quantifying flood resilience, would tend to influence the attitudes of homeowners by promoting the uptake of resistance and resilience measures as well as by developing their understanding of how to raise existing levels of resilience. By investing in resistance and resilience measures they could avoid claims or make claims with lesser value which can help maintain access to insurance. All of these implications will help support the government policy of setting out strategies to encourage the adoption of property-level flood protection which is to complement the more traditional focus on flood defence. The framework would also support the wider flood resilience agenda, and would also help to inform future government policy on flood risk management.

The framework has the potential to be extended to flood resilience measurement at larger scale applications i.e. at the community level, regional level and even national level after it has been fully developed, that is, developed and tested at individual property level. It also has the potential to be applied to non-residential properties and public buildings such as commercial properties, retail buildings and schools. The framework provides the opportunity for application in other countries and developing countries through modification of framework to represent the resilient features prevalent in the country of application. This could encourage transfer of knowledge between countries.

There exists the prospect of a user interface through the development of a mobile application for the implementation of framework by potential users. This application will help design a platform that makes the framework accessible to stakeholders through mobile devices such as smartphones and tablets devices.

References

Adedeji, T. J., Proverbs, D. G., Xiao, H., & Oladokun, V. O. (2018). Towards a conceptual framework for property level flood resilience. *International Journal of Safety and Security Engineering, 8*(4), 493–504.

American Psychological Association. (2014). *The road to resilience*. Washington, DC: American Psychological Association.

Bruneau, M., et al. (2003). A framework to quantitatively assess and enhance the seismic resilience of communities. *Earthquake Spectra, 19*(4), 733–752.

Cutter, S. L., et al. (2008). A place-based model for understanding community resilience to natural disasters. *Global Environmental Change, 18*(4), 598–606.

de Bruijn, K., et al. (2017). Resilience in practice: Five principles to enable societies to cope with extreme weather events. *Environmental Science and Policy, 70,* 21–30.

DEFRA. (2005). *Making space for water: Taking forward a new Government strategy for flood and coastal erosion risk management in England*. London: Defra Publications.

DEFRA. (2006). *Flood Risks to People—Phase 2 project record—F2321/PR*. London: Environment Agency and Department for Environment, Food and Rural Affairs.

Dhonau, M., et al. (2016). *Homeowners guide to flood resilience a living document*. England: MDA.

Ecofys & BioIntelligence. (2010). *Study to support the impact assessment for the EU energy saving action plan*: Ecorys.

Edmonds, T. (2017). *Household flood insurance*. United Kingdom: House of Commons Library.

Environment Agency. (2014). *Flood and coastal erosion risk management Long-term investment scenarios (LTIS),* Bristol, England: Environment Agency.

Eriksen, S. H., & Kelly, P. M. (2007). Developing credible vulnerability indicators for climate adaptation policy assessment. *Mitigation and Adaptation Strategies for Global Change, 12,* 495–524.

Extreme Events and Health Protection. 2014. *Flooding and mental health: Essential information for front-line responders.* England: Public Health.

Few, R., Ahern, M., Matthies, F. & Kovats, S. (2004). *Floods, health and climate change: A strategic review Norwich.* UK: The Tyndall Centre for Climate Change Research.

Fikretoglu, D., & McCreary, D. R. (2012). *Psychological resilience: A brief review of definitions, and key theoretical, conceptual, and methodological issues*. Toronto, Ontario, Canada: Defence Research and Development Canada.

Fletcher, D., & Sarkar, M. (2013). Psychological resilience: A review and critique of definitions, concepts and theory. *European Psychologist, 18,* 12–23.

Folke, C. (2006). Resilience: The emergence of a perspective for social–Ecological systems analyses. *Global Environmental Change, 16,* 253–267.

Friedli, L. (2009). *Mental health, resilience and inequalities*. Denmark: World Health Organisation.

Garvin, S. (2012). *Flood Resilient Building—Part 2: Building in flood-risk areas and designing flood-resilient buildings*. Watford: BRE Press.

Graber, R., Pichon, F. & Carabine, E. (2015). *Psychological resilience: State of knowledge and future research agendas.* London.

Gunderson, L. (2010). Ecological and human community resilience in response to natural disasters. *Ecological and Society, 15*(2), 18.

Hashimoto, T., Stedinger, J. R., & Loucks, D. P. (1982). Reliability, resiliency, and vulnerability criteria for water resource system performance evaluation. *Water Resources Research, 18*(1), 14–20.

Holling, C. (1973). Resilience and stability of ecological systems. *Annual Review of Ecology and Systematics, 4,* 1–23.

Hollnagel, E. (2006). Resilience: The challenge of the unstable. In E. Hollnagel, D. D. Woods, & N. Leveson (Eds.), *Resilience engineering: Concepts and precepts*. Aldershot, UK: Ashgate.

Hollnagel, E., Memeth, C. P., & Dekker, S. (2008). *Resilience engineering perspectives. Remaining sensitive to the possibility of failure. volume* (1st ed.). Vermont, USA: Ashgate, Burlington.

Jha, A. K., Bloch, R., & Lamond, J. (2012). *Cities and flooding: A guide to integrated urban flood risk management for the 21st century*. Washington DC: The World Bank.

Joseph, R. D. (2014). *Development of a comprehensive systematic quantification of the costs and benefits (CB) of property level flood risk adaptation measures in England. Ph.D., University of the West of England.* Bristol, England: University of the West of England.

Joseph, R., Proverbs, D., & Lamond, J. (2015). Homeowners' perception of the benefits of property level flood risk adaptation (PLFRA) measures: The case of the summer 2007 event in England. *International Journal of Safety and Security Engineering, 5*(3), 251–265.

Joseph, R., Proverbs, D., Lamond, J., & Wassell, P. (2011). An analysis of the costs of resilient reinstatement of flood affected properties: a case study of the 2009 flood event in Cockermouth. *Structural Survey, 9*(4), 279–293.

Kallaos, J., Wyckmans, A. & Mainguy, G. (2014). *Synthesis review on resilient architecture and infrastructure indicators*: RAMSES Project.

Kazmierczak, A., & Connelly, A. (2011). *Buildings and Flooding: a risk-response case study*. EcoCities project, Manchester, UK: University of Manchester.

Kreibich, H., et al. (2005). Flood loss reduction of private households due to building precautionary measures—Lessons learned from the Elbe flood in August 2002. *Natural Hazards and Earth System Sciences, 5,* 117–126.

Kropp, S. (2012). *The influence of flooding on the value of real estate,* s.l.: Rom, Italy, May 6–10, 2012.

Lamond, J. E. (2008). *The impact of flooding on the value of residential property in the UK*. Wolverhampton, UK: University of Wolverhampton.

Lamond, J., Proverbs, D., & Hammond, F. (2010). The impact of flooding on the price of residential property: A transactional analysis for the UK. *Housing Studies, 25*(3), 335–356.

Lamond, J., Rose, C., Proverbs, D. & Defra, (2016). *Supporting the uptake of low cost resilience: FD2682 rapid evidence assessment final report.* London: Defra.

Lock, S. et al. (2012). *Secondary stressors and extreme events and disasters.* PLOS Disasters.

Luthar, S., Cicchetti, D., & Becker, B. (2000). The construct of resilience: A critical evaluation and guidelines for future work. *Child Development, 7,* 543–562.

May, P., et al. (2015). *Surveying for flood resilience in individual properties: Guidance for home-owners*. London: Defra.

McAslan, A. (2010). *The concept of resilience: understanding its origins, Meaning and Utility.* Australia: Strawman.

McNulty, A., & Rennick, K. (2015). *The experience of flooding in the UK—A research study*. UK: British Red Cross.

Neria, Y., Nandi, A., & Galea, S. (2008). Post-traumatic stress disorder following disasters: A systematic review. *Psychological Medicine, 38*(4), 467–480.

Norris, F. H. (2010). *Behavioral science perspectives on resilience*. Oak Ridge: Community and Regional Resilience Institute.

ODPM. (2003). *Preparing for Flood: Interim guidance for improving the flood resistance of domestic and small business properties*. London, UK: Office of the Deputy Prime Minister.

Oladokun, V., Proverbs, D., & Lamond, J. (2017). Measuring flood resilience: A fuzzy logic approach. *International Journal of Building Pathology and Adaptation, 35*(5), 470–487.

Pitt, M. (2008). *Learning lessons from the 2007 floods*. London: Cabinet Office.

Proverbs, D., & Lamond, J. (2017). *Flood resilient construction and adaptation of buildings*. USA: Oxford University Press.

Queensland Government. (2002). *Guidance on the assessment of tangible flood damages*. Queensland: Queensland Government.

Rose, C., et al. (2016). Improving the uptake of flood resilience at the individual property level. *International Journal of Safety and Security Engineering, 6*(3), 607–615.

Sirochmanová, L., Kozlovská, M., & Bašková, R. (2016). The importance of the criteria of residential buildings from the perspective of future users. *Journal of Civil Engineering, 11*(1), 97–106.

Smith, K., & Ward, R. (1998). *Physical process and human impacts*. England: Wiley.

Stanke, C. et al. (2012). The effects of flooding on mental health: Outcomes and recommendations from a review of the literature. *PLOS Currents Disasters*, May, 30.

Tapsell, S., Rowsell, E., Tunstall, S. M., & Wilson, T. (2002). Vulnerability to flooding: Health and social dimensions. *Philosophical Transactions of the Royal Society, London A, 360*(1796), 1511–1525.

Tierney, K., & Bruneau, M. (2007). Conceptualizing and measuring resilience, a key to disaster loss reduction. *TR News, 250,* 14–17.

USACE. (1988). *Flood proofing tests—Tests of materials and systems for flood proofing structures*. USA: US Army Corps of Engineers.

VanBreda, A. D. (2001). *Resilience theory: A literature review*. Pretoria, South Africa: South African Military Health Service, Military Psychological Institute.

Wang, C., & Blackmore, J. M. (2009). Resilience concepts for water resource systems. *Water Resources Planning and Management, 135*(6), 528–536.

Werner, E. E., & Smith, R. S. (1992). *Overcoming the odds: High risk children from birth to adult hood*. Ithaca, NY: Cornell University Press.

Wingfield, J., Bell, M., & Bowker, P. (2005). *Improving the flood resilience of buildings through improved materials, methods and details*. Leeds: Leeds Metropolitan University.

Resilience-Based Design for Blast Risk Mitigation: Learning from Natural Disasters

Shady Salem, Manuel Campidelli, Wael W. El-Dakhakhni and Michael J. Tait

1 Introduction: Risk in the Built Environment and the Need for Resilience

The modern characteristics of the built environment are increasingly determined by a system of buildings and supporting infrastructure that is growing in size, interconnectedness, vulnerability, and risk exposure. The size of cities and their critical infrastructure—including transportation and telecommunication networks, water and wastewater systems, energy, food and agriculture, health care, and finance—is growing to meet the demand imposed by global demographic trends (UN 2004), migration patterns, and the tendency to relocate from rural to metropolitan areas (Van Riper 1997). As the need for efficient and cost-effective services increases, so does the connectivity between once separate systems in what are now termed as "smart cities," where many critical infrastructure networks are strongly interlinked. Interdependencies are expressed as physical, cyber, geographical, and logical bidirectional relationships characterized by feedback and feedforward paths between two or more systems (Rinaldi et al. 2001); as they develop, they carry the unprecedented risk of failures spreading from one system to another. In fact, when interdependence reaches a critical threshold, a condition usual termed hyper-connectivity, the system becomes prone to hyper-risk (Helbing 2013), wherein new vulnerabilities emerge from systemic coupling and effects of local deficiencies may spread from the host

---

S. Salem (✉)
Civil Engineering Department, The British University in Egypt, Cairo 11837 - P.O. Box 43, Suez Desert Road, El-Sherouk City, Cairo, Egypt
e-mail: salemsh@mcmaster.ca

Department of Civil Engineering, McMaster University, 1280 Main St. W, Hamilton L8S 4L7, ON, Canada

M. Campidelli · W. W. El-Dakhakhni · M. J. Tait
Institute for Multi-Hazard Systemic Risk Studies—Interface, Department of Civil Engineering, McMaster University, 1280 Main St. W, Hamilton L8S 4L7, ON, Canada

system/network in which they originated to others, in a series of progressive, cascading failures. This already challenging state of affairs is further exacerbated by a multi-hazard environment, which threatens modern metropolitan areas in a multitude of ways, from earthquakes and flooding to deliberate acts of terrorism. In terms of sheer impact on the global economy, the most pressing hazards identified by the World Economic Forum (WEF 2018) are classified under the rubric of weapons of mass destruction, extreme weather events, natural disasters, failure of climate change adaptation, food and water crises, ecosystem collapse, large-scale migration, and pandemics. Extreme weather in the US alone accounts for up to 16 billion-dollars in damages every year as the result of drought, flooding, freeze, severe storm, tropical cyclone, wildfire, and winter storm.

In addition to these stressors, other risk factors, subtler and more pernicious, can emerge from the interaction between human endeavors and the environment. In this respect, an especially confounding source of risk has its roots in the flawed, yet dominant, conception of natural disasters, one that obfuscates how commonplace human endeavors can lead to disaster when undermined by scarcely predictable natural phenomena. In fact, the very expression "natural disaster" may be misleading in that it ignores the ever-present interaction between the natural environment and the built infrastructure. Based on historical records of seismic activity, flooding, and other natural hazards, to denote their negative impact on the affected populations as natural appears to be a category mistake. Available case studies of past disasters—for example, the 2005 Hurricane Katrina (Louisiana, US)—suppot this point of view.

In Louisiana, the Hurricane Protection Project proposed in the Flood Control Act of 1965 had the purpose of building a series of control structures, such as floodwalls and levees, to provide hurricane protection in areas around Lake Pontchartrain and the Mississippi watershed. The cost of the project, initially estimated to be approximately $85 million, grew to $738 million in 2005, about 72% of which was covered by the US Federal Government; similarly, the time of completion had grown from 13 to 50 years (USACE 2005). In addition, a system of subsidized flood insurance was in place. When Hurricane Katrina struck, it caused the destruction of more than 283,000 homes and 1500 lives in Louisiana alone; overall, direct economic losses and insured losses were estimated in the amounts of $125 billion and $40.6 billion, respectively (FEMA Mitigation Assessment Team 2006). These losses have been partly ascribed to the land development policies underpinning the Hurricane Protection Project, whose benefits were assumed to come, in the extraordinary proportion of 79%, from new urban development protected by the enhanced levee system (Burby 2006).

The case of Hurruicane Katrina demonstrates the interaction between the natural and built environments. However natural the leading cause of a disaster may be, its destructive character is bestowed by the agency of human settlers, via policies of land development, urban planning, and construction codes, which historically had far too often the effect of increasing the risk by moving entire communities in harm's way. In his analysis, Burby (2006) identified the "safe development" and "local government" paradoxes. The first explains why measures for mitigating risk led to its increase—via intensive development of a system of levees and floodwalls in areas of Louisiana highly vulnerable, as made apparent by Hurricane Betsy, and

policies of subsidized flood insurance—all of which conspired to greatly increase the population density in flood-prone areas, prop up a false sense of security in the residents, and dissuade property owners from taking action to improve the buildings' safety. The second paradox reveals a recurring pattern in the decision making of local officials who, when tasked with the safety of their communities, repeatedly resisted federal projects aimed at the improvement of storm protections in order to avoid their share of the associated costs. This phenomenon may have several causes, as noted in Burby (2006): Chief amongst them is the perception that mitigation costs are immediate while the benefits are uncertain, likely not to be manifest during the tenure of elected officials, and often overshadowed by short-term concerns about housing, transportation, etc.

1.1 Blast Risk

Buildings of strategic and symbolic importance, as well as infrastructure, are increasingly susceptible to emergent forms of risk, including cyber and physical attacks. Sensors and information systems can significantly improve safety, health, and convenience in "smart buildings" while saving electricity and water usage (Dell EMC 2017); they can, however, serve as a beacon for the most malicious and deliberate forms of aggression, which can breed dramatic and enduring consequences. These systems have the potential to increase a building's vulnerability against anthropogenic hazards, in a way that is analogous to what observed in the case of natural phenomena. Terrorist attacks on civilian facilities, in the manner of bombings and the dissemination of harmful biological agents, are known to have a disproportionate impact on a population's morale and its economy. A few glaring examples in recent memory include the Oklahoma City bombing, the 9/11 attacks on the World Trade Center and the subsequent anthrax attacks (Bier et al. 2005; Morrill et al. 2004). The insured costs of the 9/11 attacks have been estimated in the amount of US$ 40 billion, that is to say twice as much as the insured losses claimed for the largest natural catastrophe ever reported until that time in the United States (Fitzpatrick 2005). The challenge presented by terrorism, however, reaches beyond mere insurance premiums. As reported by Swiss Re Ltd. (2016), acts of violence in the pursuit of political goals receive limited coverage from insurance policies, even though, as of 2015, they accounted for 15% of the aggregate casualties worldwide caused by anthropogenic disasters. The reason behind this lack of coverage lies in the overwhelming difficulty, faced by actuaries, to assess second–order effects following the immediate quantifiable damage caused by an attack. Traditional risk assessment schemes—e.g. the probabilistic risk assessment (PRA) methodology introduced by Grant and Stewart (2012, 2015) with specific applications to facilities involved in blast events of a malicious origin—however necessary and instrumental to the determination of best expectations of meaningful loss metrics, prove insufficient when domino effects on the public at large and indirect costs can dwarf direct losses. To manage seemingly intractable uncertainties, engineering resilience into the economic, financial, and physical systems

is the only viable option on the horizon. From the perspective of resilient thinking, losses associated with all plausible disaster scenarios are to be expected, planned for, and recover from in an efficient fashion on the basis of the intelligent design of structure and infrastructure and well–defined resilience metrics (objectives) such as financial loss, casualties, and downtime. Therefore, the following section is dedicated to a cursory summary of well-established definitions and concepts associated with the resilience of the built environment.

1.2   Resilience as a Mitigation Strategy

In engineering disciplines, despite a proliferation of definitions (Ayyub 2015), there is a general consensus on the meaning of resilience, which is focused on investigating the methodologies more apt to make engineered systems less prone to failure and more adaptable to events potentially disruptive of their functionality. Although not comprehensive, the definition provided by the National Infrastructure Advisory Council (NIAC 2010) is sufficiently broad: NIAC defines infrastructure resilience as "[enhancing] the ability of critical infrastructure systems, networks, and functions to withstand and rapidly recover from damage and disruption and adapt to changing conditions." In qualitative terms, the dimensions of resilience include robustness, rapidity, resourcefulness, and redundancy (Bruneau et al. 2003). Of these, robustness and rapidity are the key factors that can be translated in quantitative terms, clearly defined on the basis of the function that measures a desirable feature of a system. If the case of a suspension bridge is taken as an example, its purpose is to grant passage over an obstacle, which can be quantified by the traffic capacity, i.e. the number of vehicles able to cross the bridge per unit time. Assuming a full capacity of 100 vehicles/minute, the bridge robustness would be determined by the number of vehicles able to transit after the impact of known stressors—including landslide, hurricane, earthquake as well as blast and ballistic loading. If, for instance, 20 vehicles/minute were able to safely transit over the superstructure after a ballistic attack, then $20/100 = 20\%$ would be the measure of bridge robustness. Rapidity would relate to the time—measured in days, weeks, and months—required to "bounce back" and restore full functionality, i.e. a pre-disaster traffic flow. Resourcefulness and redundancy are seen as necessary precursors, as they relate to the resources available to increase both robustness and rapidity. A possible definition of bridge redundancy is "the capability of a bridge superstructure to continue to carry loads after the damage or the failure of one of its members" (Ghosn and Moses 1998). In statically indeterminate structures, the latter objective is accomplished via stress redistribution. Subsuming all four dimensions, resilience has been proposed as an overall measure of how a system can withstand the impact of several hazards and remain functional. In Bruneau et al. (2003), the loss of resilience is defined as the loss of functionality integrated over the time of recovery, while more direct definitions of the "resilience index" refer to the mean functionality over the time of recovery (Attoh-Okine et al. 2009). These differences notwithstanding, it is worth noting that no one mathematical
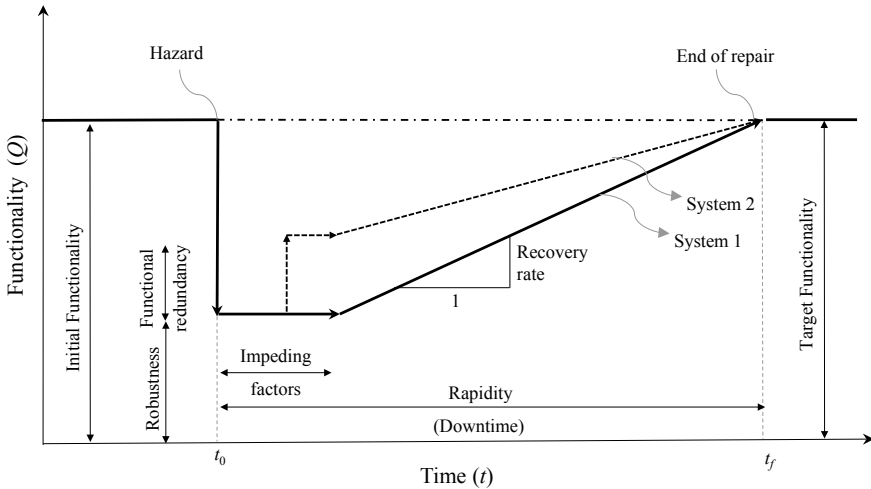
Fig. 1 Idealized resilience triangle with linear recovery path: system 1 features no redundancy, which would expedite recovery, and significant impending factors that delay the onset of recovery; system 2 benefits from some measure of redundancy and less impending factors

definition of a resilience index can comprehensively replace the full representation of the diminished functionality during recovery, i.e. the functional history from the time of event/hazard occurrence to the time of complete recovery, as schematically represented in Fig. 1.

The ultimate objective of resilience, i.e. functional restoration in the shortest amount of time, can be articulated in more detail, depending on the design requirements. In the REDiTM roadmap to resilience (Almufti and Willford 2013), three states are considered as sensible resilience targets compliant with basic safety requirements, i.e. re-occupancy (no utilities available), pre-disaster functionality (recovery of all primary functions), and full recovery (including aesthetics). The means to engineer and expedite recovery range from organizational (contingency planning), to ambient (risk mitigation through apt design of the surroundings), to retrofit strategies (structural damage mitigation) and extend to optimization tools aimed at minimizing the combined cost of multiple risk mitigation measures. A typical problem in blast risk mitigation is depicted in Fig. 2, where the tradeoff between two types of interventions is presented. On the one hand, the erection of barriers to protect the perimeter—in the form of anti-ram barriers, fences, controlled gates, bollard lines, etc.; on the other, structural strengthening of the exposed façade—in the form of fiber reinforced polymer retrofitted columns, installation of blast–resistant glazing systems provided with polyvinyl butyral interlayer, etc. Any suitable optimization tool would consider all viable options and determine the combinations that achieve the Pareto front in terms of all sensible resilience metrics, including the cost of the intervention, economic losses in the immediate aftermath of a blast event, losses associated with downtime during recovery, and human casualties.
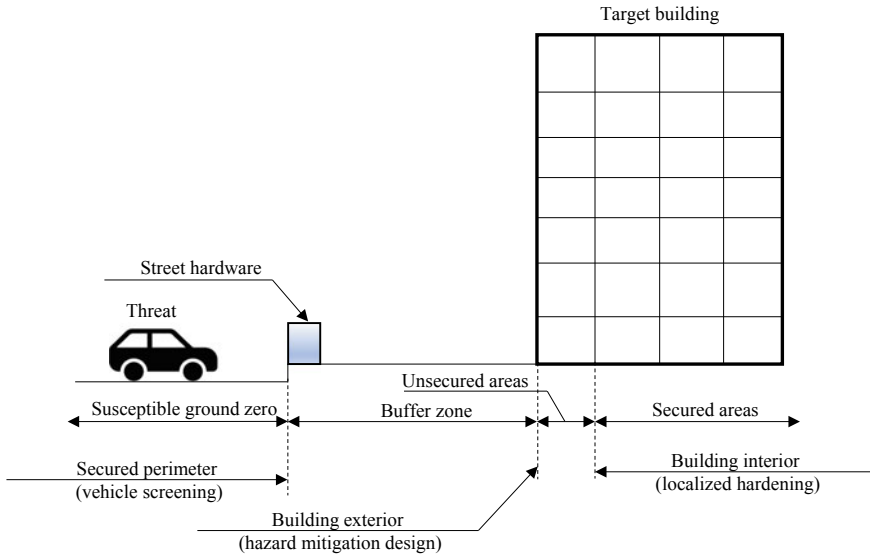
Fig. 2 Schematic defensive strategies for blast protection. Adapted from FEMA 427

2 Framework for Resilience-Based Blast Design

Within the context of blast-resistant design, two resilience–based frameworks have been put forth. The first, introduced by Quiel et al. (2016) and Marjanishvili (2017), focuses on the probabilistic prediction of system robustness when subjected to a blast threat, but does not consider the rapidity attribute of resilience. The second framework was proposed by Salem et al. (2017, 2018) to provide a deterministic estimate of post-blast functionality and downtime experienced by any system amenable to structural analysis. In this section, previous work by Salem et al. (2017, 2018) is further expanded for optimal deployment of mitigation measures against blast risk. Two indices have been proposed as comprehensive resilience metrics, namely, the functionality loss index (I_F) and resilience indicator (I_R): I_F is related to robustness, i.e. the ratio between residual post–blast functionality in the immediate aftermath of an attack and the system functionality under ordinary conditions, while I_R is the functionality loss integrated over the downtime. For example, the functionality of office buildings is computed using a functionality loss indicator (λ), a binary indicator that represents the accessibility of each area of the building after the hazard and is based on the expected performance of the façade components surrounding each architectural unit (bay) affected by blast waves. A bay is defined as a space of the building delimited by architectural components that have either a functional or an aesthetic purpose (Strong 2000). A bay is considered functional (i.e. $\lambda = 0$) if all its surrounding components experience a level of damage no greater than superficial. By definition, superficial damage may or may not be visible and may require cosmetic

repair, if any at all, which allows for a bay to remain serviceable. Conversely, the bay is considered out of service (i.e. not function, $\lambda = 1$) whenever one or more of its pertinent façade components experience any damage greater than superficial. This framework does not account for the initiation of progressive collapse in that it deliberately excludes hazardous and blow out damage states; however, it may be extended to cases wherein non–structural components experience extreme damage, as their failure would not compromise the global structural integrity. For structural components, the λ–indicator and I_F are formulated as shown in Eqs. (1), (2) and (3) (Salem et al. 2018),

$$\lambda = \begin{cases} 0 & \text{Bay incurring superficial damage} \\ 1 & \text{Bay incurring moderate or heavy damage} \\ \text{N/A} & \text{Bay incurring hazardous damage or blowout} \end{cases} \tag{1}$$

$$I_{fi} = A_i I_i \lambda_i \tag{2}$$

$$I_F = \frac{\sum_{i=1}^{n} I_{fi}}{\sum_{i=1}^{n} A_i I_i} \tag{3}$$

where I_{Fi} denotes the localized functional loss incurred by the i-th bay, which can be used for mapping the damage distribution over the affected facade; A_i and I_i are the area and importance factor of the i-th bay, respectively; and λ_i is the loss indicator defined in Eq. (1).

Regarding the time of recovery, needed to restore the system to full functional capacity, the work of Almufti and Willford (2013) introduces a distinction between downtime and repair time. Repair time is the time required to repair or replace all damaged components, whereas downtime also accounts for impeding factors—e.g. the delay between hazard occurrence and the initiation of repairs—and utility disruption—e.g. the time required for the recovery of backup systems. The effects of impending factors and functional redundancy on the recovery path are shown in Fig. 1: Impending factors are likely to delay and flatten the rate of recovery, whereas functional redundancy has the opposite effect and may be engineered via comprehensive contingency/emergency plans. In the following discussion, given the lack of information pertaining to impeding factors, the downtime is simply assumed to coincide with the time of repair, which is calculated using the baseline repair estimate recommended in FEMA P-58 (FEMA 2012a) in case of a seismic event. The FEMA estimate is based on the total labor repair cost divided by the average hourly rate; in turn, the labor cost is calculated using the labor production commencement time ($LPCT$), that is the ratio of labor cost to total repair cost. The methodology is summarized in Eq. (4).

$$Baseline\ estimate\ (hr) = \sum \frac{Repair\ cost\ (\$) \times labor\ production\ commencement\ time\ (\%)}{Effective\ hourly\ rate\ (\$/hr)} \tag{4}$$
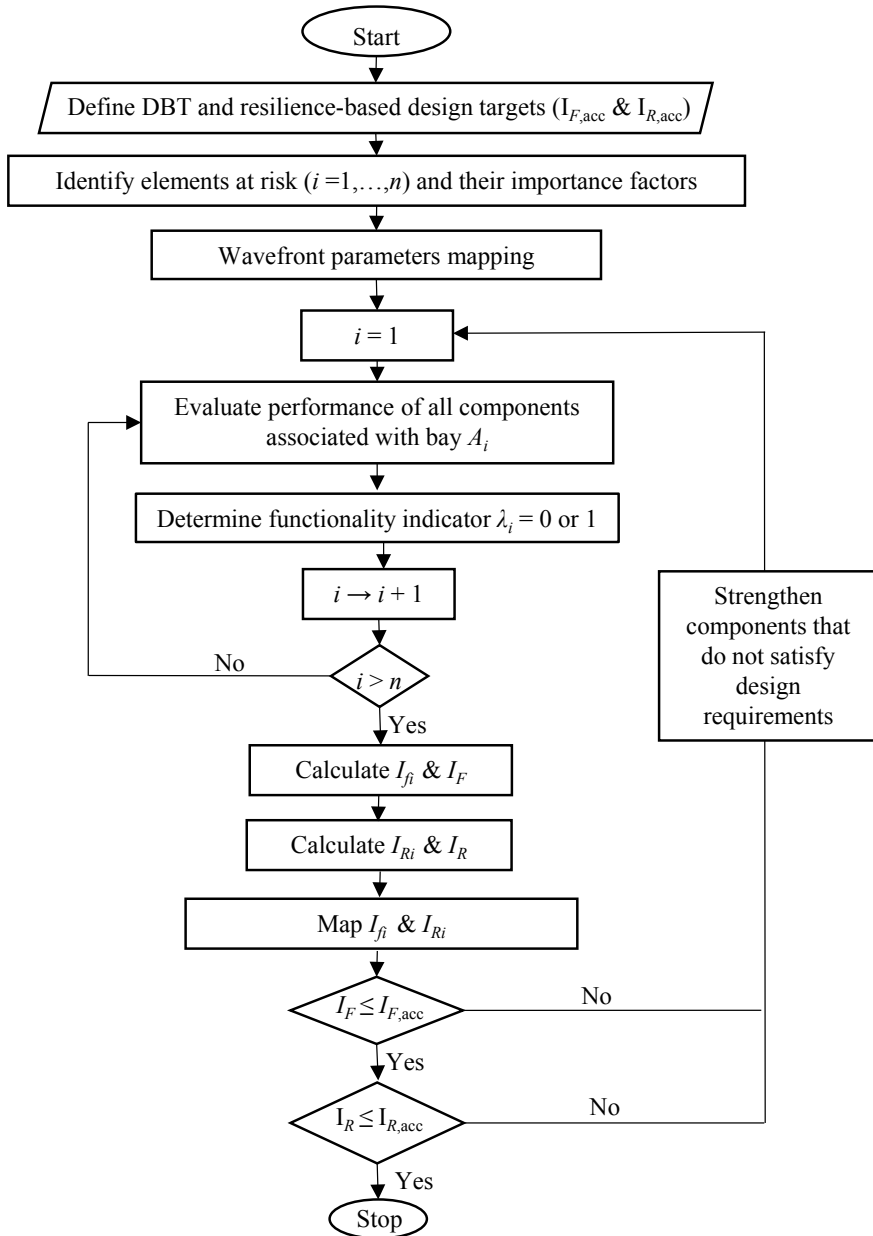
Fig. 3 Proposed blast resilience framework

As mentioned earlier, the I_R proposed by Salem et al. (2017, 2018) is used to aggregate losses over the time of recovery, as per Eq. (5),

$$I_R = \frac{1}{2}(t_f - t_0)I_F \qquad (5)$$

where t_0 is the time of blast event occurrence; t_f is the time at which full functionality is restored; and I_F is the functionality loss index from Eq. (4). I_R can be used in conjunction with I_F to provide stakeholders with a more comprehensive understanding of the consequences of a blast event. To monitor localized cumulated losses, a local resilience indicator (I_{Ri}) can be used instead, in which the subscript i denotes the i-th bay:

$$I_{Ri} = \frac{1}{2}(t_f - t_0)I_{fi} \qquad (6)$$

Figure 3 illustrates a flow chart of the proposed blast–resilience framework. The process begins with identifying a suitable design basis threat (DBT), in compliance with applicable standards, and the resilience-based design targets, i.e. acceptable values for the functionality index and resilience indicator. Then, the elements at risk are identified and importance factors are established based on decision-makers' priorities. Afterwards, the wavefront parameters are mapped over the building's envelope based on the selected DBT; the structural response of each member is calculated, and the localized functional loss I_{fi} is mapped across the building façade using Eq. (2). Localized cumulated losses I_{Ri} are also mapped—using Eq. (6)—to visualize the influence of façade components vulnerability on the overall functional loss.

# 3 Application of Resilience-Based Blast Design Concepts to Office Buildings

The following example presents an application of the proposed framework for optimizing the allocation of resources directed at the mitigation of blast risk. The example illustrates the procedure for mapping functional loss, downtime, and the local resilience index of a typical mid/high–rise administrative building. The adopted features are those of a nine-story governmental complex adapted from the Alfred P. Murrah federal building, as shown in Fig. 4 (Corley et al. 1996; Sozen et al. 1998). Figure 4a illustrates the building elevation, while Fig. 4b, c depict the building plan for the first two floors and the typical plan for the third through ninth floors, respectively. Figure 4b, c also highlight the façade facing the explosion and its egress spaces, which provide access redundancy. Figure 5 shows the distribution of importance factors across the exposed façade, which range from 0.1 to 2.0. For example, the importance factor of each egress space is set equal to 0.1, because its twin space is designed to fulfill the demand of the entire building; however, the importance of

the upper storey is 2.0, because there reside the top managerial offices, which are vital to productivity.

Two blast scenarios are considered as a representation of different threat types—shown in Fig. 6 (Salem et al. 2018). The first scenario (scenario 1) represents a person–borne threat, with an explosive charge weighing 50 kg, while the second scenario (scenario 2) represents a vehicle-borne threat, with a relatively larger charge of 500 kg. The screening zone set up to grant access to employees and visitors is assumed to be 10 m wide, which is the minimum distance that any person–borne threat should be able to reach without detection, based on FEMA's guidelines (FEMA-426 2011), whereas the vehicle screening area has an outer perimeter at 25 m from the façade, which is the closest distance that can be reached by an undetected vehicle-borne threat. Accordingly, both threats are positioned along the associated screening lines following a uniform probability distribution, with the purpose of simulating the worst-case scenarios. Figure 7 shows the variation of specific impulse distribution for scenario 1 due to the variability of threat location—identified as R_1 through R_7.

In this example, the lost functionality accounts for the serviceability of architectural units adjacent to damaged components in the façade, while a wide range of phenomena—including blast wave propagation inside the building core as well as primary and secondary fragmentation—are neglected. However, these phenomena can, in principle, be incorporated within the proposed framework. Furthermore, to avoid distraction with inessential geometrical details, the exposed façade (at axe "A") is assumed fully covered by non–load bearing, reinforced concrete masonry panels. All panels are constructed using $390 \times 190 \times 190$ mm concrete masonry units having 20 MPa average compressive strength; they are vertically reinforced with No. 5 rebars (average cross-sectional area $= 200$ mm^2) every three cells (600 mm rebar spacing) and horizontally reinforced with No. 3 rebar (average cross-sectional area $= 71$ mm^2) every other course. Figure 8 reports P–I diagrams that show the performance of the CMU panels with reference to different damage states (USACE 2008). According to the current standards for blast protection (ASCE 2011; CSA 2012), the two selected scenarios yield a "very low" level of protection (LOP), which can be ascribed to the low resistance of the panels. For this example, the repair cost of masonry walls is adopted from FEMA P-58 (FEMA 2012a), based on the 90th percentile associated with the repair of special reinforced masonry walls, flexure controlled, 200–300 mm (8–12″) thick, and no taller than 3.67 m (12′). The costs are $100.43/m^2 and $487.93/m^2 for the first and second damage states (DS1 and DS2), respectively, while the repair cost for the third and fourth damage states (DS3 and DS4) is assumed to be $906.00/m^2, as both states would require wall replacement (Salem et al. 2018).

Figure 9 shows a detailed distribution of resilience parameters across the façade generated by three distinct threat locations (R_1, R_4, and R_7) as well as the envelope of the three. The envelope represents an imaginary scenario illustrating aggregated losses caused by the variability in threat location and can be of use for optimizing resources. Figure 9a, b, and c report functional loss, downtime (repair time), and the local resilience indicator, respectively. It should be noted that I_{Ri} is based on the assumption of a linear recovery path, which implicitly presupposes a con-

(a) Elevation

Investigated façade
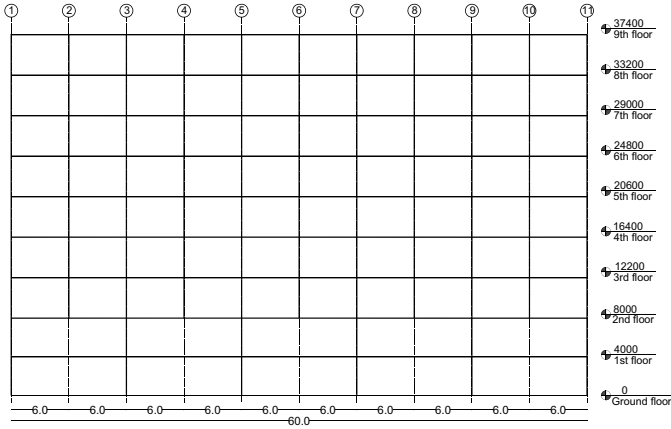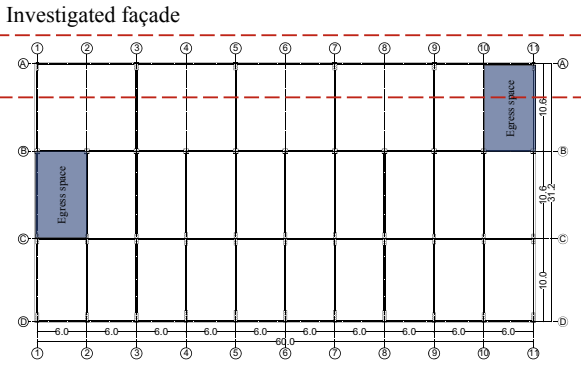
(b) Plan of ground and second floors

Investigated façade
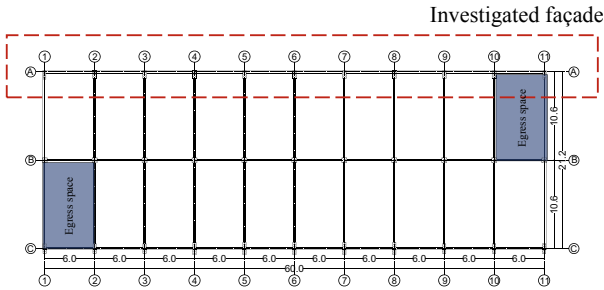
(c) Plan of third through ninth floor

Fig. 4 Administrative building archetype. Adapted from the Alfred P. Murrah federal building

Fig. 5 Map of functionality importance factors

Fig. 6 Secured areas in threat scenarios 1 and 2
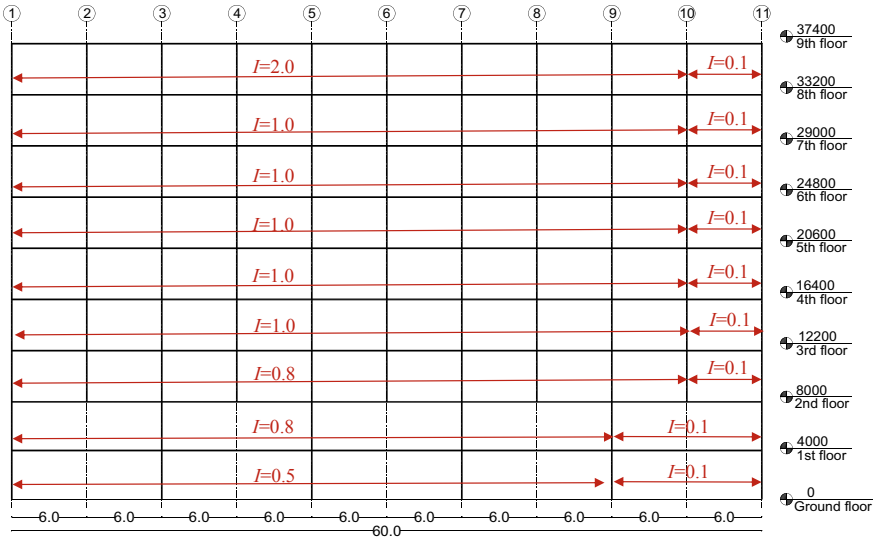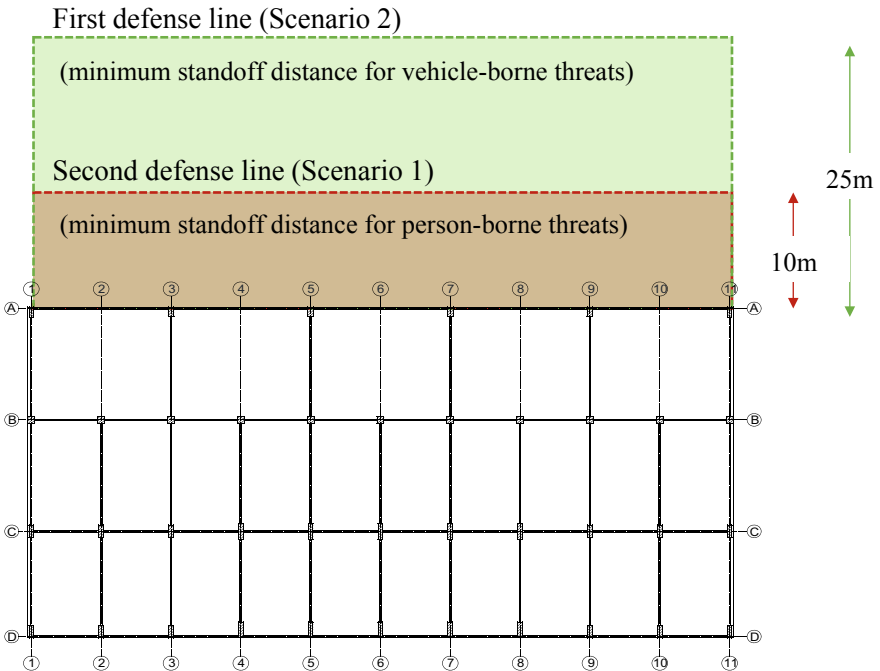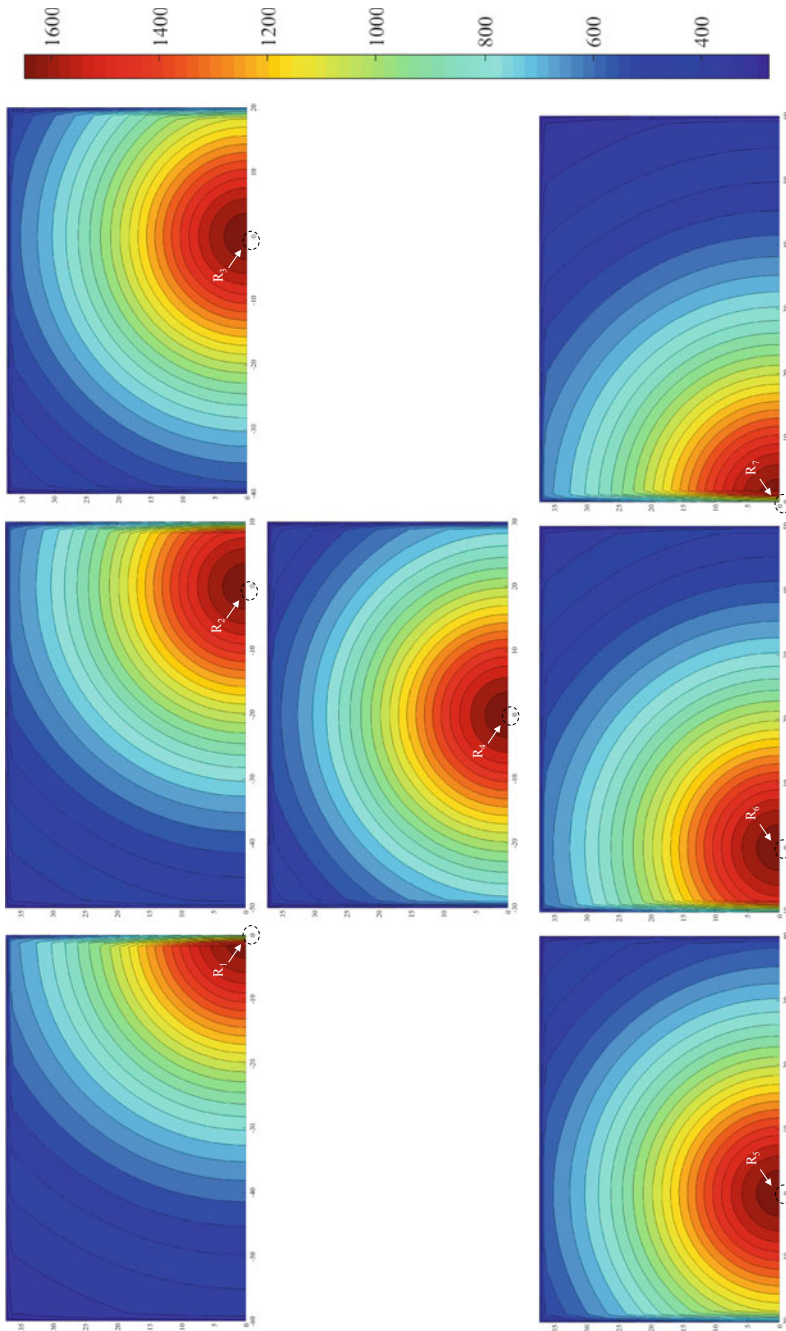
Fig. 7 Variation of specific impulse caused by threat location uncertainty in scenario 1
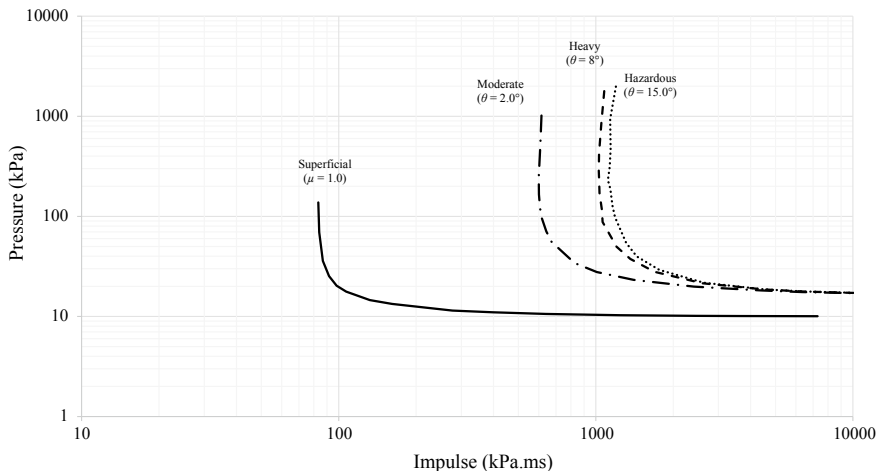
Fig. 8 Pressure-impulse diagrams of the exposed façade generated by SBEDS software (USACE 2008)

stant supply rate of resources. For the sake of simplicity, a series repair scheme is assumed—wherein repair activities are conducted floor by floor, one at a time—and the number of repair workers is set to eight (one crew), based on FEMA P-58 (FEMA 2012a, b) guidelines, which recommend one worker each 92 m^2 (1000 ft^2) at the rate of \$255/hr and a labor production commencement time LPCT = 69%.

The envelope in Fig. 9a displays the variation of functional loss across the façade, which accounts for the vulnerability of the façade components to the threat as well as the area and importance factor of each affected bay. The envelope in Fig. 9b depicts the downtime required to repair each façade component, depending on the applicable damage state. The color coding underscores the different envelopes obtained for functional loss and downtime: Façade components critical to the function loss are at the upper floor, owing to its importance, while the components at the ground level are the most critical to the downtime, because the smaller standoff distance causes greater damage. From these results, it can be inferred that, generally, it is not possible to minimize both functional loss and downtime. To overcome this dilemma, the I_{Ri} envelope in Fig. 9c, which integrates the functional loss over time, can be used as a final arbiter in the decision-making process. Finally, Fig. 10 illustrates the envelope distribution of resilience parameter across the façade in scenario 2. The similarity between functional loss envelopes of scenarios 1 and 2 is apparent and it is attributed to the fragility of the façade components in relation to the assumed explosive charges, in that all components experienced damage greater than DS1 in both scenarios. However, the downtime resulting from scenario 2 is significantly longer than that from scenario 1, as a greater number of elements are damaged in the former, with consequent increment in both repair time and local resilience indicator.

Fig. 9 Resilience parameters for scenario 1 and three different threat locations: **a** functional loss; **b** downtime; **c** local resilience indicator

(a)

0.99	0.99	0.99	0.99	0.99	0.99	0.99	0.99	0.99	0.05
0.49	0.49	0.49	0.49	0.49	0.49	0.49	0.49	0.49	0.05
0.49	0.49	0.49	0.49	0.49	0.49	0.49	0.49	0.49	0.05
0.49	0.49	0.49	0.49	0.49	0.49	0.49	0.49	0.49	0.05
0.49	0.49	0.49	0.49	0.49	0.49	0.49	0.49	0.49	0.05
0.49	0.49	0.49	0.49	0.49	0.49	0.49	0.49	0.49	0.05
0.49	0.49	0.49	0.49	0.49	0.49	0.49	0.49	0.49	0.05
0.40	0.40	0.40	0.40	0.40	0.40	0.40	0.40	0.40	0.05
0.79		0.79		0.79		0.79			0.10
0.49		0.49		0.49		0.49			0.10

(b)

33.3	33.3	33.3	33.3	33.3	33.3	33.3	33.3	33.3	33.3
61.8	61.8	61.8	61.8	61.8	61.8	61.8	61.8	61.8	61.8
61.8	61.8	61.8	61.8	61.8	61.8	61.8	61.8	61.8	61.8
61.8	61.8	61.8	61.8	61.8	61.8	61.8	61.8	61.8	61.8
61.8	61.8	61.8	61.8	61.8	61.8	61.8	61.8	61.8	61.8
61.8	61.8	61.8	61.8	61.8	61.8	61.8	61.8	61.8	61.8
61.8	61.8	61.8	61.8	61.8	61.8	61.8	61.8	61.8	61.8
61.8	61.8	61.8	61.8	61.8	61.8	61.8	61.8	61.8	61.8
117.7		117.7		117.7		117.7			117.7
117.7		117.7		117.7		117.7			117.7

(c)

16.46	16.46	16.46	16.46	16.46	16.46	16.46	16.46	16.46	0.82
15.28	15.28	15.28	15.28	15.28	15.28	15.28	15.28	15.28	1.53
15.28	15.28	15.28	15.28	15.28	15.28	15.28	15.28	15.28	1.53
15.28	15.28	15.28	15.28	15.28	15.28	15.28	15.28	15.28	1.53
15.28	15.28	15.28	15.28	15.28	15.28	15.28	15.28	15.28	1.53
15.28	15.28	15.28	15.28	15.28	15.28	15.28	15.28	15.28	1.53
15.28	15.28	15.28	15.28	15.28	15.28	15.28	15.28	15.28	1.53
12.22	12.22	12.22	12.22	12.22	12.22	12.22	12.22	12.22	1.53
46.56		46.56		46.56		46.56			5.82
29.10		29.10		29.10		29.10			5.82

Fig. 10 Envelop resilience parameters for scenario 2: **a** functional loss; **b** downtime; **c** local resilience indicator

4 Conclusions

The need for an integrated approach to blast-resistant design becomes apparent when the broader consequences of terrorism are to be estimated in the context of a complex system of structures and infrastructure that is growing in size, interconnectedness, vulnerability, end threat exposure. As the history of natural disaster has shown, human endeavors have often begotten the unintended consequence of moving communities in harm's way, under the allure of "safe development" projects. When the focus is shifted to smart buildings of symbolic and/or strategic importance, current technological developments in sensors and information systems have significantly contributed to improving safety, health, and convenience. They can, however, serve as a beacon for terrorist attacks in the manner of bombings, which are known to have a disproportionate impact on a population's morale and its economy. Traditional risk assessment schemes—with specific applications to facilities involved in blast events of a malicious origin—prove insufficient when domino effects on the public at large and indirect costs dwarf direct losses. To manage seemingly intractable uncertainties, engineering resilience into every economic, financial, and physical system is the only viable option on the horizon. In the case of individual buildings, this chapter has introduced a viable framework for their design and assessment under the threat of blast loading. The metrics adopted to support the decision–making process include, primarily, functional loss and downtime. When faced with the problem of optimizing resources, the analyst may investigate the Pareto front generated by these two variables. In alternative, a simpler approach can be suggested in the form of a global resilience indicator, which can synthesize the information generated by resilience-based analysis into one single number—easily actionable by stakeholders and authorities having jurisdiction.

References

Almufti, I., & Willford, M. (2013). *REDiTM rating system: Resilience-based earthquake design initiative for the next generation of buildings*. Arup Co.

ASCE. (2011). *Blast protection of buildings. ASCE 59–11*, (American Society of Civil Engineers, ed.), American Society of Civil Engineers, Reston, VA, VA.

Attoh-Okine, N. O., Cooper, A. T., & Mensah, S. A. (2009). Formulation of resilience index of urban infrastructure using belief functions. *IEEE Systems Journal, 3*(2), 147–153.

Ayyub, B. M. (2015). Practical resilience metrics for planning, design, and decision making. *ASCE-ASME Journal of Risk and Uncertainty in Engineering Systems, American Society of Civil Engineers, 1*(3), 1–11.

Bier, V. M., Nagaraj, A., & Abhichandani, V. (2005). Protection of simple series and parallel systems with components of different values. *Reliability Engineering & System Safety, 87*(3), 315–323.

Bruneau, M., Chang, S. E., Eguchi, R. T., Lee, G. C., O'Rourke, T. D., Reinhorn, A. M., et al. (2003). A framework to quantitatively assess and enhance the seismic resilience of communities. *Earthquake Spectra, 19*(4), 733–752.

Burby, R. J. (2006). Hurricane Katrina and the paradoxes of government disaster policy: Bringing about wise governmental decisions for hazardous areas. *The ANNALS of the American Academy of Political and Social Science, 604*(1), 171–191.

Corley, W. G., Sozen, M. A., Thornton, C. H., & Mlakar, P. F. (1996). *The Oklahoma City bombing: Improving building performance through multi-hazard mitigation.*

CSA. (2012). *CSA S850-12 Design and assessment of buildings subjected to blast loads*. Mississauga, ON, Canada: Canadian Standards Association.

Dell EMC. (2017). *Smart cities and communities—GDT Smart City Solutions on Intel®-based Dell EMC infrastructure*. Hopkinton, MA, USA.

FEMA-426. (2011). *BIPS 06/FEMA 426: Reference manual to mitigate potential terrorist attacks against buildings*. U.S. Department of Homeland Security.

FEMA. (2012a). *Seismic performance assessment of buildings. Volume 3—Performance assessment calculation tool (PACT) version*. Federal Emergency Management Agency, Redwood City, California.

FEMA. (2012b). *Seismic Performance Assessment of Buildings. Volume 2—Implementation Guide*. Federal Emergency Management Agency, Redwood City, California.

FEMA Mitigation Assessment Team. (2006). Hurricane Katrina in the Gulf Coast building performance observations, recommendations, and technical guidance. Federal Emergency Management Agency (FEMA).

Fitzpatrick, J. H. (2005). The Impact of a new large-scale terrorism attack on insurance, reinsurance and the economy. *Workshop Session at the World Economic Forum in Davos*, 2001–2003.

Ghosn, M., & Moses, F. (1998). *Redundancy in highway bridge superstructures*.

Grant, M., & Stewart, M. G. (2012). A systems model for probabilistic risk assessment of improvised explosive device attacks. *International Journal of Intelligent Defence Support Systems, 5*(1), 75.

Grant, M., & Stewart, M. G. (2015). Probabilistic risk assessment for improvised explosive device attacks that cause significant building damage. *Journal of Performance of Constructed Facilities, 29*(5), B4014009.

Helbing, D. (2013). Globally networked risks and how to respond. *Nature, 497*(7447), 51–59.

Marjanishvili, S. (2017). Resilient bridge design to extreme events. In Y. Bazilevs & J. S. Chen (Eds.), *Engineering Mechanics Institute Conference.* San Diego, California, USA.

Morrill, K. B., Malvar, L. J., Crawford, J. E., & Ferritto, J. M. (2004). Blast resistant design and retrofit of reinforced concrete columns and walls. *Structures 2004* (pp. 1–8). American Society of Civil Engineers, Reston, VA.

NIAC (National Infrastructure Advisory Council). (2010). *A framework for establishing critical infrastructure resilience goals*. Department of Homeland Security, Washington, D.C.

Quiel, S. E., Marjanishvili, S. M., & Katz, B. P. (2016). Performance-based framework for quantifying structural resilience to blast-induced damage. *Journal of Structural Engineering, 142*(8), C4015004.

Rinaldi, S., Peerenboom, J., & Kelly, T. (2001). Identifying, understanding, and analyzing critical infrastructure interdependencies. *Control Systems, IEEE*.

Salem, S., Campidelli, M., El-Dakhakhni, W., & Tait, M. (2017). *Blast resilient design of infrastructure subjected to ground threats. Volume 4: Fluid-Structure Interaction*, ASME, Hawaii, USA, V004T04A018.

Salem, S., Campidelli, M., El-Dakhakhni, W. W., & Tait, M. J. (2018). Resilience-based design of urban centres: Application to blast risk assessment. *Sustainable and Resilient Infrastructure, 3*(2), 68–85.

Sozen, M. A., Thornton, C. H., Corley, W. G., & Sr., P. F. M. (1998). The Oklahoma city bombing: Structure and Mechanisms of the Murrah building. *Journal of Performance of Constructed Facilities*, *12*(3), 120–136.

Strong, E. E. (2000). *Repetition: A study of the structural bay. The proposal of a concert hall for the Virginia Symphony on Belle Isle, Richmond, Virginia*. Virginia Polytechnic Institute and State University.

Swiss Re Ltd. (2016). *Natural catastrophes and man-made disasters in 2015: Asia suffers substantial losses*. Zurich, Switzerland: Swiss Re Ltd.

UN (United Nations). (2004). *World Population to 2300*. (U. Nations, ed.), Department of Economic and Social Affairs, Population Division, New York, NY.

USACE, U. A. C. of E. (2005). *Lake Pontchartrain and Vicinity Hurricane Protection*. Washington, DC.

USACE, U. A. C. of E. (2008). *User's guide for the single-degree-of-freedom blast effects design spreadsheets (SBEDS)*. ACE Protective Design Centre, USA, PDC TR-06-01 Rev 1, Omaha, NE.

Van Riper, P. (1997). *A concept for future military operations on urbanized terrain*. Quantico, VA: Gazette.

WEF (World Economic Forum). (2018). *The global risks report 2018* (13th Ed.). World Economic Forum, Geneva, Switzerland.

Seismic Mitigation Framework for Non-engineered Masonry Buildings in Developing Countries: Application to Malawi in the East African Rift

Viviana Novelli, Panos Kloukinas, Raffaele De Risi, Innocent Kafodya, Ignasio Ngoma, John Macdonald and Katsuichiro Goda

1 Introduction

Earthquakes are the major cause of deaths in comparison with other natural hazards, such as floods, tsunamis, volcanic eruptions, winds and droughts (Shapira et al. 2018). Fatalities due to seismic events amount to about 60,000 people a year, and around 90% of deaths occurs in developing countries (OECD 2018). Moreover, in the latest seismic events in developing countries, fatalities are largely associated with the collapse of non-engineered masonry buildings (Guragain et al. 2018; Lang et al. 2018), which are poorly constructed and highly at risk in seismic prone regions (Arya 2018).

Clearly, to minimise building collapses in developing countries, reduce human losses, and increase resilience through effective mitigation, it is important to assess

V. Novelli (✉) · R. De Risi · J. Macdonald
Department of Civil Engineering, University of Bristol, Bristol BS8 1TR, UK
e-mail: vn18530@bristol.ac.uk

R. De Risi
e-mail: raffaele.derisi@bristol.ac.uk

J. Macdonald
e-mail: john.macdonald@bristol.ac.uk

P. Kloukinas
Faculty of Engineering & Science, University of Greenwich, Chatham ME4 4TB, UK
e-mail: p.kloukinas@greenwich.ac.uk

I. Kafodya · I. Ngoma
University of Malawi, The Polytechnic, Blantyre, Malawi
e-mail: ikafodya@poly.ac.mw

I. Ngoma
e-mail: ingoma@poly.ac.mw

K. Goda
Department of Earth Sciences, Western University, London N6A 5B7, Canada
e-mail: kgoda2@uwo.ca

seismic risk and propose solutions to mitigate seismic damage (Habieb et al. 2017; Fulzele and Aggarwal 2018; Gilani and Miyamoto 2018). Indeed, in developed countries, such as the USA, New Zealand, Japan and most of the seismic prone areas in Europe, numerous efforts have been made to standardise approaches for both building assessment and seismic mitigation (ATC 20, ATC 20-2, NZSEE 2016; JBDPA 1990; CEN. 2004; European Standard EN 1998-1-2004). In contrast, in developing countries the same efforts have not been committed due to a lack of resources and expertise to draw up seismic design codes (Arendt et al. 2017; Zepeda 2018). Hence, either seismic design codes do not exist or, if they are available, as it is the case for India (Bureau of Indian Standards 2015 and IS:1893, Part 1, 2002), Nepal (NBC 105, 1994), China (Guo-Xing 2003), East Africa (Lubkowski et al. 2014), and Latin America, (Chavez et al. 2012), these codes are based on international standards for engineered buildings (e.g. Eurocodes and North American standards). This leads, in the latter case, to standards recommending the use of techniques and materials which are not cost effective in developing countries. Therefore, local communities opt to construct non-engineered masonry buildings with low quality materials and poor construction practice (Bhagat et al. 2017). Subsequently, when informal settlements are highly populated by non-engineered masonry buildings, they may be exposed to potentially destructive seismic events, and evidently, there is a need for methods to assess seismic risk and reduce damage probability through low-cost retrofitting solutions. Currently, an approach which combines assessment and retrofitting of non-engineered masonry buildings does not exist, justifying the promotion of research activities on implementing seismic risk assessment methodologies in recent years (Novelli et al. 2015; Yepes-Estrada et al. 2016; Goda et al. 2016, 2018; Di Meo et al. 2018; Nassirpour et al. 2018; Spacone et al. 2019).

The current chapter aims to address this gap in the existing literature by offering a guidance for assessing non-engineered masonry buildings and identifying suitable mitigation solutions to increase seismic resilience in developing countries. This guidance consists of a seismic mitigation framework for collecting data, classifying buildings in typologies, estimating building performance and recommending low-cost retrofitting interventions. In this framework, building features and related typologies are identified with procedures based on existing global datasets or locally collected data. Since non-engineered masonry buildings are characterised by low structural integrity, the framework introduces an extensive classification approach based not only on structural and geometric features but also on data related to deficiencies, needed to address low-quality materials and poor building practice.

Building performance is evaluated using existing risk assessment methods. Since these methods are mainly developed to assess engineered buildings or buildings within specific regions, they are not always applicable to different regional contexts and environments. To overcome limitations of existing approaches, these methods are reviewed by discussing their potential applicability in developing countries, and their capacity to identify highly vulnerable non-engineered building typologies, which require mitigation plans to enhance their actual structural performance. Due to the scarce economic resources and the potential lack of technical expertise in the developing countries, in this framework, mitigation is based on low-cost retrofitting

interventions. Notably, the proposed solutions underline how retrofitting of buildings should be done and does not necessarily involve (or require) great cost, but essentially requires correct and simple practices.

The entire methodology of the seismic mitigation framework is presented in Sect. 2 and its applicability in a real context is presented in Sect. 3, where the proposed framework was applied to a case study in Malawi. The case study focuses upon a representative location in the country, where the expansion of informal settlements has been occurring rapidly. The case study is useful for not only validating the discussed methodology but also analysing issues and solutions adopted to overcome inconsistencies between multiple sources including global databases [e.g. PAGER (Jaiswal and Wald 2008; World Housing Encyclopedia 2002)] local archives (e.g. census data (National Statistical Office of Malawi 2008) and data collected onsite through rapid surveys (as part of Step 1). Building classifications for the constructions in Malawi were derived using data collected through the surveys, which were conducted to record more detailed information related to geometrical/structural features and building quality, as advised in Step 2. According to the collected data, three typologies of different vulnerability were identified and adopted in Step 3, where the mechanical method FaMIVE: Failure Mechanism Identification and Vulnerability Evaluation (D'Ayala and Speranza 2003) has been used to derive fragility curves and failure mode distribution. Retrofitting interventions were identified according to both observed deficiencies and estimated failure modes, and they were recommended as solutions to improve building performance and actual building practice. The effectiveness of the proposed low-cost engineering interventions was also discussed by comparing building capacities assessed before and after retrofitting interventions.

2 Methodology

The seismic mitigation framework is presented in four steps, as introduced in Fig. 1. Brief descriptions of the procedure are:

- Step 1 examines which types of data can be collected from local databases and archives and how these data can be used to gain deeper understanding of non-engineered masonry building practice. It also explains how preliminary on-site investigations should be organised and performed to identify locations of major interest, which require detailed investigations within structural campaigns.

Step 1: Local data acquisition and preliminary visits
Step 2: Building typology classification
Step 3: Derivation of fragility curves
Step 4: Seismic mitigation program

Fig. 1 Seismic mitigation framework

- Step 2 implements the classification for non-engineered masonry buildings and the structural survey plan to identify the critical factors that significantly affect seismic performance of non-engineered masonry buildings. These factors cover a variety of parameters defined to assess structural/geometric features, to rank the quality of materials and structural components and to record the presence of damage and deficiencies. Among the defined parameters, some are defined as the minimum required parameters to classify non-engineered masonry building typologies. Moreover, it specifies how surveys are planned and how parameters are assessed at different levels of detail and then used to classify building typologies.
- Step 3 discusses the possibility to derive seismic fragility curves for non-engineered masonry buildings using existing methods available in the literature. Since existing methods are subjected to different limitations and uncertainties, a critical review of the methods relying on (1) expert-opinion based approaches and (2) analytical model-based approaches is offered to illustrate their applicability in developing countries. For existing methods, their levels of accuracy and sophistication are discussed and their different options to fuse global data available in international datasets with local data collected from rapid/detailed surveys are shown.
- Step 4 provides guidance to plan retrofitting solutions for a mitigation plan to reduce seismic risk and increase resilience. The proposed retrofitting solutions are based on low-cost engineering strategies and they are proposed to improve construction techniques adopted for non-engineered masonry buildings.

The seismic mitigation framework is presented in the following sub-sections, to describe the details of each step mentioned above.

2.1 Step 1: Local Data Acquisition and Preliminary Visits

Step 1 describes local data collection and how these data can be employed to reach improved understanding of local construction techniques. Some of these local data, when available, may lack consistency; therefore, these gaps and discrepancies are also discussed.

Local data can be collected from archives and sources available from the literature. These data are needed for the following objectives: (1) identifying city/village sizes and building distribution, and (2) understanding local construction techniques. These can be fulfilled using maps and urban plans to identify locations of cities, towns, and villages, as well as locations of informal settlements where non-engineered masonry buildings are mostly found. Informal settlements are not always distinguishable, since they are constructed outside of both formal planning and building permit processes, and therefore typically have a chaotic building distribution in urban areas, and a more spread distribution in rural areas. These types of settlements are the main residential developments in rural areas, while in urban environments, informal settlements always coexist with formal ones.

To identify building settlements with the highest population density, census data, providing information related to the number of inhabitants and households, data related to agriculture and business, and building typologies (e.g. structural type, height, year of construction) are useful. However, reliability of census data depends on how they are gathered and how often they are updated. In developing countries where data collection is an issue due to lack of local economic and technological resources, census data do not always provide an accurate database (Corburn and Riley 2016; Ezeh et al. 2016; Satterthwaite et al. 2018).

Building settlements should not only be characterised with reference to the population but also to building constructions and their related distribution, as this allows it to be identified where vulnerable building typologies are located. Within this scope, local seismic standards are normally the first document that should be consulted, to gain deep knowledge about building constructions and construction techniques adopted in the country. However, in developing countries, and particularly in informal settlements, standards cannot be used for this purpose, since there is often great discrepancy between actual building/construction practice and recommendations given by the standards in place. This occurs because international standards, such as Eurocodes and North American codes, based on techniques for engineered buildings, are sometimes merely nominal references in developing countries and therefore residents build houses using available and affordable materials and techniques.

To overcome this lack of compliance with recommended standards, in many developing countries, guidelines for non-engineered constructions are often developed and provided for local communities. In these guidelines, which are an important source to have access to information about local construction techniques, non-technical information about how non-engineered buildings should be constructed to be seismically resilient are provided. However, although these guidelines propose low-cost engineering practices, they are not always followed, since in some low-income developing countries, local communities struggle to obtain good quality materials. Furthermore, there is also the problem of identifying and disseminating the best building practice in guidelines, since many experts recommend use of technologies, that may not be either adequate to improve building performances or relevant under the economy and social environment of a specific country (Shah et al. 2018a). At the same time, since dissemination of new building practice is not in place, householders and local builders are often unaware of existing guidelines and therefore build houses according to local skills and experience (Fulzele and Aggarwal 2018).

To overcome deficiencies in the existing databases, on-site visits and direct inspection of local buildings are the most effective means. These visits should be planned, realising that it is not feasible to survey all buildings. It is also important to recognise the difficulty in relying on local resources due to lack of local skills and expertise in case collected information on a building sample is not complete or more detailed surveys are required. During preliminary visits, rapid walk-through surveys are usually effective as no measurements are required, and a large number of buildings can be inspected in relatively short time. In conducting walk-through surveys, GPS tools and cameras are useful to record locations and take photos of the most common types of buildings observed on site.

2.2 Step 2: Building Typology Classification

Since buildings belonging to the same typology are expected to have the similar seismic performance, it is reasonable to classify buildings into building typologies by ensuring uniform treatment and interpretation of the data (Coburn and Spence 2003; Abrahamczyk et al. 2013). Building typologies can be identified using different approaches. In case data are limited and there is no possibility to carry out structural surveys, buildings can be classified using global data available in international datasets (e.g. PAGER (Jaiswal et al. 2011); World Housing Encyclopedia (http:// www.world-housing.net/), and Global Earthquake Model (Silva et al. 2014)). These classifications are based on specific regions and rely on limited data, which are adopted to extrapolate classifications to other nearby regions, where data are not available. Since these extrapolations are usually based on expert judgment and lack of knowledge of the building environment in a specific region limits the possibility to validate these methods, the applicability of the global datasets may be difficult to be justified.

To assign accurate building typologies, it is proposed to classify non-engineered masonry buildings with reference to a set of parameters defined in Fig. 2. These parameters largely affect seismic building performance and are selected according to field experience of the authors. The parameters are classified into (1) "structural system" describing both the types of construction materials and the roof/floor system, (2) "geometry" describing plan, elevation, and opening layout, (3) "structural irregularity" describing irregularity in plan (e.g. re-entrant corner), in elevation (e.g. portico, additional floors), and identifying the presence of protruding elements (e.g. chimneys, columns, and canopy parapets), (4) "strengthening elements" describing the presence of elements constructed to improve structural detailing (e.g. buttresses; timber or steel wall plates, timber or concrete ring beams), (5) "quality" describing construction building quality in terms of materials and structural detailing (e.g. neat or chaotic brick distribution, poor or high quality brick texture, good or bad connections between walls and roof/floors), (6) "deficiencies" identifying shortcomings due to lack of maintenance exhibited by the presence of moisture, vegetation, roof/floors/walls damage, or loss of material, and (7) "seismic damage" identifying presence of cracks, which can be associated to seismic failure modes in case of the building being damaged by an earthquake.

To collect information related to the parameters in Fig. 2 and to derive building typologies, structural surveys may be necessary: (1) by inspecting a sufficient number of buildings, which allow the typologies to be characterised and (2) at specific locations (or settlements) selected as the most typical ones in the region of study, as defined in Step 1. Surveys can be conducted efficiently if the survey team uses inspection forms (either PC-tablet-based or hardcopy paper-based). The tools used in data collection should have flexible architecture, in a way that when they are adopted for buildings in a regional context, characterised by parameters which are not included in the original version of such tools, the same tools can be adapted and expanded (Novelli et al. 2015). Before starting a structural campaign, surveyors need
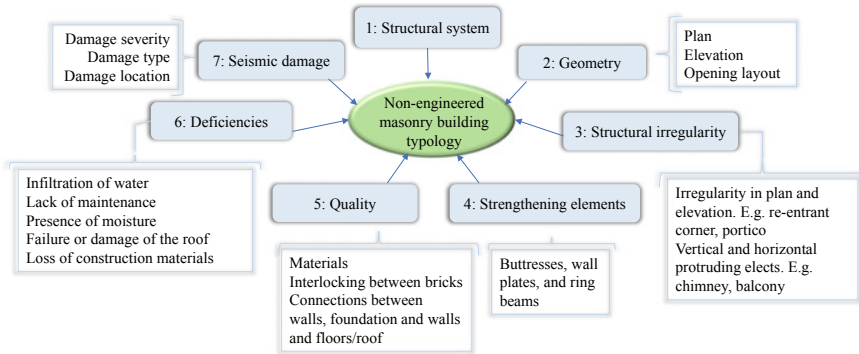
Fig. 2 Building typology classification for non-engineered buildings

be trained to be familiarised with (1) how buildings in the region are constructed, and (2) which parameters among the ones in Fig. 2 require attention and need to be surveyed carefully.

2.3 Step 3: Derivation of Fragility Curves for Building Typologies

Nowadays, various seismic fragility assessment methods are available in the literature. Many of them are based on empirical procedures, while others rely on more sophisticated numerical models (Lang 2002; Calvi et al. 2006; D'Ayala et al. 2014; Rossetto et al. 2014; Pitilakis 2015). The common goal of these procedures is to assess buildings and their structural performance under earthquake loading. Seismic fragility functions characterise the probability of exceeding damage levels for different earthquake excitation levels. These methods are generally developed to assess building typologies within specific contexts. Consequently, they may not be suitable to assess specific buildings. Furthermore, since existing fragility assessment methods are often implemented to estimate seismic performance of engineered constructions, they are not directly applicable to non-engineered masonry buildings, constructed with weak materials and under poor quality control, resulting in premature seismic failures. This underlines the need to review existing methods, and identify the ones capable of striking the best balance in terms of: (1) inaccuracy deriving from limited or incomplete (global or local) data, adopted to characterise non-engineered building typologies, (2) ambiguity arising from partial (or a lack of) information on how non-engineered constructions behave under seismic loads, in particular if seismic data from past earthquakes are not available, and (3) uncertainty arising from intrinsic randomness of the seismic phenomenon. Within this scope, in this chapter, the review is focused on existing methods relying on expert-opinion and numerical

approaches based on engineering mechanics. A review to discuss their applicability to non-engineered masonry building typologies in developing countries is provided in the following subsections.

2.3.1 Methods Relying on Expert Judgement-Based Approach

The methods described in this section rely on expert judgement-based approaches. For these types of procedures (e.g. MSK 64 Scale (Medvedev et al. 1965), ATC-13 Classification (1985), EMS 98 Scale (Grünthal 1998), FEMA 154 (2002), PAGER (Jaiswal et al. 2011), World Housing Encyclopedia (http://www.world-housing.net/), and Global Earthquake Model (Silva et al. 2014)), fragility functions are pre-defined for building typologies located in specific regions and are provided in global datasets, where damage distributions are defined against different ground motion levels (Lang 2002; Calvi et al. 2006; Rossetto et al. 2014). These fragility functions are derived using statistical models, which employ a few structural and geometrical parameters used to identify building typologies and an actual damage distribution for a wide range of ground motions. The use of these pre-defined fragility functions is highly favoured in developing countries, particularly, when data to characterise building typologies and seismic damage from past earthquakes are not available (Schultz et al. 2010), and therefore there is no possibility to derive specific fragility curves based on local data.

It should be noted that classifying buildings with reference to a global dataset is not straightforward because most of the classifications are defined for the USA and Europe, and therefore they are not easily adaptable in developing countries. To overcome this issue and to extend global datasets to developing countries, many researchers employ modifiers defined based on expert opinion (Maqsood et al. 2013; Naguit 2017; De Silve et al. 2018; Shah et al. 2018b). To avoid the use of modifiers, which are highly dependent on engineering judgment, several global datasets (PAGER (Jaiswal et al. 2011), World Housing Encyclopedia (www.world-housing.net), and Global Earthquake Model (Silva et al. 2014) have been introduced with the scope of covering the fragility of the entire world. However, since these datasets use data obtained from specific locations to extrapolate fragility for nearby regions, clearly, their applicability is still questionable and can be misleading (Schultz et al. 2010; Naguit 2017).

2.3.2 Methods Relying on Numerical/Analytical Model-Based Approach

These methods are developed to assess seismic fragility using analytical models of different accuracy and complexity. Numerical model-based approaches relying on Finite element models (Mendes and Lourenço 2009; McKenna 2011; Lagomarsino et al. 2013; Chaibedra et al. 2017; Choudhury and Kaushik 2018; Mendes et al. 2018), are adopted to assess masonry building performance by modelling index buildings representative of typologies. However, these approaches, to be reliable,

should be employed on a considerable amount of structural and geometrical data. Furthermore, even if these approaches are broadly used, they have a significant drawback in capturing complex behaviour and failure modes of masonry structures. Most of them perform only in-plane analysis for buildings characterised by well-connected walls and floors, while only a small fraction of them can perform both in-plane and out-of-plane analysis on buildings characterised by well (or poorly) connected walls and floors (Novelli et al. 2015).

Among the analytical approaches there are also methods based on mechanical models which have the advantage of being capable of assessing seismic performance of a masonry building for both in-plane and out-of-plane failure modes. These approaches (Bernardini el at. 1990; D'Ayala and Speranza 2003; Restrepo-Vélez and Magenes 2004; Addessi et al. 2014) aim at estimating collapse load factor multipliers of a given configuration of macro-elements and loads by imposing kinetic energy equations. These methods present the benefit of requiring a few input parameters, which can be collected with semi-rapid on-site investigations to estimate collapse load factor multipliers and to identify of possible failure modes.

2.4 Step 4: Seismic Mitigation Programs

A seismic mitigation is a programme which employs the most cost-effective retrofitting solutions to reduce causalities and loss of properties in case an earthquake occurs in the future. In developing countries, cost-effective solutions promote: (1) low-cost engineering actions which are affordable to local communities; (2) simple retrofitting interventions which do not require high expertise; (3) transferable retrofitting strategies to different typologies and sites; and (4) innovative self-sustaining construction techniques based on using local materials and local resources which benefit the economy of the region under study. To ensure the success of a mitigation plan, building capacities before and after retrofitting need to be assessed and compared. When the comparison shows an improvement in the performance of retrofitted buildings, the mitigation programme is viable and can be implemented.

3 Case Study: Malawi

Malawi is located in Sub-Saharan Africa and shares borders with Mozambique, Zambia, and Tanzania (see Fig. 3). Although, in the last decades, the country has been made important economic reforms to accelerate the economic growth, poverty remains prevalent (OECD 2018). The country is ranked as the third poorest country in the world (FAO, IFAD, and WFP 2015; World Bank 2017), where the main economic sector is agriculture, which is often negatively affected by adverse environmental disturbances and hazards (e.g. hot weather, health, heavy rain, wind, and flood).
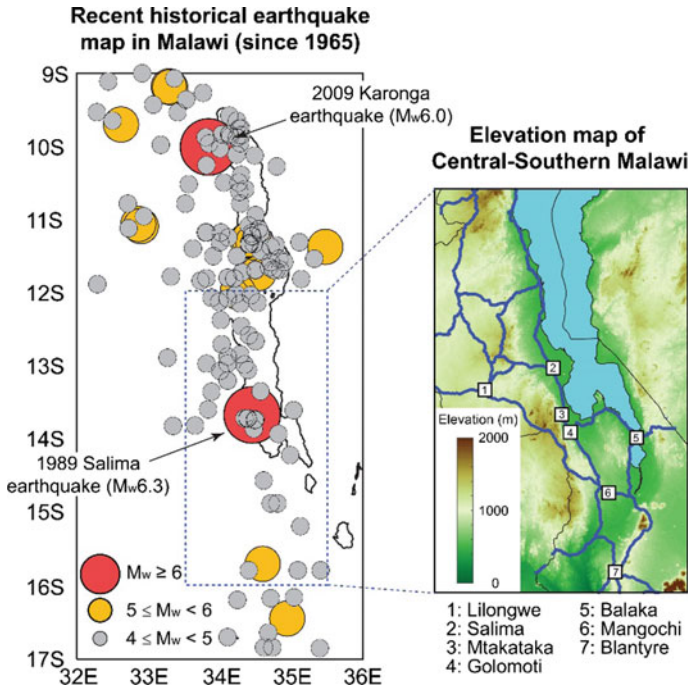
Fig. 3 Map of Malawi, and identification of the sites of interest. *Source* MASDAP (http://www.masdap.mw/) for road data, and SRTM (https://www2.jpl.nasa.gov/srtm/) for elevation data

Malawi is also a seismic-prone country within the southern branch of the active East Africa Rift System, where M_w 7.0 (or greater) earthquakes can occur near major geological faults. The most significant earthquake in the country in recent history occurred in 1989 with M_w 5.7, making 50,000 people homeless in the centre of Malawi (Midzi and Manzunzu 2014). The Karonga earthquake sequence of 2009 with M_w 4.9–6.0 is also remembered as one of the most recent major seismic events in the country; 300 people or more were injured and about 4000 dwellings were destroyed or damaged (Hayashi 2014).

In Malawi, non-engendered masonry buildings are the most popular construction adopted for dwellings, as is the case for most countries in East Africa and most developing countries around the world. Houses of this type are built informally by local artisans using poor quality materials and structural detailing. In addition to this poor construction practice, lack of quality control underlines a need to investigate seismic building performance through methods capable of estimating damage probability and identifying effective retrofitting solutions to prevent failures due to future seismic events.

In this section, seismic performance of masonry houses in Malawi were evaluated by following the framework proposed in Sect. 2. Different building stocks of non-engineered masonry buildings, located in informal settlements, were selected by inspecting population/household numbers in the Malawi Housing and Population Census (National Statistical Office of Malawi 2008) and Google Earth images (https://earth.google.com/web/). To obtain realistic proportions of the building distribution in the selected informal settlements, preliminary surveys were conducted in Central and Southern Malawi. Data collected in this phase, as indicated in Step 1 of the framework, were used to understand building distribution/typologies and local practice indicated in (1) available urban plans (2) the existing demographic information that is available from the 2008 Malawi Housing and Population Census (National Statistical Office of Malawi 2008), and (3) the World Housing Encyclopaedia (2002) and (4) PAGER (Jaiswal et al. 2011) and (5) Safer Housing Construction Guidelines for non-engineered buildings (Bureau TNM 2016). To enrich the available data and characterise buildings structurally, onsite campaigns were carried out and 40 buildings were inspected through semi-detailed structural surveys. Data for these buildings, as discussed in Step 2 of the framework, were recorded qualitatively and used to characterise only some of the parameters shown in Fig. 2; the recorded parameters were the ones which had a significant impact on the structural behaviour of the inspected buildings. Successively, the collected data were used to identify three different building typologies for non-engineered masonry buildings, which differ in construction material, roof type, quality of structural detailing, irregularity, and observed deficiencies.

To assess the seismic risk of the selected regions, the seismic vulnerability of the three building types were evaluated by using the mechanical approach FaMIVE (D'Ayala and Speranza 2003). The method belongs to the class of analytical approaches based on simplified numerical models, introduced in Step 3. The approach was used to understand building seismic performance in terms of both capacity and damage probability, providing fragility curves at different damage thresholds for each of the identified non-engineered building typologies.

Results from FaMIVE were adopted for identifying most likely failure modes in the case of intense ground shaking and facilitate the selection of suitable mitigation solutions for Malawi from an economic and technical point of view (Step 4). The proposed solutions were based on low-cost engineering interventions, as advised in the framework, and they were mainly adopted to prevent out-of-plane failure modes, which had mainly occurred in the non-engineered masonry buildings with poor construction standards, damaged by the Karonga earthquake in 2009 (Kushe et al. 2017). To highlight the benefit of the proposed solutions, capacities for the building typologies before and after the retrofitting plan proposed for Malawi were evaluated and compared.

3.1 Step 1: Local Data Acquisition and Preliminary Visits in Malawi

The first data collection for Malawi, as proposed in Step 1, were performed using information taken from local archives and available datasets, which were used to gather information related to non-engineered masonry building distribution and typologies and to gain a deeper understanding of local building codes and construction techniques. Within this scope, the accessible sources in Malawi included:

- Urban plan used to derive building settlement location (UN-HABITAT, United Nations High Commissioner for Refugees (UNHCR), and International Federation of Red Cross (IFRC) (2010–2012))

In Malawi, the total population is more than 18.5 million and is growing at a high annual rate of about 4.02% (UN-HABITAT, United Nations High Commissioner for Refugees (UNHCR), and International Federation of Red Cross (IFRC) (2012)). Due to the population growth there is a rapid expansion of informal settlements not only in small cities and rural villages, but also in major cities, such as Lilongwe and Blantyre. For these settlements, urban plans are not regularly updated, due to lack of proper management framework or residential development. This happens because in formal settlements new property developments are registered at the local city council or district council, while in informal settlements new houses are built outside the formal planning and building permit processes. Detailed figures on these aspects are provided in UN-HABITAT, United Nations High Commissioner for Refugees (UNHCR), and International Federation of Red Cross (IFRC) (2010), where the rapid, and uncontrolled expansion of informal settlements is highlighted as the main challenge for housing sector and built environment management in the country.

- Local/global datasets used to identify building classification:

  - National census database (National Statistical Office of Malawi 2008)
    The last census database was made locally available in 2008. The entire country is divided into small Enumeration Areas (EA). The population and number of households in the census are reported with reference to each identified EA in the country. The same database also includes information about building types, which are classified as: (a) traditional, typically consisting of sun-dried brick walls, mud floors, and grass thatch, (b) semi-permanent, being built of any combination of sun-dried and fired bricks, and (c) permanent, being made of fired bricks and iron roofs. In the census the proportions of traditional, semi-permanent, and permanent dwelling types were 28, 44, and 28% nationwide, respectively.
  - World Housing Encyclopaedia (2002)
    This global classification refers to data gathered from the Malawi National Census database of 1998, and modified by expert judgement, following findings of field surveys (Ngoma and Sassu 2002). According to this dataset, Malawian houses are classified in three main types, where 35% of the dwellings are in

rammed earth (traditional type in the context presented above), 45% are adobe in unburnt brick masonry (could be either traditional or semi-permanent type) and 5% in wattle and daub (traditional type). The remaining 15% are unclassified and are assumed to belong to the permanent housing type.

– PAGER (Jaiswal and Wald 2008)

According to this global dataset, Malawian houses consists of: 15% mud wall houses, 19% adobe block houses, 1% rubble stone, 14% unreinforced fired brick and 51% unreinforced concrete block masonry (Jaiswal and Wald 2008). These values were extrapolated from the UN-HABITAT, United Nations High Commissioner for Refugees (UNHCR), and International Federation of Red Cross (IFRC) (2007), global report which refers to data taken from the 2004 National Census in Tanzania and modified by expert judgement (Jaiswal and Wald 2008).

- Local design codes used to understand local building practice

The official code of practice is MS791-1:2014 (Malawi Bureau of Standards, 2014). This code, based on the British Standards, and is not usually complied with, requiring high construction skills and extensive economic resources. Specifically, for informal settlements, Safer Housing Construction Guidelines (Bureau TNM 2016) are available and developed to provide guidance on good practice to construct low cost masonry buildings. Although the Guidelines are a significant source of information to understand how buildings in informal settlements should be built, communities do not always opt for such solutions because they are not relatively affordable. Furthermore, since a dissemination plan of the existing guidelines is not in place, householders and local builders are often unaware of these guidelines which are currently only available in a digital format.

- Preliminary visit carried out to overcome gaps in existing data

Evidently, the data summarised above underline inconsistencies due to (1) lack of control of residential development affecting the existing urban plan (2) discrepancies between local/global datasets, highlighted by the different criteria adopted to classify buildings and derived building typology distributions and (3) non-compliance with design standards and guidelines leading to a high expansion of informal houses built using poor materials and low quality construction techniques. These gaps and irregularity were also confirmed by preliminary visits carried out on site in eight EAs of Central and Southern Malawi, selected as representative sub-areas by inspecting population/household numbers in the Census (National Statistical Office of Malawi 2008) and Google Earth images (https://earth.google.com/web/). The eight EAs covered five different locations: Salima, Mtakataka, Golomoti, Balaka, and Mangochi (see Fig. 3). In this phase, the selected eight EAs were inspected by conducting a quick walk-through survey in 2017. Compared with the 2008 Census data, the distribution of building types had significantly changed, especially in urban areas, where the proportions of permanent houses had increased, while the proportions of traditional ones had decreased significantly in both urban and rural areas. However, from

the structural vulnerability point of view, this increment in the proportion of permanent buildings cannot necessarily be related to a capacity improvement of the housing stock overall. For example, houses made of burnt brick but with low-quality mud (or even cement) mortars or houses with iron-sheet roofs but no proper connections to the walls were not necessarily more robust than adobe ones (or "semi-permanent" in the Malawi Census classification (National Statistical Office of Malawi 2008)). As a conclusion of the preliminary survey, there was a need for more detailed information to be collected and interpreted wisely to allow a more appropriate building classification, directly linked to the quality of materials and structural details. This leads to the next section, where Malawian houses are described in detail and classified in typologies according to data collected through on-site structural surveys.

3.2   Step 2 Building Typologies Identified in Malawi

Semi-rapid structural surveys were carried out, as proposed in Step 2 of the framework, to characterise the parameters shown in Fig. 2. 40 non-engineered buildings located in the EAs selected in Step 1 (see Fig. 3) were inspected by (1) taking a few measurements, (2) recording the presence of irregularities, and (3) collecting information related to structural deficiencies and maintenance issues. For each building, data was collected only for two orthogonal façades, since parallel walls in the inspected buildings had similar opening layout.

Most of the inspected constructions were made of fired (clay) bricks, since these are materials which are relatively cheap to source on-site, and they do not require high construction skills (Fig. 4a). Regarding mud brick, although this was the traditional material adopted to construct houses in Malawi; there was still a considerable number of buildings inspected on-site, which were made of mud bricks, as observed on site (Fig. 4b). The most observed type of mortar was mud, and cement is slowly taking over, but was still limited in use for the surveyed informal settlements (Fig. 4a and b). The majority of the inspected houses (63%) were built with single-skin walls with a thickness varying from 100 to 160 mm, while houses with double skin walls had a thickness varying from 210 to 260 mm. Regarding building roofs, these were made of timber rafters supporting thatch or light metallic corrugated sheets (Fig. 4c and d). Both roof types can be classified as light systems, as they are not fully rigid along the entire plane; and therefore, they do not act as rigid diaphragms. Furthermore, it was observed that roofs generally were not connected to the bearing walls, therefore they were not able to provide restraints against lateral movements of the walls due to winds or earthquakes. Timber wall plates, to support roof structures, were used only occasionally on the top of the longest external walls of the inspected houses, and the use of timber ring beams to tie bearing walls was not part of the construction methods observed on site.

Positively from a seismic point of view, the vast majority of houses in the surveyed areas were one storey high, constructed as isolated buildings, and had rectangular shapes in plan (typical plan dimensions 8 m × 6 m). On the other hand, negatively
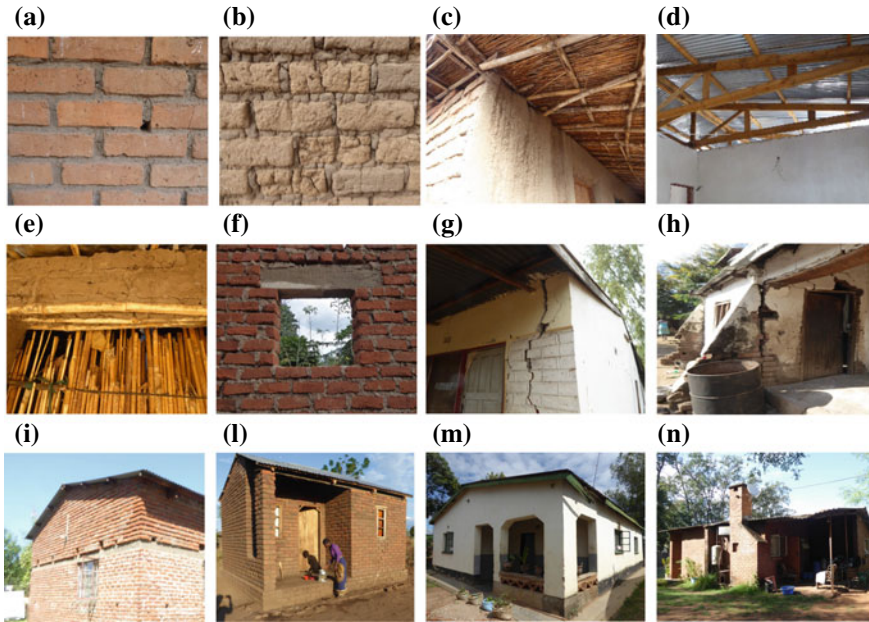
Fig. 4 Typical buildings in Malawi **a** fired bricks with cement mortar; **b** mud bricks with mud mortar; **c** thatched roof, **d** light metallic sheets supported by timber rafters, showing a lack of connection between walls and roof, and absence of both wall plates and ring beams; **e** bamboo lintel; **f** concrete lintel, **g** house with poor connection between walls; **h** lack of connection between buttress and wall; **i** concrete ring beam; **l** re-entrant corner; **m** portico; **n** chimney

from a seismic point of view, the poor construction detailing observed in the houses significantly compromised the building performance. For instance, lintels on top of openings were rarely in place, and only window frames made of timber planks with small cross Sections (10 cm × 5 cm) were used. In case lintels were adopted, they were often made with bamboo according to traditional techniques, while concrete lintels were used in buildings constructed by wealthy families (Fig. 4e and f). The poor detailing was also underlined by the lack of connections between walls (Fig. 4g), and between walls and floors/roof, which could lead to brittle failures during earthquakes. In particular, in inspected houses of single-skin walls, connections between different elements were poor. For inspected houses with double-skin walls, connections between walls and between the walls and roof were better constructed, and thus they are supposed to provide a higher structural stability to the entire building. To improve the quality of connections between walls, in a small percentage of the inspected houses (12%), buttresses or ring beams were adopted (Fig. 4h and i). Buttresses were made with fired bricks and are frequently used in newly constructed houses, although these strengthening elements rarely worked well to prevent overturning of walls, since they were often disconnected from the entire building. With regard to ring beams, they were constructed in reinforced concrete and placed on top

Table 1 Definition of building typologies in the inspected houses in Malawi

Building typology			A	B	C
Structural system	Vertical system type	Masonry type	Unburnt (mud) bricks/ fired (clay) bricks	Fired (clay) bricks	Fired (clay) bricks
		Mortar type	Mud	Mud	Cement
	Roof type		Thatch supported by timber elements (rafters)	Metallic corrugated sheets supported by timber elements (rafters)	Metallic corrugated sheets supported by timber elements (rafters)
Geometry	Rectangular plan - Typical size (8 m x 6 m)		Smaller than typical size (commonly)	Typical size (commonly)	Larger than typical size (commonly)
Structural irregularity	Portico		No	Possible	Possible
	Re-entrant corner		Possible	Possible	Possible
	Chimney		No	Possible	Possible
Strengthening elements	Buttresses, concrete ring beams		No	Possible	Possible
Quality	Materials		Poor	Medium	Good
	Connections between walls and roof		Poor	Medium or good	Good
Maintenance			Poor	Medium or good	Medium or good

of openings and function as a lintel for distributing loads from the spandrels to the adjacent piers, and as a belt for ensuring connection between the tops of walls.

Seismic performance of the inspected houses was also likely to be vastly affected by the presence of irregular elements (e.g. re-entrant corner, portico, chimney, see Fig. 4 l, m and n), observed in some new houses with good materials. Furthermore, structural shortcomings in these types of constructions were caused not only by low construction skills, but also by lack of maintenance. This was underlined by the presence of cracks and material loss which were often observed in inspected buildings, resulting in notable deterioration and damage (Fig. 4g and h).

To derive typologies based on the buildings observed on site, in Table 1, structural and geometrical factors, which highly varied, were ranked in terms of poor-good quality scales, defined with respect to the minimum and maximum quality levels observed on site. With reference to Table 1, three different non-engineered typologies A, B and C (shown in Fig. 5) were identified, and added successively in the existing Malawian building classification of the World Housing Encyclopedia of 2002, discussed in Sect. 3.1 (Novelli et al. 2018).

(a)   (b)   (c)

Fig. 5 Typical one-storey masonry building in Malawi. **a** typology A; **b** typology B; **c** typology C

Typology A was representative of 23% of the inspected buildings. These were made of poor fired and unfired bricks and poor mud mortar. Generally, these houses had smaller plan geometry than the typical plan geometry of 8 m × 6 m. Most of these houses had thatch supported by light timber rafters, low quality materials, and poor structural detailing (e.g. lack of connection between walls and between the walls and roof). 46% of buildings were of typology B, the most common of the typologies observed in Malawi. These buildings were made of fired bricks and mud mortar. These houses had a typical plan geometry of 8 m × 6 m. These houses had thatch or corrugated metallic sheets supported by light timber rafters. The construction detail varied significantly, therefore factors related to connections, quality material, and maintenance level were defined as medium. The presence of irregularities (e.g. portico and re-entrant corner) was recorded. The typology C covered 31% of the inspected houses. These were made of fired bricks and cement mortar. Generally, these houses had a larger plan geometry than the typical plan. Due to the extended plan size, irregularities were likely to occur (e.g. portico and re-entrant corner). Most of these houses had corrugated metallic sheets supported by timber rafters or truss, good quality material, and good structural detailing (e.g. adjacent walls and walls/roof are connected). The good structural quality of these houses was also given by the presence of strengthening elements (e.g. buttresses, and ring beams).

Using the expert judgements, and on-site observations, the authors had assigned a different level of vulnerability with reference to EMS scale (Grünthal 1998) for each of the identified typologies, (low, medium and high to A, B and C, respectively) as recently updated by the authors in the World Housing Encyclopedia (Novelli et al. 2018). In the next sections, the failure mode distribution and the actual level of vulnerability are estimated analytically and expressed in terms of acceleration and drift for each of the identified typology.

3.3 Step 3 Derivation of Seismic Fragility Curves
for Building Typologies in Malawi

The seismic performance of the derived typologies was estimated using FaMIVE (D'Ayala and Speranza 2003; Casapulla and D'Ayala 2006; Novelli et al. 2015). In the past, this approach has been applied to assess the seismic performance of masonry buildings in Italy, Spain, Turkey, India, Iran and Nepal. The method was adapted to consider different construction types as well as a large variety of failure modes, both in-plane and out-of-plane. The past case studies have demonstrated good agreement between estimated seismic building performance and observed damage. The approach is based on a mechanical procedure, which calculates collapse load factor multipliers for different failure modes, defined as all possible collapse mechanisms that can occur for a masonry building subjected to earthquake shaking. Collapse load factor multipliers are calculated for each inspected façade of a building, taking into account the geometrical/structural features of the orthogonal walls and their quality of connections, as this allows assessing the structural interaction between walls and their mutual response under seismic loads. Among the computed collapse load factor multipliers, the failure mode with the smallest multiplier is considered to occur on a façade (as the weak link).

In the present case study, possible failure modes, which can occur on non-engineered buildings in Malawi, were identified on images taken during the reconnaissance surveys carried out after the 2009 Karonga earthquake by the authors. These failure modes, as illustrated in Fig. 6a, were classified in three major classes: (1) OOP: Out-Of-Plane, predominantly occurs on single-skin walls with a low-quality material and low-quality connection with orthogonal walls and roof, causing overturning of a single façade; (2) IP: In-Plane, predominantly occurs on single/double-skin walls with a medium-quality material and a good-quality connection with orthogonal walls and roof; causing shear failure of a single façade and (3) CORNER: Corner failure, predominantly occurs on double-skin walls with good-quality material and good-quality connection with orthogonal walls and roof, causing the overturning of at least two orthogonal façades.

With reference to the possible collapses for the houses inspected in Malawi, the failure mode distribution estimated with FaMIVE is illustrated in Fig. 6b. As expected from the on-site surveys, since a lack of connection between the walls and roof and low-quality construction materials were frequently observed in the inspected buildings, OOP with a percentage of 69% is the most likely failure mode for the inspected facades belonging to typology A and B. Regarding IP (19%) and CORNER (12%), these were mainly estimated for the inspected façades of buildings belonging to typologies B and C which were better constructed and therefore had higher resistance to seismic loads, compared to typology A.

The capacity curves of the building typologies (A, B, and C) and failure mode classes (OOP, IP, and CORNER) were computed based on the collapse load factor multipliers (D'Ayala 2005; D'Ayala and Novelli 2014). Since the load factor multipliers in FaMIVE were calculated for façade, multiple capacity curves, one for each
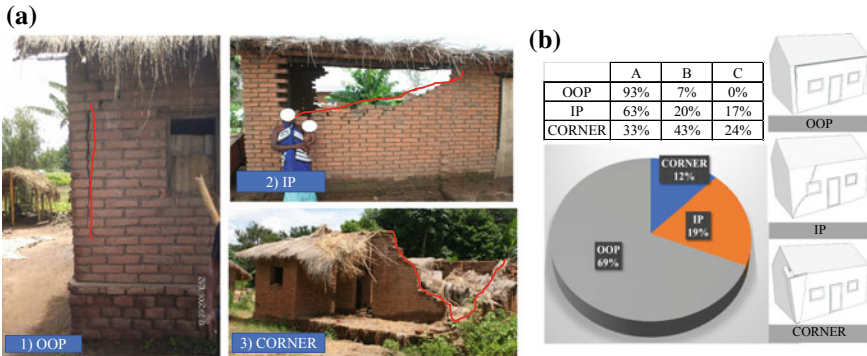
Fig. 6 **a** Typical failure modes observed after the 2009 Karonga earthquake Source of image 1: authors; source of image 2: (http://www.aaronmoore.com.au/malawi-earthquake-relief#/i/1) taken by Aaron Moore, used with permission and source of image 3: (http://www.aaronmoore.com.au/malawi-earthquake-relief#/i/2) taken by Aaron Moore, used with permisson; and **b** failure modes estimated for single inspected facade (expressed in percentages)

analysed façade, were derived for a single building. The minimum capacity curve among all examined façades was adopted as the capacity curve for the entire building. With regards to the strength capacity, the acceleration (%g) coincided, for each façade, with the collapse load factor obtained with FaMIVE. The minimum capacity curve among all examined façades was adopted as the capacity curve for the entire house. The elastic limit displacement at the top of each façade was calculated as a function of the elastic stiffness and the mass of the façade, involved in the activated failure mode. The ultimate displacement was defined as the displacement that determined the geometrical instability of the façade and hence its collapse. Computed the displacements, the drift was derived with the respect to the height of the single inspected façade. With reference to the definition of strength and drift given above, the different levels of seismic resistance of the three typologies are illustrated in Fig. 7a, showing the comparison of the median capacity curves derived in terms of building typologies (A, B, and C) and failure mode classes (OOP, IP, and CORNER). The four identified points on the curves were associated to corresponding damage state (ds_i) as proposed in Fig. 7a, where the capacity curves for the identified building typologies are presented. For each curve, the following ds_i are reported: LD, Light Damage, corresponding to the elastic lateral capacity, SD, Structural Damage, corresponding to the peak capacity, NC, Near Collapse, corresponding to incipient or partial collapse, and C, Collapse, corresponding to the total collapse. As expected from the definition of the three typologies, it is noticeable that building typology A (class of buildings characterised by low-quality materials and construction details) has the lowest values of acceleration and drift compared to B and C with the highest peak capacities. The three building typologies are characterised by an almost linear behaviour up to maximum capacity and a very modest ductile range. Clearly, the estimated capacity curves are capable to capture different vulnerability levels,
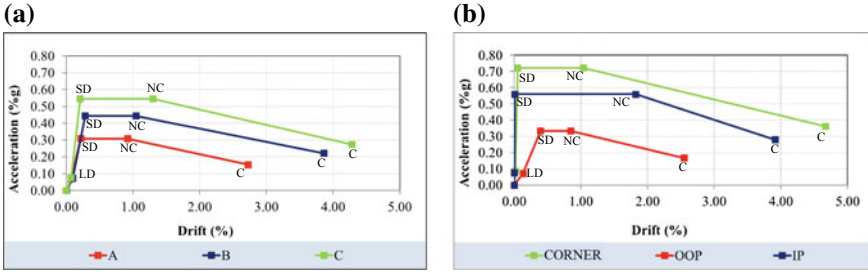
(a)

(b)

Fig. 7 Median capacity curves for **a** the building typologies: A, B and C and **b** failure mode classes: OOP, IP and CORNER

highlighted by the different identified peak capacities, which can be associated to the three vulnerability levels (low, medium and high to A, B and C, respectively) assessed by expert judgements by the authors in the World Housing Encyclopedia (Novelli et al. 2018). The effect of classifying the inspected buildings with reference to the estimated failure modes (OOP, IP, CORNER, see Fig. 6b) are investigated in Fig. 7b. It is important to state that this classification typifies buildings not according to their geometric/structural features but according to the estimated seismic response. This entails the definition of classes OOP and IP made of buildings of typologies A, B and C and class CORNER with buildings of typologies B and C, as indicated in the table of Fig. 6b. As expected in Fig. 7b, the results show that class OOP has similar capacity curves of typology A, since most of these buildings are collapsing for overturning as illustrated in Fig. 6b. In addition, the smaller ductile range of OOP respect to IP and COMB underline the high brittleness of this failure mode. On the other hand, the differences on the peak capacities observed for IP and COMB compared to OOP (differences are more than 30 and 50% respectively) highlight a robust seismic response. Consequently, the CORNER and IP failure modes are relatively favoured collapse mechanisms, in the sense that they occur only for buildings built with good/medium construction practice (in other terms for buildings of typology B and C), which are evidently higher resistant to seismic events, and therefore have a lower probability to collapse.

In agreement with the N2 method (Fajfar 2000), fragility curves for different damage states (ds_i) for LD, SD, NC and C, as defined in the Global Earthquake Model (GEM) guidelines (D'Ayala et al. 2014), were obtained by computing the median and standard deviation values of the displacements estimated for each damage state of the typologies (A, B and C) and failure mode classes (OOP, IP, and CORNER). The median and standard deviation were used to derive equivalent lognormal distributions indicated as (S_d) in the fragility curves. To this end, fragility curves were obtained as follows:

$$\hat{S}_{d, ds_i = e^{\bar{\mu}_i}} \quad \text{with} \quad \bar{\mu}_i = \frac{1}{n} \sum_{j=1}^{n} \ln \bar{S}_{d, ds_i}^{j} \tag{1}$$

and the corresponding standard deviation as:

$$\beta_{ds_i} = e^{\bar{\mu}_i + \frac{1}{2}\sigma_i^2} \sqrt{e^{\sigma_i^2} - 1} \quad \text{with} \quad \sigma_i = \sqrt{\frac{\sum \left(\ln \bar{S}_{d,ds_i}^j - \ln \hat{S}_{d_{ds_i}}^j\right)^2}{n}} \tag{2}$$

Results of Eqs. (1) and (2) are shown in Tables 2 and 3 and fragility curves for typologies A, B, and C, and OOP, IP and CORNER for damage state C (Collapse) are reported in Fig. 8.

Clearly, the median S_d identified for OOP and A have very similar values. This happens because although buildings in each typology are classified according to different criteria, most of the buildings in A, also fail in OOP, therefore both typolo-

Table 2 Median displacement thresholds and their corresponding dispersion for building typologies (A, B and C) due to the variability of capacity curves in the sample

	LD		SD		NC		C	
	Median S_d (cm)	b_{dsi}	Median S_d (cm)	b_{dsi}	Median S_d (cm)	b_{dsi}	Median S_d (cm)	b_{dsi}
A	0.1729	1.3090	0.5186	1.3090	2.0417	2.0203	6.1250	2.3420
B	0.1399	0.9486	0.4198	0.9486	2.5333	1.4871	7.6000	1.3425
C	0.0361	1.0666	0.1084	1.0666	3.4500	1.4546	14.0000	1.6105

Table 3 Median displacement thresholds and their corresponding dispersion for failure modes (OOP, IP, and CORNER) due to the variability of capacity curves in the sample

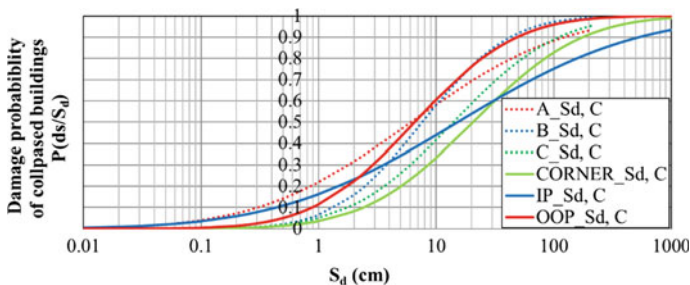|	LD		SD		NC		C	
	Median S_d (cm)	b_{dsi}	Median S_d (cm)	b_{dsi}	Median S_d (cm)	b_{dsi}	Median S_d (cm)	b_{dsi}
OOP	0.2525	1.0800	0.7576	1.0800	2.2000	1.5689	6.6000	1.5689
IP	0.0062	1.0795	0.0187	1.4589	4.6667	1.4078	15.3333	2.7736
CORNER	0.0003	1.2535	0.0009	1.2535	3.4500	1.6778	20.7000	1.6778

Fig. 8 Fragility functions for building typology (A, B, and C) and failure modes (CORNER, IP, and OOP)

gies are composed by the same buildings. However, the related fragility curves in Fig. 8 show a significant variation in the probability of collapsed buildings starting from a S_d greater 0.1 cm, where it results for low values of S_d (smaller than 10 cm) that buildings collapsing for in OOP are more than the ones classified in A. Furthermore, the effect of using different building classifications (based on the geometrical/structural features or failure modes), is mainly underlined by the drastic difference of the probability of damage between B and IP (medium vulnerability) and C and CORNER (low vulnerability) where the differences in the median S_d are more than 50 and 33% respectively. Noticeably, C/CORNER are the typologies that have the less severe earthquake damage (e.g., for Sd = 5 cm, number of collapsed buildings in C/CORNER are around 40 and 60% less than collapsed buildings in B/IP, and A/OOP). This is because the collapse fragility functions have from a gentler to a steeper slope going from a lower to higher vulnerable typology.

3.4   Step 4 Seismic Mitigation Programs for Malawi

Several types of interventions based on low-cost engineering solutions can be suggested to improve the structural performance of the inspected non-engineered masonry buildings in Malawi. Descriptions of recommended retrofitting interventions include:

- Wall plates (see Fig. 9a and b).

These elements are made as horizontal timber bands installed along the tops of walls under the roof to provide a fixing point at the ends of the rafters and to ensure connection between the tops of walls and the roof. These elements are fixed to walls through steel or timber pegs. In the inspected houses in Malawi these elements were rarely used under the rafters, which generally seated directly on top of walls, which often resulted in severe local damage to the walls by the rafters due to stress concentration. To prevent high stress concentration at rafter-wall contact points and
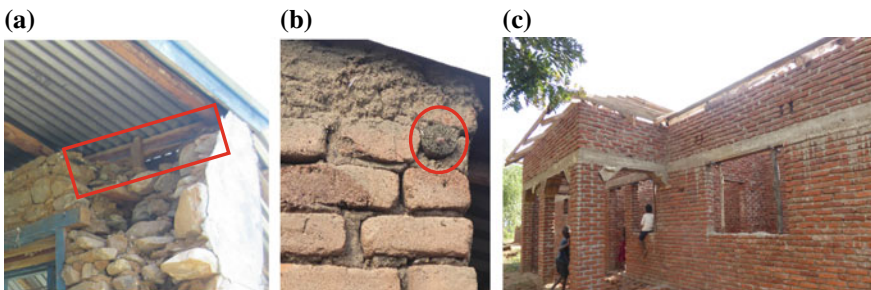
(a)   (b)   (c)

Fig. 9 **a** Timber wall plate of rectangular section, **b** timber wall plate of circular section, and **c** concrete ring beam

to improve connections between walls and the roof structure, wall plates are highly recommended.

- Ring beams (see Fig. 9c).

Ring beams (also known as a crown, collar, band or tie beams or seismic beams) are made of reinforced concrete or timber and are located as a belt at roof and/or lintel level. These elements are used to ensure that gravitational/seismic loads are properly transferred, and connections on top of walls prevent out-of-plane failure modes. In this respect, in the Safer Housing Construction Guidelines (Bureau TNM 2016), there is a specific section for ring beams, where it is advised to combine ring beams at lintel and roof levels as only one beam, which should be located at roof level. This has been suggested to reduce complexity and cost in the building process. In practice, as discussed in Sect. 3.2, concrete ring beams are rarely used, and they are only placed at lintel level, supporting spandrels, which can be highly vulnerable under earthquakes, if they are deep in height. The observed ring beams were often under-designed to support gravitational/seismic loads and since they were not connected directly to roofs, these were not capable of constraining roof structures. Existing ring beams need to be inspected and substituted with new ones, if they are deficient. Furthermore, it is strongly advised that ring beams be placed both at lintel and roof levels, or only at the lintel level, if spandrels are not significantly deep in height. Use of ring beams at roof level only should be considered, if lintels on the top of openings are also adopted.

- Buttresses (Fig. 10a)

These structural elements are made with fired bricks and are located along walls. Buttresses have the functions to increase stability of buildings, limit the vibration and prevent out-of-plane failure modes in the wall located in the orthogonal direction respect to the buttresses (Ortega et al. 2018).

The out-of-plane failure mode is the most common collapse mechanism that can occur in non-engineered masonry buildings (D'Ayala 1999; Karantoni and Bouckovalas 1997; Tomazevic 1999). This was confirmed by failure modes observed
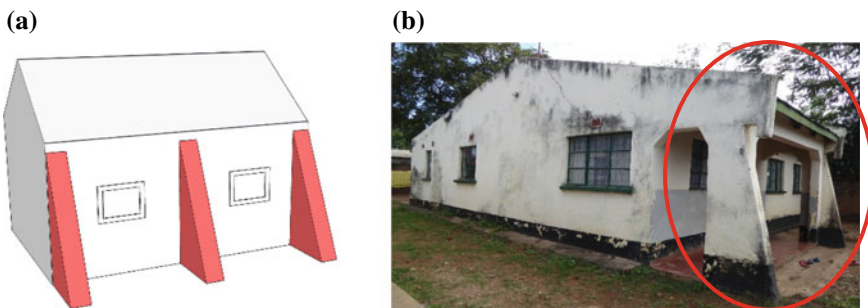

(a)   **(b)**

Fig. 10 **a** Buttresses: structures made of stones or bricks, built against walls, to prevent overturning **b** buttresses observed on-site during structural surveys

during the 2009 Karonga earthquake by the authors as well as the failure mode distribution shown in Fig. 6 assessed for the inspected non-engineered masonry buildings in Malawi. Since out-of-plane failure modes are caused by lack of connections between walls (Giuffre 1993a, b) and buttresses are the most adequate low-cost engineering solution to prevent such failure modes, their benefit is assessed running a further analysis where inspected buildings failing for OOP are assumed to be strengthened using the intervention, illustrated in Fig. 10a. Improvements achieved by the added buttresses are significant. The results are shown in Fig. 11a and b, where the effectiveness of the buttresses is presented in terms of both failure mode distribution and capacity curves. The use of buttresses, since it limits overturning collapse of buildings, favours IP and CORNER failure modes, which occur for 56% and 44% of the inspected façades respectively, preventing OOP successfully. With regards to capacity curves, the positive role of the buttresses is mainly highlighted by the increment of acceleration in both typologies A and B. Since most of the buildings in these typologies fail in OOP (93% and 63 in A and B respectively, as illustrated in Fig. 6), the presence of buttresses rises their strengths from 0.31 (%g) in A and 0.42 (%g) in B before retrofitting to 0.41 (%g) in A and 0.51 (%g) in B after retrofitting. With reference to typology C, only 33% fails in OOP, as illustrated in Fig. 6, therefore the effect of the buttresses is only limited to a few buildings which increase the mean capacity of typology C with 7% of growth in the peak acceleration before and after retrofitting.

With the demonstrated positive impact, buttresses are highly recommended to prevent overturning. In addition, it is also important to mention that buttresses have an important role to prevent overturning in houses with poorly connected walls, only if they are located along the length of the longest walls, which are generally the most vulnerable to OOP compared to the short ones. Therefore buttresses only located on one side of a façade, as the one indicated in Fig. 10b, showing a typical Malawian house with veranda made of buttresses, are not capable to prevent the overturning of the entire wall, if the side of the façade without buttresses is not properly connected with the orthogonal wall. Consequently, it is advised to inspect existing houses in Malawi, add buttresses, if walls are poorly connected, and replace buttresses, if they are not connected to the buildings.
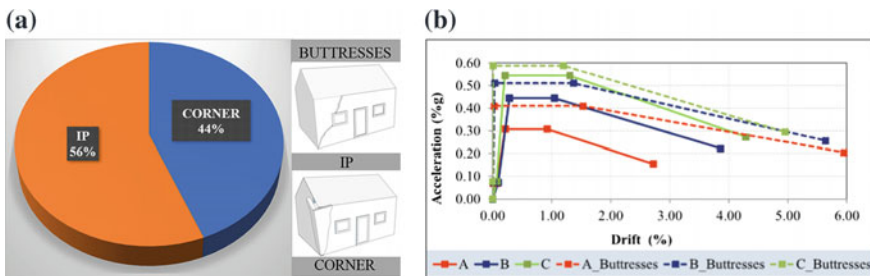

Fig. 11 a) Failure modes distribution after buildings inspected in Malawi have been strengthened b) Capacity curves before and after strengthening with buttresses

4 Conclusions

This chapter has described a seismic mitigation framework for assessing non-engineered masonry buildings. It facilitates the identification of suitable mitigation solutions to increase seismic resilience of non-engineered masonry buildings in developing countries. The application of the framework has been demonstrated by focusing on Central-Southern Malawi, selected as a representative country in the East African Rift region, where rapid expansion of informal settlements is occurring. The developed framework integrates effective guidance with regard to collecting data, classifying non-engineered masonry buildings in main typologies, estimating building performance, and identifying adequate low-cost retrofitting strategies. Moreover, the seismic mitigation framework can offer notable advantages of using mitigation solutions to increase seismic resilience in developing countries by deriving failure mode distribution and fragility curves of non-engineered masonry buildings before and after a mitigation plan is employed. In the future, the framework could be further extended to a risk assessment tool and could serve to implement performance-based earthquake engineering methods in developing countries.

References

Abrahamczyk, L., Schwarz, J., Langhammer, T., Genes, M. C., Bikÿe, M., Kaÿin, S., et al. (2013). Seismic risk assessment and mitigation in the Antakya-Maras region (SERAMAR): Empirical studies on the basis of EMS-98. *Earthquake Spectra, 29,* 683–704. https://doi.org/10.1193/1.4000163.

Addessi, D., Mastrandrea, A., & Sacco, E. (2014). An equilibrated macro-element for nonlinear analysis of masonry structures. *Engineering Structures, 70,* 82–93.

Arendt, L., Hortacsu, A., Jaiswal, K., Bevington, J., Shrestha, S., Lanning, F., et al. (2017). Implementing Nepal's national building code: A case study in patience and persistence. *Earthquake Spectra, 33*(S1), S167–S183.

Arya, A. S. (2018). Disaster risk reduction for buildings. In *Advances in Indian Earthquake Engineering and Seismology* (pp. 367–381). Springer, Cham.

ATC-13 (Applied Technology Council-13). (1985). Applied Technology Council. Earthquake damage evaluation data for California Applied Technology Council, Redwood City.

Bernardini, A., Gori, R., & Modena, C. (1990). An application of coupled analytical models and experiential knowledge for seismic vulnerability analyses of masonry buildings. In A. Koridze (Ed.), *Engineering aspects of earthquake phenomena* (Vol. 3, pp. 161–180). Oxon: Omega Scientific.

Bhagat, S., Buddika, H.S., Adhikari, R.K., Shrestha, A., Bajracharya, S., Joshi, R., Singh, J., Maharjan, R. and Wijeyewickrema, A.C. (2017). Damage to cultural heritage structures and buildings due to the 2015 Nepal Gorkha earthquake. *Journal of Earthquake Engineering*, pp. 1–20.

Bureau TNM. (2016). Safer house construction guidelines. Available at https://issuu.com/saferconstructionguidelines/docs/no-crocini.

Calvi, G. M., Pinho, R., Magenes, G., Bommer, J. J., Restrepo-Vélez, L. F., & Crowley, H. (2006). Development of seismic vulnerability assessment methodologies over the past 30 years. *ISET Journal of Earthquake Technology, 43*(3), 75–104.

Casapulla, C., & D'Ayala, D. (2006). *In-plane collapse behaviour of masonry walls with frictional resistances and openings*. New Delhi: Structural Analysis of Historic Constructions.

CEN. (2004). *European standard EN 1998-1-2004: "Eurocode 8: Design of structures for earthquake resistance—Part 1: General rules, seismic actions and rules for buildings*. Bruxelles: Comité Europèen de Normalisation.

Chaibedra, B., Benanane, A., & Boutaraa, Z. (2017). Numerical multi-modeling and seismic analysis of historical URM building. *Asian Journal of Civil Engineering (BHRC), 18*(8), 1341–1351.

Chavez, J., Khemici, O., Khater, M., & Keshishian, P. (2012). Building codes and relative seismic vulnerability in Latin American Countries. 15WCEE Lisboa.

Choudhury, T., & Kaushik, H. B. (2018). Seismic fragility of open ground storey RC frames with wall openings for vulnerability assessment. *Engineering Structures, 155,* 345–357.

Corburn, J., & Riley, L. (Eds.). (2016). Slum health: From the cell to the street. Univ. of California Press.

D'Ayala, D. (1999) Correlation of seismic damage between classes of buildings: churches and houses. In: A. Bernardini (Ed.) *International workshop on measures of damage to masonry buildings* (pp. 41–58). Balkema: Rotterdam.

D'Ayala, D. (2005). Force and Displacement Based Vulnerability Assessment for Traditional Buildings. *Bulletin of Earthquake Engineering, 3*(3), 235–265.

D'Ayala, D., & Novelli, V. (2014). Seismic Vulnerability Assessment: Masonry Structures. *Encyclopedia of Earthquake Engineering*, 1–20.

D'Ayala, D., & Speranza, E. (2003). Definition of collapse mechanisms and seismic vulnerability of historic masonry buildings. *Earthquake Spectra, 19*(3), 479–509.

D'Ayala, D., Meslem, A., Vamvatsikos, D., Porter, K., Rossetto, T., Crowley, H., & Silva, V. (2014). Guidelines for analytical vulnerability assessment of low/mid-rise buildings: Methodology. Vulnerability global component project.

De Silva, S., De Silva, G. S., & Padmal, H. M. S. S. (2018). Assessment method for seismic vulnerability of old masonry buildings in Sri Lanka. *Procedia Engineering, 212,* 61–68.

Di Meo, A., Borzi, B., Faravelli, M., Pagano, M., Ceresa, P., Monteiro, R., et al. (2018). Seismic vulnerability assessment of the urban building environment in Nablus, Palestine. *International Journal of Architectural Heritage, 12*(7–8), 1196–1215.

Ezeh, O., Gordon, M. H., & Niranjan, K. (2016). Enhancing the recovery of tiger nut (Cyperus esculentus) oil by mechanical pressing: Moisture content, particle size, high pressure and enzymatic pre-treatment effects. *Food Chemistry, 194,* 354–361.

Fajfar, P. (2000). A nonlinear analysis method for performance-based seismic design. *Earthquake spectra, 16*(3), 573–592.

FAO, IFAD & WFP. (2015). Achieving Zero Hunger. The critical role of investments in social protection and agriculture. Rome, FAO.

FEMA 154. (2002). Rapid visual screening of buildings for potential seismic hazards. Federal Emergency Management Agency, Washington, D.C.

Fulzele, S. A. T. U., & Aggarwal, G. (2018). Earthquake recovery management for long-term development and community resilience. *Journal of Global Resources, 4*(01), 12–17.

Gilani, A. S., & Miyamoto, H. K. (2018). Seismic collapse probability of structures with viscous dampers per ASCE 7-16: Effect of large earthquakes.

Giuffè, A. (Ed.). (1993a). Sicurezza e conservazione dei centri storici—Il caso Ortigia, Ed. Laterza (In Italian).

Giuffrè, A. (1993b). Sicurezza e conservazione dei centri storici. Il caso Ortigia. Bari: Laterza, 1993. Valluzzi MR, Cardani G, Binda L, Modena C. Analysis of the seismic vulnerability of masonry buildings in historic centres and intervention proposals. In *Proceedings of the 6th Int. Symp. on the Conservation of Monuments in the Mediterranean Basin*, Lisbon, Portugal, April 7–10, 2004 (6 pp. to appear).

Goda, K., Gibson, E. D., Smith, H. R., Biggs, J., & Hodge, M. (2016). Seismic risk assessment of Urban and rural settlements around lake Malawi. *Frontiers in Built Environment, 2,* 30. https://doi.org/10.3389/fbuil.2016.00030.

Goda, K., Kloukinas, P., De Risi, R., Hodge, M., Kafodya, I., Ngoma, I., et al. (2018). Scenario-based seismic risk assessment for Malawi using improved information on earthquake sources and local building characteristics. 16th European Conference on Earthquake Engineering, Thessaloniki, Greece.

Grünthal, G. (1998). *European Macroseismic Scale 1998 (EMS98)* (p. 15). Cahiers du Centre Européen de Géodynamique et de Sismologie: Council of Europe.

Guo-Xing, C. (2003). The evolution and prospect of the code for seismic design of buildings in China. *Journal of Seismology, 1,* 017.

Guragain, R., Shrestha, S. N., Maharjan, D. K., & Pradhan, S. (2018). Lessons from building damage patterns during April 25, 2015 Gorkha Earthquake in Nepal. In *Living Under the Threat of Earthquakes* (pp. 79–93). Springer, Cham.

Habieb, A. B., Milani, G., & MILANI, F. (2017). Seismic performance of a masonry building isolated with low-cost rubber isolators. *WIT Transactions on the Built Environment*, 172, 71–82.

Hayashi, Y. (2014). Low-income groups and living environment in the cities of the Republic of Malawi. A direct survey about formal and informal settlements. L'architettura delle città-The Journal of the Scientific Society Ludovico Quaroni, 2(3-4-5).

IS:1893. Indian Seismic code. (2002). Criteria for Earthquake resistant design of structures, General provisions and buildings, Bureau of Indian Standards, New Delhi.

Japan Building Disaster Prevention Association, JBDPA. (1990, revised in 2001, 2015). Standard for post-earthquake damage level classification of reinforced concrete building.

Jaiswal, K. S., & Wald, D. J. (2008). *Creating a global building inventory for earthquake loss assessment and risk management (open-file report 2008-1160)* (p. 103). Reston, VA: US Geological Survey.

Jaiswal, K., Wald, D., & D'Ayala, D. (2011). Developing empirical collapse fragility functions for global building types. *Earthquake Spectra, 27,* 775–795. https://doi.org/10.1193/1.3606398.

Karantoni, F. V., & Bouckovalas, G. (1997). Description and analysis of building damage due to Pyrgos, Greece earthquake. *Soil Dynamics and Earthquake Engineering, 16*(2), 141–150.

Kushe, J., Manda, M., Mdala, H., & Wanda, E. (2017). The earthquake/seismic risk, vulnerability and capacity profile for Karonga town. *African Journal of Environmental Science and Technology, 11*(1), 19–32.

Lagomarsino, S., Penna, A., Galasco, A., & Cattari, S. (2013). TREMURI program: an equivalent frame model for the nonlinear seismic analysis of masonry buildings. *Engineering Structures, 56,* 1787–1799.

Lang K. (2002). Seismic vulnerability of existing buildings; Institute of Structural Engineering (IBK), ETH Zurich, Report No. 273, vdf Hochschulverlag, Zurich.

Lang, D. H., Kumar, A., Sulaymanov, S., & Meslem, A. (2018). Building typology classification and earthquake vulnerability scale of Central and South Asian building stock. *Journal of Building Engineering, 15,* 261–277.

Lubkowski, Z., Villani, M., Coates, K., Jirouskova, N., & Willis, M. (2014, August). Seismic design considerations for East Africa. In *Second European Conference on Earthquake Engineering and Seismology*, Istanbul (p. 12).

Malawi Bureau of Standards Board. (2014). The structural use of masonry—Code of practice, Part 1: Unreinforced masonry walling, MS791.

Maqsood, S. T., Schwarz, J., & Edwards, M. (2013). Application of the European macroseismic scale—1998 in the Asia-Pacific region. In *Proceedings: Vienna Congress on Recent Advances in Earthquake Engineering and Structural Dynamics* (pp. 28–30).

McKenna, P. (2011). Earthquake engineer: Earthquakes don't kill, but buildings do. *New Scientist, 210*(2813), 23.

Medvedev, S.V., Shponkhoier, V., & Karnik V. (1965). Shkala seismicheskoi intensivnosti MSK-64 (MSK-64 Seismic Intensity Scale). Moscow: MGK Akad. Nauk SSSR. In Mishatkin, V.N.,

Zakharchenko, N.Z., & Chebrov, V.N.(Ed.), *Hardware for the seismic subsystem of the tsunami warning service, Seism. Instrum.*, 2012, (Vol. 48, no. 1, pp. 16–33).

Mendes, N., & Lourenço, P. B. (2009). Seismic assessment of masonry "Gaioleiro" buildings in Lisbon, Portugal. *Journal of Earthquake Engineering, 14*(1), 80–101.

Mendes, N., Zanotti, S., & Lemos, J. V. (2018). Seismic performance of historical buildings based on discrete element method: An adobe church. *Journal of Earthquake Engineering*, pp. 1–20.

Midzi, V., & Manzunzu, B. (2014). Large recorded earthquakes in sub-Saharan Africa. *Extreme Natural Hazards, Disaster Risks and Societal Implications, 1,* 214.

Ngoma, I., & Sassu, M. (2002). Rural mud wall building-Nyumba yo mata or ndiwula-rep. n 43.

Naguit, M. (2017). Towards Earthquake-resilient buildings: Rupture process and exposure/damage analysis of the 2013 M7. 1 Bohol Philippines Earthquake.

Nassirpour, A., Galasso, C., & D'Ayala, D. (2018, June). A mobile application for multi-hazard physical vulnerability prioritization of schools. In *16th European Conference on Earthquake Engineering (16ECEE)* (Vol. 16). European Association of Earthquake Engineering (EAEE).

National Statistical Office of Malawi. (2008). *Population and housing census 2008*. Zomba, Malawi: National Statistical Office.

Nepal National Building Code (NBC)-105. (1994). Nepal national building code for seismic design of buildings in Nepal, ministry of housing and physical planning, Department of Buildings, Kathmandu, Nepal.

Novelli, V., Kloukinas, P., Ngoma. I., Kafodya, I., Macdonald, J., and Goda, K. (2018). Unreinforced masonry houses made of fired clay bricks (Report 205). World Housing Encyclopedia, Earthquake Engineering Research Institute, California, USA.

Novelli, V. I., D'Ayala, D., Makhloufi, N., Benouar, D., & Zekagh, A. (2015). A procedure for the identification of the seismic vulnerability at territorial scale. Application to the casbah of Algiers. *Bulletin of Earthquake Engineering, 13*(1), 177–202.

NZSEE (New Zealand National Society for Earthquake Engineering). (2016). Section C8—Seismic assessment of unreinforced masonry buildings technical guidelines for engineering assessment. The seismic assessment of existing buildings.

OECD (Organisation for Economic Co-operation and Development). (2018). PISA 2015 Results in Focus. Retrieved from https://www.oecd. org/pisa/pisa-2015-results-in-focus.pdf.

Ortega, J., Vasconcelos, G., Rodrigues, H., & Correia, M. (2018). Assessment of the efficiency of traditional earthquake resistant techniques for vernacular architecture. *Engineering Structures, 173,* 1–27.

Pitilakis K. (2015) Chapter 3 earthquake risk assessment: certitudes, fallacies, uncertainties and the quest for soundness. In A. Ansal (Ed.), Perspectives on European Earthquake engineering and seismology, geotechnical, geological and earthquake engineering 39. https://doi.org/10.1007/978-3-319-16964-4_3.

Restrepo-Vélez LF, Magenes G. (2004). A mechanics-based procedure for the seismic risk assessment of masonry buildings at urban scale. In *Proceedings of the XI Convegno Nazionale ANIDIS*, Genova.

Rossetto, T., Ioannou, I., Grant, D. N., & Maqsood, T. (2014). Guidelines for the empirical vulnerability assessment.

Satterthwaite, D., Sverdlik, A., & Brown, D. (2018). Revealing and responding to multiple health risks in informal settlements in sub-saharan African Cities. *Journal of Urban Health*, 1-11.91(3), 1059–1074.

Schultz, M. T., Gouldby, B. P., Simm, J. D., & Wibowo, J. L. (2010). Beyond the factor of safety: Developing fragility curves to characterize system reliability (No. ERDC-SR-10-1). Engineer research and development center vicksburg ms geotechnical and structures lab.

Shah, H. C., Dong, W., Stojanovski, P., & Chen, A. (2018a). Evolution of seismic risk management for insurance over the past 30 years. *Earthquake Engineering and Engineering Vibration, 17*(1), 11–18.

Shah, M. F., Kegyes-B, O. K., Ray, R. P., Ahmed, A., & Al-ghamadi, A. (2018b). Vulnerability assessment of residential buildings in Jeddah: A methodological proposal. *International Journal, 14*(44), 134–141.

Shapira, S., Levi, T., Bar-Dayan, Y., & Aharonson-Daniel, L. (2018). The impact of behavior on the risk of injury and death during an earthquake: a simulation-based study. Natural Hazards.

Silva, V., Crowley, H., Pagani, M., Monelli, D., & Pinho, R. (2014). Development of the OpenQuake engine, the Global Earthquake Model's open-source software for seismic risk assessment. *Natural Hazards, 72*(3), 1409–1427.

Spacone, E., Brando, G., Peruch, M., Mazzanti, C., Sovero, K., & Tarque, N. (2019). An Extensive Survey of the Historic Center of Cusco for Its Seismic Vulnerability Assessment. In *Structural Analysis of Historical Constructions* (pp. 1257–1267). Springer, Cham.

Tomaževič, M. (1999). *Earthquake-resistant design of masonry buildings*. London: Imperial College Press.

UN-HABITAT, United Nations High Commissioner for Refugees (UNHCR), and International Federation of Red Cross (IFRC). (2007). Situation analysis of informal settlements in Kampala. Nairobi, Kenya: UN Habitat. Available at http://www.unmalawi.org/agencies/unhabitat.html.

UN-HABITAT, United Nations High Commissioner for Refugees (UNHCR), and International Federation of Red Cross (IFRC). (2010). The Malawi urbanisation challenge.

UN-HABITAT, United Nations High Commissioner for Refugees (UNHCR), and International Federation of Red Cross (IFRC). (2012). Shelter Projects 2010: Malawi 2009 Earthquake. Available at http://www.sheltercasestudies.org/shelterprojects2010/A17-Malawi-2010.pdf.

World Housing Encyclopedia. (2002). World housing encyclopedia database for Malawi. Available at http://db.world-housing.net/list.

World Bank. (2017). World Bank Annual Report 2017 (English). Washington, D.C.: World Bank Group. http://documents.worldbank.org/curated/en/143021506909711004/World-Bank-Annual-Report-2017.

Yepes-Estrada, C., Silva, V., Rossetto, T., D'Ayala, D., Ioannou, I., Meslem, A., et al. (2016). The global earthquake model physical vulnerability database. *Earthquake Spectra, 32*(4), 2567–2585.

Zepeda, S. (2018). Structural Design for School Administration Block in Zimbabwe. Journeyman International | Zimbabwe Rural Schools Development Programme (ZRSDP).

Double and Triple Impulses for Capturing Critical Elastic-Plastic Response Properties and Robustness of Building Structures Under Near-Fault Ground Motions

Kotaro Kojima, Kohei Fujita and Izuru Takewaki

1 Introduction

Near-fault ground motions have been recorded recently through widely distributed recording networks. After detailed investigations, it was clarified that such ground motions have special characteristics. The effects of near-fault ground motions on the response of building structures have been investigated extensively (Hall et al. 1995; Sasani and Bertero 2000; Alavi and Krawinkler 2004; Kalkan and Kunnath 2006; Khaloo et al. 2015). The fling-step and forward-directivity are two types and are utilized to characterize such near-fault ground motions (Kalkan and Kunnath 2006; Mavroeidis and Papageorgiou 2003). As representative ground motions, Northridge earthquake in 1994, Hyogoken-Nanbu (Kobe) earthquake in 1995 and Chi-Chi (Taiwan) earthquake in 1999 provided many earthquake structural engineers with useful and precious data.

The fling-step and forward-directivity inputs are well characterized by a few wavelets. Some useful research works have been presented. Mavroeidis and Papageorgiou (2003) clarified the characteristics of this class of ground motions and proposed some simple models. Sasani and Bertero (2000) proposed one-cycle and 1.5-cycle sinusoidal waves as the ground motion models for the fling-step and forward-directivity inputs, respectively (also in Kalkan and Kunnath 2006).

K. Kojima
Faculty of Design and Architecture, Kyoto Institute of Technology, Kyoto 606-8585, Japan
e-mail: Kojima61@kit.ac.jp

K. Fujita · I. Takewaki (✉)
Department of Architecture and Architectural Engineering, Kyoto University, Kyoto 615-8540, Japan
e-mail: takewaki@archi.kyoto-u.ac.jp

K. Fujita
e-mail: fm.fujita@archi.kyoto-u.ac.jp

In this chapter, new approaches using the double impulse (Kojima and Takewaki 2015a) and the triple impulse (Kojima and Takewaki 2015b) are explained for various models which represent important nonlinear vibration phenomena and the intrinsic response characteristics under the near-fault ground motion are made clear. The common underlying concept is the modeling of simple sinusoidal waves into a few impulses with the equivalent power and the use of energy balance for the derivation of closed-form expressions of the maximum elastic-plastic response. The energy balance provides many advantages because the impulses cause only free vibration and complicated treatment by forced input can be avoided. It should be reminded that the relative response velocity is zero at the maximum deformation and the strain energy is zero at the second impulse timing in the case of critical double impulse. These properties enable the derivation of closed-form expressions of the maximum elastic-plastic response in a simple way (Kojima and Takewaki 2015a, b, c; 2016a, b, c; Takewaki and Kojima 2017; Takewaki et al. 2017). The present approach is expected to overcome the difficulty in the nonlinear structural dynamics (Caughey 1960; Iwan 1961). Then the closed-form expressions for the elastic-plastic responses under the series of impulses are applied to the soil-structure interaction problem and the base-isolated building. Furthermore, these closed-form solutions are used for evaluating the robustness of building structures (Kanno et al. 2017; Fujita et al. 2017; Hayashi et al. 2018).

2 Modeling of Main Part of Near-Fault Ground Motion into Double Impulse and Triple Impulse

The main portions of most near-fault ground motions can be represented by a few pulse-like waves as shown in Fig. 1. As far as the maximum response is concerned, the response resulting from such pulse-like waves plays an important role. In this chapter, the main portion of the pulse-like ground motions is simulated by the double impulse (see Fig. 2a) or the triple impulse (see Fig. 2b).

In this chapter, the magnitude of the double or triple impulse is determined so that the maximum Fourier amplitude of the double or triple impulse is equal to that of the corresponding one-cycle sine wave or one and half-cycle sine wave. This adjustment is introduced to guarantee the good response correspondence between the one-cycle sine wave or one and half-cycle sine wave and the double or triple impulse. The correspondence of the Fourier amplitudes between the one-cycle sine wave (or one and half-cycle sine wave) and the double impulse (or triple impulse) is shown in Fig. 3a, b. V and V_y denotes the input velocity level of the double impulse and the reference velocity level giving just yield deformation after the first impulse. These parameters will be explained later. Figure 3c shows the correspondence of the restoring force-deformation characteristics under the critical double impulse and the one-cycle sine wave. Figure 3d also illustrates the correspondence of the restoring
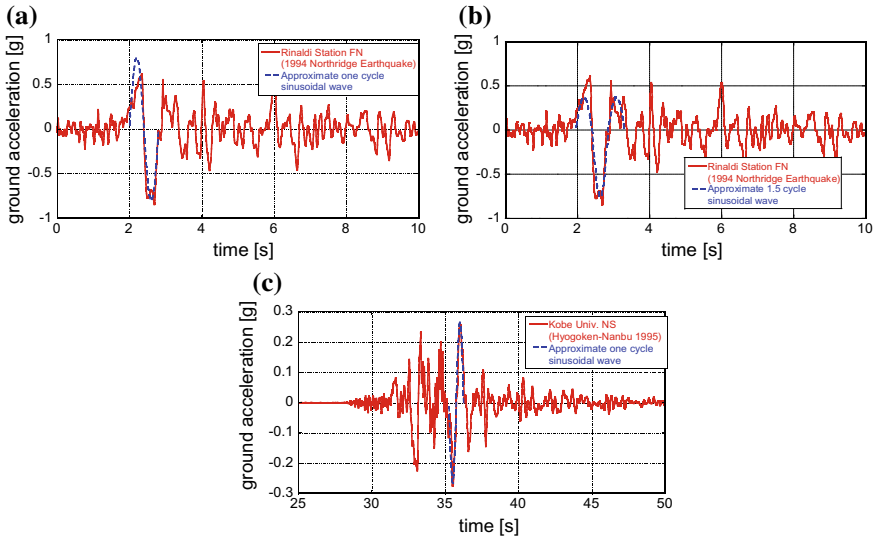
Fig. 1 Modeling of main part of pulse-type recorded ground motion into the corresponding one-cycle or one and a half cycle sinusoidal input: **a** Rinaldi station fault-normal comp. (Northridge earthquake 1994) (one-cycle), **b** Rinaldi station fault-normal comp. (one and a half cycle); **c** Kobe University NS comp. (almost fault-normal) (Hyogoken-Nanbu (Kobe) earthquake 1995) (Kojima and Takewaki 2016a)
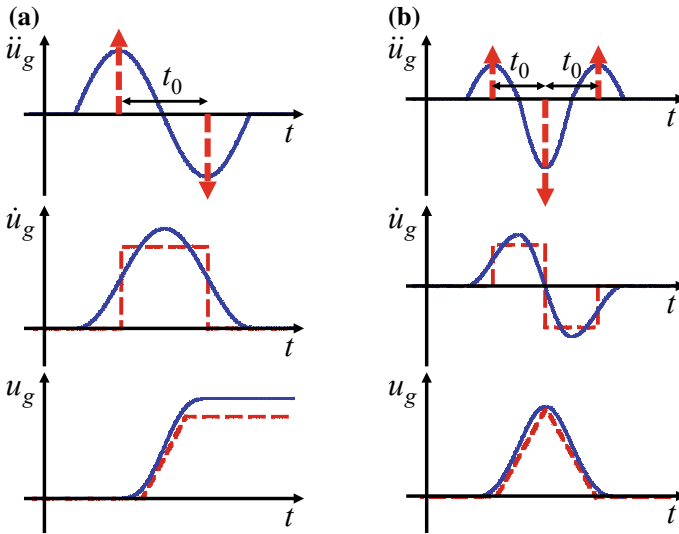

Fig. 2 Modeling of pulse-like ground motions: **a** Fling-step input (one-cycle sine) and double impulse, **b** Forward-directivity input (one and half-cycle sine) and triple impulse (Kojima and Takewaki 2015a, b)
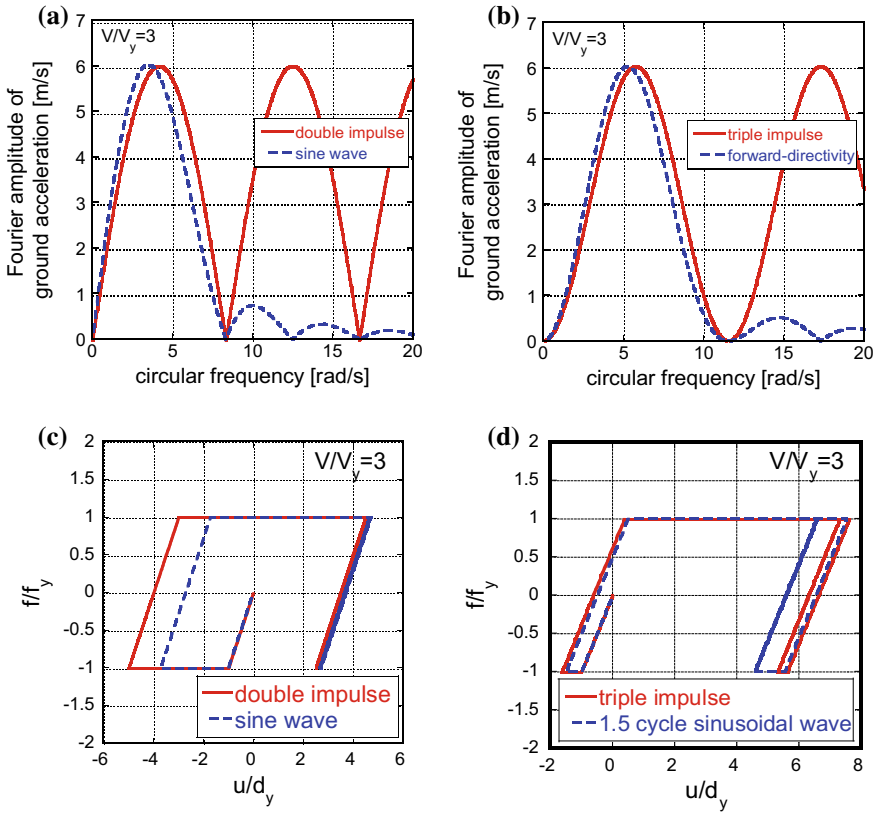
Fig. 3 Adjustment of input level of double and triple impulses to the corresponding one-cycle and one and half-cycle sine wave based on Fourier amplitude equivalence and response correspondence under double and triple impulses: **a** double impulse, **b** triple impulse, **c** restoring force-deformation correspondence under double impulse, **d** restoring force-deformation correspondence under triple impulse (Kojima and Takewaki 2015a, b)

force-deformation characteristics under the critical triple impulse and the one and a half-cycle sine wave.

3 Closed-Form Elastic-Plastic Response to Critical Double Impulse

Figure 4 shows an overview of the process of the response of an elastic-perfectly plastic single-degree-of-freedom (SDOF) model under the critical double impulse. The critical double impulse implies the double impulse which causes the maximum response under the conditions of a constant velocity amplitude and a variable impulse
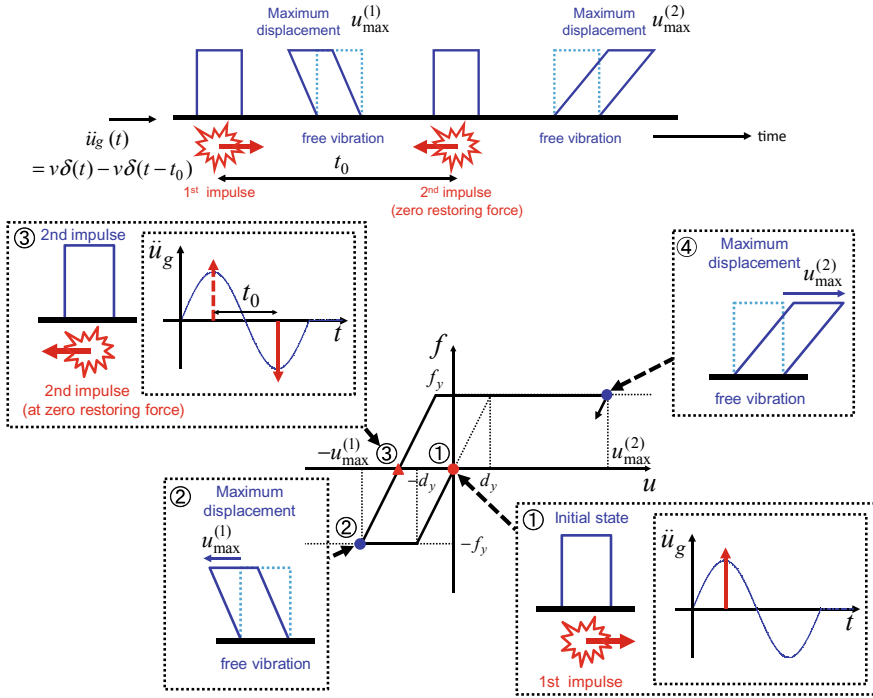
Fig. 4 Overview of elastic-plastic response process of SDOF model to critical double impulse

interval (Drenick 1970; Takewaki 2007). It should be emphasized that the critical timing of the second impulse is the time when the restoring force becomes zero in the first unloading process (Kojima and Takewaki 2015a). The parameters u and f denote the displacement of the structural mass relative to the ground motion and the restoring force of the system. d_y and f_y denote the yield deformation and the yield force, respectively. u_{max1} and u_{max2} denote the maximum deformation after the first impulse and the second impulse, respectively. $u_{max} = \max(u_{max1}, u_{max2})$ denotes the maximum deformation. V denotes the input velocity level of the double impulse (the instantaneous change of velocity of the structural mass) and V_y is the product of the natural circular frequency ω_1 of the SDOF system and d_y. V_y is the reference velocity level giving just yield deformation after the first impulse. Figure 5 shows the normalized maximum deformation under the critical double with respect to the normalized input velocity level. In Fig. 5, CASE 1 is the elastic case, CASE 2 is the case where the system goes into the yielding stage only after the second impulse and CASE 3 is the case where the system goes into the yielding stage even after the first impulse.

Fig. 5 Maximum
deformation under critical
double impulse with respect
to input velocity level
(Kojima and Takewaki
2015a)
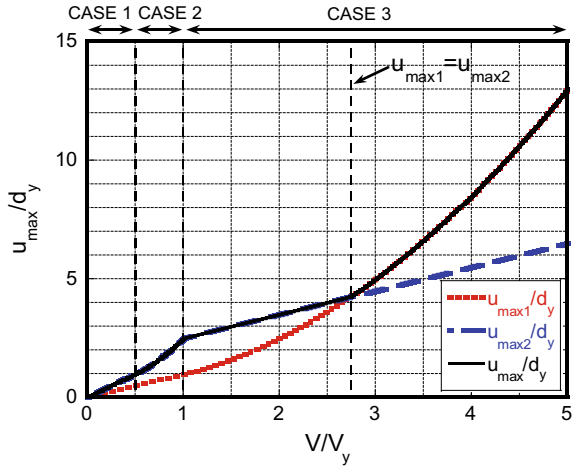
4 Closed-Form Elastic-Plastic Response to Critical Triple Impulse

In comparison with the response to the double impulse, the derivation process of the critical timing is somewhat complicated in the triple impulse. Figure 6 shows following four cases depending on the input level. CASE 1 is the case of elastic response during all response stages, where $u_{\max 3}$ is the largest. CASE 2 is the case of plastic deformation only after the third impulse, where $u_{\max 3}$ is the largest. CASE 3 is the case of plastic deformation after the second impulse, where $u_{\max 2}$ or $u_{\max 3}$ is the largest. CASE 4 is the case of plastic deformation even after the first impulse, where $u_{\max 2}$ is the largest. Then CASE 3 is divided into CASE 3-1 and CASE 3-2. CASE 3-1 is the case where the timing of the third impulse acts in the unloading stage and CASE 3-2 is the case where the timing of the third impulse acts in the yielding (loading) stage. $u_{\max 1}$, $u_{\max 2}$ and $u_{\max 3}$ denote the maximum deformation after the first impulse, the second impulse and third impulse, respectively. It is assumed here that the critical impulse has the second impulse timing at the zero restoring force in the first unloading process. It can be understood that the third impulse timings are different in CASE 3 and CASE 4.

Figure 7 shows an overview of the response process of an elastic-perfectly plastic SDOF model to the critical triple impulse in CASE 4. On the other hand, Fig. 8 illustrates the maximum deformation of the undamped elastic-perfectly plastic SDOF system under the critical triple impulse with respect to the input velocity level.

Figure 9 shows the maximum deformation to the triple impulse for varied time interval t_0. t_0^c in Fig. 9 denotes the critical time interval of the triple impulse and t_0^c is defined as the zero restoring force timing just after the first impulse. From Fig. 9, the response to the triple impulse is maximized at $t_0 = t_0^c$ when V/V_y is smaller than 2. When V/V_y is larger than 2, the response to the triple impulse is maximized at the
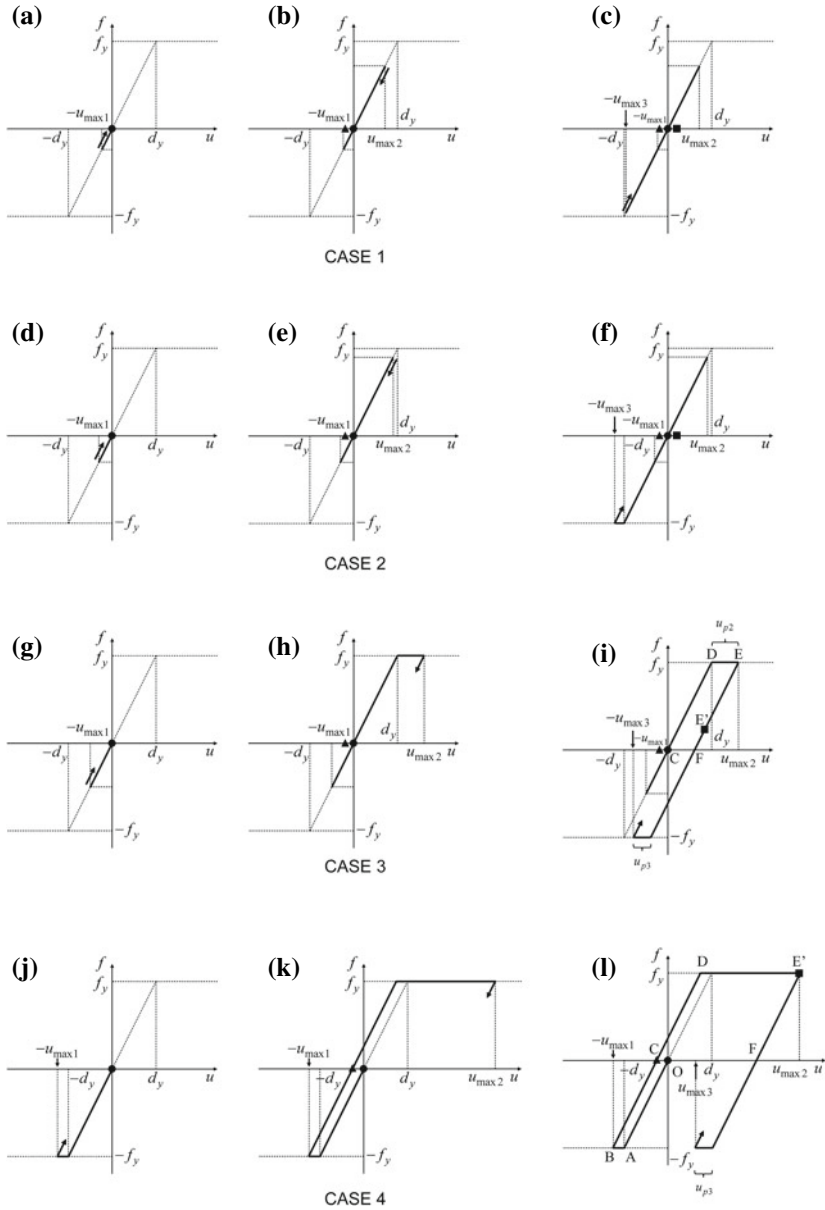
Fig. 6 Maximum deformation of elastic-perfectly plastic system under the critical triple impulse (Kojima and Takewaki 2015b)
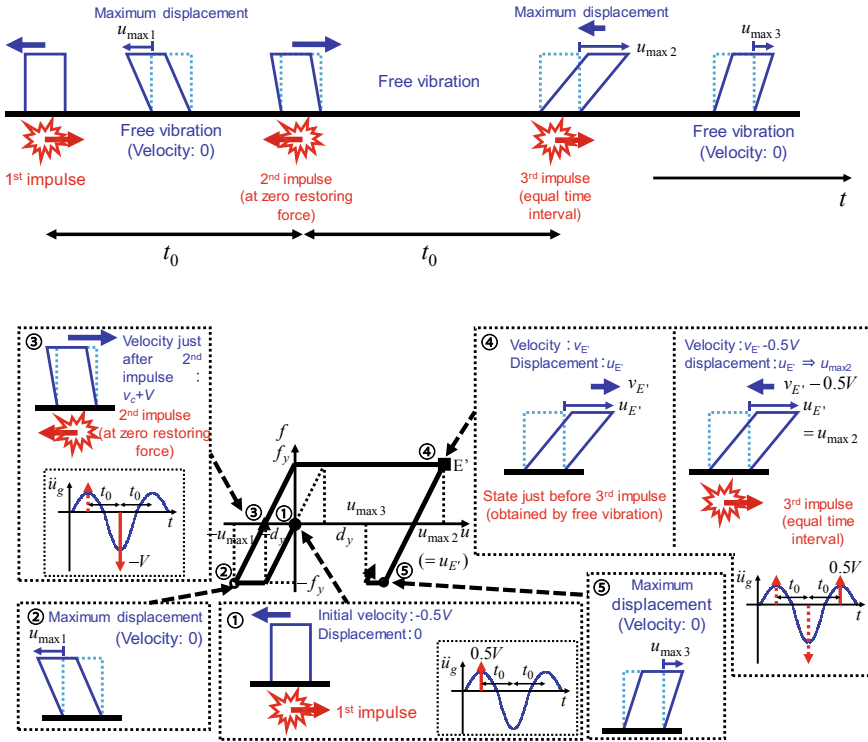
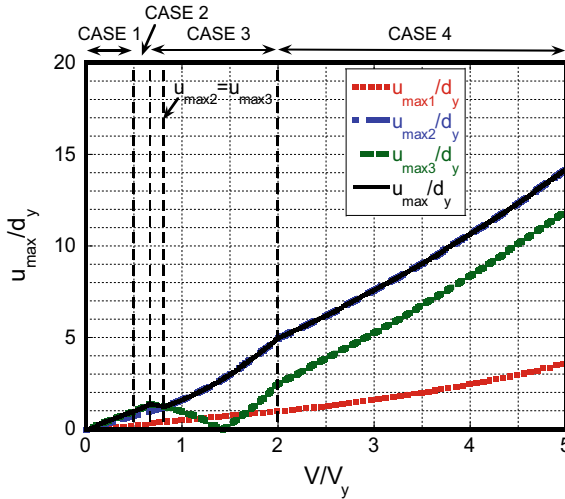**Fig. 7** Overview of elastic-plastic response process of SDOF model to critical triple impulse

Fig. 8 Maximum deformation under critical triple impulse with respect to input velocity level (Kojima and Takewaki 2015b)
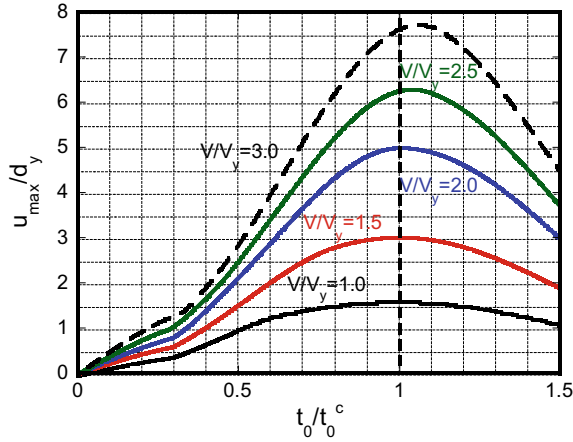
Fig. 9 Maximum deformation under triple impulse with constant velocity level for varied time interval
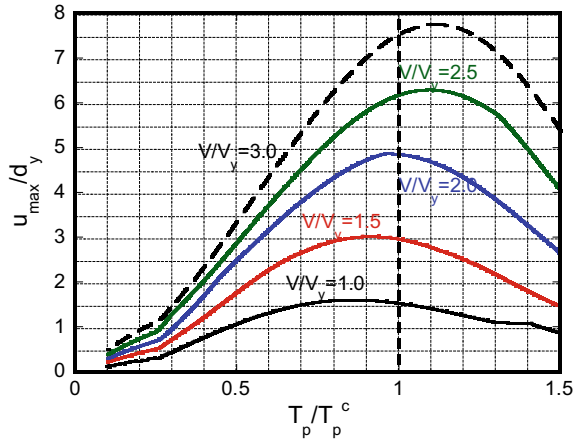
Fig. 10 Maximum deformation under 1.5-cycle sinusoidal wave with constant velocity amplitude for varied input period

time interval t_0 slightly larger than t_0^c. Figure 10 presents the maximum deformation to the corresponding 1.5-cycle sinusoidal wave with the constant velocity amplitude for varied input period T_p. T_p/T_p^c is equal to t_0/t_0^c because $T_p = 2t_0$ and $T_p^c = 2t_0^c$. From Fig. 10, the response to the 1.5-cycle sinusoidal wave is maximized near $T_p = T_p^c$ and $T_p^c = 2t_0^c$ is a fairly good approximate of the critical period of the 1.5-cycle sinusoidal wave for a specific velocity amplitude.

5 Comparison of Maximum Deformation Under Critical Double Impulse and that Under Critical Triple Impulse

Figure 11 shows the comparison of the maximum deformation of an undamped elastic-perfectly plastic SDOF system under the critical double impulse and that under the critical triple impulse. The maximum deformations of an undamped linear elastic SDOF system under both the critical double impulse and the critical triple impulse are $u_{max}/d_y = 2(V/V_y)$. $u_{max}/d_y = 2(V/V_y)$ is equal to the maximum deformation under the critical double impulse or the critical triple impulse in CASE 1. From Fig. 11, the maximum deformation under the critical double impulse is larger than that under the critical triple impulse in the range $0.5 \leq V/V_y < (4 + 2\sqrt{22})/9$. On the other hand, when V/V_y is larger than $(4 + 2\sqrt{22})/9$, the maximum deformation under the critical triple impulse is larger than that under the critical

Fig. 11 Comparison of maximum elastic-plastic response under critical double impulse and that under critical triple impulse, **a** original one, **b** magnified one
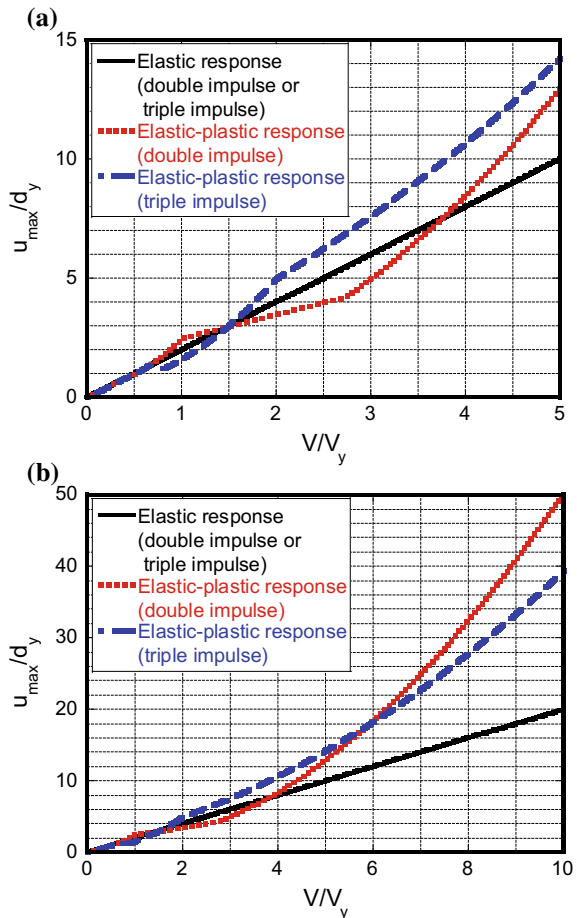
double impulse. This is because the maximum deformation after the first impulse of the critical double is larger than that after the second impulse when the input velocity level V/V_y is larger than $1 + \sqrt{3} \simeq 2.7320$, and the maximum deformation after the second impulse of the critical triple impulse is largest when the input velocity level V/V_y is larger than $2(1 + \sqrt{35})/17 \simeq 0.8137$. The boundary input level $V/V_y = (4+2\sqrt{22})/9 \simeq 1.4868$ can be obtained by using the closed-form solutions for the maximum responses under the critical double impulse and triple impulse.

The maximum deformation under the critical double impulse is larger than that under the critical triple impulse when the input velocity level is larger than about 6. When the input velocity level V/V_y is larger than about 6, the ductility factor is larger than about 18. This input level range is only considered for base-isolation building in Sect. 8.

6 Applicability of Closed-Form Solution for Elastic-Plastic Response Under Critical Triple Impulse to Actual Recorded Near-Fault Ground Motion

In this section, the possibility is investigated whether the triple impulse can be used as substitute for the fault-normal near-fault ground motions and the applicability of the proposed theory using the triple impulse to the actual recorded fault-normal near-fault ground motions is discussed. In order to investigate the applicability of the proposed theory, the elastic-plastic response under the critical triple impulse is compared with the critical response under the Rinaldi station fault-normal component during the Northridge earthquake in 1994. Figure 12 shows the accelerogram of the Rinaldi station fault-normal component during the Northridge earthquake in 1994. The main part of this accelerogram is modeled by the 1.5-cycle sinusoidal wave as shown in Fig. 12. The maximum velocity and the period of the corresponding 1.5-cycle sinusoidal wave are denoted by V_p and T_p. $V_p = 1.05$[m/s] and $T_p = 0.8, 0.85, 0.9, 0.95$ [s] are adopted for the Rinaldi station fault-normal component. Although the critical triple impulse is determined for the structural parameter V_y, the

Fig. 12 Rinaldi station fault-normal component and corresponding 1.5-cycle sinusoidal wave
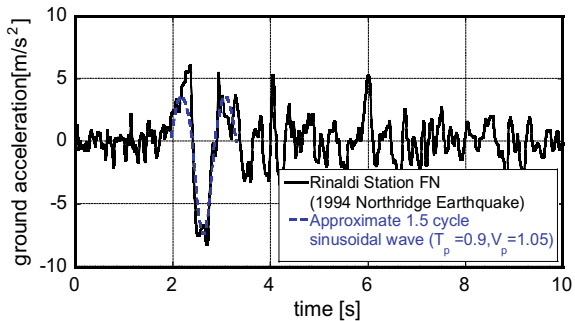
structural parameter V_y is selected for the input velocity level of the actual recorded ground motion to maximize the elastic-plastic response under the actual recorded ground motion because the recorded ground motion is fixed (the input velocity level is fixed). This procedure is similar to the elastic-plastic response spectrum (changing the strength parameter), which was developed in 1960–1970 (Veletsos et al. 1965).

Figure 13 shows the comparison of the elastic-plastic response under the critical triple impulse and the critical elastic-plastic response under the Rinaldi station fault-normal component. The critical elastic-plastic response under the Rinaldi station fault-normal component is obtained by the time-history response analysis. The ordinate axes in Fig. 13a, b present the maximum deformation and the maximum

Fig. 13 Comparison of the elastic-plastic response under the critical triple impulse and that under the Rinaldi station fault-normal component, **a** maximum deformation, **b** maximum deformation amplitude
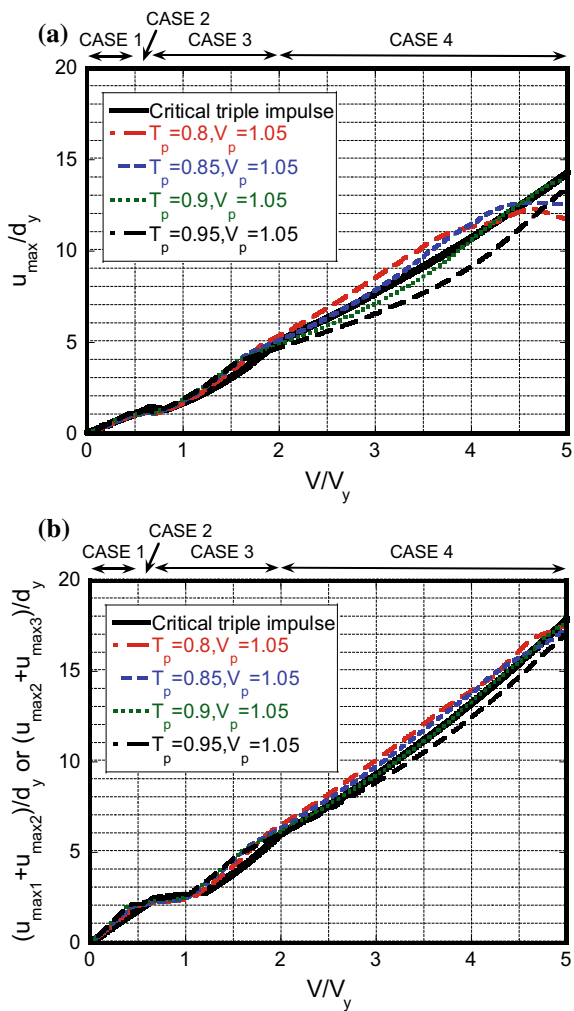
amplitude of deformation. The abscissa is the normalized input velocity level V / V_y. The input velocity level V of the triple impulse as substitute for the Rinaldi station fault-normal component is $V = 1.687 [m/s]$. From Fig. 13a, b the response under the critical triple impulse corresponds to the critical elastic-plastic response under the recorded fault-normal near-fault ground motion (Rinaldi station fault-normal component) regardless of some variation of the parameter of the sinusoidal wave.

7 Application of Elastic-Plastic Response Under Critical Double Impulse and Triple Impulse to Swaying-Rocking Model

In this section, the closed-form expressions for the maximum elastic-plastic responses to the critical double and triple impulses are applied to a structure on flexible ground. The building is modeled by an SDOF system and the stiffness of the ground is modeled by using the sway and rocking springs. The SDOF system supported by the swaying and rocking springs is called the simplified swaying-rocking model (SR model). Figure 14 shows the maximum deformation of the building on the flexible ground under the critical double and triple impulses with respect to the normalized input velocity level. The shear wave velocities of soil type 1, 2 and 3 are $V_S = 200 [m/s]$, $V_S = 133 [m/s]$, $V_S = 100 [m/s]$, respectively. The mass of the building is $m = 800 \times 10^3 [kg]$ and the natural period of the building with fixed base is 1.0[sec]. A 10-story building is assumed here for the super structure. The yield deformation is $d_y = 0.16[m]$, the equivalent height is $H = 40 \times 0.7 = 28[m]$, and the equivalent radius of the foundation $r = 8[m]$. The mass density of ground is $\rho = 1.8 \times 10^3 [kg/m^3]$ and the Poisson's ratio is $\nu = 0.35$.

From Fig. 14a, it can be understood that, in the case of a smaller input level of the double impulse to the structural strength (CASE 1 and 2 for the double impulse), as the ground stiffness becomes larger, the maximum deformation also becomes larger. On the other hand, in the case of a larger input level (CASE 3 for the double impulse), as the ground stiffness becomes larger, the maximum deformation becomes smaller when $u_{max1} < u_{max2}$ and the maximum deformation becomes larger when $u_{max1} > u_{max2}$.

From Fig. 14b, it can be realized that, in case of a smaller input level of the triple impulse (CASE 1 and CASE 2 for the triple impulse), as the ground stiffness becomes larger, the maximum deformation also becomes larger. In the case of a middle input level (CASE 3 for the triple impulse), as the ground stiffness becomes larger, the maximum deformation becomes smaller when $u_{max2} < u_{max3}$ and the maximum deformation becomes larger when $u_{max2} > u_{max3}$. In the case of a larger input level (CASE 4 for the triple impulse), as the ground stiffness becomes larger, the maximum deformation becomes smaller.
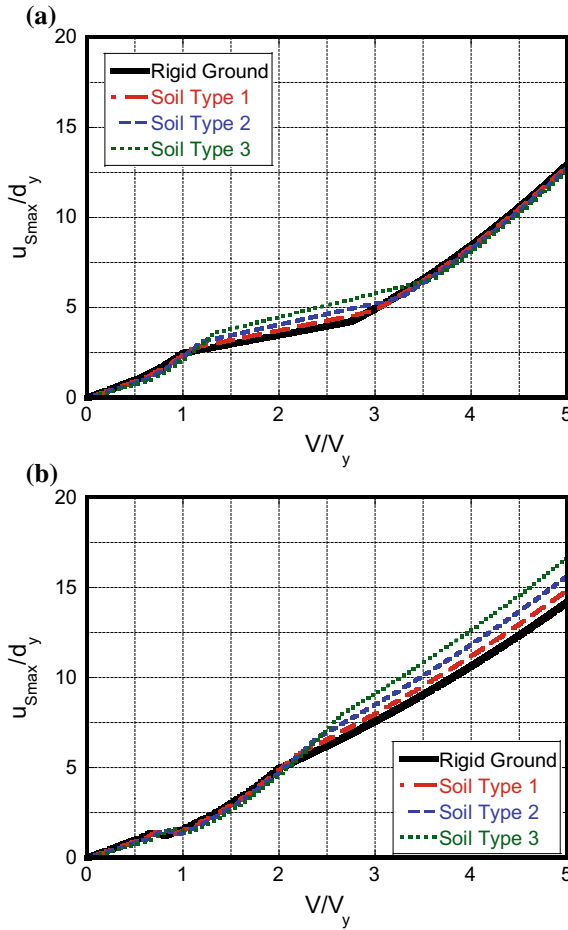
Fig. 14 Maximum deformation of superstructure on flexible ground, **a** double impulse, **b** triple impulse

This is because the elastic strain energy stored in the swaying and rocking springs becomes smaller as the ground stiffness becomes larger. For example, in CASE 4 for the triple impulse, as the ground stiffness becomes smaller, the elastic strain energy stored in the ground springs during the plastic deformation of the superstructure after the first impulse becomes larger and the velocity just after second impulse (the kinetic energy just after second impulse) becomes larger. Then the maximum deformation after the second impulse becomes larger. Therefore, the maximum deformation becomes larger in CASE 4, as the ground stiffness becomes smaller.

8 Application of Elastic-Plastic Response Under Critical Double and Triple Impulses to Base-Isolated Building

In this section, the closed-form solution for the elastic-plastic response to the critical double and triple impulses is applied to base-isolated buildings with nonlinear isolators. The base-isolated building is modeled by a two-degree-of-freedom system (SDOF superstructure and base-isolation story). The base-isolation story is assumed to consist of lead rubber bearings and modeled by a shear spring with elastic-perfectly plastic restoring-force characteristic. In order to apply the closed-form solution for the SDOF system, the two-degree-of-freedom system is transformed into the SDOF system by neglecting the mass on the base-isolation story and introducing the series spring model. Figure 15 shows the maximum deformation in the base-isolated story of the 10-story and 20-story base-isolated buildings under the critical double and

Fig. 15 Maximum deformation in the base-isolation story to critical double impulse and triple impulse, **a** 10-story base-isolated building, **b** 20-story base-isolated building
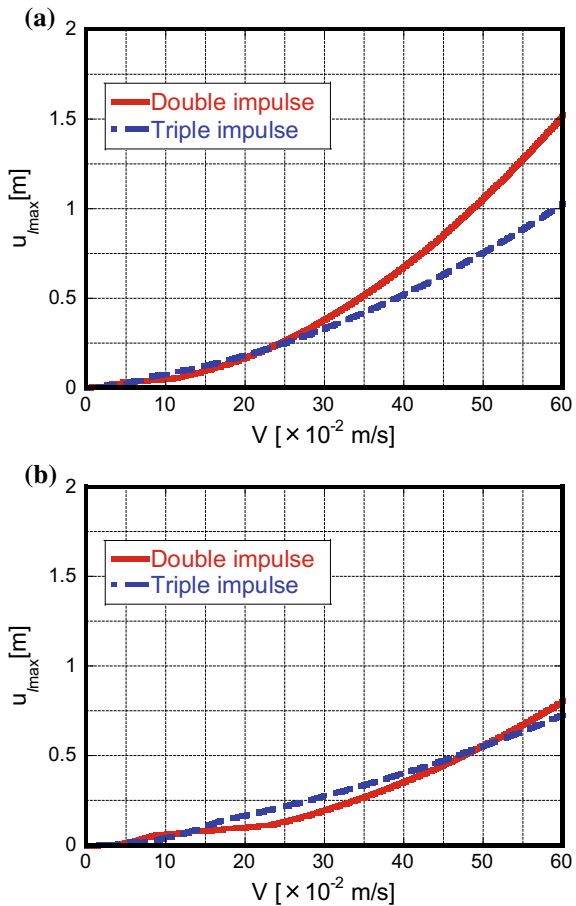
triple impulses with respect to the input velocity level $V[\times 10^{-2}\text{m/s}]$. $u_{I\max}$ denotes the maximum deformation in the base-isolation story. The model parameters of the 10-story and 20-story base-isolated buildings are summarized as follows.

[10-story base-isolated building model]

The mass of the superstructure is $m = 800 \times 10^3$[kg] and the natural period of the superstructure with fixed base is 1.0[sec]. The mass on the base-isolation story is $m_I = 160 \times 10^3$[kg], the fundamental natural period of the rigid superstructure on the base-isolation story is $T_I = 2.0$[sec] and the yield deformation of the base-isolation story is $d_y = 0.01$[m].

[20-story base-isolated building model]

The mass of the superstructure is $m = 1600 \times 10^3$[kg] and the natural period of the superstructure with fixed base is 2.0[sec]. The mass on the base-isolation story is $m_I = 160 \times 10^3$[kg], the fundamental natural period of the rigid superstructure on the base-isolation story is $T_I = 1.4$[sec] and the yield deformation of the base-isolation story is $d_y = 0.01$[m].

From Fig. 15a, b, in the case of a larger input level, the base-isolation story to the critical double impulse is larger than that to the critical triple impulse.

9 Robustness Evaluation by Critical Double and Multiple Impulses

New evaluation methods for the robustness of buildings considering the critical double impulse have been proposed recently. Kanno et al. (2017) proposed the method for evaluating the robustness of SDOF elastic-perfectly plastic systems under the critical double impulse by considering uncertainties of the yield deformation and the stiffness of the SDOF system (Kanno et al. 2017). Subsequently Fujita et al. (2017) modeled a base-isolated building by an SDOF system and evaluated the robustness of the base-isolated high-rise building under the critical double impulse (Fujita et al. 2017). Figure 16 shows an example of robustness in terms of robustness functions proposed by Ben-Haim (2006). It can be understood that the robustness of the base-isolated building depends strongly on the nominal yield deformation in the base-isolation story.

Furthermore Hayashi et al. (2018) proposed a simple method for evaluating the response for the hybrid control structural system of base-isolation and building-connection under the critical multi impulse as a substitute for the long-period and long-duration ground motion (Hayashi et al. 2018). It was confirmed that the hybrid control system is highly robust and can resist both impulsive earthquake ground motions (near-fault ground motions) and long-period and long-duration ground motions. Extension to the critical triple impulse may be possible with minor changes.
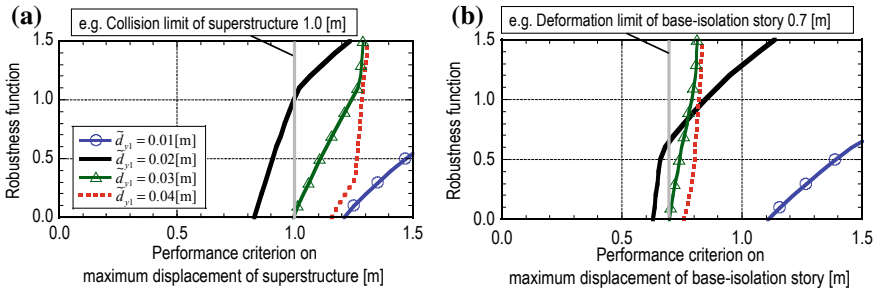
Fig. 16 Comparison of robustness functions for maximum displacement of models with various nominal yield deformations, **a** superstructure, **b** base-isolation story (Fujita et al. 2017)

10 Conclusions

It has been demonstrated that a good approximation of the maximum elastic-plastic responses of various structural models to near-fault ground motions can be derived by using the responses to the corresponding double and triple impulses. A simple but elaborated energy approach played a central role in the derivation of such good approximate closed-form expressions. The closed-form expressions for the elastic-plastic responses under the critical double impulse and the critical triple impulse are applied to the swaying-rocking model considering soil-structure interaction and the model of base-isolated buildings. Furthermore, the robustness evaluation methods considering the critical double impulse have been introduced.

References

Alavi, B., & Krawinkler, H. (2004). Behaviour of moment resisting frame structures subjected to near-fault ground motions. *Earthquake Engineering and Structural Dynamics, 33*(6), 687–706.

Ben-Haim, Y. (2006). *Information-gap decision theory: Decisions under severe uncertainty* (2nd ed.). London: Academic Press.

Caughey, T. K. (1960). Sinusoidal excitation of a system with bilinear hysteresis. *Journal of Applied Mechanics, 27*(4), 640–643.

Drenick, RF. (1970). Model-free design of aseismic structures. Journal of the Engineering Mechanics Division, ASCE, *96*(EM4), 483–493.

Fujita, K., Yasuda, K., Kanno, Y., & Takewaki, I. (2017). Robustness evaluation of elastic-plastic base-isolated high-rise buildings under critical double impulse. *Frontiers in Built Environment, 3,* 31.

Hall, J. F., Heaton, T. H., Halling, M. W., & Wald, D. J. (1995). Near-source ground motion and its effects on flexible buildings. *Earthuake Spectra, 11*(4), 569–605.

Hayashi, K., Fujita, K., Tsuji, M., & Takewaki, I. (2018). A simple response evaluation method for base-isolation building-connection hybrid structural system under long-period and long-duration ground motion. *Frontiers in Built Environment, 4,* 2.

Iwan, W. D. (1961). *The dynamic response of bilinear hysteretic systems* (Ph.D. Thesis). California Institute of Technology.

Kalkan, E., & Kunnath, S. K. (2006). Effects of fling step and forward directivity on seismic response of buildings. *Earthquake Spectra, 22*(2), 367–390.

Kanno, Y., Yasuda, K., Fujita, K., & Takewaki, I. (2017). Robustness of SDOF elastoplastic structure subjected to double-impulse input under simultaneous uncertainties of yield deformation and stiffness. *International Journal Non-Linear Mechanics, 91,* 151–162.

Khaloo, A. R., Khosravi1, H., & Jamnani, H. H. (2015). Nonlinear interstory drift contours for idealized forward directivity pulses using "Modified Fish-Bone" models. *Advances in Structural Engineering, 18*(5), 603–627.

Kojima, K., & Takewaki, I. (2015a). Critical earthquake response of elastic-plastic structures under near-fault ground motions (Part 1: Fling-step input). *Frontiers in Built Environment, 1,* 12.

Kojima, K., & Takewaki, I. (2015b). Critical earthquake response of elastic-plastic structures under near-fault ground motions (Part 2: Forward-directivity input). *Frontiers in Built Environment, 1,* 13.

Kojima, K., & Takewaki, I. (2015c). Critical input and response of elastic-plastic structures under long-duration earthquake ground motions. *Frontiers in Built Environment, 1,* 15.

Kojima, K., & Takewaki, I. (2016a). Closed-form critical earthquake response of elastic-plastic structures on compliant ground under near-fault ground motions. *Frontiers in Built Environment, 2,* 1.

Kojima, K., & Takewaki, I. (2016b). Closed-form dynamic stability criterion for elastic-plastic structures under near-fault ground motions. *Frontiers in Built Environment, 2,* 6.

Kojima, K., & Takewaki, I. (2016c). A simple evaluation method of seismic resistance of residential house under two consecutive severe ground motions with intensity 7. *Frontiers in Built Environment, 2,* 15.

Mavroeidis, G. P., & Papageorgiou, A. S. (2003). A mathematical representation of near-fault ground motions. *Bulletin of the Seismological Society of America, 93*(3), 1099–1131.

Sasani, M., & Bertero, V.V. (2000). Importance of severe pulse-type ground motions in performance-based engineering: historical and critical review. In *Proceedings of the Twelfth World Conference on Earthquake Engineering*, Auckland, New Zealand.

Takewaki, I. (2007). *Critical excitation methods in earthquake engineering.* Elsevier, Second edition in 2013.

Takewaki, I., & Kojima, K. (2017). Double, triple and multiple impulses for critical elastic-plastic earthquake response analysis to near-fault and long-duration ground motions. In N. Chouw, R. P. Orense & T. Larkin (Eds.), *International Workshop on Seismic Performance of Soil-Foundation-Structure Systems, Seismic Performance of Soil-Foundation-Structure Systems*. The University of Auckland, New Zealand (pp. 123–135). CRC Press/ Taylor & Francis Group. November 21–22, 2016.

Takewaki, I., Taniguchi, R., & Kojima, K. (2017). Critical response of elastic-plastic structures to near-fault ground motions and its application to base-isolated building structures, Chapter 6. In *International Symposium in Earthquake Engineering and Structural Dynamics* in memory of late Professor Ragnar Sigbjörnsson, Conference in Reykjavik—June 2017, Earthquake Engineering and Structural Dynamics in Memory of Ragnar Sigbjörnsson (pp. 123–141).

Veletsos, A. S., Newmark, N. M., & Chelapati, C. V. (1965). Deformation spectra for elastic and elasto-plastic systems subjected to ground shock and earthquake motions. In *Proceedings of the Third World Conference on Earthquake Engineering*. New Zealand.

Multi-objective Performance-Based Design Optimization of a Controlled Rocking Steel Braced Frame System

Henry V. Burton, Ji Yun Lee, Saber Moradi and Shahrzad Dastmalchi

1 Introduction

Controlled rocking steel braced frames (CRSBFs) have been developed as an alternative to conventional lateral force resisting systems with the goal of providing enhanced seismic performance. CRSBFs seek to reduce the potential for permanent structural damage through rocking response with post-tensioned (PT) strands used to provide self-centering action, thereby reducing or eliminating residual drifts. Localized yielding and energy dissipation in replaceable fuses serve to reduce drift demands. Rocking behavior is achieved by allowing the braced frame columns to uplift at the base. The frame elements, including the columns, braces, beams and all connections, are designed using capacity-design principles and are expected to respond elastically during moderate-to-severe earthquake shaking. Ultimately, the overall goal of CRSBFs and other types of earthquake protective systems is to reduce the socioeconomic and environmental life cycle seismic impacts in buildings.

Prior research on CRSBFs has primarily focused on experimental (e.g. Eatherton and Hajjar 2010; Ma et al. 2011; Wiebe et al. 2013) and numerical investigations (Hall et al. 2010; Eatherton and Hajjar 2011; Steele et al. 2017) to evaluate their

H. V. Burton (✉) · S. Dastmalchi
Department of Civil and Environmental Engineering, University of California Los Angeles, Los Angeles, USA
e-mail: hvburton@seas.ucla.edu

S. Dastmalchi
e-mail: shdstm@ucla.edu

J. Y. Lee
Department of Civil and Environmental, Washington State University, Pullman, USA
e-mail: jiyun.lee@wsu.edu

S. Moradi
Department of Civil Engineering, Ryerson University, Toronto, USA
e-mail: s.moradi@ryerson.ca

performance and develop simplified design procedures (e.g. Eatherton et al. 2014; Wiebe and Christopoulos 2015). Experimental studies have demonstrated the predictable response and viability of CRSBFs as an enhanced seismic system, including the ability to achieve self-centering action after being subjected to high drift demands. Numerical investigations have provided insights into how the CRSBF structural behavior is affected by key design parameters such as the response modification factor, flag shape height ratio and ambient building resistance. Conceptual design principles and simplified analysis methods provide guidelines for selecting and sizing key CRSBF elements. A cost-benefit evaluation was performed by Dyanati et al. (2017) in which the CRSBF annualized losses were compared to that of a conventional concentric braced frame (CBF) system. The losses due to drift-sensitive component damage were found to be lower in the CRSBF compared to the CBF. However, the opposite was found to be true for losses triggered by damage to acceleration sensitive components. For a 6-story building case, the CRSBF experienced lower overall losses compared to the CBF, whereas for a 10-story building , the overall CRSBF losses were found to be higher.

The current study seeks to evaluate the seismic performance of a 6-story CRSBF building and determine the optimal design parameters that will minimize the combined upfront cost (of the CRSBF only) and earthquake-induced economic losses and environmental impacts. The structural design parameters to be optimized include the rocking frame dead load, initial PT force, fuse strength and frame aspect ratio. The performance criteria are based on minimizing earthquake-induced economic losses and greenhouse gas emission over the service life of the building and the added environmental and economic cost that is needed to achieve more robust designs. Surrogate models are used to establish a statistical link between the structural design parameters and earthquake impacts. Design parameter combinations are determined using the design of experiment methodology. Structural models corresponding to these parameter combinations are analyzed using nonlinear response history analyses (NRHAs) and the resulting engineering demand parameters (EDPs) are used as inputs into the earthquake impact assessment. Once the surrogate models have been trained and validated, they are used to optimize the building performance considering individual and multiple objectives.

2 Performance-Based Assessment and Design Optimization Methodology

Figure 1 shows an overview of the adopted seismic performance assessment and design optimization methodology. Central to the overall framework is the development of surrogate models that can reasonably approximate the combined upfront (initial construction of CRSBF only) and earthquake-induced impacts over a predefined structural design domain (structural parameter ranges and combinations). These surrogate models are then used to determine optimal designs for individual and multiple performance objectives.
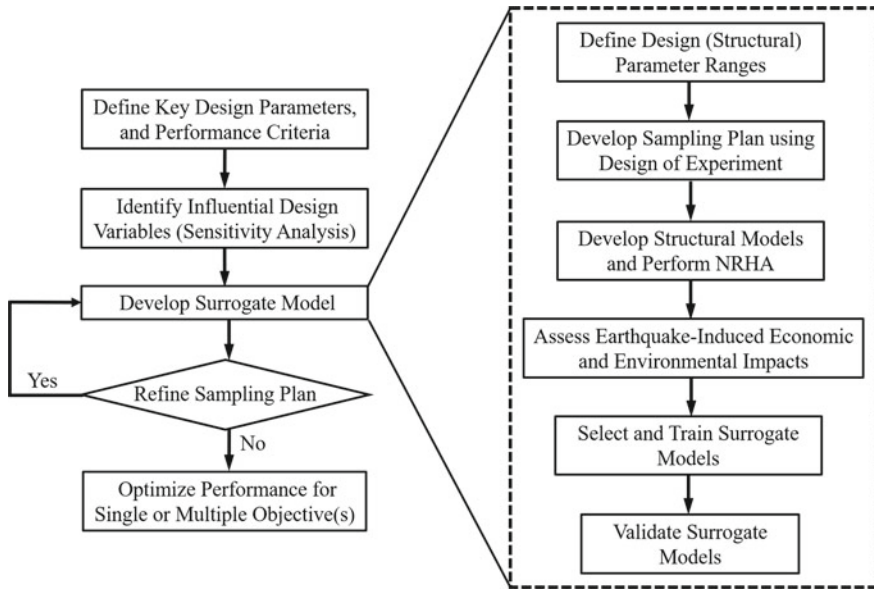
Fig. 1 Overview of performance-based assessment and design optimization methodology

The first step in the overall process is to identify relevant design variables and performance criteria. Four factors that have been shown in prior studies to have a significant influence on the seismic performance of CRSBFs (e.g. Eatherton and Hajjar 2011; Hall et al. 2010) are considered as the structural design parameters. They include the dead load on the rocking frame (P_D), initial PT force (F_{PT}), fuse yield strength (F_{yf}) and the frame aspect ratio (i.e., the bay width-to-height ratio) (B/H).

Service-life seismic performance is described in terms of earthquake-related economic and environmental impacts. Economic impacts are defined based on the cost of repairing earthquake damage to structural and non-structural components as well as equipment. The FEMA P58 methodology (FEMA 2012) is used to assess earthquake-induced economic losses. The Economic Input-Output Life Cycle Assessment (EIO-LCA) (Weber et al. 2009) method is used to quantify greenhouse gas emissions associated with the repair and replacement construction activities that result from earthquake damage.

Once the primary design variables and performance objectives have been established, the surrogate models are developed. Surrogate models are compact representations of the approximate multivariate input/output behavior of the CRSBF. They represent the statistical link between the identified primary structural design parameters and the building service-life seismic performance. In the context of this study, their role is to mimic the complex structural response behavior that is simulated using NRHAs, the damage and financial loss assessed as part of the FEMA-P58 methodology, as well as the EIO-LCA-based environmental impacts.

As shown in Fig. 1, multiple sub-steps are needed to develop the surrogate model. The applicability domain is defined in the first step, whereby the input parameter ranges of the surrogate model are established. Within the context of the surrogate model development, the design space comprises all possible combinations of the considered input parameters. However, performing a "mechanistic" assessment (NRHA + FEMA P58 + EIO-LCA) of all possible design cases is unfeasible. Therefore, a choice must be made about which designs or parameter combinations will be evaluated to construct the surrogate model. This process is referred to as the sampling plan development or design of (physical and computational) experiments (DOE). For this purpose, the central composite design is adopted, whereby each variable (structural design parameter) is associated with a discrete value (or factor level) and a subset of the complete set of factor combinations is used as the sampling points.

Once the sampling points have been established, each design is evaluated using the mechanistic assessment and a performance point is obtained for each metric. Here, the performance point refers to the economic and environmental impact associated with initial construction of only the CRSBF and earthquake-damage occurring during the building's service life. Note that the upfront costs of the non-CRSBF building components are excluded from the optimization because the assumption is that they are constant across all CRSBF design cases. This assumption also enables an isolation of the effect of the CRSBF design and behavior on the building service life performance.

The selection and training of the surrogate model is the next step in the process. Selection involves choosing the type of model that will be used to statistically represent the relationship between the design variables and the performance points. The surrogate models are trained using a subset of the sampling points (training data) with the remaining points (testing data) used for model validation. This enables an assessment of their predictive capabilities away from the training data.

To develop the surrogate model, the design space is defined before the relationship between the design variables, constraints and performance outcome is known. Once the surrogate model has been developed and this relationship has been established, a refinement of the sampling plan may be necessary depending on the results from the validation. The surrogate-model-development step (including all sub-steps) must be repeated if the sampling plan is redefined. Once the surrogate model is finalized, performance optimization is conducted.

3 Description of Baseline Building Case and CRSBF Configuration

The baseline building case is based on the 6-story design developed by Ma et al. (2011) (identified as A6-20 in Ma et al.). A typical plan view and CRSBF elevation are shown in Fig. 2. All bays are 6.1 m wide with six in the longitudinal direction and four in the transverse direction. The building weight is 37,931 kN and the typical
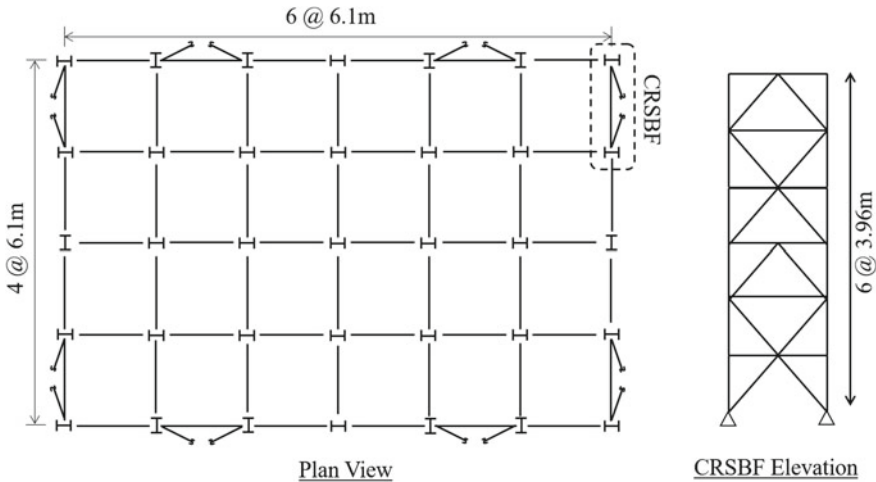
Fig. 2 Typical plan view and elevation for CRSBF building (based on Ma et al. 2011)

story height is 3.96 m. The response modification factor is taken to be $R = 8$. Four perimeter CRSBFs are used in each direction. A site class D location in Los Angeles with $S_s = 1.5g$ and $S_1 = 0.6g$ was used to design the building. The CRSBF PT is aligned in the center of the bay and the fuse is placed at the ground level, also at the center of the bay. Capacity design principles were used to design the braced frame members (beams, columns and braces), with the goal that they remain essentially elastic under maximum considered earthquake (MCE) level shaking. The details of the frame member sizes are summarized in Ma et al. (2011).

4 Development of Sampling Plan Using Design of Experiments

Four input parameters related to the design of CRSBFs are used as predictors for the surrogate models. These factors include the dead load on the rocking frame, initial PT force, and fuse yield strength normalized by the tributary seismic weight, $\frac{P_D}{W}$, $\frac{F_{pt}}{W}$ and $\frac{F_{yf}}{W}$, respectively, as well as the frame aspect ratio, B/H, which is defined as the ratio of the frame bay width to height (Table 1). The parameter ranges, which are defined by an upper and lower limit, are selected based on previous studies of CRSBFs. The center levels are the average of the upper and lower levels.

The sampling plan is established using the design of experiment, which is a statistical method for efficient and systematic experiment planning (including data sampling), analysis, and interpretation (Montgomery 2013). In the design of experiment terminology, 'experiment' is a measurement, observation or computation of a response variable (y). An experiment (or a run) in the current study corresponds to an

Table 1 Normalized input factors and their ranges used to develop the surrogate models

Factor	Lower level (−1)	Center level (0)	Upper level (+1)
P_D/W	0.10	0.30	0.50
F_{pt}/W	0.10	0.15	0.20
F_{yf}/W	0.10	0.30	0.50
B/H	0.20	0.35	0.50

Table 2 Central composite design with additional runs in coded units

Combination No.	Input parameter			
	P_D/W	F_{pt}/W	F_{yf}/W	B/H
1	−1	−1	−1	−1
2	1	−1	−1	−1
3	−1	1	−1	−1
4	1	1	−1	−1
5	−1	−1	1	−1
6	1	−1	1	−1
⋮	⋮	⋮	⋮	⋮
36	0	1	0	0
37	0	0	−1	0
38	0	0	1	0
39	0	0	0	−1
40	0	0	0	1
41	0	0	0	0

initial construction and service-life impact (economic and environmental) assessment for a single CRSBF structural model with one of the factor combinations generated using the design of experiment. The parameter combinations are generated using the central composite design, which is commonly used for developing response surface models. Table 2 shows the adopted set of parameter combinations (experimental design), which includes 25 runs (required for a regular central composite design and with 1 center point) as well as 16 additional runs (which will improve the prediction capability of the surrogate models). Each factor in this design has three levels (lower, center, and upper levels listed in Table 1). For each factor combination in Table 2, the economic and environmental impacts of CRSBF initial construction and building service-life earthquake damage, are assessed using the methodologies described later in the paper. It is important to note that the CRSBF member (beams, columns and braces) sizes are highly dependent on the value of the four input parameters. Therefore, for each sampling point, the CRSBF beams, columns and braces are sized using the methodology developed by Steele and Wiebe (2016). This variation in member size also captures the differences in the economic and environmental cost of the CRSBF structure within the sampling plan.

5   Structural Modeling, Ground Motions and Nonlinear Response History Analyses

5.1   Structural Modeling

Two-dimensional structural models are developed in *OpenSees* (McKenna 1999) for each input factor combination (Fig. 3). Fiber cross sections that incorporate the *Steel02* material with 0.3% strain hardening are used to represent the beams and columns. The connections between beams and columns are modeled as flexurally rigid. Force-based nonlinear beam-column elements are used for the braces, which also have the S*teel02* material with 0.3% strain hardening. Buckling is captured by applying initial imperfections and corotational transformations in the braces. The recommendations by Uriz et al. (2008) are used to discretize the brace elements along
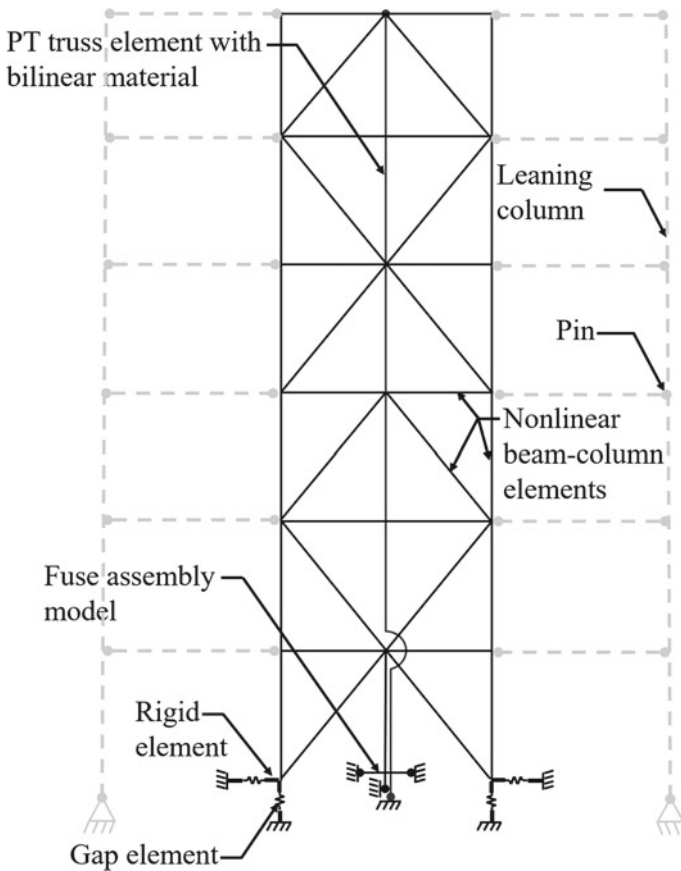

**Fig. 3** Schematic representation of CRSBF numerical model in OpenSees

the length and are also the basis for the selected numbers of fibers and integration points. Brace fracture is not incorporated in the structural model. Pinned connections are used at the brace ends and rigid elastic elements are placed at the ends of beams, columns and braces in the region of the gusset plate. Rayleigh damping corresponding to 2% of critical damping in the first and third modes is applied. Truss elements with a bilinear material model (Ma et al. 2011) are used for the PT strands. The assembly model proposed by Ma et al. (2011) is used to represent the behavior of the energy-dissipating fuses. The fuse link components include a truss element to capture axial stiffness and a beam element with large flexural stiffness and rotational springs on each end to simulate flexural behavior. P-Δ effects originating in the gravity loads on the frames not included in the structural model are captured by placing a leaning column on each side of the rocking frame and the two are connected using pin-ended strut elements. Compression-only gap elements are used to simulate the rocking behavior at the base of each column. These gap elements are near rigid in compression but have zero tensile stiffness.

5.2 Ground Motions and Nonlinear Response History Analyses

The EDPs needed for the economic loss assessment are obtained from NRHAs performed on the structural models corresponding to the individual sampling point or input factor combination. The set of 44 (22 pairs) far-field ground motion records specified in the FEMA P695 guidelines (FEMA 2009) are used for the structural analyses. The response spectra for the suite of unscaled ground motions are shown in Fig. 4. The geometric average of the spectral accelerations over a range of periods, Sa_{avg}, is used as the ground motion intensity measure. Compared to other intensity measures (e.g. 1st mode spectral acceleration), Sa_{avg} has been shown to be more suffi- cient and efficient in predicting the response of rocking building systems (Shokrabadi and Burton 2017). Following the recommendation of Eads et al. (2015), the period range for computing Sa_{avg} is taken to be $0.2T_1$ to $3T_1$. For the 6-story building used in this study, the period corresponding to Eq. 12.8-7 of ASCE 7-16 (ASCE 2016) is com- puted to be 0.74 s. For a period range of $0.2T_1$ to $3T_1$, Sa_{avg} corresponding to the max- imum considered earthquake (MCE), $Sa_{avg,MCE}$, is 0.81g. It is worth noting that the spectral acceleration corresponding to $T = 0.74$ s is $Sa_{T1,MCE} = 1.22g$. The ground motions are scaled individually such that their Sa_{avg} matches the target intensity.

Incremental dynamic analyses (IDAs) are performed for Sa_{avg} intensities ranging from 0.2 to 2.0 $Sa_{avg,MCE}$, using increments corresponding to 0.2 $Sa_{avg,MCE}$. An additional analysis case is performed at 5% $Sa_{avg,MCE}$ to ensure that responses, damage and losses at low hazard events are considered in the numerical integration. The maximum drift ratio in each story, the peak acceleration corresponding to each floor level and the residual drift demand in each story, are obtained from each analysis. The analysis results are also used to generate collapse intensity statistics for each

Fig. 4 Response spectra for the unscaled ground motions
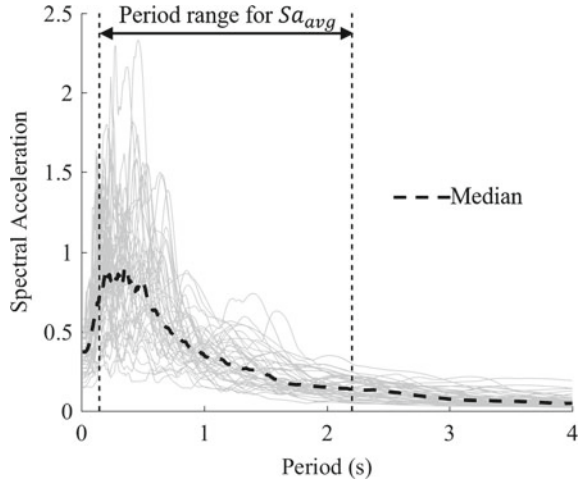
sampling point, which are needed for the economic loss assessment. The collapse criteria include the occurrence of dynamic instability (slope of the IDA curve is very small) or when the story drift ratio exceeds 0.1 (Steele and Wiebe 2017). The building is assumed to be irreparable when the residual story drift ratio exceeds 0.01 (FEMA 2012). At each intensity level, the fraction of collapsed and irreparable damage cases is taken as the empirical probabilities of collapse and demolition, respectively. The maximum likelihood method (Baker 2015) is then applied to the empirical data to obtain lognormal fragility curve parameters (median and log standard deviation) for collapse and demolition.

6 Initial Construction and Service-Life Earthquake-Impact Assessment

6.1 Economic Impact Assessment

For each sampling point or input factor combination, the earthquake induced economic losses corresponding to each ground motion intensity level is obtained by applying the FEMA P58 methodology. The probabilistic distributions of structural response parameters together with component-level damage fragility curves are used to generate probabilistic descriptions of physical damage, which are then combined with component-level loss functions to produce economic impacts. The *Seismic Performance Prediction Program (SP3)* (https://www.hbrisk.com) is used to perform the intensity-based loss assessments where the cost of demolition is included. The damageable structural and non-structural components are summarized in Table 3. Note that, for the elements of the braced frame (beams, columns and braces), the

Table 3 Damageable components used in economic loss assessment

Building component	Unit	EDP	Quantity per story
CRSBF	Each	SDR[a]	8
Gravity connections	Each	SDR	27
Curtain walls	30 ft^2	SDR	180
Partition walls	100 ft	SDR	10
Wall partition finishes	100 ft	SDR	0.8
Suspended ceiling	250 ft^2	PFA[b]	40
Independent pendant lighting	Each	PFA	30
Traction elevator	Each	PFA	3[c]
Potable water piping	1000 ft	PFA	1.7
Potable water pipe bracing	1000 ft	PFA	1.7
HVAC ducting	1000 ft	PFA	1.0
Fire sprinkler water piping	1000 ft	PFA	2.0
Fire sprinkler drop	×100	PFA	0.9

[a]*SDR* Story drift ratio
[b]*PFA* Peak floor acceleration
[c]Entire building

drift demands due to rigid body rotation are excluded from the damage assessment. The cost of the building is taken to be 235 US dollars per square foot, which corresponds to a total cost of 13.6 million US dollars. All economic losses are normalized by the building's replacement cost excluding the cost of demolition. The demolition cost, which includes the removal of debris, is taken as 25% of the initial construction cost (FEMA 2012).

More robust CRSBF designs will ultimately lead to reduced service-life earthquake impacts, however, the upfront environmental and economic costs will be greater. This tradeoff between enhanced robustness and increased initial impacts is considered by quantifying an environmental and economic "cost premium" that will be added to the service-life earthquake impacts. For each sampling point, this cost premium is defined as the initial-construction-impact (environmental and economic) of the controlled rocking braced frame members normalized by that of the entire building, C_{CRBF}http://eproof ing.springer.com/books$_v$2/images/ok.png. This distribution is shown in Fig. 5, where C_{CRBF} ranges from 2.4 to 8.4% of the replacement value. It is not surprising that building (or sampling point) 1, which corresponds to the lower-level value (see Table 1) for all four input factors, has the lowest C_{CRBF}. In contrast, the highest C_{CRBF} corresponds to building 32, which has all upper-level input factor values.

A site-specific seismic hazard curve based on Sa_{avg} is shown in Fig. 6. The Sa_{avg} hazard curve was obtained using the approach suggested by Eads et al. (2015), which involves making small modifications to the already-available ground motion prediction equations for period-based spectral accelerations. Based on the expected

Fig. 5 Distribution of normalized (by building replacement value) upfront cost of the controlled rocking braced frame (C_{CRBF}) for the adopted sampling plan
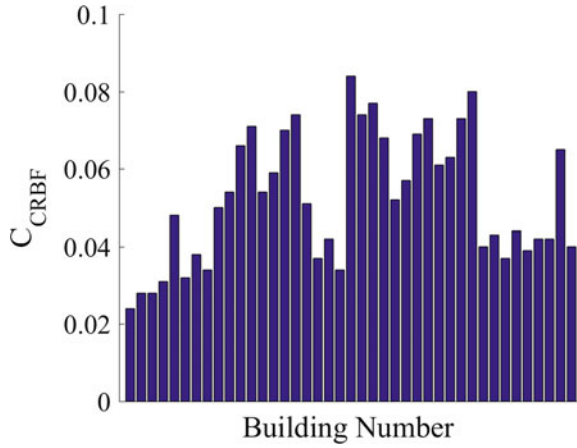
Fig. 6 Hazard curve used to compute life cycle impacts
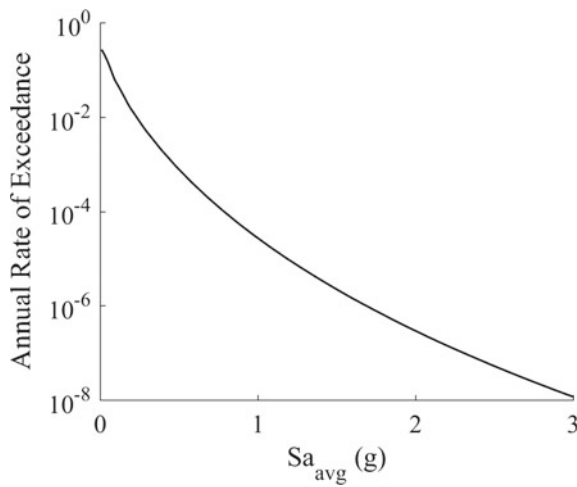
losses conditioned on ground motion intensity combined with the hazard curve, the expected annual losses are estimated. The earthquake-induced building economic losses over an assumed 50-year service life is computed using an annual discount rate of 5%, a value that is within the range commonly used in engineering decision making (2.5–6%) (Lee and Ellingwood 2015).

6.2 Environmental Impacts

The EIO-LCA method is used to assess the environmental impacts of the initial CRSBF construction and the repair and replacement activities that follow earthquake

damage. The method divides an entire economy into distinct sectors and constructs an input-output transaction matrix that represents the interactions among sectors. Using linear algebra models, the direct, indirect, and total effect of changes to the economy and the environment are assessed. More detailed descriptions of the EIO-LCA method are summarized in Hendrickson et al. (1998), Ochoa et al. (2002), and Sharrad et al. (2008).

The 2002 EIO-LCA benchmark model of the United States economy, which is available in the Carnegie Mellon University's EIO-LCA tool (http://www.eiolca.net/), is used to obtain environmental impacts. This model employs the 428×428 input-output matrix compiled by the Bureau of Economic Analysis of the US Department of Commerce based on various census data sources (Weber et al. 2009). The cumulative earthquake induced economic losses resulting from the repair and replacement construction activities are used as the required input of this model. The losses corresponding to each intensity level are disaggregated into the damageable structural and non-structural components shown in Table 3. Each component is again disaggregated into more specific materials and associated economic sectors, and their relative contribution to the repair and replacement costs of each component are obtained from RS Means (www.rsmeans.com). Combined with the seismic hazard curve, the expected cumulative contributions of each sector are summed up to generate the expected service-life economic costs of the associated component due to earthquake repair and replacement activities (EIO-LCA input), which is then used to obtain the environmental impacts of that component (EIO-LCA output). The total cumulative environmental impact of a building is the aggregation of the environmental impacts of each of the components listed in Table 3. The greenhouse gas emission due to earthquake repair and replacement normalized by the amount associated with initial construction of the building (26,376 tons), is the considered environmental metric.

The environmental impact of the initial CRSBF construction is also included in the performance-based optimization. This impact parameter is taken to be the normalized (by the building replacement value) greenhouse gas emission due to initial CRSBF construction, $CO_{2,CRBF}$. Recall that the greenhouse gas emissions are obtained from the economic costs of the building components (EIO-LCA method). Therefore, the distribution of $CO_{2,CRBF}$ (not shown) is similar to (although not exactly the same as) C_{CRBF} (Fig. 5).

6.3   Intensity-Based Earthquake Impacts for Center-Level Sampling Point

Figure 7 shows the normalized (by replacement costs and emissions) expected losses and emissions conditioned on the ground motion intensity (Sa_{avg}) for the sampling point where the center-level (see Table 1) is used for each of the four input factors (i.e. $P_D/W = 0.30$, $F_{pt}/W = 0.15$, $F_{yf}/W = 0.30$ and $B/H = 0.35$). The
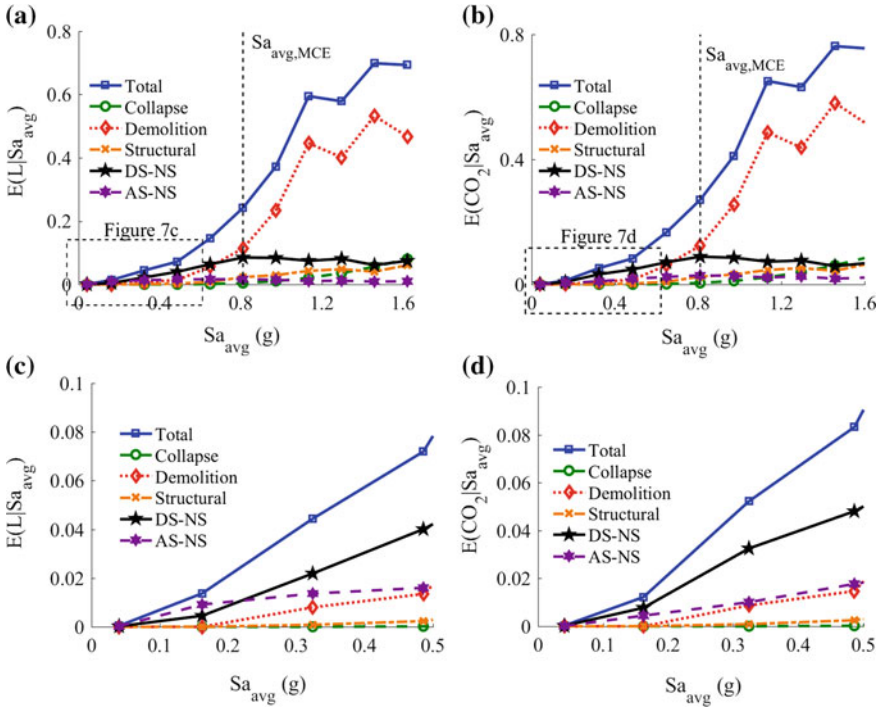
Fig. 7 Normalized (by replacement values) and disaggregated expected economic losses (**a**, **c**) and CO_2 emissions (**b**, **d**), conditioned on the ground motion intensity for the "center-level" sampling point

losses, $E(L|Sa_{avg})$, and emissions, $E(CO_2|Sa_{avg})$, are disaggregated based on contributions from collapse, demolition, structural damage, drift-sensitive non-structural damage (DS-NS) and acceleration-sensitive non-structural damage (AS-NS). Note that the "dip" in demolition-related (and total) economic/environmental impacts between 120 and 140% $Sa_{avg,MCE}$, which appears odd, is a result of the higher levels of dispersion in the residual drifts at the higher intensity.

While the same overall trend is observed for the intensity-based economic (Fig. 7a, c) and environmental (Fig. 7b, d) impacts, there are some subtle differences that are important to the design optimization. When normalized by the replacement impact, the CO_2 emissions for a given intensity are slightly higher than the associated economic losses. For instance, at the MCE hazard level, the expected losses are 24% of the replacement cost, whereas, expected CO_2 emissions are 27% of the replacement emissions. Overall, DS-NS components and residual drifts (demolition) components dominate both impacts at lower and higher intensities, respectively. However, it can be observed in Fig. 7c that, unlike CO_2 emissions, AS-NS components (mostly the elevator) play a significant role at the lowest intensity levels where annual rates of

Fig. 8 Normalized (by replacement values) and disaggregated service-life impacts for all sampling points: **a** economic losses and **b** CO_2 emissions

exceedance are highest. This observation has implications to the service-life impacts described in the next section.

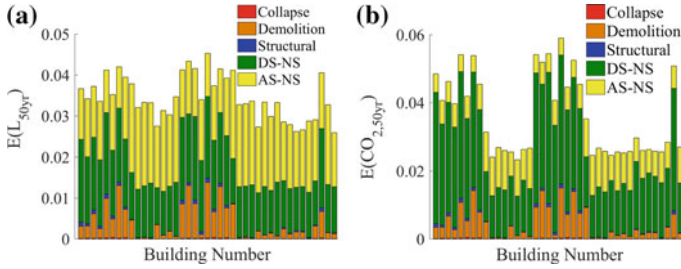The normalized and disaggregated service-life impacts for all sampling points are presented in the form of bar charts in Fig. 8. Recall that for each sampling point, a different combination of input parameters (P_D/W, F_{pt}/W, F_{yf}/W and B/H) is used. The normalized earthquake-induced economic losses, $E(L_{50yr})$, which are shown in Fig. 8a, range between 2.5 and 4.5% of the building replacement cost. In other words, for the adopted sampling plan, the selected input parameters can change the service-life economic losses by a factor of up to 1.8. There is also significant variation in the distribution of losses across the different categories. Collapse and structural component losses are negligible across all sampling points and losses caused by demolition vary between almost zero and approximately 1.3%. At first glance, the low service-life contribution of demolition-related impacts may seem surprising since Fig. 7a, b show that demolition dominates the impacts at higher levels (MCE and greater). However, Fig. 7c, d show that demolition-related impacts are not as significant at the low-to-moderate intensities, which are associated with high hazard levels.

Economic losses are almost equally dominated by AS-NS and DS-NS components. However, from one sampling point to the next, there are variations in which of these two types of components account for most of the service life losses. This set of observations highlights the effect of the choice of input parameters on both the total and distribution of service life economic losses.

The dispersion (as measured by the coefficient of variation) in expected service life CO_2 emissions, $E(CO_{2,50yr})$ (Fig. 8b) across all sampling points is generally higher compared to $E(L_{50yr})$, with the former ranging from 2 to 6% of the building replacement emissions. Therefore, compared to economic losses, service-life environmental impacts are found to be more sensitive to the selected CRSBF design parameters. There are other subtler differences in how the input factor combinations affect these two metrics. For instance, the lowest $E(L_{50yr})$ and $E(CO_{2,50yr})$ occur in different sampling points: 41, and 14, respectively. Moreover, while there are variations in whether AS-NS or DS-NS components dominate $E(L_{50yr})$ from one sampling point to the next, the DS-NS components dominate $E(CO_{2,50yr})$ across all

sampling points. These differences in the effect of the choice of input parameters on the two service-life impact metrics will affect the multi-objective optimal design presented later in the paper.

7 Surrogate Model Development and Verification

Surrogate models are developed and verified for the economic and environmental impacts (i.e. response variables) using the design of experiment method. Each surrogate model represents the relationship between the input parameters (e.g. P_D/W) and a response variable (e.g. $E(L_{50yr})$). A quadratic polynomial model is used to fit the data generated by the adopted experimental design. The quadratic model for each surrogate model is in the form of Eq. 1:

$$y = \beta_0 + \sum_{i=1}^{k} \beta_i x_i + \sum_{i=1}^{k} \sum_{j=1}^{k} \beta_{ij} x_i x_j + \varepsilon \tag{1}$$

where β's are the unknown regression coefficients, x's are the independent predictors (factors), and ε is the random error (or the residual) term, that is the difference between the actual (y_l) and predicted ($\widehat{y_l}$) response ($\varepsilon_l = y_l - \widehat{y_l}$) and is obtained for each design point or factor combination ($l = 1, 2, \ldots, n$). The unknown coefficients (the β's) are estimated using the method of least squares, which minimizes the sum of the squares of the errors ($\sum_{l=1}^{n} \varepsilon_l^2$) (Montgomery 2013). Surrogate models are developed to predict both the service-life ($E(L_{50yr})$ and $E(CO_{2,50yr})$) and total ($E(L_{50yr}) + C_{CRBF}$ and $E(CO_{2,50yr}) + CO_2$) impact metrics. The goal here is to highlight the differences between the optimal design parameters with and without the consideration of the upfront cost of the CRSBF. The coefficients for the four surrogate models are summarized in Table 4 and their prediction capability is assessed in the following subsection.

To assess the predictive performance of the surrogate models, 10 additional factor combinations are generated and used as testing data. Table 5 lists the coded form of these additional sampling points, which are different from the training data originally used to develop the surrogate models. Nonlinear structural models of CRSBFs with these factor combinations are analyzed and the actual impact values (initial plus service-life) are compared with the predictions from the surrogate models. Figure 9 shows the actual versus predicted service-life impact quantities for each surrogate model where the training and testing data are distinguished from each other.

Quantitative measures of the surrogate models' ability to predict the testing dataset are summarized in Table 6. The coefficient of determination (R^2) is computed as the ratio of the sum of squares from the surrogate model responses to that of the actual responses. The R^2 values are generally higher for greenhouse gas emission metrics where the variance across the sampling plan impact values in the training dataset was observed to be higher compared to the economic loss metrics. The ability of the

Table 4 **a** β_i's for all the response variables, **b** β_{ij}'s for $E(L_{50yr})$ and $E(CO_{2,50yr})$, **c** β_{ij}'s for $E(L_{50yr}) + C_{CRBF}$ and $E(CO_{2,50yr}) + CO_2$

i	Input parameter, x_i	$E(L_{50yr})$	$E([CO]_{(2,50yr)})$	$E(L_{50yr}) + C_{CRBF}$	$E([CO]_{(2,50yr)}) + [CO]_{(2,CRBF)}$
0	Intercept	0.074	0.121	0.175	0.147
1	B/H	−0.267	−0.444	−0.693	−0.444
2	P_D/W	−0.024	−0.051	−0.076	−0.051
3	F_{yf}/W	−0.016	0.006	0.079	0.006
4	F_{pt}/W	0.151	0.088	−0.019	0.088

i	Input parameters, $(x_i$ and $x_j)$	$\beta_{(i's)}$ "for" $E(L_{50yr})$				$\beta_{(i's)}$ "for" $E([CO]_{(2,50yr)})$			
		B/H	P_D/W	F_{yf}/W	F_{pt}/W	B/H	P_D/W	F_{yf}/W	F_{pt}/W
1	B/H	0.358				0.513			
2	P_D/W	0.026	0.001			0.054	0.012		
3	F_{yf}/W	−0.052	0.018	0.022		−0.040	0.0060	−0.009	
4	F_{pt}/W	0.012	0.027	0.093	−0.654	0.048	0.061	0.083	−0.536

i	Input parameters, $(x_i$ and $x_j)$	$\beta_{(i's)}$ "for" $E(L_{50yr}) + C_{CRBF}$				$\beta_{(i's)}$ "for" $E([CO]_{(2,50yr)}) + [CO]_{(2,CRBF)}$			
		B/H	P_D/W	F_{yf}/W	F_{pt}/W	B/H	P_D/W	F_{yf}/W	F_{pt}/W
1	B/H	0.941				0.513			
2	P_D/W	0.117	0.022			0.054	0.012		
3	F_{yf}/W	−0.195	0.0002	0.028		−0.040	0.0060	−0.009	
4	F_{pt}/W	0.643	0.102	0.022	−0.619	0.048	0.061	0.083	−0.536

Table 5 The coded design used for verification

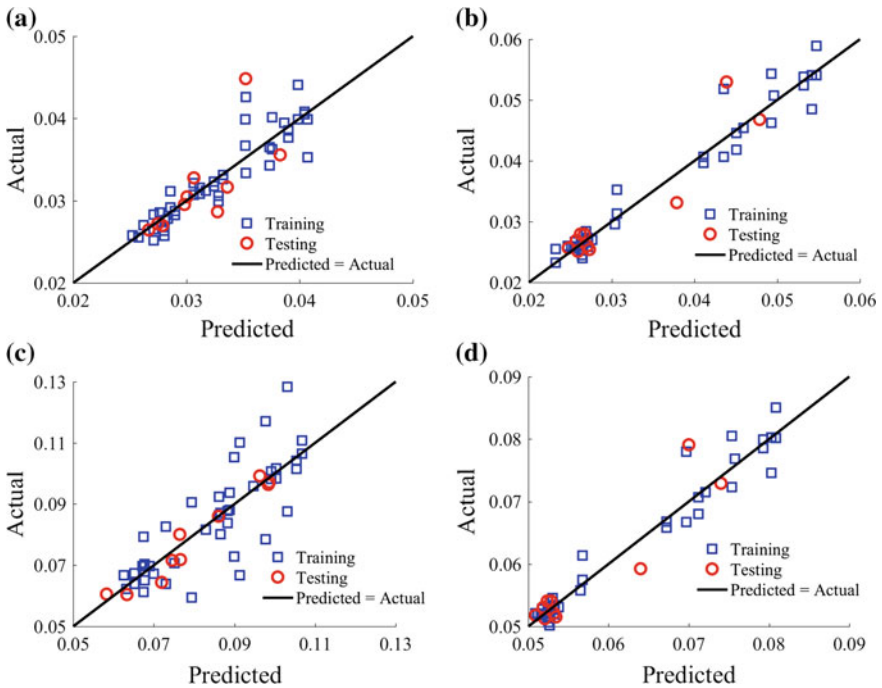| Combination No.	Input parameter			
	P_D/W	F_{pt}/W	F_{yf}/W	B/H
1	0	0	−1	−1
2	1	1	0	−1
3	0	0	1	1
4	1	0	−1	1
5	−1	1	0	1
6	1	0	−1	−0.8
7	0.4	−1	0	1
8	0	−1	−1	0
9	1	0	1	0
10	0	1	1	0

Fig. 9 Actual versus surrogate-model-predicted impacts: **a** $E(L_{50yr})$, **b** $E(CO_{2,50yr})$, **c** $E(L_{50yr})+$ C_{CRBF} and **d** $E(CO_{2,50yr}) + CO_2$

Table 6 Surrogate model verification details

Response variable	R^2	$MARD$
$E(L_{50yr})$	0.84	0.048
$E(CO_{2,50yr})$	0.96	0.045
$E(L_{50yr}) + C_{CRBF}$	0.67	0.040
$E(CO_{2,50yr}) + CO_2$	0.96	0.023

surrogate models to accurately predict the response variables in the testing dataset is quantitatively summarized using the median absolute relative deviation (*MARD*), which is computed as the median of the absolute difference between the predicted and actual response variables normalized by the actual values (Sun et al. 2017). The *MARD* value for the four surrogate models ranges from 0.023 to 0.048, indicating good overall prediction accuracy.

8 Sensitivity of Impacts to Individual Predictors

To further investigate the differences in how the aggregated (initial plus service life) metrics are affected by the CRSBF design, their sensitivity to variations in the individual structural input parameters is evaluated. The surrogate models are used to compute aggregated impacts based on the two metrics, with each input parameter incrementally varied between the upper and lower levels (Table 1) while the other three are sampled from a uniform distribution. Figure 10 shows the effect of each input parameter on the aggregated impact metrics.

Among the four input parameters, the aspect ratio is observed to have the greatest effect on both metrics. However, there are variations in the extent and manner in which each metric is affected. $E(L_{50yr}) + C_{CRBF}$ is highest at the upper level, $B/H = 0.5$, and the minimum impact occurs at $B/H = 0.32$ (Fig. 10a). The impact at the lowest level, $B/H = 0.2$, is approximately 87% of the maximum impact. The
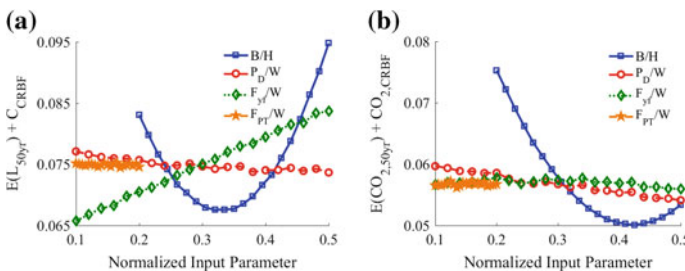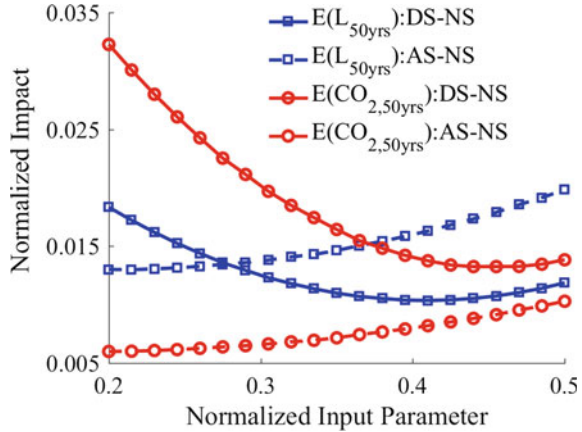

Fig. 10 Sensitivity of impact metrics to individual structural parameter variations: **a** $E(L_{50yr}) + C_{CRBF}$ and **b** $E(CO_{2,50yr}) + CO_{2,CRBF}$

Fig. 11 Comparing
sensitivity of DS-NS and
AS-NS components
$E(L_{50yr})$ and $E(CO_{2,50yr})$
to aspect ratio variations

overall trend of the effect of aspect ratio on $E(CO_{2,50yr}) + CO_{2,CRBF}$ is similar to $E(L_{50yr}) + C_{CRBF}$, however, there are differences in the extent to which each impact is affected. The maximum and minimum $E(CO_{2,50yr}) + CO_{2,CRBF}$ vary by a factor of approximately 1.5 compared to 1.4 for $E(L_{50yr}) + C_{CRBF}$. Additionally, the B/H corresponding to the minimum impact is 0.32 and 0.43 for $E(L_{50yr}) + C_{CRBF}$ and $E(CO_{2,50yr}) + CO_{2,CRBF}$, respectively. Lastly, the maximum $E(L_{50yr}) + C_{CRBF}$ occurs at the upper-level B/H, whereas, the maximum $E(CO_{2,50yr}) + CO_{2,CRBF}$ occurs at the lower level.

The differences in the effect of the aspect ratio on aggregated economic and environmental impacts can be explained by comparing its effect on DS-NS and AS-NS components service-life impacts. Figure 11 shows that, while DS-NS components impacts decrease with increasing B/H, the opposite is true for the impacts caused by AS-NS components. Generally, a larger aspect ratio will increase the strength and stiffness of a rocking system, which will lead to higher floor acceleration demands. It is therefore not surprising that the expected service-life impacts caused by damage to AS-NS components increases with the CRSBF aspect ratio. It is also noted from Fig. 11 that, relative to the total impacts, B/H has a much smaller effect on $E(CO_{2,50yr})$ due to AS-NS components damage compared to DS-NS components, which is consistent with results shown in Fig. 8a, b. Although not as influential as the aspect ratio, the dead load on the rocking frame, P_D/W, reduces the impacts for both metrics. Moreover, while negligible for $E(CO_{2,50yr}) + CO_{2,CRBF}$, the effect of the fuse yield force, F_{yf}/W, is fairly substantial and positively correlated with $E(L_{50yr}) + C_{CRBF}$. The initial PT force, F_{PT}/W, has the lowest overall impact on both metrics.

The contrast between the effect of strength/stiffness on the impacts caused by damage to DS-NS and AS-NS components is a key challenge in achieving optimal designs. Moreover, the disparities in the extent to which the various CRSBF parameters affect different impact metrics (service-life and aggregated) are important when seeking to optimize the performance based on multiple objectives.

9   CRSBF Design Optimization

The surrogate models are used to optimize the aggregated and service-life performance of the CRSBF where the goal is to obtain design parameter values (regions of the statistical design space) that minimize the considered impacts. The optimization problems are defined to address both synergistic and conflicting objectives with the ultimate goal of achieving the best holistic performance. For instance, the current study seeks to minimize the aggregated impacts of the CRSBF building, which includes both the initial construction and service-life emissions/costs. However, minimizing the service-life seismic impacts requires more robust designs with higher initial costs/emission. As described in the previous section, another source of conflict is the difference in the sensitivity of each impact metric to the various design parameters. In other words, an optimal condition for one impact metric may not coincide with that of another. Single- and multi-objective performance optimization is conducted using a desirability function approach, which is described in the next sub-section followed by the optimization objectives and discussion of the results.
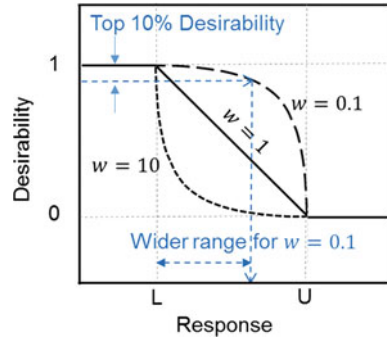
9.1   Desirability Function Approach

The desirability function approach is used for the single- and multiple-objective optimization problems (Myers et al. 2009). First, a desirability function (d_i) is assigned to each response variable (y_i) or optimization objective (e.g. economic costs). The desirability function value (d_i) ranges from 0 to 1, representing the least to the most desirable condition, respectively. For the goal of minimizing the response, the desirability function (Derringer and Such 1980) is obtained from Eq. 2.

$$d_i = \begin{cases} 1 & y_i < L_i \\ \left(\frac{U_i - y_i}{U_i - L_i}\right)^{w_i} & L_i \leq y_i \leq U_i \\ 0 & y_i > U_i \end{cases} \tag{2}$$

where U_i and L_i are the upper and lower bounds for the response or objective i, which are the maxima and minima values of each response variable observed in the experimental design (i.e. maxima and minima values of each response observed for the training data or parameter combinations), w_i is a *weight value* for response i, which changes the shape of the associated desirability function. As shown in Fig. 12, the desirability function is linear when $w_i = 1$. In the case of $w_i > 1.0$, more stringent constraints are placed on the optimization target (the lower bound when minimization is the objective). In other words, the rate at which the desirability decreases moving from L_i to U_i is higher. In contrast, a lower value of w_i (near 0.1) reduces the constraints associated with achieving a desirable response. To illustrate this, consider a minimization problem where the goal is to achieve a lower bound for the response. As shown in Fig. 12, assuming the top 10% desirability value as

Fig. 12 Desirability
function d_i for the goal of
minimization

the optimal condition, the desirability function with $w_i = 0.1$ leads to a much wider range for the response variable compared to when $w_i = 10$. Hence, using a higher weight for an optimization objective results in a narrower optimal range.

The desirability function (d_i) for each response variable (impact category) is then combined to compute an overall desirability function (D) for the optimization problem:

$$D = \left(d_1^{r_1} \times d_2^{r_2} \times \cdots \times d_n^{r_n}\right)^{1/\sum r_i} \tag{3}$$

where n is the number of response variables and r_i is an importance value assigned to response i. The importance value specifies the relative priority for achieving an objective and it ranges from 1 (the least important objective) to 5 (the most important objective). The optimization problem then involves maximization of the overall desirability function (D).

9.2 Results from Single- and Multiple-Objective Design Optimization

Several optimization objectives are explored to determine the parameter combinations or regions that lead to optimal conditions for each impact category when studied separately and the simultaneous minimization of all impact categories with the same importance value.

The results for six optimization problems are summarized in Table 7. A weight of $w_i = 10$ is used for all cases and an importance value $r_i = 5$ is applied to each impact category for the multi-objective optimization case. The sensitivity analyses showed that the aspect ratio had the highest influence on the overall performance of the CRSBF system (Fig. 10). From Table 7, it can be observed that the optimal value of B/H ranges from 0.32 to 0.44, which corresponds to the minimization of $E(L_{50yr}) + C_{CRBF}$ and $E(CO_{2,50yr}) + CO_{2,CRBF}$, respectively. Earlier,

Table 7 Single- and multi-objective optimization problems and associated parameter values

Optimization problem: minimize	Design parameter value			
	B/H	P_D/W	F_{yf}/W	F_{pt}/W
$E(L_{50yr})$	0.38	0.36	0.37	0.20
$E([CO]_{2,50yr})$	0.40	0.35	0.11	0.18
$E(L_{50yr}) + C_{CRBF}$	0.32	0.30	0.12	0.11
$E([CO]_{2,50yr}) + [CO]_{(2,CRBF)}$	0.44	0.24	0.50	0.20
$E(L_{50yr}) + E([CO]_{2,50yr})$	0.38	0.31	0.19	0.20
All	0.36	0.50	0.14	0.11

the acceleration sensitive damage was shown to have a smaller influence on environmental impacts compared to economic losses (Fig. 11). This is consistent with $E(CO_{2,50yr}) + CO_{2,CRBF}$ being minimized with a higher B/H, which corresponds to a higher stiffness and floor accelerations. When the goal is to simultaneously minimize economic and environmental aggregated impacts, the optimal $B/H = 0.36$. The sensitivity analyses also showed both types of impacts (economic and environmental) decreased monotonically with P_D/W (Fig. 10). It is therefore not surprising that the optimal P_D/W for minimizing *All* impacts corresponds to the upper-level value of 0.50. The optimal F_{pt}/W and F_{yf}/W values are highly dependent on the performance criteria, spanning their full range of values for the six objective functions. However, to simultaneously minimize *All* impacts, the optimal F_{pt}/W and F_{yf}/W are 0.11 and 0.14, respectively.

Plots of the desirability, D, (computed using Eq. 3) as a function of pairs of input parameters for the performance criteria of minimizing *All* impacts, are shown in Fig. 13. The optimal set of input parameters are the values that produce the maximum desirability. Figure 13 shows how D is affected by the interaction between parameters. For instance, Fig. 13a shows that the effect of the B/H on D is minimally influenced by F_{yf}/W. In other words, for a given value of B/H, the relative change in D as a function of F_{yf}/W is minimal. While not shown in Fig. 13, this observation holds true for the interaction between B/H and the other two parameters (P_D/W and F_{pt}/W). This also explains why the optimal values for B/H are comparable to the values that minimize $E(L_{50yr}) + C_{CRBF}$ and $E(CO_{2,50yr}) + CO_{2,CRBF}$ in Fig. 10. In contrast, P_D/W has a significant impact on how F_{yf}/W influences D (Fig. 13b) and vice versa. Figure 13b shows that D is maximized when F_{yf}/W and P_D/W are approximately at their lower- and upper-level values, respectively. This is consistent with prior studies, which have shown that the residual drifts in CRSBFs are minimized when the contribution to overturning resistance from the fuse is low relative to the combined contribution from the dead load and the post-tensioning (e.g. Ma et al. 2011). The effect of the interaction between P_D/W and F_{pt}/W on the desirability is also observed to be fairly significant. Figure 13d shows that D is maximized near the upper- and lower-level values of P_D/W and F_{pt}/W, respectively.
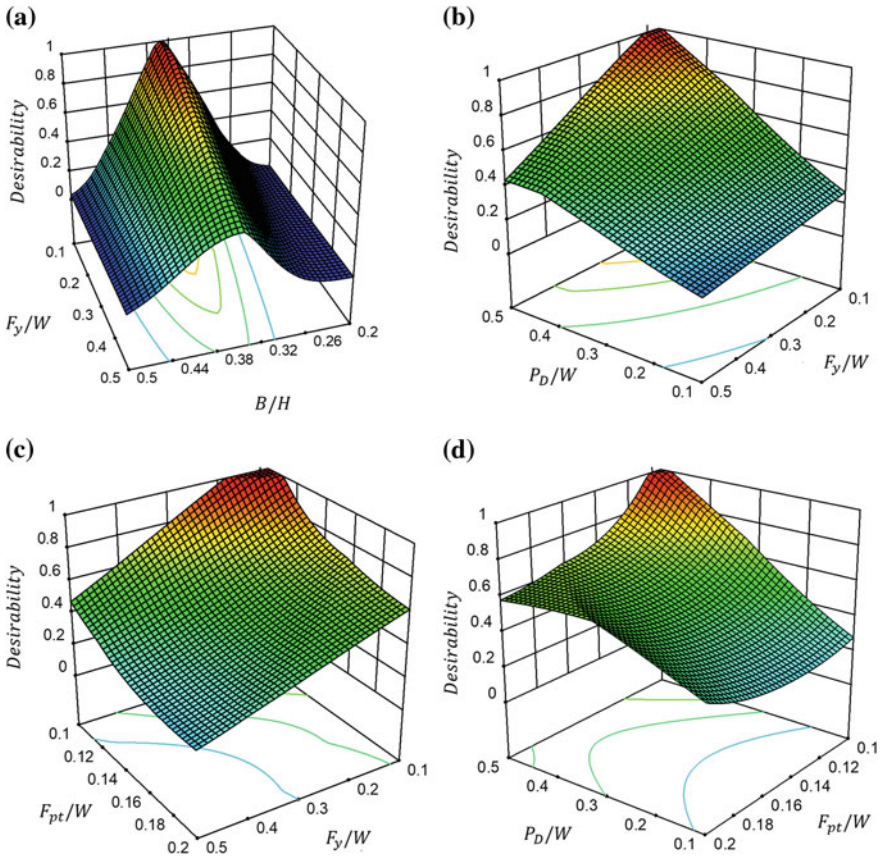
Fig. 13 Desirability as a function of pairs of input parameters for the goal of minimizing *All* impacts: **a** B/H and F_{yf}/W, **b** P_D/W and F_{yf}/W, **c** F_{pt}/W and F_{yf}/W and **d** P_D/W and F_{pt}/W

10 Conclusion

This chapter presented a seismic performance assessment and multi-objective design optimization of a 6-story controlled rocking steel braced frame (CRSBF) building. Service-life performance is quantified based on earthquake-induced economic losses and greenhouse gas emissions. The ultimate goal is to determine the optimal structural design parameter values that will minimize upfront (CRSBF only) and earthquake-induced economic and environmental impacts. The considered structural design parameters include the frame aspect ratio (bay width to height ratio), B/H, the dead load on the rocking frame, (P_D), initial post-tensioning (PT) force (F_{pt}), and fuse strength (F_{yf}). The latter three parameters are normalized by the tributary seismic weight (W).

Nonlinear response history analyses (NRHAs) of two-dimensional structural models of the CRSBF are used to generate engineering demand parameters (EDPs). Earthquake-induced economic losses over the service life of the building are assessed using the FEMA P58 methodology and the EDPs obtained from the NRHAs. Greenhouse gas emissions are computed using the Economic Input-Output Life Cycle Assessment (EIO-LCA) method. Surrogate models are developed and used to establish a statistical link between the structural design parameters and the economic and environmental impacts. The sampling plan (of the input parameter combinations) for the surrogate model is generated using the design of experiment method. After validation, the surrogate models are used to conduct single- and multi-objective optimization of the building performance using a desirability function approach.

For the intensity-based assessments (i.e. impacts conditioned on ground motion intensity level), residual drifts (demolition) dominated both economic and environmental impacts at higher intensities [maximum considered earthquake (MCE) level and higher]. At low-to-moderate intensities (less than MCE) where the seismic hazard is highest, drift sensitive non-structural components (DS-NS) had the greatest influence on both impact metrics. Acceleration-sensitive non-structural components (AS-NS) contributed the most to economic losses at the lowest intensities. However, this observation did not hold true for CO_2 emissions. In other words, AS-NS component damage was not the biggest contributor to CO_2 emissions at the lowest intensities.

Compared to economic losses, $E(L_{50yr})$, the CO_2 emissions over a 50-year service-life, $E(CO_{2,50yr})$, was found to be more sensitive to the selected CRSBF design parameters. Across all sampling points, $E(L_{50yr})$ ranged from 2.5 to 4.5% compared to 2 to 6% for $E(CO_{2,50yr})$. Moreover, $E(L_{50yr})$ was almost equally dominated by AS-NS and DS-NS component damage. In contrast, $E(CO_{2,50yr})$ associated with DS-NS component damage was consistently higher than the emissions from AS-NS component damage. Among the considered structural design parameters, B/H had the greatest influence on both $E(L_{50yr})$ and $E(CO_{2,50yr})$ while F_{pt}/W had the smallest effect. Furthermore, DS-NS component damage impacts increased with B/H but the opposite was observed for AS-NS impacts.

The optimal value of B/H for individually minimizing the aggregated (CRSBF initial plus building service-life) economic and environmental impacts was found to be 0.32 and 0.44, respectively. When the goal is to (at the same time) minimize both economic and environmental aggregated impacts, the optimal B/H is 0.36. For the other three parameters, the optimal values for minimizing (at the same time) economic and environmental aggregated impacts are $F_{pt}/W = 0.11$, $F_{yf}/W = 0.14$ and $P_D/W = 0.50$.

References

ASCE. (2016). *Minimum design loads for buildings and other structures*. ASCE 7-16, Reston, VA.

Baker, J. W. (2015). Efficient analytical fragility function fitting using dynamic structural analysis. *Earthquake Spectra, 31,* 579–599.

Derringer, G., & Suich, R. (1980). Simultaneous optimization of several response variables. *Journal of Quality Technology, 12*(4), 214–219.

Dyanati, M., Huang, Q., & Roke, D. (2017). Cost-benefit evaluation of self-centering concentrically braced frames considering uncertainties. *Structure and Infrastructure Engineering, 13*(5), 537–553.

Eads, L., Miranda, E., & Lignos, D. G. (2015). Average spectral acceleration as an intensity measure for collapse risk assessment. *Earthquake Engineering and Structural Dynamics, 44*(12), 2057–2073.

Eatherton, M., & Hajjar, J. (2010). *Large-scale cyclic and hybrid simulation testing and development of a controlled-rocking steel building system with replaceable fuses*. NSEL-025, Department of Civil and Environmental Engineering, University of Illinois at Urbana-Champaign.

Eatherton, M. R., & Hajjar, J. F. (2011). Residual drifts of self-centering systems including effects of ambient building resistance. *Earthquake Spectra, 27*(3), 719–744.

Eatherton, M. R., Ma, X., Krawinkler, H., Mar, D., Billington, S., Hajjar, J. F., & Deierlein, G. G. (2014). Design concepts for controlled rocking of self-centering steel braced frames. *Journal of Structural Engineering*. https://doi.org/10.1061/(asce)ST.1943-541X.0001047.

FEMA (Federal Emergency Management Agency). (2009). *Quantification of building seismic performance factors* (FEMA P695). Redwood City, CA.

FEMA (Federal Emergency Management Agency). (2012). *Seismic performance assessment of buildings* (FEMA P-58, Vols. 1 and 2). Redwood City, CA.

Hall, K. S., Eatherton, M. R., & Hajjar, J. F. (2010). *Nonlinear behavior of controlled rocking steel-framed building systems with replaceable energy dissipating fuses*. Newmark Structural Engineering Laboratory, University of Illinois at Urbana-Champaign.

Hendrickson, C., Horvath, A., Joshi, S., & Lave, L. (1998). Economic input-output models for environmental life-cycle assessment. *Environmental Science and Technology, 32*(7), 184A–191A.

Lee, J. Y., & Ellingwood, B. R. (2015). Ethical discounting for civil infrastructure decisions extending over multiple generations. *Structural Safety, 57,* 43–52.

Ma, X., Krawinkler, H., & Deierlein, G. G. (2011). *Seismic design and behavior of self-centering braced frame with controlled rocking and energy dissipating fuses*. John Blume Earthquake Engineering Center, TR 174, Stanford, CA.

Mckenna, F. T. (1999). *Object-oriented finite element programming: Frameworks for analysis, algorithms and parallel computing* (Ph.D. dissertation, University of California, Berkeley).

Montgomery, D. C. (2013). *Design and analysis of experiments*. Hoboken: Wiley.

Myers, R. H., Montgomery, D. C., & Anderson-Cook, C. M. (2009). *Response surface methodology: Process and product optimization using designed experiments* (3rd ed.). New York: Wiley.

Ochoa, L., Hendrickson, C., & Matthews, H. (2002). Economic input-output life-cycle assessment of US residential buildings. *Journal of Infrastructure Systems, 8*(4), 132–138.

Sharrard, A. L., Matthews, H. S., & Ries, R. J. (2008). Estimating construction project environmental effects using an input-output-based hybrid life-cycle assessment model. *Journal of Infrastructure Systems, 14*(4), 327–336.

Shokrabadi, M., & Burton, H. V. (2017). Ground motion intensity measures for rocking building systems. *Earthquake Spectra, 33*(4), 1533–1554.

Steele, T. C., & Wiebe, L. D. A. (2016). Dynamic and equivalent static procedures for capacity design of controlled rocking steel braced frames. *Earthquake Engineering and Structural Dynamics, 45*(14), 2349–2369.

Steele, T. C., & Wiebe, L. D. A. (2017). Collapse risk of controlled rocking steel braced frames with different post-tensioning and energy dissipation designs. *Earthquake Engineering and Structural Dynamics, 46*(13), 2063–2082.

Sun, H., Burton, H. V., Zhang, Y., & Wallace, J. W. (2017). Interbuilding interpolation of peak seismic response demands using spatially correlated demand parameters. *Earthquake Engineering Structural Dynamics, 47*(5), 1168–1188.

Uriz, P., Filippou, F. C., & Mahin, S. A. (2008). Model for cyclic inelastic buckling of steel braces. *Journal of Structural Engineering, American Society of Civil Engineers, 134*(4), 619–628.

Weber, C., Matthews, D., Venkatesh, A., Costello, C., & Matthews, H. (2009). *The 2002 US benchmark version of the economic input-output life cycle assessment (EIO-LCA) model*. Green Design Institute, Carnegie Mellon University.

Wiebe, L., & Christopoulos, C. (2015). Performance-based seismic design of controlled rocking steel braced frames. I: Methodological framework and design of base rocking joint. *Journal of Structural Engineering, 141*(9), 04014226.

Wiebe, L., Christopoulos, C., Tremblay, R., & Leclerc, M. (2013). Mechanisms to limit higher mode effects in a controlled rocking steel frame: Large amplitude shake table testing. *Earthquake Engineering and Structural Dynamics, 42*(7), 1069–1086.

Seismic Performance Assessment of Reinforced Concrete Columns in Regions of Low to Moderate Seismicity

Saim Raza, Hing-Ho Tsang, Scott J. Menegon and John L. Wilson

1 Introduction

Seismic resilience is the ability of a structure to withstand dynamic responses caused by ground shaking to an acceptable level, such that the structure retains its vertical load carrying capacity, and hence avoids collapse and loss of life. Further, it ensures the community's ability to function with minimal disruption immediately following an earthquake.

The imposed energy demand on a building due to earthquake ground accelerations is dissipated by displacement of its lateral load resisting system. The columns in a building can either form an integral part of its lateral load resisting system or they can be 'gravity' columns, which are not usually designed for lateral load and just need to be able to maintain the corresponding drift demand the lateral load resisting system undergoes without collapsing. Collapse of a column becomes imminent when the drift demand exceeds its collapse drift capacity, i.e. the drift at which column ceases to support the applied vertical loads. Collapse of one or more columns can eventually trigger the collapse of the entire building and as such, proper design with the consideration of the drift capacity of columns is vitally important to the seismic resilience of the building.

In low to moderate seismic regions, limited ductile detailing practice results in RC columns that can possess low collapse drift capacity and as such are considered to be less resilient for rare or very rare earthquake events. This chapter discusses the seismic resilience of such limited ductile RC columns and presents a 'two-tier' assessment procedure (Wilson and Lam 2006; Wilson et al. 2009) for evaluating the seismic resilience of RC columns in regions of low to moderate seismicity using

S. Raza · H.-H. Tsang (✉) · S. J. Menegon · J. L. Wilson
Swinburne University of Technology, Melbourne, VIC, Australia
e-mail: htsang@swin.edu.au

S. J. Menegon
Wallbridge Gilbert Aztec, Melbourne, VIC, Australia

269

a piecewise lateral force-displacement model presented herein. The chapter begins by providing a brief overview of the differences between limited ductile and ductile detailing of RC columns in the light of confinement requirements stipulated in various concrete design standards around the world. This is followed by a discussion about design parameters affecting lateral force-displacement behaviour of RC columns. The paper is concluded with different examples of how the aforementioned lateral force-displacement model can be used to demonstrate seismic compliance of limited ductile columns in regions of low to moderate seismicity.

2   Confinement Requirements for Different Ductility Levels

The displacement capacity of an RC column is dependent on a number of factors such as aspect ratio of the column, amount of transverse reinforcement, concrete compressive strength, transverse reinforcement yield strength and axial load ratio (Raza et al. 2018a). However, two parameters that largely influence the displacement capacity of an RC column are the amount of transverse reinforcement and axial load ratio. The transverse reinforcement in an RC column, besides preventing buckling of longitudinal bars and avoiding shear failure, also provides confinement to the concrete core, which in turn significantly affects deformability of the RC column. The lateral confinement of the concrete core, particularly in the plastic hinge region, enhances the deformation capacity of the RC column by increasing crushing strength and ultimate strain of the concrete core. Moreover, it also restrains the dilatation or expansion of the concrete core by imposing lateral confining pressure. Therefore, the amount of confinement reinforcement is one of the major parameter affecting ductility of an RC column and it serves as the basis for classifying an RC column as limited ductile, moderately ductile or fully ductile.

Due to the perceived lower seismic risk in regions of low to moderate seismicity, confinement reinforcement is widely spaced, thereby resulting in a limited ductile RC column. On the other hand, ductile detailing prevalent in high seismic regions results in a confinement reinforcement that is very closely spaced. Table 1 provides a comparison of the confinement requirements for different ductility levels of normal-strength RC (NSRC) and high-strength RC (HSRC) columns in accordance with the specifications of reinforced concrete design standards.

Limited ductile detailing requirements, specified by design standards of Australia AS 3600 (2018), Canada CSA A23.3 (2014) and Europe (Eurocode 8-DCL) are compared with moderately ductile and ductile detailing requirements of US ACI 318 (2014), New Zealand NZS 3101-1 (2006) and Europe (Eurocode 8-DCM and Eurocode 8-DCH). A comparison of transverse reinforcement spacing requirements for different ductility levels of NSRC columns indicates that transverse reinforcement in moderately ductile columns is approximately two times more closely spaced than corresponding limited ductile columns. Likewise, transverse reinforcement in fully ductile columns is 3–4 times more closely spaced than limited ductile columns.

Table 1 Confinement requirements of reinforced concrete design standards for different ductility levels

Standard	Spacing in critical region (s≤)		Minimum transverse reinforcement ratio by area/volume ($\rho_h/\rho_s \geq$) for confinement in critical region	
	NSRC	HSRC	NSRC	HSRC
AS 3600 (2018) (limited ductile)	D_c, $15d_b$	$0.6D_c$, 300 mm	–	$\frac{0.01 f'_c}{f_{yr} k_e}$
CSA A23.3 (2014) (limited ductile)	D_c, $16d_b$, $48d_t$, 300 mm	$0.75D_c$, $12d_b$, $36d_t$, 225 mm	–	
EN 1998-1 (2004) Eurocode 8 DCL (limited ductile)	$0.6D_c$, $12d_b$, 240 mm			
EN 1998-1 (2004) Eurocode 8 DCM (moderately ductile)	$0.5D_o$, $8d_b$, 175 mm		$\rho_s = \frac{30\mu_\varnothing \varepsilon_{sy,d}}{k_e}\ \frac{P}{f'_c A_g}\ \frac{D_c}{D_o} - 0.035$	
EN 1998-1 (2004) Eurocode 8 DCH (ductile)	$0.33D_o$, $6d_b$, 125 mm		$\rho_s = \frac{30\mu_\varnothing \varepsilon_{sy,d}}{k_e}\ \frac{P}{f'_c A_g}\ \frac{D_c}{D_o} - 0.035$	
ACI 314 (2014) (ductile)	$0.25D_c$, $6d_b$, $100 + \frac{350-h_x}{3}$		$\rho_h = 0.3\left(\frac{A_g}{A_{ch}} - 1\right)\frac{f'_c}{f_{yt}}$ (1a) $\rho_h = 0.09\frac{f'_c}{f_{yt}}$ (1b) $\rho_h = 0.2 k_f k_n \frac{P}{f_{yt} A_{ch}}$ (1c) Greater of (1a) and (1b) for $P \leq 0.3\,A_g f'_c$ and $f'_c \leq 70$ Greater of (1a), (1b) and (1c) for $P > 0.3\,A_g f'_c$ or $f'_c > 70$	
NZS 3101-1 (2006) (ductile)	$0.25D_c$, $6d_b$		$\rho_h = \frac{(1.3-\rho_t m)}{3.3}\ \frac{A_g}{A_c}\ \frac{f'_c}{f_{yt}}\ \frac{P}{\varnothing f'_c A_g} - 0.006$ where $m = \frac{f_{yt}}{0.85 f'_c}$	

where s = spacing, D_c = smaller column dimension, D_o = minimum dimension of concrete core, d_b = diameter of the longitudinal bar, h_x = maximum center-to-center spacing of longitudinal bars laterally supported by corners of crossties or hoop legs around the perimeter of the column, f'_c = compressive strength of concrete, f_{yt} = transverse reinforcement yield strength, A_g = gross area of concrete section, A_{ch} = cross-sectional area of a member measured to the outside edges of transverse reinforcement, P = design axial load, k_f = confinement effectiveness factor, k_n = concrete strength factor, ρ_t = ratio of longitudinal column reinforcement, $\varnothing$ = strength reduction factor, $\mu_\varnothing$ = curvature ductility factor, $\varepsilon_{sy,d}$ = yield strain of tensile steel

It is also noted that, while spacing requirements for HSRC columns are reduced relative to NSRC columns in limited ductile detailing, they remain the same in ductile detailing specifications. This may be in particular, because spacing requirements for ductile detailing are already so stringent that any further reduction may not be practically viable as it may lead to congestion and placement problems.

In addition to reducing the spacing requirements, design standards also specify an expression for determining a minimum transverse reinforcement ratio for moderately to fully ductile detailing of RC columns. A notable thing that can be observed in these expressions is the inclusion of the axial load ratio, in determining the minimum amount of transverse reinforcement for the confinement of concrete core in ductile columns. These expressions indicate that the amount of transverse reinforcement in ductile columns is proportional to the axial load ratio of the column. Thus, columns supporting higher axial load ratios are provided with more amount of transverse reinforcement in order to ensure ductile behaviour. ACI 314 (2014) goes to a further extent in this regard and provides separate expressions based on the limiting values of axial load ratio and concrete compressive strength, thereby resulting in even more stringent confinement requirements for high-strength RC columns with higher axial load ratios >0.3. This is in particular due to the extremely brittle nature of high-strength concrete at high axial load ratios. Recent experimental testing conducted by authors also demonstrated extremely brittle failure of high-strength RC columns especially at high axial loads (Raza et al. 2018b).

In order to illustrate the difference between different ductility levels, confinement reinforcement for a high-strength RC column is designed in accordance with the requirements of different concrete design standards for axial load ratio (n) of 0.2 and 0.4. Table 2 summarises the design details of the column and also presents the results of the comparison. It can be observed in Table 2 that the minimum amount of transverse reinforcement required for moderate ductility is around 3 times of the amount required for limited ductile behaviour at an axial load ratio of 0.2. Furthermore, as the axial load ratio is doubled, the amount of transverse reinforcement required to ensure moderately ductile behaviour of RC column also increases more than twice. In a similar manner, a fully ductile column has approximately 5 times higher transverse reinforcement at low axial load ratio (n = 0.2) and about 9 times higher transverse reinforcement at high axial load ratio (n = 0.4), than a corresponding limited ductile column. This underscores the significance of axial load ratio in reducing the ductility level of an RC column as such that significantly higher transverse reinforcement is required to compensate for the loss in ductility due to higher axial load ratio. It is also evident from Tables 1 and 2 that limited ductile RC columns have the same amount of transverse reinforcement irrespective of the axial load ratio, which implies that seismic resilience of limited ductile columns supporting a higher axial load can be at serious risk as their ductility which is already limited, is further reduced due to high axial load. A comparison of the transverse reinforcement ratios for different ductility levels in Table 2 also indicates that confinement requirements for ductile behaviour stipulated by New Zealand standard results in an amount of transverse reinforcement that is almost equivalent to the amount required to maintain moderately ductile behaviour in Eurocode 8.

Table 2 Minimum transverse reinforcement ratio for different ductility levels—a case study example

Column properties	Design standard	Minimum transverse reinforcement ratio by area ρ_h (%)	
		n = 0.2	n = 0.4
Cross-section = 250 × 250 mm Concrete compressive strength = $f_c' = 70$ MPa Longitudinal rebars = 6N16 Transverse reinforcement rebar = N10 Transverse reinforcement yield strength = $f_{yh} = 500$ MPa Concrete cover = 20 mm	AS 3600 (2018) (limited ductile)	0.42	0.42
	CSA A23.3 (2014) (limited ductile)	0.34	0.34
	Eurocode 8 DCL (limited ductile)	0.42	0.42
	Eurocode 8 DCM (moderately ductile)	1.1	2.4
	Eurocode 8 DCH (ductile)	1.89	3.78
	ACI 314 (2014) (ductile)	1.75	3.17
	NZS 3101-1 (2006) (ductile)	1.0	2.62

3 Seismic Assessment of Limited to Moderately Ductile RC Columns

It is imperative to understand the influence of various design parameters on the drift capacity of an RC column in order to ensure its seismically resilient design. This section first provides an overview of the design parameters affecting drift capacity of an RC column and then presents a piecewise lateral force-displacement model for NSRC and HSRC columns.

3.1 Design Parameters Affecting Drift Capacity

The post-peak drift behaviour of RC columns has been studied using a database of 190 RC columns (111 NSRC and 79 HSRC) from the literature (Raza et al. 2018a). The influence of six design parameters, namely, aspect ratio (*a/h*), longitudinal reinforcement ratio (ρ_v), transverse reinforcement ratio (ρ_h), transverse reinforcement yield strength (f_{yh}), concrete compressive strength (f_c') and axial load ratio (n) on the drift capacity of the RC column is summarised below:

- *Aspect Ratio*: Aspect ratio is the ratio of shear span length (a) of the column to the depth of its cross-section (h). Aspect ratio primarily controls the failure mode of RC column and is used for classifying RC column as flexure dominated (*a/h* > 2) or shear dominated (*a/h* ≤ 2). The drift behaviour of shear-critical RC columns is generally dependent on aspect ratio as such that increase in aspect ratio increases the drift capacity of the column, however, aspect ratio does not exhibit a significant influence on the drift behaviour of flexure-critical columns.

- *Longitudinal Reinforcement Ratio*: The amount of longitudinal reinforcement doesn't have any significant effect on the drift capacity of RC columns, hence, no direct correlation could be established between drift capacity of RC column and the amount of the longitudinal reinforcement.

- *Transverse Reinforcement Ratio*: A very strong correlation exists between the amount of transverse reinforcement and the drift capacity of RC columns. This is because confinement of the concrete core by transverse reinforcement increases the crushing strength and ultimate strain of the concrete. Therefore, with all other parameters being constant, a column with a higher amount of transverse reinforcement will have a high drift capacity.

- *Transverse Reinforcement Yield Strength*: Lateral load failure drift (drift at 20% degradation of lateral strength) of RC column shows a very slight increase with the increasing yield strength of transverse reinforcement. However, axial load failure drift (collapse drift) of an RC column delineates more substantial increase with the increase of transverse reinforcement yield strength. This is because transverse reinforcement usually yields close to axial load failure point and thus provides an enhanced confinement resulting in a high axial load failure drift capacity.

- *Concrete Compressive Strength*: Brittleness of concrete increases with the increase in compressive strength. Hence, high-strength RC columns will exhibit a lower drift capacity in contrast to normal-strength RC columns if all other design parameters are kept the same.

- *Axial Load Ratio*: Axial load ratio $\left(\frac{P}{f'_c A_g}\right)$ is the ratio of axial load to the product of concrete compressive strength with the gross cross-sectional area of an RC column. Amongst all the design parameters, the axial load ratio has the most significant effect on the drift capacity of the RC column. RC columns designed for higher axial loads have a significantly lower drift capacity as compared to the ones supporting lower axial load ratios.

3.2 Piecewise Lateral Force-Displacement Prediction Model

The piecewise lateral force-displacement prediction model presented here is defined by five points (Wilson et al. 2015), namely, cracking strength, yield strength, ultimate strength, lateral load failure (20% lateral strength degradation) and axial load failure (50% lateral strength degradation) as shown in Fig. 1.

- *Point A* (*Cracking Strength*): A reinforced concrete column starts developing cracks after reaching the cracking point on the lateral force-displacement model. The principles of basic mechanics can be used to determine the lateral strength and corresponding drift at the cracking point.

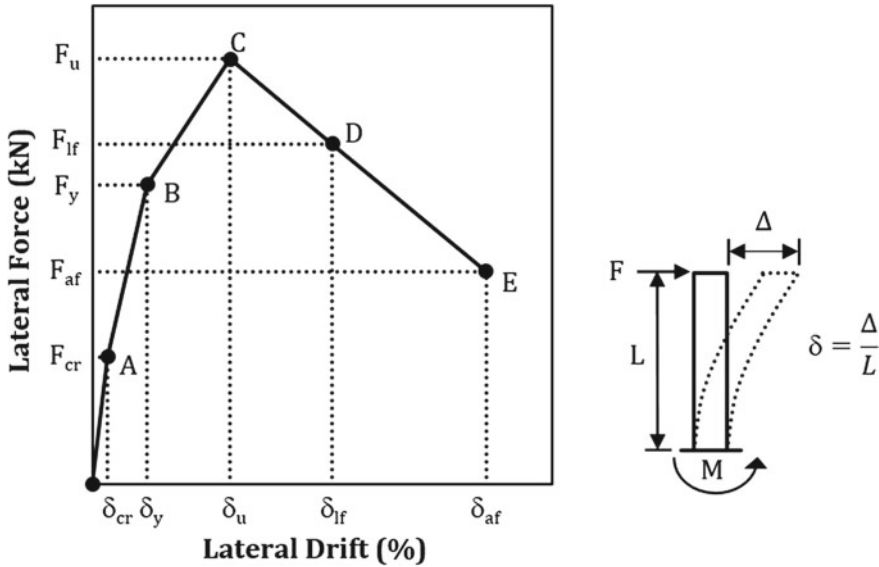$$F_{cr} = \frac{M_{cr}}{L} \tag{2a}$$

Fig. 1 Piecewise lateral force-displacement model

$$M_{cr} = \left(f_t + \frac{P}{A_g} \right) \frac{I_g}{y} \tag{2b}$$

$$\delta_{cr} = \frac{M_{cr} L}{3 E_c I_g} \tag{2c}$$

where F_{cr} = cracking strength, M_{cr} = cracking moment, δ_{cr} = drift at cracking, A_g = gross area of column, flexural tensile strength of concrete = $f_t = 0.6\sqrt{f_c'}$ (AS 3600 2018), P = axial load, L = shear span of the column, E_c = elastic modulus of concrete, y = distance to the neutral axis and I_g = gross moment of inertia of column cross-section.

- *Point B* (*Yield Strength*): A column maintains elastic behaviour up to the point of yield strength on lateral force-displacement model. Classical working stress method can be used to determine the yield strength of an RC column. The corresponding yield drift can be calculated using Eq. (3b) that employs classical curvature methods or Eq. (3c) that uses elastic drift approach and an effective second moment of area as described in FEMA 356 (FEMA 2000) or Paulay and Priestley (1992):

$$F_y = \frac{M_y}{L} \tag{3a}$$

$$\delta_y = \frac{1}{3} \varnothing_y L \tag{3b}$$

$$\delta_y = \frac{M_y L}{3 E_c I_{eff}} \tag{3c}$$

where F_y = yield strength, M_y = yield moment, δ_y = drift at yield, $\varnothing_y$ = yield curvature and I_{eff} = effective second moment of area given by:

(a) FEMA 356 (2000)

$$I_{eff} = 0.7\, I_g \text{ for axial load ratio } n \geq 0.5$$
$$= 0.5 \text{for axial load ratio } n \leq 0.3$$

For $0.3 \leq n < 0.5$, the value of I_{eff} should be interpolated.
(b) Paulay and Priestley (1992)

$$I_{eff} = \left(\frac{100}{f_y} + n\right) I_g \tag{3d}$$

- *Point C* (*Ultimate Strength*): The point at which column reaches its maximum strength is termed as ultimate strength point in the lateral force-displacement model. Ultimate flexure strength of an RC column can be determined using the ultimate strength design method. The ultimate drift may be calculated as the sum of elastic and plastic drift. The elastic drift is the yield drift, whereas the plastic drift is calculated using ultimate curvature and plastic hinge length.

$$F_u = \frac{M_u}{L} \tag{4a}$$

$$\delta_u = \delta_y + \delta_{pl} \tag{4b}$$

$$\delta_{pl} = (\varnothing_u - \varnothing_y) L_p \tag{4c}$$

where F_u = ultimate strength, M_u = ultimate moment, δ_u = ultimate drift, δ_{pl} = plastic drift, $\varnothing_u$ = ultimate curvature from ultimate strength analysis, L_p = plastic hinge length = $0.5D$, D = column width.
- *Point D* (*Lateral Load Failure*): Lateral load failure point corresponds to 20% degradation in peak lateral strength of RC column. Lateral load failure is taken as the conventional failure point in regions of high seismicity. The drift at lateral load failure of flexure-critical NSRC and HSRC columns can be predicted using the following empirical expressions (Raza et al. 2018a):

$$\left(\delta_{lf}\right)_{flexure} = 3(1 - 2n) + \left(\rho_h \sqrt{\frac{f_{yh}}{f_c'}}\right) \tag{5}$$

where $\left(\delta_{lf}\right)_{flexure}$ = drift at lateral load failure for flexure-critical columns (in %), n = axial load ratio, ρ_h = transverse reinforcement ratio by area (in %),

f_{yh} = transverse reinforcement yield strength (MPa), f_c' = concrete compressive strength (MPa).

The proposed empirical expressions are applicable within the following range of parameters: $12.1 \leq f_c' \leq 104.3$ MPa, $0.07\% \leq \rho_h \leq 1.0\%$, $f_{yh} \leq 500$ MPa and $0.027 \leq n \leq 0.5$.

- *Point E* (*Axial Load Failure*): It is the point at which column loses 10% or more of its axial load carrying capacity and collapses. The strength at axial load failure is conservatively taken as 50% of the peak lateral strength, whereas axial load failure drift of NSRC and HSRC columns can be predicted using the following empirical expressions developed by the authors (Raza et al. 2018a):

$$\delta_{af} = 5(1 - 2n) + \left(\rho_h \sqrt{\frac{f_{yh}}{f_c'}} \right) \tag{6}$$

where δ_{af} = drift at axial load failure (in %), n = axial load ratio, ρ_h = transverse reinforcement ratio by area (in %), f_{yh} = transverse reinforcement yield strength (MPa), f_c' = concrete compressive strength (MPa).

The proposed empirical expressions are applicable within the following wide range of parameters: $13.5 \leq f_c' \leq 104.3$ MPa, $0.07\% \leq \rho_h \leq 0.92\%$, $240 \leq f_{yh} \leq 1360$ MPa and $0.05 \leq n \leq 0.5$.

Equations (5) and (6) have been developed and calibrated using an extensive database of uni-directional tests of NSRC and HSRC columns from the literature. The drift predictions by the models are also in a very good agreement with the results of recent experimental testing conducted by the authors (Raza et al. 2018b). The expressions cover a wide range of concrete compressive strength and are equally applicable to both NSRC and HSRC columns. It is noted that these models give the drift predictions for RC columns which are subjected to uni-directional actions predominately. It is suggested to factor the expressions (5) and (6) with 1/2 for columns which are expected to undergo strong bi-directional actions. This factor of 1/2 is in accordance with the results of bi-directional experimental testing conducted by authors (Raza et al. 2018c) recently, in which the collapse drift capacity of a high-strength RC column is found to be approximately half of the corresponding drift capacity under uni-directional cyclic testing.

The expressions (5) and (6) relate the drift capacity of an RC column with the design parameters such as axial load ratio, transverse reinforcement ratio, transverse reinforcement yield strength and concrete compressive strength and hence provide a convenient tool to design engineers for assessing the displacement capacity of the RC column at an early design stage. It is quite evident from the above expressions that drift capacity of an RC column will be high at low axial load ratio, less concrete compressive strength and more amount of high-strength transverse reinforcement.

3.3   Case Study Example

The influence of design parameters on the drift capacity of an RC column, as discussed previously in Sect. 3.1, is further illustrated with the help of a case study example. The piecewise lateral force-displacement prediction model is used to predict lateral force-displacement (pushover) curves for a high-strength RC column with a cross-section of 500×500 mm. The design properties of the column are summarised in Table 3. The column is designed with limited ductile detailing in accordance with the specifications of AS 3600 (2018). The variable parameter for this case study is axial load ratio i.e. $n = 0.15, 0.3$ and 0.45. The column is a cantilever with a height of 2 m.

   The lateral force-displacement curves of the case study example are shown in Fig. 2 and the drift capacity values are presented in Table 4. The results show a drastic effect of axial load ratio on drift capacity of an RC column. As the axial load ratio

Table 3 Design properties of case study column

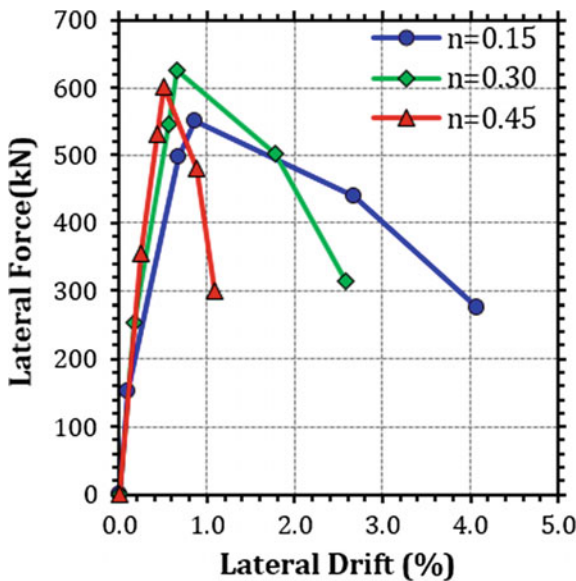| Width × depth × height (mm)	Aspect ratio	Concrete grade strength f_c' (MPa)	Longitudinal rebars (ρ_v, %)	Stirrups (mm) ρ_h (%) (by area)	Transverse reinforcement yield strength f_{yh} (MPa)
$500 \times 500 \times 2000$	4	65	12N28 (2.96)	4-legged N10@300 (0.21)	500

Fig. 2 Lateral force-displacement (pushover) curves for case study example

Table 4 Drift predictions for case study RC column

Point	Drift capacity		
	$n = 0.15$	$n = 0.3$	$n = 0.45$
Cracking point	0.1% (2.0 mm)	0.2% (4.0 mm)	0.3% (6.0 mm)
Yield point	0.7% (14.0 mm)	0.6% (12.0 mm)	0.4% (8.0 mm)
Ultimate point	0.9% (18.0 mm)	0.7% (14.0 mm)	0.50% (10.0 mm)
Lateral load failure	2.7% (54.0 mm)	1.8% (36.0 mm)	0.9% (18.0 mm)
Axial load failure (collapse)	4.1% (82.0 mm)	2.6% (52.0 mm)	1.1% (22.0 mm)

increases from 0.15 to 0.45, the collapse drift capacity (axial load failure) of the case study column reduces from around 4–1%. Moreover, the difference between lateral load failure and axial load failure drift is reduced at high axial load ratios, which implies that heavily loaded columns may collapse suddenly after 20% degradation in strength. This has an important implication from the design perspective, as the architectural requirements generally compel structural engineers to design RC columns with a smaller cross-section. This requirement is fulfilled by the use of high-strength concrete, furthermore, in order to create more floor space, columns are designed to support higher axial load so that less number of columns are needed. The results of this case study highlight the possible dangers associated with such a practice for limited ductile RC columns especially in the scenario of a very rare earthquake, as the seismic displacement demand under such a scenario would be higher than the displacement capacity of the column.

4 Applications of the Lateral Force-Displacement Prediction Model

This section discusses potential applications of the proposed lateral force-displacement model for limited ductile RC columns.

4.1 Two-Tier Seismic Assessment of Soft-Storey Buildings

The piecewise lateral force-displacement model can be used to evaluate the seismic performance of soft-storey buildings. A storey that has less stiffness and is weaker than the adjacent storeys is called a soft storey. Soft-storeys can often exist in the ground floor of residential buildings, due to architectural requirements for the provision of open space so that parking garages, swimming pools, etc. can be accommodated. Typical soft-storey buildings shown in Fig. 3 indicate that large open space is created by providing columns in the ground storey, thereby reducing the whole

Fig. 3 Typical soft-storey buildings (photos taken by Hing-Ho Tsang)

structure to a rigid block of heavy mass supported on columns at the bottom. Thus, columns in the soft-storey not only serve the purpose of providing vertical support to the building but also act as lateral load resisting mechanism under seismic actions.

During an earthquake, energy and displacement demands tend to concentrate in the bottom columns of the soft-storey structures. Moreover, all the levels of a soft-storey structure displace by a similar amount, hence it is possible to idealize it as a single degree of freedom system. Seismic performance of such soft-storey structures can be reasonably assessed by evaluating the performance of its bottom storey columns. The next sub-section presents a two-tier assessment procedure to evaluate the seismic performance of soft-storey buildings using the proposed lateral force-displacement model.

4.1.1   Tier 1 Assessment

Lateral force-displacement model proposed in Sect. 3.2 of the chapter can be used with 'two-tier' assessment approach proposed by Wilson and Lam (2006) to assess seismic performance of soft-storey structures in regions of low to moderate seismicity.

A 'first-tier' simple check is to compare peak displacement demand (PDD) for a rare or very rare earthquake event with the axial load failure drift (δ_{af}) capacity of the soft-storey columns. A soft-storey structure can be considered resilient against collapse if the drift corresponding to axial load failure of the soft-storey columns is greater than the peak displacement demand during an earthquake. Peak displacement demand for any region can be obtained directly from the respective seismic design code of that region. As an illustration, peak displacement demands for a rare earthquake event (return period of 500 years) determined in accordance with Australian earthquake standard, AS 1170.4 (2007) are summarised in Table 5 for different soil sites for a seismic hazard factor of 0.08 g, which is the minimum threshold value for Australia (Lam et al. 2016).

Table 5 Peak displacement demands for a seismic hazard factor (Z) of 0.08 g on different soil sites

Return period	Rock (mm)	Shallow soil (mm)	Soft soil (mm)	Very soft soil (mm)
500	26	36	58	90

Table 6 Drift predictions for case study soft storey building

Point	Drift capacity (mm)
Cracking point	6.0
Yield point	19.0
Ultimate point	22.0
Lateral load failure	58.0
Axial load failure (collapse)	83.0

The application of 'first-tier' assessment procedure is demonstrated herein using a case study building that has a soft-storey at the ground floor. The case study resists lateral earthquake loads using two columns with a 500×500 cross-section (matching the properties of the example presented in Sect. 3.3) and an inter-storey height of 3.2 m, which are bending in double curvature. The column is assumed to be provided in the ground floor of a soft-storey structure in a low seismic region (hazard factor, Z = 0.08 g) and is supporting an axial load ratio, n = 0.3. The drift capacity of the soft-storey column is summarised in Table 6. As explained earlier, a soft-storey structure is essentially a rigid block of heavy mass supported on columns at the bottom, so its performance can be assessed by simply assessing the performance of its ground storey columns as seismic displacement demands in such a structure accumulates at the bottom. This case study column has an axial load failure drift of 83 mm, which is greater than the peak displacement demand for the rock, shallow soil and soft soil sites summarised in Table 5. This means the building can achieve a collapse prevention performance objective for a 500-year return period event on these sites. However, since the maximum displacement is less than the peak displacement demand of 90 mm for a very soft soil site, the building is potentially vulnerable on sites of this nature.

4.1.2 Tier 2 Assessment

If a soft-storey column fails the 'first-tier' check, an advanced 'second-tier' assessment comprising of the capacity spectrum method can be employed. In the capacity spectrum method, the structural capacity curve and seismic demand curves are superimposed on each other to get the performance point of the structure. The performance point represents the maximum acceleration and displacement demands on the structure during the earthquake. If the capacity and demand curves intersect, then a structures performance can be deemed satisfactory. The lateral force-displacement model presented in this chapter gives the capacity curve of an RC column, whereas

Fig. 4 Second tier
assessment of the case study
soft-storey structure
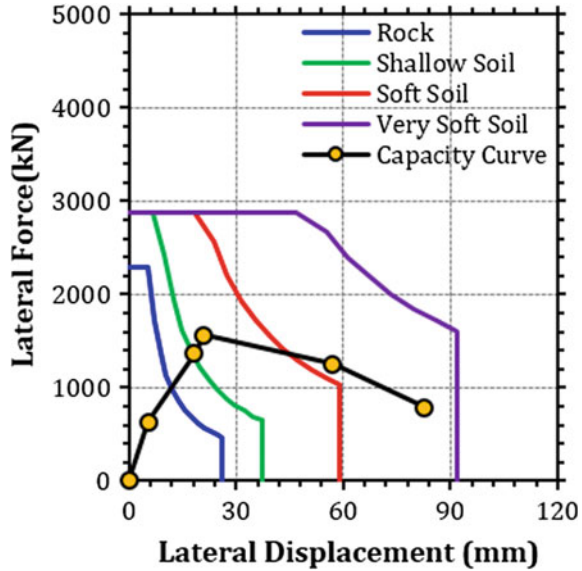
seismic demand curve is site-specific and region dependent and can be obtained from
the design response spectrum of the relevant seismic design codes.

The application of second-tier check is demonstrated on the soft-storey column
mentioned previously, by plotting the capacity curve of the column obtained in
Sect. 3.3 against seismic demand curves of rock, shallow soil, soft soil and very
soft soil sites for a rare earthquake event, as shown in Fig. 4. Because the soft storey
has two columns, the lateral forces calculated for one column are multiplied by two.
The seismic demand curve in Fig. 4 is in accordance with the requirements of AS
1170.4 (2007) and has been converted into the force-displacement format by multi-
plying acceleration with the mass of the structure, which is assumed to be 1000 tons
for the purpose of this illustration. The damping ratio for response spectrum is 5%.

The second-tier assessment shows that the soft-storey building is able to meet
the strength and displacement requirements on rock, shallow soil and soft soil sites,
hence it can be deemed practically safe on these sites. However, both the strength
and displacement demands are exceeding the structure's capacity on a very soft soil
site, thereby making it vulnerable to collapse in a rare earthquake event.

The outcomes from the second-tier assessment are in agreement with those from
the simplified first-tier check. When analysing a large building stock, the first-tier
approach can allow designers to quickly assess and eliminate the less valuable build-
ings. Thus allowing the more complex analysis to be performed on the truly vulner-
able buildings.

4.1.3   Seismic Performance Level of Soft-Storey Buildings

The piecewise lateral force-displacement model can also be used to assess the performance level of soft-storey buildings during earthquakes in low to moderate seismic regions. Table 7 relates each point on the piecewise lateral force-displacement model with a corresponding performance level specified in Vision 2000 document drafted by Structural Engineers Association in California (SEAOC).

Table 7 can serve as a convenient tool for the design engineers to assess the performance level of a soft storey building in a particular earthquake scenario, as the performance of a soft-storey building is largely dependent on the performance of its bottom storey columns, which can be evaluated by using the proposed lateral force-displacement model. For instance, seismic performance levels of the soft-storey building previously evaluated using the two assessment methods for a rare earthquake scenario are summarised in Table 8.

The performance levels stated in Table 8 are in accordance with the results of Tier 1 and Tier 2 assessment of the soft storey building analysed in the previous section. For example, under Tier 1 assessment, rock soil has a peak displacement demand of 26 mm, which is close to the 'ultimate' displacement capacity of the soft storey column i.e. 22 mm (refer Table 6), hence the performance level is considered to be 'life safety'. However, under Tier 2 assessment, capacity and demand curves of the soft-storey structure intersect close to the yield point for a rock site, hence the performance level is specified as operational/immediate occupancy. The performance levels for other soil sites are also determined accordingly.

It can be observed in Table 8 that the performance levels of the case study building determined in accordance with Tier 1 assessment are generally more conservative as compared to Tier 2 assessment. This implies that Tier 1 assessment is simple,

Table 7 Correlation between performance levels and the lateral force-displacement model

Performance level	Corresponding limiting point of the lateral force-displacement model
Fully operational	Cracking point
Operational/immediate occupancy	Yield point
Life safety	Ultimate point
Near collapse	Lateral load failure point
Collapse	Axial load failure point

Table 8 Predicted seismic performance levels of the case study soft-storey building

Soil site	Performance level-tier 1	Performance level-tier 2
Rock	Life safety	Operational/immediate occupancy
Shallow soil	Near collapse	Life safety
Soft soil	Near collapse	Near collapse
Very soft soil	Collapse	Collapse

yet conservative, and hence, can be employed as a quick safety check to assess the seismic performance of the soft storey structures at the design stage.

4.2 Non-linear Analysis of RC Structures

The proposed lateral force-displacement model can also be used for non-linear analysis of RC structures. Most of the earthquake design standards require non-linear analysis for the seismic design of structures with high importance levels. Realistic models of stress-strain, moment-curvature and force-displacement behaviour are required to capture the non-linear response of structures reliably. The proposed lateral force-displacement model can be employed by structural design engineers for non-linear analysis of RC structures due to its simplicity, a wide range of applicability (both NSRC and HSRC columns) and accuracy, especially in capturing post-peak displacement behaviour of RC columns prevalent in regions of low to moderate seismicity. This can be achieved by using the proposed model to define the force-displacement behaviour of RC columns in the commercial design software packages such as ETABS, SAP2000 etc. while conducting a non-linear analysis of the RC structures.

4.3 Gravity Columns in RC Wall Buildings

The majority of low-, mid- and high-rise buildings in Australia are RC wall buildings (Menegon et al. 2017), which utilise RC rectangular walls and building cores as the primary lateral load resisting system of the building. This is a common practice observed in many other regions of low to moderate seismicity. Buildings of this nature are generally designed for lateral loads using 3D linear elastic analysis programs (e.g. ETABS) with all the columns as 'pin-ended' elements. Using this approach, all the lateral load is distributed to the walls and buildings cores and the columns 'go the ride' when the floor diaphragrm displaces and moves as the walls and building cores resist the lateral earthquake loads.

The seismic compliance of the columns can quickly be assessed by determining the maximum displacement of the columns from the analysis model and then ensure that it is less than the axial load failure displacement of the respective column (i.e. Eq. 6). However, it should be noted that when force-based seismic analysis procedures are adopted, the maximum displacement of the columns is not the maximum displacement in the 3D linear elastic analysis model, but rather the displacement from the model multiplied by the force reduction factor (i.e. $R_f = \frac{\mu}{S_p} = 2.6$ for limited ductile RC structures, according to AS 1170.4 2007) adopted when calculating the seismic actions. The force reduction factor is used to account for inelastic behaviour in the structure.

5 Conclusions

This chapter has presented the factors affecting displacement behaviour of an RC column in detail and provided an overview of a piecewise lateral force-displacement model that can be used for reliable assessment of drift capacity of limited ductile RC columns in regions of low to moderate seismicity. The application of the proposed model in assessing the seismic performance of soft-storey structures is demonstrated with the help of a case study example. The proposed model is not only simple to use but also has a wide range of applicability in terms of design properties of RC columns. The proposed model can also serve as a tool for conducting a reliable non-linear analysis of RC buildings through its use in commercial design software packages for defining the force-displacement behaviour of an RC column.

References

ACI Committee 318. (2014). *Building code requirements for structural concrete (ACI 318M-14) and commentary (ACI 318RM-14)*. Farmington Hills, MI: American Concrete Institute.

AS 3600. (2018). *Concrete structures*. Standards Australia.

AS 1170.4. (2007). *Structural design actions, Part 4: earthquake actions in Australia*. Standards Australia.

CSA A23.3. (2014). *Design of concrete structures*. Ontario, Canada: Canadian Standards Association.

EN 1998-1. (2004). *Eurocode 8: Design of structures for earthquake resistance—Part 1: General rules, seismic actions and rules for buildings*. Brussels: European Committee for Standardisation.

FEMA 356. (2000). *Prestandard and commentary for the seismic rehabilitation of buildings*. Washington, DC.: Federal Emergency Management Agency.

Lam, N. T. K., Tsang, H. H., Lumantarna, E., & Wilson, J. L. (2016). Minimum loading requirements for areas of low seismicity. *Earthquakes and Structures, 11*(4), 539–561.

Menegon, S. J., Wilson, J. L., Lam, N. T. K., & Gad, E. F. (2017). RC Walls in Australia: Reconnaissance survey of industry and literature review of experimental testing. *Australian Journal of Structural Engineering, 18*(1), 24–40.

NZS 3101-1. (2006). *Concrete structures standard—The design of concrete structures*. Wellington: Standards New Zealand.

Paulay, T., & Priestley, M. (1992). *Seismic design of reinforced concrete and masonry structures*. New York, USA: Wiley.

Raza, S., Tsang, H.-H., &Wilson, J. L. (2018a). Unified models for post-peak failure drifts of normal- and high-strength RC columns. *Magazine of Concrete Research, 70*(21), 1081–1101.

Raza, S., Menegon, S. J., Tsang, H.-H., & Wilson, J. L. (2018b). Experimental testing program to investigate the collapse drift capacity of limited ductile high-strength RC column. In *Proceedings of the 25th Australasian Conference on the Mechanics of Structures and Materials, ACMSM25*, Brisbane, Australia.

Raza, S., Menegon, S. J., Tsang, H.-H., & Wilson, J. L. (2018c). Experimental testing of limited ductile high-strength reinforced concrete columns under bi-directional cyclic actions. In *Proceedings of Australian Earthquake Engineering Society, AEES*, Perth, Australia.

Structural Engineers Association of California (SEAOC). (1995). *Vision 2000: Performance based seismic engineering of buildings*. Sacramento, CA: Californian Office of Emergency Services.

Wilson, J., & Lam, N. (2006). Earthquake design of buildings in Australia using velocity and displacement principles. *Australian Journal of Structural Engineering, 6*(2), 103–118.

Wilson, J., Lam, N., & Rodsin, K. (2009). Collapse modelling of soft-storey buildings. *Australian Journal of Structural Engineering, 10*(1), 11–23.

Wilson, J. L., Wibowo, A., Lam, N. T. K., & Gad, E. F. (2015). Drift behaviour of lightly reinforced concrete columns and structural walls for seismic design applications. *Australian Journal of Structural Engineering, 16*(1), 62–74.

Part II
Resilience in Infrastructure

Achieving Resilience of Large-Scale Engineered Infrastructure Systems

Wolfgang Kröger

1 Introduction

By definition, "systems" consist of numerous, often-diverse elements, interacting in multiple ways, within operational contexts and boundaries that need to be defined. The focus of this chapter is on large-scale, human-engineered systems and infrastructures, in particular, that function synergistically to provide vitally important goods (such as energy including electricity, water, and data) and services (such as transportation, banking, and health care). Such networked infrastructure systems "constitute the very foundation of all prospering societies" (Rosas-Casals et al. 2007). They are termed critical, if their continuous functionality "is essential for … vital societal functions, health, safety, security, economic or societal well-being of people, and the disruption or destruction of which would have impact … as a result of the failure to maintain those functions" (Council Directive 2008/114/EC). Among others, physical engineered critical infrastructures include the electric power grid, fresh water and sewage system, rail, road and air transportation systems, and the Internet; all together they provide the very "backbone" of Western economies and societies (Vugrin et al. 2010). They have grown to meet increasing demand, have been subject to major technical and organizational changes and evolved, often in an uncontrolled manner.

Local failures or disruptions of their operations, respectively, often evolve into unexpected cascade patterns with trans-industry, large scale effects and result in substantial societal and economic damage. For example, the blackout in the north eastern part of the USA on 14 August 2003 affected 55 million people and caused a loss of US\$ of 250–300 billion (Wang and Rong 2009). Due to continued, even growing integration and mutual dependencies as well as a decreasing heterogeneity, they have gradually become more and more complex and developed into a dynamic "system-of-systems" and need to be understood as such. As humans interact with these systems

W. Kröger (✉)
ETH Zurich, Zürich, Switzerland
e-mail: kroeger@ethz.ch

individually and collectively they are an essential part of them; therefore we understand them as socio-technical systems and have to take a variety of influencing factors and behaviors into account, rather than examining purely technical system (Häring et al. 2016). Moreover, critical infrastructure systems (CIS) are making intensively use of digital systems for monitoring and control, turning them into cyber-physical systems and augmenting (inter-) dependencies within and among those systems. As they can form and be influenced by their operating environment and merge, as some argue (Heinimann and Hatfield 2017), into a socio-ecological-technical system.

Many countries like the U.S. and EU Member States as well as Switzerland have established programs to protect CIS. Traditionally, they applied the concept and policy of physical protection and hardening, i.e. prevention and mitigation of disruptive events, to increase safety and security of infrastructure assets. However, this in isolation turned out to be a brittle strategy, almost impossible to define an end state and extremely expensive. Thus "resilience became a priority, meaning that systems should have "soft landing/bolstering" capabilities and maintain functionality following disruptions" (Vugrin et al. 2010).

2 Definition of Some Key Terms

Being aware of the "non-technical" dimension of **risk** accounting for social and psychological aspects, we focus on the "technical" dimension, i.e. the normative, mathematically formulated risk concept. Accordingly, we define risk as the occurrence of some negative specified consequences, potentially arising from the faulty operation of considered systems or activities and associated uncertainties. For quantification of risk, we measure consequences of undesirable events in terms of "real" losses, i.e. damages to health of people and/or to the environment; we express uncertainty in terms of associated probabilities (frequencies) of undesired events of all different kinds, following the rules of probability calculus. For critical infrastructures the term risk may include the probability of loss of goods and services with its resulting consequences for the people and other systems affected (see also Zio 2016). We acknowledge that new perspectives of risk have been developed, which add the dimension of knowledge to the risk description (Aven and Krohn 2014), as for example the values of probability in two different situations could be the same, but may be based on quite different knowledge and eventually assumptions.

The risk concept aims to avoid/prevent, reduce and control/manage risks, meanwhile risk analysis is a formalized subject for the purpose of revealing potential failures modes and/or identifying hazard triggering events and induced event sequences (scenarios), as well as estimating specified consequences and associated likelihoods/frequencies, before they manifest, and thus provide risk-based information for potential corrections by decision makers.

Vulnerability was long considered as being closely similar to risk, if only with a broader interpretation. Some limit vulnerability to "the degree a system is able to withstand specific loads" (SRA glossary 2016) or "as the exposure and sensitivity

of a (socio-technical-ecological) system towards certain stressors minus resilience" (Berkes et al. 2004; Adger 2000). In contrast, others define vulnerability as the properties of a system that may weaken or limit its ability to survive and perform its mission in the presence of threats that originate both within and outside the system boundaries (Einarsson and Rausand 1998). We basically follow this interpretation and understand the concept of vulnerability as a global system property (Kröger and Zio 2011) that describes (a) to which degree a system is affected by a specific risk source (hazards) and is able to withstand specific loads/hostile environments, respectively, (b) the degree of exposure to hazards including the likelihood of being exposed and the susceptibility to suffering losses and damages, and (c) the degree of resilience by taking after-shock response behavior and recovery into account.

One of the first attempts for defining **resilience** dates back to Holling in 1973 for ecological systems, based on which various definitions have arisen in different disciplines and domains. In general they can be interpreted as "the ability of a system to anticipate and withstand external shocks, bounce back to its pre-shock state as quickly as possible and adapt to be better prepared to future catastrophic events" (Panteli et al. 2017). However, with regard to making the concept operable a more specific, detailed definition is recommendable. Focusing on technical systems, and physical engineered critical infrastructure systems in particular, we define resilience as the ability to resist/absorb the adverse effects of a disruptive force (either sudden or creeping, including all possible hazards and threats) with decreasing performance (but not collapsing), and the ability and speed to recover and return to an appropriate level of functionality (under budgetary constraints)—by adapting through self-organization and learning and eventually bouncing back or transforming into a different state (see also p. 52 in Kröger 2017). The traditional risk concept, with focus on the identification of obvious and, most importantly, hidden weaknesses in the system design, seeks to "harden" vulnerable components, and thus strives for prevention and mitigation, whereas the resilience concept aims at post-event/after shock, "soft landing" strategies (Linkov and Palma-Oliveira 2017) by strengthening inherent properties of the system, that are the absorptive, adaptive and restorative capacity, or the ability of the system to recover as a function of time and costs.

Resilience is mainly regarded as positive feature in infrastructures, maybe in conflict with other concepts. For instance redundancy may make systems more resilient while "sustainability" calls for most efficient use of resources.

Resilience engineering is still a relatively new and evolving concept. According to (Hollnagel et al. 2006) "a central idea is that failure is not necessarily a consequence of malfunction or poor design; rather it is the result of "the web of ongoing interactions and adaptations" that characterizes complex system behavior in the real world". Madni and Jackson (2009) point "to a growing recognition that tragic accidents and catastrophic failures (like the Columbia space shuttle accident of 2003) can be traced to organizational factors that create conditions that invite disaster". Therefore, resilience engineering is regarded as a proactive approach that looks for ways to enhance the ability of organizations to explicitly monitor risks, and make appropriate tradeoffs between required safety levels and production and economic pressure, see also Fig. 1 for a conceptual framework.
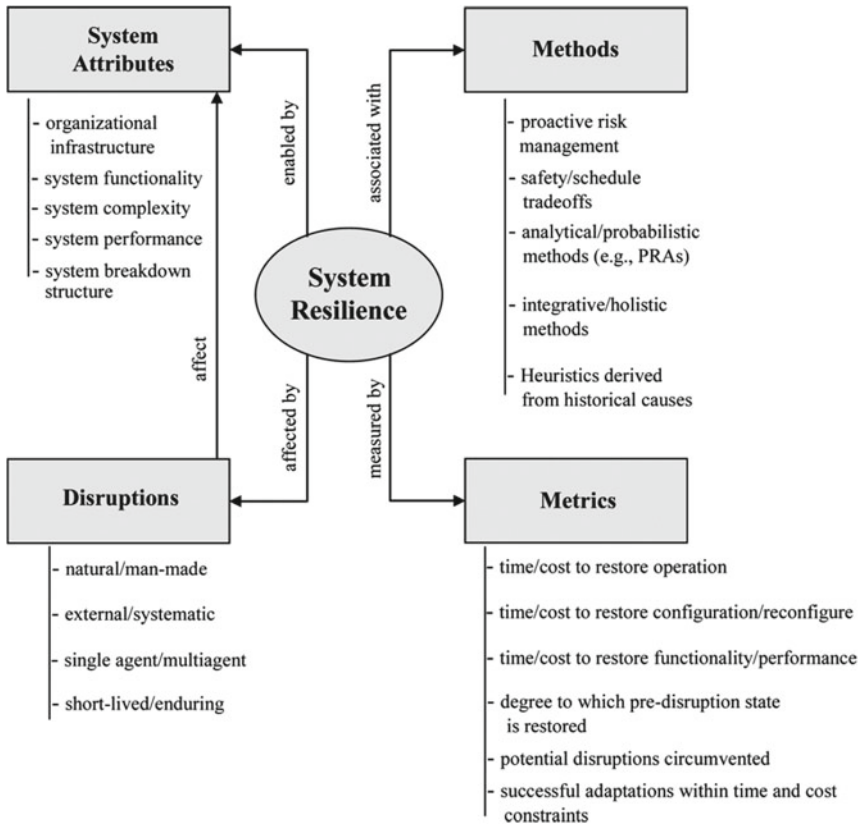
Fig. 1 Conceptual framework for resilience engineering that is based on four key pillars: disruption, system attributes, methods, and metrics (Madni and Jackson 2009)

3   Frameworks and Metrics for Critical Infrastructure Resilience Assessment

Numerous frameworks for resilience assessments have been developed for and named after domains, notably the social, organizational, economic, and technical domain. The latter includes physical systems that are engineered and operated by humans like the power grid. However, the development of sufficiently comprehensive/holistic frameworks is challenging and still in its infancy as they have to integrate the available knowledge on safety and cyber-security, human interactions/interventions and complex networks and address all possible failures and threats, and potential stressors or shocks, respectively (Zio 2018). Besides traditional reliability[1] indices, such

---

[1]In the engineering domain reliability deals with the ability of the system to perform required functions under stated conditions over a specified period of time.
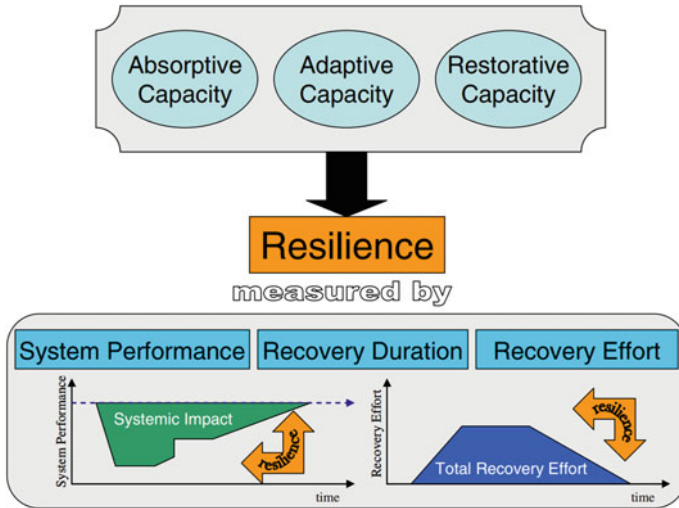
Fig. 2 Capacities and measures of system resilience (Vugrin et al. 2010)

as Loss of Load Frequency or Load Expectations (LOLF or LOLE), various metrics have been proposed aiming to specifically quantify resilience, for example measuring the difference between the real (post-disruptive event) and the target performance curve, either by the areas below or ratio of the curves. A few selected examples of proposed framework provide more detailed information.

Sandia National Laboratories developed a general framework for assessing the resilience of all types of critical infrastructure and economic systems involving the systemic impact (defined as the difference between the targeted performance level and an actual performance level following the disruptive event) and the total recovery effort (amount of resources expended during recovery processes). The framework is composed of (1) a definition of system resilience that focuses on the factors that need to be considered, (2) a quantitative methodology to evaluate these factors and measure system resilience, and (3) a qualitative analysis to examine resilience capabilities and enhancement features to explain or replace quantitative results, see Fig. 2 for illustration. For quantitative analysis they proposed to apply the optimal control method and to develop optimal feedback control laws by using mathematical formulations. Among others this concept was used for the assessment of the resilience of 18 regional critical infrastructures and key resources to an earthquake scenario.

Panteli et al. (2017) proposed to replace the "resilience triangle" (Tiernay and Bruneau 2007), modeled in the majority of studies, by the "resilience trapezoid" to depict all phases that a critical infrastructure, including the power system, might reside in during an event, as well as the transitions between these states, see Fig. 3 for comparison. The trapezoid clearly includes three phases: (I) disturbance progress, (II) post-disturbance, and (III) restorative state.
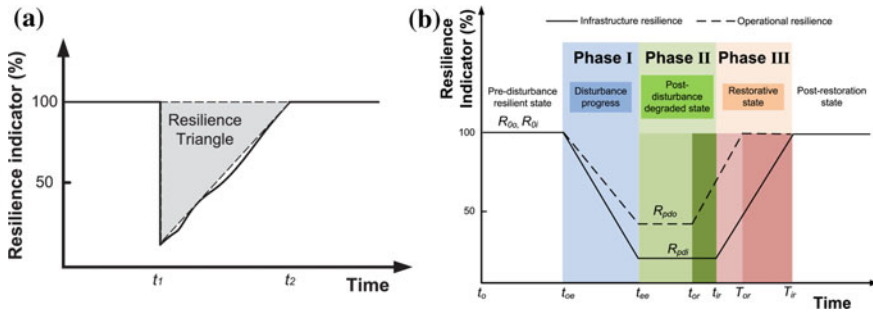
Fig. 3 **a** The resilience triangle, **b** the multi-phase resilience trapezoid (Panteli et al. 2017)

A resilience metric system, its mathematical formulation and expression of the linearized trapezoid areas have been defined.

The concept was applied to assess the resilience of a test version of the British transmission grid to a large-scale windstorm with three different wind profiles and scenarios. Simplifying assumptions were:

– Node demands fluctuate and vary in time in simulations
– Wind impact on transmission lines and towers modeled by use of fragility curves
– Mean-time-to-repair approach for recovery, no restoration during windstorm, the number of repair crews as an important parameter
– Cascading caused by thermal overloads and tripping by (all undamaged) protective devices, reconnection of islands the next hour, no transients considered.

Nan et al. (2016) developed a framework and integrated metric to quantify the resilience of interdependent infrastructure systems. They distinguished, as usual, four phases, namely the original steady state phase, the disruptive phase with absorptive system capabilities, the recovery phase coined by adaptive and restorative capabilities of the system, and finally the new steady state phase. Besides "robustness", which represents the absorptive capability by measuring the minimum performance level, two additional measures are introduced, i.e. the "rapidity" and "performance loss" during both the disruptive and recovery phase. The term rapidity is referred as the capability to achieve prioritized goals in a timely manner in order to contain losses and avoid further disruption; it can be quantified as average rapidity by the slope of performance level or by adopting the method of ramp detection to be more accurate. The performance loss can be interpreted/quantified as the area bounded by the graph of the performance measure before and after occurrence of effects caused by the disruptive event, which can also be denoted as the system impact area. The newly attained steady state level may equal or differ from the original steady state level. In order to consider this a quantitative measure, the "recovery ability", is developed. To allow a combination of all these measures and comparison among different systems and system configurations, a general resilience metric is proposed[2] that differs
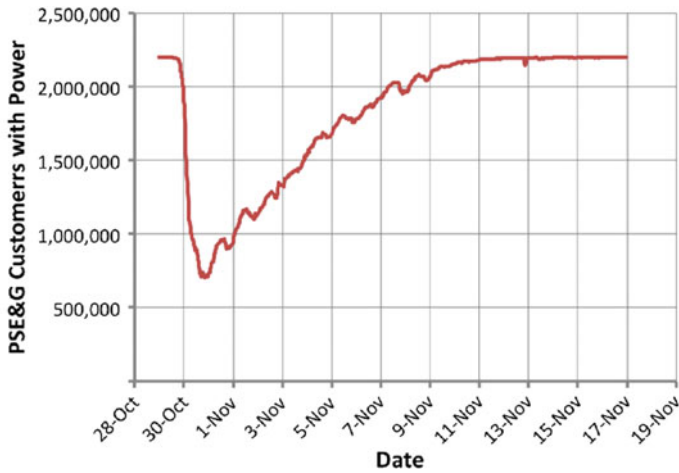

Fig. 4 PSE&G customers across NJ after outage caused by Hurricane Sandy (Henry and Ramirez-Marquez 2016)

from previous ones in that it is time-dependent and able to integrate all essential capabilities. The overall approach pretends to be neither model nor domain specific.

Ouyang and Fang (2017) provided a nice overview on metrics and frameworks used to assess and maximize resilience in various domains (including transportation and distribution networks) and proposed a framework to optimize the resilience of critical infrastructures against intentional malicious attacks. They defined resilience to an attack as the joint ability of a critical infrastructure system to resist the attack, to absorb the initial damage and quickly recover to normal operation; resilience is quantified as the ratio of the integral of the real performance curve over the time period [0, T] to the integral of the target performance curve during the period. The modeling framework includes three elements, a network model based on graph theory and two types of flow mechanisms, a three level defender-attacker-defender model, and the consideration of system restoration processes by allocating limited repair groups; some simplifying assumptions were made and stated.

Moreover a thorough resilience-based analysis was carried out (Henry and Ramirez-Marquez 2016) on the power outages to over eight million customers across 21 states, which lasted for days and even weeks, when Hurricane Sandy hit the US East Coast in October 2012. Figure 4 shows the power grid behavior, with PSE&G customers power across NJ over time as metrics, and nicely illustrates the resilience pattern outlined before, starting with the disruptive force, the resisting phase with a decline of performance to about 30% of the pre-event level, the re-stabilization and recovery phase to the initial performance level after more than about eight days. This real-world case also helped to identify measures to improve resilience, i.e. to achieve a faster cost-effective rebound while the number customers affected should be less.

4 Comparing the Resilience Concept with the Traditional Risk Management Concept

Although having the same philosophical background both concepts are different in focus. As mentioned before, the focus of the traditional risk concept is on the identification of obvious and, most importantly, of hidden weaknesses in the system design. It seeks to "harden" vulnerable components, and thus strives for prevention and mitigation. By contrast the resilience concept aims at post-event/after shock, "soft landing" strategies (Linkov and Palma-Oliveira 2017), particularly by strengthening four inherent properties of the system, that are absorptive and adaptive capacity and the ability of the system to recover quickly. Risk analysis can integrate recovery and adaption but it is not the main objective. Therefore, better resilience can be achieved by enhancing one or more of the four capacities and can result in increased inherent system's ability to withstand disturbances and cope with the unexpected (Thoma et al. 2016), in general. That's why some recent research (e.g., Linkov et al. 2014) claims that resilience is better suited than risk for threats that are unknown, unquantifiable, systemic, and unlikely/catastrophic and *in short* to deal with "deep uncertainty". Others oppose (e.g., Baum 2016) and find both concepts comparably suitable to deal with those threats and that the resilience paradigm suffers from insensitivity to probabilities and consequences and should be supplemented with these quantities. However, interest in infrastructure resilience can be concerned with existing technical, logistic, political, and operational mechanisms, relating to selected potential disasters. Kovalenko and Sornette (2013) denote the concept of risk and resilience as complementary measures of stress.

To recap, when the hazard/threat itself and the impact on the system, typically from an exogenous viewpoint, are mainly in focus, risk and risk analysis appear to be the most suitable approach. In contrast, when the concern is with the system itself, the consideration must became more comprehensive and shift to include endogenous aspects, which would definitely require to deal with concepts of vulnerability or resilience (Johnson and Gheorghe 2013). It is commonly agreed that the resilience quantification is less mature than its peer methodology in traditional risk assessment (see also Linkov and Palma-Oliveira 2017).

5 Characterizing Critical Infrastructure Systems and Development Trends

Large-scale critical infrastructure systems (CIS) like for the energy, fresh water or data supply or transportation of passengers or goods are composed of a plethora of mostly heterogeneous components/subsystems of great physical and functional diversity, which interact in multiple ways in a networked structure. CIS are multi-layered, embedded in a multi-facetted social-political-economical-natural environment, usually managed by different kinds of actors often with different objectives and logics.

Further, we have to consider that most complex infrastructure systems are "living" or operated in a rather dynamic than quasi-static environment, they are responsive to environmental dynamics including conditions, opportunities and constraints, etc., make internal adjustments and have the ability to learn from experience.

Modern CIS often have a hierarchical structure, consisting of a physical layer, which comprises devices that interact with the physical process, and the cyber layer, which comprises information and communications hard- and software needed to monitor and control the physical process. The resulting type of systems often shows complex-adaptive, in part autonomous and chaotic behavior thus it is often called non-deterministic system or "System of the Third Kind" (Ring and Tenorio 2012).

CIS are usually geographically distributed and spatially connected, open to the environment, in which they operate. Most CIS, the power grid in particular, were basically designed in the past, have evolved structurally and technologically over times and extended their capacity to meet increasing service demands. Presently, they are often operated in a competitive market (instead of a former monopolistic) structure—beyond original design parameters and safety margins.

CIS are subject to many types of hazards/threats of different nature: They range from random mechanical/electrical/material failures and potential common cause failures (including design flaws, aging, etc.) to natural hazards such as earthquakes, tsunamis/floods, landslides, avalanches, and extreme weather situations; they include soft- and hardware failures and human errors at different points in time and levels (political-strategic, design/manufacturing, operation, maintenance and repair, organizational deficits) as well as intentional malevolent physical and cyber attacks as potential new triggers of hazards. Depending on the site conditions and spatial extension civilian impacts such as chemical explosions or aircraft crashes may have to be considered. From a longer term perspective the spectrum of natural hazards and human-made threats may widen and include negative effects of climate change. As CIS are increasingly interconnected globally, anything and everything could be exposed to large-scale cyber attacks/cyber risks (World Security Report 1/2 2018).

Those systems, and their elements within, are vulnerable to different degrees and may pose risks themselves, i.e. the lines of a high-voltage power transmission system are inherently vulnerable—while related buses appear robust and defendable—and may cause harm in case of break or physical contact.

Most of the infrastructure systems have witnessed tighter integration and closer coupling and growing (inter-) dependencies, respectively: The loss of power supply, if sufficiently long, may cause the failure of the information and communication system which in return may impede black-start of the power system. This development trend will (probably to an increasing extent) continue. Besides globalization and extension to new domains (e.g., from pure use of electricity to mobility) the pervasive use of cyber-based, digital host technologies for supervisory, control and data acquisition (SCADA) serve as major driver.

The power supply system, unconfined one of the most important critical infrastructures, consists of multiple generators of different size and at different power levels, extra high/high voltage long distance transmission grids and low voltage
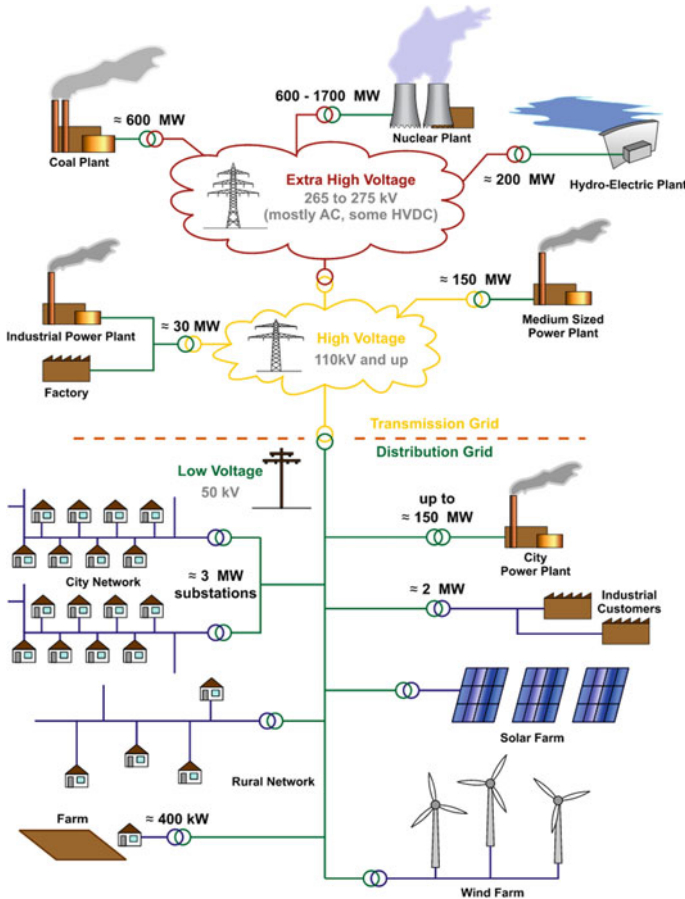
Fig. 5 General layout of electricity networks (voltage and power levels as well as depictions of electrical lines are typical for Germany and other European states)

regional/local distribution grids, each with pertinent lines and substations (transformers), and of numerous loads (points to consumers), see Fig. 5 for general layout.

> The European Transmission System (ENTSO-E power grid), for example, is the backbone of electricity supply to roughly 534 million citizens in Europe. It consists of five large synchronous areas, is operated by 41 Transmission System Operators from 34 countries according to commonly agreed, legally binding rules (ENTSO-E Operation Handbook), out of which the "N-1 criterion" is key. It says, that any probable single event leading to a loss of a power system element should not endanger the security of the whole interconnected system, e.g., redistribution of the physical flow should not cause a tripping cascade. Thus, serious blackout events are often rare or unprecedented as the likely and anticipated failures are already routinely accounted for in systems basic design and operation.

If properly implemented, the mainly deterministic framework has been successful in ensuring historical high performance and reliability, respectively, of

power transmission systems in most Western countries. However, it seems insufficient to cope with combined failures, tripping scenarios, and influencing operational/organizational factors, which go clearly beyond the current N-1 security requirements, but have played a significant role in major outages/blackouts (Kröger 2017, update 2018). History comprises a list of about 115 major[3] blackouts for the time period from mid 1999 to the end of 2017; 26 major and three other special events have been selected for further characterization, particularly of the main causes and mechanisms. Unsurprisingly, this evaluation emphasizes the dominating role of natural hazards including extreme weather triggering disturbances (at least 13 out of 29 events) but circumstantiates also the important role of organizational/contextual factors including demand and generation inadequacies (roughly 7 out of 29), since roughly five major outages were triggered by purely technical failures including a software bug and additional two outages followed fires. It is important to note that we experienced—besides one military (?) attack in Pakistan—three cyber attacks on power grids—two in 2015 and 2016 in the Ukraine, after careful observation and planning.

A statistical analysis of a series of blackouts of the North American power transmission system from 1984 to 1998 (www.nerc.com) has proven that the probability distribution of blackout sizes does not decrease exponentially, but rather follows a power law, with an exponent between -1 and -2. Thus, evaluated data suggest that large blackouts are much more likely than expected, which is a clear indication that the power system is a complex system, designed and operated near a critical point, and that overall loading and stress—relatively close to operating limits—is a key factor affecting the risk of cascading failure (Dobson et al. 2007). Most major blackouts had rippling effects on customers' activities, industries, and other infrastructure sectors, because of their dependence on electricity.[4]

Generally, the electricity supply system has adapted to steadily increasing demand and has undergone various changes, technologically, structurally, and organizationally. In Europe, it was mostly a loosely coupled network of local systems with regionally and vertically structured monopolies, responsible for the whole supply chain from generation to consumption. In recent years the system was unbundled and replaced by an intricate evolving market structure, often with stressing operation modes. The grid was originally not designed for such conditions, i.e. may render preventively designed safety margins insufficient. This comes along with increasingly

---

[3]Events are termed "major" as the outages (a) were not planned (at the date of occurrence) by the service provider, (b) affected at least 1,000 people and lasted at least one hour, and (c) must be at least 1,000,000 person-hours of disruption (visit [*en.wikipedia.org/wiki/List_of_majorpower_outages*]).

[4]For example, the "Northeast blackout" on August 14, 2003 hit parts of the Northeastern (including NYC) and Midwestern USA and the Canadian province of Ontario when a manageable local blackout cascaded into a collapse of the entire power grid. 508 generating units at 265 power plants shut down, the total load dropped from 28,700 to 5,716. Telephone services generally remained operational, but the increased demand left many circuits overloaded. Cellular phone services were disrupted and a large number of factories closed. Water systems in several cities lost water pressure because pumps lacked power. Electrified railway services were interrupted, passenger screening at some airports ceased, leading to a closure of airports and flight cancellations, etc.

short-term trading and cross-border electricity transport/exchange. Other major challenges comprise:

1. The necessary integration of a growing share of intermittent energy sources, harvesting wind and solar at most suitable sites, into the existing largely heterogeneous network at different voltage levels. Those "renewables" are highly disperse but at large-scale dense in remote regions ("farms"), requiring massive transfers; they are non-controllable and show significant temporal and seasonal swings. The necessity of base load and back-up power generation remains, depending on the development of the entire system and storage capacities, in particular.

2. Besides re-conceptualization of the current grid, increasing "smartness" of the grid is sought with more homogeneous, often clustered distribution of more heterogonous production sources, leveraging stochastic output patterns, including smart meters and new devices for increased controllability for consumers, as well as on-line monitoring, observation and control systems.

3. Such smart energy networks come along with the idea of decentralized, maybe autonomous cellular structures, involving concurrent local power producer/consumers and operation control largely away from central units, therefore converting the grid from operated as designed for into a flexible, adaptive system.

4. Besides new structural characteristics, automation devices (intelligent sensors and switches) may speed up the service restoration within the affected section in case of power interruptions through strengthened "self-healing capabilities".

5. Intensified security issues, i.e. potential of detrimental cyber attacks including manipulation, due to digital cyber-based information and communication host technology. These systems often link different domains such as control, operation and trading and use commercial hard- and software including the public Internet, with entry points for attacks.

In short: We are witnessing socio-technical changes and transitions, which may further increase systems' complexity, make them more efficient and controllable but add entry points for cyber attacks.

6 Challenges to Understand and Analyze Complex System Behavior

6.1 Coping with Complexity

As outlined before, in recent years most of the engineered critical infrastructure systems (CIS) have witnessed growing integration and connectedness as well as dramatic technological and organizational changes with globalization and digitalization as key drivers. Thus, most CIS evolved themselves into a highly complex networked system and associated behavior. Moreover, they pooled their resources and capabilities together to obtain an even more complex "system-of-systems", with functions

and behaviors as well as operational environments completely different from the past. Thus, it is key to understand and cope with "complexity" and complex behaviors of critical infrastructure systems.

There is no absolute definition of the term complexity. However, a characterization of what is complex, appears possible, generally by "something with many parts where those parts interact with each other in multiple ways culminating in a higher order of emergence,[5] greater than the sum of its parts" (www.wikipedia.org) or "if it is not possible to establish an accurate prediction model of system based on knowing the specific functions and states of its individual components" (SRA glossary 2016). Therefore, it is commonly agreed, that classical methods of technical risk analysis, mainly based on reductionist methods and linear causal chains without feedback loops, are likely to fail at capturing the collective behavior of complex systems and how they interact and form relationships with their environments. Elements/components/parts can be manifold, physical-engineered, human, logical or contextual, etc. The boundary of the system(s), either at micro (components—subsystems), macro (entire system) or global (network of entire systems) level, needs to be defined.

Regarding physical-engineered systems, like critical infrastructures, we follow the distinction of two groups of complexity, namely structural/topological and dynamic, the former being intrinsic in the system design and the latter emerging from system operation (and response to imbalances) (Zio 2016). Structural complexity is coined by a number of characteristics:

1. Heterogeneity, which refers to the differences in the large number of elements, the scale of their interconnections and roles within the system structure, often going along with high-connected core elements and low-connected periphery nodes.
2. System architecture, which defines the topological and/or logic structure, linking the system elements through their interrelations (interdependencies.
3. Divisibility of the system structure into subsystems and elementary parts.

Dynamic complexity discloses through the emergence of (even unexpected) system behavior in response to changes in the environmental and operational conditions of its components. Depending on their characteristics, most complex engineered infrastructure systems exhibit highly dynamic, non-linear behavior with positive (not damping) feedback loops. Small changes of initial conditions/local disturbances often accelerate and trigger cascades with initial load (stress) condition as important parameter. Analysis across (non-technical) networks and experience have revealed that some systems with a huge number of interacting components are likely to have critical thresholds ("tipping points") where their behavior, if reached, changes abruptly ("regime shifts") and that homogeneity/heterogeneity and connectivity/modularity seem to be the dominating features (Scheffer et al. 2012).

---

[5]A phenomenon whereby larger entities arise through interactions among smaller or simpler entities such that the larger entities exhibit properties the smaller/simpler entities do not exhibit (www.wikipedia.org).

Without doubt, the electric power supply system, and the high-voltage transmission grid in particular, exhibit key attributes of complex systems: It is made up of a large, non-trivial number of different parts and relations between them,[6] it is embedded in and interacting with a non-trivial, continuously changing operational and organizational environment, technical and non-technical (human) components have memory (aging, poor maintenance; experience, training, etc.) and include feedback loops. Further, the system is sensitive to initial stress/load conditions because interactions between component failures are stronger when components are highly loaded as shown by experience and theoretical analysis.[7] With regard to outlined characteristics of complexity, these systems have shown emergent behaviors in collective ways, difficult to predict from the superposition of single elements and difficult to manage, and being subject to large uncertainties (Zio 2016). Indeed, system breakdowns often emerged from relatively small congestions followed by a cascade of failures. For example, when component operating limits are exceeded, protection acts and the component, e.g., a line, "fails" in the sense of not being available to transmit power, which causes a transient and power flow to be redistributed to other components throughout the network, rather than being limited to adjacent network components. Depending on initial load conditions such failures can lead to large-scale consequences and even propagate to one or more other systems, due to dependencies.

Extending deliberations on the electric power grids one must consider a further evolution towards the most complex engineered systems. We assume that the variety of power sources and generators, of controls (with a more active role of users, new devices for increased controllability, etc.) and loads as well as the extent of the interconnectedness will further increase complexity (Zio 2016), unless corrective measures are taken. Moreover, the continuously growing role of computer-based information and communication technology (ICT) and use of commercial hard- and software, all about the same in most critical infrastructures, may turn the electric power supply system, and the electric power grid in particular, into a typical construct of a complex system-of-systems.

6.2 Challenges to Methods of Risk Analysis

Methods of risk analysis developed in parallel to the development of systems, basically aiming at providing answers to the triplet of questions " what can go wrong" or "what can happen", "how likely will an event happen" and "if it does happen, what are the consequences" (Kaplan and Garrick 1981). In other words, aiming at identification and characterization of undesired events/event scenarios, estimation

---

[6]As an example, the Swiss high-voltage power transmission grid has been modeled by 587 technical and non-technical interacting agents.

[7]A time-stepped model based on a two layer agent-based approach resulted in a cumulative frequency versus size of lost power; the curve changed its shape from exponential to power law for load levels exceeding 100% (Schläpfer et al. 2012).

of expected adverse consequences and associated uncertainty, in general. Methods of probabilistic risk assessment (PRA) emerged in the 1970s, with the "Rasmussen Study" to estimate the risks caused by the operation of—rather complicated than complex—nuclear power plants as most prominent example. The probabilistic approach allowed for a relaxation of the deterministic assumptions by introducing uncertainties and quantifying them through "expected values", which are the products of probabilities of undesired events/event scenarios, and various metrics of consequences.

As mentioned before current infrastructure systems like the power grid are rather complex than just complicated and push us to another level of insufficient knowledge, characterized by unexpected changes and behaviours. Large blackouts are typically caused by long, intricate sequences of all possible rare events and interactions for which combinatorial analysis gets overwhelmed (Dobson et al. 2007). Given the complexity of the systems and/or processes simulation has been advocated to handle a large, combinatorial set of possible events and scenarios, of which only a few lead to "critical" situations. Currently, simulation can also be exploited to estimate the accident scenarios probabilities; generally, for this Monte-Carlo methods of stochastic discrete event simulation have been accepted as good standard (Zio 2018).

Methods, helping us to develop a detailed and comprehensive understanding of their susceptibility to disturbances and complex behaviors after they have occurred, are exposed to major challenges:

1. Multifaceted interactions with intervening variables of a plethora of heterogeneous components, organized in a hierarchy of subsystems, often results in behaviors related with non-linear feedback mechanisms, self-organizing processes and adaptive learning.
2. The collective behavior of the system is more than the sum of individual behaviors of its elements, thus a holistic theoretical approach is needed to analyze the system as a whole.
3. Small changes of initial conditions can accelerate, lead to cascades within the system and across boundaries, and have big global effect.
4. Depending on their topological structure and initial stress level, critical thresholds may be reached, leading to bifurcations, and potentially abrupt system collapse.
5. Most such systems are multi-layered, technologically and structurally evolving and strongly coupled, they are large-scale open and subject to a widening set of natural hazards and man-made threats; damages can be caused directly and indirectly.
6. A set of socio-economic factors, either operational or organizational, intertwined with purely technological factors, as well as the interplay of the system with its operational environment need to be taken into account.

The analysis of these systems cannot be carried out only by use classical probabilistic methods such as fault trees, based on decomposition, and event trees, based on quasi-static causal chains (Zio 2016) as well as human factor analysis, based on human reliability assumptions (Leveson 2014). Moreover, they cannot ensure sufficient completeness under the existing uncertainties, do not account for unexpected failure modes and relationships that govern the behaviour of such systems "of the

third kind" (see also Heinimann and Hatfield 2017) and face some fundamental limitations (Kröger and Sornette 2013). Moreover, standard probabilistic techniques like event trees, which assume independence between events, imply exponential probability distributions and are not applicable in principle to systems that exhibit power tails as the electric power grids (Dobson et al. 2007).

6.3 Approaches and Available Methods

Currently, a variety of advanced methods, models and tools has been developed and applied to **single** engineered **infrastructure systems**. Those methods, either qualitative or quantitative, can be divided into two categories: empirical and predictive (Johansson and Hassel 2010; Ouyang 2014).

The **empirical/statistical** approach aims to identify failure mechanisms and patterns of cascading failure, thereby assisting learning from the analysis of previous near misses and serious events. As most critical infrastructures have been operated over a long period of time and are continuously operating under self-surveillance, sufficient knowledge and huge datasets are available, in principle. However, reliable statistical data are rare as systems experienced major technological, operational, and organizational changes and available rich data may not sufficiently reflect the situation of interest at present and in the future.

The **predictive quantitative** approach mainly refers to modeling and simulating the major characteristics of critical infrastructure systems through reasonable simplification. Several, mainly predictive research methods are regarded representative and expatiated as follows (see also Kröger and Zio 2011 for further details and a comparative summary). These "advanced" methods are, by nature, either (a) structural/topological/state-related like Complex Network Theory, Petri-Net and Bayesian-Net, (b) logical like hierarchical trees, (c) phenomenological/functional like Agent-based Modeling, or (d) flow-focused like Input-output Inoperability Modeling and System Dynamics; the two most common methods are briefly explained below:

- **Complex Network Theory** (CNT): A widely used method, formed by classical graph theory, which aims to understand the structure of components' interactions, characterize the topology of the system and study its generic properties such as vulnerability by removal of elements or changing physical components from operable to inoperable, respectively—either randomly or targeted. The underlying assumption is that the structure of a system affects its function, e.g., the topology of the power grid affects the stability of power transmission.

  Before building the adjacency matrix, constituents of a real system are mapped into N nodes and K unweighted edges (arcs, links), see Fig. 6 for illustration. The structural properties and a drop of performance, in particular, are represented by a group of topology-based metrics such as (i) node degree k, i.e. number of links, and node degree probability distribution $P(k)$, giving the probability that a node
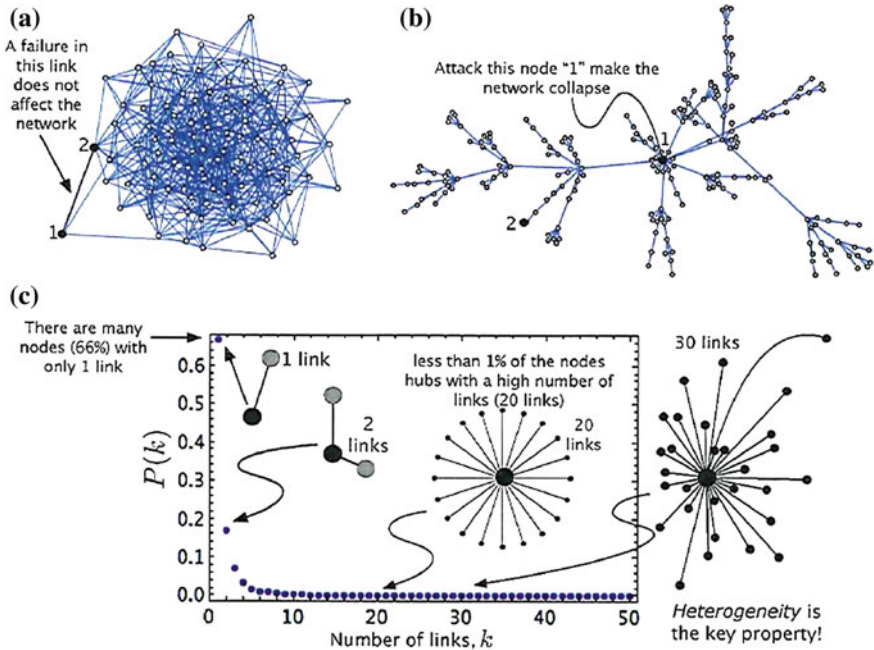
Fig. 6 Illustration and results of Complex Network Theory: **a** robust network; **b** example of a scale-free, i.e. neither completely regular or random, network like many real world networks, vulnerable to attacks on nodes with many links; **c** node degree probability density function P(k) of a network similar to that represented in (**b**) (Cuadra et al. 2015)

is connected to *k* other nodes, (ii) characteristic path length, i.e. number of edges in the shortest path between two nodes, and clustering coefficient as well as (iii) degree, topological closeness and betweenness centrality. For example, the degree (connectivity) distribution allows for dividing complex networks into two major classes: If P(k) peaks at an average <k> and decays exponentially for large *k* we speak of exponential, fairly homogenous networks; in contrast, if P(k) decays by following a power law, we speak of "scale-free", typically heterogeneous, real-world networks. This characterization provides an indication of the robustness of a complex system against random failures or targeted attacks.

The analysis of the topological properties of the network representing critical infrastructure systems can also reveal useful information about the structure property including growth mechanisms, points and causes of vulnerability. However, this method alone lacks the ability to capture uncertain characteristics of critical infrastructure systems when the behavior of single components is rather continuous than discrete and dynamical physical processes occur, acting on the network. However, various approaches have been introduced at different level of abstraction of the physical system to overcome this constraint, e.g., by adding simple models to include the dynamics of flow of physical quantities (such as electricity) like
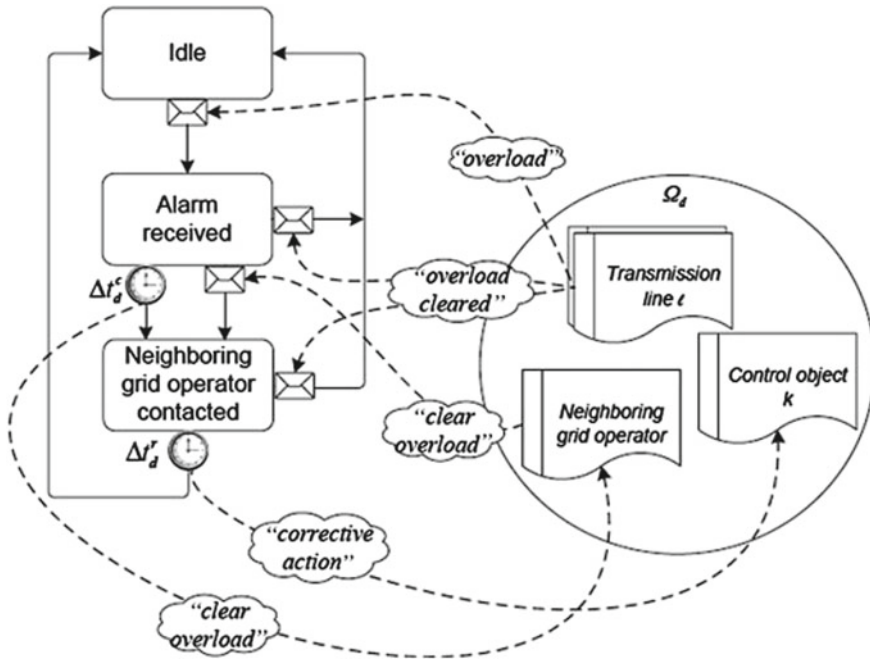
Fig. 7 Agent-based modeling approach—finite state machine to include the response of the transmission system operator to line overload (Schläpfer et al. 2012)

DC load flow calculations, or multi-state models to describe different degrees of degradation of the individual components. Furthermore, unweighted graphs have been replaced by weighted graphs to characterize the strength of a connection and network. Often CNT methods are applied to help guiding and focusing more detailed analyses in critical areas.

- **Agent-Based Modeling** (ABM): A relatively new approach aiming at simulating complex, adaptive systems composed of different types of interacting, autonomous agents with the capability to adapt. Agents are heterogeneous and thus can model both diverse technical and non-technical (social and human) components. Agents are built with information of a geographical location, specified functions, capabilities including knowledge, learning and memory and rules of behaviors, see Fig. 7 for the "finite state machine" to model a human agent within the power sector, i.e. the transmission grid operator. As a modification and further development of Object-Oriented Modeling (OOM), the ABM multi-layer approach is capable of including physical laws (e.g., to calculate load flow redistribution after a line failure of the power grid) and emulate the behavior of the entire system emerging from the behaviors of individual agents and their interactions. Non-technical agents may include decision-making algorithms or behavioral (error) probabilities.

The ABM is mostly used to study phenomena such as self-organization, adaptation or responsive behavior. It allows the explicit integration of highly non-linear, time dependent effects and supports the interdependency assessment process, e.g., by introducing interconnected agents, and allows achieving a closer representation of system behaviors. However, this approach demands large number of parameters defined for each agent, which require thorough knowledge of studied systems and sufficient data. As most real world systems like critical infrastructures entail a large number of agents the computational burden is high and needs to be reduced, e.g., by focusing on specific aspects to simplify the model.

In general, those predictive methods are different by capabilities and scope as well as by area of application and objectives. They are mostly targeted at vulnerability and risk assessment, as said before, for existing infrastructure systems with fixed topological structure. They are limited to the operational level, although sometimes extending to the industrial-planning level, e.g., to study the effects of structural-topological changes like decentralization. The above mentioned methods can vary with analytical granularity, data availability, model sophistication, etc. and can be expanded or complemented with "less advanced" methods such logic trees as well as "simple" methods like HAZOP or FMEA. Thus, a framework is often needed to integrate a number of methods capable of viewing the "complexity problem" from different perspectives under existing uncertainties and making optimal use of them. Some argue that evaluating vulnerabilities in power networks by using purely topological metrics (like CNT) and not taking physical realities of electrical power flow into account can be misleading (Hines et al. 2010; Eusgeld et al. 2009).

The **human factor** and its contribution to system's performance needs to be included in the analysis of critical infrastructure systems as human behavior may initiate failures and cascades, in particular, and may aggravate or diminish the impact of such events even, if not being the very cause. Early, so-called first generation methods aim at predicting and quantifying the likelihood of human error. They based on reductionisms, i.e. breaking down the given task into subtasks, prior to considering the potential impact of modifying factors under which it is performed such as time pressure, equipment design, and stress. As they focused on the skill and rule-based level of human actions they were often criticized for failing to consider the impact of the contextual-organizational factors and errors of commission (the latter means doing something different from what they should). So-called second generation techniques attempt to overcome these shortcomings by representing the effects of the environment on the execution of the task by introducing "Performance Shaping or Influencing Factors" (PSFs or PIFs) before assigning human error probabilities. They are still under (slowed down) development and deserve further validation (see also Kröger and Zio 2011 for details). Thus, methods to include the human factor and performance in risk and vulnerability assessment still deem insufficient and are aligned with large uncertainties.

In practice, there is still no "all by one" approach. Instead, it has proven necessary to integrate different types of methods and modeling approaches into one simulation

tool as a hybrid approach, to fully utilize the advantages of each method/approach and optimize the efficiency of the overall simulation (Kröger and Nan 2014).

Real-world interdependent networks pose even harder challenges to methods than single networks while many of their challenges remain (Havlin et al. 2012). Unfortunately, single applications of most of the quite advanced methods (some introduced before) still address interdependencies within or among those networks in a rather limited, often simplified idealized way. For example, complex network theory (CNT) has been extended to capture interdependencies by introducing additional layers and couplings, analogous to interactions between particles in statistical physics (Kenett et al. 2014). However, there are some combined applications, like the CIMS architecture, developed by Idaho National Laboratories in the early 2000s, uses an agent-based (ABM) approach to model infrastructure elements, the relation between them, and individual behavior in a simplified way, whereas each network within the simulation is modeled as a connected graph. Pederson et al. (2006) and Ferrario et al. (2016) proposed a Hierarchical Graph combined with Monte-Carlo simulation to evaluate the robustness of (inter-) dependent critical infrastructures.

To overcome limitations and to capture non-local spreads, physical response behavior and key failure mechanisms/parameters, in short to achieve a closer representation of interdependent critical infrastructure systems, a comprehensive "all by one" modeling approach would be necessary. This turned out to be extremely difficult to achieve and moreover inefficient or a challenge to resources including compute power. Instead, and as an interim solution, it has proven more promising to integrate different kinds of single approaches into one simulation tool and, thereby fully utilizing the advantages of each single method (and created model), meanwhile the effective data exchange needs to be ensured, e.g., by two commonly used frameworks, High Level Architecture (HLA) standard and distributed interactive simulation (DIS) (Nan et al. 2013); a simulation test-bed was created by adopting the HLA standard and dividing the overall simulation tool into different domain-specific simulation modules, i.e. the physical system under control and the system control and data acquisition (SCADA) system.

Most up-to-date approaches focus on physical-engineered networks as such and include some of the contextual factors only implicitly, e.g., by comprehensive data assignment. More sophisticated/novel methods aiming to more realistically capture the behavior of complex interdependent critical infrastructures and their interaction with the operational environment as well as a widened spectrum of triggering events including malicious attacks and the behavior of modern "smarter" system designs are worldwide subject of an active field of research and development.

Resilience analysis and **quantification**, respectively, is less mature than its peer methodology in traditional risk assessment, which otherwise has decades of practical use. This is also because resilience is particularly relevant for dealing with uncertain threats (and ambiguous and unexpected system response behaviors under extreme conditions), which are always difficult, if not impossible, to quantify (Linkov and Palma-Oliveira 2017). Processes and frameworks for comprehensive resilient system behavior assessment have been proposed, e.g., by (Heinimann and Hatfield 2017), who framed resilient system behavior in three classes of generic functions (biophysi-

cal, enabling and cognitive) and raised a set of 10 questions to be answered—instead of the three in case of risk analysis.

The (evolving) resilience concept has also been applied to physical-engineered critical infrastructures and the electricity supply system, in particular. Extensive surveys on methods, suitable to analyze resilience, have been provided and knowledge gaps have been identified: (Häring et al. 2017) offer a taxonomy of "methods up to method classes suitable for….resilience quantification". Out of those graph (complex network) theory, agent-based modeling and combinations with other analytical methods as well as coupling techniques for sufficient data exchange are recommended, although varying in purpose and scope. Besides another differently structured survey on methods, (Heinimann and Hatfield 2017) identified knowledge gaps for future scientific investigations including the domains of context and framing, disruption identification and "bio-physical" resilience analysis; the need to find ways to better understand system-specific conditions which ferment regime shifts may serve as an example.

7 Ways to Increase Resilience of Future Infrastructure Systems

As resilience of large-scale technical systems is a fairly new concept and resilience engineering is an evolving discipline, there are no commonly agreed principles and means to increase resilience, yet. As resilience is a comprehensive strategy such principles and means must comprise physical (including cyber)–engineered, operational (including human), organizational and socio-economic aspects and realize that these aspects and related issues are intertwined.[8]

From the author's perspective some recommendations can be given and should be followed:

- Define subject including boundaries, level/problem space and time scale as well as metrics.
- Distinguish between operational and physical infrastructure as the first, based on possible smart solutions (like de- and re-coupling), might be faster to recover; plan recovery actions with adequate means and resources (repair crews).
- Develop a sufficiently detailed model to identify weak points, study/understand complex system behavior and the effect of measures; widen hazards and threats and triggered scenarios to all imaginable, notably to include cyber attacks (manipulations).

---

[8]A recent study, carried out within the project of three German academies on "Future Energy Systems", proposed a package of measures to create a more resilient energy system, meaning that it is a socio-technical system, and addressed explicitly new stress and vulnerabilities caused by malicious attacks, natural hazards due to climate change, scarcity of raw material due to international political risks, and inadequate energy infrastructure due to wrong investment incentives (Leopoldina et al. 2017).

- Increase heterogeneity and modularity; balance currently favored decentralized structures against centralized structures.
- Strive for robust topology, i.e. optimize robustness of structures against random failures and targeted attacks (e.g., by using topology metrics including node degree/degree distribution).
- Aim at reducing complexity and, if not practically feasible, balance complexity (avoid too little/too high) and/or develop more complex ways of exercising control.
- Balance automation and human control (keep humans in the loop for the unforeseen).
- Provide real time information by digital monitoring and control systems but secure devices and processes.
- Develop and implement switching installations as well as defensive decoupling and reconnecting strategies to avoid local disturbances to develop to large-scale system disruptions/collapses incorporate adequate emergency measures.
- Find ways to bridge losses, e.g., by taking small generation stand-by units into operation, and re-establish sufficient system performance.
- Learn from the past, notice early warning signals; re-organize the system and decision-making in response to external changes.
- Allocate resource buffers, implement physical and functional redundancy or diversity, where applicable.
- Design for operation within adequate safety margins, avoid overloads and operate the system further from "critical points".

While many of the recommendations, i.e. proposed principles and means are currently favored or in line with current developments, strategies, and logics, like the use of more heterogeneous energy sources and decentralized modular topology of the grid, the last counters the trend to reduce redundancies/diversity and safety margins observable in many domains because of economic reasons. Thus, striving for increased resilience is a real challenge, which *inter alia* calls for a change of mindset and additional investments.

8   Conclusions

Large-scale (cyber-) engineered infrastructure systems like the electric power supply system/grid rely on structures and are an essential part of infrastructure systems, on which our societies and economy increasingly depend. Those systems, termed critical, have undergone major changes of all kinds and continue to do so. They are rather socio-technical than purely technical systems and have merged into a system-of-systems due to interdependencies within and among them. They exhibit different degrees of complexity and complex behaviors including non-linearities, cascades and tipping points, all hard to understand and to tackle. Although attempts to reduce complexity have been proposed and made, recently foreseeable and favored developments may even lead to growing complexity: a smart, decentralized power grid,

integrating intermittent energy sources like wind and solar and autonomous producers/consumers ("prosumers") as well as innovative mobility concepts with highly assisted/ autonomous vehicles and extended sharing models may serve as examples. Traditional methods and tools, which base on decomposition and linear causal chains, turned out to be insufficient to model complex systems; advanced modeling and simulation techniques have been developed and partly applied, although further improvements are necessary and should be subject of intensified research.

Most critical infrastructure systems, particularly in most Western countries, performed extremely well. However, we experienced unprecedented major disruptions often with surprising combinations of per se rare events, starting locally and developing sometimes to global scale. Besides natural hazards and some technical failures socio-economic and organizational factors played a dominating role as triggering events while lack of investments and of risk awareness and preparedness had a large impact on consequences. Future developments driven by pervasive use of digital communication and control systems and "smartness" in general will make systems more efficient but also expose them to new (cyber) threats. Past disasters also prove the need of focusing on after shock behavior and on precaution against events, that are unknown and hard to anticipate and imagine; absorptive, adaptive, and recovery capabilities should be amplified rather than purely hardening and preventive measures. A shift towards increased resilience is favored—a concept which has been successfully developed and applied to other than the technical domain. Therefore, a lot of conceptual and operationalizing work as well as a new engineering approach and a change of mindset are required here to enhance the resilience of physical-engineered critical infrastructure systems.

The resilience concept calls for a comprehensive system approach and a sufficiently holistic view. Multiple factors and influencing elements (including physical elements and structures) as well as the operational environment need to be considered, all this is a real challenge. Frameworks to understand and quantify resilience including metrics and methods have been proposed but are still less reliable and mature than in the field of classical risk assessment and should be further developed. A thorough application of the resilience concept and its quantification could help to provide practical means to improve critical systems; striving for extending the limits of predictability may reduce the number unknowns or "Black Swans".

References

Adger, W. N. (2000). Social and ecological resilience are they related? *Progress in Human Geography, 24,* 347–364.

Aven, T., & Krohn, B. S. (2014). A new perspective on how to understand. *Assess and Manage Risk and the Unforeseen, RESS, 121,* 1–10.

Baum, S. D. (2016). Risk and resilience for unknown, unquantifiable, systemic, and unlikely/catastrophic threats. *Environment, Systems, and Decisions, 35*(2), 229–236.

Berkes, F., Colding, J., & Folke, C. (2004). Navigating social-ecological systems: building resilience for C complexity and change. *Ecology and Society, 9*(1), 12.

Council of the European Union. (2008). COUNCIL DIRECTIVE 2008/114/EC of 8 December 2008 on the identification and designation of European critical infrastructures and the assessment of the needs to improve their protection.

Cuadra, L., Salcedo-Sanz, S., Del Ser, J., Jiménez-Fernandez, S., & Geem, Z. W. (2015). A critical review of robustness in power grids using complex network concepts. *Energies, 8,* 9215.

Dobson, I., Carreras, B. A., Lynch, V. E., & Newman, D. E. (2007). Complex systems analysis of series of blackouts: Cascading failure, critical points, and self-organization. *CHAOS, 17,* 026103.

Einarsson, S., & Rausand, M. (1998). An approach to vulnerability analysis of complex industrial systems. *Risk Analysis, 18*(5), 535–546.

Eusgeld, I., Kröger, W., Sansavini, G., Schläpfer, M., & Zio, E. (2009). The role of network theory and object-oriented modeling within a framework for the vulnerability analysis of critical infrastructures. *RESS, 94,* 954–963.

Ferrario, E., Pedroni, N., & Zio, E. (2016). Evaluation of robustness of critical infrastructures by hierarchical graph representation, clustering and Monte-Carlo simulation. *RESS, 155,* 78–96.

Förstner, U., & Köster, S. (2017). Leopoldina, acatech, and UNION. In O. Renn (Ed.), *Das Energiesystem resilient gestalten* (in German), ISBN:978-3-8047-3668-9.

Havlin, S., Kenett, D. Y., Ben-Jakob, E., Bunde, A., Cohen, R., Hermann, H., et al. (2012). *European Physical Journal Special Topics, 214*(1), 273.

Häring, I., Ebenhöch, S., & Stolz, A. (2016). Quantifying resilience for resilience engineering of socio-technical systems. *European Journal for Security Research, 1,* 21–58.

Häring, I., et al. (2017). Towards a generic resilience management, quantification and development process: general definitions, requirements, methods, techniques and measures, and case studies. In I. Linkov & J. M. Palma-Oliveira (Eds.), *Resilience and risk*. New York: Springer.

Heinimann, H. R., & Hatfield, K. (2017). Infrastructure resilience assessment, management, and governance. In I. Linkov & J. M. Palma-Oliveira (Eds.), *Resilience and risk*. New York: Springer.

Henry, D., & Ramirez-Marquez, J. E. (2016). On the impacts of power outages during Hurricane Sandy—A resilience-based approach. *Systems Engineering, 19*(1), 59.

Hines, P., Cotilla-Sanchez, E., & Blumsack, S. (2010). Do topological models provide good information about electricity infrastructure vulnerability? *CHAOS, 20,* 033122.

Hollnagel, E., Woods, D. D., & Leveson, N. (2006). *Resilience engineering (Concepts and precepts)*. Hampshire: Ashgate Publishing Ltd.

Johnson, J., & Gheorghe, A. V. (2013). Antifragility analysis and measurement framework for systems of systems. *International Journal of Disaster Risk Science, 4*(4), 159–168.

Johnson, J., & Hassel, H. (2010). An approach for modelling interdependent infrastructures in the context of vulnerability analysis. *RESS, 95,* 1335–1344.

Kaplan, S., & Garrick, B. J. (1981). On the quantitative definition of risk. *Risk Analysis, 1*(1), 11–27.

Kenett, D. Y., Gao, J., Huang, X., Shao, S., Vodenska, I., Buldyrev, S. V., et al. (2014). Network of interdependent networks: Overview of theory and applications. In G. D. Agostini & A. Scala (Eds.), *Networks of networks: The frontier of complexity* (pp. 3–36). Cham: Springer.

Kovalenko, T., & Sornette, D. (2013). Dynamical diagnosis and solutions for resilient natural and social systems. *GRF Davos Planet @ Risk, 1*(1), 7–33.

Kröger, W., & Zio, E. (2011). *Vulnerable systems*, Springer, ISBN978-0-85729-655-9.

Kröger, W. (2017). Securing the operation of socially critical systems from an engineering perspective: New challenges enhanced tools and novel concepts. *European Journal for Security Research, 2,* 39–55.

Kröger, W., & Nan, C. (2014). Addressing interdependencies in complex technical networks. In G. D. Agostini & A. Scala (Eds.), *Networks of networks: The frontier of complexity* (pp. 279–309). Cham: Springer.

Kröger, W., & Sornette, D. (2013). *Reflections on limitations of current PSA-methodology*. Columbia, SC, USA, CD-ROM: ANS International Topical Meeting on Probabilistic Safety Assessment and Analysis.

Leveson, N. (2014). A new accident model for engineering safer systems. *Safety Science, 42*(4), 237–270.

Linkov, I., & Palma-Oliveira, J. M. (2017). An introduction to resilience for critical infrastructures. In I. Linkov & J. M. Palma-Oliveira (Eds.), *Resilience and risk*. New York: Springer.

Linkov, I., Bridges, T., Creutzig, F., Decker, J., Fox-Lent, C., Kröger, W., et al. (2014). Changing the resilience paradigm. *Nature Climate Change, 4,* 407–409.

Madni, A. M., & Jackson, S. (2009). Towards a conceptual framework for resilience engineering. *IEEE Systems Journal, 3*(2), 85.

Nan, C., Eusgeld, I., & Kröger, W. (2013). Analyzing vulnerabilities between SCADA system and SUC due to interdependencies. *RESS, 113,* 76–93.

Nan, C., Sansavini, G., & Kröger, W. (2016). Building an integrated metric for quantifying the resilience of interdependent infrastructure systems. In C. G. Panayiotou et al. (Ed.), *CRITIS 2014* (pp. 159–171). New York: Springer.

Ouyang, M. (2014). Review on modeling and simulation of interdependent critical infrastructure systems. *RESS, 121,* 43–60.

Ouyang, M., & Fang, Y. (2017). A Mathematical framework to optimize critical infrastructure resilience against intentional attacks. *Computer-Aided Engineering, 32*(11), 909–929.

Panteli, M., Mancarella, P., Trakas, D. N., Kyriakides, E., & Hatziargyriou, Hatziargyriou N. D. (2017). Metrics and quantification of operational and infrastructure resilience in power systems. *IEEE Transactions on Power Systems, 32*(6), 4732.

Pederson, P., Dudenhoeffer, D., Hartley, S., & Permann, M. (2006). *Critical infrastructure interdependency analysis: A survey of U.S. and international research*. Idaho: Idaho National Laboratory.

Ring, J., & Tenorio, T. (2012). Systems of the third kind: Distinctions, implications, and initiatives. *INCOSE Insight, Special Feature, 15*(2), 10.

Rosas-Casals, M., Valverde, S., & Solé, R. V. (2007). Topological vulnerability of the European power grid under errors and attacks. *International Journal of Bifurcation and Chaos, 17*(07), 2465–2475.

Scheffer, M., Carpenter, S. J., Lenton, T. M., Bascompte, J., Brock, W., Dakos, V., et al. (2012). Anticipating critical transitions. *Science, 338,* 344–348.

Schläpfer, M., Kessler, T., & Kröger, W. (2012). *Reliability analysis of electric power systems using an object-oriented hybrid modeling approach*. arXiv preprint arXiv:1201.0552.

Society for Risk Analysis. (2016). *SRA glossary*, SRA publication platform.

Thoma, K., Scharte, B., Hiller, D., & Leismann, T. (2016). Resilience engineering as part of security research: Definitions, concepts and science approaches. *European Journal for Security Research, 1,* 3–19.

Tiernay, K., & Bruneau, M. (2007). Conceptualizing and measuring resilience: A key to disaster loss reduction. *TR news, 250,* 14–17.

Vugrin, E. D., Warren, D. E., Ehlen, M. A., & Camphouse, R. C. (2010). A framework for assessing the resilience of infrastructure and economic systems. In K. Gopalakrishnan & S. Peeta (Eds.), *Sustainable and resilient critical infrastructure systems* (pp. 77–116). New York: Springer.

Wang, J.-W., & Rong, L.-L. (2009). Cascade-based attack vulnerability on the US power grid. *Safety Science, 47*(10), 1332–1336.

World Security Report 1/2. (2018).

Zio, E. (2016). Critical infrastructures vulnerability and risk analysis. *European Journal for Security Research, 1,* 97.

Zio, E. (2018). The future of risk assessment. *RESS, 177,* 176–190.

Seismic Resilience of Existing Infrastructure: Mitigation Schemes for Soil–Structure Systems Subjected to Shaking and Faulting, and Crisis Management System

Ioannis Anastasopoulos, Athanasios Agalianos, Lampros Sakellariadis and Liam Jones

1 Introduction

Throughout history, earthquakes in populated areas have caused tremendous damage and severe direct and indirect losses. Dramatic reminders are the consecutive seismic events that completely razed the ancient hilltop towns and villages of Amatrice in Central Italy and the powerful M7.8 event that shook the coast of Ecuador in 2016 leaving 7,000 buildings destroyed and more than 26,000 people in shelters. Even if of low probability, a large-scale failure can occur sooner or later anywhere in the world bringing immense direct and indirect losses.

But when earthquakes occur in developing countries, they are invariably followed by immeasurable humanitarian calamities. A plethora of major events worldwide confirm this reality: the 2004 Sumatra earthquake and tsunami disaster was accountable for the loss of 240,000 human lives; the death toll of the 2010 Haiti earthquake rose to 250,000; the 2005 Pakistan earthquake killed 80,000 people; the 1990 Western Iran quake claimed 50,000 lives and left over 400,000 homeless. Although the list is merely indicative, the number of victims is still rising whenever such events take place.

Today, both the built environment and populations continue to increase and so their exposure to seismic hazard. Infrastructure systems are amongst the first impacted and

I. Anastasopoulos (✉) · A. Agalianos · L. Sakellariadis · L. Jones
ETH Zurich, Zurich, Switzerland
e-mail: ixa@ethz.ch

A. Agalianos
e-mail: agaliana@ethz.ch

L. Sakellariadis
e-mail: lampross@ethz.ch

L. Jones
e-mail: jonesli@ethz.ch

there is currently no doubt that their failures can have direct impacts on the quality of life, as well as economic growth and viability. At the same time, the rapid expansion of urbanized regions is inevitably followed by the need to enlarge the capacity of infrastructure (the population in urbanized regions will rise from 51% to nearly 65% in 2050) at a time when the world strives to secure infrastructure maintenance funding.

Even if new infrastructure could be constructed to be immune to disasters (a knowingly utopic scenario given—above all—the resource constraints), the vast amount of existing networks would be operating at sub-standard—if not unsafe—service levels. According to several directives, scientific reports and industry analysts, action must be taken to increase the resilience of existing infrastructure systems in order to handle the needs of the future and be ready for unexpected (unknown) events that may occur.

Within this context, this chapter presents some recent advances in the development of innovative seismic hazard mitigation solutions. Focusing on the enhancement of resilience of existing infrastructure, it deals with three different components of the seismic problem: (a) seismic shaking; (b) seismic faulting; and (c) post-seismic crisis management. In the first case, a novel seismic retrofit technique is presented, taking advantage of nonlinear soil-structure interaction to increase seismic resilience. In the second case, the resilience against large tectonic deformation is enhanced by installing "smart" barriers and sacrificial members. In the last case, a rapid response system is outlined, aiming to enhance post-seismic resilience by allowing optimized response and swift post-seismic recovery.

2 Seismic Shaking

The first part of this chapter outlines some recent developments on the retrofit of existing buildings, bridges, and quay walls. In the first two cases, the mitigation technique takes advantage of nonlinear soil response. In the case of the quay wall a simple, yet effective, solution is outlined.

2.1 *Building Retrofit*

2.1.1 Introduction

Current seismic codes recognize that the avoidance of structural damage is not always possible. To that end, they aim to ensure that loads that are in excess of capacity can be sustained without leading to collapse. The concepts of ductility and capacity design are employed for this purpose, materialized by appropriate reinforcement detailing (Park and Paulay 1975). A further substantial enhancement of seismic design codes has been achieved through performance-based design principles (Bertero 1996; Calvi

1999; Priestley 2000). However, the vast majority of the current building stock has been designed and constructed on the basis of outdated seismic codes. The seismic vulnerability of the building stock is mainly governed by that of older structures, thus compromising its seismic resilience.

The seismic vulnerability of existing buildings has been proven in several occasions during major earthquakes, such as Northridge 1994 (Trifunac et al. 1998); Kobe 1995 (Nakamura et al. 1996); Kocaeli 1999 (Barka 1999); Chi-Chi 1999 (Chen et al. 2001); L'Aquila 2009 (Chiarabba 2009) and more recently Christchurch 2010 (Cubrinovski et al. 2011). What is even worse is that the structural integrity of existing building can be compromised, even under moderate intensity seismic shaking. The 1999 M_s5.9 Athens earthquake is a dramatic such example. Despite its moderate magnitude, it led to the collapse of about 100 buildings and severe damage of 13,000 structures in total (Stavrakakis et al. 2002). The need to devise novel retrofit techniques for existing structures that enhance their resilience is evident.

Current seismic codes do not allow strongly nonlinear soil response. The foundation is capacity-designed to ensure that plastic response will be contained in the structural system, practically disallowing mobilization of foundation bearing capacity. However, there is a large number of relevant studies, which demonstrate that strongly nonlinear foundation response can offer substantial benefits in terms of response, cutting off the inertia loading that can transmitted to the structure (Paolucci 1997; Pecker 1998, 2003; Gazetas et al. 2003; Gajan et al. 2005; Apostolou et al. 2007; Pender 2007; Paolucci et al. 2008; Gajan and Kutter 2008, 2009; Shirato et al. 2008; Vassiliou and Makris 2012; Panagiotidou et al. 2012). Such *rocking isolation* at the soil-foundation level offers increased energy dissipation, thus enhancing the safety of the foundation-structure system, even for levels of seismic shaking exceeding the design by a large margin (Anastasopoulos et al. 2010b; Gelagoti et al. 2012; Kourkoulis et al. 2012). Figure 1 schematically compares conventional capacity design to rocking isolation for a frame resting on shallow foundations.

2.1.2 Studied System and Physical Modeling

As shown in Fig. 2, an idealized reinforced concrete (RC) building is studied. The selected 3-storey structure is considered to be representative of structures that were built in Mediterranean European countries in the 70s. As depicted in Fig. 2a, the structure is characterized by asymmetry in both directions.

An equivalent "slice" of the soil–foundation–structure system is simulated, which corresponds to 1/3 of the structure (Fig. 2b). Based on the calculated bending moment capacities M_{RD} of its columns and beams (Rontogianni 2011), the structure does not comply with capacity–design principles (a typical for that time strong beam-weak column design) and is therefore prone to soft-storey collapse.

The existing building is retrofitted by adding RC shear walls, one for each loading direction. With reference to the equivalent slice being considered for the simulation (Fig. 2b), the RC shear wall is placed next to the middle column (on its left side). The retrofit was designed according to modern seismic code provisions (KANEPE

2010), considering design acceleration $A = 0.24$ g and behavior factor $q = 3.5$. This led to shear walls of 1.5 m in length and 0.25 m in width. Their reinforcement was computed according to current RC codes (EKOS 2000).

The seismic performance of the existing and the retrofitted building was studied through shaking table testing (Anastasopoulos et al. 2015b). The tests were conducted at the Laboratory of Soil Mechanics of the National Technical University of Athens (NTUA). Regarding the foundation of the RC shear walls of the retrofit, two different options are considered: (a) conventional design; and (b) rocking isolation. While the conventional design follows the current code provisions, in the case of rocking isolation full mobilization of foundation moment capacity is promoted, simply by reducing the foundation width.
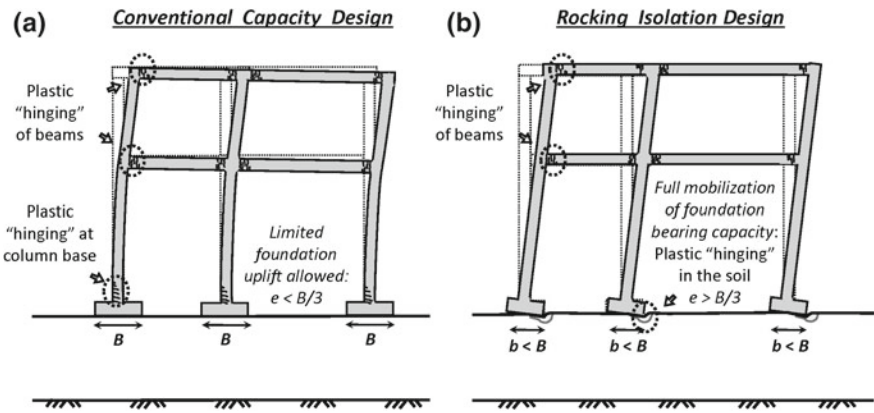

Fig. 1 Design concepts for a frame resting on shallow foundations: **a** current capacity design; and **b** rocking isolation
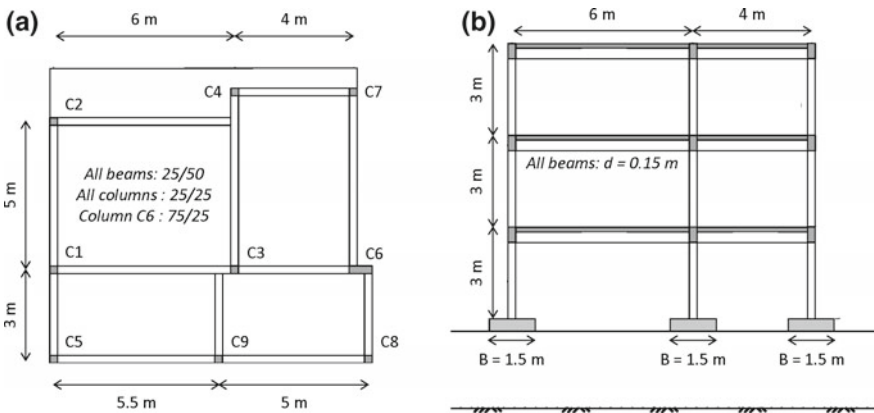

Fig. 2 Geometry of the 3-storey building: **a** plan view; and **b** cross-section

The physical model comprised two identical 2-bay frames for stability. The two frames were connected to each other using steel plates having mass equal to that of each floor. Taking account of the dimensions of the strong box that was used for the tests (which is a function of the capacity of the equipment), a scaling factor $N = 10$ was employed. The footings were modeled with thick (to be rigid) aluminum plates. Similar aluminum plates, but of appropriate dimensions in order to maintain stiffness similarity were used to model beams and columns (Gibson 1997). Instead of relying to material nonlinear response, the beam-column connections were modelled with custom–built artificial plastic hinges (APH).

As illustrated in Fig. 3c, each artificial plastic hinge consists of an aluminum alloy housing and bearing assembly. Special setscrews are used to prevent the bearing from rotating inside the housing unit. The torque at which sliding rotation takes place is a function of the radial pressure acting the bearing, which is a function of the applied torque on the setscrew. Therefore, by adjusting the torque on the setscrew, the radial pressure acting on the bearing can be adjusted, therefore controlling the bending moment capacity M_{RD} of each structural member. More details on the calibration method of the APHs can be found in Anastasopoulos et al. (2015b).
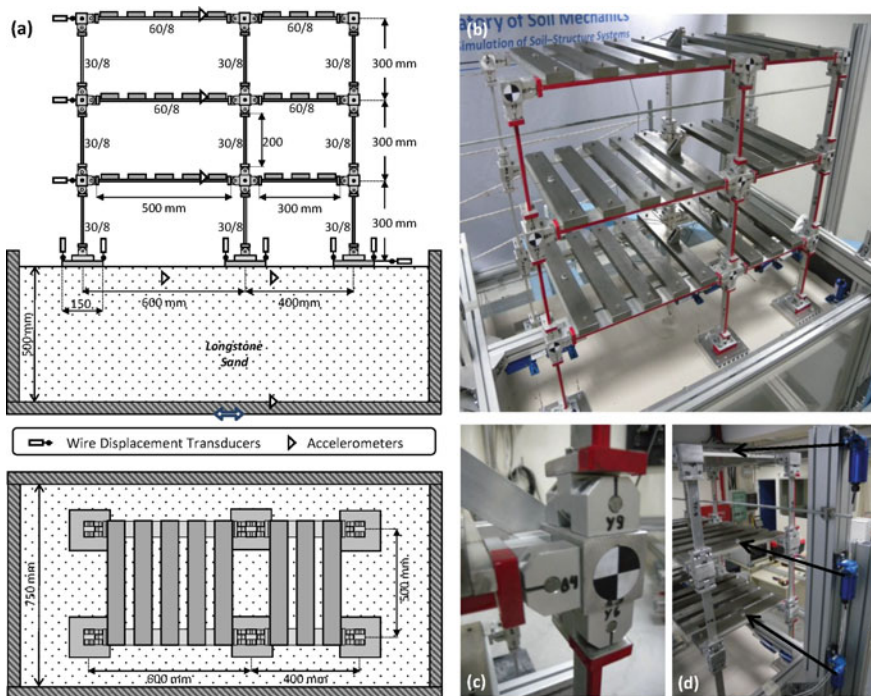

Fig. 3 Physical model of the existing building: **a** model cross-section and plan view, along with structural member properties and instrumentation (mm); **b** image of the physical model; **c** image of an artificial plastic hinge; and **d** locations of displacement sensors

With respect to soil conditions, a layer of dry Longstone sand was considered. The utilized soil material is a fine-grained quartz sand, having an average grain size $d_{50} = 0.15$ mm (Anastasopoulos et al. 2010c). To explore the effect of soil stiffness, the relative density D_r was varied from 45 to 93%, covering the entire range from loose to dense sand. To focus on the comparative assessment of the retrofit alternative, the discussion focus on dense sand. As shown in Fig. 3d, various sensors were installed both on the superstructure and inside the soil. The main scope of the instrumentation was to measure the seismic response in terms of inter-storey drifts and foundation rotation, swaying, and settlement.

An ensemble of recorded seismic motions were used as base excitation. They were selected in order to cover a wide range of seismic intensities and strong motion characteristics. The seismic vulnerability of the existing structure was investigated using moderate intensity records from Greece and Turkey. The same records were then employed to verify the enhanced resilience of the retrofit solution for seismic shaking within the design limits. Then, a set of very strong records were used to compare the safety margins of the investigated retrofit alternatives to seismic shaking in excess of the design levels. These include the Rinaldi record, from the 1994 Northridge earthquake; and the JMA and Takatori records, from the devastating 1995 Kobe earthquake. The employed earthquakes sequences are summarized in Table 1. More details on the shaking sequences can be found in Anastasopoulos et al. (2015b).

2.1.3 Seismic Vulnerability of the Original Building

The original building was initially tested to confirm its vulnerability. The first sequence of Table 1, consisting of mainly moderate intensity records, was used

Table 1 Shaking sequences employed in the experimental series

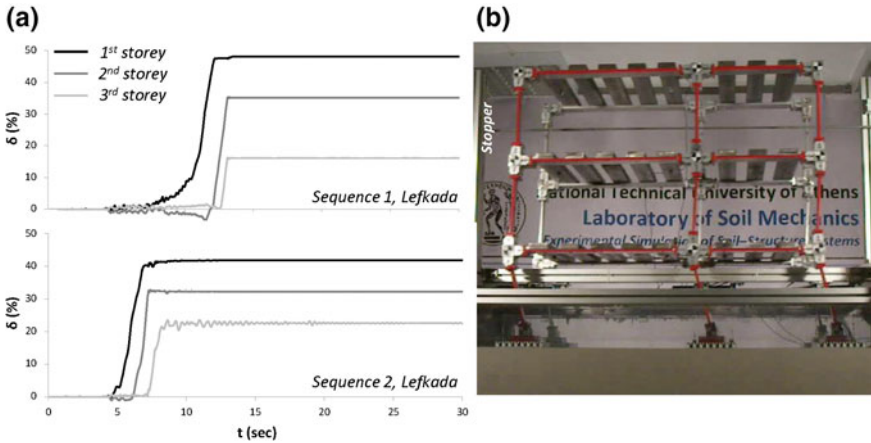| Sequence 1		Sequence 2		Sequence 3		Sequence 4	
Record	α_{max} (g)	Record	α_{max} (g)	Record	α_{max} (g)	Record	α_{max} (g)
MNSA	0.51	Sin—4 Hz	0.10	MNSA	0.51	JMA	0.82
Aegion	0.38	Sin—2 Hz	0.20	Aegion	0.38	Rinaldi	0.83
Kalamata	0.24	Sin—1 Hz	0.20	Kalamata	0.24	Takatori	0.61
Lefkada	0.35	MNSA	0.51	Lefkada	0.35		
		Aegion	0.38	Sakarya	0.36		
		Kalamata	0.24	JMA	0.82		
		Lefkada	0.35	Rinaldi	0.83		
		Sakarya	0.36	Takatori	0.61		
		JMA	0.82				
		Rinaldi	0.83				
		Takatori	0.61				

Fig. 4 Response of the original building subjected to the Lefkada record: **a** drift ratio δ time histories for Sequence 1 (top) and Sequence 2 (bottom); and **b** snapshot of soft-storey collapse

for these tests. Subjected to the Lefkada record, the original building sustained soft-storey collapse. Figure 4a offers a summary of the results, with emphasis on the performance of the superstructure. The time histories of drift δ are indicative of a soft-storey collapse mechanism. The building accumulates drift during the first few seconds of shaking, with most of it being localized within the first floor. Subsequently, an abrupt increase was observed. As the collapse mechanism is initiated, the structure starts accumulating excessive drift, which is always concentrated at the first floor. For $t \approx 11$ s, the 1st floor drift ratio exceeds 20%; the collapse mechanism is clearly seen in the snapshot of Fig. 4b. The building is subsequently arrested by stoppers, and therefore the drift of the first floor cannot possibly increase further. The second and the third storeys continue to accumulate drift, until they are also arrested by the stopper.

To investigate the effect of preceding seismic excitations, the model was also subjected to Sequence 2 (Table 1). In this case, when the model was subjected to the Lefkada record, it had also sustained 3 sinusoidal excitations in addition to the MNSA, Aegion, and Kalamata records. The collapse mechanism remained unaltered, however taking place a few seconds earlier (Fig. 4a, bottom). This difference is attributed to the previous shaking events, due to which the accumulated drift was higher at the onset of the Lefkada seismic excitation. Despite the qualitative similarities in terms of failure mechanism, the seismic sequence can be seen to have measurable effect on seismic performance.

2.1.4 Verification of Conventional Retrofit

The experiments confirmed the inadequacy of the original structure, when considering modern seismic design provisions. As previously discussed, the retrofit comprises a 1.5 long RC shear wall per loading direction. The latter were modelled with an aluminum plate, which was monolithically attached on all 3 storeys. The bending moment capacity of the shear wall was simulated with an appropriately calibrated APH, installed at its base. The necessary increase of the width of the corresponding foundation was achieved by an extension of the aluminum plate on both sides. For the conventionally-designed retrofit solution, the foundation was capacity designed (according to current seismic codes): $B = 6$ m.

A first set of tests were conducted to verify the adequacy of the conventionally-designed retrofit solution for shaking within the design limits. The conventionally-designed retrofitted building was subjected to Sequence 1, which mostly contains excitations of moderate intensity. The test verified the efficiency of the conventionally-designed retrofitted structure, which sustained the entire shaking sequence not only without collapsing, but also with a limited amount of inter-storey drift δ. The drift time histories of all three stories were more-or-less identical, thanks to the homogenizing action of the shear walls (Anastasopoulos et al. 2015b). Being stiffer and stronger than the columns and the beams of the original structure, the shear walls tend to force the system to follow their deformation, which resembles rigid-body rotation with respect to the plastic hinge at the base. This leads to the observed homogenization of drift, which is almost evenly distributed between the three floors. Even if the bending moment capacity of the shear wall is reached, soft-–storey collapse will remain quite improbable. In conclusion, the testing verified the efficiency of the conventional retrofit for seismic motions that do not exceed the design.

2.1.5 Conventional Retrofit Versus Rocking Isolation

In the case of conventional design, the shear wall foundation was *over-designed* by a factor of 1.4, following current capacity design provisions. In the context of rocking isolation, exactly the opposite is required: the foundation width needs to be reduced to allow full mobilization of its bearing capacity, promoting rocking response (Anastasopoulos et al. 2010b; Gelagoti et al. 2012). As demonstrated by the previously shown results, the conventionally-retrofitted building exhibited a good performance when subjected to moderate intensity shaking. To comparatively assess the safety margins of the two design schemes, a series of testing were conducted employing the stronger records.

Figure 5 offers a comparison of the performance of the two retrofit schemes subjected to the Rinaldi record, which can be seen as an example of shaking that substantially exceeds the design limits. As depicted in Fig. 5 (left), the conventionally-designed system sustains excessive distortion with its δ reaching 8%. The latter is mainly due to the flexural distortion of the shear wall δ_c.
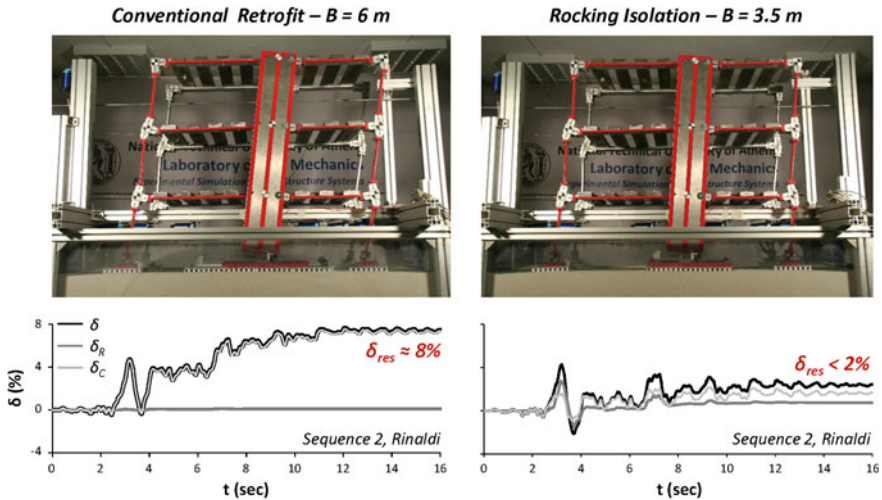
Fig. 5 Comparison of the performance of the two retrofit schemes subjected to the Rinaldi record (Sequence 2). Snapshots of the model and time histories of drift ratio δ of the shear wall: total drift δ; drift δ_R due to rotation; and due to flexural distortion δ_C

As shown in Fig. 5 (right), the performance of the rocking-isolation scheme is much better as the maximum δ remained lower than 4% (50% reduction). The residual drift was practically negligible. Most of the observed δ is related to foundation rotation (δ_R), with the flexural distortion component (δ_C) being negligible. The rocking-isolation retrofit offers superior performance, with its only drawback being the somehow larger settlement (Anastasopoulos et al. 2015b). The rocking foundation acts as a "fuse", setting a limit to the moment that can find its way to the shear wall. Provided that the toppling rotation is not reached (something which highly unlikely given the width of the foundation), gravity acts as a restoring mechanism.

2.1.6 Retrofit Using Variable-Geometry Foundations

Rocking isolation of the added RC walls was shown to offer a viable retrofit alternative, offering improved seismic performance by reducing the maximum and residual inter-storey drift. Despite the fact that the settlements were acceptable (partly thanks to the dense sand that was used in the testing sequence), permanent settlement is typically the price to pay. Moreover, residual foundation rotation may in some cases not be negligible, raising post-seismic serviceability issues.

Figure 6 depicts a novel concept of a variable geometry foundation, aiming to alleviate such drawbacks. As discussed in more detail in Anastasopoulos et al. (2015b), the effective foundation width varies with rotation. The smaller width b is engaged under moderate seismic shaking, offering maximum rocking isolation. Under severe seismic shaking, the rotation increases leading to mobilization of a larger width B.

Fig. 6 Schematic illustration of the hybrid variable-geometry foundation concept
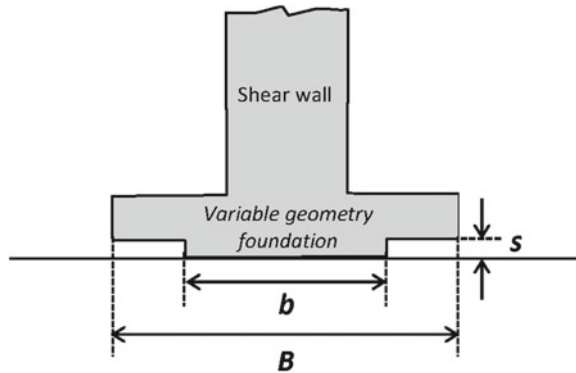
The rotation θ at which B is engaged is a function of the difference $(B-b)$ and the height s of the transition. And since the toppling rotation θ_u is a function of foundation width, this will lead to a progressively more stable system. In addition, the accumulation of settlement can be reduced, as the footing will become progressively larger with the increase of rotation. A stepped transition was employed in the tests of (Anastasopoulos et al. 2015b), but a (linear or parabolic) ramp transition that would lead to a progressive increase of effective foundation width is also envisioned.

The shaking table tests were repeated to explore the performance of such variable-geometry foundations. Figure 7 offers a comparison of the rocking–isolated retrofit using one of the a variable-geometry foundation ($B = 3.5$ m, $b = 2$ m, $s = 0.05$ m), to the already discussed retrofit schemes (conventional, $B = 6$ m; and rocking-isolated, $B = 3.5$ m) and the original structure in terms of distribution of residual drift δ_{res} with height. It is reminded that the original structure sustained soft-storey collapse when excited by the Lefkada record (Fig. 7a). For moderate intensity shaking, the δ_{res} of the conventionally–retrofitted structure was negligible, becoming however excessive when subjected to strong shaking (Fig. 7b). With $\delta_{res} \approx 14\%$ for the Takatori record, the building would probably collapse in reality. The rocking-isolated system with a constant-width $B = 3.5$ m footing performed much better (Fig. 7c), with δ_{res} not exceeding 4% for the notorious Kobe JMA record. Still though, when subjected to the Takatori record, δ_{res} did exceed 11%. In the case of the variable-geometry footing, δ_{res} was 1% for JMA, however still reaching 9% for Takatori.

In Fig. 7c, d, it is interesting to observe the distribution of δ_{res} with height. In the case of JMA and Rinaldi, δ_{res} is almost constant with height, as expected thanks to the homogenizing effect of the shear walls. This is not at all the case for Takatori, something that is attributed to sliding of the foundation of the shear wall. In contrast to the shear wall, the columns have a substantially lower moment capacity, and therefore their footings do not sustain large enough lateral loading that could lead to sliding. The result of this is differential displacement, a problem that can easily be mitigated through addition of tie beams.
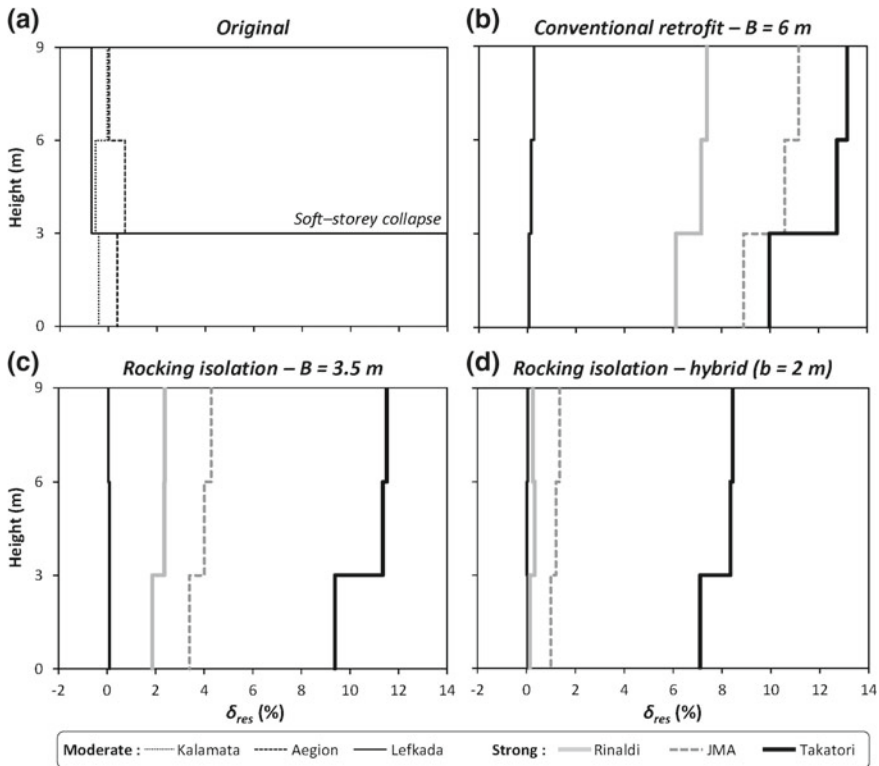
Fig. 7 Distribution of residual drift δ_{res} with height for Sequence 2: **a** original structure; **b** conventional retrofit ($B = 6$ m); **c** rocking–isolated retrofit ($B = 3.5$ m); and **d** rocking–isolated retrofit, with variable geometry foundation ($B = 3.5$ m, $b = 2$ m, and $s = 0.05$ m)

2.1.7 Hinged Tie Beams

The use of tie beams may be efficient in minimizing differential displacements, but at the same time, may also hinder the beneficial effects of rocking isolation. With the goal of reducing the differential (sliding-related) displacements, while maintaining rocking isolation, a concept of hinged tie beams (Fig. 8, left) was introduced in Anastasopoulos et al. (2013a). By introducing such a *hinged* connection, the rocking of the shear wall foundation is not restrained, while at the same time the lateral differential displacements are restrained by the axial rigidity of the tie beams.

The efficiency of such a solution was explored numerically in Anastasopoulos et al. (2013a) and experimentally verified in Anastasopoulos et al. (2015b). In the shaking table tests, steel rods were used to model the tie beams, connected to the footings with a hinged connection. As illustrated in Fig. 9 (right), the rocking-isolated retrofitted structure performed exceptionally with the hinged tie beams, even under severe seismic excitation with the notorious Takatori record. This is confirmed by
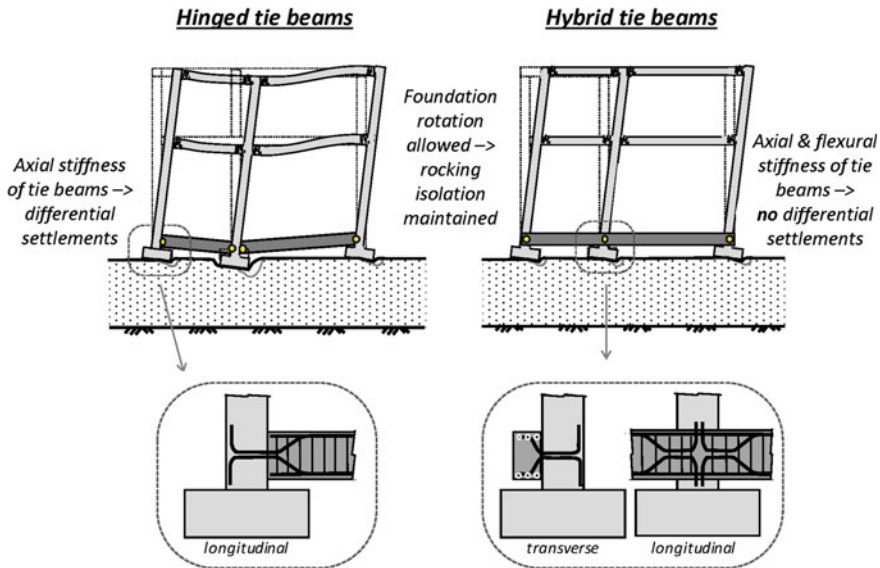
Fig. 8 Novel concepts for the seismic retrofit of existing buildings through addition of: hinged tie beams (left); and hybrid tie beams (right)

the drift ratio time histories, according to which the incorporation of the hinged tie beams lead to roughly 50% decrease of δ_{res} (from the previously discussed 9% to roughly 4.5%).

2.1.8 Hybrid Tie Beams

A further improvement can be achieved through the hybrid concept of Fig. 8 (right), which aims to combine the advantages of conventional (fully-fixed) and hinged tie beams. It consists of a continuous tie beam, placed behind the columns and connected with external hinges. The simplest way to materialize such an external hinge is to connect the tie beam with the columns using centrally-placed steel reinforcement, as sketched in Fig. 8 (right). Through such an arrangement, the flexural rigidity of the tie beams can be adequately mobilized, homogenizing the settlements of the three footings and reducing the differential settlements, while at the same time preserving the benefits of rocking isolation.

The efficiency of the hybrid concept was numerically investigated for the asymetric two-storey frame of Fig. 1 in Anastasopoulos et al. (2013a). Figure 10 presents the settlement–rotation (w–θ) response of the three footings for very strong seismic shaking with a Tsang–type excitation of $PGA = 1g$. The differential settlement between the middle and the edge footings is markedly reduced to 2.5 cm (Fig. 10b), as opposed to 11.5 cm for the case of hinged tie beams (Fig. 10a). This is considered
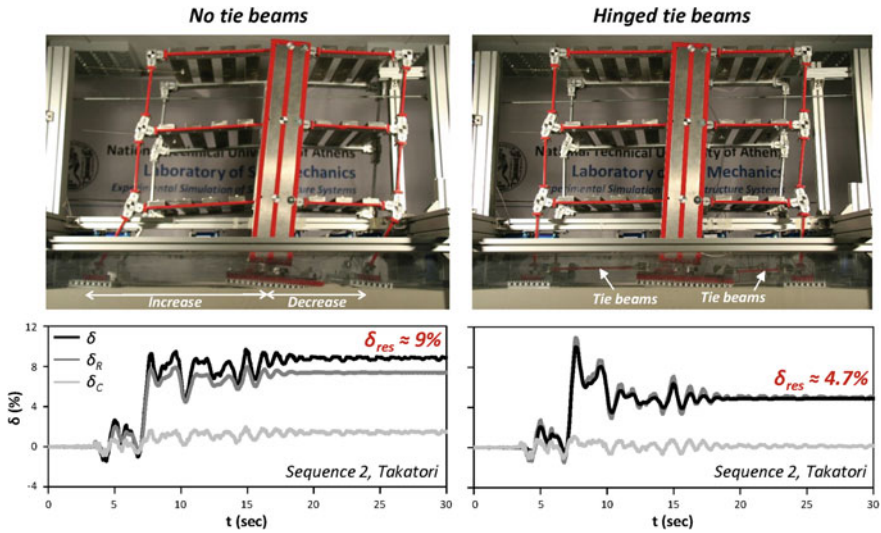
Fig. 9 Rocking–isolated retrofit equipped with variable-geometry footing ($B = 3.5$ m, $b = 2$ m, $s = 0.05$ m), subjected to the Takatori record (Sequence 2). Images of the model (top) and drift ratio time histories (bottom): without tie beams (left); and with hinged tie beams (right)

a remarkable improvement, given the extreme seismic excitation (10 strong motion cycles of $1g$ at a period of 0.5 s). Such decrease of differential settlements, while maintaining the benefits of rocking isolation, may lead to a substantial enhancement of the seismic resilience of existing buildings.

2.2 Quay Wall Retrofit

2.2.1 Introduction

As with the current building stock, the vast majority of existing quay walls were built several decades ago according to outdated seismic codes. Typically composed of simply supported multiple blocks, such quay walls may be particularly vulnerable to strong seismic shaking. Their economic and societal importance is not to be underestimated, as they constitute critical components of commercial and passenger ports, waterfront industrial facilities and terminals. Their seismic vulnerability has been proven in several large magnitude earthquakes, such as the 1995 $M_w 7$ Kobe earthquake in Japan. The failure of quay walls may have a severe impact on the functionality of the port, affecting the economy at a national or even international level. The Port of Kobe is a dramatic such example: 24 years after the Kobe earthquake, it has not yet fully recovered, proving that the indirect damage can be much more substantial than the direct one.

2.2.2 Studied Quay Wall and Experimental Setup

The main scope of the current Chapter is to outline novel concepts of enhancing the seismic resilience of structures. In this context, the seismic response of an existing multi-block quay wall is explored. The studied quay wall is inspired from the Port of Piraeus in Athens (Greece). A set of dynamic centrifuge model tests were conducted at the University of Dundee geotechnical beam centrifuge (Anastasopoulos et al. 2015c). As depicted in Fig. 11a, the quay wall is composed of 8 RC blocks, resting on top of each other without any shear connection. The height of the real quay wall is 17.4 m, but a reduced version of 13.86 m height was tested in the centrifuge given its shaking capacity and the size of the ESB container. An idealized soil layer of dense sand ($D_r = 80\%$) was used for the tests.

The deformation of modern single-block quay walls involves seaward displacement, settlement and rotation. The response can become much more complicated in the case of multi-block quay walls, as the absence of shear connection between the blocks may also lead to relative displacements and rotations between the blocks. These may increase the seismic vulnerability of the system, something that was proven by the experimental results (Anastasopoulos et al. 2015c). Even medium intensity seismic excitations may lead to accumulation of large displacements, practically leading to failure in terms of serviceability.

A novel retrofit concept was proposed in Anastasopoulos et al. (2015c), with the aim of reducing the residual lateral displacement of the quay wall. As shown in Fig. 11b, the retrofit consists of connecting the blocks and anchoring the top of the quay wall at an appropriate distance. In the experiments, the connection was
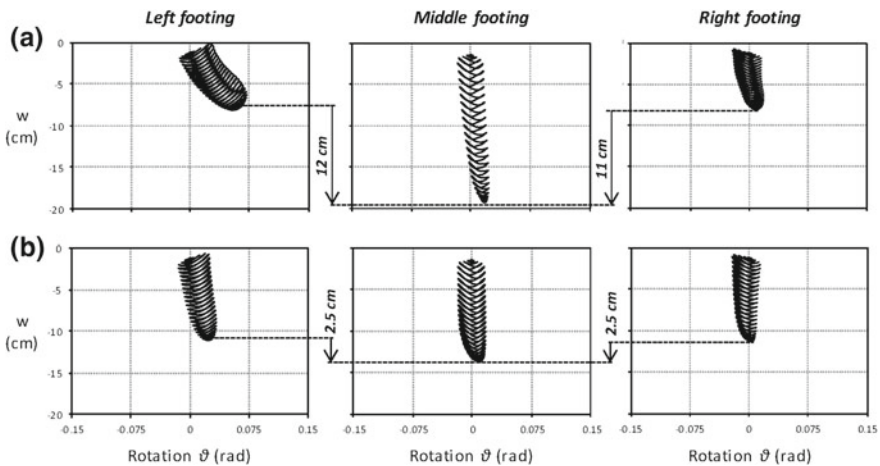

Fig. 10 Rocking-isolated asymmetric building fitted with **a** hinged tie beams; and **b** hybrid tie beams, in terms of settlement-rotation response of the three footings when subjected to very strong shaking (Tsang-type excitation of $a_{max} = 1$ g)
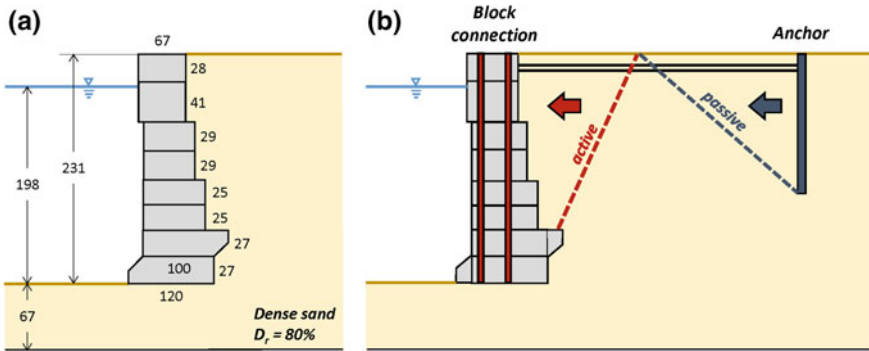
Fig. 11 Enhancing the resilience of existing multiple-block quay walls: **a** geometrical attributes of the reduced multi-block quay wall of Piraeus Port in Athens, Greece (dimensions in mm, model scale 1:60); and **b** sketch of the retrofit solution

implemented with tie rods; in reality boreholes would be required, through which steel reinforced members would be installed.

2.2.3 Indicative Results

The centrifuge model was subjected to a sequence of moderate to strong seismic excitations, including real records from Greece (Lefkada, 2003; Kefalonia, 2014), Italy (L'Aquila, 2009), the US (Northridge, 1994), and Japan (Kobe, 1995). Figure 12 compares the performance of the retrofitted to that of the existing quay wall, subjected to the L'Aquila record. The horizontal displacement at the top of the wall (Fig. 12a) has two components: (a) the translational movement, which also includes sliding between the blocks (a mechanism which governs the performance of the existing quay wall); and (b) the rotational movement of the wall (which is the most important for the retrofitted quay wall). The efficiency of the retrofit is evident, as it leads to almost 50% reduction of the residual displacement.

As illustrated in Fig. 12b, due to the connection of the blocks, the rotational movement dominates the response of the retrofitted wall. This is a key difference to the existing quay wall, where the blocks are free to slide relative to each other. Figure 12c, d compare the response in terms of settlements. Although the retrofitted system experiences somehow increased settlement compared to the existing wall (something that is attributed to its rotational response and to some mobilization of the bearing capacity failure mechanism), the performance of the retrofitted system is advantageous in terms of settlement Δw (see sketch of Fig. 12) relative to the backfill. Δw is considered as a much more representative measure of the potential distress of structures and lifelines supported on the quay wall. The retrofit is shown to allow its reduction by about 50%, thus confirming its efficiency in enhancing system resilience.
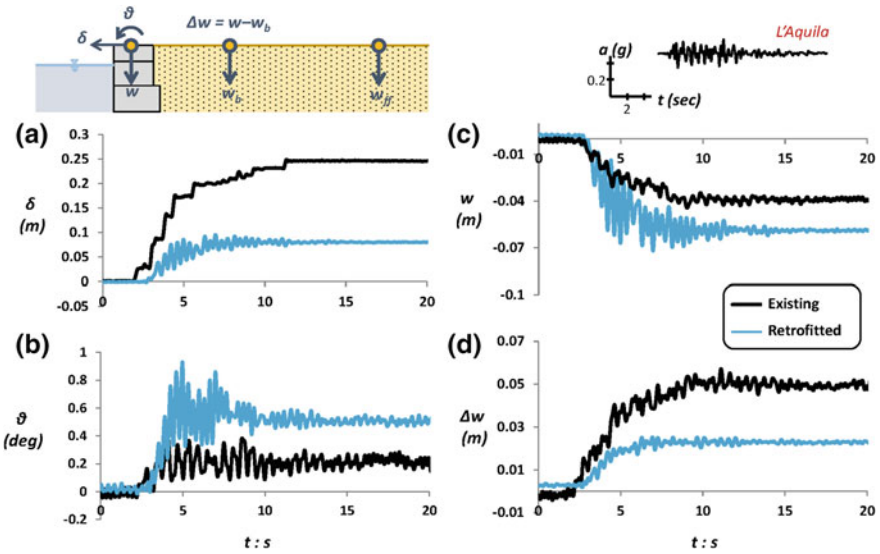
Fig. 12 Comparison of the performance of the retrofitted to that of the existing quay wall subjected to the L'Aquila record in terms of: **a** horizontal displacement at the top of the wall; **b** rotation; **c** settlement; and **d** differential settlement with respect to the backfill

2.3 Bridge Retrofit

2.3.1 Introduction

The adaptation of existing motorway infrastructure to increasing mobility demands represents a worldwide challenge. The remediation of bottlenecks can be achieved by adding traffic lanes, calling for widening of existing bridges. Such widening is directly associated with an increase of dead- and live-loads, necessitating retrofit of piers and foundations. In most cases, the widened bridge needs to be designed according to current seismic design provisions, leading to further increase of the seismic actions that need to be considered.

In contrast to superstructure retrofit, which is relatively straightforward, foundation retrofit can be challenging, costly, and time–consuming. Partial excavation in the vicinity of the existing foundation is necessary, followed by enlargement of the existing foundation, and installation of additional pile rows in the case of pilegroups. This entails a number of challenges related to accessibility and interruption of ongoing traffic. Such technical challenges and their financial and time-related implications should not be underestimated.

Given the typically high degree of conservatism in foundation design, exploiting nonlinear soil-structure interaction (SSI) is worth considering. By allowing nonlinear SSI, a "do nothing" approach may constitute a viable option, provided that the seismic performance is within acceptable limits in terms of permanent deformations. Within

this context, this section presents a comparative assessment of current design practice, which is based on "elastic" foundation design, to an alternative design approach that allows exploitation of nonlinear response.

Foundations are typically designed to remain elastic under all load combinations (e.g. EC8 2000). Foundation capacity design is used to ensure that the foundation moment capacity is larger than that of the bridge pier, thus guiding plastic hinging to the superstructure. However, relatively recent research suggests that soil–foundation plastic response during seismic shaking may actually be beneficial (e.g., Paolucci 1997, Kutter et al. 2003). Furthermore, the current design philosophy has been shown to have some shortcomings, especially in case of extreme seismic events substantially exceeding the design. One such example it the collapse of the Fukae bridge in Japan during the 1995 Kobe earthquake (Iwasaki et al. 1995). Designed in the 1960s, its pilegroup foundations had a much higher conventional moment capacity than the bridge piers. Plastic hinges formed at the piers, leading to a dramatic collapse of 18 spans.

Within this context, this chapter presents two case studies of motorway overpass bridges, founded on shallow and piled foundations, exploring the possibility of exploiting nonlinear SSI, as an alternative to conventional "elastic" retrofit design. Both cases refer to existing bridges in Greece, assumed to be widened to accomodate increased traffic demands. In both cases, conventional foundation retrofit is compared to the "do nothing" approach, i.e., keeping the existing foundation by allowing full mobilization of its bearing capacity during seismic loading.

2.3.2   Bridge Founded on Shallow Foundations

An existing Attiki Odos motorway (Athens, Greece) overpass bridge is used as an illustrative example. The A01-TE23 bridge is an asymmetric 5-span structural system, of 115.6 m total length. The continuous 10.4 m wide deck is of hollow cross-section. The deck is resting on cylindrical RC piers of 1.8 m diameter. The bridge is designed according to the provisions of the Greek Seismic and RC Codes. Figure 13 offers an overview of the bridge and the details of the finite element (FE) model. More details can be found in Agalianos et al. (2017a).

The bridge piers are founded on square shallow footings. The soil consists of an idealized homogenous clay layer of undrained shear strength $S_u = 150$ kPa. Two design solutions are considered: (a) conventional design, leading to footings of 7 m (P1 and P2) and 8 m (P3 and P4) width; and (b) allowing nonlinear SSI and foundation rocking, with footings of 3.5 m (P1 and P2) and 4 m (P3 and P4). The deck is sitting on 4 elastomeric bearings at each abutment.

In the case of rocking foundations, the moment capacity of the foundation is smaller than that of the corresponding piers. Thus, failure of the RC piers cannot possibly occur, as the foundation will act as a "safety valve". This implies that the apparent safety factor against seismic loading (FS_E) is lower than 1. Naturally, it is ensured that the safety factor against vertical loading (FS_v) remains larger than 2.5 to
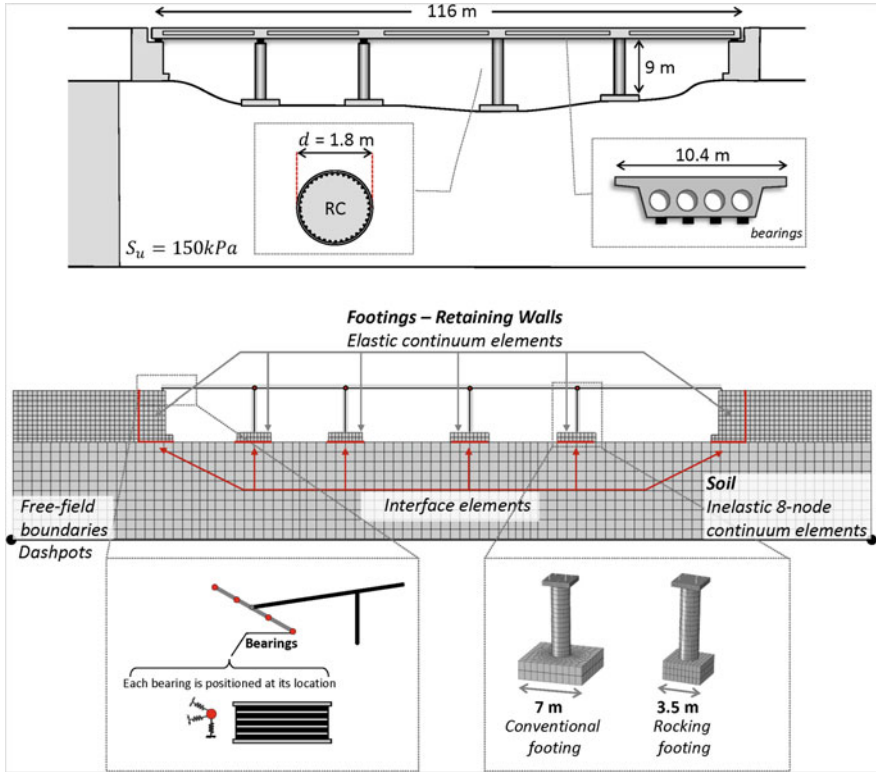
Fig. 13 Key attributes of the A01-TE23 overpass bridge of the Attiki Odos motorway and details of the 3D FE model of the entire bridge-foundation-abutment-soil system

comply with current codes. A schematic illustration of the two solutions is presented in Fig. 14.

The performance of the two solutions is compared under severe seismic shaking, using the Takatori record from the 1995 Kobe earthquake as seismic excitation. Indicative results are depicted in Fig. 15, corresponding to the pier P4, which experiences the most severe damage. The comparison is in terms of deck drift (δ) time histories, pier moment–rotation (M–θ) response, and time histories of foundation settlement (w).

In the case of the conventionally designed footing, the maximum flexural displacement reaches 46 cm (Fig. 15a), substantially exceeding its ductility capacity (31 cm). Evidently, such severe seismic loading does not only lead to yielding of the piers, but may also lead to collapse, something which is confirmed by the M–θ response of the pier section (Fig. 15c). At the same time, foundation rotation remains negligible and the settlement does not exceed 1 cm (Fig. 15d).

In the case of the rocking foundation, although the total drift still reaches 40 cm, collapse is avoided. As shown in Fig. 15b, the major component of drift is the one
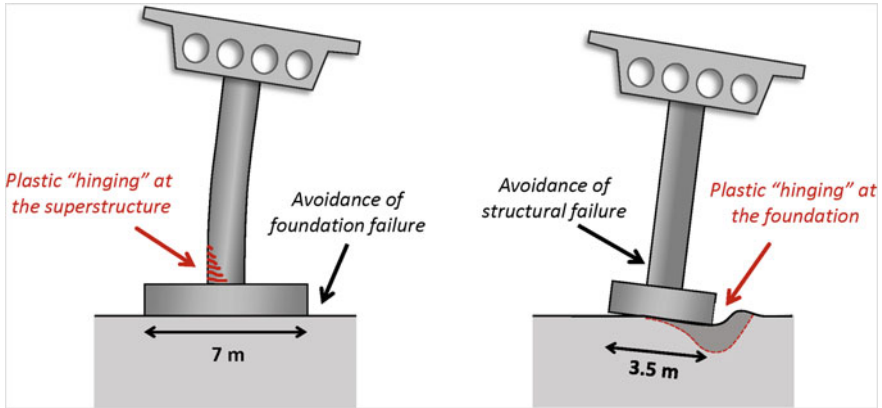
Fig. 14 Schematic illustration of the two solutions: conventional design, larger foundation (left); compared to the rocking, smaller foundation approach (right)
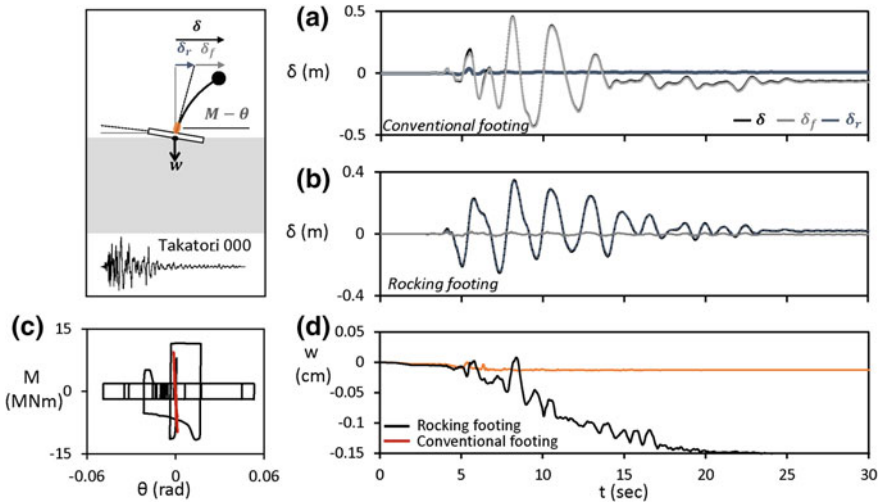

Fig. 15 Comparison of the two design alternatives using the Takatori record as seismic excitation: **a** time history of deck drift for the conventional footing (distinguishing between total, flexural, and rotational drift) compared to **b** deck drift for the rocking footing; **c** comparison of pier moment–rotation response; and **d** time histories of settlement

due to rocking. The total bending moments at the base of pier P4 never exceed the moment capacity (Fig. 15c), but as revealed by Fig. 15d the inelastic behaviour of soil results to accumulation of settlements. The residual rotation remains negligible, but the settlement reaches 15 cm which can be seen as the price to pay for the superior levels of seismic safety and the reduced damage of piers.

2.3.3 Bridge Founded on Pilegroups

The second example refers to an overpass bridge founded on a pilegroup. The existing Ladopotamos bridge (Greece) is founded on a 3×5 pilegroup. As shown in Fig. 16, it is 2-span bridge with a continuous RC box-girder deck, supported on a single multicolumn thin-walled RC pier of width $B = 7$ m and height $h = 20$ m. The reinforcement of the RC piers is calculated according to the Greek Seismic and RC Codes. The pier is rigidly connected to the deck, which is supported by 4 elastomeric bearings at each abutment. The deck is assumed to be widened in order to serve two additional traffic lanes, resulting to roughly 50% increase of dead- and live-loads. To that end, the RC piers are retrofitted (Fig. 16).
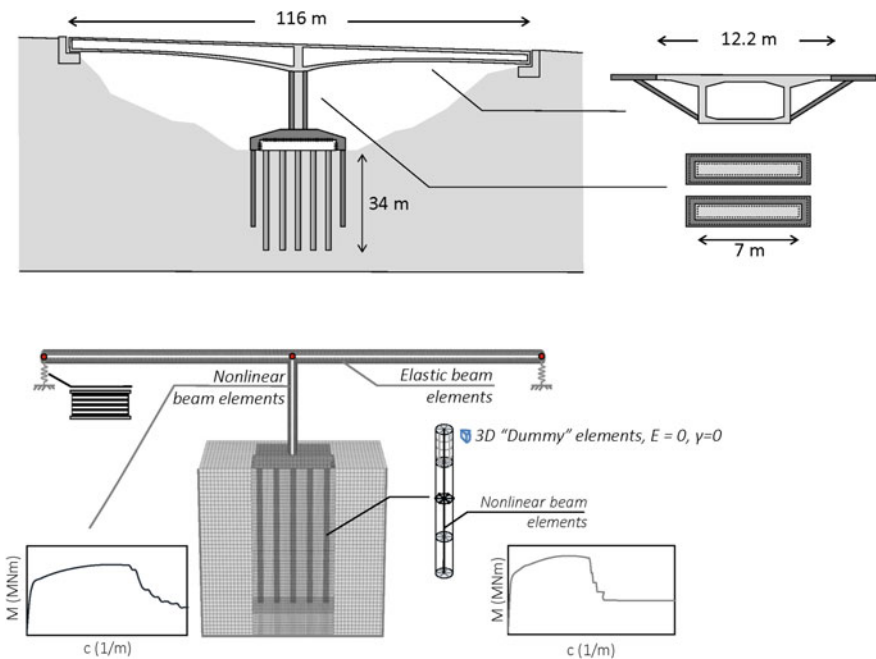

Fig. 16 Key attributes of the Ladopotamos overpass bridge and details of the 3D FE model of the entire bridge-pilegroup-soil system

Table 2 Synopsis of static and dynamic safety factors for each design consideration

Scenario	Initial pile group	Retrofitted pile group
Static	$V_{s,d}/V_{e,d} = 1.1$	$V_{s,d}/V_{e,d} = 1.6$
Seismic	$M_{el,d}/M_{e,d} = 0.8$	$M_{el,d}/M_{e,d} = 1.02$

The bridge is founded on a layered clay stratum determined on the basis of in situ Standard Penetration Tests (SPT). An overview of the system under consideration and the key components of the FE model are presented in Fig. 16. The existing foundation is evaluated according to current code provisions with respect to the increased static loads ($V_{e,d}$) and the seismic actions ($M_{e,d}$). The design moment capacity ($M_{el,d}$) is determined assuming an elastic approach: it corresponds to the moment at which the edge piles reach their design axial resistance. The acting loads and the pile resistance are summarized in Table 2 for the widened bridge. Although the design axial loads are lower than the design capacity of the pilegroup under static conditions, in the earthquake load combination the design moment is higher than the elastic moment capacity, calling for pilegroup retrofit.

The common practice of attaching additional pile rows is chosen for the case examined. Two rows, each consisting of three piles are added in the transverse direc-
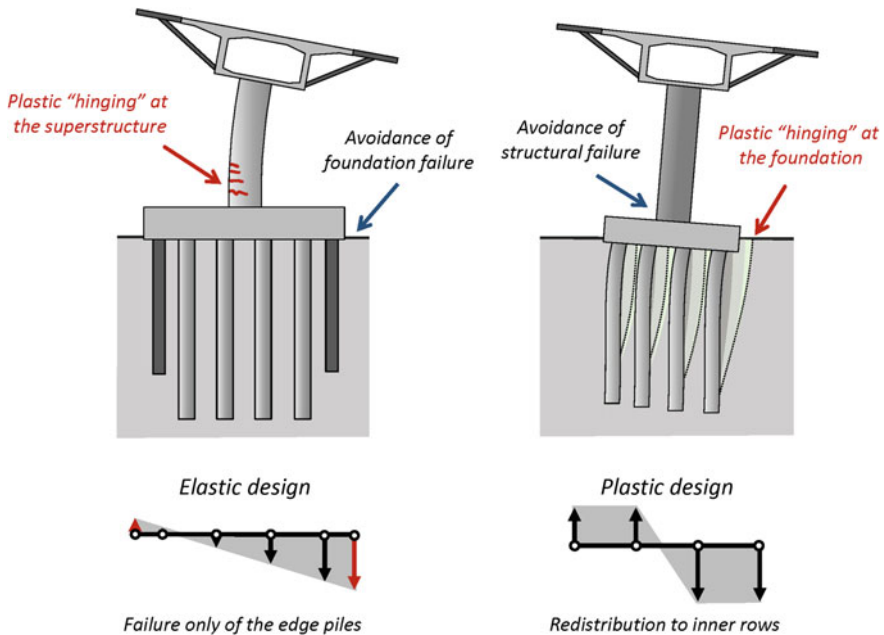

Fig. 17 Schematic illustration of the retrofitted pilegroup applying conventional capacity design (plastic "hinging" at the superstructure), compared with the non-retrofitted foundation applying the ductility design concept (plastic "hinging" at the soil-foundation system)

tion. The new piles have the same diameter but a smaller total length following an optimization process. This retrofit solution increases both the static axial resistance, $V_{s,d}$, and the conventionally-defined moment capacity of the pile group, $M_{el,d}$, which reaches the required safety level for the critical case of the seismic load combination ($M_{el,d}/M_{ed} = 1.02$).

As previously, capacity design aims to ensure that the pilegroup capacity is larger than that of the pier, thus guiding plastic hinging to the superstructure. On the contrary, a plastic design approach allows full mobilization of pilegroup moment capacity, by allowing load redistribution to the inner rows after the edge piles have fully mobilized their (vertical) bearing capacities. The two different approaches, along with the corresponding failure mechanisms, are illustrated in Fig. 17.

The performance of the retrofitted and of the non-retrofitted foundation is compared under nonlinear dynamic time history analysis. The TCU-068NS record of the 1999 M_w7.7 Chi-Chi earthquake in Taiwan is used as seismic excitation. The motion was scaled to PGA so that it approaches the design spectrum of the examined system (exceeding the design spectrum at the frequency range of interest). Therefore, the two foundation alternatives are assessed for a record in a similar range to their design considerations. The results of the comparison are summarized in Fig. 18 in terms of deck drift (δ) time histories, pier section moment–curvature (M–c) response, and foundation settlement (w) time histories.

Although the bridge with the non-retrofitted pilegroup experiences larger total deck drift δ, it shows a slightly better response in terms of structural deflection (Fig. 18a, b). The retrofitted pilegroup acts almost as a fixity, experiencing limited
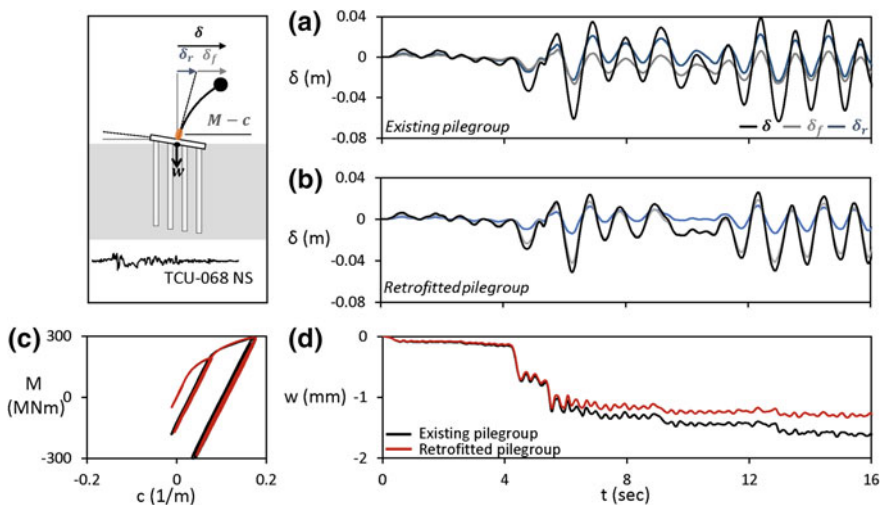

Fig. 18 Comparison of the two design alternatives using TCU-068NS record as seismic excitation in terms of: **a** time history of deck drift for the existing pilegroup (distinguishing between total, flexural, and rotational drift) compared to **b** deck drift for the retrofitted pilegroup; **c** comparison of pier moment–curvature response; and **d** time histories of settlement

nonlinearity. On the contrary, the non-retrofitted pilegroup is subjected to highly nonlinear response, with over 50% of the total deck drift being due to foundation rotation. The latter acts as a "fuse" for the superstructure, thanks to the activated energy dissipation mechanisms associated with soil yielding.

Consistently to the drift time histories, the bridge with the non-retrofitted pilegroup experiences slightly lower pier curvature and therefore somehow decreased structural damage (Fig. 18c) but with somehow larger total settlements (Fig. 18d). In contrast to the shallow foundation example, the settlements are practically negligible. Overall, the benefits of pilegroup retrofit are not evident. The total drift is reduced, but the flexural component is actually increased due to the stiffer foundation response. This implies increased pier damage, while the improvement in terms of settlements is negligible.

3 Seismic Faulting

3.1 Introduction

It is well known that earthquakes occur as a result of sudden movement of tectonic plates, releasing a large amount of energy in the form of seismic waves. Besides shaking, this dislocation of the seismic fault may propagate to the ground surface and cause severe damage or collapse of overlying structures. The fault rupture may appear at the ground surface in the form of a fault scarp or ridge, that can be several meters in height, extending several kilometers in length. When such fault cropping takes place directly underneath or in the immediate vicinity of a structure, it may lead to severe distress due to the imposed tectonic deformation.

Being a highly localised problem, smaller, disperse structures are generally less affected by faulting-induced deformations. This is not the case for large and long structures, particularly those with a very large physical footprint such as bridges, dams and power stations, which have a much higher probability of being "hit" by an outcropping fault rupture, and are also in general much less resilient to large ground deformations (Kung et al. 2001; Ulusay et al. 2002; Ural 2001).

The propagation of a seismic fault towards the ground surface is further complicated by the presence of soil, whose stress-dependent characteristics drastically alter the propagation trajectory. Moreover, the presence of an overlying structure alters the stress field, further complicating the phenomenon. An interaction with the propagating fault rupture and the soil develops, which may lead (under certain conditions) to partial or even complete diversion of the fault rupture path (Anastasopoulos et al. 2008; Bray et al. 1994). As it will be shown later on, such mechanisms can be exploited to enhance the resilience of structures against faulting.

The design against seismic faulting is a major challenge for designers and planners, due to the large uncertainty over both the location and the magnitude of such tectonic deformation. Improving the resilience of structures to seismic faulting can

be performed following two different strategies: (i) structural strengthening of the foundation and the superstructure to sustain the imposed tectonic deformation; or (ii) diversion of the fault rupture through modification of the soil in the vicinity of the structure, aiming to avoid the tectonic deformation.

3.2 Behavior of Structures Subjected to Faulting

The behavior of foundation-structure systems subjected to faulting-induced deformation is largely a function of their foundation type and dead load. Piled systems are in general sensitive to tectonic deformation, as they tend to transmit the deformation to the superstructure. Measures to improve performance include design of the piles for large ductility demands, or alternatively preventing the transmission of large bending moments to the superstructure by physically decoupling the pile from the cap by introducing a hinged-connection. A detailed description and analysis of such systems can be found in Anastasopoulos et al. (2013b).

The performance of foundation slabs is highly dependent on their stiffness and the surcharge load applied by the structure. Lightly-loaded structures do not significantly alter the propagation path and are therefore subjected to larger distress. If the foundation slab is rigid enough, it may lose contact with the soil, and end up acting as a cantilever or simply supported beam, depending on the type and location of the fault outcrop (Fig. 19). Such loss of support will in turn induce significant sagging or hogging deformation of the foundation slab. Unless designed for such stressing, this may lead to failure of the foundation and of the overlying structure (Anastasopoulos 2005).

When the foundation slab is heavily loaded, a more interesting phenomenon may take place. Since the propagation of the fault rupture is essentially a shear failure problem, the rupture will always propagates along the minimum energy path, i.e. it will "try" to avoid areas of higher shear strength. And since the shear strength of soil
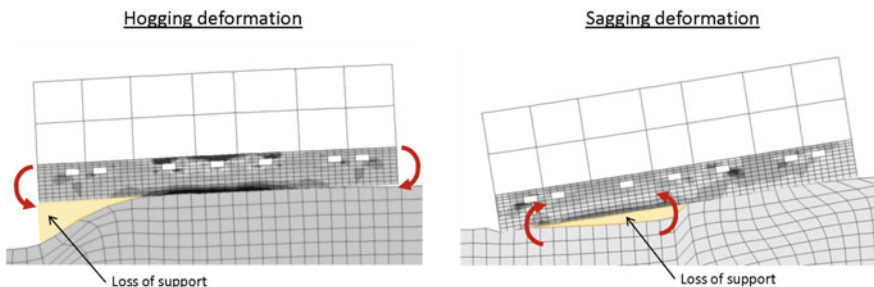

Fig. 19 Typical observed behavior for structures founded on a foundation slab subjected to dip-slip faulting. Depending on the location of the fault rupture, the foundation structure system may be subjected to either hogging (left) or sagging (right) deformation

is a function of the confining stress, the rupture will tend to avoid propagating through areas of increased stresses, such as the area underneath a heavily loaded foundation slab. Under such conditions, fault rupture diversion is possible, as it has been observed both in the field and in the laboratory (Anastasopoulos 2005; Anastasopoulos and Gazetas 2007a; Anastasopoulos et al. 2007, 2009).

Such phenomena have been investigated for both normal and reverse (dip-slip) faults (Tolga Yilmaz and Paolucci 2007; Anastasopoulos and Gazetas 2007b; Anastasopoulos et al. 2008a, b), including case histories, analysis methods, and design recommendations. It is these interaction mechanisms that form the basis for improving the resilience of structures to faulting, either by improving their resistance to loss of support or by actively diverting the potential fault rupture.

3.3 Foundation–Structure Retrofit

Strengthening of the foundation system is a first obvious possibility. Through such strengthening, the foundation slab can be designed to safely sustain the bending moments associated with the previously discussed loss of support. Given the difficulties in predicting the precise location of the fault outcrop, the design should be performed on the basis of envelopes of loading (including both hogging and sagging deformation), considering all possible locations of the fault rupture. A second possibility is to increase the dead load of the foundation–structure system to promote fault rupture diversion.

Such methods have been shown to greatly improve life safety of new structures, and have been applied to new constructions (Gazetas et al. 2008; Anastasopoulos et al. 2010a). However, in the context of improving resilience of existing structures, applying such measures can be costly and technically challenging. The cost of such retrofit, involving complete renovation of the foundation system, may be comparable to the cost of re-building the entire structure. Furthermore, such measures, while vastly improving life safety, are less effective at preserving serviceability, which may be just as critical for important structures related to lifelines or those of historic or social significance. An additional problem is related to the settlements under normal static conditions, which can become excessive due to the direct or indirect increase of the dead load of the system. For new structures, such considerations can be incorporated at the design stage, but for existing ones additional complications may arise.

It must also be pointed out that, although performance can be improved by such methods, the permanent rigid-body rotations cannot be avoided. In most cases, the associated rotations vastly exceed those permissible by modern design standards, rendering the structure unfit for purpose after faulting (Ulusay et al. 2002; Faccioli et al. 2008). Despite their obvious significance in avoiding casualties, these measures may prove to do little to affect the direct and indirect costs. This is particularly problematic in the case of critical infrastructure, where ensuring serviceable and fit for purpose is paramount to ensuring the wellbeing of the population at large.

3.4   Mitigation Through Weak Barriers

An alternative mitigation technique is introduced to enhance the resilience of existing critical structures, overcoming the previous problems, avoiding retrofit, greatly improving serviceability, and also being insensitive to the foundation type. The method aims at altering the fault rupture path by installing a weak wall barrier close to the structure that requires protection (Fig. 20). In the previously discussed case of the heavily-loaded foundation, the high surcharge load produced a bulb of increased strength material beneath the foundation, which tends to be "avoided" by the propagating shear band.

Exactly the opposite is achieved by the weak barrier, which introduces a weak preferential rupture path that acts as an "attractor" for the fault rupture, directing it up and away from the structure. The barrier acts as a "fuse", diverting the fault rupture and absorbing much of the faulting-induced deformation, thus efficiently protecting the structure. It has been shown that such a concept may offer adequate protection in terms of structural integrity, in addition to reduction of permanent rotation. It should
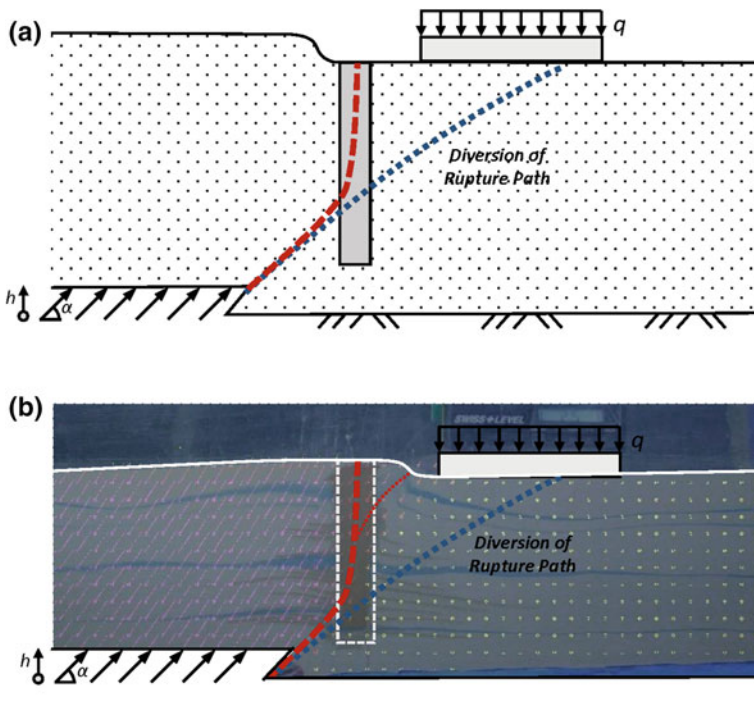

Fig. 20 Mitigation through weak wall barrier for a foundation subjected to reverse faulting: **a** sketch of the main concept; and **b** experimental image of the response of such a wall using the Soil Bentonite Wall (SBW) concept (Fadaee et al. 2013)

be noted that the method discussed herein is applicable to reverse faulting, but similar methods could be conceived for other types as well.

The performance of such a weak wall barrier can be simulated satisfactorily using the FE method, employing a soil constitutive model capable of reproducing softening of the soil at large strains. Both the ability to model soil softening and appropriate considerations for the mesh used for the analysis are essential to reproducing the highly localised shear bands in the soil which characterise the fault rupture propagation problem (Anastasopoulos et al. 2007). Such a simplified analysis technique is presented in Anastasopoulos et al. (2008a). The analyses discussed herein employ such a strain softening constitutive model, assuming plane strain conditions.

As shown in Fig. 20b, a weak wall barrier can be materialized by means of a Soil Bentonite Wall (SBW) (Fadaee et al. 2013). Such walls are typically used for seepage control or contaminant mitigation, and are constructed using diaphragm wall machinery. Having a lower strength (of the order of $S_u = 0.3$ kPa) than the surrounding soil, the soil-bentonite mixture produces a "fuse", which can both divert the fault rupture and absorb a substantial part of the deformation. Through a combined numerical and experimental study, it was shown that such a barrier is able to divert the fault rupture away from the structure, offering a very good level of protection.

The mitigation concept was further developed to overcome some of the weaknesses of the SBW system, regarding the predictability of its long-term performance, and reliability. The introduced "smart" barrier is similar in concept to the SBW, but the "fuse" is realised by a series of elastoplastic elements at increments of depth within the soil. Such a system is far easier to predict and tailor to specific requirements. In order to understand how such a system works, and how to specifically design such a "smart" barrier for a project, it is worth understanding the specific mechanisms of the fuse system.

In this context, let's consider the "smart" barrier as a series of elastoplastic elements, placed at vertical increments as shown in Fig. 21. Three stages of response can be distinguished:

(1) <u>Before faulting</u>, each element must elastically resist the geostatic lateral earth pressures due to the weight of the soil and the structure without undergoing any significant deformation.
(2) <u>During faulting</u>, the fuse elements must compress and deform plastically before the soil foundation system fails, i.e., before the fault rupture is able to fully mobilise the shear resistance of the soil underneath the foundation.
(3) <u>After faulting</u>, the now-deformed device must resist the new static stresses without significant deformation, just as before loading.

Therefore, the basic design criteria for such a device is to resist the in situ lateral earth pressures, with some factor of safety, and to deform plastically soon after these pressures are exceeded.

Using these basic principles a design methodology for such devices can be formulated using an analogy to active and passive conditions (Fig. 21). Before faulting, the wall is subjected to active or at-rest earth pressures, depending on the excavation sequence (Fig. 21a). When subjected to reverse faulting-induced deformation, the
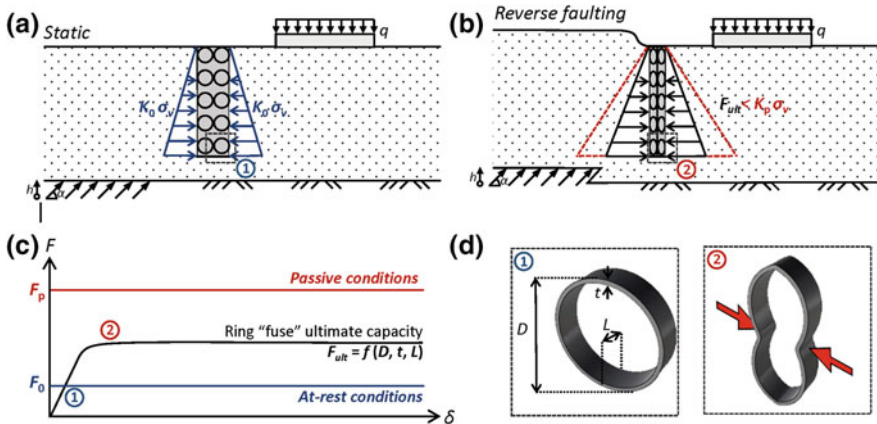
Fig. 21 Concept of a "smart" barrier: **a** static loading, in situ (K_0) earth pressures; **b** reverse faulting, tendency to develop passive (K_p) earth pressures; **c** force-displacement response of a ring-fuse; and **d** key dimensions and illustration of compressive ring fuse failure

earth pressures will tend towards passive (Fig. 21b). Each row of rings with plastic failure capacity F_{ult} can be designed to have an adequately large factor of safety against static loading:

$$FS_{st} = F_{ult}/F_a \geq 1.5 \tag{3.1}$$

where: F_a is the lateral force due to active conditions. In a similar manner, each row of rings can be designed for an adequately small "apparent" factor of safety against passive conditions:

$$FS_f = F_{ult}/F_p \leq 1/1.5 \tag{3.2}$$

where: F_p is the lateral force due to passive conditions. If the rings are designed to yield under such compressive loading, F_p will never develop and this is why FS_f is an "apparent" factor of safety.

As long as the faulting-induced lateral force along the wall remains below its passive value, passive conditions will not develop, and the fault rupture will not propagate towards the structure. Instead, the wall will be compressed, "absorbing" the faulting-induced deformation by compressive failure of the sacrificial elements.

As discussed in more detail in Anastasopoulos and Jones (2018), the simplest form of such perfectly elastoplastic sacrificial members consists of steel rings of diameter D, out-of-plane length L, and thickness t. The ultimate capacity F_{ult} is simply a function of geometry and steel strength. Such sacrificial devices can be constructed from standard construction materials, consisting of circular hollow sections (CHS) layered between sheet pile walls and again installed like a diaphragm wall.

Such schemes have been shown to improve the performance of structures subjected to reverse faulting. An example is shown in Fig. 22, referring to a rigid $B = 10$ m foundation with $q = 20$ kPa subjected to $h = 1$ m thrust faulting with free field outcropping $s = 5$ m (mid-way beneath the foundation), propagating through an idealized dense sand layer of $H = 20$ m thickness.

The unprotected reference case (Fig. 22, top), is compared to protection with a SBW (Fig. 22, middle) and to the "smart" barrier with sacrificial rings (Fig. 22, bottom). The "smart" barrier and the SBW are effective at diverting the fault rupture away from its initial trajectory (which would intersect with the foundation). The sacrificial devices fail plastically soon after the faulting deformation begins (in the specific case, plastic capacity is reached at $h/H \approx 2\%$). Further evidence of the schemes effectiveness can be seen in the induced rotations. The unprotected foundation sustains a rotation $\theta \approx 3°$, a value that is clearly beyond any reasonable serviceability limit. The SBW-protected foundation performs appreciably better, with its rotation θ not exceeding 0.4°. The performance of the "smart" barrier is even better, with $\theta \approx 0.2°$.
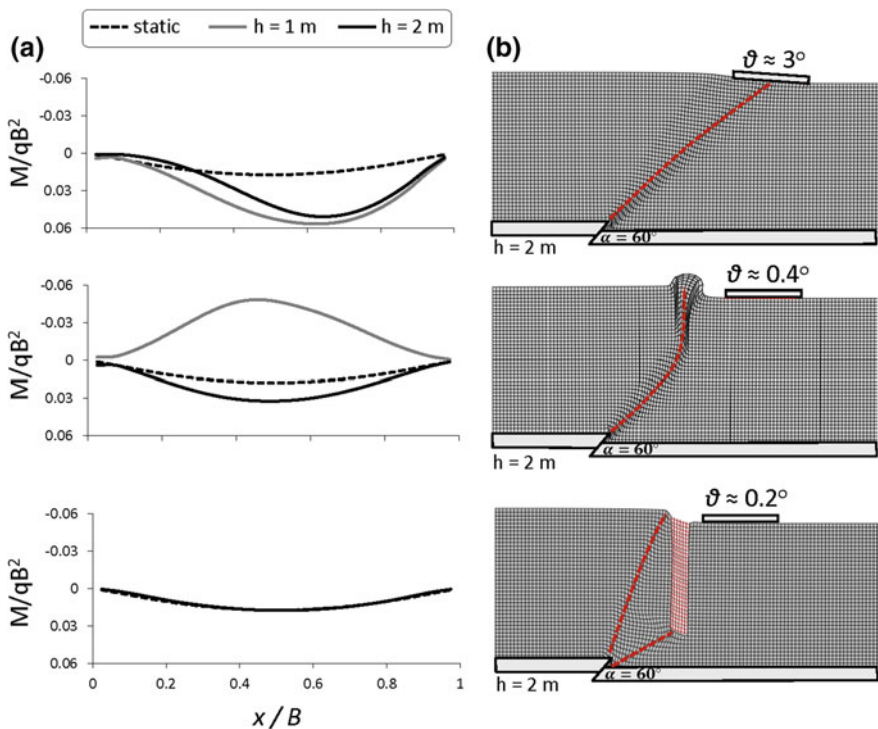

Fig. 22 Mitigation using a $B_w = 3$ m "smart" barrier for a $B = 10$ m foundation carrying $q = 20$ kPa surcharge load, at distance $s = 5$ m. Comparison of the unprotected case (top) to a SBW (middle) and a "smart" barrier (bottom). Foundation distress is shown by normalized foundation bending moment M/qB^2, along with the deformed mesh and foundation rotations for $h = 2$ m

As shown in Fig. 22, the same conclusions can be drawn based on the normalized foundation bending moments M/qB^2. Without mitigation (Fig. 22, top), the bending moment is almost 5 times larger than its static value, something that would imply failure. The SBW reduces substantially the distress of the foundation (Fig. 22), but still M/qB^2 is about 2 times larger than the initial static value. The "smart" barrier demonstrates the most dramatic improvement, with the bending moments in the foundation practically indistinguishable from the static case.

The "smart" barrier offers a potentially simple and cost effective path to improve the resilience of structures subjected to tectonic faulting, making use of controlled failure and the concept of sacrificial members ("fuses") to redirect and control large tectonic deformations.

3.5   Application of Sacrificial Members to Bridges

Similar sacrificial members can be used to protect bridges from faulting-induced deformation. Instead of trying to divert the fault around the bridge foundations, the "fuses" can be installed directly on the structure. The main concept is the same, aiming to guide plastic deformations at strategically located points (i.e., the sacrificial members), protecting the bridge structure from damage. One investigated concept involves the installation of the previously discussed ring-type sacrificial elements between the deck and the piers.

The rings can be designed to remain elastic under normal design loads, yielding in a controlled manner when the bridge is subjected to tectonic deformation, so as to absorb a big part of the imposed deformation protecting the bridge deck. Such a solution can be particularly effective for long continuous deck systems, which have been shown to be extremely sensitive to tectonic deformation (Anastasopoulos et al. 2008c). The performance can be improved by switching to a multi-span simply supported deck, but this is neither efficient for static loads nor is it practical for existing structures. Instead, the replacement of existing bearings with sacrificial devices offers a relatively inexpensive route to enhance the resilience of such existing structures.

The sacrificial rings can be installed as shown in Fig. 23. The example refers to an actual motorway bridge having a continuous prestressed concrete deck over 5 spans of 115.6 m total length. In the initial design, the deck is rigidly connected to piers P3 and P4, resting on sliding bearings at piers P1 and P2, and on four elastomeric bearings at each abutment. Such indeterminate structural systems are known to be sensitive to differential displacements, and a simple remedy is the adoption of a determinate system with simply-supported decks (Anastasopoulos et al. 2008c). However, such a solution requires multiple joints, capable of sustaining large deformations, and is not the most efficient for all other types of loading.

Figure 23 offers an example comparison, considering a reverse fault of vertical offset $h = 1$ m emerging at the ground surface between P3 and P4. The mitigation scope is to minimize the stressing of the continuous deck, by directing plastic deformation onto the sacrificial rings. As shown in Fig. 23a, when subjected to tectonic
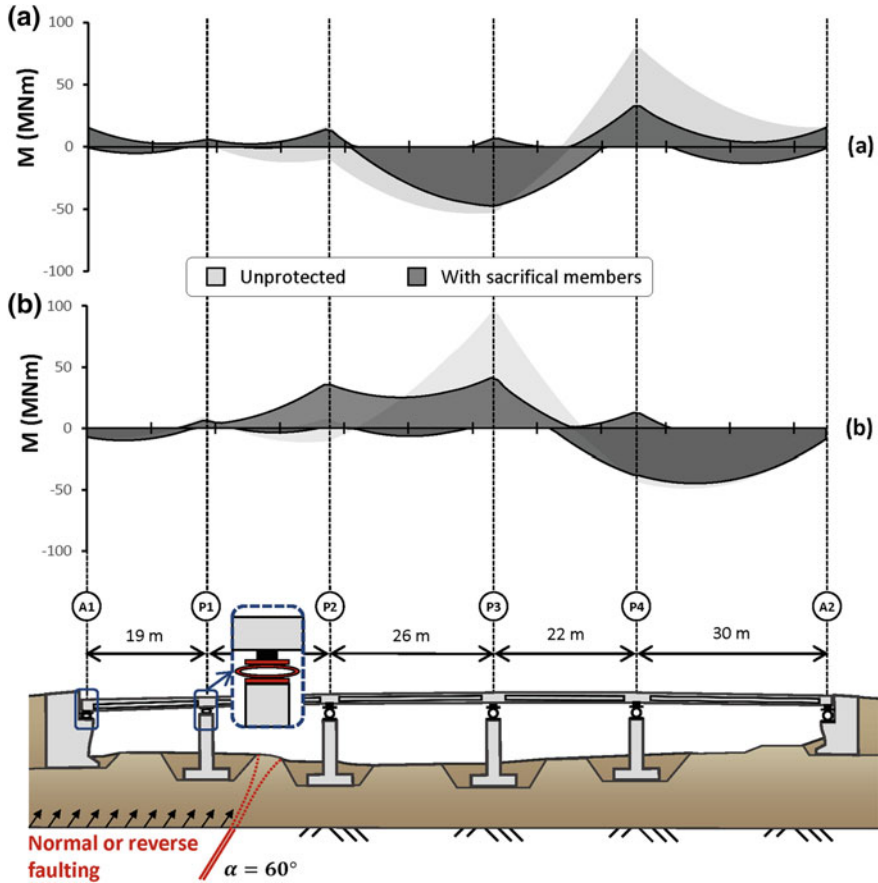
Fig. 23 Installation of sacrificial members to enhance the resilience of on existing continuous deck bridge subjected to $h = 1$ m normal and reverse faulting. Bending moment envelopes for fault outcropping between piers P1 and P2 for: **a** normal; and **b** reverse faulting. The sketch at the bottom is indicative of reverse faulting

deformation, the sacrificial ring at P4 yields, reducing the imposed deck flexural distortion. As a result, the peak (i.e., absolute maximum) deck bending moments are reduced with the sacrificial rings (Fig. 23b) to 30 MNm, as opposed of 80 MNm without any protective devices. It may therefore be concluded that the addition of such sacrificial rings may be employed to enhance the resilience of existing continuous deck bridges.

4   Earthquake Crisis Management

4.1   Introduction

The previous sections presented retrofit concepts and mitigation techniques targeting at enhancing the resilience of existing structures against seismic shaking and faulting. The key scope of such approaches is to minimize the direct consequences of a major seismic event. The indirect consequences of an earthquake, such as the deterioration of the serviceability of transportation and lifeline networks can be equally, or in many cases even more, detrimental. The latter can either be due to a decrease of network capacity (due to damage of critical infrastructure), or due to the increased demand triggered by the damage within the neighbouring urban environment. In the 1999 $M_s 5.9$ Athens earthquake, for example, the transportation network was severely affected, although its infrastructure remained unscathed.

   In contrast to the direct consequences of a strong earthquake, which cannot always be avoided due to monetary constraints, the indirect consequences can be effectively mitigated employing a coordinated crisis management system. Evidently, inspection of the affected infrastructure will be essential after a strong seismic event. However, an immediate estimate of the seismic damage of critical structural components is necessary: (i) to decide on the needs of emergency inspection; and (ii) to optimize allocation of inspection teams. At a larger scale, such an estimate enables a first quantification of the damage distribution, facilitating the detection of sensitive areas.

   After a major earthquake, the main dilemma will be whether there is a need for interruption of network operation. While preemptive motorway closure until post-seismic inspection may seem as a safe option, it will unavoidably obstruct operation of rescue teams, and may actually lead to increased indirect losses. On the other hand, maintaining the network in operation without inspection may have dramatic consequences, as depicted in Fig. 24.

Fig. 24 Damage of motorway bridges during the 1994 Northridge earthquake (left); and a bus marginally stopping before a collapsed bridge of Hanshin Expressway Route No. 3 (right)

In a similar manner, at a bigger urban scale, immediate coordinated actions with respect to critical facilities (hospitals, schools, etc.) or lifelines (water storage facilities, power plants, etc.) are essential in efficiently mitigating the indirect losses after a strong seismic event. Even if the structural damage of critical infrastructure is not substantial, the lack of coordinated action will increase the feeling of insecurity to the affected groups, hence proliferating the generalized sense of panic and causing potentially further losses or even additional injuries.

In the following sections, a simple method for real-time seismic damage assessment is outlined, followed by an example application of a crisis management system to a major motorway in Athens, Greece.

4.2   Real-Time Seismic Damage Assessment

A key component of a crisis management system is a method to estimate the seismic damage of critical structures in real time. The seismic vulnerability of infrastructure can be estimated using fragility curves. The latter relate the probability of an element at risk to reach or exceed a specific damage state with seismic intensity, which is typically expressed by a seismic intensity measure (IM). A comprehensive review of the state of the art on the subject can be found in Pitilakis and Crowley (2014). An alternative approach is Incremental Dynamic Analysis (IDA), according to which the numerical model of the structure is subjected to one or more seismic excitations, progressively scaled to different levels of increasing intensity (Vamvatsikos and Cornell 2002). The resulting IDA curves correlate a damage index (DI) with a single IM.

Recognizing that PGA and PGV are not sufficient indices of seismic intensity, many researchers have proposed a variety of intensity measures, such as the Housner Intensity (Housner 1952) and the Arias Intensity (Arias 1970). Although such IMs are much more efficient, their correlation to seismic damage is not always adequate (Garini and Gazetas 2013). This implies that a single IM is possibly not adequate to capture all of the characteristics of a seismic motion. An alternative approach was introduced in Anastasopoulos et al. (2015a), where instead of selecting an optimum IM, advanced econometric modeling is employed to combine an appropriate number of statistically significant IMs.

Through such an approach, a simple method for real time seismic damage assessment was developed, initially on the basis of an idealised single degree of freedom (SDOF) system. Despite its simplicity, such a SDOF equivalent can be considered as a reasonable approximation for a variety of structures, such as overpass bridges, storage tanks, and wind turbines (Fig. 25). The method requires a large number of nonlinear dynamic time history analyses, using multiple seismic records as seismic excitation. Based on the results of the analyses, advanced econometric modelling is applied to develop multivariate equations, expressing seismic damage as a function of statistically significant intensity measures (IMs).
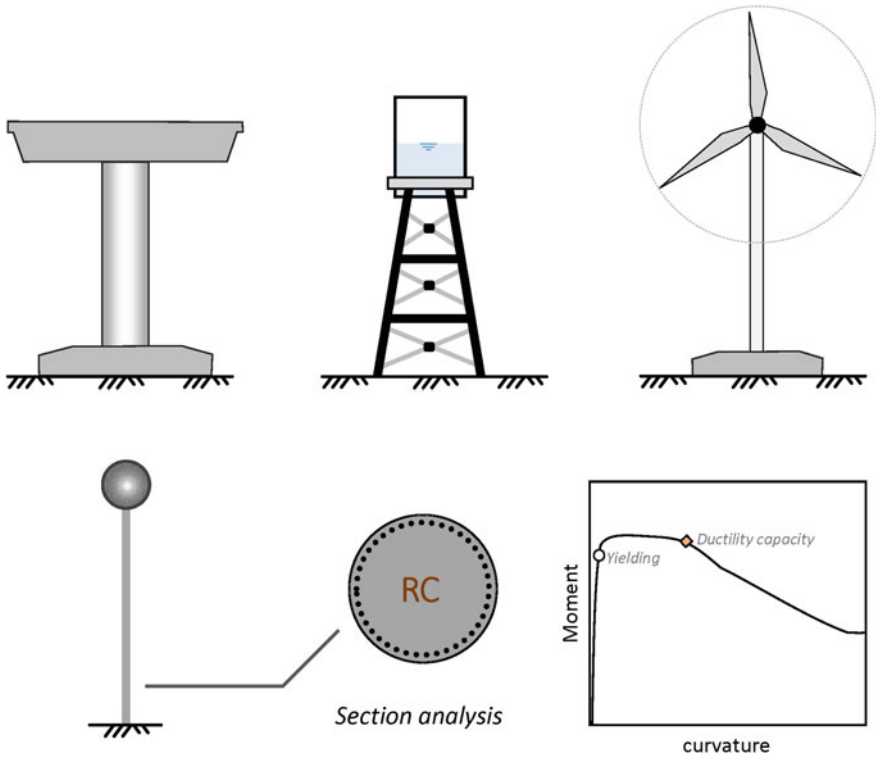
Fig. 25 Critical infrastructure that can be simplified as a nonlinear SDOF system

Aiming to have a wide enough range of strong motion characteristics, 29 seismic records were selected and used as seismic excitation. For each one of these records, the PGA (peak ground acceleration) was scaled from 0.1 to 1.2 g, leading to a total of 348 acceleration time histories that were used to examine the response of the equivalent SDOF system to different levels of seismic excitation. The maximum drift ratio, $\delta_{r,\max}$ (%), can be used as a damage index (DI):

$$\delta_{r,\max} = \frac{\delta_{\max}}{h} * 100\% \tag{4.1}$$

where: $\delta_{\max}$ is the maximum lateral displacement at the top of the cantilever, and h is the height of the SDOF system.

Within the context of a crisis management system, the damage needs to be further classified in damage states (no damage, small damage, serious damage, and severe damage up to collapse). An example showing the correlation between $\delta_{r,\max}$, as obtained from the 348 analyses, and one of the most efficient IMs (the Velocity Spectrum Intensity, VSI (Von Thun et al. 1988)) is presented in Fig. 26. Evidently, a single IM is a poor index of seismic damage. It is worth observing that for VSI=
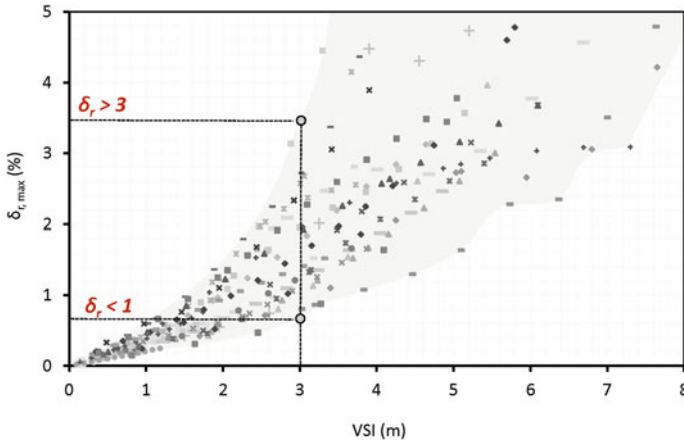
Fig. 26 Correlation of $\delta_{r,\max}$ with one of the most efficient IMs examined (VSI)

3 m, $\delta_{r,\max}$ varies from less than 1% (minor damage) to over 3% (severe damage or collapse). Such differences of the damage state for the same IM indicate the importance of the characteristics of the seismic excitation. The frequency content, duration, and so on, may have a significant effect on the performance of a structure and cannot be ignored.

Despite the fact that PGA and PGV (Peak Ground Velocity) are commonly used as IMs, it is acknowledged that a large PGA alone does not always result to severe structural damage, and the same applies to a large PGV. Other indices, such as the Peak Ground Displacement (PGD), the strong motion duration (T_d), spectrum intensity (SI), and spectral characteristics, can be simultaneously considered in damage estimation. Within this context, a total of 19 IMs were selected, each one describing different characteristics of the seismic motion (Garini and Gazetas 2013). All IMs were tested individually and the obtained correlations are similar to the one of Fig. 26, confirming that a single IM cannot be used for reliable damage prediction.

A nonlinear regression model was estimated for the selected DI, and all the 19 examined IMs were tested for potential inclusion in the model. The nonlinear regression model is of the form:

$$Y_i = EXP[\beta_0 + \beta_1 * X_{1_i} + \varepsilon_i] \qquad (4.2)$$

where: Y_i is the dependent variable (i.e., the damage index $\delta_{r,\max}$) which is a function of a constant term β_0 and a constant β_1 times the value X_1 of independent variable X (i.e., the IMs) for observation $i(i = 1, 2, …, n)$ plus a disturbance term ε.

All explanatory parameters included in the models are statistically significant at 0.90 level of confidence (with most of them being statistically significant at 0.99 level of confidence). Finally, the effect of an IM on the DI may not be of a linear form. Hence, several transformations (power forms, logarithmic relationships, etc.) were
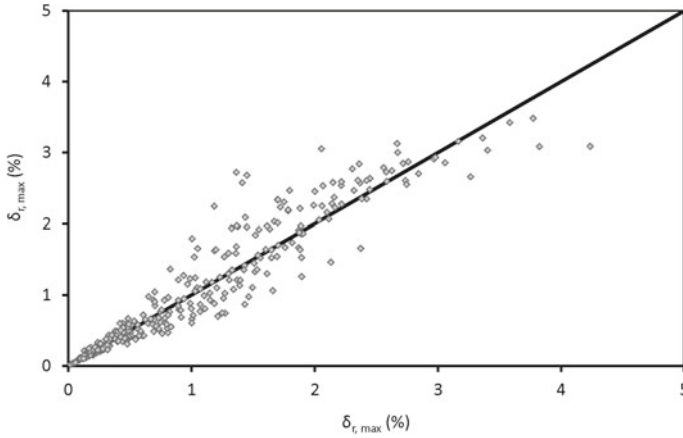
Fig. 27 Observed (FE analysis) maximum drift ratio $\delta_{r,max}$ versus predicted using the nonlinear regression model equation

tested, with the ones presented below, providing the best statistical fit and forecasting accuracy potential. The resulting linear regression model equation for the selected DI is as follows:

$$\delta_{r},\max = e^{\left[\begin{array}{c} \beta_1*LN(PGA)+\beta_2*\frac{1}{PGV}-\beta_3*\frac{1}{\sqrt{PGD}}-\beta_4*A_{RMS}^2+\beta_5*\frac{1}{\sqrt{D_{RMS}}}-\beta_6*\frac{1}{\sqrt{I_c}}-\beta_7*\frac{1}{\sqrt{S_E}}+\beta_8*\frac{1}{CAV} \\ +\beta_9*\sqrt{VSI}-\beta_{10}*\sqrt{H_I}-\beta_{11}*\frac{1}{SMA}+\beta_{12}*\frac{1}{SMV}+\beta_{13}*LN(T_P)-\beta_{14}*\frac{1}{T_{mean}}+\beta_{15}*\sqrt{D_{sig}} \end{array}\right]}$$

(4.3)

The derived equation includes 15/19 IMs, which were found to be statistically significant. The efficiency of the proposed nonlinear regression model equation was examined comparing the predicted damage of the SDOF system by using the corresponding equation to the observed one, as obtained from the numerical analysis. Figure 27 presents an overview of the 348 FE analyses. The overall statistical fit of the model can be assessed through the Adjusted R-squared, as follows:

$$R_{adjusted}^2 = 1 - [(n-1)/(n-p)] * \left[\left(\sum_{i=1}^{n} \left(Y_i - \hat{Y}_i\right)^2 \right) / \left(\sum_{i=1}^{n} (Y_i - \bar{Y})^2 \right) \right] = 0.949 \quad (4.4)$$

where Y and $\hat{Y}$ are the observed and predicted values, respectively, of the dependent variable (i.e., DI) for observation $i(i = 1, 2, …, n)$, $\bar{Y}$ is the observed mean value of the dependent variable, and p is the number of explanatory model parameters. More details on the development of the model can be found in Anastasopoulos et al. (2015a).

The efficiency of the nonlinear regression model equation is demonstrated more clearly in Fig. 28, where the observed damage states of the numerical analysis are compared to the predicted ones using the nonlinear regression model equations. The damage states considered are based on typical values of drift ratio for each damage

Fig. 28 Efficiency of nonlinear regression model equations for the 29 historic records used. Observed, using the FE model (1st column) versus predicted, using the nonlinear regression model equation (2nd column) damage state based on maximum drift ratio $\delta_{r,\max}$

state with reference to Response Limit States (Priestley et al. 1996). It is also shown on how many of the total of the 348 dynamic analyses the observed damage state is the same with the predicted one and on how many there is one state difference.

The efficiency of the nonlinear regression model equation is further examined using a set of 15 out-of-sample records. In Fig. 29, the observed damage states of the numerical analysis are compared to the predicted ones using the nonlinear regression model equation. It is also shown on how many of the total of 15 dynamic analyses the observed damage state is the same with the predicted one. The nonlinear regression model equations offer a satisfactory way to estimate the structural damage of SDOF systems, within the context of real time damage assessment.

The same analysis can be conducted using a different, possibly more sophisticated, FE model and/or a different set of IMs. The purpose of this section was to demonstrate the efficiency of the proposed method in a relatively simple manner. In the next section the same concept is applied to more complicated systems as part of an application of a crisis management system on a metropolitan motorway.
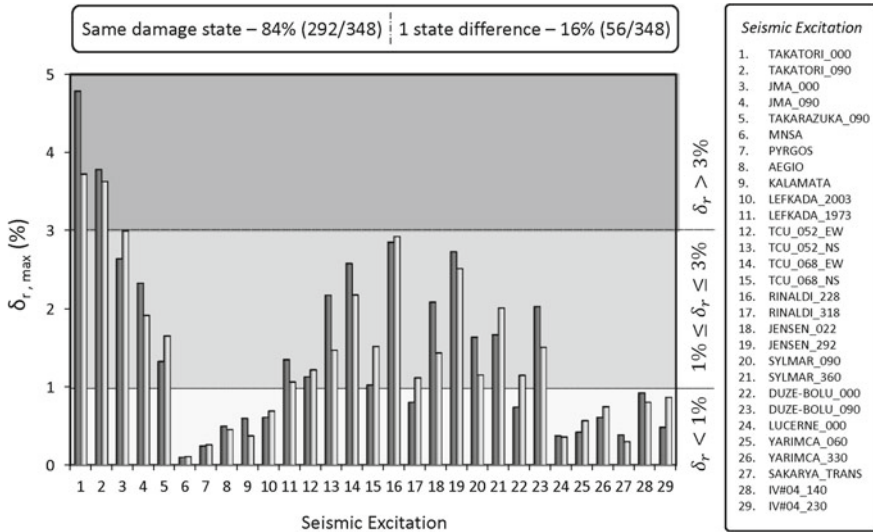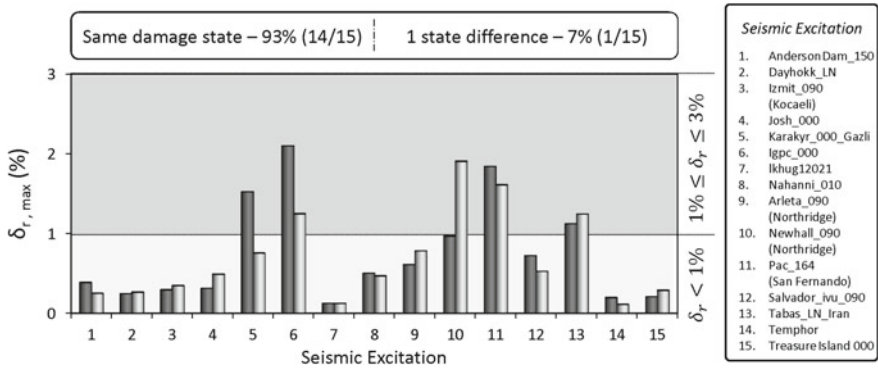
Fig. 29 Efficiency of nonlinear regression model equations for 15 out-of-sample historic records. Observed, using the FE model (1st column) versus predicted, using the nonlinear regression model equation (2nd column) damage state based on maximum drift ratio $\delta_{r,\mathrm{max}}$

4.3 Example Application: Attiki Odos Motorway—Athens, Greece

Several emergency response systems have been developed worldwide (e.g., Erdik et al. 2011) and with respect to transportation networks, there have been some attempts to apply seismic risk assessment to motorway systems, such as the one in the Friuli-Venezia Giulia region of NE Italy (Codermatz et al. 2003). A rapid response (RARE) system for motorway bridges is discussed herein as part of a European research project, applying the previously discussed simple method for real-time seismic damage assessment using the Attiki Odos Motorway (Athens, Greece) as a case study (Anastasopoulos et al. 2015a, d).

The large number and complexity of the bridges encountered in motorways is a particular challenge for such an endeavor. A motorway typically includes a few hundreds of bridges and therefore a classification scheme is necessary in order to examine specific representative cases instead of every single bridge. Even if a few representative bridges are selected, the development the previously discussed nonlinear regression model equations requires a large number of dynamic time history analyses. The computational effort to perform such a set of analyses using detailed 3D FE models (such as the one of Fig. 30a) is currently prohibitive. However, the use of oversimplified SDOF models may lead to gross errors (Anastasopoulos et al. 2015d).

Therefore, there is a need for development of simplified, yet realistic models. Such a simplified method was outlined in Anastasopoulos et al. (2015d), considering an equivalent SDOF system of the most vulnerable pier with appropriate springs and dashpots at its top and bottom to account for key structural components and nonlinear SSI. The latter was extended to account for abutment stoppers and was validated for different bridge typologies. It was shown to compare fairly well with detailed FE

models of the entire bridge-foundation-abutment-soil system, and was subsequently used to derive nonlinear regressions model equations. An overview of the simplified model is shown in Fig. 30, and more details can be found in Agalianos et al. (2017b), Sakellariadis et al. (2018).

The previously discussed nonlinear regression modeling methodology is applied for one of the representative cases examined. The extended simplified model of the A01-TE20 overpass bridge of Attiki Odos motorway (Fig. 30c) was subjected to real seismic excitations, scaled to PGA ranging from 0.1 to 1.2 g in order to derive the necessary dataset. The output of the numerical analyses refers to the structural damage of the bridge, expressed in terms of $\delta_{r,\max}$, as a function of the 19 IMs. The results are then used to develop nonlinear regression model equation, correlating $\delta_{r,\max}$ with statistically significant IMs:

$$\delta_{r,max} = e^{\left[\beta_1 LN(PGA)+\beta_2 \frac{1}{PGV}-\beta_3 \frac{1}{\sqrt{PGD}}-\beta_4 A_{RMS}^2+\beta_5 \frac{1}{\sqrt{D_{RMS}}}+\beta_6 \frac{1}{SMV}+\beta_7 LN(T_P)-\beta_8 \frac{1}{T_{mean}}+\beta_9 \sqrt{D_{sig}}\right]}$$
(4.5)

In this particular example, only 9/19 IMs were found to be statistically significant. The efficiency of the nonlinear regression model equation is examined comparing the predicted structural damage (using the derived equation) to the observed one (as obtained from the FE analyses employing the simplified model). The comparison, for all dynamic time history analyses, is summarized in Fig. 31a while the overall statistical fit can be assessed through the Adjusted R-squared:
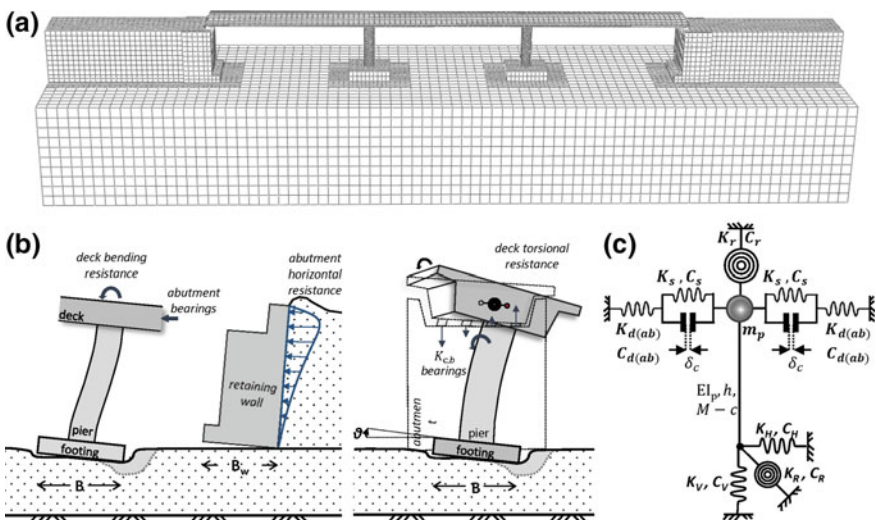

Fig. 30 Outline of simplified modelling technique: **a** detailed 3D FE model of bridge A01-TE20 used as benchmark; **b** illustration of key mechanisms; and **c** simplified model

$$R_{adj}^2 = 0.96 \qquad\qquad\qquad\qquad (4.6)$$

The predicted damage compares satisfactorily well with the observed damage for all of the examined seismic excitations. However, the developed nonlinear regression model equations were developed using the same dataset. Therefore, it is important to verify the predictive accuracy of the derived model equations using out-of-sample data. Such a verification was performed using a set of 5 out-of-sample seismic records. The latter were used to conduct a new set of dynamic analyses, this time using as a benchmark the rigorous 3D model of the A01-TE20 bridge (Fig. 30a).

At this point, it is should be pointed out that the nonlinear regression model equation was developed on the basis of dynamic analyses employing the simplified model. Its verification using out-of-sample data against the detailed 3D model is therefore a nontrivial test. Figure 31b summarizes the comparison in terms of predicted (equation) versus observed (detailed 3D FE model) $\delta_{r,\max}$. This comparison offers a simultaneous verification of the simplified model, and of the nonlinear regression method. Finally, in the same graph, both the observed (detailed 3D model) and the predicted (equation) structural damage is characterised according to typical damage states. The nonlinear regression model equation predicts correctly the damage state in all cases examined. Therefore, overall, the nonlinear regression model equation offers a satisfactory estimate of the structural damage in the context of a crisis management system.

The 190 bridges of Attiki Odos were subdivided in 6 classes and for each class a representative bridge was selected and analysed in both directions of seismic loading. The classification scheme and the details of the bridges can be found in Anastasopoulos et al. (2015d, 2018). The analysis followed the same procedure as for the A01-TE20 bridge, resulting to 6 nonlinear regression model equations for each direction of seismic loading. This outcome was the key step for the (pre-seismic) implementation of a crisis management system.
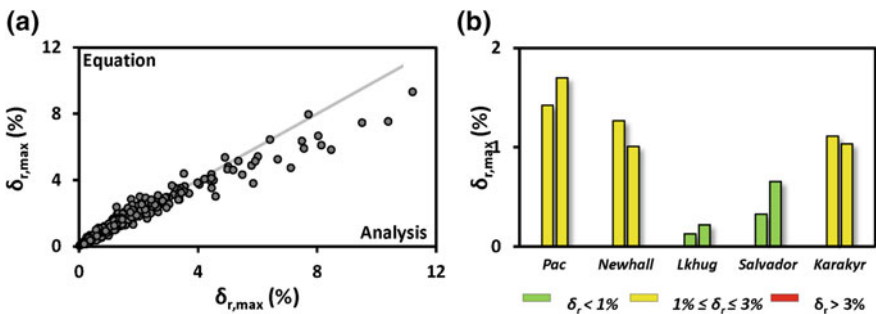
Fig. 31 **a** Summary of dynamic time history analyses in predicted (nonlinear regression model equation) versus observed (FE analysis using the simplified model) structural damage expressed with $\delta_{r,\max}$; efficiency of nonlinear regression model equation for 5 out-of-sample historic records in terms of $\delta_{r,\max}$ and the resulting damage state
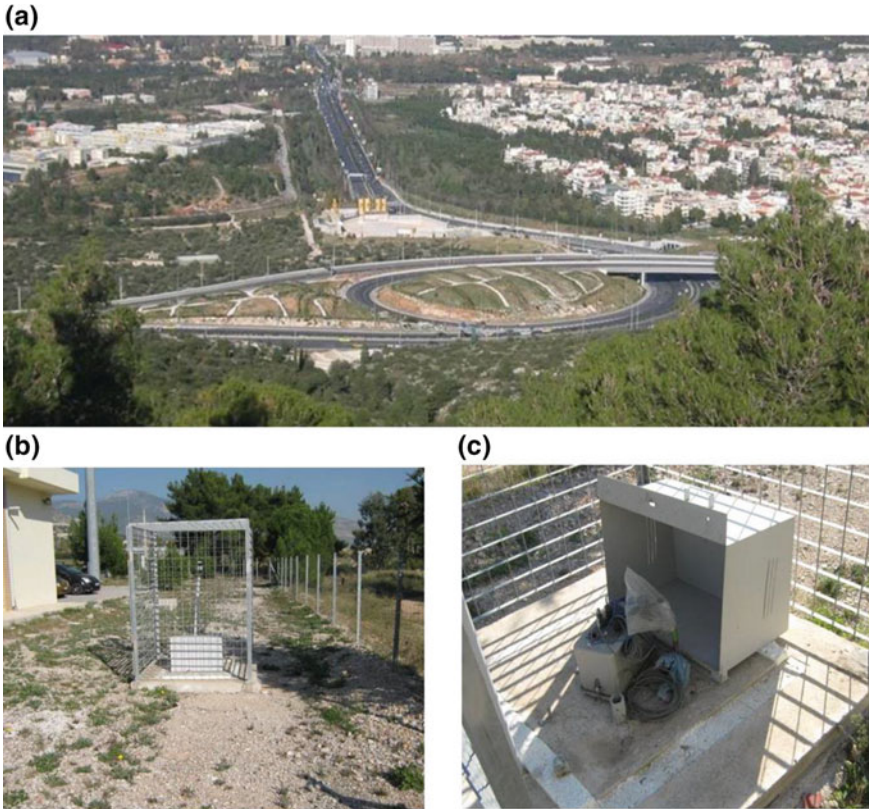
Fig. 32 View of one accelerograph station: **a** the highway section monitored; **b** the station with the GPS antenna; and **c** close-up of recording instruments and wiring

The further steps needed, include the development of a comprehensive GIS database of motorway infrastructure (including information related to motorway infrastructure) and the installation of an accelerograph network which will record the seismic motions at characteristic locations along the motorway.

A network of 8 accelerographs was installed at "free field" positions along the highway (Fig. 32). The criteria considered to define the optimum location for each instrument along the motorway are:

(a) Proximity to a highway facility (e.g., toll plaza), to facilitate power supply;
(b) Absence of any major structure in close vicinity, so that the recorded shaking may be characterized as "free field"; and
(c) Even distribution along the motorway, so that each one records the shaking affecting structures within a radius of 6–8 km around it.

In accord with the concept described in the previous sections, the network was installed so that the recording of each accelerograph may be considered represen-
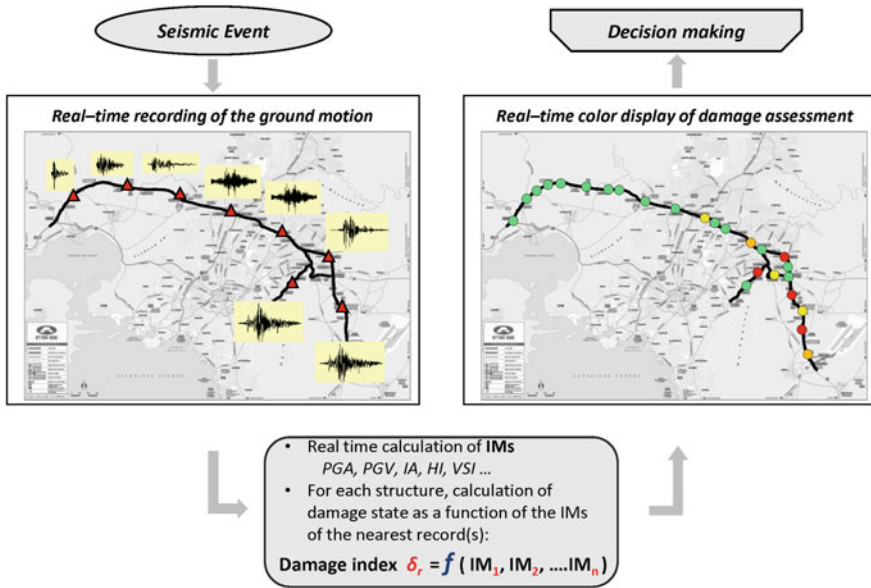
Fig. 33 Schematic illustration of the application of the RARE system during a seismic event

tative of free field shaking of a different section of the motorway. As such, the free field demand exerted upon each structure is calculated using the readings of the two closest accelerographs. All readings are tagged both in time and space domain within a database maintained in the control unit and administered by the motorway administrator. Hence, they may be manipulated in real time in order to calculate the DI of each structure following the methodology presented previously.

Under operation, during a seismic event the real-time system will record seismic accelerations at various locations along the motorway. In this way, the seismic motion will be available in real time, right after the occurrence of the earthquake. For each bridge, the nearest record(s) will be used to assess the seismic damage employing the proposed real-time damage assessment system. Finally, the estimated damage will be the characterised based on typical damage states, offering to an immediate estimate of the damage distribution along the network.

The direct knowledge of the seismic excitation along the motorway is a major difference to traditional risk assessment, in which case the seismic excitation cannot possibly be predicted, and hence probabilistic approaches are much more appropriate. A schematic illustration of the application of the RARE system during an earthquake is presented in Fig. 33.

References

Agalianos, A., Psychari, A., Vassiliou, M. F., Stojadinovic, B., & Anastasopoulos, I. (2017a). Comparative assessment of two rocking isolation techniques for a motorway overpass bridge. *Frontiers in Built Environment, 3,* 47.

Agalianos, A., Sakellariadis, L., & Anastasopoulos, I. (2017b). Simplified method for the seismic response of motorway bridges: Longitudinal direction–accounting for abutment stoppers. *Bulletin of Earthquake Engineering, 15*(10), 4133–4162.

Anastasopoulos, I. (2005). Fault rupture–soil–foundation–structure interaction.

Anastasopoulos, I., et al. (2008). Simplified approach for design of raft foundations against fault rupture. Part I: Free-field. *Earthquake Engineering and Engineering Vibration, 7*(2), 147–163.

Anastasopoulos, I., Anastasopoulos, P. C., Agalianos, A., & Sakellariadis, L. (2015a). Simple method for real-time seismic damage assessment of bridges. *Soil Dynamics and Earthquake Engineering, 78,* 201–212.

Anastasopoulos, I., Anastasopoulos, P. C., Sakellariadis, L., Agalianos, A., Kourkoulis, R., Gelagoti, F., et al. (2018). Development of RApid Response (RARE) system for motorway bridges: Overview and pilot application to Attiki Odos motorway. *ISSMGE International Journal of Geo-engineering Case Histories, 4*(4), 306–326.

Anastasopoulos, I., Antonakos, G., & Gazetas, G. (2010a). Slab foundation subjected to thrust faulting in dry sand: Parametric analysis and simplified design method. *Soil Dynamics and Earthquake Engineering, 30*(10), 912–924.

Anastasopoulos, I., Drosos, V., & Antonaki, N. (2015b). Three-storey building retrofit: Rocking isolation versus conventional design. *Earthquake Engineering and Structural Dynamics, 44*(8), 1235–1254.

Anastasopoulos, I., & Gazetas, G. (2007a). Foundation–structure systems over a rupturing normal fault: Part I. Observations after the Kocaeli 1999 earthquake. *Bulletin of Earthquake Engineering, 5*(3), 253–275.

Anastasopoulos, I., & Gazetas, G. (2007b). Foundation–structure systems over a rupturing normal fault: Part II. Analysis of the Kocaeli case histories. *Bulletin of Earthquake Engineering, 5*(3), 277–301.

Anastasopoulos, I., Gazetas, G., Bransby, M. F., Davies, M. C., & El Nahas, A. (2009). Normal fault rupture interaction with strip foundations. *Journal of Geotechnical and Geoenvironmental Engineering, 135*(3), 359–370.

Anastasopoulos, I., Gazetas, G., Loli, M., Apostolou, M., & Gerolymos, N. (2010b). Soil Failure can be used for earthquake protection of structures. *Bulletin of Earthquake Engineering, 8*(2), 309–326.

Anastasopoulos, I., Gelagoti, F., Spyridaki, A., Tz, Sideri, & Gazetas, G. (2013a). Seismic rocking isolation of asymmetric frame on spread footings. *Journal of Geotechnical and Geoenvironmental Engineering, ASCE, 140*(1), 133–151.

Anastasopoulos, I., Georgarakos, T., Georgiannou, V., Drosos, V., & Kourkoulis, R. (2010c). Seismic performance of bar-mat reinforced-soil retaining wall: Shaking table testing versus numerical analysis with modified kinematic hardening constitutive model. *Soil Dynamics & Earthquake Engineering, 30*(10), 1089–1105.

Anastasopoulos, I., & Jones, L. (2018). On the development of novel mitigation techniques against faulting–induced deformation: "Smart" barriers and sacrificial members. *Soil Dynamics and Earthquake Engineering*.

Anastasopoulos, I., Loli, M., Antoniou, M., Knappett, J., Brennan, A., & Gazetas, G. (2015c). Centrifuge testing of multi-block quay walls. In *Proceedings of SECED 2015 Conference: Earthquake Risk and Engineering towards a Resilient World*, 9–10 July, Cambridge, UK.

Anastasopoulos, I., Sakellariadis, L., & Agalianos, A. (2015c). Seismic analysis of motorway bridges accounting for key structural components and nonlinear soil–structure interaction. *Soil Dynamics and Earthquake Engineering, 78,* 127–141.

Anastasopoulos, I., et al. (2007). Fault rupture propagation through sand: Finite-element analysis and validation through centrifuge experiments. *Journal of Geotechnical and Geoenvironmental Engineering, 133*(8), 943–958.

Anastasopoulos, I., et al. (2008a). Numerical analyses of fault–foundation interaction. *Bulletin of Earthquake Engineering, 6*(4), 645–675.

Anastasopoulos, I., et al. (2008b). Simplified approach for design of raft foundations against fault rupture. Part II: Soil-structure interaction. *Earthquake Engineering and Engineering Vibration, 7*(2), 165–179.

Anastasopoulos, I., et al. (2008c). Design of bridges against large tectonic deformation. *Earthquake Engineering and Engineering Vibration, 7*(4), 345–368.

Anastasopoulos, I., et al. (2013b). Interaction of piled foundation with a rupturing normal fault. *Geotechnique, 63*(12), 1042–1059.

Apostolou, M., Gazetas, G., & Garini, E. (2007). Seismic response of slender rigid structures with foundation uplifting. *Soil Dynamics and Earthquake Engineering, 27*(7), 642–654.

Arias, A. (1970). A measure of earthquake intensity. In R. J. Hansen (Ed.), *Seismic design for nuclear power plants* (pp. 438–483). Cambridge: MIT Press.

Barka, A. A. (1999). 17 August 1999 earthquake. *Science, 258,* 1858–1859.

Bertero, V. V. (1996). Establishment of design earthquakes—Evaluation of present methods. In *International Symposium on Earthquake Structural Engineering*, August 1976, St. Louis, Missouri, USA.

Bray, J. D., et al. (1994). Earthquake fault rupture propagation through soil. *Journal of Geotechnical Engineering, 120*(3), 543–561.

Calvi, G. M. (1999). A displacement-based approach for vulnerability evaluation of classes of buildings. *Journal of Earthquake Engineering, 3*(3), 411–438.

Chen, Y.-G., Chen, W.-S., Lee, J.-C., Lee, Y.-H., Lee, C.-T., Chang, H.-C., et al. (2001). Surface rupture of 1999 Chi-Chi earthquake yields insights on active tectonics of central Taiwan. *Bulletin of the Seismological Society of America, 91*(5), 977–985.

Chiarabba, C., et al. (2009). The 2009 L'Aquila (central Italy) M_W6.3 earthquake: Main shock and aftershocks. *Geophysical Research Letters, 36*: L18308, 6 p.

Codermatz, R., Nicolich, R., & Slejko, D. (2003). Seismic risk assessments and GIS technology: Applications to infrastructures in the Friuli-Venezia Giulia region (NE Italy). *Earthquake Engineering & Structural Dynamics, 32,* 1677–1690.

Cubrinovski, M., Bray, J. D., Taylor, M., Giorgini, S., Bradley, B., Wotherspooon, L., et al. (2011). Soil liquefaction effects in the central business district during the February 2011 Christchurch Earthquake. *Seismological Research Letters, 82*(6), 893–904.

EC8. (2000). Design provisions for earthquake resistance of structures, Part 5 Foundations, Ret. Str. and Geot. aspects. Brussels., 1998-5 Eur. Com. for Standard.

EKOS. (2000). Greek code for reinforced concrete. Org. of Seismic Planning and Protection: Athens.

Erdik, M., Sesetyan, K., Demircioglu, M. B., Hancılar, U., & Zulfikar, C. (2011). Rapid earthquake loss assessment after damaging earthquakes. *Soil Dynamics and Earthquake Engineering, 31*(2), 247–266.

Faccioli, E., et al. (2008). Fault rupture–foundation interaction: Selected case histories. *Bulletin of Earthquake Engineering, 6*(4), 557–583.

Fadaee, M., et al. (2013). Soil bentonite wall protects foundation from thrust faulting: Analyses and experiment. *Earthquake Engineering and Engineering Vibration, 12*(3), 473–486.

Gajan, S., & Kutter, B. L. (2008). Capacity, settlement, and energy dissipation of shallow footings subjected to rocking. *Journal of Geotechnical and Geoenvironmental Engineering, ASCE, 134*(8), 1129–1141.

Gajan, S., & Kutter, B. L. (2009). Effects of moment-to-shear ratio on combined cyclic load-displacement behavior of shallow foundations from centrifuge experiments. *Journal of Geotechnical and Geoenvironmental Engineering, ASCE, 135*(8), 1044–1055.

Gajan, S., Kutter, B., Phalen, J., Hutchinson, T., & Martin, G. (2005). Centrifuge modelling of load-deformation behaviour of rocking shallow foundations. *Soil Dynamics and Earthquake Engineering, 25,* 773–783.

Garini, E., & Gazetas, G. (2013). Damage potential of near-fault records: Sliding displacement against conventional "Intensity Measures". *Bulletin of Earthquake Engineering, 11,* 455–480.

Gazetas, G., Apostolou, M., & Anastasopoulos, I. (2003). Seismic uplifting of foundations on soft soil, with examples from Adapazari (Izmit 1999, Earthquake). In *BGA International Conference on Foundations Innovation, Observations, Design & Practice*, BGA, University of Dundee, Scotland, September 25, pp. 37–50.

Gazetas, G., et al. (2008). Preliminary design recommendations for dip-slip fault–foundation interaction. *Bulletin of Earthquake Engineering, 6*(4), 677–687.

Gelagoti, F., Kourkoulis, R., Anastasopoulos, I., & Gazetas, G. (2012). Rocking isolation of frame structures founded on separate footings. *Earthquake Engineering and Structural Dynamics, 41,* 1177–1197.

Gibson, A. D. (1997). *Physical scale modeling of geotechnical structures at One-G*. Report no. SML 97-01. Pasadena, CA: California Institute of Technology, p. 413.

Housner, G. W. (1952). Spectrum intensities of strong motion earthquakes. In *Proceedings of the Symposium on Earthquake and Blast Effects on Structures*. Oakland California: EERI; pp. 20–36.

Iwasaki, T., Fujino, Y., Iemura, H., Ikeda, S., Kameda, H., Katayama, T., et al. (1995). Report on highway bridge damage caused by the Hyogo-ken Nanbu earthquake of 1995. Committee on Highway Bridge Damage caused by the Hyogo-Ken Nambu Earthquake, Japan.

KANEPE. (2010). Greek code for seismic retrofit, Org. of Seismic Planning and Protection: Athens.

Kourkoulis, R., Gelagoti, F., & Anastasopoulos, I. (2012). Rocking isolation of frames on isolated footings: Design insights and limitations. *Journal of Earthquake Engineering, 16*(3), 374–400.

Kung, C.-S., Ni, W.-P., & Chiang, Y.-J. (2001). Damage and rehabilitation work of Shih-Kang dam. In *Proceedings of Workshop on Seismic Fault-Induced Failures*, Tokyo.

Kutter, B. L., Martin, G., Hutchinson, T. C., Harden, C., Gajan, S., & Phalen, J. D. (2003). Status report on study of modeling of nonlinear cyclic load-deformation behavior of shallow foundations. In: PEER Workshop, University of California, Davis.

Nakamura, Y., Uehan, F., & Inoue, H. (1996). *Waveform and its analysis of the 1995 Hyogo-Ken-Nanbu Earthquake* (II), Railway Technical Research Institute.

Panagiotidou, A. I., Gazetas, G., & Gerolymos, N. (2012). Pushover and seismic response of foundations on stiff clay: Analysis with P-Delta effects. *Earthquake Spectra, 28*(4), 1589–1618.

Paolucci, R. (1997). Simplified evaluation of earthquake induced permanent displacement of shallow foundations. *Journal of Earthquake Engineering, 1*(3), 563–579.

Paolucci, R., Shirato, M., & Yilmaz, M. T. (2008). Seismic behaviour of shallow foundations: shaking table experiments versus numerical modelling. *Earthquake Engineering and Structural Dynamics, 37,* 577–595.

Park, R., & Paulay, T. (1975). *Reinforced concrete structures*. New York: Wiley.

Pecker, A. (1998). Capacity design principles for shallow foundations in Seismic Areas. In *Proceedings of 11th European Conference on Earthquake Engineering*. A.A. Balkema Publishing.

Pecker A. (2003). Aseismic foundation design process, lessons learned from two major projects: The Vasco de Gama and the Rion Antirion bridges. In *ACI International Conference on Seismic Bridge Design & Retrofit*, La Jolla, CA.

Pender, M. (2007). Seismic design and performance of surface foundations. In *4th International Conference on Earthquake Geotechnical Engineering*, Thessaloniki, Greece (CD-ROM).

Pitilakis, K., & Crowley, H. (2014). Recommendations for future directions in fragility function research. In K. Pitilakis, H. Crowley, & A. Kaynia (Eds.), *SYNER-G: Typology definition and fragility functions for physical elements at seismic risk*. Geotechnical, geological and earthquake engineering (Vol. 27). Dordrecht: Springer.

Priestley, M. J. N. (2000). Performance based seismic design. In *Proceedings of 12th World Conference on Earthquake Engineering* (12WCEE), Auckland, New Zealand, Paper No. 2831.

Priestley, M. J. N., Seible, F., & Calvi, G. M. (1996). *Seismic design and retrofit of bridges*. New York: Wiley.

Rontogianni, A. (2011). *Seismic rehabilitation of an existing 3-storey building: Conventional design and rocking isolation system*. Diploma Thesis, National Technical University of Athens.

Sakellariadis, L., Agalianos, A., & Anastasopoulos, I. (2018). Simplified method for real-time seismic damage assessment of motorway bridges: Transverse direction—Accounting for abutment stoppers. *Earthquake Engineering & Structural Dynamics, 47,* 1496–1521.

Shirato, M., Kouno, T., Asai, R., Nakani, N., Fukui, J., & Paolucci, R. (2008). Large-scale experiments on nonlinear behaviour of shallow foundations subjected to strong earthquakes. *Soils and Foundations, 48*(5), 673–692.

Stavrakakis, G. N., Chouliaras, G., & Panopoulou, G. (2002). Seismic source parameters for the M_L = 5.4 Athens Earthquake (7 September 1999) from a new telemetric broad band seismological network in Greece. *Natural Hazards, 27,* 47–60.

Tolga Yilmaz, M., & Paolucci, R. (2007). Earthquake fault rupture—Shallow foundation interaction in undrained soils: A simplified analytical approach. *Earthquake Engineering & Structural Dynamics, 36*(1), 101–118.

Trifunac, M. D., Todorovska, M. I., & Lee, V. W. (1998). The Rinaldi strong motion accelerogram of the Northridge, California, earthquake of 17 January, 1994. *Earthquake Spectra, 14*(1), 225–239.

Ulusay, R., Aydan, Ö., & Hamada, M. (2002). The behaviour of structures built on active fault zones: Examples from the recent earthquakes of Turkey. *Structural Engineering/Earthquake Engineering, 19*(2), 149s–167s.

Ural, D. (2001). The 1999 Kocaeli and Duzce earthquakes: Lessons learned and possible remedies to minimize future Losses. In *Proceedings Workshop on Seismic Fault Induced Failures*, Tokyo, Japan.

Vamvatsikos, D., & Cornell, C. A. (2002). Incremental dynamic analysis. *Earthquake Engineering & Structural Dynamics, 31,* 491–514. https://doi.org/10.1002/eqe.141.

Vassiliou, M. F., & Makris, N. (2012). Analysis of the rocking response of rigid blocks standing free on a seismically isolated base. *Earthquake Engineering and Structural Dynamics, 41*(1), 177–196.

Von Thun, J. L., Rochim, L. H., Scott, G. A., & Wilson, J. A. (1988). Earthquake ground motions for design and analysis of dams. Earthquake engineering and soil dynamics II–recent advances in ground-motion evaluation. Geotechnical Special Publication 20, ASCE; pp. 463–481.

Bridging Multi-hazard Vulnerability and Sustainability: Approaches and Applications to Nepali Highway Bridges

Rabindra Adhikari, Dipendra Gautam, Pratyush Jha, Bikalpa Aryal, Kamal Ghalan, Rajesh Rupakhety, You Dong, Hugo Rodrigues and Gokarna Motra

1 Introduction

Highway bridges are important infrastructures for the economic mobility of any region. Obstruction in the transport system due to bridge damage may cause huge losses in the economy. The East-West Highway (EWH) in Nepal is very crucial

R. Adhikari · B. Aryal · K. Ghalan
Department of Civil Engineering, Cosmos College of Management and Technology,
Pokhara University, Pokhara, Nepal
e-mail: rabindraadhi@cosmoscollege.edu.np

R. Adhikari
Interdisciplinary Research Institute for Sustainability (IRIS), Kathmandu, Nepal

D. Gautam (✉)
Structural and Geotechnical Dynamics Laboratory, StreGa, University of Molise,
Campobasso, Italy
e-mail: dipendra.gautam@unimol.it

P. Jha
Digicon Engineering Consult, Lalitpur, Nepal
e-mail: pratyush0119@gmail.com

R. Rupakhety
Earthquake Engineering Research Center, University of Iceland, Selfoss, Iceland
e-mail: rajesh@hi.is

Y. Dong
Department of Civil Engineering, The Hong Kong Polytechnic University, Hung Hom, Kowloon,
Hong Kong, China
e-mail: you.dong@polyu.edu.hk

H. Rodrigues
RISCO-School of Management and Technology, Polytechnic Institute of Leiria, Leiria, Portugal
e-mail: hugo.f.rodrigues@ipleiria.pt

G. Motra
Department of Civil Engineering, Institute of Engineering, Pulchowk Campus, Lalitpur, Nepal
e-mail: gmotra@ioe.edu.np

for the national economy and transport system as Nepal basically relies on ground transport. Across the world, several natural hazards have reflected the performance and damage scenarios of highway bridges. Witzany et al. (2008), Hong et al. (2012), Wang et al. (2014), among others, have presented the effect of floods on bridges. Similarly, Gautam and Dong (2018) presented the account of flood damage to a bridge in central Nepal due to the 2017 flash flood. Effect of other natural hazards, e.g. earthquake, to bridges, is extensively discussed in the existing literature. The 1993 flood and landslide events in Nepal destroyed 16 bridges in central and eastern Nepal (For details see: https://reliefweb.int/report/nepal/nepal-floodslandslides-jul-1993-un-dha-situation-reports-1-8). In every monsoon, dozens of bridges become defunct in Nepal due to flood and landslides but the multi-hazard effects in bridges are seldom discussed. Gautam (2017a, b) presented the seismic vulnerability of highway bridges in the EWH. Previous studies on highway bridges highlight that Nepali bridges are very vulnerable to various natural hazards (e.g. Gautam 2017a, b; Gautam and Dong 2018).

Flooding is a global issue causing huge losses of lives and damage to infrastructures annually. For instance, 2016 flooding at Missouri caused damage to homes, roads, bridges, and other structures; eight of eleven counties in the basin were declared a Federal Disaster Area (USGS 2016). Similarly, Nepal has faced increasing severity and frequency of floods over the past few decades. The 2017 monsoon observed torrential precipitation within a few weeks and resulted in severe flooding in the southern plains of Nepal. As reported by the National Planning Commission (NPC), the flood impact was severe in 18 districts which caused enormous losses of lives and properties (NPC 2017). The flood damage was prevalent in 35 districts of Nepal and the overall loss was estimated to be 393 million Nepali rupees (NPC 2017) [1 US$ ≈ 115 Nepali rupees as of September 16, 2018]. The effects of natural hazards such as 2001, 2008, and 2017 floods demonstrate Nepal's high vulnerability to natural hazards which underscores the need for identification of damage scenario, preparedness initiatives, and resilient solutions. A continuous exposure of physical infrastructure to floods leads to degradation of these assets. Over the years, roads and bridges provide a reduced level of service and efficiency, affecting all economic activities. This has serious implications for not only regional development of the Terai region, but also to the country as a whole. The physical infrastructures, therefore, need to be reconstructed with more stringent specifications owing to the vulnerability scenario. The Department of Roads under the government of Nepal occasionally conducts monitoring and maintenance of highway bridges, however, to the best of authors' knowledge, there is no specific guideline for post-disaster damage evaluation and damage grading of the highway bridges. To fulfill this gap, this study aims to develop a guideline for post-flood damage assessment and evaluation of vulnerability and deterioration. Multi-hazard vulnerability is accounted considering flood and earthquake scenario. The developed methodology is implemented in 50 highway bridges along the EWH affected by the 2017 flood.

2 Multi-hazard Vulnerability of Highway Bridges in Nepal

2.1 Flood Vulnerability

More frequent than large earthquakes, flood events impose hydrodynamic and hydrostatic loads as torrential precipitation occurs almost annually. Due to a lack of periodic or seasonal maintenance, especially in developing countries like Nepal, aggravation of deterioration is commonly observed. Upon accumulation of such deterioration, higher damage states would usually occur. However, higher damage may occur in case of earthquake). Nepali rivers are well known to carry high sediment loads, thus the damage during floods is usually unpredictable. Due to lack of information and parameters for more rigorous numerical/mechanical modelling, especially in the case of Nepali bridges, this study focuses on an empirical survey to understand the relation between damage level and depth of inundation.

During field reconnaissance, several damage modes were documented. Sedimentation and scouring were observed in almost every bridge visited in central and eastern Nepal. Figure 1a shows the scouring mechanism developed in the pier of an RC bridge. Similarly, Fig. 1b highlights the common sedimentation problem in Nepali highway bridges.

Apart from scouring and sedimentation, approach slab damage was commonly observed during the field reconnaissance as shown in Fig. 2a. It appears that approach slabs are more vulnerable than bridge decks. Scouring damage to the pier base was another common problem identified during the field reconnaissance; an example is shown in Fig. 2b. Even though the damages in these cases were not serious, lack of immediate repairs can lead to damage accumulation and eventual loss of functionality or even stability of these bridges.

Due to continued use without repairs, plaster spalling in piers was observed in some cases. This may be due to environmental actions as well as construction quality. Figure 3a reflects the environmental attack on the pier along with the spalled plaster.

(a) Scouring

(b) Sedimentation in the bridge piers
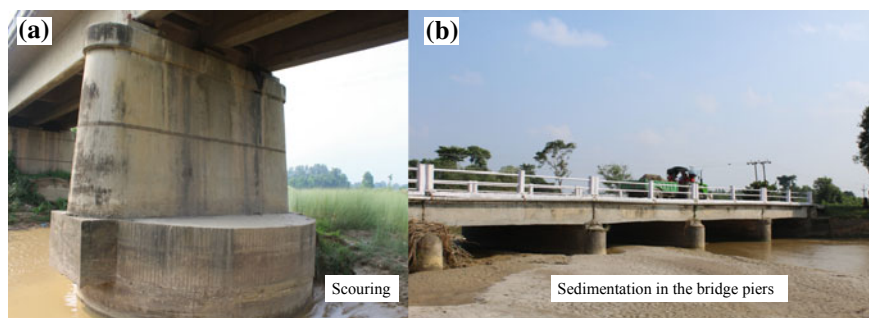
Fig. 1 **a** Scoured pier base, **b** sedimentation of the piers and raised river bed along with deposited debris
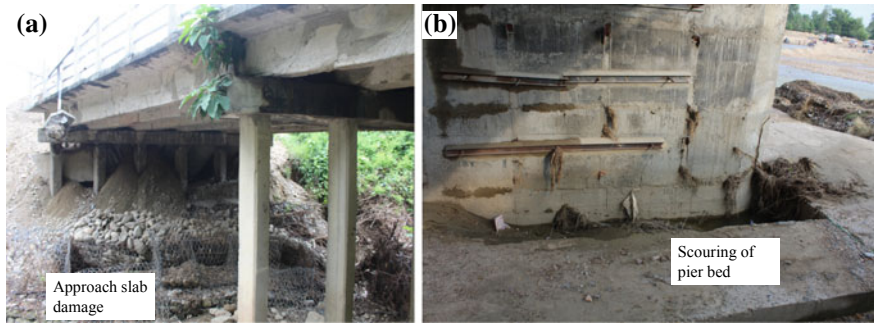
Fig. 2 **a** Approach slab damage due to the flood, **b** scouring of pier base

Fig. 3 **a** Spalling of plaster due to 2017 flood, **b** exposed re-rebar due to flooding

Similarly, in Fig. 3b, exposed rebars are shown. Exposure of rebars was due to the erosion of plaster and concrete cover. The thickness of concrete cover was under-calculated in design, or the construction quality was not good enough.

Two of the major bridges along the East-West Highway of Nepal were heavily damaged due to the 2017 flash flood. As shown in Figs. 4 and 5, some piers of the bridges reflected large settlement due to localized erosion. Localized erosion is common in Nepali rivers due to channel shifting. As can be seen from the figures, no direct damage is reported in any of the piers or superstructure, however, the major problem is arising from the foundation.

A rapid damage assessment campaign was conducted on 2–5 September 2017. Figure 6 shows the stretch of East-West Highway covered during the field investigation. Out of 50 assessed bridges, only seven reflected notable damage. To the best of authors' knowledge, relation between inundation depth and damage in Nepali highway bridges is hitherto unknown. The depth-damage curves constructed from the observations is presented in Fig. 7. In Fig. 7 damage ratio is the extent of damage noted in situ based on visual inspection. The damage extent was assigned to a bridge from the component-based damage extents.

Fig. 4 Dudhaura bridge damaged due to settlement and scouring in Bara district, central Nepal

Fig. 5 Ratu bridge damaged due to settlement and scouring in Mahottari district, central Nepal

As can be seen from Fig. 7, a linear depth-damage curve was formulated. When formulating the depth-damage curve, the outliers with relatively high values of depth without any damage were not considered. As the data was relatively scattered due to variation in precipitation, nature of river bed and sedimentation, the outliers were manually removed using judgment without any parametric basis. The governing equation of the depth-damage curve with the coefficient of determination is also given in Fig. 7.
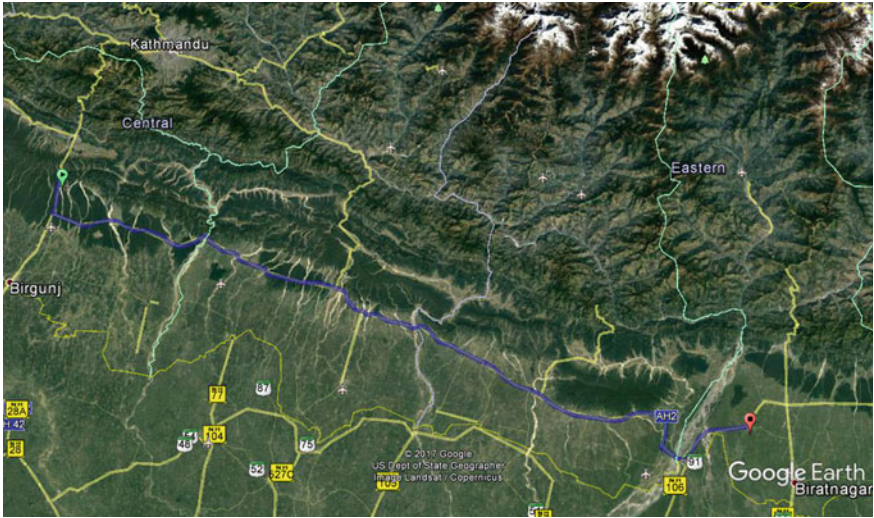
Fig. 6 The section of East-West Highway covered during field reconnaissance
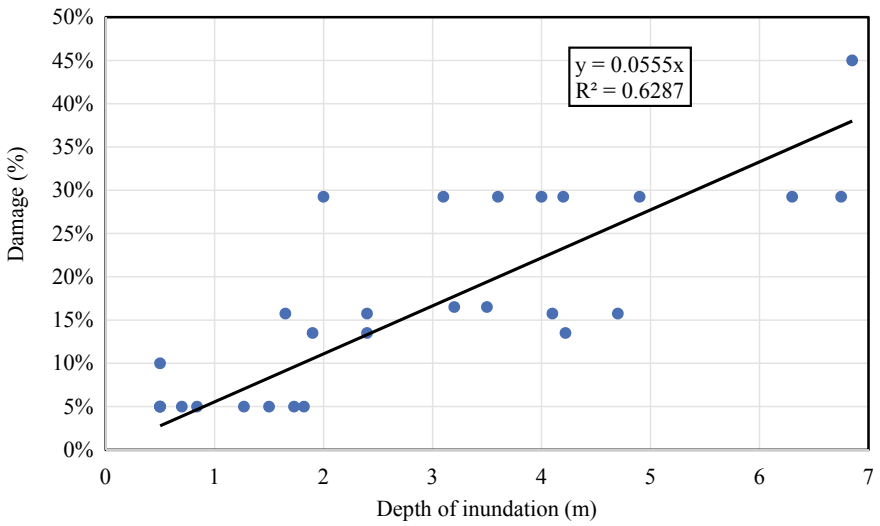
Fig. 7 Depth-damage curve for the highway bridges

2.2 Seismic Vulnerability

During the field reconnaissance, seismic fragility of bridges was estimated according to a pre-defined form. Four damage states, namely minor damage (<5% damage ratio), major damage (5–40% damage ratio), severe damage (40–70% damage ratio), and collapse (>70%), are classified in the form. The mean and lower bound estimates of peak ground accelerations corresponding to these damage states were estimated from experts through a questionnaire. Similarly, to accommodate the multi-hazard, separate forms were used to identify the most likely peak ground acceleration for each damage states when earthquake and flood occur at a time. The mean and lower bound PGA for each four damage states (minor, major, severe, and collapse) were noted during the field reconnaissance for earthquake and earthquake followed by a flood equivalent to the 2017. From the recorded judgments, the two Gaussian parameters were estimated for each bridge. After that, averaging of estimated PGA from two experts was done for the bridges and the median and lognormal standard deviation were used to create the fragility functions based on heuristic method. Further details regarding the methods of creating fragility functions is available in Porter et al. (2007). Readers are also referred to consult the heuristic methods applied to create fragility functions in ATC-13 (1985) and ATC-40 (1996) for further details. A simplified methodology to derive heuristic fragility functions for buildings as suggested by Gautam et al. (2018) is presented in Fig. 8. Following the steps as depicted in Fig. 8, combined lower bound PGA (λ) for a particular damage state (i) can be calculated using Eq. (1) as:

$$\lambda = \frac{\sum_{i=1}^{n} w_i^{\alpha} \lambda_i}{\sum_{i=1}^{n} w_i^{\alpha}} \qquad (1)$$

Similarly, combined median PGA (θ) for each damage state was estimated by using Eq. (2) as follows:

$$\theta = \frac{\sum_{i=1}^{n} w_i^{\alpha} \theta_i}{\sum_{i=1}^{n} w_i^{\alpha}} \qquad (2)$$

In Eqs. (1) and (2), w_i is the weight assigned to the lower bound PGA value (λ_i) judged by expert i, $\alpha = 1.5$, n is the total number of expert judgements available, and θ_i is the median PGA value judged by expert i. Once the combined lower bound and median PGAs are estimated, the logarithmic standard deviation (γ) can be estimated as:

$$\gamma = \frac{\ln\left(\frac{\theta}{\lambda}\right)}{1.28} \qquad (3)$$
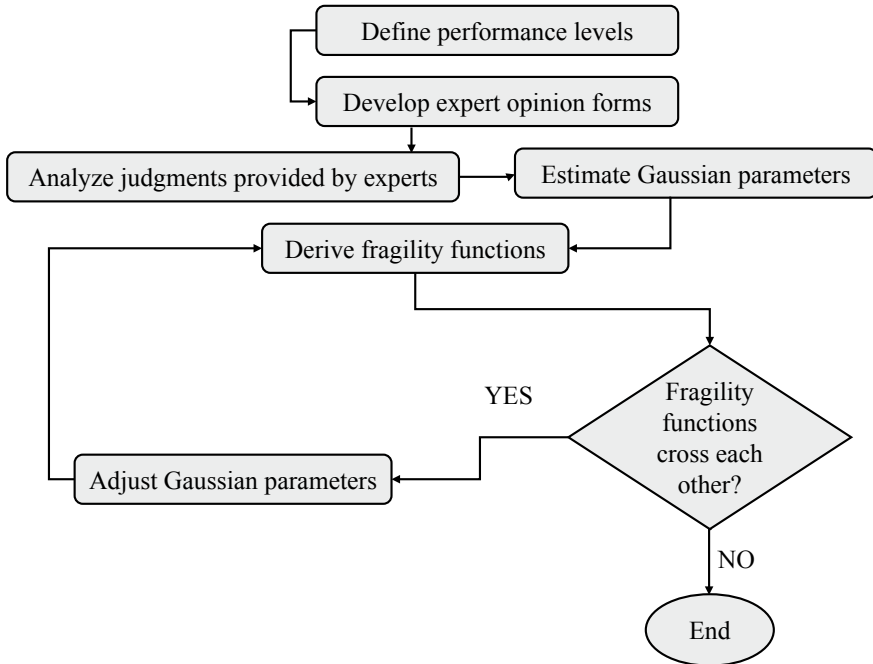
Fig. 8 Methodology to derive heuristic fragility functions (modified from Gautam et al. (2018))

In the case of heuristic fragility functions, it is crucial to note that the logarithmic standard deviation should not be less than 0.4 (Porter et al. 2007), thus the median value should be adjusted as follows:

$$\theta_i = 1.67\,\lambda_i \big[if\,\gamma_i < 0.4 \big] \tag{4}$$

Two sets of fragility functions were derived for the highway bridges in Nepal using the heuristic approach as depicted above. Judgment forms were filled up in situ together with the damage assessment campaign. Two separate forms were used to estimate the damage level considering seismic vulnerability alone and designated flood (similar to the August 2017 flood) followed by an earthquake. Figure 9 highlights occurrence of major, severe, and collapse damage states and 15–25% lower PGA when seismic vulnerability was considered along with the flood.

As highway bridges are the engineered constructions with better construction precautions than that of residential buildings, seismic vulnerability is usually expected to be lower. However, even minor or major damages would lead into inoperability of highway bridges. For instance, the collapse damage state has nearly 12% probability of exceedance at 1 g when seismic action is considered alone, but when seismic action together with the flood event as that of 2017 was considered, the probability of exceedance of the collapse damage state is 28%. Except the minor damage state, both
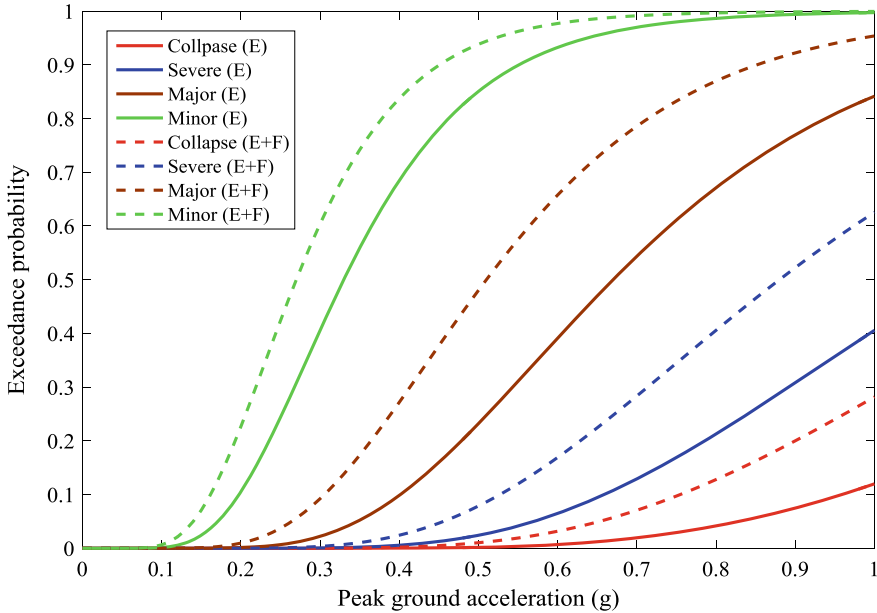
Fig. 9 Fragility functions considering earthquake (denoted by (E) in figure) and multi-hazard, i.e. flood followed by an earthquake (denoted by (E+F) in figure) for the RC highway bridges of Nepal

major and severe damage states depict similar variation for earthquake alone, and flood followed by an earthquake. The variation in minor damage could be observed as less than 10%, meanwhile other damage states have the variation higher than that.

3 Condition Assessment of Bridges: New Approach and Application

Condition assessment of highway bridges is crucial to monitor the status of operation as well as to plan repair/rehabilitation priorities. Condition assessments are done usually by skilled technicians; however, great care is needed to determine the exact status of the bridge. As repair/rehabilitation priorities demand high investment, accurate condition assessment is important. To assess the condition of the entire bridge, component-level condition assessment is important. We presented a new condition assessment system based on component level observations. Pile/footing, pier/abutment (piers, abutment, wing-wall), bearing (bearings, expansion joint), girder/beam, deck (deck, railings, kerb, overall superstructure), river training work (retaining structures, river training works), and utilities (approach road, other utilities) were considered for component-level condition assessment. Two field investigation forms were developed to record damage and deterioration. All types of natural as well

as anthropogenic hazards were considered when developing the assessment forms. The forms are presented in the Appendix. The first form provides general description of the bridge with a sketch and damage classification system as well as deterioration classification system. The second form depicts the component level damage and possible interventions.

Damage to structural and other crucial elements are given higher weights in computing overall condition. We used dozens of field observations to quantify the weightages which could be directly used when performing condition assessment. As shown in Table 1, the pile/footing could contribute 100% damage to the bridge leading to inoperability. That is, if severe damage/collapse of pile/footing occurs, the bridge should be understood to be inoperable leading to major repairs or partial reconstruction of the bridge. Piers and abutments are given 90% weightage contribution in overall damage, girders/beams contribute 50%, bearings, deck, and river training works contribute 20% each. Damage to utilities are not considered in estimating the overall condition the bridges. The overall damage is taken as the largest weighted damage of the different components. Deterioration weightages are also provided to assess the deterioration level of bridges in situ. Pile/footing is assigned with 15% weightage, piers/abutments with 40% weightage, bearings with 10%, girders with 15%, deck with 10%, river training works with 5%, and utilities with 5% weightages. Deterioration scores are the weighted sum of the deterioration scores of the different components. A generic method to designate the damage/deterioration is presented in Table 2. In Table 2, σ denotes the standard deviation of the damage/deterioration score obtained from field reconnaissance. A mandatory aspect of this method is that the application of the method is possible only if several forms are filled up in situ. Thereafter, the mean value for the damage/deterioration score along with the standard deviation can be estimated. Further decision can be taken based on the convention provided in Table 2. As the method is generic one, the numerals before the standard deviation could be adjusted per the severity and necessity. A similar application of the mean and standard deviation based vulnerability grading can be also found in the paper by Gautam (2017a, b).

Overall bridge damage, in most cases, was dominantly contributed by piers and abutments as shown in Fig. 10. Bridge damage was significant due to damage of river-training works followed by pile or footing and then bearing. However, overall bridge deterioration was mostly contributed due to deterioration of piers or abutments and minor contributions were also made by bearings and girders. These observations show that piers and river-training works should get higher attention for bridge strengthening or new design.

River training works were the most vulnerable component as shown in Fig. 11. Piers/abutments are highly susceptible to minor to moderate damage as can be seen from Fig. 11. Similarly, piers/abutments were the most deteriorated components in bridges (Fig. 12). Prolonged use without maintenance may lead to accumulate and aggravate the damage. Intervention and future design should thus focus on deterioration resistance. Decks were also significantly deteriorated but to minor extents only. However, deteriorations may accumulate over time in lack of regu-

Table 1 Component level weightages for damage and deterioration

Components (i)	Maximum damage contribution to the system (W_i) (%)	Deterioration contribution to the system (T_i) (%)	Damage score	Deterioration score
Pile/footing	100	15	Corresponding to max. ($W_i \times D_i$)	Sum of ($W_i \times T_i$)
Piers/abutments	90	40		
Bearings	20	10		
Girders/beams	50	15		
Deck	20	10		
River training works	20	5		
Utilities	–	5		
Total	–	100		

Table 2 A framework to categorize the damage/deterioration level and possible intervention

Classification	Damage/deterioration level	Possible intervention	Traffic condition/operational condition
>1.5 σ	Critical	Emergency repairs	Closed
0.5 σ to 1.5 σ	Severe	Immediate repairs	Closed
−0.5 σ to 1.5 σ	Major	Immediate repairs	Closed
−1.5 σ to −0.5 σ	Minor	Repairs	Partly closed
<−1.5 σ	Low	Minor repairs	Partly closed/uninterrupted
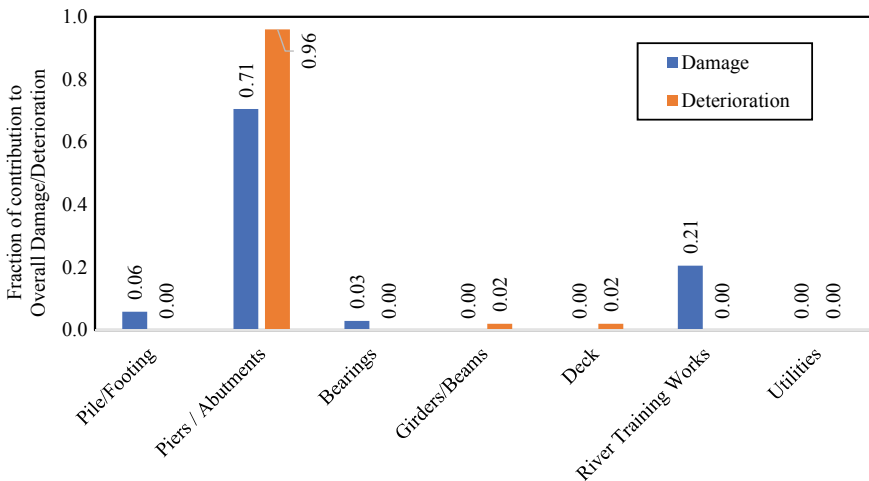
Fig. 10 Most critical component of bridges corresponding to damage and deterioration
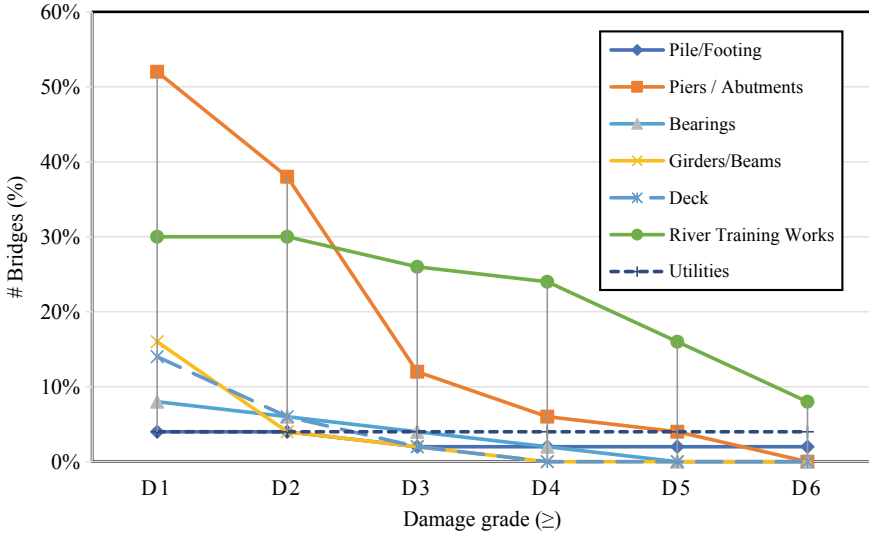
Fig. 11 Damage condition of different bridge component (% of bridges with their component at particular damage state or higher)
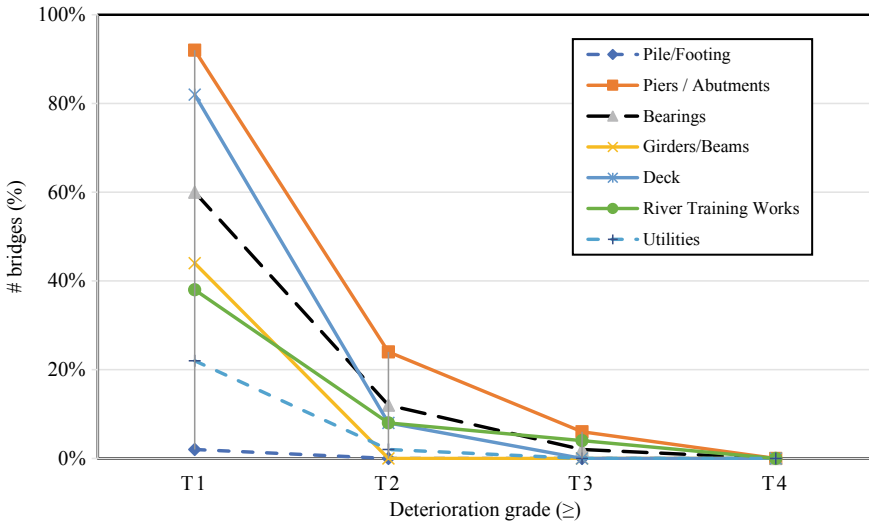
Fig. 12 Deterioration condition of different bridge component (% of bridges with their component at particular damage state or higher)

lar repair/maintenance. Bearings were found to be deteriorated significantly which may be due to frequent flow of water through bearings.

To formulate a relationship between damage and deterioration, the field observations were plotted together as in Fig. 13. As shown in Fig. 13, significant relation
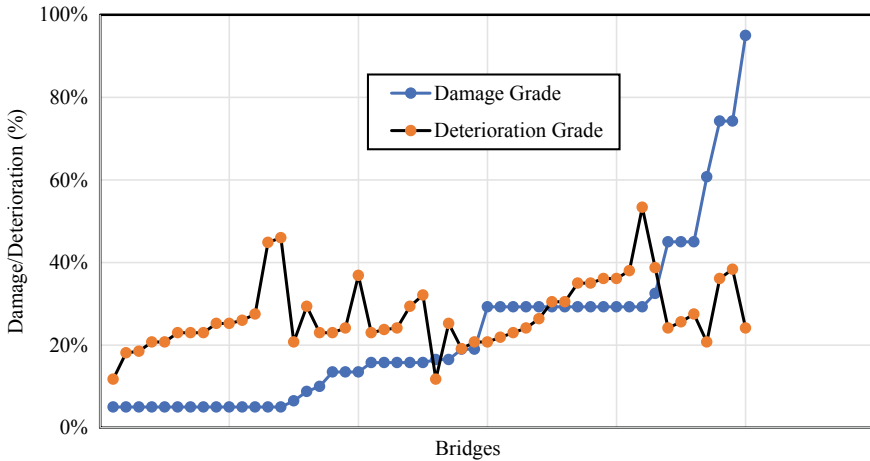
Fig. 13 Damage versus deterioration relationship of highway bridges

between damage and deterioration was not achieved. In some bridges, damage was high even if the deterioration was low. While in some other bridges, damage was low even in the case of relatively higher deterioration. Meanwhile, Fig. 13 should be carefully judged as it is constructed from the empirical data of a single event. It should be noted that deterioration is expected to be relevant for seismic vulnerability, thus Fig. 13 does not represent the scenarios exhaustively.

4 Futurism: Sustainability of Bridges

Sustainable structural engineering is gaining considerable momentum worldwide. Due to increased attention towards climate change impacts and limited resources availability, structural engineers are paying attention to sustainability in residential buildings to large infrastructures. (see e.g.: Sabatino et al. 2015; Dong and Frangopol 2016; Frangopol et al. 2017; Zheng et al. 2018; among others). Due to its geopolitical location and resource constraints as well as the impact of climate change, both structural and infrastructural development in Nepal may face resource constraints soon. Moreover, exposure and vulnerability associated with natural hazards are growing in the due course, thus a sustainable and multi-hazard resilient framework is of the utmost need of now. As highlighted recently by Gautam and Dong (2018) a single flash flood in central Nepal swept a newly constructed bridge. This is so emblematic that all further bridge constructions should be aware of the torrential rainfall and subsequent flash floods in the mountainous terrains. With these shreds of evidences, it would be pertinent to formulate a preliminary sustainability framework for Nepali highway bridges for possible incorporation in the bridge design guide-

lines as well as to establish a milestone for further research in sustainable bridge engineering. Figure 14 shows a sustainability framework which is modified and localized for Nepali bridges considering similar studies presented by Dong et al. (2013). Further investigations pertaining to each component are required to quantify the sustainability framework in detail. Primarily, three major natural hazards, viz. earthquake, flood, and landslide/debris flow/mass movement, either triggered or independent are considered. As highlighted before, both deterioration and damage in highway bridges would be gravely affected by component level performance, thus the multi-hazard fragility functions to each component would be pertinent to formulate alongside. Thereafter, the fragility functions should be integrated with the depth-damage curves as suggested in this study. Empirical depth-damage curve as in this study would be the most representative due to underlying uncertainties in the simulation where creation of exacting matching environment may not be necessarily assured. With the outputs of hazard and risk assessment campaigns, a loss estimation framework could be effectively developed. Once loss estimation scenario to a defined bridge class is known, sustainability analysis could be performed in eight parameters and the results could be later integrated. Life-cycle assessment (LCA), which is relatively new and not in practice Nepal, is inevitable to address sustainability issues. Further details regarding LCA can be found in the book published by American Society of Civil Engineers (2010). Similarly, Dong and Frangopol (2017) present a life-cycle-cost-benefit analysis (LCCBA), and similar framework could
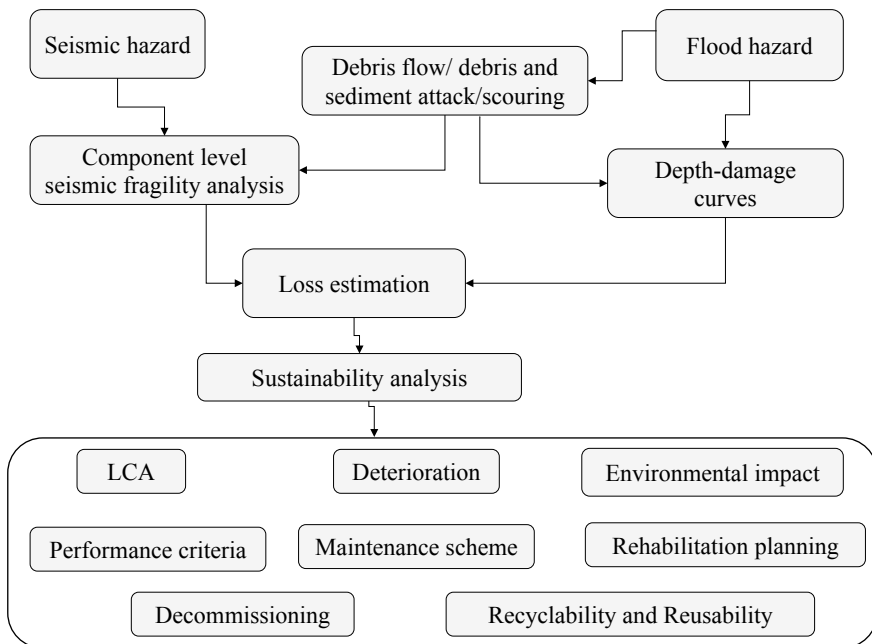
Fig. 14 Sustainability framework for Nepali highway bridges

be effectively implemented to Nepali highway bridges. Due lack of timely mainte-nance, Nepali highway bridges are often subject to deterioration, which in turn may lead to much higher damage when exposed to earthquake, or landslide although the single event records from 2017 floods do not reflect the same. Continuous scouring of foundation and piers was frequently observed during the field reconnaissance. Nepali highway bridges are exposed to greater loads than the designed one thus the performance criteria would not be assured. A mandatory framework which restricts the vehicle type per the bridge class can resolve the issue of exposure to greater than designed load. Nepali highway bridges were constructed primarily since the 1970s and now is the time for effective rehabilitation planning. Cost-benefit analysis and LCA can be effective tools at this moment. Moreover, decommissioning planning is also required for some strategic network bridges due to traffic flow nature as well as suitability of bridge type. Due to environmental concerns, recyclability and reusabil-ity criteria should be encapsulated in the design and construction phases of highway bridges. If sustainability framework is well recognized and endorsed in design and construction of highway bridges, together with the multi-hazard risk assessment, better performance against multiple hazards can be expected.
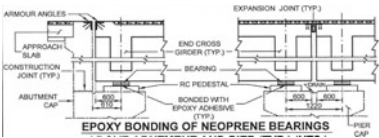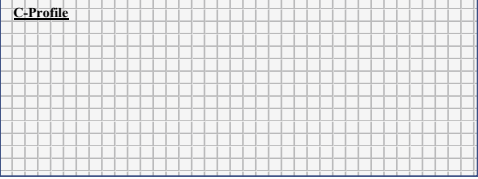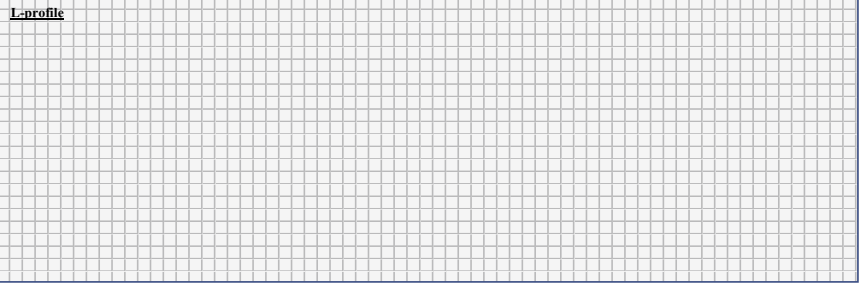
5 Concluding Remarks

To understand multi-hazard damage to highway bridges, a reconnaissance mission was conducted after the 2017 central Nepal flash flood. After the detailed assessment of 50 highway bridges, depth-damage curve is constructed in this chapter. A new methodology of condition assessment of the highway bridges was formulated and the same was implemented in situ. Moreover, a sustainability framework for the highway bridges considering possible multi-hazards is proposed for implementation. Damage and deterioration both are crucial issues in highway bridges, thus weightage-based damage and deterioration assessment systems are proposed, and possible interven-tions are suggested. Besides, scenario bridge operations are assigned to each dam-age/deterioration states. The heuristic fragility functions constructed in this chapter show that seismic vulnerability increases after major floods.

This chapter mostly used empirical and heuristic approaches to construct fragility functions as well as depth-damage curves. Further investigations in terms of analyt-ical modeling may be used in future to calibrate and generalize the multi-hazard risk of Nepali highway bridges. Further investigations are also needed to quantify each component of the sustainability framework.

Appendix: Data Collection Forms

District / Place:		Form ID: T___|
Date/Time: 2017-09-	*Inspection Team:*	*Insp. Side: (facing upstream)* *Left / Right*
Const. Year (BS): *Location (N, E):*	*Bridge Type:* *S-Girder / S-Truss / C-T-Beam / C-Arch / Other _____*	*Bridge Name:* *River Name:*
Span Nos: *Span Length:* *Bridge Length:*	*Lanes No:* *Carriageway w (m):* *Footpath w (L, R):*	*Overall Det#/Damage* Rating:* *a) Super-Structure: ___/___* *b) Substructure: ___/___* *c) Overall: ___/___*

Comments (including construction deficiencies, seating, design issues):

#Deterioration Grades (except due to flooding):	*Damage Grades:
T0: *No deterioration*; T1: *Minor Deterioration* (some seepage, non-structural cracks/spalling, corrosion patches, etc); T2: *Major Deterioration* (heavy corrosion/erosion of material, dislocation of non-structural element, Non-functional non-structural components; T3: *Severe Deterioration* (heavy erosion/corrosion with loss of section>20%, dislocation of structural-element, corrosion/exposure or rebar, spalling of structural concrete, etc.)	D0: *No damage*; D1: *Minor Damage* (hairline cracks, slight damage immediately operable); D2: *Extended Damage* (minor damage-extended cracks & operable but needs repairs) [<1mm]; D3: *Moderate Damage* (extended cracks, dislocation of non-structural components: traffic flow need to be controlled to prevent the damage aggravation); D4: *Major Damage* (extended damage: damage to structure and traffic should not be allowed; needs major repairs); D5: *Severe Damage* (significant damage to structural components); D6: *Collapse*
Utilities (describe size also):	Depth of Abutment-base from Bridge-Deck (m): Depth of Bearing (Abut-top) from Bridge-Deck (m): Depth of HFL (Above/Below bridge Deck) (m):

Pipelines/ Electric cables / Communication Cable / Canal / Other

C-Profile

L-profile

OBSERVED FLOOD DAMAGE		(Right / Left) ; FormID: _____	
COMPONENT (+NDT Test Results)	**Details of damage (+photo no)**	**Extent (in scale of 5)** **Damage grade*** **Det. grade***	**Suggested repair technique**
Superstructure		Extreme: Moderate: Minor: Dam-G: Det-G:	
		Extreme: Moderate: Minor: Dam-G: Det-G:	
		Extreme: Moderate: Minor: Dam-G: Det-G:	
		Extreme: Moderate: Minor: Dam-G: Det-G:	
		Extreme: Moderate: Minor: Dam-G: Det-G:	
		Extreme: Moderate: Minor: Dam-G: Det-G:	

References

American Society of Civil Engineers. (2010). *ASCE. Sustainability guidelines for the structural engineer*. Reston, VA: Structural Engineering Institute. https://ascelibrary.org/doi/book/10.1061/9780784411193.

ATC-13. (1985). *Earthquake damage evaluation data for California, ATC-13*.

ATC-40. (1996). *Seismic evaluation and retrofit of concrete buildings, ATC-40*.

Dong, Y., & Frangopol, D. M. (2016). Life-cycle multi-hazard risk assessment of highway bridges. In *Maintenance, Monitoring, Safety, Risk and Resilience of Bridges and Bridge Networks—Proceedings of the 8th International Conference on Bridge Maintenance, Safety and Management, IABMAS* (pp. 158–62).

Dong, Y., & Frangopol, D. M. (2017). Probabilistic life-cycle cost-benefit analysis of portfolios of buildings under flood hazard. *Engineering Structures, 142,* 290–299. https://doi.org/10.1016/j.engstruct.2017.03.063.

Dong, Y., Frangopol, D. M., & Saydam, D. (2013). Time-variant sustainability assessment of seismically vulnerable bridges subjected to multiple hazards. *Earthquake Engineering and Structural Dynamics, 42*(10), 1451–1467. https://doi.org/10.1002/eqe.2281.

Frangopol, D. M., Dong, Y., & Sabatino, S. (2017). Bridge Life-cycle performance and cost: Analysis, prediction, optimisation and decision-making. *Structure and Infrastructure Engineering, 13*(10), 1239–1257. https://doi.org/10.1080/15732479.2016.1267772.

Gautam, D. (2017a). Assessment of social vulnerability to natural hazards in Nepal. *Natural Hazards and Earth System Sciences, 17*(12). https://doi.org/10.5194/nhess-2017-137.

Gautam, D. (2017b). On seismic vulnerability of highway bridges in Nepal: 1988 Udaypur earthquake (M W 6.8) revisited. *Soil Dynamics and Earthquake Engineering, 99*(August), 168–171. https://doi.org/10.1016/j.soildyn.2017.05.014.

Gautam, D., & Dong, Y. (2018). Multi-hazard vulnerability of structures and lifelines due to the 2015 Gorkha Earthquake and 2017 Central Nepal Flash Flood. *Journal of Building Engineering, 17*. https://doi.org/10.1016/j.jobe.2018.02.016.

Gautam, D., Chaulagain, H., Rupakhety, R., Adhikari, R., Neupane, P., & Hugo, R. (2018). *Vernacular masonry construction in Nepal: History, dynamics, vulnerability and sustainability*. In Masonry: Design, Materials and Techniques.

Hong, J.-H., Chiew, Y.-M., Lu, J.-Y., Lai, J.-S., & Lin, Y.-B. (2012). Houfeng bridge failure in Taiwan. *Journal of Hydraulic Engineering*. https://doi.org/10.1061/(asce)hy.1943-7900.0000430.

NPC. (2017). Post flood recovery need assessment. Kathmandu. https://www.npc.gov.np/images/category/PFRNA_Report_Final.pdf.

Porter, K., Kennedy, R., & Bachman, R. (2007). Creating fragility functions for performance-based earthquake engineering. *Earthquake Spectra, 23*(2), 471–489. https://doi.org/10.1193/1.2720892.

Sabatino, S., Frangopol, D. M., & Dong, Y. (2015). Sustainability-informed maintenance optimization of highway bridges considering multi-attribute utility and risk attitude. *Engineering Structures, 102,* 310–321. https://doi.org/10.1016/j.engstruct.2015.07.030.

USGS. (2016). Preliminary peak stage and streamflow data at selected U.S. Geological Survey streamgages for flooding in the Central and Southeastern United States during December 2015 and January 2016. https://pubs.er.usgs.gov/publication/ofr20161092.

Wang, H., Hsieh, S.-C., Lin, C., & Wang, C.-Y. (2014). Forensic diagnosis on flood-induced bridge failure. I: Determination of the possible causes of failure. *Journal of Performance of Constructed Facilities*. https://doi.org/10.1061/(asce)cf.1943-5509.0000419.

Witzany, J., Cejka, T., & Zigler, R. (2008). Failure resistance of historic stone bridge structure of Charles bridge. II: Susceptibility to floods. *Journal of Performance of Constructed Facilities*. https://doi.org/10.1061/(asce)0887-3828(2008)22:2(83).

Zheng, Y., Dong, Y., & Li, Y. (2018). Resilience and life-cycle performance of smart bridges with shape memory alloy (SMA)-cable-based bearings. *Construction & Building Materials, Elsevier, 158,* 389–400.

Systems Thinking Approach for Resilient Critical Infrastructures in Urban Disaster Management and Sustainable Development

Md. Shahab Uddin, Jayant Kumar Routray and Pennung Warnitchai

1 Introduction

Disasters are dynamic processes (Alexander 1993). It can create physical damages and reduce the capacity of functioning in unpredictable ways. There is no place, and no system conclusively immune to disasters (Haddow et al. 2017). However, it is possible to reduce the consequences of disasters by reducing the vulnerabilities and timely response. Disaster damage is a function of hazards and vulnerabilities. Hazards are considered as an external force whereas; vulnerabilities are negative forces inherent in the system. Some vulnerabilities can easily be recognized while some lay in the system complexity. In absence of proper treatment, such vulnerabilities can rise up as secondary hazards. Latent vulnerabilities are very difficult to recognize, most of the time they remain out of sights, and create unpredictable consequences when the system is in chaos.

Modern cities are complex and dependent system. Functionality of an urban system is highly dependent upon the infrastructures system (Menoni et al. 2002). Infrastructures system is more than just an aggregation of individual facilities. They are mutually interconnected and interdependent. According to Elliott and McDonough (1999), the affinity existing between infrastructures is responsible for the growing intricacy of the "system of systems" and the subsequent disaster brought by the damage to the individual facility in an urban system. The philosophy of Perrow

Md. S. Uddin (✉)
Disaster Preparedness, Mitigation and Management, Asian Institute of Technology, Khlong Luang, Thailand
e-mail: shamimmsu@gmail.com

J. K. Routray
Regional and Rural Development Program, Asian Institute of Technology, Khlong Luang, Thailand

P. Warnitchai
School of Engineering & Technology, Asian Institute of Technology, Khlong Luang, Thailand

(2011) stated that disruption in complex system is inevitable but more importantly, the patterns of incidence are unpredictable. Aristotle's famous axiom that in a complex system "the whole is more than the sum of its parts" (Duncan 1979; Kane and Higham 2015) bears some similarity to the statement of Perrow.

Well-reported disasters around the world (Great Japan earthquake 2011, Hurricane Katrina 2005, Canada Blackout 2003, September 11 2001, Kobe Earthquake 1995, Loma Prieta Earthquake 1989, and others) have highlighted the vulnerability of power, transportation, communication, water, fuel and essential systems and their importance in response to the injury, death and damage which are an inevitable consequence of significant events in urban or city areas. Resilient infrastructures can build up a resilient city. Jha et al. (2013) defined infrastructure resilience as the decline in the vulnerability of built structures, such as buildings, lifelines and essential facilities. Resilience also refers to better management of resources and quick recovery. As a complex system, proper understanding of connectivity and interdependence between the components are also vital for the resilient critical infrastructures system (Rinaldi et al. 2001).

Resilience is the building block of sustainability. The major phases of resilience concept are planning and preparedness for initial shock absorption, emergency response for adaptive management, and the third is restoration for bouncing back to normalcy or even better. As cities are growing faster, their dependency on infrastructures is increasing dramatically. Moreover, due to incomplete understanding of interdependencies between infrastructures, capability to protect critical infrastructure still remains as a challenge for a resilient city (Mussington 2002; Javanbarg and Scawthorn 2012).

This chapter is an effort to use the knowledge of systems thinking for the operation and management of urban critical infrastructures system and disaster resilience. In the beginning, this chapter elaborated the importance of critical infrastructures in urban emergency response, and their vulnerabilities from internal (inherent complexities) and external (natural and manmade hazards) factors. This chapter is followed by a comparison between complex urban system and elaboration of the importance of system thinking in urban emergency response, disaster resilience and future sustainability. Finally, this chapter introduced many theories, tools, and models related to systems thinking and their potentials for modeling complex connectivity and interdependence among the infrastructures in an urban system. For disaster resilience and future sustainability city managers adopt systems thinking approach and computer aided decision support system for emergency response, disaster management and new development.

2 Critical Infrastructures (CIs) System

Urban systems are a mesh of complex connectivity and interdependence between the infrastructures (Fig. 1). In our daily life, the intricate systems have become an unavoidable part, almost like an omnipresent entity. When this dependence is
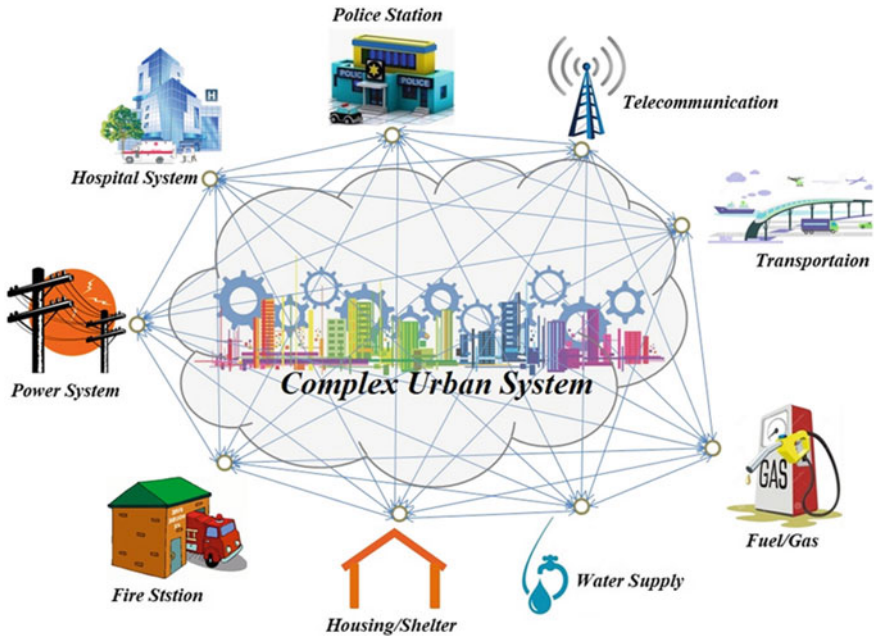
Fig. 1 Urban critical infrastructures system; a complex system (Constructed by the first author)

disrupted and brings forth the reality of our extreme reliance on the systems, only then we come to understand the extent of our dependency on the systems. For example: if there is a disruption in power supply, it will affect the functionality of all other systems and ultimately the entire society will sustain a certain level of miseries.

In general, urban infrastructures are grouped into two classes, (1) physical and (2) socio-economic. Physical infrastructures include all critical systems such as electricity and water supply, waste (water) management, transport and ITC systems. On the other hand, socio-economic infrastructures are important for health, safety and security, economy, culture and other social standards. Hospitals, schools, public administration, police station, fire station, bank, and esthetic areas belong to this class (Fourie 2006; Kabiru 2016).

2.1 Definitions of CIs System

Infrastructures are system or facility that provide basic services for the wellbeing of the society. The dictionary of American Heritage has defined the word 'infrastructure' for standard operation as: "The basic facilities, services, and installations needed for the functioning of a community or society, such as transportation and communications systems, water and power lines, and public institutions including

schools, post offices, and prisons" (Hildick-Smith 2005). All the basic facilities and services essential for the functioning of the urban society is collectively termed as Critical Infrastructures (CIs) system (Chapman et al. 2013).

According to Brunsdon (2003) critical infrastructure comprises the essential services and facilities on which communities depend. These can be further subdivided as follows:

- Lifeline services: water supply, wastewater system, electricity, gas supply and ITC
- Transportation services: road, rail, port, and airport facilities and networks
- Essential services: hospitals, police stations, fire stations, and emergency management center.

The following section reviews definitions of Critical Infrastructures use by different countries and organizations with a list of major critical facilities. This section is collected from the works of Brunner and Suter (2008) and Ritter and Weber (2004). In addition, government websites of the respective countries were also reviewed (Table 1).

2.2 Characteristics of CIs System

2.2.1 General Features

Studer (2000) divided critical infrastructure systems into object-oriented systems (OS) such as hospital and network-oriented systems (NS) such as electricity system. In geographic information system (GIS) such facilities are normally illustrated using point and line features to present locations (hospital, fire station) and networks (road network, pipeline system). Similarly, in graph theory, nodes are used to characterize an entity and links are used to illustrate the relationship between the facilities. Nodes, links and their spatial location are the key features to analyze the complex mutual connectivity and interdependence in the entire system. Critical infrastructures are parts of an urban environment, Similarly, they also generate an environment for themselves and the society (Fig. 2).

2.2.2 Interdependence

Urban critical infrastructures are complex, mutually connected and interdependent system. They are also called "Complex Adaptive System" and "System of Systems". The interdependence between critical infrastructures are generally bilateral. Many scholars defined the interdependence into many classes. The most common classification was proposed by Rinaldi and co-workers (2001). They divided critical infrastructures interdependence into four classes, namely

Cyber: This type of dependency is very vital in this modern world. Most of the organizations relay on information sharing between infrastructures. This type of

Table 1 Definition and list of critical infrastructures adopted by different countries and organizations

Country	Definition	List
United States of America	"Systems and assets, whether physical or virtual, so vital to the United States that the incapacity or destruction of such systems and assets would have a debilitating impact on security, national economic security, national public health or safety, or any combination of those matters"	IT, telecom, chemicals, commercial facilities, dams, nuclear, government facilities, transportation systems, emergency services, postal and shipping, agriculture and food, healthcare, water systems, energy, banking and finance, national monuments and icons
United Kingdom	"… comprise those assets, services and systems that support the economic, political and social life of the UK whose importance is such that loss could: (1) cause large scale loss of life; (2) have a serious impact on the national economy; (3) have other grave social consequences for the community; or (3) be of immediate concern to the national government"	Communications, emergency services, energy, finance, food, government and public services, public safety, health, transport, water
Australia	"Critical infrastructure is defined as those physical facilities, supply chains, information technologies and communication networks which, if destroyed, degraded or rendered unavailable for an extended period, would significantly impact on the social or economic well-being of the nation, or affect Australia's ability to conduct national defense and ensure national security"	Banking, (tele-) communication, energy and utility, transportation and distribution, other critical government services (Including defense and emergency services)
Japan	"Critical infrastructures are formed by business entities providing highly irreplaceable services and are essential for people's social lives and economic activities. If an infrastructure's function is suspended, reduced or unavailable, people's social lives and economic activities will be greatly disrupted"	Communication, government and administrative services, finance, civil aviation, railways, logistics, electricity, gas, medical services, water
Germany	"Critical infrastructures are organizations and facilities of major importance to the community whose failure or impairment would cause a sustained shortage of supplies, significant disruptions to public order or other dramatic consequences"	Banking and finance, (tele-) communication, energy and utilities, public administration, public health, rescue services, transport

Sources   https://publicwiki-01.fraunhofer.de/CIPedia/index.php/Critical_Infrastructure_Sector; https://www.dhs.gov/critical-infrastructure-sectors;   https://www.cpni.gov.uk/critical-national-infrastructure-0;   https://www.tisn.gov.au/Pages/Critical_infrastructure.aspx;   https://www.nisc.go.jp/eng/;   https://www.bmi.bund.de/EN/topics/civil-protection/critical-infrastructure-protection/critical-infrastructure-protection-node.html
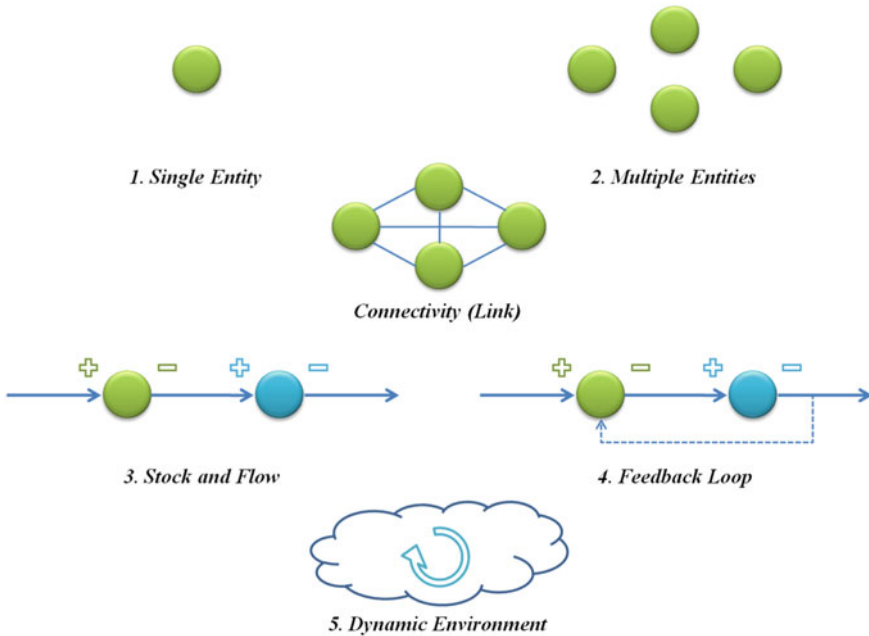
Fig. 2 General features of critical infrastructures system (Constructed by the first author)

dependence comprises and depend on Information and Telecommunication (ITC) systems.

Geographical: This type of interdependence is also called 'co-location' interdependence. When two or more infrastructure systems are located in the same neighborhood and close physical proximity, any disruption in the locality or any infrastructure system can affect components across multiple infrastructures due to physical proximity.

Physical: Physical interdependence is the most common and visible among all other types. Output from one is an input for other infrastructures. Electricity from power supply system is vital for the functionality of all other infrastructures and facilities.

Logical: Logical interdependence is also called 'decision interdependence'. Government or organizational policies, plans, and decisions can reshape the mutual interdependence between the systems and attributes of individual systems.

The same categories as Rinaldi et al. (2001) was adopted by Peerenboom et al. (2001). Dudenhoeffer et al. (2006) and Pederson et al. (2006) introduce policy and societal interdependence. Zhang and Peeta (2011) summarize the classification schemes of interdependencies among the infrastructure systems as following: (1) functional, (2) physical, (3) budgetary, and (4) market and Economic. Table 2 summarized common types of interdependence, simple definition and references.

Table 2 Types and definitions of critical infrastructures interdependence

Type of Interdependence	Generalized definition
Physical	For functioning, one facility needs supplies from other(s)[a,b]
Cyber	The dependency for information transmission through the information infrastructure[a,b]
Logical	Dependency on social, political, financial decisions, and policy intervention[a,b,c,d,e]
Geographic	Spatial proximity between the infrastructures[a,b,f]
Societal	The relationship between the infrastructures and community[c,d]
Functional	One infrastructure system needs inputs from other(s) for operation[e,f]
Budgetary	Dependency on money for development, maintenance, and recovery[e,f]

[a]Rinaldi et al. (2001); [b]Peerenboom et al. (2001); [c]Dudenhoeffer et al. (2006); [d]Pederson et al. (2006); [e]Zhang and Peeta (2011); [f]Zimmerman (2013)

Many other types of interdependence were reported in different articles, such as (1) restoration interdependence (Kameda 2000; Wong and Isenberg 1995), (2) Cascade interaction (Kameda 2000; Yao et al. 2004), and (3) General interaction (Yao et al. 2004). Wallace et al. (2001) and Lee et al. (Lee II et al. 2007) classified interdependence as input, mutual, shared, exclusive, and co-located.

2.3 CIs System Vulnerabilities

Oliver-Smith (2013) expressed vulnerability as the conceptual nexus linking people's relationship with their environment to social forces and institutions and the cultural values that sustain or contest them. Vulnerability generally defines the inherent properties and sensitivities of a system and its components under the impact of hazard or stress (Cardona 1999). Comfort (1999) defined vulnerability as those circumstances which place people at risk by reducing their means of response or denying them existing protection.

Vulnerability of urban critical infrastructures is multifaceted. System complexity, connectivity and interdependence, inadequate capacity, management incompetence, community dependency, and aging facilities are major concerns for critical infrastructure vulnerability assessment. Eusgeld et al. (2008) listed flaws in design, imple-
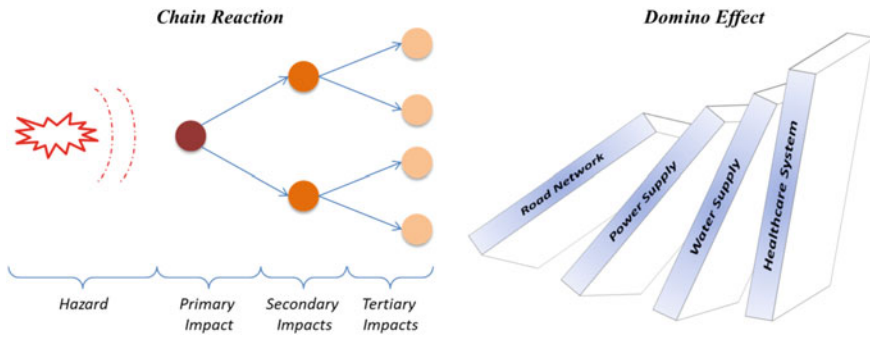
Fig. 3 Complexity and interdependence induced vulnerabilities in urban critical infrastructures system (Constructed by the first author)

mentation, operation and/or management of a system as the reasons for increasing the sensitivity to internal and external threats, despite its absorbing and recovering ability.

Minciardi et al. (2006) divides vulnerability into two types; (1) physical vulnerability and (2) functional vulnerability. Here, physical vulnerability is similar to static vulnerability and functional vulnerability represents dynamic or systemic vulnerability. Menoni et al. (2007) divided the factors of critical infrastructures vulnerability into three types such as functional vulnerability, organizational vulnerability and physical vulnerability. According to Little (2004), in major urban areas, infrastructure systems are intrinsically interconnected and open to complex system failures. Interdependence induced damage cascade or domino effects are major vulnerabilities in disaster emergencies. In a complex interdependent system, the effects of a disaster propagate within the system in chain reaction and creates primary to tertiary level interventions (Fig. 3).

2.4   CIs and Past Disasters

The critical interdependence between the disrupted infrastructures during emergency was first reported after the 1906 San Francisco Earthquake (O'Rourke et al. 2006; Scawthorn et al. 2006). O'Rourke (2007) reported the consequences of electric power disruption on community and other facilities after the 1994 Northridge Earthquake. In the recent years many disasters such as Haiti Earthquake (Kovacs 2010), Hurricane Katrina (Price 2006; McDaniels et al. 2007), Great Japan Earthquake 2011 (Norio et al 2011; Bouchon and Di Mauro 2012), September 11, 2001 (Seiferst 2002; Luiijf and Klaver 2011), Canada Blackout 2003 (McDaniels et al. 2007; Chai et al. 2011), Marmara Earthquake 1999 (Comfort and Sunger 2001), German Blackout 2005 (Bach et al. 2013), Ice Storm 1998 (Chang et al. 2007), Florida Hurricane 2004 (Bigger et al. 2009), Hurricane Sandy 2012 (Heidemann et al. 2012; Beck

Table 3 Patterns of functionality disruption on CI systems in disasters

Facility	Reasons/patterns of functionality disruption
Schools	1. Physical damages (structural and non-structural) 2. Inadequate water and waste water systems
Hospitals	1. Physical damages (structural and non-structural) 2. Insufficient manpower 3. Damage of lifeline facilities (power, water, gas, telecommunication) 4. Scarcity of fuel supply for backup generator 5. Damage of road network 6. Scarcity in logistics supply
Fire station	1. Structural and non-structural damage 2. Damage of fire trucks 3. Damage of lifeline facilities (power, water, telecommunication) 4. Scarcity of fuel supply for backup generator and fire trucks 5. Damage of road network
Police station	1. Structural and non-structural damage 2. Damage of vehicles 3. Limited fuel supply
EOC/local govt. office	1. Structural and non-structural damage 2. Damage of lifeline facilities (power, water, telecommunication) 3. Scarcity of fuel supply for backup generator and fire cars
Electric power	1. Damage/shutdown of generation plants 2. Damage of distribution center 3. Damage of distribution network (cable, poles, transformers) 4. Lack of water for cooling system 5. Inadequate supply of fuels (gas, oil, coals)
Water	1. Breaks and leakages in underground pipeline systems 2. Damage/shutdown of pump station 3. Damage/shutdown of water purification plants 4. Damage of underground/overhead reservoir tank 5. Damage of wastewater lift station and treatment plant
Telecom	1. Damage of towers and facility stations 2. Shutdown of cooling system (lack of water) 3. Inadequate electric supply and fuel for backup generator 4. Shutdown due to extreme overloads
Gas/fuel	1. Damage of underground pipeline system 2. Damaged/shutdown of petroleum purification plant 3. Damage/shutdown of compressor 4. supply disruption due to lack of accessibility
Transportation	1. Damage due to ground rapture 2. Damage due to soil liquefaction 3. Damage due to bridge collapse 4. Damage due to falling down of overpass and elevated highways 5. Blockage due to landslide debris 6. Blockage due to collapsed buildings debris 7. Shutdown of traffic signal system 8. Heavy traffic due to mass movement, road damaged and traffic signals

2012; Comes and Van de Walle 2014), Hurricane Hugo 1989 (Griswold et al. 1990), South China Snow Storm 2008 (Wang et al. 2012), Kobe Earthquake 1995 (Goto et al. 2008), Chile Earthquake (Kovascs 2010), Hurricane Haiyan 2013 (Lum and Margesson 2014) very clearly demonstrated the vulnerabilities of critical infrastructures against natural and man-made disasters. All those events also demonstrated the significance of cascading failure in the total disruption from the hazards. Table 3 documented ranges of damage pattern in critical infrastructures from the past disasters.

3   CIs System Management

Operation and management of critical infrastructures are very challenging and their services are vital for all the phases of disaster management cycle. During the new development, existing risk mitigation, and preparedness planning system thinking approach can help to find the optimum number and suitable sites for new construction, optimizing the utilization of available resources and developing suitable communication and coordination mechanism among the organizations. Generally, the overall situation gets more dynamic and chaotic during the emergency and disaster. The situation demands huge efforts for response and recovery. Timely initiatives can reduce the damage and loss significantly. The necessity for systems thinking is more critical in emergency response and recovery than the normal condition.

3.1   *Location Allocation*

Location theory has long been of interest for determining optimum sites of infrastructures such as fire stations, hospitals, airports, or warehouses. It has a well-developed theoretical background (Pace and Shieh 1988; Asami and Isard 1989). Owen and Daskin (1998) identified facility location problem as an important research issue in spatial data analysis in 1998 as it deciphers problems of balancing the demand and supply by using sets of objectives and relevant constrictions.

The idea of location allocation was first introduced in 1909 to find the best site for a warehouse to optimize travel distance (Başdemir 2004). Other seminal location publications include: Hotelling (1990), Christaller (1966), Cooper (1963), Hakimi (1964, 1965), Balinski (1965), ReVelle and Swain (1970), Toregas et al. (1971), and Church and ReVelle (1974), Badri (1999). Service area covering problems are one of the principal problems in location theory (Daskin 1997; Brandeau and Chiu 1989; ReVelle and Eiselt 2005). Badri (1999) combined Analytic Hierarchy Process and multi-objective goal-programming to support decision making for locating optimum site for facility planning. Church and ReVelle (1974) and Erdemir et al. (2008) worked on Maximum Covering Location Problem for locating fixed number of facilities that will provide maximum coverage.

3.2 Resource Optimization

The Patriot Act of 2001 legally defined the Concept and Practice of Critical Infrastructure Protection (CIP), and the US Presidential Directive HSPD-7 in 2003 broadened as "the Identification, prioritization, and protection of the physical and virtual systems that are so vital to the United States that the incapacity or destruction of such systems and assets would have a debilitating impact on security, national economic security, national public health or safety" (Moteff 2007).

Since it is impossible to protect all CI sectors, assets, systems and networks with limited resources, prioritizing efforts are required to focus better on protection planning, inform resource allocation decisions, and support effective incident management, including where risk management programs should be instituted and which measures offer the greatest return on investment (Boin and McConnell 2007).

Management of widespread disruption and chaos is solely dynamic process when the situations evolve over time and creates state of uncertainty. Traditional management approaches may not be able to take control of the situation, rather can push the situation from bad to worse. Management approach need to adapt with the ever-changing dynamic situations. Such adaptive management approach demands very clear knowledge on the attributes and attitudes of all the components involved in the system.

Rist et al. (2013) defined adaptive management as "a structured, iterative process which aims to reduce uncertainty by increasing knowledge and understanding, thus enabling improved management decisions over time". Many scholars (Williams and Brown 2016; Allen et al. 2011; Rehme et al. 2011; Prato 2007; Parma 1998; Kohm and Franklin 1997; Walters 1986; Holling 1978) stated adaptive management the appropriate approach for handling uncertainty and change over time.

3.3 Priority Restoration

Restoration is the process of bringing back a disrupted society to its essential normal functioning. The restoration process normally begins immediately after any hazard event and mainly focuses on the establishment of repairable essential facilities and services. The process can last for few weeks to months depending on the nature and scale of the devastation and capacity of the affected community (Amaratunga and Haigh 2011).

All the components in our society are interconnected and interdependent, and function simultaneously as a single complex system. Any change in one component has the potential to influence the whole system. Sharkey et al. (2015) stated "A restoration interdependency occurs when a restoration task, process, or activity in an infrastructure is impacted by a restoration task, process, or activity (or lack thereof) in a different infrastructure". In their research, they also documented five types of restoration interdependency observed during the restoration process on Hurricane Sandy 2012. Based on the experiences from 11 September 2001, Prieto (2002) sug-

gested the importance of support environment functionality for effective restoration and recovery. Restoration of damaged critical facilities in Kobe Earthquake took much longer times (5–10) than hazards because of cascade effects and complex interactions (Pitilakis et al. 2008).

3.4 Organizational Coordination

Hazard events management is eventually a dynamic playground of multiple organizations (Waugh 1993). All the organization need to understand and communicate among each other to synchronize their activities for an effective response and management (Paton and Flin 1999; Janssen et al. 2010; Waugh and Streib 2006; Kapucu and Garayev 2011). Information is the key to effective emergency response but rarely available (Horan and Schooley 2007; Kapucu et al. 2010; Comfort et al. 2004; Weber and Khademian 2008).

According to Waugh and Streib (2006) collaborative management approaches have become an unavoidable tool for urban emergency response and disaster management. According to Bardach (1998), collaboration is the effort to join potential mutual activities of two or more agencies to increase the value of ultimate outcomes. In collaborative approach people from different organizations work for a single goal through joining labors, capitals, knowledge, and share rights of the final product (Kamensky and Burlin 2004). Communication, cooperation and coordination are vital for effective collaboration. The efficiency of emergency response can be significantly improved with the support of quality information (Horan and Schooley 2007; Kapucu et al. 2010). A harmonic performance is impossible without proper coordination among the organizations in emergency response (Paton and Flin 1999).

Since emergency situation is full of complication, urgency, and indecision (Aldunate et al. 2005; Comfort 1999; Danielsson and Ohlsson 1999) it is crucial to have a clear idea about goals, roles, capabilities, authorities, inputs and outputs of all participating organizations before any devastation. In the past, emergency collaboration was mainly focused on the post disaster situation. Emergency collaboration can be significantly improved by networking the core emergency responders before any disaster and continue as a normal practice by mainstreaming it in organizational practices.

4 Urban Disaster Management

4.1 Urban System

Urban centers are at the heart of development, commerce, education and innovation (Shaw et al. 2009). Urban critical infrastructures are like vital organs in a body (Turoff et al. 2014). Infrastructure services are essential to support economic pros-

perity and quality of life (Rinaldi et al. 2001; Kröger 2008). Currently, more than 50% of the world population are living in complex urban system (UN-Habitat 2011) and projected as 60% by 2030 (Doytsher et al. 2010). For the safety and security of this huge population, future urban systems need to be resilient against disasters. Urbanization is inevitable (Teriman et al. 2008); hazards are unavoidable; but disasters/emergencies could be preventable. Increasing dependency of urban systems on critical infrastructures and technology (Menoni et al. 2002), and ever-increasing complexity among the urban subsystems (Gencers 2013) are growing concerns about their undesirable effects in disaster situation.

4.2   Infrastructure, City, and Hazard

Cities are becoming highly prone to disasters by both natural and manmade hazards. Lives and livelihoods of a city solely relies on the services from their basic or critical infrastructures system. Critical infrastructures must stay functional in all situation. However, such facilities do not stay in isolation. They are equally victimized during massive devastations. In absence of effective and timely recovery, lives in city can worsen without basic services. To reduce the probability of such happening, city managers need to think for resilient infrastructures system along with a resilient city. Hazard can create threats for infrastructures system. On the other hand, properly designed infrastructure can reduce the risk of disasters and sometime prevent it. Faultily designed and managed infrastructures can create additional threats and disaster. Similarly, we can see that, urban systems are not only victims of disasters/hazards, they are also the background reason for frequent disasters. Unplanned urbanization and climate change are key reasons for the suffering of urban communities from disasters. Figure 4 illustrated the interrelationships between infrastructure, urban system, and hazard in urban disaster continuum.

4.3   CIs in Disaster Continuum

The modern society is highly reliant on services from the infrastructures system for their lives and livelihoods. Services from critical infrastructures are vital for disaster management and emergency response. Moreover, malfunctioned critical infrastructures system can create service disruption and push the entire society to a disastrous situation. Disaster emergency response and management, usual lives and livelihood, and development, all solely rely on the performance of critical infrastructures system. Resilient critical infrastructures are the key to disaster resilience and future sustainability.

Critical infrastructures are vital for the functioning of urban system, they are also very important for managing crisis in the urban system (Fig. 5). In case of crisis/disaster they are the primary responders for protecting the society from dev-
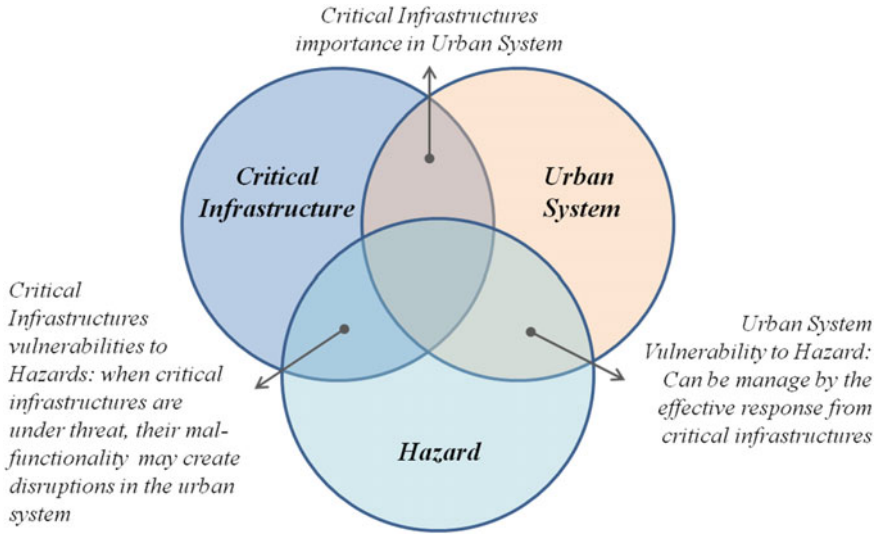
Fig. 4 Interrelationships between hazard, urban system and critical infrastructure (Constructed by the first author)
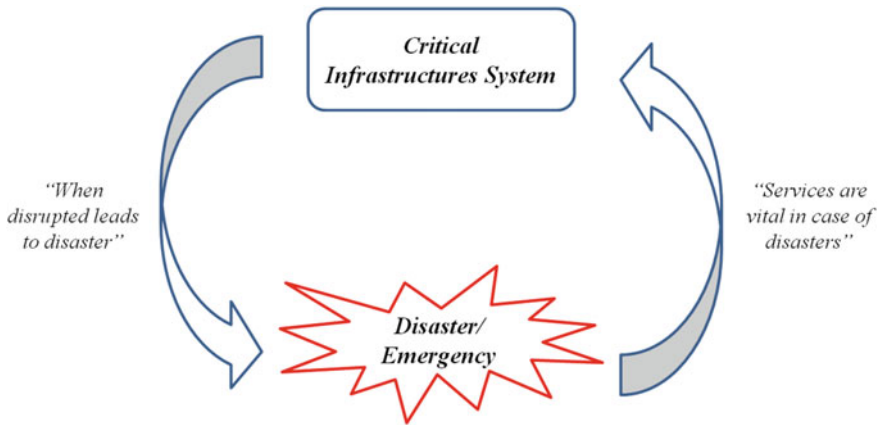
Fig. 5 Critical Infrastructure and disaster (Adopted from 'Bouchon 2006')

astation. On the other hand, malfunctional critical infrastructures and disrupted vital services can push the society to chaos and sufferings (Bouchon 2006). The role of critical infrastructure and their protection are vital for public safety, emergency response and disaster management (Stangl et al. 2012). Post disaster recovery of community, basic services, and economy also rely on the capacity and resilience of infrastructures (Jha et al. 2013).

Resilient urban system is highly dependent on resilient critical infrastructures system (Javanbarg and Scawthorn 2012; Oh et al. 2012). One of the challenging

issues in building critical resilience is their complex connectivity and interdependency (Mussington 2002; Shinozuka et al. 2007; Dueñas-Osorio and Vemuru 2009; Ouyang and Dueñas-Osorio 2011; Rosato et al. 2008). Since, all the infrastructure facilities perform as a team, even if each facility is resilient, the system may still remain vulnerable in absence of a coordinated management approach (Auersward et al. 2006; Waugh and Streib 2006). Again, due to incomplete understanding of interdependencies between infrastructures, capability to protect critical infrastructure remains as a challenge for a resilient urban system (Mussington 2002; Javanbarg and Scawthorn 2012).

5   Urban Emergency Response

5.1   Emergency Response

Every hazard prompted event or incident starts with emergency: a state of confusion. Scholars characterized emergency by complexity, urgency, and uncertainty (Chen et al. 2008; Aldunate et al. 2005; Comfort 1999; Danielsson and Ohlsson 1999). The situation demands huge amount of decisions with limited information. Correct management approach may help to stop/control damage propagation and bring the situation back to normalcy first. Wrong or improper initiatives may lead the situation to the worst such as disaster or catastrophe (Fig. 6).

The very common nature of any hazards disruptions is, they reduce the capacity (C) of the affected system and escalates the demands (D) significantly. Such sudden fluctuations in capacity and demand can create bottlenecks to event man-
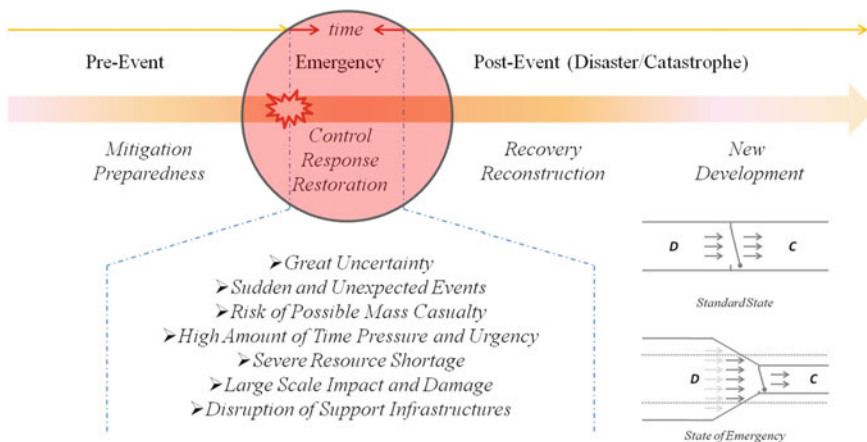
Fig. 6 Uncertainty and other challenges in emergency response (Constructed by the first author)

agement (Fig. 6). In absence of timely and effective action to take care of such situation workloads may increase with time and lead the system to progressive collapse. Effective emergency response can miraculously improve the state of chaos from being deteriorated and increase resilience.

5.2 Disaster Resilience

According to Holling (1973), resilience is a "measure of the persistence of systems and their ability to absorb change and disturbance and still maintain the same relationships between populations or state variables". Many scholars also considered the rate of recovery as an indicator of resilience (Campanella 2006; Wallace and Wallace 2008 ; Cutter et al. 2008). The very basic concept of sustainability is the ability to be maintained at a certain rate or level. In the realm of development, the concept of sustainability provides the idea of development without obstructing the rights of future generations (Brundtland 1987). In chaos or hazard events management, sustainability refers to the capacity of remedial from hazard devastations and positive progression. Theoretically, sustainable and resilient communities are able to withstand extreme disruptions and recover rapidly (Tobin 1999).

Resilience is the key to sustainability whereas chaos is an integral part of our society. We may not prevent, but we can manage effectively to reduce losses and damages, and recover quickly. Quicker response results in better chaos control (Waugh and Streib 2006). Resilient communities have the capacity to absorb shock, response fast, recover quickly and get back to normalcy, or better (Holling 1973). A resilient system is an adaptive system, which can learn from the part and act better in future. The ultimate outcome of resilience is sustainability. From a cyclic rise and falls over long period, a resilient system maintains net achievement and supports sustainability (Fig. 7).

5.3 Disaster Sustainability

Sustainability is the long-term outcome initiated from effective disaster management, adaptive learning, and building resilience. Resilience is the building block of sustainability, while adaptive learning is the process of building resilience. However, the most important thing in disaster management is emergency response. Disaster sustainability also depends on the event severity and community capacity. Small disasters can help the community to buildup resilience gradually from positive adaptive learning. Whereas, a catastrophic event-level of devastation is far beyond the capacity of the affected community-can push the community to ground zero, and make the community settings more miserable and vulnerable. The sense of sustainability in real-life disaster is quite different than the concept in development studies. Disaster sustainability is a parallel thought of sustainable development.
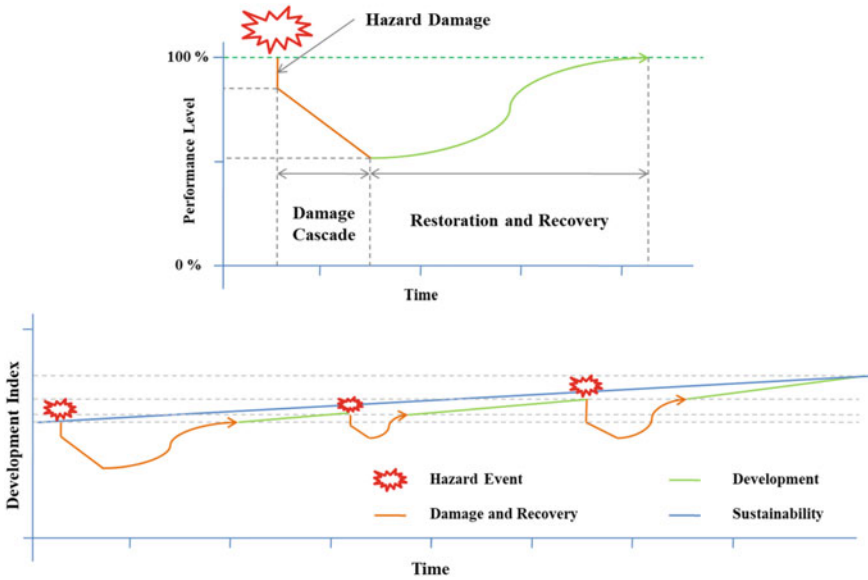
Fig. 7 Conceptual links between emergency response, resilience and sustainability (Constructed by the first author)

6 Systems Thinking

6.1 Basic Concepts

Our society is becoming complex with new developments and interventions of new technologies. All the issues and problems in the society are interconnected and mutually dependent (Uddin et al. 2018). In the current circumstances, it is not possible to make a safe and efficient social system by treating the constituents of the system independently. The management practice needs a paradigm shift from managing social issues individually to collectively. Disaster is the result of complex interactions between the physical world, the natural and built environment, organizational settings, and activates (Quarantelli 2005; Cuny 1993; Davis and Wall 1992). Latent risk can be materialized into real disasters when a triggering event meets the vulnerabilities and crosses the threshold (Maskrey 1993; ICSU-LAC 2010). Vulnerability is the state of an 'element at risk' that reflects susceptibility, the conditions that favor or facilitate damage (Khazai et al. 2015).

Urban systems are like mutually connected multiple gas balloons. Exerting external pressure on one of them will change the pressure dynamics in all the connected balloons. To understand the flow dynamics in the complex urban system, the concept of 'entropy' can be used. According to the second law of thermodynamics thermal energy flows from higher gradient to lower gradient to reach the equilibrium. While
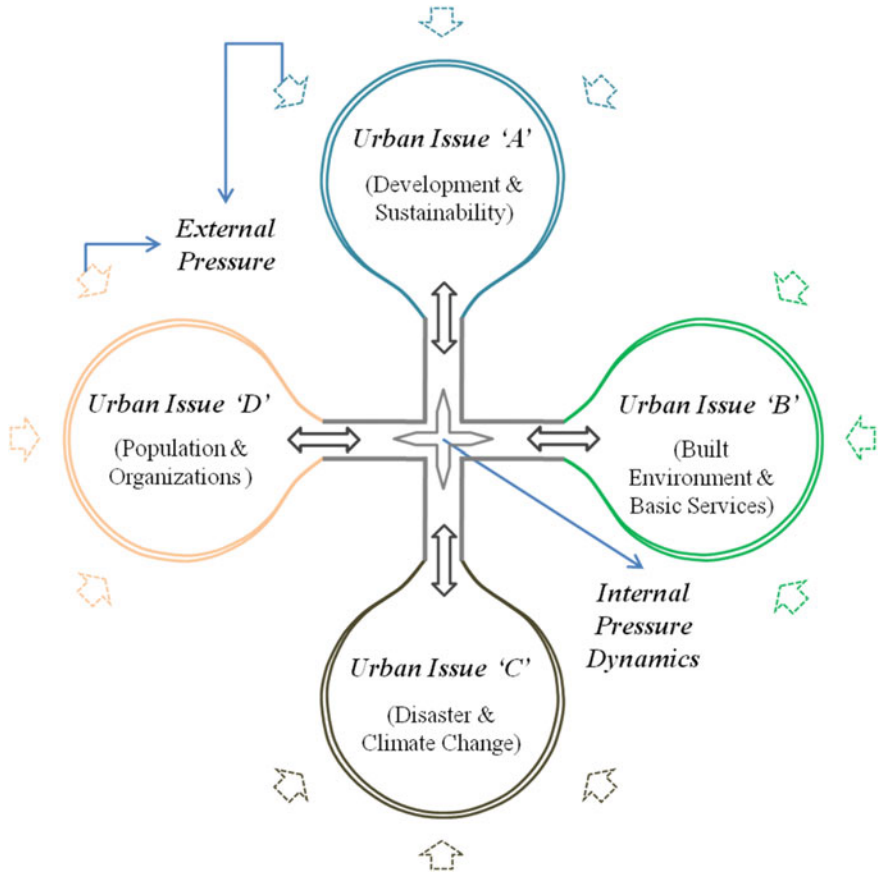
Fig. 8 Conceptual model for systems thinking in urban management (Uddin et al. 2018)

the thermal system is trying to find a balance state, it is also creating imbalances with the surrounding environment which exceed the net gain of equilibrium. In complex urban system, when we are trying to solve one issue without treating the system as a whole, it can create more problems than the solution. Figure 8 is a conceptual illustration of an urban system, which demonstrated complexity of the system, and pointed out that it is impossible to solve a problem individually without taking issues directly or indirectly connected with the target problem into consideration. All the elements in the urban system are connected and mutually dependent. They conjointly share internal pressure fluxes among them. In the mutually connected complex system, urban critical infrastructures system is one of the most important balloons.

6.2 Systems Thinking for CIs Management

Complex systems are collection of a number of interacting parts that perform in a non-linear way, and displays 'emergent' phenomena (Ramalingam 2013). Event progression in the complex systems relies on their initial conditions, often called the 'butterfly effect'. Butterfly effect creates large effects from small causes in a complex system (Smith 1998; Stewart 1997). Another principle of the complex system is 'bifurcation', where the system evolves in a nonlinear way with successive disruption (Mathews et al. 1999; Williams 2014). Cities are the complex systems (Montenegro 2010), where system's complexity is one of the challenging issues for the authority in disaster response (Griinewald and Binder 2010; Satterthwaite and Dodman 2013). Managing large data, understanding system dynamics, forecasting and planning, smart decision making, organizational management, and rational plan and policies are six potential scopes of system thinking for better urban governance (Orr 2014).

7   System Theories, Tools and Models

A system is an integration of many individual elements with unique features performing together in harmony to produce a collaborative goal(s). Generally, a system has an input, a processing unit, and an output. Since, system consists of many components and their connectivity, they are essentially complex. In a controlled complex system (computer, internet, etc.), where all the connected elements act based on predefined roles and relationship, system outputs for specific inputs are simply predictable. However, in an organic complex system, all the elements behave naturally and freely. Even though, connectivity and interdependence in an organic complex system are equally important as the controlled one, elements in organic complex system rarely considered the influences of each action on the overall system performance. In a complex system, relationships between the facilities are mostly non-linear. And most of the time it is impossible to capture the dynamics by adopting an approach. The following section elaborated a list of theories, tools and models suitable for modeling the interdependence and dynamic behaviors of complex infrastructures systems.

The field of operations research introduced a number of advanced analytical techniques in order to solve complex problems and make organizational decisions. Figure 9 illustrated a list of common ideas and their hierarchy of implementation. The subsequent sections elaborated all the theories, tools and models and their suitability in the understanding and management of complex urban and critical infrastructures.
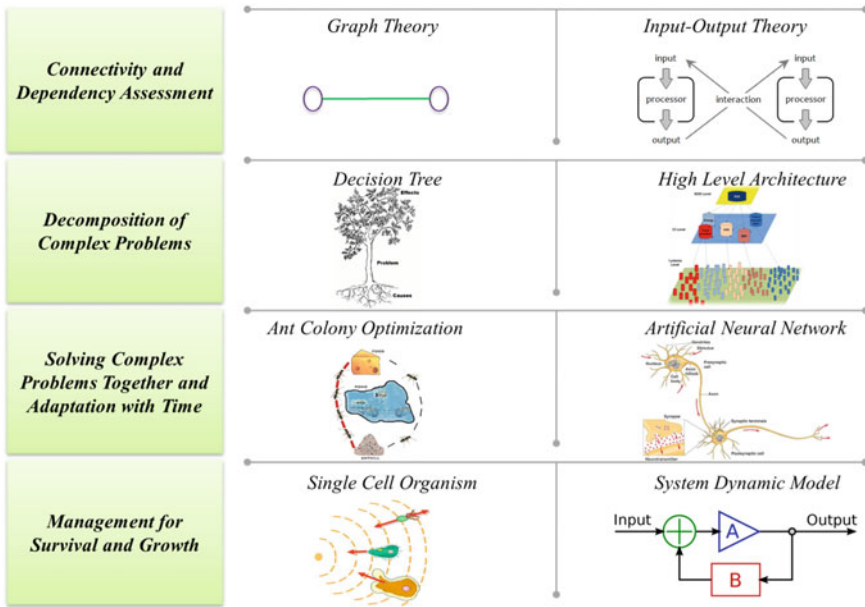
Fig. 9 Different approaches for different level of analysis (Constructed by the first author)

7.1 Theories

7.1.1 Graph Theory

Graph theory is one of the basic tools for network analysis. Basically, a graph consists of node (vertex) and link (edge). Nodes are basic element of a graph. Each node has its own properties. A link is the connection between two nodes. Based on the relationship (unilateral and bilateral) between two nodes a graph can be directed or undirected graph. Not only direction, types of graph also depends on the strength of relationship between the nodes (Bollobás 2012). Graph theory is the simplest theory for visualizing the connectivity and interdependence among the target entities. In graph theory infrastructure system are illustrated in networks where nodes represent individual infrastructure and links represent connectivity and interdependence among them.

7.1.2 Decision Tree

Decision Tree is one of the simple ideas for breaking down a complex problem into simple cause-effect chains. The approach is user friendly, flexible, less technical, and can handle non-linear relationships in complex system (Friedl and Brodley 1997). In contrast to other tools, it is quick and easy to train decision trees, and are rapid in exe-

cution (Jacobsen et al. 1999). It consists of three basic parts: (1) causes, (2) problems, and (3) effects. This idea can adopt both top-down (decomposition) and bottom-up (aggregation) approaches. Decision tree can be a very suitable to synthesize problems in urban infrastructures and solve them more naturally.

7.1.3 High Level Architecture

High Level Architecture (HLA) is a technique for modeling and simulating complex distributed systems (Kuhl et al 2000; Dahmann et al. 1997). This approach breaks down the complex system into many simple interconnected sub-systems. HLA offers many advantages for modeling and simulation of dynamic behavior of complex urban infrastructures system. The idea was developed originally by the US Department of Defense (DoD) (Nan and Eusgeld 2011; Eusgeld et al. 2011). The main idea of the approach was to facilitate the reuse and the interoperability of simulations (Kuhl et al. 2000). There are lots of existing domain-wise models. HLA ideas is to integrate them to solve new problems with higher potentials.

7.1.4 Ant Colony Optimization

Ants are social insects. Although, individually ant possesses only limited cognitive abilities, each is equipped with basic set of behavioral rules and collectively they can solve complex problems (Dorigo and Birattari 2011; Yaseen and Al-Slamy 2008). Rather than performing individually, ant's colony performs as a team based on some predefined rules and goals. Ant foraging is a prime example of so-called emergent behavior. When ants move for searching food, they release pheromone and create a trail to attract other ants to a food source. The learnings from ant colony optimization can significantly help optimized and collaborative management of urban infrastructures.

7.1.5 Artificial Neural Network

Artificial Neural Network (ANN) is an idea that roughly copied the human brain. ANN is the fundamental idea of artificial intelligence. This theory is developed to solve complex problems through systematic organization and utilization of previous experience (Schalkoff 1997; Haykin 2009). This approach is attractive to a large scale of problems belonging to different domains (Bishop 2007). It is designed to use segregated pieces of knowledge and information to solve complex problems. Urban critical infrastructures, as a system of systems can adopt ANN for making decisions to solve their complex problems more effectively.

7.1.6 System Dynamics

System Dynamics is the approach for studying and understanding the processes of a complex system over time. The method diagram includes stocks (the processing unit), flows (inputs and outputs) and information (the relationships between stock and slows) (Sterman 2000). The flows in system dynamics can be presented in two basic diagrams: (a) causal-loop diagrams and (b) stock-and-flow diagrams (Kirkwood 1998; Min et al. 2007). System dynamics is an effective tool for strategy assessment and policy evaluation (Sterman 2000). This approach is also used in environmental modeling, in economics, and in analysis of infrastructure interdependencies (LeClaire and Reilly 2005; Conrad et al. 2006; Min et al 2007). Feedback loops indicate connection and direction of effects between CI components (Stergiopoulos et al. 2016).

7.1.7 Input-Output Theory

Input–output model is another famous idea for modeling infrastructure interdependences (Haimes et al. 2005; Santos and Haimes 2004; Leung et al. 2007). The basic principle is based on an economic theory. It was proposed by Leontief in 1973. His model simplifies the analysis of the interdependence between the facilities and forecast possible changes in the entire system for any local perturbation. The model formulation is given by:

$$q = Aq^* + c$$

The above equation is simple idea of capturing complex interdependencies between the critical infrastructures. In the equation 'q' in the ultimate functionality levels of different infrastructures (0 to 1); 'q*' is the standardized level of functionality (typically 1); 'A' is the generalized interdependency matrix; and 'c' is the recovery rate following a disaster.

7.1.8 Agent Based Model

Agent-based models (ABM) is the approach for producing valuable information about dynamically interacting complex real-world system (Bonabeau 2002). ABM simulates aggregate performance of the constituents of the complex system. In this approach all the agents work for a collaborative goal, rather than for achieving individual goals. Individual infrastructure system can be viewed as agents. Decisions and actions of an individual agent are always influenced by the connected agents and governed by the ultimate goals of the system. Hence, the modeling and simulation of critical infrastructure interdependencies is the key advantage of the ABM approach (Stergiopoulos et al. 2016). ABM is one of the methods that emerged in the

early phase of modeling complex interdependence in critical infrastructures (Tolk and Uhrmacher 2009; Tomita et al. 1998; Amin 2002; Batty 2007). This method can seizure all types of the interdependencies among the critical infrastructures system (Ouyang 2014).

7.1.9 Markov Process

In Markov process, the initial situation of a certain system is assumed as an input. If the moment n is regarded as the "current", the moment 0, 1, …, n − 1 as the "past", and the moment n + 1 as the "future", Markov property indicates that when the "current" situation of a certain system is known, the situational probability of any "future" situation of the system is independent to its "past" situations. The system will transfer among the potential situations with a certain probability distribution. That is, the "future" situation features stochasticity, which is similar to the efficiency variation of emergency system, resulted from the restriction of emergency capacity and other uncertain factors (Gilks et al. 1995; Doucet et al. 2001).

7.1.10 Fuzzy Set Theory

Binary (0/1) system is not always suitable for solving all the real-world problems. In binary system, an infrastructure can only have one of the two possible states of functionality (functioning or not functioning) following a major hazard event. In reality, infrastructures sustain different level of damages and different levels of functionality loss. Effective decision-making models for critical infrastructure management should be able to tolerate fuzziness or ambiguity (Yu 2002). To solve the problems of such nature Zadeh (1965) introduced fuzzy set theory, and since then it has been applied in varieties of research in applied science (Izadi and Mohammadi 2013). In comparison with traditional binomial approach, fuzzy idea is much advanced for modeling interdependence functionality in complex system during disaster emergencies.

7.2 Tools

7.2.1 Social Network Analysis

Social Network Analysis (SNA) is the approach to analyze and visualize the relationships among actors (Scott 1988; Knoke and Yang 2008). The origin of SNA has deep roots in anthropology and sociology (Moreno 1934). SNA generally calculates betweenness, closeness, and degree centrality measures to provide different perspectives on the social or organizational relationships within the network (Freeman 1978).

Degree Centrality: Degree centrality is the simplest measure of node connectivity. It assigns an importance weight based on the number of links held by each node. This assessment is for finding the entities based on the potentials of their influence on the overall system.

Closeness Centrality: The measure is to find the entities who are best placed to influence the entire network most quickly. Closeness centrality assesses the shortest paths between all nodes, then assigns each node a weight based on its sum of shortest paths. The basic idea is that an entity 'x' is central if it can easily interact with all other entities within the network.

Betweenness Centrality: This measure identifies which entities act as 'bridges' between nodes in a network. These entities are also called gatekeeper entities. It measures the number of paths that pass through each entity.

7.2.2 Analytical Hierarchy Process

Analytical Hierarchy Process (AHP) is a frequently used tool for formulating and analyzing multicriteria decisions. AHP was introduced by Saaty (1972) to support decision making process for complex judgmental issues. AHP assistances decision makers to convert qualitative experience of experts into quantitative numbers by making trade-offs among them. The process conducts pair-wise comparisons to assess the relative rank of one activity to the other using the scale (Saaty 1977). Saaty argues that human mind can make more reasonable decision in comparing two things than to compare many. AHP is a suitable tool for setting priority of facilities in critical infrastructures system to reach a targeted goal. A inclusive list of the key applications of AHP, along with a explanation of the technique, can be found in Saaty (1980), Ramanathan (2001), Weiss and Rao (1987), Javanbarg et al. (2012), and Zahedi (1986).

7.2.3 DEMATEL Process

DEMATEL is a multicriteria decision-making tool for analyzing complicated and intertwined problems (Tsai et al. 2009). The concept of the tool was originally developed by the Science and Human Affairs Program of the Battelle Memorial Institute of Geneva (Wu 2008). The DEMATEL (Decision-Making Trial and Evaluation Laboratory) technique was adopted to visualize the influence propagation in a complex system representing direct relationship map (Falatoonitoosi et al. 2012). DEMATEL approach collects data from expert opinion survey following the concept 'Pairwise Comparison' (Saaty 1980), analyzes them following the concept of Markov Chain and graph theory (Geyer 1992).

7.3 Models

7.3.1 HAZUS-MH by FEMA

HAZUS-MH is a GIS based software has been developed by the Federal Emergency Management Agency (FEMA) to analyzes potential losses from disasters such as earthquakes, flood, and cyclone. It can analyze the severity of an earthquake by estimating the physical damage, economic loss and social impact (Schneider and Schauer 2006, Kircher et al. 2006). The software has separate physical damage and recovery models for individual structures and infrastructures (Dueñas-Osorio et al. 2007). HAZUS restoration curves are functions of 'damage states' of the facility and restoration schedule only considered non-emergency situation, where all other facilities are functioning normal. For restoration modeling, HAZUS used data from ATC-13 (ATC 1985; FEMA 1994, 2011). However, during a real-world hazard disruption rather than a single facility the whole society experiences disruptions. HAZUS model failed to illustrate the critical infrastructure interdependency and its uses are only limited to proactive disaster risk reduction and preparedness planning.

7.3.2 Syner-G by EC

Systemic Seismic Vulnerability and Risk Assessment of Complex Urban, Utility, Lifeline Systems and Critical Facilities (SYNER-G) has developed by European Commission Directorate-General for Research under Framework Programme-7 is slightly advanced than the HAZUS model in context of critical infrastructure interdependency. This model added the concept of usability. The concept usability not only considered physical damage of a facility but also dependency of the facility on other facilities (Cavalieri et al. 2012; Pitilakis and Kakderi 2011; Pitilakis et al. 2014a, b). The model slightly touched the issue of interdependency and proposed future development of their research through integration of cascading effects and emergency recovery process; these are absent in the current model.

7.3.3 Business Recovery Model by MCEER

A similar research has been developed by MCEER (Multidisciplinary Center for Earthquake Engineering Research) at the State University of New York at Buffalo. MCEER primarily works on restoration modeling of lifeline systems and has conducted relevant research on multiple infrastructures, while their aim is to establish disaster-resilient communities (Shinozuka et al. 2004). The main objective on MCEER was to increase the seismic resilience of the community through effective rehabilitation and recovery strategies. The MCEER recovery model is characterized by the attributes and behaviors of economic agents within a community (Chang and

Miles 2003). In spite of physical restoration and recovery of infrastructure systems, MCEER model mainly focused on business recovery and resilience for the analysis.

7.3.4 I2Sim Model by UBC

To estimate the effect of interdependence I2Sim used the following matrix procedures. This mathematical formulation also allows performing sensitivity analysis to determine the strongest interdependencies and the most vulnerable points. I2Sim's core solution is based on network partitioning techniques (Anderson 2010) implemented on a PC-cluster environment. Systems of thousands of variables are solved in seconds of computer time allowing for instant feedback on the evolution of the system dynamics (Marti et al. 2008).

There is another famous simulator named as I2Sim (Infrastructure Interdependency Simulator) developed by The University of British Columbia (UBC) and Other Five Universities in Canada under Joint Infrastructure Interdependencies Research Program (JIIRP). The model explicitly explained the functional interdependency of a facility on other facilities to aid in decision making during disasters (Ventura et al. 2010; Martí et al. 2008). Even though I2Sim is the most advanced simulator for critical infrastructure interdependency among the three discussed above, still lacks integrated recovery, facility management, organizational coordination and information management.

8   Ongoing Research

An extensive research effort is essential for understanding and management of complexities in the urban system to support decision making for disaster resilience and future sustainability. The first author of the chapter is currently working on "System Thinking for Urban Resilience: Modeling and Management of Critical Infrastructures Interdependence for Urban Emergency Response". The main target of the research is to create a "virtual city" in GIS platform using the information from a real one. The main methodological approach is to identify key entities (critical infrastructures), their location, individual attributes/behavior, mutual connectivity and interdependence between the entities (inputs-outputs), their cumulative behavior, and most importantly the priority of their services for the welfare of the community.

The integrated model is a system of three interconnected and interdependent models, namely facility functional interdependence model, dynamic restoration model, and adaptive management model for resource optimization (Fig. 10). The integrated model is designed to behave like the real city and generate scenarios based on a predefined condition for decision support. The decision-making is the human component of the system. This section is not only responsible in making decisions supported by the model generated alternative scenarios, but also in collecting, validating, and feed-
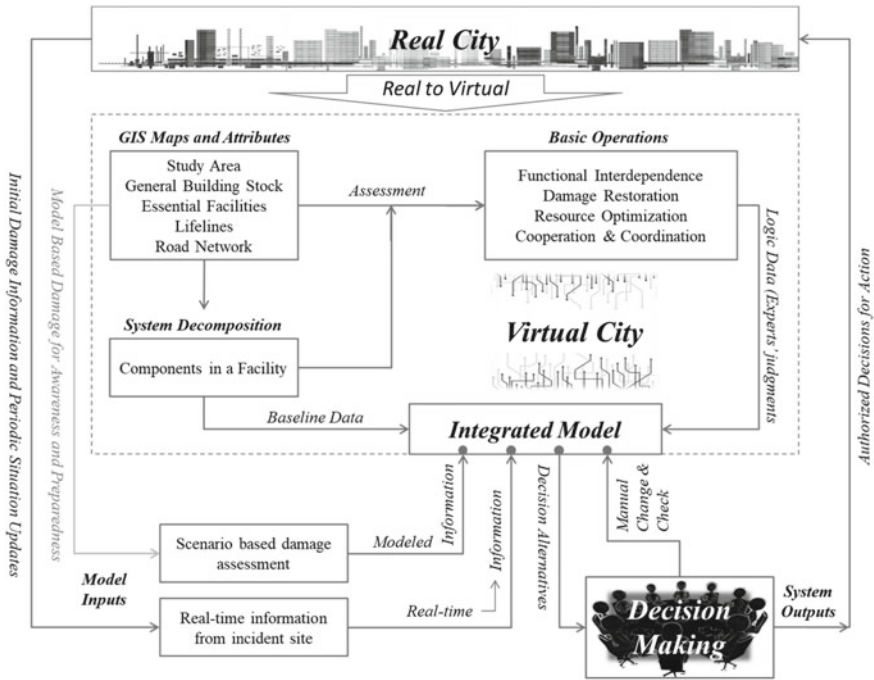
Fig. 10 The architecture of the proposed Emergency Response Support System (ERSS) (Constructed by the first author)

ing real-time information, and updating models' algorithms based on new learning from past events.

9   Conclusion

Critical infrastructures in an urban system need to be planned properly before constructing, protected from both natural and manmade threats and kept functional in all the circumstances. As complex-adaptive system, operation and management of such facilities must adopt the approaches of system thinking for maximizing overall performance and optimizing utilization of available resources. According to standard definitions, disaster is a situation while communities are unable to cope using their own resources. Most of the research blamed scarcity of resources for the suffering in disaster situation. But in reality, optimal utilization of available resources is the bigger challenge than scarcity. Disaster in an urban system significantly alter the input-output flows and supply-demand balances. Other than creating resources scarcity, disaster reassigns the weight of supplies and demands in the system. Hence, a contemporary mechanism for operation and management of urban infrastructures

and other constituents may not meet the needs of emergencies in future urban complex environment.

Cities are becoming complex with new developments and technological interventions. And subsequently harvesting the latent threats for many impending disasters. In the current social system where economy and lifestyle largely depend on the contribution of the basic infrastructures system, disaster resilience of an urban system has become an essential issue to be noted. It is a function of its resilient infrastructures system. Enhancing the resilience of infrastructure systems is critical to the sustainability of the society. As a complex system, CIs needs to adopt system-thinking approach and computer aided decision support system for their resilience and sustainability. CIs system can only provide services to the community in any situation when they are resilient enough to deal with any calamities without any sacrifice in their vital functionality.

It may not be possible to develop a single model, tool or theory for solving the problems in the operation and management of critical infrastructures in complex urban system. But it is feasible to breakdown the complex problem into simple identical segments, solve them independently with reference to a standard boundary conditions and later put them together to work as a single unit. For solving an independent simple problem, it is easy to get a suitable tool or theory and modify them as needed. This chapter described a set of theories, tools and models which have the potentials of solving the issues in complex urban system. A suitable combination and arrangement of these theories and tools can significantly contribute in the operation and management of critical infrastructures in a complex urban setting, especially in the context of emergencies. Modeling and management of critical infrastructures are comparatively a filed of academic intervention. The field has immense scopes of fundamental and operational research. Traditional urban management and emergency response approaches may not meet the needs of the future cities. Cities are not only growing faster but also becoming prone to hazards. It is very important to understand the dynamics in cities and prepare accordingly for the future safety and security of the urban areas and the half of the world population inhabiting in them. City managers and decision makers need to focus on treating problems in the urban system as a whole rather than treating them in parts. for effective urban emergecy response, disaster management, and future sustainability.

References

ATC. (1985). *Earthquake damage evaluation data for California*. Applied Technology Council.

Aldunate, R. G., Pena-Mora, F., & Robinson, G. E. (2005). Collaborative distributed decision making for large scale disaster relief operations: Drawing analogies from robust natural systems. *Complexity, 11*(2), 28–38.

Alexander, D. (1993). *Natural disasters* (p. 632). New York: UCL Press and Chapman & Hall.

Allen, C. R., Fontaine, J. J., Pope, K. L., & Garmestani, A. S. (2011). Adaptive management for a turbulent future. *Journal of Environmental Management, 92*(5), 1339–1345.

Amaratunga, D., & Haigh, R. (2011). *Post-disaster reconstruction of the built environment: Rebuilding for resilience*. Wiley.

Amin, M. (2002). Toward secure and resilient interdependent infrastructures. *Journal of Infrastructure Systems, 8*(3), 67–75.

Anderson, R. J. (2010). *Security engineering: A guide to building dependable distributed systems*. Wiley.

Asami, Y., & Isard, W. (1989). Imperfect information, uncertainty and optimal sampling in location theory: An initial reexamination of Hotelling, Weber, and von Thünen. *Journal of Regional Science, 29*(4), 507–521.

Auerswald, P. E., Branscomb, L. M., La Porte, T. M. and Michel-Kerjan, E. O. (Eds.). (2006). *Seeds of disaster, roots of response: how private action can reduce public vulnerability*. Cambridge University Press.

Bach, C., Gupta, A. K., Nair, S. S., & Birkmann, J. (2013). Critical infrastructures and disaster risk reduction. In *National Institute of Disaster Management and Deutsche Gesellschaft für internationale Zusammenarbeit GmbH (GIZ)*, New Delhi (72p).

Badri, M. A. (1999). Combining the analytic hierarchy process and goal programming for global facility location-allocation problem. *International Journal of Production Economics, 62*(3), 237–248.

Balinski, M. L. (1965). Integer programming: Methods, uses, computations. *Management Science, 12*(3), 253–313.

Bardach, E. (1998). *Getting agencies to work together: The practice and theory of managerial craftsmanship*. Brookings Institution Press.

Batty, M. (2007). *Cities and complexity: Understanding cities with cellular automata, agent-based models, and fractals*. The MIT press.

Başdemir, M. M. (2004). Locating search and rescue stations in the aegean and western mediterranean regions of Turkey. *Journal of Aeronautics and Space Technologies, 1*(3), 63–76.

Beck, C. (2012). *Critical infrastructure resilience: What we can learn from hurricane Sandy*. Security Center-Center for National Policy.

Bigger, J. E., Willingham, M. G., Krimgold, F., & Mili, L. (2009). Consequences of critical infrastructure interdependencies: Lessons from the 2004 hurricane season in Florida. *International Journal of Critical Infrastructures, 5*(3), 199–219.

Bishop, C. M. (2007). *Pattern recognition and machine learning*. New York, USA: Springer.

Boin, A., & McConnell, A. (2007). Preparing for critical infrastructure breakdowns: The limits of crisis management and the need for resilience. *Journal of Contingencies and Crisis Management, 15*(1), 50–59.

Bollobás, B. (2012). *Graph theory: An introductory course* (Vol. 63). Springer Science & Business Media.

Bonabeau, E. (2002). Agent-based modeling: Methods and techniques for simulating human systems. *Proceedings of the National Academy of Sciences, 99*(suppl 3), 7280–7287.

Bouchon, S., & Di Mauro, C. (2012). Resilience? Insights into the role of critical infrastructures disaster mitigation strategies. *TeMA Journal of Land Use, Mobility and Environment, 5*(3), 103–117.

Bouchon, S. (2006). The vulnerability of interdependent critical infrastructures systems: Epistemological and conceptual state of the art. Institute for the Protection and Security of the Citizen, Joint Research Centre, European Commission (pp. 99).

Brandeau, M. L., & Chiu, S. S. (1989). An overview of representative problems in location research. *Management Science, 35*(6), 645–674.

Brundtland, G. (1987). Our common future: Report of the 1987 World Commission on Environment and Development (Vol. 1, p. 59). Oslo: United Nations.

Brunner, E. M., & Suter, M. (2008). *An inventory of 25 national and 7 international critical information infrastructure protection policies, International CIIP Handbook 2008/2009*. ETHZurich: Center for Security Studies.

Brunsdon, D. (2003). *Critical infrastructure and earthquakes: Understanding the essential elements of disaster management*. New Zealand: Wellington.

Campanella, T. J. (2006). Urban resilience and the recovery of New Orleans. *Journal of the American Planning Association, 72*(2), 141–146.

Cardona, O. D. (1999). Environmental management and disaster prevention: Two related topics: A holistic risk assessment and management approach. *Natural Disaster Management,* 151–153.

Cavalieri, F., Franchin, P., Gehl, P., & Khazai, B. (2012). Quantitative assessment of social losses based on physical damage and interaction with infrastructural systems. *Earthquake Engineering and Structural Dynamics, 41*(11), 1569–1589.

Chai, C. L., Liu, X., Zhang, W. J., & Baber, Z. (2011). Application of social network theory to prioritizing Oil & Gas industries protection in a networked critical infrastructure system. *Journal of Loss Prevention in the Process Industries, 24*(5), 688–694.

Chang, S. E., McDaniels, T. L., Mikawoz, J., & Peterson, K. (2007). Infrastructure failure interdependencies in extreme events: Power outage consequences in the 1998 Ice Storm. *Natural Hazards, 41*(2), 337–358.

Chang, S. E., & Miles, S. B. (2003). Resilient community recovery: Improving recovery through comprehensive modeling. *MCEER Research Progress and Accomplishments: MCEER, 3,* 139–148.

Chapman, L., Azevedo, J. A., & Prieto-Lopez, T. (2013). Urban heat & critical infrastructure networks: A viewpoint. *Urban Climate, 3,* 7–12.

Chen, R., Sharman, R., Rao, H. R., & Upadhyaya, S. J. (2008). Coordination in emergency response management. *Communications of the ACM, 51*(5), 66–73.

Christaller, W. (1966). *Central places in southern Germany*. Prentice Hall.

Church, R., & ReVelle, C. (1974, December). The maximal covering location problem. In *Papers of the Regional Science Association* (Vol. 32, No. 1, pp. 101–118). Springer-Verlag.

Comes, T., & Van de Walle, B. (2014). Measuring disaster resilience: The impact of hurricane sandy on critical infrastructure systems. *ISCRAM, 11,* 195–204.

Comfort, L. (1999). *Shared risk: Complex systems in seismic response*. New York: Pergamon Press.

Comfort, L. K., Ko, K., & Zagorecki, A. (2004). Coordination in rapidly evolving disaster response systems: The role of information. *American Behavioral Scientist, 48*(3), 295–313.

Comfort, L. K., & Sungu, Y. (2001). *Organizational learning from seismic risk: The 1999 Marmara and Duzce, Turkey Earthquakes*. Working Paper 2001–5, Graduate School of Public and International, Affairs, University of Pittsburgh.

Conrad, S. H., LeClaire, R. J., O'Reilly, G. P., & Uzunalioglu, H. (2006). Critical national infrastructure reliability modeling and analysis. *Bell Labs Technical Journal, 11*(3), 57–71.

Cooper, L. (1963). Location-allocation problems. *Operations Research, 11*(3), 331–343.

Cuny, F. C. (1993). Introduction to disaster management: Lesson 2—Concepts and terms in disaster management. *Prehospital and Disaster Medicine, 8*(1), 89–95.

Cutter, S. L., Barnes, L., Berry, M., Burton, C., Evans, E., Tate, E., et al. (2008). A place-based model for understanding community resilience to natural disasters. *Global Environmental Change, 18*(4), 598–606.

Dahmann, J. S., Fujimoto, R. M., & Weatherly, R. M. (1997, December). The department of defense high level architecture. In *Proceedings of the 29th Conference on Winter Simulation* (pp. 142–149). IEEE Computer Society.

Danielsson, M., & Ohlsson, K. (1999). Decision making in emergency management: A survey study. *International Journal of Cognitive Ergonomics, 3*(2), 91–99.

Daskin, M. (1997). Network and discrete location: Models, algorithms and applications. *Journal of the Operational Research Society, 48*(7), 763–764.

Davis, I., & Wall, M. (1992). *Christian perspectives on disaster management*. Middlesex, UK: IRDA.

Dorigo, M., & Birattari, M. (2011). Ant colony optimization. In *Encyclopedia of machine learning* (pp. 36–39). Boston, MA: Springer.

Doucet, A., De Freitas, N., & Gordon, N. (2001). An introduction to sequential Monte Carlo methods. In *Sequential Monte Carlo methods in practice* (pp. 3–14). New York, NY: Springer.

Doytsher, Y., Kelly, P., Khouri, R., McLaren, R., & Potsiou, C. (2010). Rapid urbanization and mega cities: The need for spatial information management. *Research study by FIG Commission, 3*.

Dudenhoeffer, D. D., Permann, M. R., & Manic, M. (2006, December). CIMS: A framework for infrastructure interdependency modeling and analysis. In *Proceedings of the 38th Conference on Winter Simulation* (pp. 478–485).

Dueñas-Osorio, L., Craig, J. I., & Goodno, B. J. (2007). Seismic response of critical interdependent networks. *Earthquake Engineering and Structural Dynamics, 36*(2), 285–306.

Dueñas-Osorio, L., & Vemuru, S. M. (2009). Cascading failures in complex infrastructure systems. *Structural Safety, 31*(2), 157–167.

Duncan, J. (1979). Divided attention: The whole is more than the sum of its parts. *Journal of Experimental Psychology: Human Perception and Performance, 5*(2), 216–228.

Elliott, W. M., & McDonough, P. (1999). Optimizing post-earthquake lifeline system reliability. In *Proceedings of the 5th U.S. Conference on Lifeline Earthquake Engineering*, Seattle, Washington.

Erdemir, E. T., Batta, R., Spielman, S., Rogerson, P. A., Blatt, A., & Flanigan, M. (2008). Location coverage models with demand originating from nodes and paths: Application to cellular network design. *European Journal of Operational Research, 190*(3), 610–632.

Eusgeld, I., Nan, C., & Dietz, S. (2011). "System-of-systems" approach for interdependent critical infrastructures. *Reliability Engineering & System Safety, 96*(6), 679–686.

Eusgeld, I., Henzi, D., & Kröger, W. (2008). Comparative evaluation of modeling and simulation techniques for interdependent critical infrastructures. *Scientific Report, Laboratory for Safety Analysis, ETH Zurich* (pp. 6–8).

FEMA. (1994). *Assessment of the state-of-the-art earthquake loss estimation methodologies*. Washington: Federal Emergency Management Agency.

FEMA. (2011). *Hazus: FEMA's methodology for estimating potential losses from disasters*. Washington: Federal Emergency Management Agency.

Falatoonitoosi, E., Leman, Z., & Sorooshian, S. (2012). Casual strategy mapping using integrated BSC and MCDM-DEMATEL. *Journal of American Science, 8*(1), 125–155.

Fourie, J. (2006). Economic infrastructure: A review of definitions, theory and empirics. *South African Journal of Economics, 74*(3), 530–556.

Freeman, L. C. (1978). Centrality in social networks conceptual clarification. *Social networks, 1*(3), 215–239.

Friedl, M. A., & Brodley, C. E. (1997). Decision tree classification of land cover from remotely sensed data. *Remote Sensing of Environment, 61*(3), 399–409.

Gencer, E. A. (2013). Natural disasters, urban vulnerability, and risk management: A theoretical overview. In *The interplay between urban development, vulnerability, and risk management* (pp. 7–43). Berlin, Heidelberg: Springer.

Geyer, C. J. (1992). Practical Markov chain Monte Carlo. *Statistical Science, 7*(4), 473–483.

Gilks, W. R., Richardson, S., & Spiegelhalter, D. (Eds.). (1995). *Markov chain Monte Carlo in practice*. CRC press.

Goto, Y., Suzuki, T., Suetomi, I., Shoji, Y., Tsuruta, M., Kataoka, S., & Suzuki, H. (2008). Damage propagation caused by interdependency among critical infrastructures. In *The 14th World Conference on Earthquake Engineering*.

Griinewald, F., & Binder, A. (2010). *Inter-agency real time evaluation in Haiti: 3 months after the earthquake*. Report, Groupe URD and Global Public Policy Institute.

Griswold, J. S., Lightle, T. L., & Lovelady, J. G. (1990). Hurricane Hugo: Effect on state government communications. *IEEE Communications Magazine, 28*(6), 12–17.

Habitat, U. N. (2011). *For a Better Urban Future: A Mission for the 21st Century*. Nairobi: United Nations Human Settlements Programme.

Haddow, G., Bullock, J., & Coppola, D. P. (2017). *Introduction to emergency management*. Butterworth-Heinemann.

Haimes, Y. Y., Horowitz, B. M., Lambert, J. H., Santos, J., Crowther, K., & Lian, C. (2005). Inoperability input-output model for interdependent infrastructure sectors. II: Case studies. *Journal of Infrastructure Systems, 11*(2), 80–92.

Hakimi, S. L. (1964). Optimum locations of switching centers and the absolute centers and medians of a graph. *Operations Research, 12*(3), 450–459.

Haykin, S. (2009). *Neural networks and learning machines*. (Vol. 3). Prentice Hall, New Jersey, USA.

Heidemann, J., Quan, L., & Pradkin, Y. (2012). *A preliminary analysis of network outages during hurricane sandy*. University of Southern California, Information Sciences Institute.

Hildick-Smith, A. (2005). Security for critical infrastructure scada systems. In *SANS Reading Room, GSEC Practical Assignment, Version, 1* (pp. 498–506).

Holling, C. S. (1973). Resilience and stability of ecological systems. *Annual Review of Ecology and Systematics, 4*(1), 1–23.

Holling, C. S. (1978). *Adaptive environmental assessment and management*. Wiley.

Horan, T. A., & Schooley, B. L. (2007). Time-critical information services. *Communications of the ACM, 50*(3), 73–78.

Hotelling, H. (1990). Stability in competition. In *The collected economics articles of harold hotelling* (pp. 50–63). New York, NY: Springer.

ICSU-LAC. (2010). Science for a better life: Developing regional scientific programs in priority areas for Latin America and the Caribbean. In M. K. T. Arroyo, R. Dirzo, J. C.Castillas, F. Cejas, & C. A. Joly (Eds.), *Biodiversity in Latin America and the Caribbean: An assessment of knowledge, research scope and priority areas ICSU-LAC/CONACYT, Rio de Janeiro and Mexico City* (Vol. 1, p. 332).

Izadi, L., & Mohammadi, G. (2013). Group decision making process for contractor selection based on SWOT in fuzzy environment. *International Journal of Computer and Information Technology, 2*(1), 142–151.

Jacobsen, C., Zscherpel, U., & Perner, P. (1999, September). A comparison between neural networks and decision trees. In *International Workshop on Machine Learning and Data Mining in Pattern Recognition* (pp. 144–158). Berlin, Heidelberg: Springer.

Janssen, M., Lee, J., Bharosa, N., & Cresswell, A. (2010). Advances in multi-agency disaster management: Key elements in disaster research. *Information Systems Frontiers, 12*(1), 1–7.

Javanbarg, M. B., Scawthorn, C., Kiyono, J., & Shahbodaghkhan, B. (2012). Fuzzy AHP-based multicriteria decision making systems using particle swarm optimization. *Expert Systems with Applications, 39*(1), 960–966.

Javanbarg, M. B., & Scawthorn, C. (2012). UILLIS: Urban infrastructure and lifelines interactions of systems. In *15 World Conference on Earthquake Engineering, Lisbon, Portugal*.

Jha, A. K., Miner, T. W., & Stanton-Geddes, Z. (Eds.). (2013). *Building urban resilience: Principles, tools, and practice*. The World Bank.

Kabiru, S. A. (2016). Socio-economic infrastructure and national development: An analytical assessment from Nigerian perspective. *Journal of Humanities and Social Science, 21*(10), 36–42.

Kameda, H. (2000). Engineering management of lifeline systems under earthquake risk. *Bulletin of the New Zealand Society for Earthquake Engineering, 33*(3), 248–264.

Kamensky, J. M., & Burlin, T. J. (Eds.). (2004). *Collaboration: Using networks and partnerships*. Rowman & Littlefield Publishers.

Kane, E. A., & Higham, T. E. (2015). Complex systems are more than the sum of their parts: Using integration to understand performance, biomechanics, and diversity. *Integrative and Comparative Biology, 55*(1), 146–165.

Kapucu, N., Arslan, T., & Demiroz, F. (2010). Collaborative emergency management and national emergency management network. *Disaster Prevention and Management: An International Journal, 19*(4), 452–468.

Kapucu, N., & Garayev, V. (2011). Collaborative decision-making in emergency and disaster management. *International Journal of Public Administration, 34*(6), 366–375.

Khazai, B., Bendimerad, F., Cardona, O. D., Carreño, M. L., Barbat, A. H., & Buton, C. G. (2015). A guide to measuring urban risk resilience: Principles, tools and practice of urban indicators. *Earthquakes and Megacities Initiative (EMI), The Philippines*.

Kircher, C. A., Whitman, R. V., & Holmes, W. T. (2006). HAZUS earthquake loss estimation methods. *Natural Hazards Review, 7*(2), 45–59.

Kirkwood, C. W. (1998). *System dynamics methods*. College of Business Arizona State University USA.

Knoke, D., & Yang, S. (2008). *Social network analysis* (Vol. 154). Sage.

Kohm, K. A., & Franklin, J. F. (Eds.). (1997). *Creating a forestry for the 21st century: The science of ecosytem management*. Island Press.

Kovacs, P. (2010). *Reducing the risk of earthquake damage in Canada: Lessons from Haiti and Chile*. Toronto: Institute for Catastrophic Loss Reduction.

Kröger, W. (2008). Critical infrastructures at risk: A need for a new conceptual approach and extended analytical tools. *Reliability Engineering & System Safety, 93*(12), 1781–1787.

Kuhl, F., Dahmann, J., & Weatherly, R. (2000). *Creating computer simulation systems: An introduction to the high level architecture*. Upper Saddle River: Prentice Hall PTR.

LeClaire, R. J., & O'Reilly, G. (2005, July). Leveraging a high fidelity switched network model to inform system dynamics model of the telecommunications infrastructure. In *Proceedings of 23rd International System Dynamics Conference*. Boston, MA.

Lee II, E. E., Mitchell, J. E., & Wallace, W. A. (2007). Restoration of services in interdependent infrastructure systems: A network flows approach. *IEEE Transactions on Systems, Man, and Cybernetics, Part C (Applications and Reviews), 37*(6), 1303–1317.

Leung, M., Haimes, Y. Y., & Santos, J. R. (2007). Supply-and output-side extensions to the inoperability input-output model for interdependent infrastructures. *Journal of Infrastructure Systems, 13*(4), 299–310.

Little, R. (2004). A socio-technical systems approach to understanding and enhancing the reliability of interdependent infrastructure systems. *International Journal of Emergency Management, 2*(1–2), 98–110.

Luiijf, E., & Klaver, M. (2011). *Insufficient situational awareness about critical infrastructures by emergency management*. Security and Safety, The Netherlands: TNO Defence.

Lum, T., & Margesson, R. (2014). Typhoon Haiyan (Yolanda): US and international response to Philippines disaster. *Current Politics and Economics of South, Southeastern, and Central Asia, 23*(2), 209–246.

Martí, J. R., Hollman, J. A., Ventura, C., & Jatskevich, J. (2008). Dynamic recovery of critical infrastructures: Real-time temporal coordination. *International Journal of Critical Infrastructures, 4*(1), 17–31.

Maskrey, A. (1993). *Los Desastres no son Naturales! Red de Estudios Sociales en la Prevención de Desastres en América Latina*. Bogotá: Tercer Mundo Editores.

Mathews, K. M., White, M. C., & Long, R. G. (1999). Why study the complexity sciences in the social sciences? *Human Relations, 52*(4), 439–462.

McDaniels, T., Chang, S., Peterson, K., Mikawoz, J., & Reed, D. (2007). Empirical framework for characterizing infrastructure failure interdependencies. *Journal of Infrastructure Systems, 13*(3), 175–184.

Menoni, S., Pergalani, F., Boni, M. P., & Petrini, V. (2002). Lifelines earthquake vulnerability assessment: A systemic approach. *Soil Dynamics and Earthquake Engineering, 22*(9–12), 1199–1208.

Menoni, S., Pergalani, F., Boni, M. P., & Petrini, V. (2007). Lifeline earthquake vulnerability assessment. In *Managing critical infrastructure risks* (pp. 111–132). Dordrecht: Springer.

Min, H. S. J., Beyeler, W., Brown, T., Son, Y. J., & Jones, A. T. (2007). Toward modeling and simulation of critical national infrastructure interdependencies. *IIE Transactions, 39*(1), 57–71.

Minciardi, R., Sacile, R., Taramasso, A. C., Trasforini, E., & Traverso, S. (2006). Modeling the vulnerability of complex territorial systems: An application to hydrological risk. *Environmental Modelling and Software, 21*(7), 949–960.

Montenegro, M. (2010). Urban resilience. *Seed Magazine, 30*(2), 195–197.

Moreno, J. (1934). *Who shall survive?*. New York: Beacon Press.

Moteff, J. (2007, July). *Critical infrastructure: The national asset database*. Library of Congress Washington DC Congressional Research Service.

Mussington, D. (2002). *Concepts for enhancing critical infrastructure protection*. Santa Monica: RAND Corporation.

Nan, C., & Eusgeld, I. (2011). Adopting HLA standard for interdependency study. *Reliability Engineering & System Safety, 96*(1), 149–159.

Norio, O., Ye, T., Kajitani, Y., Shi, P., & Tatano, H. (2011). The 2011 eastern Japan great earthquake disaster: Overview and comments. *International Journal of Disaster Risk Science, 2*(1), 34–42.

Oh, E. H., Deshmukh, A., & Hastak, M. (2012). Criticality assessment of lifeline infrastructure for enhancing disaster response. *Natural Hazards Review, 14*(2), 98–107.

Oliver-Smith, A. (2013). Theorizing vulnerability in a globalized world: A political ecological perspective. In *Mapping Vulnerability* (pp. 29–43). Routledge.

Orr, D. (2014). Systems thinking and the future of cities. *Solutions, 5*(1), 54–61.

Ouyang, M. (2014). Review on modeling and simulation of interdependent critical infrastructure systems. *Reliability engineering & System safety, 121,* 43–60.

Ouyang, M., & Dueñas-Osorio, L. (2011). Efficient approach to compute generalized interdependent effects between infrastructure systems. *Journal of Computing in Civil Engineering, 25*(5), 394–406.

Owen, S. H., & Daskin, M. S. (1998). Strategic facility location: A review. *European Journal of Operational Research, 111*(3), 423–447.

O'Rourke, T. D. (2007). Critical infrastructure, interdependencies, and resilience. *BRIDGE-Washington-National Academy of Engineering-, 37*(1), 22.

O'Rourke, T. D., Bonneau, A. L., Pease, J. W., Shi, P., & Wang, Y. (2006). Liquefaction and ground failures in San Francisco. *Earthquake Spectra, 22*(S2), 91–112.

Pace, K., & Shieh, Y. N. (1988). The Moses-Predohl pull and the location decision of the firm. *Journal of Regional Science, 28*(1), 121–126.

Parma, A. M. (1998). What can adaptive management do for our fish, forests, food, and biodiversity? *Integrative Biology: Issues, News, and Reviews: Published in Association with The Society for Integrative and Comparative Biology, 1*(1), 16–26.

Paton, D., & Flin, R. (1999). Disaster stress: An emergency management perspective. *Disaster Prevention and Management: An International Journal, 8*(4), 261–267.

Pederson, P., Dudenhoeffer, D., Hartley, S., & Permann, M. (2006). Critical infrastructure interdependency modeling: A survey of US and international research. *Idaho National Laboratory, 25,* 27.

Peerenboom, J., Fischer, R., & Whitfield, R. (2001, September). Recovering from disruptions of interdependent critical infrastructures. In *Proceedings of CRIS/DRM/IIIT/NSF workshop on Mitigating the Vulnerability of Critical Infrastructures to Catastrophic Failures*.

Perrow, C. (2011). *Normal accidents: Living with high risk technologies-updated edition*. Princeton university press.

Pitilakis, K., Crowley, H., & Kaynia, A. M. (2014a). *SYNER-G: Typology definition and fragility functions for physical elements at seismic risk* (p. 27). Geological and Earthquake Engineering: Geotechnical.

Pitilakis, K., Alexoudi, M., Argyroudis, S., Monge, O., & Martin, C. (2008). Vulnerability and risk assessment of lifelines. In *Assessing and managing earthquake risk* (pp. 185–211). Dordrecht: Springer.

Pitilakis, K., Franchin, P., Khazai, B., & Wenzel, H. (Eds.). (2014b). *SYNER-G: Systemic seismic vulnerability and risk assessment of complex urban, utility, lifeline systems and critical facilities: methodology and applications* (Vol. 31). Springer.

Pitilakis, K. D., & Kakderi, K. G. (2011, January). Seismic risk assessment and management of lifelines, utilities and infrastructures. In *5th International Conference on Earthquake Geotechnical Engineering* (pp. 10–13).

Prato, T. (2007). Assessing ecosystem sustainability and management using fuzzy logic. *Ecological Economics, 61*(1), 171–177.

Price, P. (2006). Depends on What You Mean by "Disaster". *Mississippi Libraries, 70*(3), 56–57.

Prieto, R. (2002). *The three R's: Lessons learned from September 11, 2001*. London: Royal Academy of Engineering.

Quarantelli, E. L. (Ed.). (2005). *What is a disaster?: A dozen perspectives on the question*. Routledge.

Ramalingam, B. (2013). *Aid on the edge of chaos: Rethinking international cooperation in a complex world*. Oxford University Press.

Ramanathan, R. (2001). A note on the use of the analytic hierarchy process for environmental impact assessment. *Journal of Environmental Management, 63*(1), 27–35.

ReVelle, C. S., & Eiselt, H. A. (2005). Location analysis: A synthesis and survey. *European Journal of Operational Research, 165*(1), 1–19.

ReVelle, C. S., & Swain, R. W. (1970). *Central facilities location. Geographical analysis, 2*(1), 30–42.

Rehme, S. E., Powell, L. A., & Allen, C. R. (2011). Multimodel inference and adaptive management. *Journal of Environmental Management, 92*(5), 1360–1364.

Rinaldi, S. M., Peerenboom, J. P., & Kelly, T. K. (2001). Identifying, understanding, and analyzing critical infrastructure interdependencies. *IEEE Control Systems, 21*(6), 11–25.

Rist, L., Campbell, B. M., & Frost, P. (2013). Adaptive management: Where are we now? *Environmental Conservation, 40*(1), 5–18.

Ritter, S., & Weber, J. (2004). Critical Infrastructure Protection: Survey of world-wide Activities. *Federal Office for Information Security, Bonn, 6*(1), 17–30.

Rosato, V., Issacharoff, L., Tiriticco, F., Meloni, S., Porcellinis, S., & Setola, R. (2008). Modelling interdependent infrastructures using interacting dynamical models. *International Journal of Critical Infrastructures, 4*(1–2), 63–79.

Saaty, T. L. (1972). *An eigenvalue allocation model for prioritization and planning* (pp. 28–31). Energy Management and Policy Center: University of Pennsylvania.

Saaty, T. L. (1977). A scaling method for priorities in hierarchical structures. *Journal of Mathematical Psychology, 15*(3), 234–281.

Saaty, T. L. (1980). *The analytic hierarchy process*. New York: McGraw-Hill.

Santos, J. R., & Haimes, Y. Y. (2004). Modeling the demand reduction input-output (I-O) inoperability due to terrorism of interconnected infrastructures. *Risk Analysis: An International Journal, 24*(6), 1437–1451.

Satterthwaite, D., & Dodman, D. (2013). Towards resilience and transformation for cities within a finite planet. *Environment and Urbanization, 25*(2), 291–298.

Scawthorn, C., O'Rourke, T. D., & Blackburn, F. T. (2006). The 1906 San Francisco earthquake and fire—Enduring lessons for fire protection and water supply. *Earthquake Spectra, 22*(S2), 135–158.

Schalkoff, R. J. (1997). *Artificial neural networks* (Vol. 1). New York: McGraw-Hill.

Schneider, P. J., & Schauer, B. A. (2006). HAZUS—Its development and its future. *Natural Hazards Review, 7*(2), 40–44.

Scott, J. (1988). Social network analysis. *Sociology, 22*(1), 109–127.

Seifert, J. W. (2002). The effects of September 11, 2001, terrorist attacks on public and private information infrastructures: A preliminary assessment of lessons learned. *Government Information Quarterly, 19*(3), 225–242.

Sharkey, T. C., Nurre, S. G., Nguyen, H., Chow, J. H., Mitchell, J. E., & Wallace, W. A. (2015). Identification and classification of restoration interdependencies in the wake of Hurricane Sandy. *Journal of Infrastructure Systems, 22*(1), 04015007.

Shaw, R., Srinivas, H., & Sharma, A., (2009). *Urban risk reduction: An Asian perspective* (Vol. 1). Emerald Group Publishing.

Shinozuka, M., Dong, X., Chen, T. C., & Jin, X. (2007). Seismic performance of electric transmission network under component failures. *Earthquake Engineering and Structural Dynamics, 36*(2), 227–244.

Shinozuka, M., Chang, S. E., Cheng, T. C., Feng, M., O'rourke, T. D., Saadeghvaziri, M. A., Dong, X., Jin, X., Wang, Y., & Shi, P. (2004). Resilience of integrated power and water systems. In *Seismic Evaluation and Retrofit of Lifeline Systems, Articles from MCEER's Research Progress and Accomplishments Volumes* (pp. 65–86).

Smith, P. (1998). *Explaining chaos*. Cambridge University Press.

Stangl, R., Siedschlag, A., Silvestru, D., Fritz, F. & Jerkovic, A. (2012). Comprehensive security research to contribute to critical infrastructure protection. Contributions to security governance in disaster risk reduction. In *12th Congress INTERPRAEVENT* (pp. 585–596).

Stergiopoulos, G., Vasilellis, E., Lykou, G., Kotzanikolaou, P., & Gritzalis, D. (2016, March). Critical infrastructure protection tools: classification and comparison. In *Proceedings of the 10th International Conference on Critical Infrastructure Protection*.

Sterman, J.D. (2000). *Business dynamics: Systems thinking and modeling for a complex world*. McGraw-Hill.

Stewart, I. (1997). *Does god play dice?: The new mathematics of chaos*. Penguin UK.

Studer, J. A. (2000). *Vulnerability of infrastructure*. Zurich, Switzerland: Studer Engineering.

Teriman, S., Yigitcanlar, T., & Mayere, S. (2008). Promoting sustainable urban development in fast growing city-regions: Practices from Kuala Lumpur and Hong Kong. In *Subtropical Cities Conference 2008, Brisbane, Qld*.

Tobin, G. A. (1999). Sustainability and community resilience: The holy grail of hazards planning? *Global Environmental Change Part B: Environmental Hazards, 1*(1), 13–25.

Tolk, A., & Uhrmacher, A. M. (2009). Agents: Agenthood, agent architectures, and agent taxonomies. *Agent-directed simulation and systems engineering*, 75–109.

Tomita, Y., Fukui, C., Kudo, H., Koda, J., & Yabe, K. (1998). A cooperative protection system with an agent model. *IEEE Transactions on Power Delivery, 13*(4), 1060–1066.

Toregas, C., Swain, R., ReVelle, C., & Bergman, L. (1971). The location of emergency service facilities. *Operations Research, 19*(6), 1363–1373.

Tsai, W. H., Chou, W. C., & Hsu, W. (2009). The sustainability balanced scorecard as a framework for selecting socially responsible investment: An effective MCDM model. *Journal of the Operational Research Society, 60*(10), 1396–1410.

Turoff, M., Bañuls, V. A., Plotnick, L., & Hiltz, S. R. (2014). Development of a dynamic scenario model for the interaction of critical infrastructures. In *ISCRAM*.

Uddin, M. S., Ahmad, M. M., & Warnitchai, P. (2018). Surge dynamics of disaster displaced populations in temporary urban shelters: Future challenges and management issues. *Natural Hazards, 94*(1), 201–225.

Ventura, C. E., Juarez Garcia, H., & Marti, J. M. (2010, July). Understanding interdependencies among critical infrastructures. In *9th US National and 10th Canadian Conference on Earthquake Engineering, Toronto, Ontario, Canada*.

Wallace, D., & Wallace, R. (2008). Urban systems during disasters: Factors for resilience. *Ecology and Society, 13*(1).

Wallace, W. A., Mendonça, D., Lee, E., Mitchell, J., & Chow, J. (2001). Managing disruptions to critical interdependent infrastructures in the context of the 2001 World Trade Center attack. In *Impacts of and Human Response to the September 11, 2001 Disasters: What Research Tells Us*.

Walters, C. J. (1986). *Adaptive management of renewable resources*. Macmillan Publishers Ltd.

Wang, S., Hong, L., & Chen, X. (2012). Vulnerability analysis of interdependent infrastructure systems: A methodological framework. *Physica A: Statistical Mechanics and its Applications, 391*(11), 3323–3335.

Waugh, W. L. (1993). Coordination or control: organizational design and the emergency management function. *International Journal of Disaster Prevention and Management, 2*(4), 17–31.

Waugh, W. L., Jr., & Streib, G. (2006). Collaboration and leadership for effective emergency management. *Public Administration Review, 66,* 131–140.

Weber, E. P., & Khademian, A. M. (2008). Wicked problems, knowledge challenges, and collaborative capacity builders in network settings. *Public Administration Review, 68*(2), 334–349.

Weiss, E. N., & Rao, V. R. (1987). AHP design issues for large-scale systems. *Decision Sciences, 18*(1), 43–61.

Williams, B. K., & Brown, E. D. (2016). Technical challenges in the application of adaptive management. *Biological Conservation, 195,* 255–263.

Williams, G. (2014). *Chaos theory tamed*. CRC Press.

Wong, F. S., & Isenberg, J. (1995). Effects of lifeline interaction on seismic performance of communications networks. In *Lifeline Earthquake Engineering* (pp. 557–564). ASCE.

Wu, W. W. (2008). Choosing knowledge management strategies by using a combined ANP and DEMATEL approach. *Expert Systems with Applications, 35*(3), 828–835.

Yao, B., Xie, L., & Huo, E. (2004, August). Study effect of lifeline interaction under seismic conditions. In *Proceedings of 13th World Conference on Earthquake Engineering*.

Yaseen, S. G., & Al-Slamy, N. M. (2008). Ant colony optimization. *IJCSNS, 8*(6), 351.

Yu, C. S. (2002). A GP-AHP method for solving group decision-making fuzzy AHP problems. *Computers & Operations Research, 29*(14), 1969–2001.

Zadeh, L. A. (1965). *Fuzzy sets. Information and control, 8*(3), 338–353.

Zahedi, F. (1986). The analytic hierarchy process—A survey of the method and its applications. *Interfaces, 16*(4), 96–108.

Zhang, P., & Peeta, S. (2011). A generalized modeling framework to analyze interdependencies among infrastructure systems. *Transportation Research Part B: Methodological, 45*(3), 553–579.

Zimmerman, B. J. (2013). Theories of self-regulated learning and academic achievement: An overview and analysis. In *Self-regulated learning and academic achievement* (pp. 10–45). Routledge.

Resilience of the Built Environment to Fire and Fire-Following-Earthquake

Thomas Gernay and Negar Elhami Khorasani

1 Introduction

Amongst the hazards with which the built environment has to cope, fire is one of the most devastating. Throughout history, urban fires and conflagrations have ravaged cities (*e.g.* Rome 64, London 1666, Chicago 1871, Baltimore 1904), resulting in countless casualties and losses, even reshaping the trajectory of entire regions by diverting economic and population growth from one city to a competing one. Such conflagrations have sometimes been caused by another primary hazard, adding destruction to this primary event, such as an earthquake (*e.g.* San Francisco 1906, Northridge 1994, Kobe 1995), blast (*e.g.* Phillips disaster in Texas 1989), or bombing in wartime (*e.g.* London 1940, Dresden 1945). Over the last century, progress in construction practices, materials and technologies, as well as fire safety and prevention, have considerably reduced the likelihood of urban conflagrations of such scale [in developed countries; yet urban conflagrations still occur in informal settlements (Arup 2018)]. Yet in any society, fire remains a major societal hazard, one that drains valuable resources from the community and has the potential to disrupt major infrastructure systems. Dramatic fire events have been widely reported in the media (*e.g.* Mont Blanc Tunnel 1999, New York World Trade Center Towers 2001, London Grenfell Tower 2017, Tehran Plasco Building 2017), but structure fires are in fact a permanent and rampant hazard. In 2016 in the U.S., 475,500 structure fires caused 2,950 deaths and 7.9 billion dollars in direct property damage (Haynes 2017). This dollar cost of structure fires increases dramatically when accounting for indirect

T. Gernay (✉)
Department of Civil Engineering, Johns Hopkins University, 3400N Charles Street, Baltimore, MD 21218, USA
e-mail: tgernay@jhu.edu

N. E. Khorasani
Department of Civil, Structural and Environmental Engineering, University at Buffalo NY, 136 Ketter Hall, Buffalo, NY 14260, USA
e-mail: negarkho@buffalo.edu

losses and expenditures, with estimates at around 1% of GDP in developed countries (CTIF 2016; The Geneva Association 2010; Zhuang et al. 2017). Besides structure fires, wildfires are also taking a considerable toll on the built environment with significant direct and indirect economic and social losses, while these wildfire events are increasing in both frequency and intensity.

To mitigate the effects of fire on the built environment, building codes were developed with specific provisions against fire hazard. Actually in many jurisdictions, unsustainable fire losses were the very reason that gave the impetus for developing the first building codes. The goal of the codes was primarily to protect lives from fire in the built environment. The approach was largely prescriptive, relying on tabulated data and empirical indexing methods for designing the measures deemed adequate to reach an implicit safety level. While this approach was successful in reducing fire-related deaths and urban conflagrations, it appears to have reached its limits for a number of reasons. First, the decreasing trends in human and direct economic losses due to fire have been levelling off during the last decades; these losses remain unacceptably high. Second, it is now widely recognized that extreme hazards harm our societies not only through direct consequences, but also through indirect socio-economic losses, which largely result from the loss of functionality of buildings and infrastructure systems in the aftermath of a disaster. For instance, bridge fires have recently caught increasing attention of the engineering community for their capacity to disrupt a transportation network and cause tremendous indirect economic losses. Finally, the rising threats posed by multi-hazard cascading events in increasingly interconnected urban networks, such as fire following earthquake, as well as wildfires within the context of wildland urban interface growth and climate change, also call for new approaches to fire hazard mitigation.

Recently, new paradigms have emerged in civil engineering and risk management to meet these challenges. These new paradigms center on principles that include resilience, performance-based design, and probabilistic assessment. Beyond life safety, the goal is to design a built environment that is prepared for, able to withstand and rapidly recover from disruptions due to hazardous events. To achieve this, building codes based on empirical ad hoc approach are ill-suited. Instead, performance-based approaches based on rational and scientific analysis, which integrate uncertainty, provide the framework to assess, retrofit and design buildings and infrastructure systems for resilience to complex and changing hazards. Extensive research has been conducted over the last three decades to advance the principles of resilience, performance-based design, and probabilistic modeling, in different sub-fields of structural engineering. The seismic engineering community, for instance, has achieved great progress, materialized notably through the release of the FEMA P58 reports (FEMA 2012a) and the associated Performance Assessment Calculation Tool (PACT) (FEMA 2012b). In contrast, research in the field of structural fire engineering is still in its early stages. While the fire community is increasingly adopting the idea that applying these principles to fire safety can yield significant dividends, much remains to be done to enable a transformation of the extent of that observed in the seismic field.

In this context, this chapter focuses on the issues and recent developments in the area of resilience of the built environment to fire hazard. The point of view is that of structural engineers, i.e. the focus of discussion is towards implementing optimum designs for the structures that support the socio-economic functions of the community to minimize losses, downtime and disruption in case of fire events. The chapter starts with a description of the fire problem (Sect. 2) to clarify what is at stake. Then, it argues that the current approach to fire safety has reached its limits when it comes to delivering resilience, and that it should be complemented with a next-generation performance-based approach to overcome the identified shortcomings (Sect. 3). Thereafter, the chapter reviews the definition and implementation of resilience in other structural engineering subfields, and discusses the similarities with and specificities of fire engineering (Sect. 4). The research toward advancing the principles of resilience in structural fire engineering is examined, including current gaps in knowledge (Sect. 5). The case of multi-hazard events, and particularly fire following earthquakes, is explored (Sect. 6). Finally, the chapter concludes with perspectives on the future of the topic (Sect. 7).

2 The Fire Problem

Fire takes a heavy toll on our societies, both in terms of human lives and economic losses. Fire death rates range between 2 and 20 per million population in industrialized countries (FEMA 2011). The factors causing differences between countries are unclear, but could be related to differences in lifestyle, cultural attitudes towards fire, fire prevention practices and education, and building practices and regulations. The U.S. fire death rate is in the worst half among the studied countries at around 10.9 in 2016 (FEMA 2018). While these rates have been continuously declining, the trend in absolute value has been levelling off and fire-caused deaths in the U.S. have been around 3,200 annually during the past 10 years, see Fig. 1a (the numbers include deaths due to structure and non-structure fires). Fire also drains considerable economic resources. A recent report prepared for the NFPA (Zhuang et al. 2017) estimated that, for 2014, the total cost of fire in the U.S. was $328.5 billion, i.e. 1.9% of the U.S. Gross Domestic Product (GDP). This total cost is defined as the collective of all net expenditure on fire protection and all net losses due to fire incidents, where the expenditures constituted $273.1 billion and the losses constituted $55.4 billion. The fire safety costs in building construction was the largest component at $57.4 billion (17.5% of total). Direct property damage is only a small part of this cost, which has hovered around $13 billion (in 2012 dollars) for nearly 25 years (Fig. 1b). The total cost has been continuously increasing in absolute value (Fig. 1c), but showed an exponentially decreasing trend in value relative to the GDP, which has hovered at around 2% (Zhuang et al. 2017). Other sources evaluate the total cost of fire at around 1% of the GDP for most industrialized countries (CTIF 2016; The Geneva Association 2010). These numbers show that fire is a significant issue, with very

high human and economic costs; furthermore, despite progress in fire mitigation, the declining trends in fire losses have been levelling off.

Regularly, dramatic accidents shed light on the potentially devastating consequences of fire. Collapses such as the NY World Trade Center in 2001 and the Tehran Plasco building in 2017 (Behnam 2018) showed that high-rise buildings are vulnerable to fire. Transport infrastructure such as tunnels and bridges are also at risk. A study of 72 historic tunnel events in road and railway tunnels between 1949 and 2010 demonstrate the majority of these events (52 cases) occurred in Europe while 10 of these events were identified in North America. These are low-probability events but with potential for high consequences. For example, in 1996, a fire broke out in the Channel Tunnel connecting France and the UK, and caused tunnel closure for 6 months, disrupting commercial business between the two countries (Kirkland 2002). The Mont Blanc Tunnel fire in 1999 caused 39 deaths and the closing down of the tunnel for 3 years. Regarding bridge fires, one well-known historic event is the MacArthur Maze I-80/I-580/I-880 interchange overpass in Oakland, California in 2007, where a tanker truck accident led to a fire that caused the collapse of a portion of the busy overpass (Garlock et al. 2012). The structure was made of steel girders with a concrete deck. The consequences of such events imply major economic losses due to a critical bridge closure within a transportation network. Chung et al. (2008) reported that the daily indirect losses associated with the MacArthur Maze overpass collapse were about $6 million, while the interchange was closed for 26 days. Such accidents indicate the fragility of our infrastructure to fire. They further demonstrate the need to carefully take into consideration the fire loading case when designing elements of the built environment, and particularly in case of large, critical or iconic structures. In addition, careful considerations are demanded when adopting novel materials, construction systems, or when extending the size and scope of existing solutions. For instance, the 2017 Grenfell Tower Fire, which caused 72 deaths, pointed the attention on the problem of façade and exterior cladding fire spread. For novel or complex buildings, for which reliance on precedence is insufficient, an adequate level of safety should be explicitly demonstrated through adequate engineering.

In an increasingly interconnected society, any disruption in the built environment may cause significant indirect costs. Infrastructure fires, such as the aforementioned tunnel and bridge fires, are relevant examples of such disruptions. In both cases, the fire resulted in the closing down of a critical link in the transportation network. Statistics show that fire represents a significant hazard to bridges, with fire-induced bridge collapses being much more frequent than, for instance, seismic-induced collapses (Garlock et al. 2012). However fire loading is not accounted for in conventional bridge design. Indeed, fire has traditionally been considered as a life safety issue rather than as a community resilience issue. Building fires also affect the functionality of the built environment, i.e. its ability to support the socio-economic functions of a community. Occupants of dwellings have to be rehoused; relatively minor fire incidents in hospitals or schools can lead to temporary closures that disrupt the social fabric; while statistics show that many businesses that experience a large fire

Fig. 1 U.S. fire hazard statistics: **a** fire related civilian deaths (Haynes 2017); **b** direct property damage (Haynes 2017); and **c** total cost (Zhuang et al. 2017). Data exclude losses that occurred from the events of 9/11/01

(a) Fire-related civilian deaths

(b) Direct property damage

(c) Total cost of fire in the U.S.
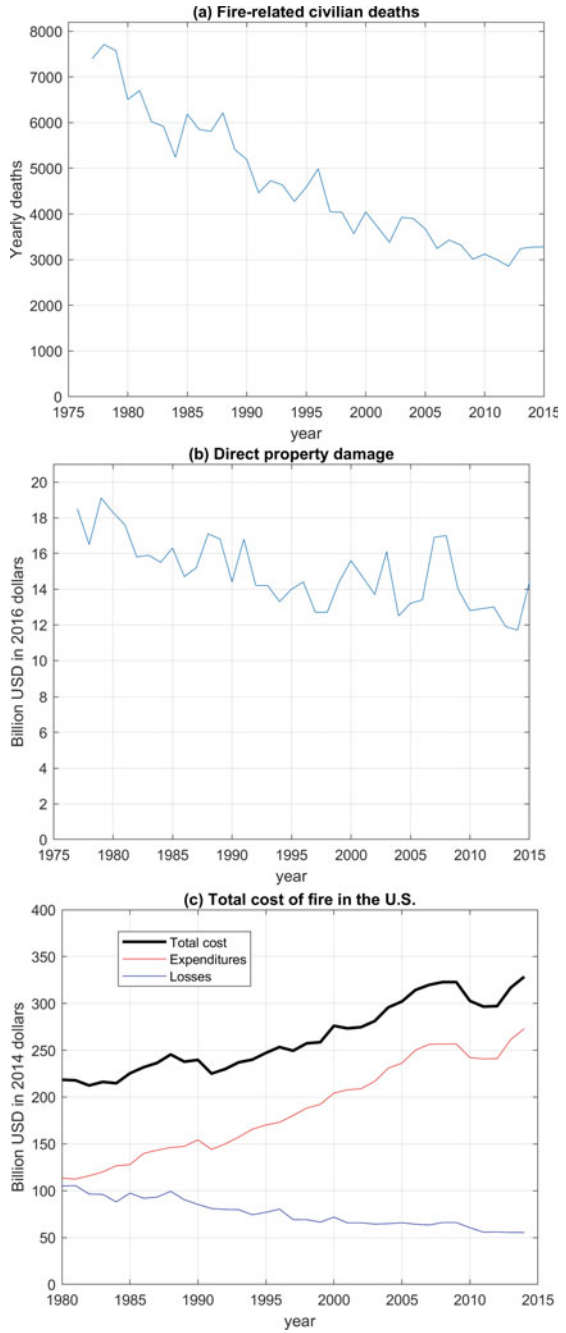
eventually go into bankruptcy due to downtime and indirect costs. Current fire provisions fail to address these issues.

There have been increasing trends in both frequency and the level of damage from wildfires across the western U.S. More than 70,000 U.S. communities, containing 46 million homes, are at the risk of Wildland Urban Interface (WUI) fires, yet only about 7,000 communities have adopted protection measures. In 2014, losses due to 25 wildfire events reached $654.3 million in direct property damage (Badger 2015). More recently, in 2017, a number of wildfires in Northern California (including the Tubbs, Nuns, and Atlas Fires) caused more than $9 billion in insured property losses, one of the costliest on the records. Potential for the loss of life and direct damage to homes and other infrastructure, as well as injuries or longer term health issues from smoke spread due to fires in the wildland and WUI communities confirm that the current approach in managing fires in communities is not sufficient. Similar conclusions can be made in case of fires following earthquake. For example, Japan's Kobe earthquake in 1995 incinerated 7.1 million sq. ft and the fire alone resulted in 500 deaths (6000 deaths total) and damaged 6900 buildings. There were 261 post-earthquake fires, 83 of these started in fire resistive buildings (Sekizawa et al. 2003). Multiple fire ignitions across the community that is already experiencing chaos due to the earthquake with possibly limited firefighting resources can lead to quick fire spread and significant damage.

3 The Need for a New Approach to Fire Safety for Buildings and Infrastructure

3.1 Description of the Current Approach for Buildings and Communities

The design process for buildings is typically accomplished by adhering to prescriptive criteria contained within codes. These criteria are meant to provide a certain level of safety and performance for the built environment. Yet, this level of performance is not explicitly evaluated, and the actual obtained performance is unknown. Arguably different buildings may end up with very different actual safety levels.

This prescriptive design process is particularly prevalent in structural fire protection design. Since the beginning of building fire codes, the design of structures for the fire loading case has mostly relied on the standard fire resistance concept. Standard fire resistance design is an empirical indexing method based on furnace testing of isolated structural components. A single standard heating exposure is used to comparatively test isolated components against predefined acceptance criteria that are intended to generalize the robustness of the protection scheme to fire exposure. For steel components, the design strategy relies entirely on insulation for fire endurance, meaning that the intent is to reduce heating of elements for mitigating the action of fire. The correlation between the criteria used in furnace testing and the performance

of the structural system in a real fire situation is very weak. Indeed, in defining the standard fire resistance, neither the anticipated in situ fire conditions nor the actual fire response of the structural system are quantified or explicitly contemplated.

Performance-based design is an alternative to the prescriptive approach. Performance-based design is a formal process that relies on the application of engineering principles and physics-based modeling for the design of buildings. It entails a specific intent to achieve defined performance objectives. The performance, which is quantified, relates to societal expectations of acceptable structural damage levels under specified loading scenarios. Systematic performance-based approaches now exist for design loads such as seismic loads that are being used in practice (FEMA 2012a).

However, performance-based design is not commonly used in the field of fire safety engineering. Despite the advances of the last decades in research pertaining to the modeling of structures at elevated temperatures, the fire protection design of the built environment rarely relies on an explicit evaluation of the demand and capacity of structural systems under fire exposure, as is done with other design loads. In order words, fire is not being considered as a load case within the load combinations when designing the structure. The performance-based approach provides a rigorous, comprehensive framework to consider the effects of fuel loads, structural insulation and other fire exposure mitigation techniques, structural capacity, etc. on explicit performance objectives. Instead, the generalized reliance on prescriptive standard fire engineering arguably results in inconsistent safety levels, stifles innovation in the field, and hinders the rational allocation of resources to mitigate fire hazard.

In addition, the current approach to fire safety is aimed at protecting life and property from the direct destructive force of fire, but does not consider indirect losses through the impact of fire on buildings, communities, and infrastructure systems' downtime. That is, the current approach does not contemplate the role of fire hazard within the societal challenge that is the need for resilience. Yet, examples abound where fire has disrupted systems and networks, for instance in the transportation and energy sectors or communities in the WUI. Buildings with strategic importance, such as hospitals, airport terminals, or data centers, ought to be designed against fire with explicit performance objectives to achieve resilience.

Finally, the current approach treats fire as an isolated hazard. Therefore, it fails to account for multi-hazard events. For instance, a fire following earthquake scenario poses significant challenges to a structure integrity. Structural and non-structural (e.g. active and passive fire protection) components may be pre-damaged while the fire action develops, which affects the structure ability to withstand the fire action (Ni and Birely 2018a; Behnam and Ronagh 2013).

3.2 Description of the Current Approach for Bridges, Tunnels and Other Infrastructure

Fire poses a hazard to infrastructure such as tunnels and bridges. Tunnel fires have received much attention by the research community compared to bridge fires. One main concern with tunnel fires relate to safety of people, as the fire and smoke can quickly spread between trucks or railway cars while people could get trapped in the tunnel. The fire scenario in a tunnel is a function of the type of fuel and available ventilation. In case of road tunnels, trucks carrying fuel, chemicals or commercial goods (categorized as heavy goods vehicles) can be a source of large fire with a relatively large heat release rate. Previous tests of large-scale railcars show that if they are on fire, they carry a heat release rate in the range of 7–77 MW (Lattimer and Ferreira 2017), this value can increase to 200 MW in the case of freight trains carrying fuel. Meanwhile, the effect of ventilation (natural or fans) cannot be ignored in determining the potential fire growth rate, fire spread, and smoke production. In addition, the effectiveness of fixed water-based suppression systems to control the fire spread has been considered, although caution must be taken when water mist systems are being used in combination with the ventilation system. A number of research projects in Europe were conducted to develop guidelines or recommendations on fire safety in the tunnels. These projects have led to a better understanding of the fire evolution in a tunnel (Li and Ingason 2012), and to develop more effective emergency egress paths for evacuation of people. However, what remains to be answered relates to the tunnel downtime and associated economic losses versus investments in structural fire design of tunnel lining including provisions for fire protection. A risk assessment framework that defines the fire scenario, the associated probability of occurrence, the level of damage due to fire, and consequences in terms of downtime and repair time can be used for informed decision-making during the design process.

Bridge fires have been less studied compared to tunnel fires, in part because bridge fires generally do not lead to fatalities. In 2017, Kodur et al. noted that "to date, there are no specific requirements in codes and standards for designing bridges to withstand fire hazard". The primary risk of fire to bridges is associated to vehicle or tanker truck crashes. The fire hazard in case of a bridge is typically characterized by a pool fire. Fire models of various complexities have been used by researchers, ranging from simple standard hydrocarbon fire curves to computational fluid dynamics. Intermediate approaches, such as the work of Quiel et al. (2015), exist where the modeling approach moves away from conservative simplified standard curves while keeping the computational costs manageable. Quiel et al. (2015) proposed a modified discretized solid flame model (MDSF) where a pool fire is represented as a solid vertical cylinder and radiation heat flux is calculated as the output. Similar to the tunnel fires, traffic interruptions in major transportation networks and significant economic losses in case of a fire justify the need to perform cost-benefit analysis and case studies on whether additional investments to increase fire resilience of the

structure should be considered or not. In addition, guidelines on post-fire assessment and systematic repair strategies need to be developed.

3.3 Limitations of the Current Approach

Clearly the current approach to fire safety for buildings and infrastructure systems fails to address the civil engineering challenges of the 21st century. The incorporation of prescriptive criteria within codes has positively impacted fire safety of the built environment over the last century, by reducing the fire related deaths, immediate property losses, and urban conflagrations. However, this prescriptive approach has reached its limits as evidenced by unacceptably high human and economic costs still attributable to fire and by the lack of consideration for the potential disruptive effects of fire on the intricate, interconnected infrastructure systems that characterize modern societies.

The limitations of the current approach stem from several paradigms that are most commonly adopted and lock the progress of the field. We define the following problems that hinder the progress of structural fire engineering toward achieving a fire resilient built environment: the *Goal problem*, the *Scale problem*, the *Uncertainty problem* and the *Hazard Scenario problem*, see Fig. 2.

The *Goal problem* refers to the fact that the prime motivation of fire mitigation efforts in the built environment has traditionally been life safety and, to a lesser extent, protection of property from direct loss. The life safety, as the performance metric, is of course sound and should remain the priority. However, relying on this metric as the only criterion to define the goal of fire mitigation does not allow contemplating larger issues at stake for society, such as downtime, indirect losses, and more broadly, resiliency. These follow-up consequences related to the loss of

Fig. 2 The need for a new approach to fire safety for buildings and infrastructure. The current approach relies on outdated paradigms regarding the definitions of the *Goal*, *Scale*, *Uncertainty*, and *Hazard scenario*
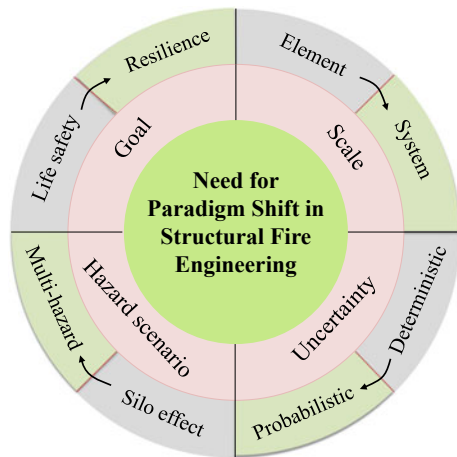
functionality may dominate the overall cost as infrastructure networks become more interconnected. Some buildings and infrastructures support critical socio-economic functions while hosting few people and property (bridges, data centers, energy plant, etc.). Meanwhile, data indicate that many businesses do not survive a major fire due to indirect losses in the weeks and months following the accident. A holistic view on fire safety needs to account for the strategic importance of buildings and infrastructures and the socio-economic costs of fire-induced downtime in defining the target safety level for the built environment. This entails redefining the goal to address a broader definition of what it means for structures and communities to be *resilient to fire*.

The *Scale problem* indicates the current inadequate focus on individual structural components rather than buildings/infrastructures and systems. The prescriptive fire resistance approach looks at individual, isolated structural components in furnace to define the fire protection. In the last two decades, research has clearly established that the behavior of structural assemblies in fire differ from that of isolated components, notably due to thermal expansion effects. This has been evidenced by large-scale structural fire tests (Lennon et al. 1999), forensic analysis of fire-induced building failure (Gann 2008), and numerical simulations (Gillie et al. 2001; Gernay and Gamba 2018). Further, due consideration of fire hazard for society entails looking at the systems of buildings/infrastructures, and the functions they serve. Cascading effects triggered by fire-induced structural failure on systems' functionality are important. Similarly, defensive actions by a small number of houses in a WUI community would not be sufficient to stop the fire spread during a wildfire event. Uniform actions taken across a neighborhood is needed to change the behavior of fire and reduce damage. Resilience to fire can only be achieved if the problem is contemplated across all scales.

The *Uncertainty problem* relates to the prevalent reliance on a deterministic approach and the lack of consideration for uncertainties in fire-structure hazard models. Uncertainties are ubiquitous when assessing structural fire safety, notably in the definition of the fire scenario, fuel loading (Elhami Khorasani et al. 2014), ventilation conditions, and material and structural response at high temperature (Gernay et al. 2018). New materials, new architectural and structural designs impact how fires grow and spread, e.g. in large open space compartments (Byström et al. 2014), or in façade fires such as in the recent Grenfell Tower Fire. Probabilistic Risk Analyses (PRA) are necessary to support explicit safety verification, particularly for uncommon fire safety designs for which the collective experience of the profession is insufficient to support an implicitly defined safety level (Hopkin et al. 2017). While other fields of structural engineering (e.g., earthquake and wind) have long embraced a probabilistic framework to assess structures performance (FEMA 2012a; Kareem 1987), probabilistic structural fire engineering is still in its infancy.

Finally, the *Hazard Scenario problem* refers to the tendency of building codes to consider hazards in isolation, adopting a silo approach to scenarios. To promote resilience, structural engineering designs must mitigate the risks to multiple hazards including multi-hazard scenarios (Gardoni and LaFave 2016). Fire can be triggered by a primary hazard such as blast or earthquake. Research indicates that the fire

response of structure is negatively affected by the previous occurrence of a blast (Liew 2008) or an earthquake (Ni and Birely 2018a). Therefore, the field needs to move beyond the silo of fire hazard and address resilience to multi-hazard scenarios involving fire if it is to create successful solutions for the built environment.

3.4 Next-Generation Performance-Based Fire Design for Resilient Built Environment

The next-generation design approach for a fire resilient built environment will need to overcome the *Goal*, *Scale*, *Uncertainty*, and *Hazard Scenario problems*. This will require adopting scientifically grounded performance-based design approaches in lieu of ad hoc prescriptive methods. In a performance-based design process, the desired performance of a building/infrastructure is stated explicitly at the outset of the project. This performance is identified jointly by all stakeholders (including owners, building officials, architect, engineers, etc.). The performance objectives that are derived state the acceptable risk of incurring damage or loss for identified fire hazards with known frequencies. As such, the risks are explicitly expressed and can account for indirect economic impact, downtime, interdependencies between infrastructure, etc. The effects of different designs on the achieved performance are determined. In this performance assessment, uncertainties in the fire severity, and limitations in our ability to accurately predict its effects, are accounted for and acknowledged. Finally, meaningful ways of communicating performance and resilience against fire to stakeholders are identified to enable decision-making. Research is underway to enable this next-generation approach, as presented in the next sections.

4 Definition of Resilience and the Context of Fire Hazard

4.1 Resilience Definition for Structural Engineers

The term resiliency has been described by many researchers and in a number of documents. The term is defined by the Presidential Policy Directive on Critical Infrastructure Security and Resilience (PPD 2013) stating that: "resiliency is the ability to prepare for and adapt to changing conditions and withstand and recover rapidly from disruptions". The National Institute of Standards and Technology (NIST) in the US has published the "Community Resilience Planning Guide for Buildings and Infrastructure" (NIST 2016). The primary argument is that a community's social institutions are essentially its 'human infrastructure' (Doerfel and Harris 2015) and as such must be supported during and after a hazard. However, safe-guarding the social functionality begins with ensuring that the largely intangible networks avoid the disruption of abrupt physical relocation, which brings the challenge back to

Fig. 3 Definition of resilience. Buildings and infrastructure systems are characterized by the functions they serve to support a society. Resiliency is the ability to minimize the effect of disruptions on this functionality
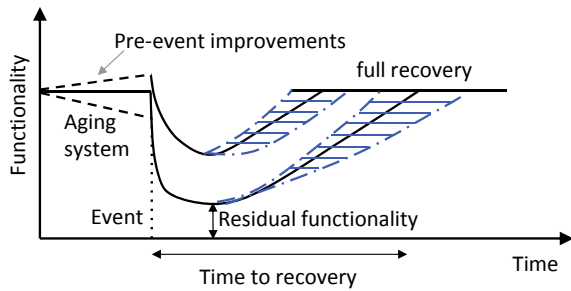
the resiliency of the physical built environments. In measuring resiliency, the guide prepared by NIST proposes an approach to identify the gaps between the desired performance goals in a community subject to hazard and anticipated performance of the built environment. The existing frameworks generally rely on risk-informed methodologies to characterize the intensity and frequency of a hazard (e.g. earthquake or floods) and assess performance of the physical infrastructure subjected to the hazard. Figure 3 shows a typical definition of resilience used by structural engineers.

In a recent paper, Koliou et al. (2018) reviewed the state of the research in community resilience and pointed out that a "tripartite view of resilience—reducing impacts or consequences, reducing recovery time, and reducing future vulnerabilities—has been prevalent over the last decade, although there are certainly variations in emphasis." Meanwhile, there has been an emphasis on how ensuring life safety does not imply resilience while maintaining functionality is key to minimize disruption and ensure resilience. Mieler and Mitrani-Reiser (2018) have studied existing definitions on functionality and deduced that functionality for buildings refers to the availability of a building facility to be used for its intended purpose. This implies the building has to maintain safety (i.e., occupants are not subjected to risk), serviceability (i.e., physical space is usable and services such as utilities are available), and accessibility (i.e., building surrounding is not damaged and building access is safe). If buildings retain functionality, the occupants, or as stated earlier, the social institution of a community, do not see the need for relocation and disruptions can be minimized. However, combining all the factors related to safety, serviceability, and accessibility of a building to simulate and quantify functionality is a complex process and it has been a challenge to establish modeling techniques to capture the complexity of the process.

4.2 Implementation of Resilience Framework for Hazards Other Than Fire

Implementation of the resilience framework for hazards other than fire, in particular earthquakes, has been the focus of a number of projects in the past few years, aiming

to reduce losses (economic and life) and minimize disruptions. For example, the literature is quite comprehensive on how to improve seismic structural performance of buildings, as one of the primary elements of a community. Most of the existing research, current building codes and standards, or frameworks such as FEMA P695 "Quantification of Building Seismic Performance Factors" (FEMA 2009) that quantifies building seismic performance, have mainly focused on the life safety criterion (and not necessarily functionality) for residential and commercial buildings. Meanwhile, current frameworks for estimating losses for entire communities, such as Hazus (FEMA 2014), take functionality or time to regain functionality into account but rely on simplified analysis. Hazus quantifies building repair time, as a function of time to clean-up and obtain financing, permits, and complete design. The Hazus approach is generally based on aggregated data rather than building specific information. The existing approaches to quantify losses at the community or building level rely on estimates of losses or restoration times as represented by fragilities. A fragility function provides the probability of exceeding a damage state for a given intensity measure. The damage states (or limit states) are generally related to the structural/non-structural performance level of a component and can be grouped into different categories ranging from no damage to collapse. The intensity measure characterizes the earthquake hazard.

The P-58 framework for seismic performance assessment of buildings (FEMA 2012a), developed by the Federal Emergency Management Agency (FEMA), is one example that provides a more robust approach to quantify seismic performance but at the building level. The P-58 framework is a step-by-step methodology to (a) quantify intensity of ground shaking, (b) deformation, acceleration, and velocity demands on structural and non-structural components of the building, (c) vulnerability of building components, and (d) the consequences and losses. After detailed information on characteristics of building structural and nonstructural components is assembled, building response is assessed using simplified or nonlinear response-history analysis. Performance metrics are defined as the number of casualties, repair and replacement cost, repair time, and unsafe placarding. The methodology incorporates uncertainties at different steps and reports building performance in terms of statistical distributions. The framework is meant to be used for risk assessment and decision-making when designing new buildings or evaluating retrofit options for existing buildings. The P-58 framework is implemented in Performance Assessment Calculation Tool (PACT) (FEMA 2012b), which provides users a platform to assemble building information and performance models and measure probabilistic loss estimates for the building.

The Advanced Technology and Research team in Arup has proposed a Resilience-based Earthquake Design Initiative (REDi) Rating system to be used by owners, architects and engineers to go beyond the current building codes and implement "resilience-based earthquake design" (Arup 2013). The REDi Rating System relies on a design that implements performance of both structural and non-structural components, including facades, building content, etc. to minimize downtime after an earthquake. The REDi Resilience Objectives rate a building into three categories of platinum (immediate re-occupancy and functional recovery of less than 72 h), gold (immediate re-occupancy and functional recovery of less than one month), and silver

(re-occupancy and functional recovery of less than 6 months). Additional criteria are provided for direction financial losses and occupant safety for each category.

In the majority of the frameworks explained above, when performance of the building is analyzed under a ground motion, the performance metrics for restoration times or vulnerabilities are quantified based on drift or acceleration of every floor in the building. Damage to structural members and most of the building components can be related to the inter-story drift that a building floor experiences, while some building contents, equipment, and furniture might be sensitive to acceleration. Therefore, studying global response of the building structural system at every floor can be used to quantify damage or restoration time.

4.3   Implementation for Fire Safety Engineering

Applying the existing frameworks on resilience to fire safety engineering is a challenging problem. Assessment of fire performance of structures involves complex multi-physics modeling and considerable uncertainties. The modeling issues pertaining to fire development, fire-structure interactions, and fire-induced damage and losses, are specific to this hazard.

It can be argued that performance-based fire engineering can be used to design and analyze the structure under fire, reduce vulnerabilities, and increase resilience. While this is possible, there is yet work to be done to establish performance-based design frameworks that are widely accepted and can be used in practice. Structural fire engineering has made significant advances in recent years in understanding performance of structural components and to some extent structural systems at elevated temperatures. However, there lacks a standard probabilistic approach for quantifying safety or reliability of a structural system under fire.

The level of uncertainty is especially large in defining the fire scenario (i.e. demand on the structure). A fire scenario not only defines the fire severity, but also captures the extent of fire spread in a building. A fire event initiated from one compartment may possibly spread between compartments in one floor or across different stories. While in earthquake engineering, performance-based design relies on a set of ground motion records from past earthquakes to cover potential design or maximum considered earthquakes, there does not exist much data on fire scenarios for structures and their frequency of occurrence. Therefore, modeling assumptions need to be made. The severity of fire and the number of compartments/floors affected by fire makes a significant difference on structural damage, and consequently on repair time, repair cost, and functionality.

Another challenge lies in the quantification of cost and time of repair given structural damage due to fire. Few studies have focused on fire-related indirect losses. In addition, it is important to study post-fire assessment of the structures and residual load capacity of members exposed to fire to have an informed decision on the conditions for re-occupancy. A recent study by Molkens et al. (2017) proposed a reliability-

based procedure that accounts for uncertainties while incorporating information from inspections, test data, and models to evaluate post-fire safety of a structure.

In summary, the current approach in practice, when it comes to decision-making about safety of a structure subjected to a fire event, follows procedures developed on ad hoc basis and engineering judgment, rather than well-established researched frameworks. The recent research aimed at advancing such frameworks is examined in Sects. 5 and 6.

5 Research Toward a Fire Resilient Built Environment

5.1 Setting up the Goals Explicitly

Research is underway to enable fire resilient designs for the built environment. A first, crucial research axis deals with the definition of the desired performance of the building or infrastructure. A performance-based design approach requires defining explicitly the performance objectives at the outset of a project jointly between the stakeholders.

Recently, performance-based design approach has started to gain traction as a means of satisfying statutory fire safety requirements with greater confidence and often in a more efficient manner than with prescriptive design, for example, case studies are presented in (Block et al. 2010; Hopkin et al. 2018). However, this approach so far has remained largely deterministic. The performance criteria used in these studies are deemed appropriately conservative based on engineering judgment and reliance on the experience of the fire safety profession. This means that the residual risk of incurring damage or loss for identified fire hazards is not evaluated as the full spectrum of consequences and their associated probabilities are not interrogated. For explicitly evaluating the residual risk associated with a given design, a Probabilistic Risk Assessment (PRA) framework can be adopted (Van Coile 2014a). This is particularly true in the context of resilience, as recovery in the wake of a fire event is dependent on the uncertain performance during fire (Molkens et al. 2017). A PRA allows evaluating the residual risk, which can then be assessed against performance objectives.

Performance objectives are generally established based on a variation of a Cost Benefit Analysis (CBA), i.e. an optimization problem. As fire is a societal safety issue, this CBA also takes into account what is both tolerable to society, and as low as is reasonably practicable (ALARP). Discussions on the performance objectives in fire engineering can be found for instance in (Fischer 2014; Van Coile et al. 2018a; Hopkin et al. 2018b). Fischer (2014) applied Lifetime Cost Optimization (LCO) to inform target reliability levels for structural fire engineering designs. LCO minimizes the lifetime costs associated with the structural fire design (or parts thereof) and fire-induced failure. The total lifetime cost is quantified as the sum of, on the one hand, upfront safety investments and maintenance costs and, on the other hand,

damage costs incurred in the uncertain event of a fire (Van Coile et al. 2014b). LCO underpins the definition of target reliability indices for buildings in the Eurocodes for normal (i.e. ambient temperature) design conditions, but such framework is not currently applied to fire design conditions. Van Coile et al. (2018a) aimed to clarify the relationship between different acceptance concepts for PRA, including comparative, absolute and ALARP concepts, as well as the different designer responsibilities associated with these different concepts. They highlighted the importance of improving the explicit safety foundation of fire safety designs and further argued that the "ALARP assessment necessarily entails a societal, risk-neutral, and scalar cost–benefit analysis, choosing between safety features so as to maximize societal welfare." Hopkin et al. (2018b) proposed the use of the J-value, derived from societal welfare considerations (the Life Quality Index), as a decision support indicator for informing decisions on fire safety.

Future works will need to focus on the incorporation of resilience considerations within decision-making frameworks such as LCO, ALARP, J-value, etc. for structural fire engineering. This is necessary to broaden the goal of fire engineering beyond life safety and thus to define performance objectives relevant for resiliency. Performance objectives focusing on functionality-recovery (Mieler and Mitrani-Reiser 2018) need to be incorporated. For instance, in a LCO framework, the damage costs incurred in the uncertain event of a fire should be broaden to include indirect costs of unavailability of societal functions. This entails a considerable amount of research to quantify the indirect costs due to fire.

Another challenge for the future development of a fire resilient built environment will consist in linking functionality-recovery performance metrics (and associated costs) directly to structural damage/response metrics in fire. In the seismic field, the resilience performance metrics are commonly measured based on drift or acceleration of a building floor under a ground motion, which is quantified by a structural analysis. In contrast, the means to link structural fire damage to resilience performance metrics are not established yet. More research is needed to understand what aspects of the structural fire response are more closely correlated to lack of functionality.

5.2 Developing the Methodology to Evaluate Performance

After selection of the performance objectives, designs must be developed and the performance capability assessed. The performance assessment of a given design must entail the definition of fire hazards, thermal-structural analyses to predict building/infrastructure response, assessment of the likely amount of damage, and probable consequences of that damage; see Fig. 4.

First, data must be gathered about the building or infrastructure under consideration. Following the methodology of FEMA P58 for earthquake loading, these data should include building/infrastructure size, replacement cost, replacement time, occupancy, vulnerable structural components and assemblies, and vulnerable non-structural systems. Part of these data is already collected and used in traditional
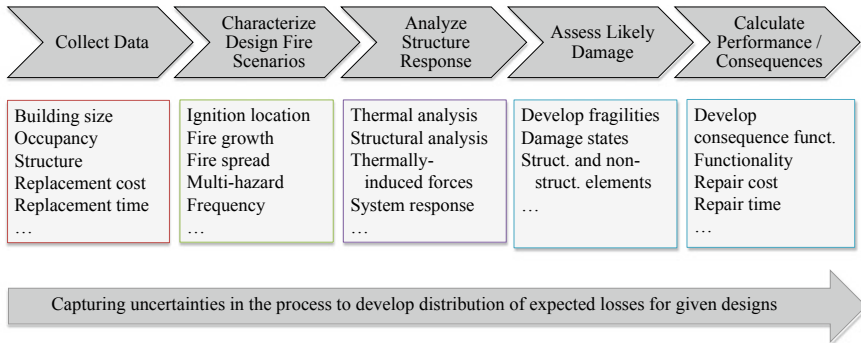
Fig. 4 Methodology for evaluating the performance of a given design under fire

structural fire engineering analyses. For instance, the building size and structural design are employed to assess the fire response. However, the amount of data used in a resilience-based analysis is larger as it includes data about costs, necessary repair actions of structural and nonstructural systems, and influence on post-fire building occupancy. Further, it is necessary to develop an understanding of the role (functionality) of the building/infrastructure at the system level to enable an accurate assessment of the economic consequences of a downtime. In earthquake engineering, data are available to assign a fragility specification to the vulnerable components in a building, with this specification including information on component damage states, fragility functions, and consequence functions in terms of restoration time and repair cost, as required in the PEER framework (the Pacific Earthquake Engineering Research (PEER) Center has established a largely used seismic engineering framework named after the Center). However, no such data is available in the fire engineering field.

Then, the performance assessment starts with the characterization of the fire hazard. This characterization relies on a combination of modeling and assumptions, as there is few data on fire scenarios for structures and their frequency of occurrence. The characterization of a design fire scenario requires assumptions on the likelihood and location of ignition. To inform assumptions about fire occurrences, statistical databases are published in some countries, e.g. in the US by the NFPA [see the analysis in (Manes and Rush 2018)]. A probabilistic fire occurrence equation is also described in the background document for the Eurocode fire load design value, see (Vassart et al. 2014). In buildings, the possibility for the fire to grow and spread beyond the compartment of origin is gauged based on engineering judgment, or accounted for in a sensitivity analysis, rather than explicitly modeled. Currently, no predictive model exists to realistically capture the fully coupled effect between the fire attacking the partitions between different fire compartments, and the failure of these partitions influencing the fire propagation in the building. Multi-compartments and/or multi-floors fire scenarios are typically considered for large projects with arbitrary propagation criteria, e.g. (Rackauskaite et al. 2017). In the end, the identi-

fication of the relevant design fire scenarios should be determined on the basis of a fire risk assessment.

Once the fire location is defined, different types of models can be applied to evaluate the thermal loading on the structure. The development and growth of a fire depends on many parameters including ventilation, fire load, geometry of the compartment, etc. For instance, open air fires attacking a bridge are very different from fires in small enclosed rooms because of the ventilation conditions and the absence of flashover. The simplest models represent the fire as a gas temperature-time curve applied on the structure, assuming a post-flashover situation in which the conditions are spatially uniform in the compartment. A commonly used example of such model is the Eurocode parametric fire (CEN 2002). The Eurocode parametric fire model provides a natural fire curve with a cooling phase as a function of the fire load density, compartment ventilation, and thermal inertia of the boundary of enclosure. This fire model has been used in several probabilistic analyses of structures in fire due to its convenience, e.g. (Gernay et al. 2018; Eamon and Jensen 2013). Where no flashover is expected to have occurred, either because the fire is in its early stage, or because the physical conditions leading to flashover are not met (e.g. in large open space compartments such as atriums or airport terminals), localized fire models accounting for spatially non-uniform heating conditions as a function of time are considered. The heating conditions are represented by thermal fluxes or temperatures. The position of the fire in a localized fire model can be either static or moving. The former case includes, for instance, the Hasemi and Heskestat models (CEN 2002). In the latter case, the term traveling fire has imposed itself in the community. Development of traveling fire model is recent (Stern-Gottfried and Rein 2012) and its physical foundations still need to be consolidated; ongoing research projects aim at addressing this question (Charlier et al. 2018). The use of localized and traveling fire models in probabilistic performance-based structural fire design appears as the next step (Teslim-Balogun et al. 2017), e.g. a case study of a steel-framed office building making use of Monte Carlo simulations considering traveling fires in open-plan spaces is presented in (Block and Kho 2018). At the more sophisticated end of the spectrum, Computational Fluid Dynamics can be used to model the fire. The CFD software Fire Dynamics Simulator (FDS), developed by NIST (McGrattan et al. 2007), is the most widely used in fire engineering. Dedicated interfaces have been developed to allow easy transfer of the results from a CFD FDS simulation to a thermo-mechanical finite element software, e.g. with SAFIR (Tondini et al. 2016). The use of FDS in structural fire engineering has gained traction in recent years, due partly to the increase in computational power. The coupling of CFD and FEM has demonstrated the potential to accurately capture the coupled fire-structure response, e.g. for reproducing localized fire tests on a steel column (Zhang et al. 2016). CFD models are particularly useful for modeling complex configurations for which no accurate simple model is available, e.g. in bridge fire applications (Alos-Moya et al. 2014). However due to computational cost, coupled CFD-FEM analyses are usually limited to the study of a few identified fire scenarios.

Uncertainties in the parameters influencing the fire severity should be accounted for in the performance assessment. In particular, the heat release rate per unit area

(Au et al. 2007) and the fire load per unit area have significant influence on the fire and involve considerable uncertainty. Data and probabilistic models for fire load densities are given in (Elhami Khorasani et al. 2014). In fact, the severity of the fire in a compartment results from a complex interaction of different parameters including the geometry, ventilation, fire load, and thermo-physical properties of the solid boundaries (Maluk et al. 2017). Notably, in compartment fires, two different regimes, known as ventilation-controlled and fuel-controlled, are observed as a function of the relative values of these parameters. Recent probabilistic studies have illustrated the sensitivity of gas temperatures to compartment size and ventilation conditions (Gernay et al. 2018; Guo and Jeffers 2015).

The next step in the performance assessment is the evaluation of the temperature evolution within the structural members. The results of the fire hazard characterization (design fires) represent boundary conditions for the heat transfer analyses within the structure. The relative position of the design fire and the structural member need to be taken into account when considering non-uniform fires. The heat transfer problem is usually solved either using simplified method, such as lumped mass approximations (Quiel et al. 2011) (particularly for steel structures), or numerical methods with a discretization of the domain (e.g. FEM) and a time integration procedure. When natural fire models are adopted, the temperature analysis of the structural members need to be made for the full duration of the fire including the cooling phase, to evaluate possible delayed failure (Gernay and Dimia 2013) and assess the residual behavior. Different uncertain parameters affect the heat transfer analysis, including the actual thickness and integrity of insulation materials (e.g. SFRM on steel sections), the thermal properties of the insulation, and that of the load-bearing materials.

Then, the building/infrastructure response is assessed under fire loading. The calculation of the mechanical behavior at elevated temperature determines the stresses, strains and displacements in the structure exposed to fire. As a result of the temperature changes, the mechanical properties of the materials are affected; hence the analysis must consider the temperature dependency of the properties. As the material properties at elevated temperature exhibit variability (Nauss 2010), some authors have proposed probabilistic temperature-dependent material models, e.g. for steel (Elhami Khorasani et al. 2015a). Yet, a well-established set of models for quantifying material properties at high temperature does not currently exist. Other effects of the temperature changes are the imposed and constrained expansions and deformations that result in thermally induced forces and moments in the structure. Advanced analyses based on numerical methods (e.g. FEM) are generally used to capture these effects.

Simulation capabilities for assessing building performance under fire loading have advanced dramatically over the last two decades. Finite element models have been used to simulate real fire-induced building failures (e.g. World Trade Center 1 and 2 (Usmani et al. 2003) and WTC 5 (LaMalva et al. 2009), Tehran Plasco building (Behnam 2018)) as well as full-scale fire tests [e.g. BRE Cardington tests (Foster et al. 2007), Ulster test (Vassart et al. 2012)]. Recently, Elhami Khorasani et al. (2019) presented a performance-based analysis of a steel-concrete composite floor subjected

to different design fire scenarios based on numerical modeling. Fire assessments of bridges (Alos-Moya et al. 2014) and tunnels (Savov et al. 2005) can also be found in the literature, although these types of structures have received less attention than buildings. More generally, a significant amount of research has been published in the last two decades to improve understanding of the behavior of structural components and structural assemblies under fire, largely based on computational studies. Advanced material models have been developed to capture the constitutive behavior at high temperature, e.g. for concrete (Gernay and Franssen 2012; Gernay et al. 2013) or aluminum (Maljaars et al. 2008). Dedicated finite element software such as SAFIR (Franssen and Gernay 2017), as well as general purpose FE software such as Abaqus and ANSYS, are available to enable studies of structures in fire. Some remaining frontiers in the deterministic performance-based modeling include the consideration of sophisticated fire scenarios and their interactions with thermal-structural response, the modeling of multi-scale problems (e.g. large buildings with high fidelity modeling of joints), and the modeling of the response of nonstructural components. Yet, the field has made considerable progress toward an established methodology for deterministic performance assessment of structural fire response.

Recently, the ability to assess performance of structures in fire in a probabilistic framework has been investigated. In 2014, Lange et al. (2014) made an important contribution by proposing an adaptation of the seismic PEER framework to the case of fire loading. This laid the groundwork for a probabilistic performance-based fire engineering framework. In 2016, the authors of this chapter (Gernay et al. 2016) proposed for the first time a methodology for constructing fragility functions for entire buildings under fire hazard. These fragility functions provide a probabilistic measure of performance for an entire building system. Hence, they can be used to evaluate a city's resilience to fire hazard, including in case of multi-hazard cascading event such as fire following earthquake (Elhami Khorasani et al. 2015b). This methodology was exemplified on a 2D multi-story steel frame studied by stochastic nonlinear finite element analyses with SAFIR using a Latin Hypercube Sampling (LHS) scheme (Gernay et al. 2016). The incorporation of the fire fragility functions in a reliability framework is discussed in (Gernay et al. 2018). Fragility functions for fire hazards have been used recently in a number of studies, e.g. for concrete columns (Rush and Lange 2017) or for multi-hazard analysis of a hospital building (Marasco et al. 2017). Yet, some theoretical questions remain such as the definition of damage states for different typologies of structures and the most proper intensity measure to characterize hazard. Furthermore, much efforts remain needed to eventually build libraries of fragility functions to assign to different types of vulnerable components and assemblies in buildings and infrastructure. Studies in uncertainty quantification of fire performance contribute to these efforts. For instance, a few reliability analyses of structural members in fire have been published for timber elements (Lange et al. 2016), steel elements (Guo and Jeffers 2014), and concrete elements (Eamon and Jensen 2013). However, a common shortcoming of current studies is their focus on isolated members and specific failure modes (e.g. pure bending of a beam, buckling of a column). This is due to the computational expense of modeling structural assemblies or entire buildings, for which advanced numerical models are required.

Therefore, another research gap for enabling probabilistic structural fire engineering lies in the development of efficient uncertainty quantification methods compatible with costly numerical models. In 2017, Van Coile et al. (2017) proposed an unbiased method, which was successfully applied to finite element models of structures in fire (Van Coile et al. 2018b), as a promising first step. In conclusion, the fire engineering community has only recently started to address the issue of probabilistic modeling and fragility specification. Developments toward this goal are encouraging, but require much more efforts over the next years if one hopes to achieve a paradigm shift in performance assessment of structures in fire.

Ideally, for a given design, variability in fire performance of the building/infrastructure is explored by considering a suite of design fires and performing a large number of thermal-structural analyses involving uncertainties. The analyses model all the structural components and assemblies, as well as possibly nonstructural systems, and result in explicit prediction of damage due to the fire. By considering a large number of realizations, one obtains a probability distribution of the consequences of fire on the considered building/infrastructure. As such a process would be cumbersome and impractical in practice, fragility functions and consequence functions can be developed for different typologies of structural components and assemblies to determine the likelihood of reaching certain damage states and compute the consequences associated with that damage. The consequence functions aim at relating the damage sustained by each component to losses. The losses should include repair cost and repair time. As a result, a distribution of expected losses could be obtained for probabilistic assessment of fire performance. From a resilience prospective, (loss of) functionality is a key aspect in this loss evaluation. Currently, no framework exists to construct consequence functions for fire hazard, and the authors are not aware of any study reporting systematic evaluations of repair cost and repair time associated with fire-induced damage. Therefore, important research efforts are needed to close this gap, including in data collection and modeling.

5.3   Enabling Decision Making and Code Implementation

The advancement of performance assessment methodologies aims at generating useful information to enable decision making. The end goal is to support policymakers and building officials in their mission, notably through implementation of new provisions in design codes that advance the principles of resilience for the built environment. Therefore, the research outlined in Sects. 5.1 and 5.2 needs to be eventually translated into practice to positively impact fire resilience.

Probabilistic performance-based fire engineering can support policymakers and building officials in multiple ways. By explicitly evaluating the residual risk of incurring damage or loss for identified fire hazards, it enables demonstrating equivalence of alternative design approaches. It also enables making informed decisions about specific building/infrastructure, such as determining if an existing building constitutes an acceptable risk, if its occupancy type can be modified and whether this entails

upgrading the fire design. At a larger scale, it provides a rational framework to perform Cost Benefit Analyses (CBA) and hence determine the efficiency of fire risk mitigation techniques. Additional upfront safety investments need to be balanced against reduction in disaster-induced damage losses to assess the net benefits and economic viability of proposed design changes. At the societal level, it is clear that resources are limited and the cost of improving resilience to fire needs to be weighed against possible life quality enhancement investments in other fields. Only risk-based analyses accounting for uncertainties can rationally inform these types of decisions.

Current building codes in Europe and in the U.S. permit the application of performance-based structural fire design to evaluate the performance of structural systems explicitly under fire exposure. In Europe, the Eurocodes have been pioneer in this approach, while in the U.S. the newly released Standard ASCE 7-16 Appendix E put forth structural fire engineering as an alternative to the code-default prescriptive method. The code framework thus exists to adopt physics-based modeling and comprehensively evaluate structural fire design variants. Explicit incorporation of uncertainties, as well as functionality objectives, in these evaluations has the potential to provide important dividends in terms of fire resilience of the built environment.

6 Accounting for Multi-hazard—The Case of Fire Following Earthquake

6.1 Fire as a Secondary Event

A fire may ignite as a secondary event following another extreme event, such as blast, impact, or earthquake. In such cases, fire could cause more damage than the initial event given that the system has already experienced a shock and is damaged to some extent. The most well-known example of collapse from fire following impact is the 2001 World Trade Center event. More recently, two buildings collapsed due to gas explosions in the Lower Manhattan (New York) in 2015, and caused a large fire that spread to other nearby buildings, which resulted in further damage (The New York Times 2015). Earthquakes can also be followed by a number of ignitions across a community due to ruptured gas lines, electric arcing, or toppled furniture inside the buildings. There have been historic cases in Japan, US, Chile, etc. where the earthquake ignited fires and caused excessive damage. These records are not limited only to the old events such as the 1906 San Francisco earthquake (where conflagration burned the city), but include others in post 1970s. For example, fires that followed the 1995 Kobe earthquake in Japan led to conflagrations and burned several blocks of houses in the city (Elhami Khorasani and Garlock 2017).

The rest of this section will focus on post-earthquake fires as a case of fire within a multi-hazard scenario. The discussion covers three aspects of hazard characterization, building response, and community response for fire following earthquake (FFE) events.

6.2 Likelihood of Ignition After an Earthquake

The study and modeling of fire following earthquake starts with characterizing the hazard and the likelihood of occurrence. While gas and electricity are the main causes of fire ignition after an earthquake, damage to walls, fire doors, sprinkler systems, etc. are the main causes of fire spread within a building when a fire starts. Ruptured gas lines (inside or outside of a building), water heaters, gas appliances such as ovens, flammable liquids, electric arcing, damaged electric wiring, and sparks during power restorations could lead to fire ignitions. Meanwhile, failure of non-structural components within buildings (e.g., sprinklers) and loss of fire compartmentation (damage to walls and doors) has also been recorded in previous earthquakes. Based on historic observations, mitigation actions such as automatic gas shut-off valves, and bracing of sprinkler systems and water heaters have been prescribed to reduce the likelihood of damage and the consequences.

A number of models have been developed to simulate post-earthquake ignitions. Lee et al. (2008) list and compare the existing ignition models in 2008 and conclude that "[FFE] data include a great deal of uncertainty, only some of which is captured in reported statistics." Ideally, it is preferred to establish a physics-based model that can be adapted for any region for simulation of post-earthquake fires. A physics-based model will require the power network, gas network, individual buildings, furniture inside the buildings, etc. to be modeled and the earthquake damage to these systems be captured. However, the complexities of developing a physics-based model for post-earthquake ignitions across a community scale make it impractical to follow such approaches. Meanwhile, Zolfaghari et al. (2009) investigated a semi-physics-based model, where causes of fire ignition (electric arcing, gas, toppled furniture, etc.) are taken into account but historic data and engineering judgment was used to arrive to the probability of ignition due to each source. Therefore, the existing models in the literature, e.g. Davidson (2009), primarily rely on historic data to assess probability of ignition after an earthquake.

The authors of this chapter have also established a data-driven probabilistic post-earthquake fire ignition model for a community. The objective was to develop a practical approach where the input information would be available to the emergency management officials. The model uses data from seven earthquakes post 1980s in California to derive the probability of ignition at a census track level given the peak ground acceleration (a measure of earthquake intensity), population density, and total square footage of buildings. Once the probability of ignition at a census track is known, the buildings in the area are categorized based on their construction type into three groups of non-combustible, wood, and mobile homes. The probability of ignition for each building is then calculated based on ignition factors for each construction type, derived again using the historic dataset. Details of the model are provided in Elhami Khorasani et al. (2017). The model can be used in a GIS-based software. Note that, since occurrence of FFE depends on environmental data such as building standards and appliances, US data-based models such as the ones in

(Davidson 2009; Elhami Khorasani et al. 2017) cannot be extrapolated for other countries.

6.3 Building Response to FFE

A well-established framework to characterize and study response of buildings to post-earthquake fires does not exist. Conducting experiments on full-scale buildings, where the structure is first subjected to earthquake shaking and then to fire, is expensive and requires special laboratory facilities and setting. Simulating the process using finite element programs would provide some insight on potential vulnerabilities of the structure. Earlier studies on the topic use different software or tools to perform non-linear numerical analyses for the earthquake and fire scenarios. Switching between programs, to conduct dynamic analysis followed by heat transfer and structural analysis at elevated temperatures implies simplifying assumptions and loss of information in transition between the models. For example, material degradation during the earthquake is ignored when analyzing the structure at elevated temperature. Therefore, a seamless and efficient transition between the two sets of analyses can enhance accuracy of the analyses. This section provides a summary of existing experimental and numerical studies on performance of buildings during post-earthquake fires.

As part of a collaborative effort, industry, government, and a number of universities came together to perform full-scale earthquake and post-earthquake fire testing of buildings. The project led by the University of California, San Diego (UCSD) studied post-earthquake fire performance of a five-story reinforced concrete frame (Hutchinson et al. 2013) and a six-story cold-formed steel (CFS) wall braced building (Hutchinson et al. 2018). The results of fire test after shaking the concrete building show that automatic sprinkler systems, fire dampers and roll-down fire doors performed well. However, separated joint seals and significant gaps between balloon framing and slabs could potentially lead to loss of compartment integrity and consequently spread of fire and smoke.

Della Corte et al. (2003, 2005) performed seismic and thermal analyses of steel moment resisting frames independently. In doing so, they categorized earthquake damage as geometric damage or mechanical damage, where the inter-story drift is the primary cause of damage and mechanical degradation is only critical at very large earthquake intensities. Their study of a multi-story frame show a 10% reduction in fire resistance when the frame is subjected to design-level earthquake, but with large intensity earthquakes, the effect in reduction of fire resistance is more significant. Behnam and Ronagh (2015) studied post-earthquake fire performance of unprotected moment resisting frames as part of a school or residential occupancy types. The earthquake effect is modeled with pushover analysis in SAP2000 and the thermal analysis is conducted in SAFIR. The results of pushover analysis, in terms of displacements, are imported to SAFIR. The results show that structures experiencing damage from earthquake have lower fire resistance (in the form of time to failure) than those in

the intact condition. Keller and Pessiki (2013) studied response of special moment frames with damaged fire protection during post-earthquake fires. The results show that softening of the beam at elevated temperatures, at regions that reach bending capacity during seismic loading, increases drift demands on the frame.

In order to be able to perform the cascading fire following earthquake analysis in one software environment while performing reliability analysis to capture uncertainties, Elhami Khorasani et al. (2015c) enhanced the thermal module in OpenSees by implementing a strain-based approach that allows for strain reversals. Elhami Khorasani et al.'s (2016) probabilistic analyses of a moment resisting frame subject to fire at lower versus upper floors, and interior versus exterior bays showed that the earthquake does not significantly change the fire resistance of the frame. Inter-story drift was the only parameter affected by the earthquake. The residual drift after the earthquake increased the total drift during fire, but this did not exceed 4%. The results implied that in case of fire, the gravity frames would be the more vulnerable part of a building. Memari and Mahmoud (2018) used a probabilistic framework to study performance of a column in a 3-story moment resisting frame and developed fragilities of steel columns considering buckling as the damage limit state. The results show that the probability of buckling in one or more columns in a story at maximum fire load density is 60% given a set of selected near- and far-field earthquake records. The developed fragility surfaces considered inter-story drift from the earthquake and fire load density as intensity measures. In summary, Chicchi and Varma (2017) provide a literature review of post-earthquake fire assessment of steel buildings in the US and Elhami Khorasani and Garlock (2017) provide an overview of existing research on response of buildings or communities to fire following earthquake.

In the studies above, it is generally assumed that steel frames are not protected. Although a conservative assumption, Braxtan and Pessiki (2011)'s experimental research confirm that spray-applied fire-resistive material (SFRM) used as fire protection is vulnerable to delamination or dislodge during seismic response. The above overview also shows that the majority of existing research has focused on steel structures. This is explained by the vulnerability of steel structures, especially unprotected, when subjected to fire, compared to concrete structures.

Another potential scenario that is of interest to the designers in earthquake prone areas is the post-fire seismic strength of structural systems. For example, Ni and Birely (2018b) studied impact of fire induced structural damage on the lateral load resistance of reinforced concrete walls. In doing so, Ni and Birely performed thermal analysis in SAFIR and obtained the maximum temperature in concrete and steel reinforcement. The residual strength and fire-damaged material properties are defined for cyclic analysis of the reinforced concrete shear wall in OpenSees. The NIST (Andres and Hoehler 2018) is conducting a test campaign on cold-formed steel shear walls to investigate the influence of fire on the seismic shear capacity.

One key aspect that needs to be further studied is related to the earthquake damage to non-structural components in a building and the potential loss of fire compartment integrity. In the Northridge and Hyogoken-Nanbu (Kobe) earthquakes, numerous building fire protection systems experienced significant damage, including up to 40% of the sprinkler systems and 30% of the fire doors. During the recent Christchurch

earthquakes, the non-structural building elements, including stairs, ceiling, facade, and fire protection systems, are reported as contributing a significant percentage of the NZ$16 Billion loss (Meacham 2015). In all these cases, damage to gypsum wall assemblies, fire doors, sprinkler systems, etc. means that active and passive fire protection systems that are provided to control fire and smoke are affected. Therefore, a holistic approach that takes into account potential fire spread inside the building is needed to measure post-earthquake fire performance of a structural system.

6.4   Community Response to FFE

Given the recent advances in community resilience studies, a fire following earthquake model is best utilized if implemented as part of a Geographic Information System (GIS) based platform, where the spatial information on the likelihood of damage from fire at a given time following the earthquake can be analyzed for regions across a certain community. The two most recognized tools for community resilience and risk management studies in the US are Hazus (FEMA 2014) and MAEViz/Ergo (2014). Hazus is developed by the Federal Emergency Management Agency and provides an inventory of data for the United States based on census tract areas. MAEViz/Ergo is an open source platform, primarily used by the researchers, developed in association with the MAE Center (Multi-hazard Approach to Engineering) at the University of Illinois, Urbana Champaign. The majority of initial efforts in advancing modeling and decision-making processes for hazard risk reductions in a region started by the earthquake engineers for seismic risk assessment. The ultimate goal and focus of many current research projects is to further incorporate economic and social losses to enable effective decisions by policy makers.

Hazus includes a fire following earthquake (FFE) module but warns the user that the available research in this area is limited and therefore, the estimated total losses from the earthquake does not include those from the fire. The FFE module includes three phases of ignition, spread, and suppression. Fire spread depends on the wind condition, spacing of buildings, their construction type, and the influence of suppression efforts. Firefighting response after an earthquake depends on water availability given post-earthquake damage to the water network, engine and crew availability given the state of emergency immediately after the earthquake, and accessibility of area for firefighters given damage to bridges and transportation network. The existing FFE module in Hazus and other available studies in the literature make simplifying assumptions regarding water availability and response time of firefighters. For example, water availability not only depends on the level of damage to pipes in the network, but also on functionality of pumps and their dependence on the power availability. Coar et al. (2018) confirmed that ignoring explicit dependence of the water network on power may provide inaccurate and unconservative predictions of the available water pressure and flow at fire hydrants after an earthquake, particularly for 'medium' to 'large' seismic events.

Yildiz and Karaman (2013) implemented an ignition model in MAEViz/Ergo to complete a scenario study in Turkey. A brief overview of their model is provided in Sect. 6.2 based on the work of Zolfaghari et al. (2009). In summary, their developed model, although it relies on a framework that groups the ignitions based on their source (gas, power, or furniture), uses site specific data and generate probability of ignition values for individual buildings that are relatively large and not realistic. Such a model is more suitable for comparison purposes to identify vulnerable areas, rather than using the absolute values of calculated probabilities.

There have been three notable scenario studies to assess seismic vulnerability and potential damage from an earthquake in the US, namely, the Shakeout (Scawthorn 2008) and HayWired (USGS 2018) earthquake scenarios in California and the Hazard Mitigation Plan seismic study of NY-NJ-CT area (NYCEM 2003). The Shakeout scenario assumed a 7.8 earthquake on Southern San Andreas Fault, which estimated 1600 fire ignitions in the region, with 1200 of which could spread and a few could possibly lead to conflagration. The most recent HayWired scenario study released in 2018 assumed a 7.0 magnitude earthquake on the Hayward Fault along the east-bay side of San Francisco Bay and concluded that the earthquake could cause 400 gas- and electric-related fires with potential conflagration. The study estimated that the fires would be directly responsible for the loss of hundreds of lives and total property losses close to $30 billion (in 2016 dollars). Finally, the tri-state NY-NJ-CT hazard study showed that a moderate earthquake could result in up to 900 fires.

In summary, the current modeling approach to fire following earthquake can be improved to reduce uncertainty in predicting losses with explicit inputs on performance of water and power networks, firefighting resources, and their response time. Decision making tools can be developed accordingly for resource allocation and implementing strategies for mitigation or response in vulnerable regions of a community.

7 Perspectives

In designing the built environment, which supports the socio-economic functions of our societies, structural engineers' objectives are evolving from a sole focus on occupant life safety toward a broader goal of resiliency and continuity of service in case of crisis. This evolution stems naturally from the development toward more dense and interconnected systems, as well as from increasing expectations from the public (as evidenced for instance after the 2011 Christchurch earthquake). Yet, even though fire is one of the most devastating hazards for buildings and infrastructures, the field of structural fire engineering has been slow to adapt to this evolution. The main reason is that, unlike earthquake or wind, fire is not traditionally contemplated as a loading case by structural engineers, but rather it is handled in a prescriptive manner at the end of the design process. As a result, the current approach to fire safety is arguably in a dead-end; draining significant resources year after year (~1–2% of GDP) while not delivering the resiliency one could expect.

   Yet, there are signs that the field of structural fire engineering is catching up. Research is gaining traction in performance-based approaches, numerical modeling capabilities, and probabilistic risk assessment; these research outcomes support the transition from empirical ad hoc approaches toward scientifically grounded analyses and designs. To be successful, new performance-based designs will have to efficiently navigate the necessary shifts in paradigm in terms of how the *Goal*, *Scale*, *Uncertainty* and *Hazard Scenario* are defined. Methods based on cost benefit analysis and lifecycle cost optimization should be used at the system scale to rationalize the use of resources to tackle the fire issue, while keeping in sight that fire is only one of many problem that society has to face (avoiding the silo effect). Importantly, other fields such as seismic engineering have paved the way, and provide methods and inspiration which can be built upon. Meanwhile, the recent evolutions of standards permitting the application of performance-based structural fire design, such as the newly released Standard ASCE 7-16 Appendix E in the U.S., will hopefully also accelerate the modernization of structural fire engineering practice. Obstacles remain, but the stakes and resources invested in fire safety are important, so that the opportunities and potential dividends in advancing the principles of fire resilience in the built environment are real.

References

Alos-Moya, J., Paya-Zaforteza, I., Garlock, M. E., Loma-Ossorio, E., Schiffner, D., & Hospitaler, A. (2014). Analysis of a bridge failure due to fire using computational fluid dynamics and finite element models. *Engineering Structures, 68,* 96–110.

Andres, B., & Hoehler, M. S. (2018). Influence of fire on the seismic shear capacity of cold-formed steel shear walls. In *Eleventh U.S. National Conference on Earthquake Engineering Integrating Science, Engineering & Policy*, Los Angeles, California, June 25–29, 2018.

Arup. (2013). *REDi rating system resilience-based earthquake design initiative for the next generation of buildings*.

Arup. (2018). *A framework for fire safety in informal settlements*. London, UK: Arup.

Au, S. K., Wang, Z. H., & Lo, S. M. (2007). Compartment fire risk analysis by advanced Monte Carlo simulation. *Engineering Structures, 29*(9), 2381–2390.

Badger, S. G. (2015). *Large-loss fires in the United States*. Report for National Fire Protection Association.

Behnam, B. (2018). Fire structural response of the Plasco building: A preliminary investigation report. *International Journal of Civil Engineering*, 1–18.

Behnam, B., & Ronagh, H. R. (2013). Performance of reinforced concrete structures subjected to fire following earthquake. *European Journal of Environmental and Civil Engineering, 17*(4), 270–292.

Behnam, B., & Ronagh, H. R. (2015). Post-earthquake fire performance-based behavior of unprotected moment resisting 2D steel frames. *KSCE Journal of Civil Engineering, 19*(1), 274–284.

Block, F. M., & Kho, T. S. (2018). Determining the fire resistance rating of buildings using the probabilistic method—A state-of-the-art approach. *The Structural Engineer: Journal of the Institution of Structural Engineer, 96*(1), 36–40.

Block, F., Yu, C., & Butterworth, N. (2010). The practical application of structural fire engineering on a retail development in the UK. *Journal of Structural Fire Engineering, 1,* 205–218.

Braxtan, N. L., & Pessiki, S. (2011). Bond performance of SFRM on steel plates subjected to tensile yielding. *Journal of Fire Protection Engineering, 21*(1), 37–55.

Byström, A., Sjöström, J., Wickström, U., Lange, D., & Veljkovic, M. (2014). Large scale test on a steel column exposed to localized fire. *Journal of Structural Fire Engineering, 5*(2), 147–160.

CEN. (2002). EN 1991-1-2. *Eurocode 1: Actions on structures—Part 1–2: General actions—Actions on structures exposed to fire*. European Standard.

Charlier, M., Gamba, A., Dai, X., Welch, S., Vassart, O., & Franssen, J. M. (2018). CFD analyses used to evaluate the influence of compartment geometry on the possibility of development of a travelling fire. In *Structures in fire* (*Proceedings of the 10th International Conference*).

Chicchi, R., & Varma A. H. (2017). Research review: Post-earthquake fire assessment of steel buildings in the United States. *Advances in Structural Engineering*, 1–17.

Chung, P., Wolfe, R. W., Ostrom, T., & Hida, S. (2008). *Accelerated bridge construction applications in California—A lessons learned report*. USA: California Department of Transportation (CALTRANS).

Coar, M., Garlock, M., & Elhami Khorasani, N. (2018). Effects of water network dependency on the electric network for post-earthquake fire suppression. *Submitted to the Journal of Sustainable and Resilient Infrastructure*.

CTIF International Assoc. of Fire and Rescue Services. (2016). *World fire statistics no 21*.

Davidson, R. (2009). *Generalized linear (mixed) models of post-earthquake fire ignitions*. Technical Report MCEER-09–2004, Multidisciplinary Center for Earthquake Engineering Research, Buffalo.

Della Corte, G., Landolfo, R., & Mazzolani, F. M. (2003). Post-earthquake fire resistance of moment resisting steel frames. *Fire Safety Journal, 38,* 593–612.

Della Corte, G., Faggiano, B., & Mazzolani, F. M. (2005). On the structural effects of fire following earthquake. In *Improvement of Buildings' Structural Quality by New Technologies: Proceedings of the Final Conference of COST Action C12*, Innsbruck, January, 20–22

Doerfel, M. L., & Harris, J. L. (2015). *Longitudinal disaster response networks: The clash of institutional and emergent organizations*. Presented at the Political Networks Conference, Portland, OR.

Eamon, C., & Jensen, E. (2013). Reliability analysis of RC beams exposed to fire. *Journal of Structural Engineering, 139,* 212–220. https://doi.org/10.1061/(ASCE)ST.1943-541X.0000614.

Elhami Khorasani, N., & Garlock, M. (2017). Overview of fire following earthquake: Historical events and community responses. *International Journal of Disaster Resilience in the Built Environment, 8*(2), 158–174.

Elhami Khorasani, N., Garlock, M., & Gardoni, P. (2014). Fire load: Survey data, recent standards, and probabilistic models for office buildings. *Engineering Structures, 58,* 152–165.

Elhami Khorasani, N., Gardoni, P., & Garlock, M. (2015a). Probabilistic fire analysis: material models and evaluation of steel structural members. *Journal of Structural Engineering, 141,* 04015050. https://doi.org/10.1061/(ASCE)ST.1943-541X.0001285.

Elhami Khorasani, N., Gernay, T., & Garlock, M. (2015b). Tools for measuring a city's resilience in a fire following earthquake scenario. In *IABSE Conference on Structural Engineering: Providing Solutions to Global Challenges*, Geneva, Switzerland (pp. 886–889).

Elhami Khorasani, N., Garlock, M., & Quiel, S. E. (2015c). Modeling steel structures in OpenSees: Enhancements for fire and multi-hazard probabilistic analysis. *Journal of Computers and Structures, 157,* 218–231.

Elhami Khorasani, N., Garlock, M., & Gardoni, P. (2016). Probabilistic performance-based evaluation of a tall steel moment resisting frame under fire following earthquake. *Journal of Structural Fire Engineering, 7*(3), 193–216.

Elhami Khorasani, N., Gernay, T., & Garlock, M. (2017). Data-driven probabilistic post-earthquake fire ignition model for a community. *Fire Safety Journal, 94,* 33–44.

Elhami Khorasani, N., Gernay, T., & Fang, C. (2019). Parametric study for performance-based fire design of U.S. prototype composite floor systems. *Journal of Structural Engineering ASCE*.

Federal Emergency Management Agency (FEMA). (2009). *Quantification of building seismic performance factors*. Federal Emergency Management Agency (FEMA) P695, Prepared by Applied Technology Council for the Federal Emergency Management Agency, Washington, D.C.

FEMA. (2011). Fire death rate trends: An international perspective. *Topical Fire Report Series, 12*(8), 1–8.

FEMA. (2012a). *Seismic performance assessment of buildings*. FEMA P-58, Prepared by Applied Technology Council for the Federal Emergency Management Agency, Washington, D.C.

FEMA. (2012b). *Performance assessment calculation tool* (PACT). Federal Emergency Management Agency. http://www.fema.gov/medialibrary/assets/documents/90380, Washington, D.C.

FEMA. (2014). *Hazus: MH 2.1 technical manual—earthquake model*. Developed by the Department of Homeland Security. Federal Emergency Management Agency. Mitigation Division, Washington, DC.

FEMA. (2018). Retrieved September 28, 2018. https://www.usfa.fema.gov/data/statistics/fire_death_rates.html.

Fischer, K. (2014). *Societal decision-making for optimal fire safety*. Bericht IBK, 357.

Foster, S., Chladná, M., Hsieh, C., Burgess, I., & Plank, R. (2007). Thermal and structural behaviour of a full-scale composite building subject to a severe compartment fire. *Fire Safety Journal, 42*(3), 183–199.

Franssen, J. M., & Gernay, T. (2017). Modeling structures in fire with SAFIR®: Theoretical background and capabilities. *Journal of Structural Fire Engineering, 8*(3), 300–323.

Gann, R. G. (2008). Final report on the collapse of world trade center building 7, Federal Building and Fire Safety Investigation of the World Trade Center Disaster (NIST NCSTAR 1A). No. National Construction Safety Team Act Reports (NIST NCSTAR).

Gardoni, P., & LaFave, J. M. (2016). Multi-hazard approaches to civil infrastructure engineering: Mitigating risks and promoting resilience. In *Multi-hazard approaches to civil infrastructure engineering* (pp. 3–12). Cham: Springer.

Garlock, M., Paya-Zaforteza, I., Kodur, V., & Gu, L. (2012). Fire hazard in bridges: Review, assessment and repair strategies. *Engineering Structures, 35,* 89–98.

Gernay, T., & Franssen, J. M. (2012). A formulation of the Eurocode 2 concrete model at elevated temperature that includes an explicit term for transient creep. *Fire Safety Journal, 51,* 1–9.

Gernay, T., Millard, A., & Franssen, J. M. (2013). A multiaxial constitutive model for concrete in the fire situation: Theoretical formulation. *International Journal of Solids and Structures, 50*(22–23), 3659–3673.

Gernay, T., & Salah Dimia, M. (2013). Structural behaviour of concrete columns under natural fires. *Engineering Computations, 30*(6), 854–872.

Gernay, T., Elhami Khorasani, N., & Garlock, M. (2016). Fire fragility curves for steel buildings in a community context: A methodology. *Engineering Structures, 113,* 259–276.

Gernay, T., Elhami Khorasani, N., & Garlock, M. (2018). Fire fragility functions for steel frame buildings: Sensitivity analysis and reliability framework. *Fire Technology*. https://doi.org/10.1007/s10694-018-0764-5.

Gernay, T., & Gamba, A. (2018). Progressive collapse triggered by fire induced column loss: Detrimental effect of thermal forces. *Engineering Structures, 172,* 483–496.

Gillie, M., Usmani, A. S., & Rotter, J. M. (2001). A structural analysis of the first Cardington test. *Journal of Constructional Steel Research, 57*(6), 581–601.

Guo, Q., & Jeffers, A. E. (2014). Finite-element reliability analysis of structures subjected to fire. *Journal of Structural Engineering, 141*(4), 04014129.

Guo, Q., & Jeffers, A. E. (2015). Finite-element reliability analysis of structures subjected to fire. *Journal of Structural Engineering, 141*(4), 04014129.

Haynes, H. J. G. (2017). *Fire loss in the United States during 2016*, NFPA.

Hopkin, D., Van Coile, R., & Lange, D. (2017). Certain uncertainty—Demonstrating safety in fire engineering and the need for safety targets. In *SFPE Europe, 07*.

Hopkin, D., Anastasov, S., McColl, B., O'Loughlin, E., & Taylor, A. (2018a). A structural fire strategy for an exposed weathering steel-framed building. *The Structural Engineer, 96*(1), 60–66.

Hopkin, D., Spearpoint, M., & Van Coile, R. (2018b). The J-value and its role in evaluating investments in fire safety schemes. *Fire Technology*, 1–18.

Hutchinson, T., Restrepo, J., Conte, J., & Meacham, B. J. (2013). Overview of the building nonstructural components and systems (BNCS) project. In *Proceedings of Structures Congress, ASCE,* Pittsburgh, PA.

Hutchinson, T. C., Wang, X., Hegemier, G., Meacham, B., & Kamath, P. (2018). Physical damage evolution during earthquake and post-earthquake fire testing of a mid-rise cold-formed steel framed building. In *Proceedings of the 11th U.S. National Conference on Earthquake Engineering*, Los Angeles, California, June.

Kareem, A. (1987). Wind effects on structures: A probabilistic viewpoint. *Probabilistic Engineering Mechanics, 2*(4), 166–200.

Keller, W., & Pessiki, S. (2013). Effect of earthquake-induced damage on the sidesway response of steel moment-frame buildings during fire exposure. *Journal of Earthquake Spectra*, *31*(1).

Kirkland, C. J. (2002). The fire in the channel tunnel. *Tunneling and Underground Space Technology, 17*(2), 129–132.

Kodur, V. K., Aziz, E. M., & Naser, M. Z. (2017). Strategies for enhancing fire performance of steel bridges. *Engineering Structures, 131,* 446–458.

Koliou, M., van de Lindt, J. W., McAllister, T. P., Ellingwood, B. P., Dillard, M., & Cutler, H. (2018). State of the research in community resilience: Progress and challenges. In *Sustainable and Resilient Infrastructure*.

LaMalva, K. J., Barnett, J. R., & Dusenberry, D. O. (2009). Failure analysis of the world trade center 5 building. *Journal of Fire Protection Engineering, 19*(4), 261–274.

Lange, D., Devaney, S., & Usmani, A. (2014). An application of the PEER performance based earthquake engineering framework to structures in fire. *Engineering Structures, 66,* 100–115.

Lange, D., Boström, L., & Schmid, J. (2016). Reliability of timber elements exposed to fire. In *Proceedings of the World Conference on Timber Engineering (WCTE)*, 22–25/08, Vienna, Austria.

Lattimer, B. Y., & Ferreira, M., (2017). A review of developing railcar design for smoke control system design. In *Proceedings of the 2017 Joint Rail Conference*, Philadelphia, U.S.A.

Lee, S., Davidson, R., Ohnishi, N., & Scawthorn, C. (2008). Fire following earthquake—Reviewing the state-of-the-art of modeling. *Earthquake Spectra, 24*, 933–967.

Lennon, T., Moore, D. B., & Bailey, C. (1999). The behaviour of full-scale steel-framed buildings subjected to compartment fires. *Structural Engineering, 77*(8), 15–21.

Li, Y. Z., & Ingason, H. (2012). The maximum ceiling gas temperature in a large tunnel fire. *Fire Safety Journal, 48,* 38–48.

Liew, J. R. (2008). Survivability of steel frame structures subject to blast and fire. *Journal of Constructional Steel Research, 64*(7–8), 854–866.

MAEViz. (2014). Hosted by the National Center for Supercomputing Applications, at the University of Illinois, Urbana. http://mae.cee.illinois.edu/software/software_maeviz.html.

Maljaars, J., Soetens, F., & Katgerman, L. (2008). Constitutive model for aluminum alloys exposed to fire conditions. *Metallurgical and Materials Transactions A, 39*(4), 778–789.

Maluk, C., Linnan, B., Wong, A., Hidalgo, J. P., Torero, J. L., Abecassis-Empis, C., et al. (2017). Energy distribution analysis in full-scale open floor plan enclosure fires. *Fire Safety Journal, 91,* 422–431.

Manes, M., & Rush, D. (2018). A critical evaluation of BS PD 7974-7 structural fire response data based on USA fire statistics. *Fire Technology*. https://doi.org/10.1007/s10694-018-0775-2.

Marasco, S., Zamani Noori, A., & Cimellaro, G. P. (2017). Cascading hazard analysis of a hospital building. *Journal of Structural Engineering, 143*(9), 04017100.

McGrattan, K., Klein, B., Hostikka, S., & Floyd, J. (2007). Fire dynamics simulator (Version 5): User's guide. National Institute of Standards and Technology (NIST).

Meacham, B. (2015). Post-earthquake fire performance of buildings: Summary of a large-scale experiment and conceptual framework for integrated performance-based seismic fire design. *Fire Technology*. Springer Science. https://doi.org/10.1007/s10694-015-0523-9.

Memari, M., & Mahmoud, H. (2018). Framework for a performance-based analysis of fires following earthquakes. *Engineering Structures, 171,* 794–805.

Mieler, M. W., & Mitrani-Reiser, J. (2018). Review of the state of the art assessing earthquake-induced loss of functionality in buildings. *Journal of Structural Engineering, 144*(3). https://doi.org/10.1061/(asce)st.1943-541x.0001959.

Molkens, T., Van Coile, R., & Gernay, T. (2017). Assessment of damage and residual load bearing capacity of a concrete slab after fire: Applied reliability-based methodology. *Engineering Structures, 150,* 969–985.

Naus, D. (2010). *A compilation of elevated temperature concrete material property data and information for use in assessments of nuclear power plant reinforced concrete structures*. US Nuclear Regulatory Commission, Office of Nuclear Regulatory Research, Washington, DC.

Ni, S., & Birely, A. C. (2018a). Impact of physical seismic damage on the fire resistance of reinforced concrete walls. *Construction and Building Materials, 182,* 469–482.

Ni, S., & Birely, A. C. (2018b). Simulation procedure for the post-fire seismic analysis of reinforced concrete structural walls. *Fire Safety Journal, 95,* 101–112.

NIST. (2016). *Community resilience planning guide for buildings and infrastructure systems*. NIST Special Publication 1190 (Vols. 1 and 2). National Institute of Standards and Technology.

NYCEM: The New York City Area Consortium for Earthquake Loss Mitigation. (2003). *Earthquake risks and mitigation in the New York, New Jersey, Connecticut Region*. Report Number MCEER-03-SP02.

PPD (Presidential Policy Directive). (2013). *Critical infrastructure security and resilience*. PPD-21. https://www.whitehouse.gov/the-press-office/2013/02/12/presidential-policy-directive-critical-infrastructure-security-and-resil.

Quiel, S. E., Moreyra Garlock, M. E., & Paya-Zaforteza, I. (2011). Closed-form procedure for predicting the capacity and demand of steel beam-columns under fire. *Journal of Structural Engineering, 137*(9), 967–976.

Quiel, S., Yokoyama, T., Bregman, L. S., Mueller, K., & Marjanishvili, S. (2015). A streamlined framework for calculating the response of steel-supported bridges to open-air tanker truck fires. *Fire Safety Journal, 73,* 63–75. (Elsevier).

Rackauskaite, E., Kotsovinos, P., & Rein, G. (2017). Structural response of a steel-frame building to horizontal and vertical travelling fires in multiple floors. *Fire Safety Journal, 91,* 542–552.

Rush, D., & Lange, D. (2017). Towards a fragility assessment of a concrete column exposed to a real fire–tisova fire test. *Engineering Structures, 150,* 537–549.

Savov, K., Lackner, R., & Mang, H. A. (2005). Stability assessment of shallow tunnels subjected to fire load. *Fire Safety Journal, 40*(8), 745–763.

Scawthorn, C. R. (2008). *The ShakeOut scenario—Fire following earthquake*. Prepared for United States Geological Survey, Pasadena, CA and California Geological Survey, Sacramento, CA.

Sekizawa, A., Ebihara, M., & Notake, H. (2003). Development of seismic-induced fire risk assessment method for a building. In *Fire Safety Science—Proceedings of the Seventh International Symposium, International Association for Fire Safety Science* (pp. 309–320).

Stern-Gottfried, J., & Rein, G. (2012). Travelling fires for structural design–Part I: Literature review. *Fire Safety Journal, 54,* 74–85.

Teslim-Balogun, A., Málaga-Chuquitaype, C., & Stafford, P. J. (2017). Assessment of efficiency of intensity measures for performance-based travelling fire design. In *IABSE Symposium Report* (Vol. 109, No. 41, pp. 1645–1648). International Association for Bridge and Structural Engineering.

The Geneva Association. (2010). *Information bulletin world fire statistics centre no. 26*.

The New York Time. (2015). *East village explosion ignites fire, fells buildings and injures at least 19*. Retrieved from https://www.nytimes.com/2015/03/27/nyregion/reports-of-explosion-in-east-village.html.

Tondini, N., Morbioli, A., Vassart, O., Lechêne, S., & Franssen, J. M. (2016). An integrated modelling strategy between a CFD and an FE software: Methodology and application to compartment fires. *Journal of Structural Fire Engineering, 7*(3), 217–233.

USGS. (2018). *The HayWired earthquake scenario—We can outsmart disaster*. U.S. Geological Survey, U.S. Department of the Interior, Fact Sheet 2018-3016.

Usmani, A. S., Chung, Y. C., & Torero, J. L. (2003). How did the WTC towers collapse: A new theory. *Fire Safety Journal, 38*(6), 501–533.

Van Coile, R., Caspeele, R., & Taerwe, L. (2014a). Reliability-based evaluation of the inherent safety presumptions in common fire safety design. *Engineering Structures, 77,* 181–192.

Van Coile, R., Caspeele, R., & Taerwe, L. (2014b). Lifetime cost optimization for the structural fire resistance of concrete slabs. *Fire Technology, 50,* 1201–1227.

Van Coile, R., Balomenos, G. P., Pandey, M. D., & Caspeele, R. (2017). An unbiased method for probabilistic fire safety engineering, requiring a limited number of model evaluations. *Fire Technology, 53*(5), 1705–1744.

Van Coile, R., Hopkin, D., Lange, D., Jomaas, G., & Bisby, L. (2018a). The need for hierarchies of acceptance criteria for probabilistic risk assessments in fire engineering. *Fire Technology*, 1–36.

Van Coile, R., Gernay, T., Elhami Khorasani, N., & Hopkin, D. (2018b). Evaluating uncertainty in steel-composite structure under fire-application of the ME-MDRM. In *10th International Conference on Structures in Fire*.

Vassart, O., Bailey, C. G., Hawes, M., Nadjai, A., Simms, W. I., Zhao, B., et al. (2012). Large-scale fire test of unprotected cellular beam acting in membrane action. *Proceedings of the Institution of Civil Engineers: Structures and Buildings, 165*(7), 327–334.

Vassart, O., Zhao, B., Cajot, L. G., Robert, F., Meyer, U., Frangi, A. (2014). *Eurocode: Background and applications. Structural fire design. Worked examples*. JRC, Luxemburg

Yildiz, S. S., & Karaman, H. (2013). Post-earthquake ignition vulnerability assessment of Kucukcekmece District. *Journal of Natural Hazards and Earth System Sciences, 13,* 3357–3368.

Zhang, C., Silva, J. G., Weinschenk, C., Kamikawa, D., & Hasemi, Y. (2016). Simulation methodology for coupled fire-structure analysis: Modeling localized fire tests on a steel column. *Fire Technology, 52*(1), 239–262.

Zhuang, J., Payyappalli, V. M., Behrendt, A., & Lukasiewicz, K. (2017). *Total cost of fire in the United States*. Fire Protection Research Foundation. Research for the NFPA mission. University at Buffalo, NY.

Zolfaghari, M. R., Peyghaleh, E., & Nasirzadeh, G. (2009). Fire following earthquake, infrastructure ignition modeling. *Journal of Fire Science, 27,* 45–79.

Part III
Resilience Concepts

Disaster Risk Reduction and Urban Resilience: Concepts, Methods and Applications

Tiago Miguel Ferreira and Paulo B. Lourenço

1 Introduction

During the past decades, there have been numerous large-scale disasters throughout the world, causing severe economic losses and affecting millions of people. These numbers, associated with a rapidly increasing rate of urbanisation, demonstrate the need for specific approaches to assess and manage natural and man-made disaster risks over these areas (Maio et al. 2018). Earthquakes, fires or floods are inevitable hazards with the potential to generate large-scale social, cultural and economic impacts and long-last disruption of the urban systems. However, these impacts can be significantly reduced through the implementation of a systematic risk assessment process. Current hazard mitigation methods applicable to reduce losses require a great effort in terms of development and implementation. This has been recently recognized as a methodology of risk management, a process of determining what should be done for a hazard, deciding which hazards and at what scale magnitude should be managed, and in what priority order. Thus, one of the most important research challenges in the field of systemic risk analysis is how to define new advanced analysis methods able to take into account the interdependencies between these different components.

The evaluation of the risk is considered essential to define strategic urban and emergency planning management actions and should be based on the analysis of the buildings, the exposed population and their emergency interaction. Such an approach is urgently needed for complex scenarios, like the historical one, but still, in many

T. M. Ferreira (✉) · P. B. Lourenço
ISISE, Institute of Science and Innovation for Bio-Sustainability (IB-S), Department of Civil Engineering, University of Minho, 4800-058 Guimarães, Portugal
e-mail: tmferreira@civil.uminho.pt

P. B. Lourenço
e-mail: pbl@civil.uminho.pt

cases around the world, historical centres scenarios are not properly investigated according this holistic risk analysis standpoint.

2 Conceptual Framework for Urban Resilience

Urban resilience is generally understood as the ability of an exposed urban area to prepare, respond and recover from the effects of multi-hazard threats, being directly connected to mitigation, preparedness, disaster, response, recovery and reconstruction disaster risk management phases (Coaffee 2008). Risk identification from natural hazards is considered the first step towards reducing their adverse effects. Several organisations such as the Global Facility for Disaster Reduction and Recovery (GFDRR) are focused on supporting governments and communities in vulnerable disaster-prone areas by increasing the perception, awareness and access to comprehensive information about physical and societal exposure to disaster risk. Hence, communities, private stakeholders and governments, are able to better estimate the potential impacts of the hazards most likely to occur and to affect people and property, as well as to carry out risk-sensitive decision-making. Moreover, these global knowledge-sharing partnerships frequently work together with the governments, the private sector and the civil society in order to create new or improve existing land-use policies, to drive investment in risk mitigation measures and to act as moderators in the dialogue between stakeholders (Arshad and Athar 2013).

There are numerous references in the literature of the positive influence of disaster risk management and planning on communities' resilient capacity. By the way of example, it is worth refereeing here the Rural Housing Reconstruction Program (RHRP), implemented in the aftermath of earthquake that struck northern Pakistan in October 2005 causing about 73,000 deaths and more than 2.8 million homeless people (Arshad and Athar 2013), the February 2010 Chile earthquake (Astroza et al. 2012) and the 22 February 2011 Christchurch earthquake (Mitchelson 2011). A particularly striking example is the 2011 Great East Japan Earthquake, a mega disaster crisis that caused about 20,000 casualties, over 130,000 building collapses and a direct economic cost estimated in $210 billion (Covello 2014). Although the level of preparedness of the Japanese community to natural hazards is internationally acclaimed and disaster risk management strategies had been developed and implemented for decades in the country, complexity resulting from the cascading effects of the 9.0 magnitude earthquake that hit the territory was simply too complex to deal with.

Civil protection bodies, in many countries, the agencies responsible for planning emergency response. In order to accomplish such task, it is essential that they be able to accurately identify which are the most vulnerable areas/zones and to prepare and put into practice logistic and field exercises aimed at simulating realistic emergency event scenarios (Goula et al. 2006). However, as highlighted by Ferreira et al. (2017b), urban risk management is often conducted by technicians and decision makers without the use of a general planning tool, which can seriously compromise

the their effectiveness since they don't have a comprehensive view of the area under investigation. An effective way of tackling this issue is to use a multi-purpose tool connected to a relational database within a Geographic Information System (GIS) platform. This kind of tools allow to perform spatially integrated analysis of the elements at risk, namely of the building stock, and to manage and integrate different types of data, such as survey information, building features, seismic vulnerability and risk scenarios. Due to this ability, these tools are of great value and usefulness for territorial planning of the city, particularly in supporting retrofitting strategies, cost-benefit analyses and the development and implementation of civil protection and local emergency plans (Neves et al. 2012).

In the pre-event phase, the primary attention should be focused on raising communities' preparedness, awareness, and perception of risks, which, in practice, can be achieved only by implementing appropriate education and communication strategies. According to Covello (2010), individual risk perception depends on a series of factors which determine how an individual responds to risk information. One of the most effective means of increasing risk awareness and assessing the risk perception of a community is through the creation and dissemination of information and communication tools and the organisation of risk awareness campaigns. Last but not least, volunteering and aiding mechanisms should be established in order to increase the response capacity during the emergency and response phase, wherein the safeguarding of human life, namely by means of the implementation of efficient safety and rescue plans, and the endowing of temporary settlement camps and infrastructures to receive homeless and injured people, should be a key priority.

Moreover, it is in the emergency and response phase that preliminary in-field technical surveys are conducted for evaluating the severity of the damage inflicted to structures and infrastructures. These surveying activities are usually developed from on a strong cooperation between the scientific community and the civil protection bodies. Even though these actions typically begin in a very early stage of the emergency and response phase, they are very likely to last for several months following the event, which increases significantly the complexity associated with their management since it involves the in-field cooperation of different players.

3   Vulnerability and Risk Evaluation Approaches for Urban Areas

Urban areas are characterized by high interference level between the buildings' vulnerabilities, the urban fabric features (complex streets network characterized by a high ratio between building height and width of facing street) and potentially high population densities, including tourists who can be unfamiliar with the environment. According to previous research (Gavarini 2001; Indirli 2009), the most influencing elements in inhabitants' safety is represented by the interactions between people and post-event environment in urban scenarios. In fact, the streets network plays a very

important role in emergency planning, especially during the evacuation phase since some urban areas can become fully or partially inaccessible due to the deposition of debris resulting from collapsed or heavily damaged buildings. In this sense, understanding urban and buildings vulnerabilities is a crucial step towards the development of more efficient and effective risk mitigation strategies. Two types of vulnerability can be distinguished (Santarelli et al. 2018):

- "Intrinsic" vulnerability, which concerns elements composing the path itself and where evaluation indices are provided for streets, public open spaces, and particular elements such as bridges;
- "Extrinsic" vulnerability, which involves the elements that do not directly belong to the path itself but that can compromise it.

Moreover, three main groups of vulnerability assessment methods are reported in the literature: empirical, analytical, and hybrid methods.

Empirical methods are particularly when a record of past events is available and building damage has been systematically collected over a significant number of events. Empirical methods can be distinguished between those purely empirical, i.e., based on post-event damage observation, and those relying on analytical formulations, in which a model of a representative building typology is defined, and its response is analysed for a certain level of action. According to Calvi et al. (2006), the stream of thought implicit in empirical methods usually fall upon damage probability matrices, vulnerability index methods, continuous vulnerability curves or screening methods.

Analytical methods are more appropriate for the cases where construction details are recorded and well understood. According to Maio et al. (2018), analytical methods tend to feature slightly more detailed and transparent vulnerability assessment algorithms with direct physical meaning, which not only allow detailed sensitivity studies to be undertaken but also the straightforward calibration to various characteristics of building stock and hazard sources. For large-scale vulnerability assessments, capacity and demand are often determined using simplified analytical methods (Mouroux and Le Brun 2006). It is worth referring the judgment-based methods, in which vulnerability is attributed to building typologies by a panel of experts selected to perform the assessment based on a common set of information and their previous knowledge. An illustrative example can be found in Porter et al. (2007). This technique may be particularly useful for generating vulnerability curves or damage probability matrices for classes of structures which are reasonably well defined in structural terms, but for which other methods cannot be applied (Rota et al. 2008).

Finally, the hybrid approaches try to overcome the main limitations of the previously described methods, making use of different sources of information combined together (Rota et al. 2010). Relevant examples of hybrid approaches are the macroseismic methods, which are based on empirical data and expert judgment or combine empirical data and analytical results.

To date, a limited number of works focuses on streets network punctual conditions and debris interactions, and, only few of them include historical scenarios through the introduction of geometric methodologies, which use the ratio between the height of

building, h, and the width of facing street, W, in order to determine the limit condition for building street interference. Since the ratio h/W is significant for the selection of pedestrians' evacuation route, this method is also used for the design of evacuation plan according to current standard methods developed in some earthquake-prone countries. It worth noting that the earthquake is one of the most influential hazards when it comes to the vulnerability of buildings in urban centres, leading to major modifications in terms of ruins production. For this reason, most of the vulnerability and debris quantification studies are related to earthquake events. Nevertheless, they can be very simply modified and adapted to other disaster events, such as fires, floods, etc.

4 Vulnerability Assessment as a Tool for Mitigating Risk in Urban Areas

The present section is aimed at discussing some of the concepts addressed in the previous sections through the application and discussion of two different large-scale vulnerability assessment approaches in two different cases studies.

In the first example, a hybrid seismic vulnerability assessment method originally developed for evaluating the seismic vulnerability of stone masonry façade walls is applied to the Historical Centre of Coimbra. The results obtained from that application are then used to estimate damage scenarios, which, in turn, are subsequently exploited to discuss emergency planning strategies. The definition of possible evacuation routes, the identification of inaccessible urban areas, as well as the number of people that, in consequence, may be affected, are some of the results presented and discussed herein.

In the second example, a simplified fire risk assessment method is applied to evaluate the fire risk in the Historical Centre of Guimarães. After being integrated into a Geographical Information System (GIS) software, the assessment results are spatially examined and discussed in the form of fire vulnerability and risk maps.

4.1 Seismic Vulnerability and Risk Analysis

Among the most frequently observed damage mechanisms in traditional masonry structures located the urban areas, the response of the facade walls is one of the most prevalent and critical ones, not only due to the direct consequences that may result from the partial or global collapse of these elements, but also because of the indirect impacts that can arise from that, such as the obstruction of evacuation routes due to the deposition of debris and ruins. Trying to tackle this issue, a new seismic vulnerability assessment method was proposed by Ferreira et al. (2014) to assess the seismic vulnerability of masonry facade walls. Such method was later extended and calibrated

by the authors (Ferreira et al. 2017a) resorting to two complementary approaches. A first based on fragility curves obtained from damage limit states defined with a simplified analytical method (Ferreira et al. 2015). The second one, based on post-earthquake damage data.

According to this vulnerability formulation, individual vulnerability is measured through an index obtained as the weighted sum of 13 evaluation parameters, listed in Table 1, each of which related to 4 classes, C_{vi}, of increasing vulnerability: A, B, C and D.

The vulnerability index of the façade wall, I_{vf}^*, can be then obtained by the weighted sum of the 13 parameters, each one of them affected by a weighting factor, p_i, which depends on the relative importance of the that particular parameter, see Eq. (1). For ease of use, the vulnerability index is normalised to range between 0 and 100, I_{vf}; the lower its value, the lower the seismic vulnerability of the façade wall.

$$I_{vf}^* = \sum_{i=1}^{13} C_{vi}\, p_i \tag{1}$$

In addition, a mean damage grade, μ_D, can be estimated for different macroseismic intensities based on the vulnerability index, I_{vf}. To this end, an analytical expression

Table 1 Vulnerability index formulation: parameters, classes and respective weights

Parameters	Class, C_{vi}				Weight
	A	B	C	D	p_i
Group 1. Façade geometry, openings and interaction					
P1. Geometry of the façade	0	5	20	50	0.50
P2. Maximum slenderness	0	5	20	50	0.50
P3. Area of openings	0	5	20	50	0.50
P4. Misalignment of openings	0	5	20	50	0.50
P5. Interaction between contiguous facades.	0	5	20	50	0.25
Group 2. Masonry materials and conservation					
P6. Quality of materials	0	5	20	50	2.00
P7. State of conservation	0	5	20	50	2.00
P8. Replacement of original flooring system	0	5	20	50	0.25
Group 3. Connection efficiency to other structural elements					
P9. Connection to orthogonal walls	0	5	20	50	2.00
P10. Connection to horizontal diaphragms	0	5	20	50	0.50
P11. Impulsive nature of the roofing system	0	5	20	50	2.00
Group 4. Elements connected to the façade wall					
P12. Elements connected to the facade	0	5	20	50	0.50
P13. Improving elements.	0	5	20	50	−2.00

that correlates hazard with the mean damage grade ($0 < \mu_D < 5$) of the damage distribution in terms of vulnerability value was developed by (Ferreira et al. 2014), Eq. (2):

$$\mu_D = 2.51 + 2.5 \times \tanh\left(\frac{I + 5.25 \times V - 11.6}{Q}\right) \qquad (2)$$

where I represents the seismic hazard described in terms of macroseismic intensity scale EMS-98 (Grünthal 1998), V is the vulnerability index obtained from Eq. (3), and Q is a ductility factor that describes the ductility of a certain constructive typology. Following the calibration made by Ferreira et al. (2014), a value of $Q = 2.0$ was assumed in this work. According to the authors, this value leads to the best approximation between mean damage grade values and post seismic damage evaluation for traditional stone masonry buildings.

$$V = 0.592 + 0.0057 \times I_{vf} \qquad (3)$$

4.1.1   Application to the Historic Centre of Coimbra

The city of Coimbra is one of the oldest and most important cities in Portugal. Besides the University of Coimbra-Alta and Sofia zone, which has been classified as a UNESCO World Heritage Site in 2013 (Vicente et al. 2015), the historical centre of Coimbra is also an outstanding cultural and touristic point. The architecture, the urban environment, the history and the cultural wealth of the area are enjoyed by the thousands of tourists who visit the city annually (Mendes da Silva 2015). A view to one of the most important streets of the historical centre of Coimbra, *Rua Ferreira Borges*, is shown in Fig. 1.

The seismic vulnerability assessment of the historical centre of Coimbra was performed by applying the above-described seismic vulnerability index methodology. A vulnerability index value, I_{vf}, was calculated for each one of the 672 façade walls that compose this case study and the vulnerability results were subsequently mapped resorting to a Geographic Information System (GIS) tool. As already discussed in Sect. 2, besides other advantages, the use of GIS allows for the spatial and organic view of the inter-connected issues associated with the study area. In this specific case, GIS was used to acquire a general overview of the level of vulnerability and risk in the study area (including damage scenarios for different seismic intensities).

The spatial distribution of the vulnerability index results over the study area is presented in Fig. 2a. In addition, Fig. 2b presents the buildings for which the corresponding vulnerability index value resulted higher than 45 and for that, consequently, a further evaluation resorting to a more detailed seismic vulnerability assessment methodology is advised.

From the analysis of Fig. 2b one can notice that there is a clear concentration of more vulnerable buildings (i.e., with higher vulnerability index values) in the north part of the study area. This result, when read together with the urban characteristics

Fig. 1 Historic Centre of Coimbra: view to *Rua Ferreira Borges*

(a)   **(b)**

Fig. 2 Vulnerability index distribution (**a**) and identification of the building façade walls with vulnerability index values equal or higher than 45 (**b**), adapted from Aguado et al. (2018)

of this area (characterised by narrow paths, alleys and streets), allows to observe that this area is one of the most problematic ones of the Historic Centre of Coimbra in terms of operational accessibility after a seismic event.

4.1.2 Analysis of Seismic Scenarios

Characterised the seismic vulnerability of the building façade walls over the study area, it is then possible to estimate and analyse damage distributions for different seismic scenarios. To do so, the above presented Eq. (2) is used to estimate individual levels of damage for different earthquake intensities which, resorting to the GIS tool, are mapped and spatially analysed. As an example, Fig. 3 presents four of these damage scenarios (for macroseismic intensities of $I_{EMS\text{-}98} = $ VI, VII, VIII and IX).

From the analysis of Fig. 3a, b, one can observed that for earthquake intensities lower than VII, most of the building façade walls present damage grade values, μ_D, ranging between 0 and 3.0. For intensities $I_{EMS\text{-}98} = $ VIII and IX the global scenario is very different, with several buildings presenting damage grades, μ_D, higher than 3.0.

4.1.3 Emergency Planning

Based on the damage scenarios given in Fig. 3, particularly of that of intensity $I_{EMS\text{-}98}$ = VIII, a proposal of potential evacuation routes for the historical centre of Coimbra is described and analysed herein. Thus, two cumulative conditions were established in order to determine if a street, alley or avenue can be used as an evacuation route in case of earthquake:

- A minimum free width of 4 meters should be guaranteed, aimed at ensuring the circulation of emergency and rescue vehicles (ambulances, fire trucks, etc.);
- The level of damage of the façade walls present along the route should be lower than 3.5 [i.e., in the range between "no damage" to "severe damage", see (Aguado et al. 2018)].

If these two conditions are met, it is plausible to assume that the route in question will be potentially free of obstacles after the earthquake event and that it can therefore be used as an evacuation route. If however one of the conditions is not satisfied, it is assumed that the pass is blocked and therefore that specific a street, alley or avenue cannot act as an evacuation route.

Following this criterion, Fig. 4a presents the three accessibility levels obtained for the Historic Centre of Coimbra, considering an intensity of $I_{EMS\text{-}98}=$ VIII (the maximum historic intensity felt in the zone). Such accessibility are represented in accordance with the following: the routes coloured in green are those where rescue vehicles can potentially circulate; the routes with restricted access (their narrowness does not allow the free circulation of the rescue vehicles) are coloured in yellow;
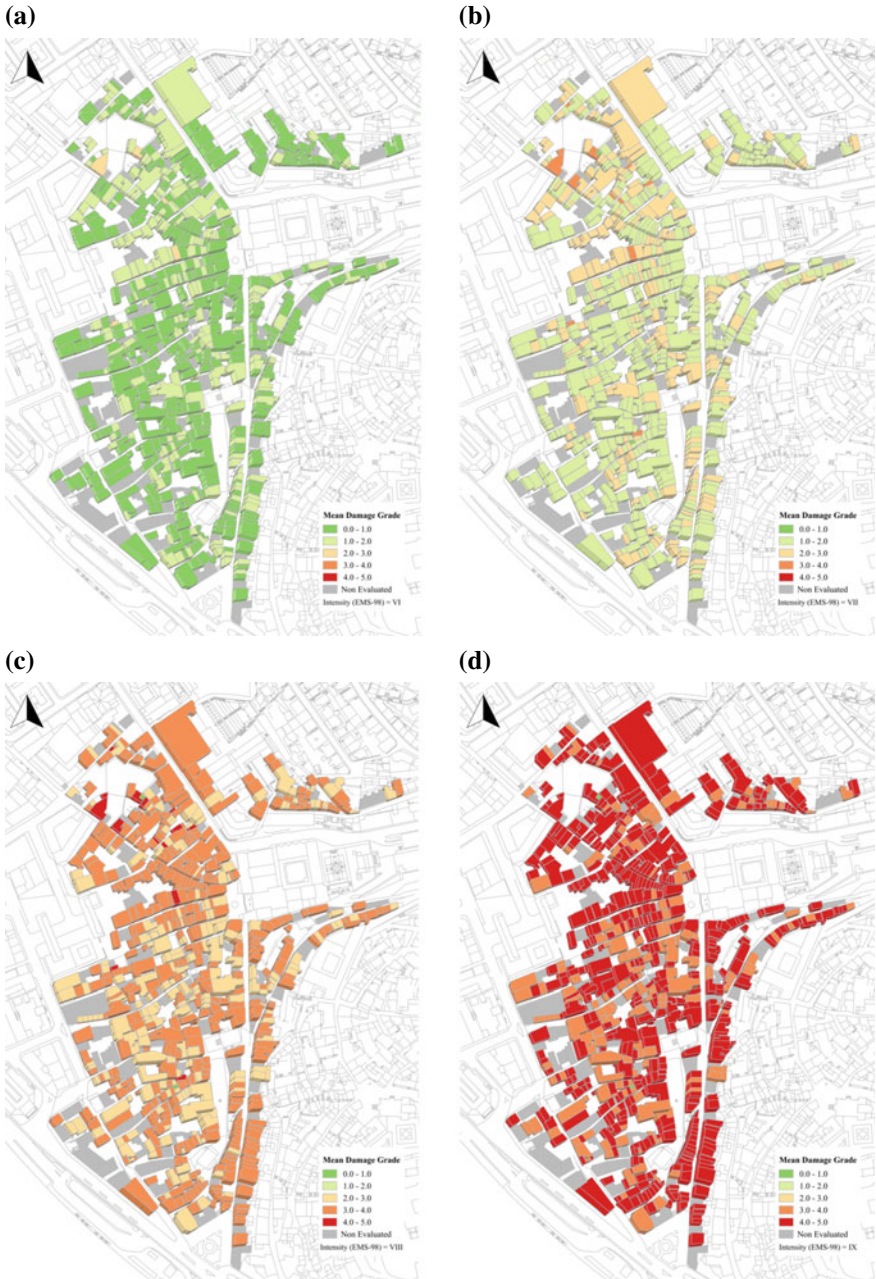
Fig. 3 Damage scenarios for macroseismic intensities $I_{EMS\text{-}98}=$ VI (**a**), $I_{EMS\text{-}98}=$ VII (**b**), $I_{EMS\text{-}98}=$ VIII (**c**) and $I_{EMS\text{-}98}=$ IX (**d**), adapted from Aguado et al. (2018)

(a) (b)

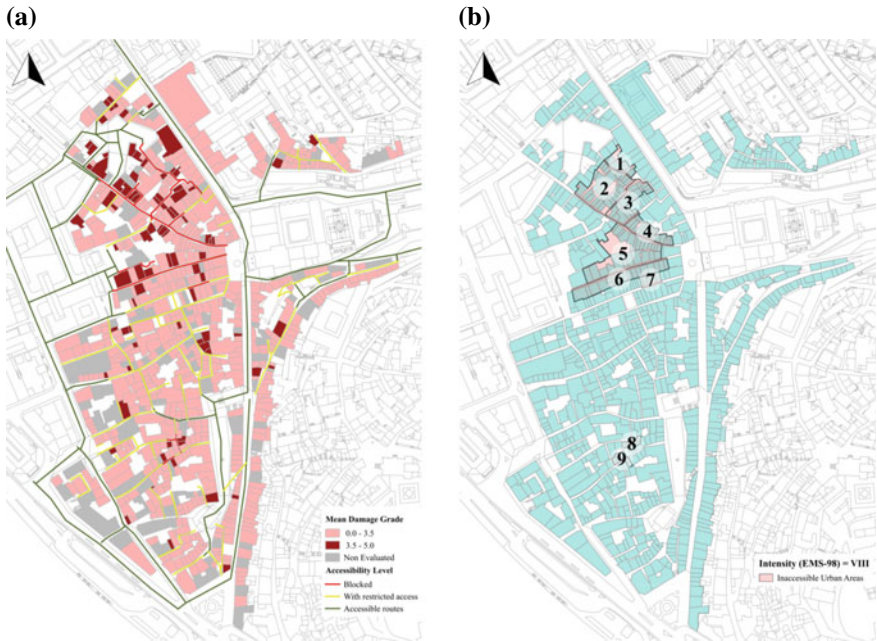**Fig. 4** Identification of potential evacuation routes (**a**); and inaccessible areas (**b**), both for an earthquake scenario of $I_{EMS\text{-}98} =$ VIII, adapted from Aguado et al. (2018)

Table 2 Number of residents living in each one of the nine urban areas analysed

Area	1	2	3	4	5	6	7	8	9	Total
No. residents	5	35	58	25	98	26	2	14	10	273

finally, the roads that will become potentially blocked for the seismic scenario considered are coloured in red.

From the result presented in Fig. 4a, it is further possible to define the urban areas that, for seismic scenario considered, may be potentially inaccessible. For this purpose, it is assumed that the urban zones located between two or more buildings for which the partial or the global collapse of their façade is expected will become isolated, as well as, as a consequence, all buildings located within its perimeter.

Following this criterion, Fig. 4b illustrates the nine areas of the Historic Centre of Coimbra that may become inaccessible for an earthquake scenario of $I_{EMS\text{-}98} =$ VIII.

Finally, the number of residents living in each one of the nine areas identified in Fig. 4b is given in Table 2.

Regarding the numbers presented in Table 2, it is important to stress that this result should be interpreted with caution, not only due to the natural uncertainty associated to data collection, but also because these numbers are largely variable throughout the day. In this case, taking into account that a considerable portion of these buildings

have commercial use at the ground floor level, the occurrence of a seismic event during the day time will very probably result in much larger numbers than those presented here, due to the many passers-by and customers potentially in the affected areas.

4.2 Fire Vulnerability and Risk Analysis

The simplified fire risk assessment methodology presented in this section, known as Fire Risk Index (FR_I) method, was proposed by Ferreira et al. (2016) aimed at providing a simpler but reliable alternative to conduct large-scale fire risk analysis, accelerating the information gathering process and optimising the risk evaluation through a "large-scale reworked and redefined assessment tool". As presented in Table 3, in terms of methodological structure the FR_I method is composed by two global factors, a global risk factor and a global efficiency factor, which, as detailed below, unfold into two sub-factors and fifteen partial factors.

The global risk factor is divided into three sub-factors devoted to evaluating fire ignition, fire propagation and evacuation phase. As for the global efficiency factor, it considers the fire combat with only one sub-factor. Furthermore, the sub-factors break-down into partial factors that assume numerical values which were defined according to an analytical hierarchy process.

Table 3 Methodological structure of the Fire Risk Index (FR_I) method, adapted from Ferreira et al. (2016)

Sub-factors		Partial factors
Global risk factor	Fire ignition, SF_I	Building conservation state
		Electric installations
		Gas installations
		Fire load nature
	Fire propagation, SF_P	Gap between aligned openings
		Safety and security teams
		Fire detection, alert and alarm
		Fire compartmentalisation
		Fire loads
	Evacuation, SF_E	Evacuation and escape routes
		Building properties
		Evacuation correction factor
Global efficiency factor	Fire combat, SF_C	Building external fire combat factors
		Building internal fire combat factors
		Security teams

Table 4 Reference Fire Risk factor (FR_R), for different types of building use

Reference risk factor	Building use	
	Residential	Service or industrial spaces, libraries and archives
FR_R	$0.19 + 0.25 \times F_c$[a]	$0.10 + 0.25 \times F_c$[a]

[a]FC is a correction factor that can assume the values of 1.10, 1.20 or 1.30, for a building of <3, <7, and 7+ floors, respectively

As presented in Eq. (1), the Fire Risk Index (FR_I) is obtained by the quotient between the weighted average of the four sub-factors described above and a reference risk factor (FR_R) that considers the type of building use, see Table 4.

$$FR_I = \frac{(1.20 \times SF_I + 1.10 \times SF_P + SF_E + SF_C)/4.0}{FR_R} \tag{1}$$

As detailed by Ferreira et al. (2016), the Fire Risk Index (FR_I) assumes the unit value as the reference value for safety verification. Thus, in a simplified manner, it is possible to say that an FR_I value higher than 1.0 suggests the need for the implementation of fire risk mitigation strategies, whereas an FR_I value lower than 1.0 suggests that the building fulfils the minimum fire safety conditions.

4.2.1 Application to the Historic Centre of Guimarães

Located in the northern region of Portugal, the Historic Centre of Guimarães is known as the cradle of the Portuguese nationality. Its historical centre, formally inscribed as a UNESCO World Heritage Site in 2001, is an exceptionally well-preserved and authentic example of the evolution of a Medieval settlement into a modern town, Fig. 5. Due to its unity, architectural characteristics, diversity of construction system, as well as due to its singular integration with the landscape setting, the Historic Centre of Guimarães represents outstanding universal values (UNESCO 2001).

Following the same logic of Sect. 4.1, the fire risk results obtained from the application of the simplified Fire Risk Index (FR_I) method described in the previous section to the Historical Centre of Guimarães are presented and discussed in the following. Also in this case, a GIS tool was developed and used to combine data regarding the characteristics of the building stock, types of use, conservation state and level of exposure and fire risk.

The first output presented in the following is the distribution of the FR_I results over the study area. On the basis of this result, which is mapped in Fig. 6, one can quickly examine the overall level of fire risk associated to each one of the buildings assessed. As detailed in Granda and Ferreira (2018), this indicator allows, in a broader and spatial manner, to identify more unsafe and critical buildings. In order to facilitate the

Fig. 5 Historic Centre of Guimarães. General view to *Largo da Oliveira*

analysis and interpretation of the results, FR_I has been divided into four levels of risk: low [0.60–1.00], moderate [1.00–1.30], high [1.30–1.65] and extreme [1.65–2.0].
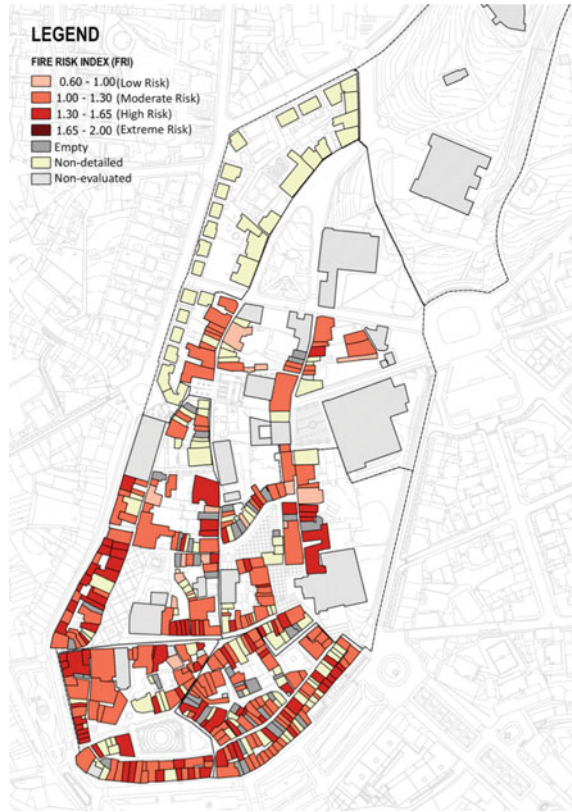
4.2.2 Risk Results Associated to Fire Ignition, Propagation, Evacuation and Combat

The sub-factor associated to Fire ignition is obtained through the average of the four partial factors indicated in Table 3: building conservation state; electric installations; gas installations; and fire load nature.

This sub-factor is particularly important insofar that old and absolute electrical installations and heating systems are included among the main sources of fire ignition in ancient buildings. In fact, such elements are particularly hazardous when associated with low conservation/maintenance levels and high fire loads, which is a frequent situation in historic city centres.

As illustrated in Fig. 7a, about 93% (253) and 6% (16) of the buildings assessed in the Historic Centre of Guimarães present a low and a moderate level of risk regarding fire ignition, respectively. It is interesting to highlight that despite the high number of buildings with non-refurbished electrical installations (69, 26%) and gas bottles placed inside the building in non-ventilated compartments (34%), the values obtained for this sub-factor were low thanks to the low hazardous nature of the materials present in most of the buildings.

As for the sub-factor associated to fire propagation, it is obtained through the
average of five partial factors: the gap between aligned openings; safety and security
teams; fire detection, alert and alarm; fire compartmentalization; and fire loads. As
can be seen in Fig. 7b, 52% of the buildings are considered in high risk of fire prop-
agation. To a large extend this is due to the lack of detection and alarm systems, the
insufficient vertical distance between aligned openings and the presence of materials
with moderate to high fire load densities. Moreover, 38% of the buildings present a
moderate risk. Regarding these latter, it is important to add that most of them have
a commercial use, which means that, they are periodically subjected to a legally
compulsory inspection process. For this reason, it seems reasonable to assume that
these buildings fully comply with the legal regulations in force. Finally, 3% of the
buildings (8) were found to be in extreme risk considering their fire propagation
characteristics.

The sub-factor associated to building evacuation results from the average of the
partial factors related to: evacuation and escape routes; building properties; and
evacuation correction factor. The distribution of the results obtained for this sub-
factor is depicted in Fig. 8a. From this result, one can notice that about 41% of

(a)   **(b)**

Fig. 7 Fire ignition and fire propagation risk results in the Historic Centre of Guimarães

buildings assessed (110) present a level of risk associated to evacuation ranging from high to extreme.

The last sub-factor that constitutes the Fire Risk Index is associated with fire combat. This sub-factor is evaluated on the basis of three partial factors: the building external fire combat; the building internal fire combat; and the existence of fire security teams. Of these, the partial factor related to the external fire combat plays a particularly relevant role in terms of urban fire risk. The result of this partial factor is linked to two key characteristics, the accessibility and the location of hydrants in the vicinity of the building, as well as the accessibility of the streets (based on the free width, the height and the slope of the access ways). As discussed by Bernardini (2017), these features play a key role in terms of fire combat due to their direct influence on the capacity of the emergency vehicles to access the buildings and to help and rescue the victims during the fire.

The Historical Centre of Guimarães does not present relevant issues related to the free height and the slope of the streets. However, regarding their free width, there is actually a potential risk resulting from the fact that much of streets located within the study area present free widths lower than 3.5 m, refer to Fig. 9a. The only exceptions are the peripheral streets of the area, whose dimensions comply with this limit of 3.5 m, see Fig. 9b.

Finally, Fig. 8b presents the distribution of the sub-factor fire combat. As one can observe in this figure, about 65% of the evaluated buildings present a level of risk in the range from high or extreme.

(a) **(b)**

Fig. 8 Evacuation and fire combat results

(a) **(b)**

Fig. 9 Mapping of accessibilities in the Historic Centre of Guimarães: street width (**a**) and different levels of accessibility (**b**)

4.2.3   Second Level Analysis: FR$_I$ with Empty Floors and Number of Building Occupants

In order to complement the analysis presented in the previous sections, the Fire Risk Index (*FR$_I$*) values obtained for the Historic Centre of Guimarães are combined and analysed in the present section with two types of exposure data: the existence of empty upper floors and total number of building occupants. In the first case, empty upper floors can contribute to facilitate fire propagation, namely due to the increased difficulty in detecting the ignition, whereas, in the second case, the number of building occupants is a fundamental indicator for estimating the number of people potentially exposed to fire.

Figure 10a presents the distribution of the empty upper floors in the Historical Centre of Guimarães, together with the individual *FR$_I$* results. As it is possible to observe, 20 of the 436 buildings evaluated in the Historic Centre of Guimarães present currently empty upper floors, being that, most of those, have a commercial use at the ground floor level.

As for the combined analysis of the *FR$_I$* and the number of building occupants, illustrated in the following Fig. 10b, about 30% of the occupants considered in this study are associated with buildings whose *FR$_I$* ranges from high to extreme (1.3–2.0). Moreover, it is worth adding that the distribution of buildings with high to extreme

Fig. 10 Second level analysis: *FR$_I$* results with empty upper floors (**a**) and number of building occupants (**b**)

fire risk is homogeneous over the whole study area, which emphasizes the need for the adoption of appropriate fire risk mitigation strategies, not only in specific locations of the Historic Centre of Guimarães, but in the whole area.

5   Conclusions

As presented and discussed in this chapter, urban disaster risk depends on several factors, some of them related to the physical characteristics of the buildings, others associated with the features of the urban space. This fact, together with the technical and practical difficulties associated with the vulnerability evaluation of existing buildings, makes the risk assessment of old urban areas a very challenging problem.

The broad conclusions and recommendation drawn from the discussion presented in this chapter converge towards the enhancement of public awareness and of the research on risk mitigation. Preferably, risk mitigation strategies should address land-use zoning (reducing exposure), planning of adequate strengthening campaigns, and the implementation of building codes suitable both for new and existing structures.

As demonstrated in the two application examples discussed in this chapter, the use of Geographic Information System (GIS) tool to integrate vulnerability and risk results constitutes a major step in the risk assessment process, enabling, in parallel, the storage of building features and survey information, and the construction of damage and risk scenarios.

The application of the seismic vulnerability assessment method presented in Sect. 4.1 to the old building stock of the Historic Centre of Coimbra allowed to obtain a broad range of relevant building vulnerability and urban risk outputs. Through the mapping of the vulnerability and loss assessment results, suitable evacuation routes associated with different levels of accessibility were mapped. Blocked, restricted access and free roads were identified considering both the façade walls prone to partial or total collapse and the narrowness of streets. Due to its practical application, this information can represent an important output for civil protection agencies. The identification of the buildings with higher risk of partial or total collapse plays a fundamental role toward the definition of the areas more prone to be inaccessible in the sequence of a seismic event.

Regarding the simplified fire risk assessment methodology presented in Sect. 4.2, it has emerged as an attempt to address and overcome some of the difficulties inherent to the evaluation of fire risk in urban areas, namely those related to time constraints and to the limited access to the interior of buildings. It is worth stressing the fire risk results presented here for the Historic Centre of Guimarães should be interpreted keeping in mind the scale and aim of the work. Nevertheless, and despite the limitations associated with this type of analysis, it allows for the identification of the most vulnerable buildings in respect to fire risk, which, from the point of view of the management of urban risks, particularly in old urban areas, represents a valuable asset.

References

Aguado, J. L. P., Ferreira, T. M., & Lourenço, P. B. (2018). The use of a large-scale seismic vulnerability assessment approach for Masonry Façade walls as an effective tool for evaluating, managing and mitigating seismic risk in historical centers. *International Journal of Architectural Heritage*, 1–17. https://doi.org/10.1080/15583058.2018.1503366.

Arshad, S., & Athar, S. (2013). *Rural housing reconstruction program post-2005 earthquake—Learning from the Pakistan experience—A manual for post-disaster housing program managers*, 116.

Astroza, M., Ruiz, S., & Astroza, R. (2012). Damage assessment and seismic intensity analysis of the 2010 (M w 8.8) Maule earthquake. *Earthquake Spectra, 28,* S145–S164. https://doi.org/10.1193/1.4000027.

Bernardini, G. (2017). Fire safety of historical buildings. Traditional versus innovative "behavioural design" solutions by using Wayfinding Systems. In *SpringerBriefs in applied sciences and technology*. Springer International Publishing.

Calvi, G. M., Pinho, R., Magenes, G., et al. (2006). Development of seismic vulnerability assessment methodologies over the past 30 years. *ISET Journal of Earthquake Technology, 43,* 75–104.

Coaffee, J. (2008). Risk, resilience, and environmentally sustainable cities. *Energy Policy, 36,* 4633–4638. https://doi.org/10.1016/j.enpol.2008.09.048.

Covello, V. T. (2014). *Learning from megadisasters: Lessons from the Great East Japan Earthquake*. The World Bank.

Covello, V. T. (2010). Strategies for overcoming challenges to effective risk communication. In R. L. Heath & H. D. O'Hair (Eds.), *Handbook of risk and crisis communication* (pp. 155–179). Routledge.

Ferreira, T. M., Costa, A. A., Vicente, R., & Varum, H. (2015). A simplified four-branch model for the analytical study of the out-of-plane performance of regular stone URM walls. *Engineering Structures, 83,* 140–153. https://doi.org/10.1016/j.engstruct.2014.10.048.

Ferreira, T. M., Maio, R., Costa, A. A., & Vicente, R. (2017a). Seismic vulnerability assessment of stone masonry façade walls: Calibration using fragility-based results and observed damage. *Soil Dynamics and Earthquake Engineering, 103*. https://doi.org/10.1016/j.soildyn.2017.09.006.

Ferreira, T. M., Maio, R., & Vicente, R. (2017b). Analysis of the impact of large scale seismic retrofitting strategies through the application of a vulnerability-based approach on traditional masonry buildings. *Earthquake Engineering and Engineering Vibration, 16,* 329–348. https://doi.org/10.1007/s11803-017-0385-x.

Ferreira, T. M., Vicente, R., Raimundo Mendes da Silva, J. A., et al. (2016). Urban fire risk: Evaluation and emergency planning. *The Journal of Cultural Heritage, 20*. https://doi.org/10.1016/j.culher.2016.01.011.

Ferreira, T. M., Vicente, R., & Varum, H. (2014). Seismic vulnerability assessment of masonry facade walls: Development, application and validation of a new scoring method. *Structural Engineering & Mechanics, 50,* 541–561. https://doi.org/10.12989/sem.2014.50.4.541.

Gavarini, C. (2001). Seismic risk in historical centers. *Soil Dynamics and Earthquake Engineering*. https://doi.org/10.1016/s0267-7261(01)00027-6.

Goula, X., Roca, A., & Oliveira, C. S. (2006). *Assessing and managing earthquake risk*. Berlin/Heidelberg: Springer-Verlag.

Granda, S., & Ferreira, T. M. (2018). Assessing vulnerability and fire risk in old urban areas: Application to the historical centre of Guimarães. *Fire Technology*. https://doi.org/10.1007/s10694-018-0778-z.

Grünthal G. (1998). *European Macroseismic Scale (EMS-98)* (Cahiers du Centre Européen de Géodynamique et Séismologie, Vol. 15). Luxembourg: European Centre for Geodynamics and Seismology.

Indirli, M. (2009). Organization of a geographic information system (GIS) database on natural hazards and structural vulnerability for the historic center of San Giuliano di Puglia (Italy) and the city of Valparaiso (Chile). *International Journal of Architectural Heritage*.

Maio, R., Ferreira, T. M., & Vicente, R. (2018). A critical discussion on the earthquake risk mitigation of urban cultural heritage assets. *The International Journal of Disaster Risk Reduction, 27,* 239–247. https://doi.org/10.1016/J.IJDRR.2017.10.010.

Mendes da Silva, J. A. R. (2015). Full and pedagogical access to a restoration site—The Tower of the University of Coimbra. In *ReUSO—III Congreso Internacional sobre Documentación, Conservación y Reutilización del Patrimonio Arquitectónico y Paisajístico*. Valencia, España (pp. 2156–2163).

Mitchelson, M. (2011). *Haiti and Christchurch earthquakes-viewed through a resilience lens*. Auckland University of Technology.

Mouroux, P., & Le Brun, B. B. (2006). Presentation of RISK-UE project. *Bulletin of Earthquake Engineering, 4,* 323–339. https://doi.org/10.1007/s10518-006-9020-3.

Neves, F., Costa, A., Vicente, R., et al. (2012). Seismic vulnerability assessment and characterisation of the buildings on Faial Island, Azores. *Bulletin of Earthquake Engineering, 10,* 27–44. https://doi.org/10.1007/s10518-011-9276-0.

Porter, K., Kennedy, R., & Bachman, R. (2007). Creating fragility functions for performance-based earthquake engineering. *Earthquake Spectra, 23,* 471–489. https://doi.org/10.1193/1.2720892.

Rota, M., Penna, A., & Magenes, G. (2010). A methodology for deriving analytical fragility curves for masonry buildings based on stochastic nonlinear analyses. *Engineering Structures, 32,* 1312–1323. https://doi.org/10.1016/j.engstruct.2010.01.009.

Rota, M., Penna, A., & Strobbia, C. L. (2008). Processing Italian damage data to derive typological fragility curves. *Soil Dynamics and Earthquake Engineering, 28,* 933–947. https://doi.org/10.1016/j.soildyn.2007.10.010.

Santarelli, S., Bernardini, G., & Quagliarini, E. (2018). Earthquake building debris estimation in historic city centres: From real world data to experimental-based criteria. *The International Journal of Disaster Risk Reduction, 31,* 281–291. https://doi.org/10.1016/j.ijdrr.2018.05.017.

UNESCO. (2001). *World cultural heritage nomination document: Historic centre of Guimarães*. UNESCO World Heritage Centre. http://whc.unesco.org/uploads/nominations/1031.pdf.

Vicente, R., Ferreira, T. M., & Mendes da Silva, J. A. R. (2015). Supporting urban regeneration and building refurbishment. Strategies for building appraisal and inspection of old building stock in city centres. *Journal of Cultural Heritage, 16,* 1–14. https://doi.org/10.1016/j.culher.2014.03.004.

Stochastic Life-Cycle Sustainability Analysis: Its Mathematical Formulation and the Role of Resilience

Paul Gharzouzi and Paolo Gardoni

1 Introduction

In recent years, there has been an increasing attention toward the evaluation of the sustainability and resilience of engineering systems throughout their service lives (Gardoni 2019). Several researchers have developed frameworks and models to assess the sustainability of various infrastructure components like bridges (Tapia et al. 2011; Mara et al. 2013), pavements (Yu and Lu 2012; Yang and Al-Qadi 2017) and infrastructure systems (Seo and Hwang 2001; Ramesh et al. 2010; Biswas 2014; Abdallah and El-Rayes 2016). In these studies, sustainability is evaluated in terms of different performance measures that include environmental, economic, and social impacts of systems. The interpretation and evaluation of sustainability depends on the context of the study. For example, in the context of modern building design, recent studies proposed frameworks that integrate the performance-based design with sustainability assessment to obtain a design that is both safe and sustainable (Welsh-Huggins and Leil 2016; Alibrandi and Mosalam 2017, 2019). In the context of disaster recovery of communities, Gardoni and Murphy (2008) conceptualized sustainable recovery in terms of individuals' capabilities as part of a Capabilities Approach to recovery.

Sustainability is also closely related to resilience (Gardoni and Murphy 2018; Gardoni 2019). The inherent resilience of a system and the work plan of activities involved in the recovery process affect the sustainability of the system when considering its life-cycle. Over the last fifteen years, resilience has become one of the most desirable feature of systems and communities (e.g., Bruneau et al. 2003; Caverzan

P. Gharzouzi · P. Gardoni (✉)

Department of Civil and Environmental Engineering, MAE Center, University of Illinois at Urbana-Champaign, Urbana, IL, USA

e-mail: gardoni@illinois.edu

P. Gharzouzi

e-mail: gharzou2@illinois.edu

and Solomos 2014; Ellingwood et al. 2016; Guidotti et al. 2016, 2019; Sharma et al. 2018; Nocera et al. 2019). A review of the literature on community resilience can be found in Koliou et al. (2018). With a more holistic perspective and going beyond the engineering domain, Doorn et al. (2018) also incorporated philosophical and social science considerations into a multidisciplinary definition of resilience that accounts for social justice. In resilience analysis, recovery curves are typically used to describe the performance or functionality of a system as a function of time as the system recovers. Different studies have proposed recovery curves of engineering systems following a hazard (e.g., Cimellaro et al. 2010; Decò et al. 2013). Most recently, Sharma et al. (2018) proposed a mathematical formulation of recovery curves based on the actual work plan of activities involved in the recovery process.

When evaluating the sustainability of a system in terms of its environmental impact over a fixed time horizon, current studies have three important limitations. First, these studies do not consider the impacts on the sustainability associated with all the processes (i.e., construction and recovery processes) that are part of the system life-cycle. Second, they do not consider the various types of engineering systems (i.e., structures or infrastructure components/systems such as buildings, bridges or pipelines). Third, they do not account for all relevant uncertainties in evaluating the sustainability of the system, such as the uncertainties in the environmental emissions associated with the material and energy needed during the system life-cycle, in addition to the uncertainties in the external conditions, among others.

This chapter proposes a formulation, named Stochastic Life-cycle Sustainability Analysis (SLCSA), for evaluating the sustainability of engineering systems throughout a time horizon of interest. The SLCSA assesses the sustainability of an engineering system in terms of its environmental impact (i.e., carbon footprint, ozone depletion or smog), for a fixed time horizon over which a system might be subject to multiple cycles of repairs. The proposed SLCSA provides a more comprehensive evaluation of the environmental impact of a system by addressing the aforementioned limitations.

First, we consider that the engineering system of interest is any structure or infrastructure. Accordingly, the environmental impact of any structure or infrastructure can be evaluated using the SLCSA.

Second, this chapter proposes state-dependent stochastic models that capture the effects and the interaction of the various processes, such as deterioration and recovery processes, in the evaluation of the environmental impact of the system. By accounting for the various processes that affect the different components of an engineering system, the environmental performance can be determined as a function of the structural performance of the system. The time-varying structural performance of the system is a function of a set of variables that characterize the system of interest (e.g., material properties, member dimensions, and imposed boundary conditions), called structural state variables. The change of these variables over time is estimated from the modeling of the relevant state-dependent stochastic processes. For instance, the modeling of the state-dependent deterioration (Jia and Gardoni 2018a, 2019) and resilience (defined by the recovery processes) (Sharma et al. 2018) aims to estimate the time-varying structural state variables of the system. The estimates of these variables can

be used to predict the structural performance of the system (that describes a certain state of the engineering system) over time (Choe et al. 2008, 2009; Simon et al. 2010; Zhong et al. 2012; Kumar et al. 2009; Kumar and Gardoni 2014a; Jia and Gardoni 2018a). The integration of the different stochastic processes, such as deterioration and recovery processes, and their effects on the structural performance is modeled following Jia et al. (2017). Following the estimation of the structural performance of the system, the environmental performance can be determined. In particular, the quantity state variables for the system are first estimated as a direct function of the structural performance. In this formulation, the quantity state variables characterize the quantities of materials and energy used during the system life-cycle. These quantity state variables are then used as inputs to the models to estimate the environmental impact of the system over time. The environmental impact is estimated using the life-cycle assessment approach, as described in the ISO 14040/14044 series (ISO 2006).

Third, to account for the relevant uncertainties in the assessment of the environmental impact of the system, the formulation adopts a simulation-based approach, such as the one developed by Jia and Gardoni (2018b). The simulation-based approach allows the propagation of the relevant uncertainties that result in a probabilistic output for the environmental impact of the system. The relevant uncertainties include those in the external conditions, such as environmental exposure and potential hazards, the system performance models, and those in the environmental emissions, associated with the material and energy inputs.

Following this introduction, this chapter is organized as follows: Sect. 2 introduces the general background that is relevant for developing the SLCSA formulation; Sect. 3 presents the proposed SLCSA formulation; Sect. 4 presents the sustainability analysis of an example reinforced concrete (RC) bridge, as an illustration of the proposed formulation; and, finally, Sect. 5 presents some conclusions.

2 Background

2.1 Life-Cycle Analysis

The life-cycle of an engineering system consists of multiple phases in which the system is in use or down (Kumar and Gardoni 2014b; Jia et al. 2017), as illustrated in Fig. 1. Within each cycle, the in use system is typically subject to various gradual and shock deterioration processes. These processes lead to the deterioration of the system state over time. The system state is described by a generic system performance measure $Q(t)$ (such as reliability or probability of failure). When $Q(t)$ is no longer acceptable, an intervention is triggered and the system is taken out of service/operation for repair or replacement/reconstruction. With reference to Fig. 1, an intervention is triggered when $Q(t)$ falls below the intervention threshold. In this case, $Q(t)$ can correspond to the reliability of a system. For example, if the probability

of failure of a system is the performance measure of interest, then an intervention is triggered whenever the probability of failure exceeds a certain intervention threshold.

The repair or replacement/reconstruction events, following an intervention, correspond to the recovery process of the system, which requires developing a specific recovery strategy to restore the system to a target performance level (Kumar and Gardoni 2014b; Sharma et al. 2018). Whether the recovery strategy corresponds to a repair or replacement/reconstruction depends on the intervention threshold, the system state at the time of intervention and the target state following the recovery process. These processes aim to prevent, mitigate or reverse the effects of the deterioration processes on the system and to increase the availability of the system. If the repair strategies would not succeed in restoring the damaged system to the desired state, then a replacement/reconstruction of the system is needed. In this chapter, we consider that a system can have multiple recovery processes during one cycle within the time horizon of interest. In particular, after a repair, the system is restored to a state that could be higher than the target performance level. In addition, a cycle ends whenever a replacement or reconstruction of the system is needed (i.e., at the end of the service life of the system). When a new cycle starts within a fixed time horizon, the system has again the initial target performance level, as illustrated in Fig. 1.

In this chapter, the duration of the generic ith cycle (see in Fig. 1) is denoted as T_{L_i} and can be written as $T_{L_i} = t_{L_i} - t_{L_{i-1}}$, where t_{L_i} is the end time of the ith cycle and $t_{L_{i-1}}$ is the end time of the $(i-1)$th cycle. An intervention event, j, within the ith
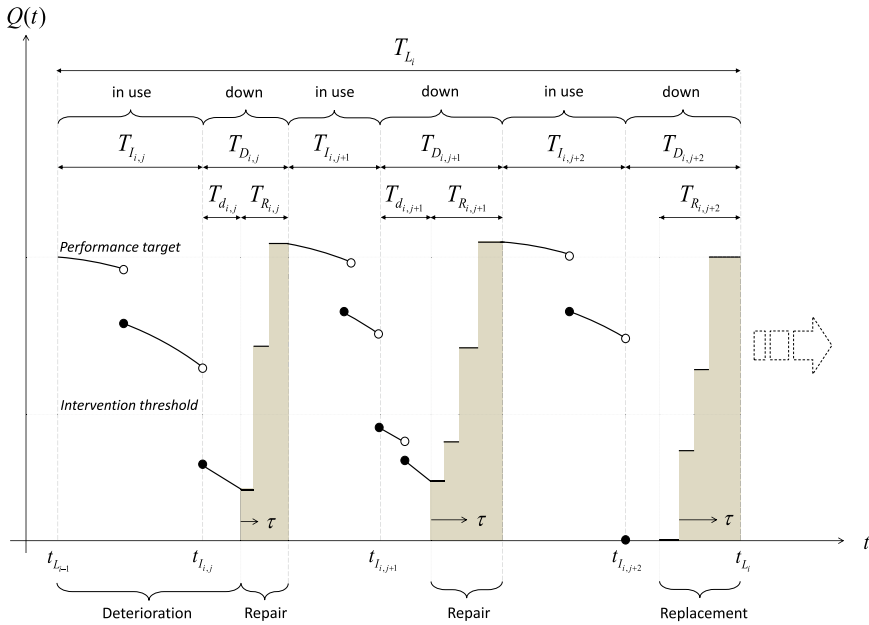

Fig. 1   Illustration of the life-cycle performance of an engineering system

cycle is denoted as $I_{i,j}$. Following the intervention event $I_{i,j}$ at time $t_{I_{i,j}}$, there might be a lag period (or a delay period), denoted as $T_{d_{i,j}}$, between the time of intervention and the start of recovery. During the lag period (i.e., from $t_{I_{i,j}}$ to $t_{I_{i,j}} + T_{d_{i,j}}$), $Q(t)$ may further degrade, for example, due to the possible occurrence of aftershocks. The subsequent recovery period is denoted as $T_{R_{i,j}}$, and the total period when the system is down following an intervention $I_{i,j}$, can be written as $T_{D_{i,j}} = T_{d_{i,j}} + T_{R_{i,j}}$.

During the time horizon of interest, every recovery strategy for the system has associated environmental impacts, in addition to the environmental impacts resulting from the construction of the system. The environmental impact associated with every process is evaluated in this chapter using the life-cycle assessment approach described in the ISO 14040/14044 series (ISO 2006). Additional life-cycle performance measures, such as the financial costs associated with these processes can also be evaluated to provide additional insight into the life-cycle performance of the system during the time horizon of interest (Gardoni et al. 2016).

3 Proposed Formulation

Figure 2 shows the flowchart of the proposed SCLSA formulation for the evaluation of the environmental performance of the system over time as a function of its structural performance. This formulation is based on the sustainability formulations proposed by Gharzouzi and Gardoni (2019a, b). Next, we discuss the modeling of the different performance measures of the system.

3.1 Structural Performance Analysis

3.1.1 Modeling the Deterioration Processes and Their Impact on the Structural Performance

Starting with the structural performance analysis, the structural external conditions/variables are modeled first. The modeling of these external conditions consists of modeling the vector of structural environmental conditions/variables (such as temperature, atmospheric pressure and relative humidity), denoted as $\mathbf{E}_{st}(t)$, and the vector of structural shock intensity measures, denoted as $\mathbf{S}_{st}(t)$. In this formulation, the vectors $\mathbf{E}_{st}(t)$ and $\mathbf{S}_{st}(t)$ constitute the vector of the time-varying structural external conditions/variables, denoted as $\mathbf{Z}_{st}(t)$, where $\mathbf{Z}_{st}(t) = [\mathbf{E}_{st}(t), \mathbf{S}_{st}(t)]$. These vectors correspond to the external conditions that the engineering system is subject to. Accordingly, the deterioration processes, that adversely affect the structural performance, are influenced by these conditions (Jia and Gardoni 2018a, 2019). Deterioration can occur both in the form of shocks due to extreme events such as earthquakes, hurricanes, floods, and blasts (i.e., shock deterioration processes) (e.g., Kumar and Gardoni 2012, 2014a, b; Kumar et al. 2009, 2015), as well as gradu-

Fig. 2 Overall flowchart for modeling the environmental performance of the system
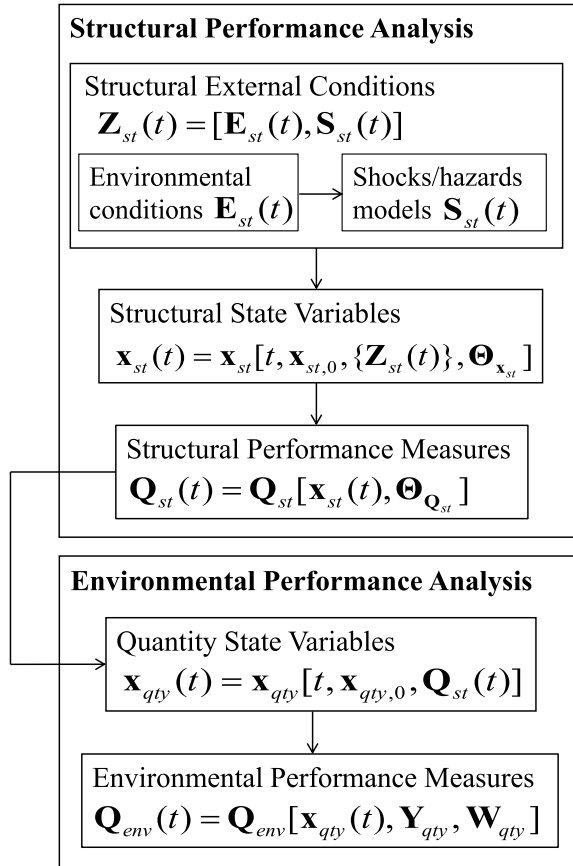
ally over time due harsh environments and regular use (i.e., gradual deterioration processes) (e.g., Choe et al. 2008, 2009, 2010; Gardoni and Rosowsky 2011). Jia and Gardoni (2018a) developed a general state-dependent stochastic formulation that models the change of the vector of structural state variables, $\mathbf{x}_{st}(t)$, over time due to deterioration processes using state-dependent stochastic models. These models can consider the likely interaction among different deterioration processes, such that their joint impact on the system state can become more significant than simply superimposing their individual impacts.

Following Jia and Gardoni (2018a, 2019), the sequence $\{\mathbf{Z}_{st}(t)\}$ of the external conditions from 0 to t is used as an input to the state-dependent stochastic models of $\mathbf{x}_{st}(t)$. The vector of structural state variables is written as $\mathbf{x}_{st}(t) = \mathbf{x}_{st}[t, \mathbf{x}_{st,0}, \{\mathbf{Z}_{st}(t)\}, \mathbf{\Theta}_{\mathbf{x}_{st}}]$, where $\mathbf{x}_{st,0}$ is the vector of structural state variables at some reference time $t = 0$, such as the time of the construction or reconstruction of the system (where $\mathbf{x}_{st,0} = \mathbf{x}_{st}(t = 0)$), and $\mathbf{\Theta}_{\mathbf{x}_{st}}$ is the vector of unknown model parameters that need to be estimated. With reference to Fig. 1, the reference time

$t = 0$ corresponds to the start of a new system cycle i, at time $t_{L_{i-1}}$, during the time horizon of interest. Because of the deterioration processes, the vector of the structural state variables changes from $\mathbf{x}_{st,0}$ to $\mathbf{x}_{st}(t)$. Following Jia and Gardoni (2018a), we write the vector of the structural state variables at time t, where $t \in [t_{L_{i-1}}, t_{I_{i,j}} + T_{d_{i,j}}]$, as

$$\mathbf{x}_{st}(t) = \mathbf{x}_{st,0} + \int_0^t \dot{\mathbf{x}}_{st}(\xi)d\xi \qquad (1)$$

where $\dot{\mathbf{x}}_{st}(\xi) = \dot{\mathbf{x}}_{st}[\xi, \mathbf{x}_{st}(\xi^-), \mathbf{Z}_{st}(\xi), \boldsymbol{\Theta}_{\mathbf{x}_{st}}]$ denotes the rate of change of the structural state variables over time, and $\mathbf{x}_{st}(\xi^-)$ is the vector of vector of state variables immediately before time ξ.

To implement this formulation for modeling the effect of the deterioration processes on $\mathbf{x}_{st}(t)$, specific models for the changes of $\mathbf{x}_{st}(t)$ need to be established and calibrated for each deterioration process. Since the formulation is general, any model for the changes of $\mathbf{x}_{st}(t)$ can be incorporated. As an example, Jia and Gardoni (2018a) proposed a non-homogenous state-dependent Markov process model for evaluating the effect of gradual deterioration on $\mathbf{x}_{st}(t)$. Such model is able to capture time/age and state-dependence in modeling the changes in $\mathbf{x}_{st}(t)$ due to gradual deterioration. As for the models due to shock deteriorations, the random occurrence of shocks and their intensities is first modeled. As an example, homogeneous Poisson processes have been used to model the occurrence of shocks with constant occurrence rate (Kumar and Gardoni 2014b). Alternatively, non-homogeneous Poisson processes have been used to model the occurrence of shocks with time-varying occurrence rate (Kumar and Gardoni 2012). After modeling the shocks, the changes in $\mathbf{x}_{st}(t)$ due to a shock with a given intensity can be modeled using, for example, probabilistic predictive models as in Kumar and Gardoni (2012, 2014a).

The changes in $\mathbf{x}_{st}(t)$ lead to changes in the state of the engineering system, characterized by a vector of structural performance measures $\mathbf{Q}_{st}(t)$. Note that this is a vector of structural performances which can include performance measures such as state of physical damage, reliability, instantaneous probability of failure and durability. We write $\mathbf{Q}_{st}(t)$ as $\mathbf{Q}_{st}[\mathbf{x}_{st}(t), \boldsymbol{\Theta}_{\mathbf{Q}_{st}}]$, where $\boldsymbol{\Theta}_{\mathbf{Q}_{st}}$ is the vector of unknown model parameters that need to be estimated. For instance, these model parameters can correspond to the parameters in the probabilistic capacity and demand models used to determine the time-varying fragility and corresponding reliability of the engineering system (Gardoni et al. 2002, 2003).

3.1.2 Modeling the Recovery Processes and Their Impact on the Structural Performance

During the system life-cycle, a recovery occurs when the engineering system is taken out of service, as a result of its structural performance measures, $\mathbf{Q}_{st}(t)$, no longer being acceptable. In this formulation, a recovery process is either a repair or a reconstruction depending on the intervention threshold, the structural performance

of the system at the time of intervention, and target structural performance following the recovery process.

A key element of the recovery modeling is the development of a recovery schedule associate to a recovery strategy. The schedule should consist ideally of all of the recovery activities needed to restore the system to a desired structural performance. In this formulation, the recovery schedule, following any intervention $I_{i,j}$, has a duration of $T_{R_{i,j}}$, as illustrated in Fig. 1. The structural state variables, $\mathbf{x}_{st}(t)$, change with the completion of the recovery activities and possible disrupting shocks that could occur during the recovery process. The recovery activities that lead to a change in the structural performance described by $\mathbf{Q}_{st}(t)$ are grouped into one recovery step. The disrupting shocks might lead to modifications in the structural performance as well as the recovery schedule.

Sharma et al. (2018) proposed a stochastic formulation to model the recovery of a system incorporating the effect of recovery activities as well as possible disrupting shocks during the recovery process. As the recovery activities progress, the associated recovery steps might introduce additional structural state variables (e.g., describing new materials used for the repair) or replace a subset of existing ones.

Following Sharma et al. (2018), we can model the structural state variables during the implementation of the recovery strategy at any time $\tau \in [0, T_{R_{i,j}}]$ as

$$\mathbf{x}_{st}(\tau) = \sum_{u=1}^{\infty} \mathbf{x}_{st}(\tau_{r,u-1})\mathbf{1}_{\{\tau_{r,u-1} \leq \tau < \tau_{r,u}\}} + \sum_{u,v=1}^{\infty} \Delta\mathbf{x}_{st}(\tau_{s,v})\mathbf{1}_{\{\tau_{r,u-1} < \tau < \tau_{r,u}, \tau_{r,u-1} < \tau_{s,v} \leq \tau\}}$$

(2)

where $\mathbf{x}_{st}(\tau)$ is the vector of structural state variables at relative time τ, measured from the beginning of the recovery process (i.e., the reference time $\tau = 0$ for the recovery schedule corresponds to $t = t_{I_{i,j}} + T_{d_{i,j}}$ following the intervention $I_{i,j}$ in the ith cycle in Fig. 1), $\mathbf{x}_{st}(\tau_{r,u-1})$ is the vector of structural state variables after completing a recovery step at time $\tau_{r,u-1}$, $\mathbf{1}_{\{A\}}$ is an indicator function, defined such that $\mathbf{1}_{\{A\}} = 1$ if A is a true statement, and $\mathbf{1}_{\{A\}} = 0$, otherwise, and $\Delta\mathbf{x}_{st}(\tau_{s,v})$ is the change of the structural state variables due to the occurrence of the vth disrupting shock at time $\tau_{s,v} \in [\tau_{r,u-1}, \tau_{r,u}]$. Note that probability distributions of $\mathbf{x}_{st}(\tau_{r,0})$ at the beginning of the recovery process can be obtained from the deterioration models.

Ultimately, these updated structural state variables can be used to determine the new structural performance of the system during and after the recovery process, as described in Sect. 3.1.1. As an example, considering RC bridges and the retrofitting with fiber reinforced polymer (FRP) as the intervention strategy, $\mathbf{Q}_{st}(\tau)$ can be determined using the probabilistic capacity and demand models developed by Tabandeh and Gardoni (2014, 2015).

3.2 Environmental Performance Analysis

With reference to Fig. 2, the environmental performance analysis of the system follows the modeling of the structural performance of the system.

The evaluation of the environmental performance of the engineering system primarily depends on modeling the vector of the quantity state variables, $\mathbf{x}_{qty}(t)$, that describes the quantities of the materials and energy used for all the processes (i.e., construction and recovery processes) associated with the engineering system over a fixed time horizon. Accordingly, the vector $\mathbf{x}_{qty}(t)$ incorporates all the quantities needed by the system over time. In this formulation, $\mathbf{x}_{qty}(t) \in \mathbb{R}_{\geq 0}^{n_q}$, where n_q is the total number of the materials and energy used during the life-cycle of the system.

In the SLCSA, $\mathbf{Q}_{st}(t)$ is used as inputs to the state-dependent stochastic models of $\mathbf{x}_{qty}(t)$. We can write the vector of quantity state variables as $\mathbf{x}_{qty}(t) = \mathbf{x}_{qty}[t, \mathbf{x}_{qty,0}, \mathbf{Q}_{st}(t)]$, where $\mathbf{x}_{qty,0}$ is the vector of quantity state variables at some reference time $t = 0$, such as the time of the construction of the system (where $\mathbf{x}_{qty,0} = \mathbf{x}_{qty}(t = 0)$). The estimated quantities of materials and energy in $\mathbf{x}_{qty}(t)$ can be considered as random variables in the evaluation of the environmental performance of the system. Because of the recovery processes during the time horizon of interest, the vector of the quantity state variables changes from $\mathbf{x}_{qty,0}$ to $\mathbf{x}_{qty}(t)$, as discussed next.

3.2.1 Modeling the Change of the Quantity State Variables Due to the Recovery Processes

For the change of the quantity state variables due to the recovery processes of the system, we write $\Delta \mathbf{x}_{qty}(\tau)$ during the implementation of a corresponding recovery strategy, at any time $\tau \in [0, T_{R_{i,j}}]$, as

$$\Delta \mathbf{x}_{qty}(\tau) = \sum_{u=1}^{n_r} \Delta \mathbf{x}_{qty}(\tau_{r,u}) \mathbf{1}_{\{\tau_{r,u-1} < \tau \leq \tau_{r,u}\}} \tag{3}$$

where $\Delta \mathbf{x}_{qty}(\tau_{r,u})$ is the change of the quantity state variables after the completion of the recovery step at time $\tau_{r,u}$, and n_r is the number of recovery steps needed to restore the system to a target performance level. From the modeling of the recovery process, discussed in Sect. 3.1.2, we can obtain the number of recovery steps, n_r, for the system. Note that n_r is a random number which makes the sum in Eq. (3) a random sum.

In this formulation, $\Delta \mathbf{x}_{qty}(\tau_{r,u})$ reflects the incremental increase in the quantities of materials and energy used during the recovery process. Accordingly, we can write the change of the quantity state variables, after the completion of the uth recovery step at time $\tau_{r,u}$, as

$$\Delta\mathbf{x}_{qty}(\tau_{r,u}) = \Delta\mathbf{x}_{qty}\big[\mathbf{x}_{qty}(\tau_{r,u-1}), \mathbf{Q}_{st}(\tau_{r,u})\big] \tag{4}$$

where $\Delta\mathbf{x}_{qty}[\mathbf{x}_{qty}(\tau_{r,u-1}), \mathbf{Q}_{st}(\tau_{r,u})] = \mathbf{x}_{qty}(\tau_{r,u}) - \mathbf{x}_{qty},(\tau_{r,u-1})$ is the change of the quantity state variables between recovery steps $(u-1)$ and u, $\mathbf{x}_{qty}(\tau_{r,u-1})$ represents the values of the quantity state variables at the $(u-1)$th recovery step, and $\mathbf{Q}_{st}(\tau_{r,u})$ represents the target structural performance after completing the uth recovery step.

Since $\Delta\mathbf{x}_{qty}(\tau)$ corresponds to an incremental change of the quantity state variables, $\mathbf{x}_{qty}(\tau)$ includes the cumulative quantities of materials and energy used during the recovery period.

3.2.2 Modeling the Environmental Impact of the System

After modeling the quantity state variables over time, $\mathbf{x}_{qty}(t)$, these variables can then be used to estimate the time-varying environmental performance measures of the engineering system, denoted by the vector $\mathbf{Q}_{env}(t)$. The vector $\mathbf{Q}_{env}(t)$ includes various environmental impacts of interest such as carbon footprint, ozone depletion or smog. We write the vector of environmental system state as $\mathbf{Q}_{env}(t) = \mathbf{Q}_{env}[\mathbf{x}_{qty}(t), \mathbf{Y}_{qty}, \mathbf{W}_{qty}]$, where $\mathbf{Y}_{qty}$ is the matrix of environmental emissions associated with $\mathbf{x}_{qty}(t)$, and $\mathbf{W}_{qty}$ is the matrix of equivalency factors needed to determine the environmental impacts of interest based on the emissions in $\mathbf{Y}_{qty}$. Determining the matrices $\mathbf{Y}_{qty}$ and $\mathbf{W}_{qty}$ are two essential steps in evaluating the environmental impacts using the life-cycle assessment approach, according to the U.S. Environmental Protection Agency (EPA) (2006) and Heijungs and Suh (2002). In this formulation, the matrix $\mathbf{Y}_{qty} \in \mathbb{R}_{\geq 0}^{n_y \times n_q}$, where n_y is the number of the environmental emissions associated with $\mathbf{x}_{qty}(t)$, and the matrix $\mathbf{W}_{qty} \in \mathbb{R}_{\geq 0}^{n_y \times n_w}$, where n_w is the number of environmental impacts of interest associated with $\mathbf{Y}_{qty}$.

In this formulation, we can consider the environmental emissions and equivalency factors in $\mathbf{Y}_{qty}$ and $\mathbf{W}_{qty}$ as random variables to account for their uncertainty when estimating the environmental impacts of the system. Ultimately, we determine the environmental impacts of interest as

$$\mathbf{Q}_{env}(t) = \mathbf{x}_{qty}^T(t) \cdot \mathbf{Y}_{qty}^T \cdot \mathbf{W}_{qty} \tag{5}$$

Using Eq. (5), we can determine the cumulative environmental impact of the system up to time t during the time horizon of interest. The expression in Eq. (5) is a generic expression to evaluate $\mathbf{Q}_{env}(t)$, following Heijungs and Suh (2002). This expression allows us to compute the environmental impacts of a system and obtain similar impacts as the ones evaluated from commercially available software for life-cycle assessment.

4 Example

As an illustration of the proposed formulation, we model the environmental performance of an example RC bridge. We consider the RC bridge with one-single column bent in Kumar and Gardoni (2014b) and Jia et al. (2017). The bridge is subject to gradual deterioration due to corrosion, and to shock deterioration due seismic excitations. Figure 3 shows the bridge configuration in addition to a schematic layout of the hypothetical seismic site of the bridge. The structural properties of the bridge can be found in Kumar and Gardoni (2014b) and Jia et al. (2017). In this example, we evaluate the environmental performance of the bridge in terms of its carbon footprint over a set time horizon of 75 years. The carbon footprint represents the total amount of carbon dioxide equivalent (CO_2eq), in kilogram (kg), as a result of all the greenhouse gases associated with the system of interest. These greenhouse gases are due to the different processes associated with the bridge throughout the 75 years. Since the carbon dioxide equivalent is evaluated over time, we express the carbon footprint in this example as $CO_2eq(t)$. In this example, we make some simplifying assumptions, since the purpose of this example is to show how the proposed formulation works.

For the evaluation of the structural performance of the bridge, we use the reliability index, $\beta(t)$, and an intervention threshold of 3.09 to determine when a recovery of the bridge is needed (i.e., when $\beta(t) \leq 3.09$). This intervention threshold corresponds to a probability of failure, $P_f(t)$, of 0.001. For the purpose of illustration, we simulate three realizations of the change of $\beta(t)$, due to corrosion and seismic excitations, and the subsequent effect on $CO_2eq(t)$, over 75 years. Accordingly, the scope of evaluating $CO_2eq(t)$ includes the contribution of the construction of the bridge and the required recovery processes over the period of interest.
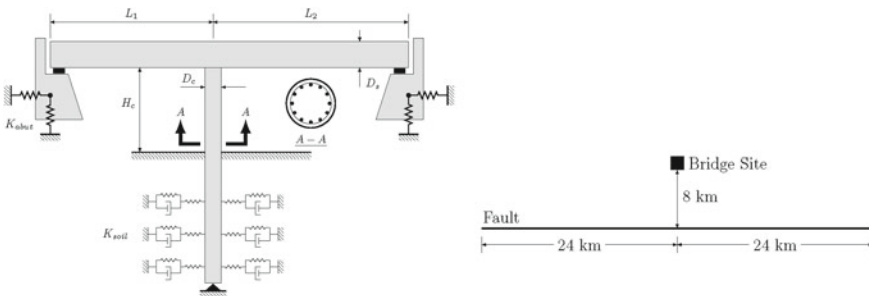

Fig. 3 The considered RC bridge and its hypothetical site (Adapted from Jia et al. 2017)

4.1 Structural Performance Analysis

The modeling of the gradual and shock deterioration processes and their impact on $\mathbf{x}_{st}(t)$ follows Jia et al. (2017). After determining $\mathbf{x}_{st}(t)$ for the realizations, we evaluate $P_f(t)$ similarly to Jia et al. (2017). Then, we can evaluate $\beta(t)$ as

$$\beta(t) = \Phi^{-1}\big[1 - P_f(t)\big] \tag{6}$$

where $\Phi^{-1}(\cdot)$ is the inverse of the standard normal cumulative distribution function (Ditlevsen and Madsen 1996; Gardoni 2017).

The recovery processes as result of the deterioration of $\beta(t)$ also follows Jia et al. (2017). We consider a repair strategy that consists of applying FRP to repair the bridge and restore it to a desired target state. Following Jia et al. (2017), we consider that the reliability index at the time of construction (i.e., $t = 0$), β_0, as the target performance level, where $\beta_0 = 3.196$. The recovery strategy is modeled with the FRP application as the sole recovery step. This means that the reliability of the bridge only improves once the FRP is applied to the bridge column. In this example, we consider a lag period, T_d, of 3 months, and a repair time, T_R, of 1 month. Based on this repair strategy, new structural state variables that characterize the FRP and its properties are introduced to $\mathbf{x}_{st}(t)$ during the recovery process. In particular in this example, we choose a carbon fiber reinforced polymer (CFRP) with a composite nominal strength of 3465 MPa, and a tensile modulus of 231 GPa for retrofitting the column of the bridge. Following the CFRP retrofit of the bridge, we do not consider the deterioration of the added CFRP, due to the lack of available models in the literature. As such, we might be overestimating the deterioration of $\beta(t)$ after a recovery process.

In case the application of FRP did not sufficiently improve the reliability of the bridge (due to accumulation of damage), then we consider a reconstruction of the bridge. This corresponds to the start of a new cycle for the bridge during the 75 years. For the reconstruction of the bridge, we consider a reconstruction time of 1.5 years.

4.2 Environmental Performance Analysis

To evaluate $CO_2eq(t)$ of the bridge for any realization, we first need to determine $\mathbf{x}_{qty}(t)$ associated with the recovery processes, in addition to $\mathbf{x}_{qty,0}$ due to the construction of the bridge at $t = 0$. In determining $\mathbf{x}_{qty}(t)$, we make some simplifying assumptions based on the available information.

For the construction of the bridge, $\mathbf{x}_{qty,0}$ is determined based on the initial bridge dimensions and material properties. To obtain $\mathbf{x}_{qty,0}$, we mainly focus on the materials and energy used for the construction of column of the bridge. That is because, in this example, we assume that the environmental impact due the construction of the bridge deck remains constant throughout the 75 years of interest, since the repair strategy

Table 1 Assumed quantities of materials and energy used for the bridge construction for all realizations

Material and Energy	Quantity	Unit
Concrete	15	m^3
Steel	0.5	m^3
Diesel (on site operations)	8	h
Diesel (transportation and hauling)	8.8	h

using CFRP mainly targets the column of the bridge (the CFRP is applied in the plastic hinge region of the column). We evaluate the volumes of concrete and steel, as well as the diesel used for the site operations and for the transportation of materials to and from the site. Table 1 shows the assumed quantities of materials and energy used for the construction of the bridge. For $\mathbf{x}_{qty}(t)$ associated with the recovery processes, we mainly determine the CFRP quantities needed to restore $\beta(t)$ to β_0. We consider a composite consisting of 65% fibers and 35% resin. In the case where a reconstruction is needed, then the additional material and energy requirements for the demolition of the bridge before its reconstruction are included in $\mathbf{x}_{qty}(t)$.

After determining $\mathbf{x}_{qty}(t)$, we can obtain $\mathbf{Y}_{qty}$ and $\mathbf{W}_{qty}$, as discussed in Sect. 3.2.2. In this example, $\mathbf{W}_{qty}$ is a vector since we are only determining the $CO_2eq(t)$ of the bridge. Using the databases in the LCA software, SimaPro (PRé Consultants 2016), we obtain $\mathbf{Y}_{qty}(t)$. The vector of $\mathbf{W}_{qty}(t)$ is obtained using the Tool for the Reduction and Assessment of Chemical and Other Environmental Impacts (TRACI v2.1) from the EPA. In this example, we assume that the environmental emissions in $\mathbf{Y}_{qty}$ are random variables and follow a lognormal distribution where each environmental emission has a mean corresponding to their value in $\mathbf{Y}_{qty}$ and a COV equal to 0.3 as a measure of the dispersion of each distribution. The simulation-based approach, from Jia and Gardoni (2018b), is used to probabilistically estimate the $CO_2eq(t)$ of the bridge for the realizations over 75 years.

4.3 Results

Figure 4 shows the change of $\beta(t)$ of the bridge due to the deterioration and recovery processes and the associated change in the expected value of $CO_2eq(t)$, denoted as $E[CO_2eq(t)]$, for the three realizations. In the first realization over 75 years (Realization 1), we observe that a total of three interventions are needed when $\beta(t) \leq 3.09$. At years 29.5, 49.2 and 61.7, a recovery strategy is required. We notice that, following the first repair strategy at year 29.5, the bridge is restored to a higher state than β_0, where $\beta(t = 29.9) = 3.47$.

However, for the second repair strategy at year 49.2, a reconstruction of the bridge is needed. This means that the repair strategy using CFRP is not sufficient to restore the bridge to a desired level in this case. This could be due to the accumulation of damage up to that time, which is not the case for the first repair strategy at a rel-
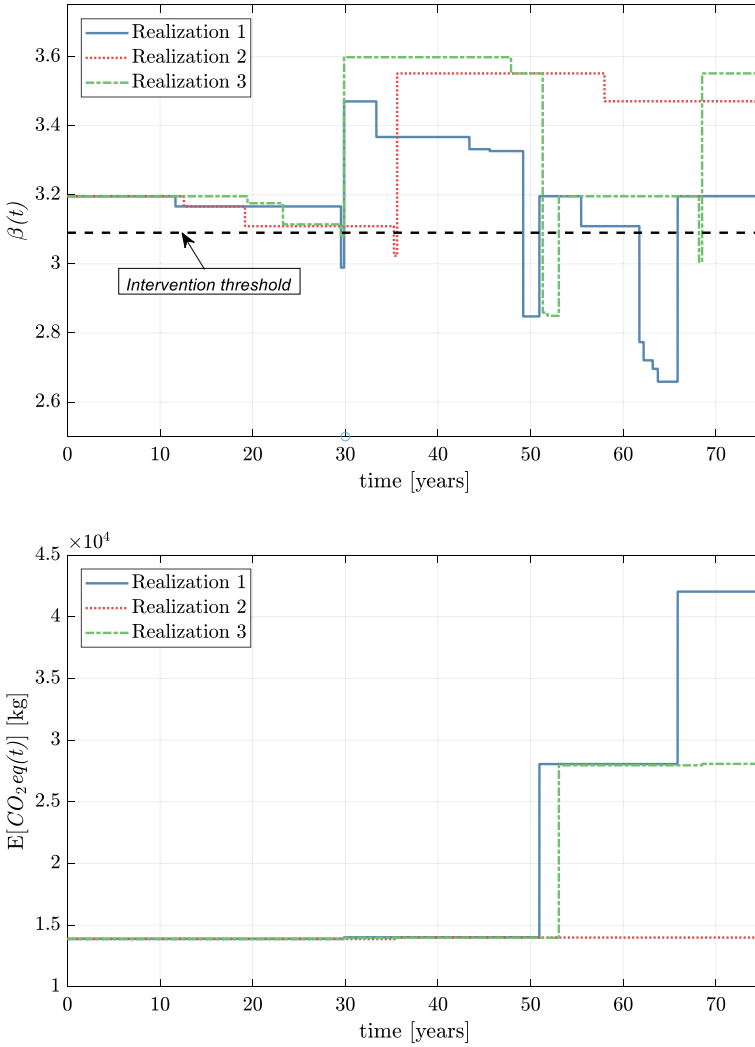
Fig. 4 The change of the bridge reliability (top plot) and the associated carbon footprint (bottom plot) during 75 years, for all realizations

atively early time in the bridge life-cycle (at year 29.5). Moreover, in some cases, additional repair and retrofitting schemes could be added to the repair strategy using CFRP to counteract the effects of the damage accumulated from the deterioration processes and further improve the structural performance of the bridge. These additional schemes, along with using CFRP, could be a solid alternative to reconstructing the bridge at year 49.2. Following its reconstruction, the bridge is again at β_0 and a new cycle begins during the time horizon of 75 years.

For the third recovery strategy at year 61.7, another reconstruction of the bridge is needed. Despite the relatively short interval of time between this reconstruction and the one at year 49.2, the bridge has deteriorated rapidly enough to require a reconstruction following the intervention. The rapid deterioration of the bridge is due to the occurrence of multiple earthquakes during this relatively short interval. In this realization, 20 aftershocks have occurred following a mainshock at $t = 61.7$ years. The continuous occurrence of aftershocks results in further deterioration of the structural state of the bridge, and subsequently in longer periods during which the bridge is down, as illustrated in Fig. 4. That is because, whenever an aftershock occurs during the recovery period following the lag period of 3 months, the reconstruction is reset from that time. And with another mainshock occurring at $t = 64.1$ years, the reconstruction of the bridge is completed at $t = 65.9$ years.

In the second realization over 75 years (Realization 2), we only observe one intervention at year 35.3. For this intervention, a repair strategy using CFRP is sufficient to restore the bridge to a significantly higher state, where $\beta(t = 35.6) = 3.55$. Despite requiring a recovery at $t = 35.3$ years, the bridge is restored to a better state compared to the first recovery at $t = 29.5$ years in Realization 1. This indicates that the bridge has sustained less damage in 35.3 years, in Realization 2, compared to the damage sustained in 29.5 years, in Realization 1. Following this repair strategy, no other repairs are needed during 75 years. This is in fact due to the low number of earthquakes that occurred during this time, for Realization 2. By comparing this realization with Realization 1, we notice the significant impact that the deterioration processes have on the state of the bridge and the associated recovery strategies.

As for the third realization (Realization 3), we observe three interventions during 75 years. The first intervention occurs at $t = 29.5$ years, similarly to Realization 1. Following the repair strategy using CFRP, the reliability of the bridge is restored to $\beta(t = 29.9) = 3.60$. From Fig. 4, we observe that the repair strategy in this realization restored the bridge to a higher state compared to the strategy in Realization 1. This further emphasizes the impact of the accumulated damage due to the deterioration processes on the recovery strategies.

For the second recovery strategy at $t = 51.3$ years, a reconstruction of the bridge is needed. As in Realization 1, the multiple aftershocks occurring following the mainshock at $t = 51.3$ years, have further deteriorated $\beta(t)$ and delayed the recovery period. The final recovery at $t = 68.2$ years consists of a repair strategy using CFRP, where $\beta(t = 68.5) = 3.55$.

For $\mathrm{E}[CO_2eq(t)]$ due to the construction and the recovery processes for Realization 1, we first observe a jump in the carbon footprint due to the construction at $t = 0$, $\mathrm{E}[CO_2eq_0]$. In Realization 1, the increase in $\mathrm{E}[CO_2eq(t)]$ due to the repair strategy using CFRP at $t = 29.9$ years is minor compared to the increase due to the reconstruction of the bridge.

Similarly for Realization 2, we first observe $\mathrm{E}[CO_2eq_0]$ and a small increase in $\mathrm{E}[CO_2eq(t)]$ due the repair strategy using CFRP at $t = 35.6$ years. As for Realization 3, we observe an increase of $\mathrm{E}[CO_2eq(t)]$ similar to $\mathrm{E}[CO_2eq_0]$ due the

reconstruction of the bridge. Moreover, we notice a small increase in $E[CO_2eq(t)]$ associated with each of the repair strategies using CFRP at years 29.5 and 68.2.

The increase in $E[CO_2eq(t)]$ at years 29.5, 35.3 and 68.2 is of similar magnitude, for all three realizations, due to the application of a similar amount of CFRP at each intervention. CFRP with thicknesses 1.35, 1.45, 1.45, and 1.35 mm are required around the plastic hinge for the repair strategies at year 29.5 (for Realization 1 and 3), 35 (for Realization 2) and 68.2 (for Realization 3), respectively. In addition, the small magnitude of the change in $E[CO_2eq(t)]$ due to these repair strategies, compared to $E[CO_2eq_0]$, reflects the difference in the contributions of the construction and each repair strategy to the overall $E[CO_2eq(t)]$.

We can observe, however, the significant increase in $E[CO_2eq(t)]$ due to the reconstruction of the bridge at different instances for Realization 1 and 3. This means that the $E[CO_2eq(t)]$ due to the multiple recovery strategies required during these 75 years exceeds the impact of the $E[CO_2eq_0]$ due to the bridge construction at $t = 0$. Accordingly, this reflects the importance of considering the deterioration of the bridge in evaluating its environmental performance, since the deterioration processes ultimately lead to the recovery processes which result in an increase of the $E[CO_2eq(t)]$ of the bridge over time.

From the simulation-based approach, we obtain a probabilistic output of the $CO_2eq(t)$ due to the construction of the bridge and the subsequent recovery processes for the three realizations, as presented in Table 2 which shows the mean and standard deviation of the $CO_2eq(t)$ during 75 years.

Table 2 Mean and standard deviation of the carbon footprint of the bridge due to construction and the recovery processes during 75 years, for all realizations

	Time (years)	Mean (kgCO$_2$ eq)	Standard Deviation (kgCO$_2$ eq)
Realization 1	0	13894	2516
	29.9	118.1	26.1
	51	14043.2	2541
	65.9	13981.9	2559.1
Realization 2	0	13868.3	2530.6
	35.6	117.6	25.8
Realization 3	0	13854.4	2564.9
	29.9	118.1	26.1
	53.1	13980.4	2550.2
	68.5	117.5	25.7

5   Conclusions

This chapter proposed a stochastic formulation for the evaluation of the life-cycle sustainability of engineering systems, named Stochastic Life-cycle Sustainability Analysis (SLCSA). In the SLCSA, the sustainability of the system is evaluated in terms of its environmental impact over a fixed time horizon. The formulation provides a more comprehensive approach to estimate the environmental impact of any structure or infrastructure, by considering the environmental impacts due to the various processes, such as the construction and recovery processes, associated with that engineering system. Moreover, the proposed formulation accounts for the relevant uncertainties, such as those in the external conditions, and those in the environmental emissions associated with the materials and energy processes used during the time horizon of interest, in determining the environmental impact of the engineering system.

   As an illustration, the life-cycle sustainability evaluation of an example RC bridge, subject to corrosion and seismic excitations, is presented. In the example, the carbon footprint due to construction of the bridge and subsequent recovery processes is evaluated for three life-cycle realizations. Based on the realizations of the bridge deterioration, the results indicated that the cumulative carbon footprint from the recovery processes can exceed the initial footprint due to construction. This is particularly the case when a repair strategy, such a CFRP retrofit scheme, is not sufficient to restore the bridge to a target state, and a reconstruction of the bridge is thus needed. The example shows the importance of considering the deterioration of engineering systems when evaluating their sustainability over a time horizon of interest. Subsequently, the estimated environmental impacts can be used in an optimization problem for the design and management of resilient and sustainable engineering systems.

References

Abdallah, M., & El-Rayes, K. (2016). Multiobjective optimization model for maximizing sustainability of existing buildings. *Journal of Management in Engineering, 32*(4), 04016003.

Alibrandi, U., & Mosalam, K. M. (2017). A decision support tool for sustainable and resilient building design. In P. Gardoni (Ed.), *Risk and reliability analysis: Theory and applications* (pp. 509–536). Cham: Springer.

Alibrandi, U., & Mosalam, K. M. (2019). Lifecycle multi criteria decision analysis of buildings using generalized expected utility. In P. Gardoni (Ed.), *Handbook of sustainable and resilient infrastructure* (pp. 770–788). Routledge: Taylor & Francis Group.

Biswas, W. K. (2014). Carbon footprint and embodied energy consumption assessment of building construction works in Western Australia. *International Journal of Sustainable Built Environment, 3,* 179–186.

Bruneau, M., Chang, S. E., Eguchi, R. T., Lee, G. C., O'Rourke, T. D., Reinhorn, A. M., et al. (2003). A framework to quantitatively assess and enhance the seismic resilience of communities. *Earthquake Spectra, 19*(4), 733–752.

Caverzan, A., & Solomos, G. (2014). Review on resilience in literature and standards codes for critical built-infrastructures. *JRC Science and Policy Report*.

Choe, D., Gardoni, P., Rosowsky, D., & Haukaas, T. (2008). Probabilistic capacity models and seismic fragility estimates for RC columns subject to corrosion. *Reliability Engineering and System Safety, 93*(3), 383–393.

Choe, D., Gardoni, P., Rosowsky, D., & Haukaas, T. (2009). Seismic fragility estimates for reinforced concrete bridges subject to corrosion. *Structural Safety, 31,* 275–283.

Choe, D., Gardoni, P., & Rosowsky, D. (2010). Fragility increment functions for deteriorating reinforced concrete bridge columns. *ASCE Journal of Engineering Mechanics, 136*(8), 969–978.

Cimellaro, G. P., Reinhorn, A. M., & Bruneau, M. (2010). Framework for analytical quantification of disaster resilience. *Engineering Structures, 32*(11), 3639–3649.

Decò, A., Bocchini, P., & Frangopol, D. M. (2013). A probabilistic approach for the prediction of seismic resilience of bridges. *Earthquake Engineering and Structural Dynamics, 42*(10), 1469–1487.

Ditlevsen, O., & Madsen, H. O. (1996). *Structural reliability methods*. New York: Wiley.

Doorn, N., Gardoni, P., & Murphy, C. (2018). A multidisciplinary definition and evaluation of resilience: The role of social justice in defining resilience. *Sustainable and Resilient Infrastructure*. https://doi.org/10.1080/23789689.2018.1428162.

Ellingwood, B. R., Cutler, H., Gardoni, P., Peacock, W. G., van de Lindt, J. W., & Wang, N. (2016). The centerville virtual community: A fully integrated decision model of interacting physical and social infrastructure systems. *Sustainable and Resilient Infrastructure, 1*(3–4), 95–107.

Environmental Protection Agency. (2006). *Life-cycle assessment: Principles and practice, EPA/600/R-06/060*. Cincinnati, Ohio, USA: Office of Research and Development.

Gardoni, P. (Ed.). (2017). *Risk and reliability analysis: Theory and applications*. New York: Springer.

Gardoni, P. (Ed.). (2019). *Handbook of sustainable and resilient infrastructure*. Routledge.

Gardoni, P., Mosalam, K. M., & Der Kiureghian, A. (2003). Probabilistic seismic demand models and fragility estimates for RC bridges. *Journal of Earthquake Engineering, 7*(1), 79–106.

Gardoni, P., & Murphy, C. (2008). Recovery from natural and man-made disasters as capabilities restoration and enhancement. *International Journal of Sustainable Development and Planning, 3,* 317–333.

Gardoni, P., & Murphy, C. (2018). Society-based design: promoting societal well-being by designing sustainable and resilient infrastructure. *Sustainable and Resilient Infrastructure*. https://doi.org/10.1080/23789689.2018.1448667.

Gardoni, P., & Rosowsky, D. (2011). Seismic fragility increment functions for deteriorating reinforced concrete bridges. *Structure and Infrastructure Engineering, 7*(11), 869–879.

Gardoni, P., Der Kiureghian, A., & Mosalam, K. M. (2002). Probabilistic capacity models and fragility estimates for reinforced concrete columns based on experimental observations. *Journal of Engineering Mechanics, 128,* 1024–1038.

Gardoni, P., Guevara-Lopez, F., & Contento, A. (2016). The life profitability method (LPM): A financial approach to engineering decisions. *Structural Safety, 63,* 11–20.

Gharzouzi, P., & Gardoni, P. (2019a). A stochastic formulation for evaluating the sustainability of engineering systems based on their structural performance. *Journal of Cleaner Production* (in preparation).

Gharzouzi, P., & Gardoni, P. (2019b). Stochastic life-cycle sustainability analysis: A stochastic formulation for evaluating the sustainability of engineering systems considering the structural and mechanical performance of their various components. *Building and Environment* (in preparation).

Guidotti, R., Chmielewski, H., Unnikrishnan, V., Gardoni, P., McAllister, T., & van de Lindt, J. W. (2016). Modeling the resilience of critical infrastructure: The role of network dependencies. *Sustainable and Resilient Infrastructure, 1*(3–4), 153–168.

Guidotti, R., Gardoni, P., & Rosenheim, N. (2019). Integration of physical infrastructure and social systems in communities' reliability and resilience analysis. *Reliability Engineering and System Safety*. https://doi.org/10.1016/j.ress.2019.01.008.

Heijungs, R., & Suh, S. (2002). *The computational structure of life cycle assessment*. Dordrecht: Springer Science + Business Media.

ISO 14040. (2006). *Environmental management—Life cycle assessment—Principles and framework*. ISO 14040:2006, International Organization of Standardization, Geneva Switzerland.

ISO 14044. (2006). *Environmental management—Life cycle assessment—Requirements and guidelines.* ISO 14044:2006, International Organization of Standardization, Geneva Switzerland.

Jia, G., Tabandeh, A., & Gardoni, P. (2017). Life cycle analysis of engineering systems: Modeling deterioration, instantaneous reliability, and resilience. In P. Gardoni (Ed.), *Risk and reliability analysis: Theory and applications* (pp. 465–494). Cham: Springer.

Jia, G., & Gardoni, P. (2018a). State-dependent stochastic models: A general stochastic formulation for modeling deteriorating engineering systems considering multiple deterioration processes and their interactions. *Structural Safety, 72,* 99–110.

Jia, G., & Gardoni, P. (2018b). Simulation-based approach for estimation of stochastic performances of deteriorating engineering systems. *Probabilistic Engineering Mechanics, 52,* 28–39.

Jia, G., & Gardoni, P. (2019). Stochastic life-cycle analysis: Renewal-theory life-cycle analysis with state-dependent deterioration stochastic models. *Structure and Infrastructure Engineering* (accepted).

Koliou, M., van de Lindt, J. W., McAllister, T. P., Ellingwood, B. R., Dillard, M., & Cutler, H. (2018). State of the research in community resilience: Progress and challenges. *Sustainable and Resilient Infrastructure*. https://doi.org/10.1080/23789689.2017.1418547.

Kumar, R., Gardoni, P., & Sanchez-Silva, M. (2009). Effect of cumulative seismic damage and corrosion on life-cycle cost of reinforced concrete bridges. *Earthquake Engineering and Structural Dynamics, 38*(7), 887–905.

Kumar, R., & Gardoni, P. (2012). Modeling structural degradation of RC bridge columns subjected to earthquakes and their fragility estimates. *Journal of Structural Engineering, 138,* 42–51.

Kumar, R., & Gardoni, P. (2014a). Effect of seismic degradation on the fragility of reinforced concrete bridges. *Engineering Structures, 79,* 267–275.

Kumar, R., & Gardoni, P. (2014b). Renewal theory-based life-cycle analysis of deteriorating engineering systems. *Structural Safety, 50*(94), 102.

Kumar, R., Cline, D., & Gardoni, P. (2015). A stochastic framework to model deterioration in engineering systems. *Structural Safety, 53,* 36–43.

Mara, V., Haghani, R., & Harryson, P. (2013). Bridge decks of fibre reinforced polymer (FRP): A sustainable solution. *Construction and Building Materials, 50,* 190–199.

Nocera, F., Gardoni, P., & Cimellaro, G. P. (2019). Time-dependent probability of exceeding a target level of recovery in resilience analysis. *ASCE-ASME Journal of Risk and Uncertainty in Engineering Systems* (accepted).

PRé Consultants. (2016). SimaPro Version 8.3, LCA Software.

Ramesh, T., Prakash, R., & Shukla, K. K. (2010). Life cycle energy analysis of buildings: An overview. *Energy and Buildings, 42*(1592), 1600.

Seo, S., & Hwang, Y. (2001). Estimation of CO_2 emissions in life cycle of residential buildings. *Journal of Construction Engineering and Management, 127*(5), 414–418.

Sharma, N., Tabandeh, A., & Gardoni, P. (2018). Resilience analysis: A mathematical formulation to model resilience of engineering systems. *Sustainable and Resilient Infrastructure, 3*(2), 49–67.

Simon, J., Bracci, J., & Gardoni, P. (2010). Seismic response and fragility of deteriorated reinforced concrete bridges. *ASCE Journal of Structural Engineering, 136*(10), 1273–1281.

Tabandeh, A., & Gardoni, P. (2014). Probabilistic capacity models and fragility estimates for RC columns retrofitted with FRP composites. *Engineering Structures, 74,* 13–22.

Tabandeh, A., & Gardoni, P. (2015). Empirical Bayes approach for developing hierarchical probabilistic predictive models and its application to the seismic reliability analysis of FRP-retrofitted RC bridges. *ASCE-ASME Journal of Risk and Uncertainty in Engineering Systems Part A: Civil Engineering, 1*(2), 04015002.

Tapia, C., Ghosh, J., & Padgett, J. E. (2011). Life cycle performance metrics for aging and seismically vulnerable bridges. *Structures Congress*.

Tool for Reduction and Assessment of Chemicals and Other Environmental Impacts (TRACI) (https://www.epa.gov/chemical-research/toolreduction-and-assessment-chemicals-andother-environmental-impacts-traci).

Yang, R., & Al-Qadi, I. L. (2017). Development of a life-cycle assessment tool to quantify the environmental impacts of airport pavement construction. *Transportation Research Record: Journal of the Transportation Research Board, 2603,* 89–97.

Yu, B., & Lu, Q. (2012). Life cycle assessment of pavement: Methodology and case study. *Transportation Research Part D, 17,* 380–388.

Welsh-Huggins, S. J., & Liel, A. B. (2016). A life cycle framework for integrating green building design and hazard resistant design: Examining the seismic impact of buildings with green roofs. *Structure and Infrastructure Engineering, 13*(1), 19–33.

Zhong, J., Gardoni, P., & Rosowsky, D. (2012). Seismic fragility estimates for corroding reinforced concrete bridges. *Structure and Infrastructure Engineering, 8*(1), 55–69.